Title
Experimental Study and Retrofit of a Non-Ductile Concrete Moment Frame Building Subjected to Biaxial Quasi-Static Seismic Loading

Author
Moore, Elham

Publication Date
2021

Peer reviewed|Thesis/dissertation

UNIVERSITY OF CALIFORNIA

Los Angeles

Experimental Study and Retrofit of a Non-Ductile Concrete Moment Frame Building Subjected to Biaxial Quasi-Static Seismic Loading

A dissertation submitted in partial satisfaction of the

requirements for the degree Doctor of Philosophy

in Civil Engineering

by

Elham Moore

2021

2021

ABSTRACT OF THE DISSERTATION

Experimental Study of a Non-Ductile Concrete Moment Frame Building

Subjected to Biaxial Quasi-Static Seismic Loading

by

Elham Moore

Doctor of Philosophy in Civil Engineering

University of California, Los Angeles, 2021

Professor John Wright Wallace, Chair

The ability of reinforced concrete (RC) columns to continue to deform with reduced capacity depends on the ability of the floor system to redistribute some of the axial load from heavily damaged element to adjacent members to prevent the collapse of the structure when that happens. Physical testing of columns, although does not fully capture the behavior of the building as a system, is the closest approach to simulate behavior of columns that undergo high constant or varying axial forces. That is by choosing boundary conditions that are representative of actual conditions, as accurately as possible. However, physical testing of a building subassembly is a more powerful tool to provide realistic information on the performance level of existing buildings under seismic loads, as well as to better demonstrate the governing failure modes of the system working together, rather than evaluating members individually.

Two large-scale beam-column-slab subassemblies were tested under biaxial quasi-static, reversed

cyclic loading are discussed in this report. The test specimens are replicas of elements from a non-ductile concrete moment frame building located on the UCLA campus, the Franz Tower (currently named the Pritzker Hall). The reinforced concrete building originally constructed in the late 60s consists of six levels with closely spaced perimeter columns supported on a transfer girder, with two open lower levels supported on a widely spaced column grid. The lateral force resisting system at the upper six levels consists of trapezoidal columns spaced at 4 ft. (1219 mm) on center along the perimeter of the structure, with trapezoidal beams spanning between the columns. Traditional retrofit techniques in accordance with the governing building codes and the *University of California Seismic Performance Rating (UCSPC)*, suggested a high cost retrofit scheme with significant disruption to the architecture of the building. This is believed to be attributed to these main reasons:

1- The governing standard for seismic evaluation and rehabilitation of existing buildings, ASCE/SEI 41-13 Seismic Evaluation and Retrofit of Existing Buildings, herein referred to as ASCE 41-13, was conservative in predicting deformation capacity of building components when subjected to lateral (seismic) loading, especially when the building components fell under the non-conforming criteria, hence underestimating their performance.

2- The cross sections of the frame beams and columns were not rectangular which is the common type of cross section for typical moment frames. As a result, there was an inherent ambiguity in the capability of the non-linear modeling parameter offered by ASCE 41-13 to predict the performance achieved by the moment frames in the Franz Tower.

3- Another uncommon characteristic of this building was the aspect ratio of the moment frames (bay width/story height), which is less than 0.3 (with the beam span of 4 ft. (1219 mm) and column height of about 12. ft 9 in. (3886 mm), while aspect ratios of more than or equal to 1 are more common. Therefore, the beams were rigid and would not be able to sustain a double curvature deformation, as common in the moment frame beams.

4- The repetitive frame system around the perimeter of the building provided a high level of redundancy that was not observed in typical buildings, nor in the test data used to derive the ASCE 41-13 modeling parameters.

To evaluate all the issues mentioned above, a detailed physical testing program was designed with an emphasis on obtaining the overall force-deformation backbone curve for the subassembly. In order to use the data obtained from the physical testing, it was imperative to recreate the experimental backbone curve in Perform-3D, by making necessary modifications to the modeling parameters of the building components. These modifications were based on the observed damage at each drift level, and at each building component, and included the plastic deformation capacity of the columns, flexural residual strength of the columns, and shear capacity of the beams. Those modifications were later applied to the Perform-3D model of the actual building in an attempt to assess its actual performance under seismic loading.

This study presents the findings of the two biaxial tests conducted on two building subassemblies and reveals that the test specimens sustained damages beyond the Collapse Prevention and Life-Safety limits of ASCE 41-13. The specimens did not lose their gravity load-carrying capacity during the test (even after exceeding 2.5% lateral drift ratio), which also provided for a higher Expected Seismic Level Performance per UCSPR, performance rating III (seismic safety policy compliant).

Finally, this study provides a holistic overview on the proposed retrofit program that includes downtime and repair costs in case of a major ground shaking, utilizing the FEMA P-58, *Seismic*

Performance Assessment of Buildings, Methodology which was developed by the Applied Technology Council (ATC) and funded by FEMA. (ATC, 2020)

This study includes building assessments per the Seismic Performance Prediction Program (SP3), including analyses per the governing standards, as well as analyses per the experimental test observations. Downtime and repair cost are of great importance to the public while not directly considered in ASCE 41-13 and other local building documents. Hence, the SP3 Risk Model Engine, was used to calculate the mean loss and time to regain function. Implementation of test data in the SP3 analysis input showed not only the retrofit program enhanced building performance in terms of life safety of the occupants, but it also showed lower expected loss, as well as significantly lower downtime in comparison to prescriptive retrofit methods.

The dissertation of Elham Moore is approved.

Thomas A. Sabol

Henry J. Burton

Saman A. Abdullah

Scott J. Brandenberg

John Wright Wallace, Committee Chair

University of California, Los Angeles

2021

To the love of my life, Alireza.

You make me a better person every day.

To my parents, Shahin and Ali.

Your unconditional love and sacrifices shaped who I am today.

To Nasrin, Kambiz, Bita, Reza, A.J., Mahsa, Cameron, Aiden, and Noyan.

You are my world.

LIST OF FIGURES

LIST OF TABLES

TABLE OF CONTENTS

LIST OF NOTATIONS

A_g = gross reinforced concrete section, neglecting the impact of reinforcement

A_s = longitudinal steel reinforcement bar cross-sectional area

A_{st} = transverse steel reinforcement bar cross-sectional area

b_w = beam web width

c_1 = dimension of rectangular or equivalent rectangular column, capital, or bracket measured in the direction of the span for which moments are being determined

c_2 = dimension of rectangular or equivalent rectangular column, capital, or bracket measured in the direction perpendicular to c_1

d = distance from extreme compression fiber to centroid of tension reinforcement

d_b = nominal diameter of steel reinforcement

E_c = Young's modulus of concrete

E_s = Young's modulus of steel

f_c' = specified (design) compressive strength of concrete

$f_{c,test}'$ = measured (tested) compressive strength of concrete at test-day age

f_y = specified (design) yield strength of reinforcement

$f_{y,e}$ = measured (tested) yield strength of reinforcement

$f_{y,L}$ = specified (design) yield strength of longitudinal reinforcement

$f_{y,t}$ = specified (design) yield strength of transverse reinforcement

f_u = measured (tested) tensile strength of reinforcement

h = column clear height

h_b = beam total depth

h_c = column total depth

I_{eff} = effective moment of inertia

I_g = gross-section moment of inertia about centroidal axis

l_n = clear span (length) of beam measured from face-to-face of wall

M_n = nominal moment strength determined in accordance with ACI 318-14 for RC beams and AISC 360-10 for SRC beams

n = modular ratio (E_s/E_c)

s = center-to-center horizontal spacing of transverse reinforcement

S_a = Pseudospectral Acceleration

S_d = Spectral Displacement

s/d_b = bar slenderness ratio computed as the ratio of center-to-center horizontal spacing of transverse reinforcement to diameter of smallest longitudinal bar

V = applied lateral load

V_u = design shear demand

$V@M_n$ = shear strength corresponding to nominal moment capacity, M_n

$V@M_{pr}$ = shear strength corresponding to probable flexural strength, M_{pr}

V_{peak} = peak (maximum) shear strength obtained during seismic testing

V_n = design (nominal) shear strength computed from ACI 318-14 Eq. 22.5.5.1 and Eq. 22.5.10.5.3

V_y = yield strength of column at first yield

ϕ = strength reduction factor taken as 0.75 and 0.9 for shear and flexural strengths of RC beams, respectively

ACKNOWLEDGEMENTS

The work presented in this research was funded by the UCLA Capital Programs as a part of their seismic evaluation and rehabilitation of potentially hazardous buildings. We are thankful to Dr. Luis Toranzo and Mark Hershberg at KPFF Consulting Engineers for their support during the testing program. Special gratitude goes to Dr. Maikol Del Carpio at KPFF for his guidance, time, and dedication during the course of writing this dissertation.

We are thankful to Thai Nguyen and Allen Hill and the construction team at PCL Construction for their special attention to this project.

We are grateful to the Haselton-Baker Risk Group for providing us with an academic license of the SP3 software (www.hbrisk.com) to be used in the performance of this work and making their technical team available when needed.

Special gratitude goes to Exponent for donating the cameras that recorded images and video through the testing program.

We also acknowledge Dr. Eric Ahlberg, Laboratory Manager and Principal Development Engineer in the Department of Civil and Environmental Engineering at UCLA, for important contributions related to instrumentation, data acquisition, and testing program.

We would also like to particularly thank Amin Safdari, a UCLA PhD candidate, for his support during construction and testing of the specimens. Special thanks go to Dr. Negin A. Tauberg for her invaluable contributions during writing of this document. Our acknowledgments extend to former UCLA PhD students (Saman Abdullah, Sofia Gavridou, Christopher Segura, Reza Ghotbi, Shahrzad Dastmalchi, and Han Sun), current PhD students (Matías Rojas León and Mehmet Emre Ünal), and undergraduate students (Christopher Law, Jordi Anggada Putra, and Marco Espinoza) for their assistance during construction, fabrication, testing, and data analysis.

VITA

2005	B.S., Civil Engineering Sharif University of Technology, Tehran, Iran
2005-2007	Mathematics and Physics Teacher and Student Mentor Malek Orphanage, Tehran, Iran
2008-2012	Senior Engineer Structural Design Plus, Los Angeles, CA
2010	Master of Building Science University of Southern California
2010	Graduate Student Researcher University of Southern California
2012-2014	Project Manager AECOM/URS Corporation, Los Angeles, CA
2012-2014	Structural Engineer Mentor ACE (Architecture, Construction, Engineering) Mentor Program Los Angeles, CA

2013-Present	Engineering Consultant EA Solutions, Los Angeles, CA
2015-2021	Graduate Student Researcher Department of Civil and Environmental Engineering University of California, Los Angeles
2016-2021	Teaching Assistant Department of Civil and Environmental Engineering University of California, Los Angeles, CA
2017-2019	Associate | Project Manager Waler P. Moore, Los Angeles, CA
2018-Present	Chair of Board of Directors Keep Children in School Foundation, Los Angeles, CA
2019-2020	Adjunct Faculty Department of Architecture Woodbury University, Burbank, CA

Chapter 1. Introduction

1.1. Background and Motivation

Reinforced concrete (RC) moment frames are commonly used to provide primary lateral seismic force-resistance for low- to mid-rise buildings located in regions with strong earthquake ground shaking. They are also highly desirable by architects due to planning flexibility and openness. Modern seismic design and evaluation building codes allow the seismic force-resisting system to experience inelastic response under design level shaking (ASCE 7-16). Research has demonstrated that concrete moment frame buildings with properly proportioned and detailed beams, columns, and joints generally perform well in strong shaking (Comartin, 2008). Seismic detailing requirements for moment frames were first introduced into the International Building Code (IBC) in 1976 and the California Building Code (CBC) in 1977. The corresponding document for concrete building design was ACI 318-71 which was based on ultimate design and introduced a commentary for the first time (ACI 318, 2019). However, there are a large number of existing concrete frame buildings in regions impacted by strong shaking that were designed prior to 1977, and hence, were designed using provisions that are known to be insufficient and make such buildings susceptible to collapse in strong shaking (Holmes, 2014).

To address the potential hazard non-ductile concrete frames built prior to IBC-1976 pose to the society in case of a major ground shaking, the City of Los Angeles passed Article 1, Division 95 of LADBS Ordinance 183893, also known as the Los Angeles Non-Ductile Concrete Retrofit Program, in 2015. This ordinance includes guidelines on the mandatory seismic evaluation of any existing concrete building built pursuant to a permit application for a new building that was submitted before January 13, 1977. For any buildings that the evaluation identifies non-conforming, a retrofit plan must be developed and implemented within 25 years.

Due to the deficiencies of ASCE 41-13 in estimating existing building performance, and the mandate of the LADBS Ordinance 183893 which requires retrofit plan, engineers are utilizing innovative approaches that enable them to predict the seismic building performance more accurately. Amongst such approaches are material strength testing, laboratory testing of building components (Taylor-Lange, et al., 2007), and when possible, a building subassembly. Physical testing of a building subassembly is a powerful tool to provide improved information on the performance of existing buildings under seismic loads, as well as to better demonstrate the governing modes of failure and important interactions that are not captured if individual components are tested. This is particularly effective for unusual systems that may not be easily categorized into conditions covered in ASCE 41-13.

Moreover, ASCE 41 and other governing documents, such as the UC Seismic Rating System (UCSRS), primarily focus on the performance of the building in terms of threat to the lives of the occupants in case of a major ground shaking, and less on the cost of repair and the time to regain function of the building after such incident. However, these two parameters are of extreme importance to the public and significantly affect the resiliency of the society after a major earthquake.

The challenges in the existing building evaluation, and other important parameters that are overlooked in the governing building codes, are the motivation for this research and discussed in the next sections.

1.1.1. ASCE 41 Deficiencies

Due to the lack of experimental data on the performance of existing buildings that were constructed prior to 1977, the current building codes highly discount the performance of such buildings; especially if the building components do not fit nicely in the defined ASCE 41 bins. The deficiencies of ASCE 41 document are discussed in detail in Chapter 2.

1.1.2. Lack of Information on Deformation Capacity of Poorly Detailed Columns

Prior to about 1977, detailing requirements (ductility) for gravity force-resisting systems were not significantly different from the requirements for lateral force-resisting systems.

For design of new buildings per current codes (ASCE 7-16), all earthquake forces are resisted by a designated lateral-force resisting system. However, for evaluation and retrofit of an existing (and likely deficient) building, neglecting resistance of the gravity system is likely to lead to overly conservative and inaccurate assessments, especially if the gravity system is detailed similarly to the lateral system. It is also important to evaluate the gravity system columns and ensure they are adequately detailed (with transverse reinforcement) to undergo lateral deformations caused by ground shakings, without collapse (deformation compatibility).

It is worth noting that detailing requirements for the lateral force-resisting elements, especially columns improved after the 1976 IBC, but lack of provisions for deformation capability of the gravity force-resisting systems caused significant damage to buildings in the 1994 Northridge Earthquake. (Gould, Kallros, & Dowty, 2019) (CUREe, 1998) The failure of the gravity system at the Zelzah parking structure (located on the California State University, Northridge campus, built in 1992), caused total collapse of the building in the 1994 Northridge earthquake, as shown in Figure 1-1. (California State University, 2019) (Todd, et al., 1994)

Figure 1-1: Collapse of Parking Structure at California State University, Northridge after the 1994 Earthquake (California State University, 2019)

However, it should be emphasized that in buildings constructed per the 1976 version of the IBC, there is not a significant difference in the detailing and placement of the transverse reinforcement in the moment frame beams and columns, and the gravity beams and columns; hence all are assumed to contribute to the stiffness of the building and resistance of the lateral forces.

1.1.3. Lack of Knowledge on Behavior of Non-Rectangular Building Components

Brutalist architecture is a style that emerged in the 1950s in Great Britain in the post-World War II era and continued throughout the 1970s. Brutalism is mainly characterized by simple and minimalistic designs, in contrast to the ornate design styles of the pre-war era, featuring the building materials, notably concrete, celebrating angular shapes and geometric building components (beams and columns) as architecture design features as shown in Figure 1-2. (Alfirevic & Alfirevic, 2017)

Many buildings requiring seismic evaluation and retrofit per LADBS Ordinance 183893, are brutalist style with odd cross-sectional geometries of building components, which ASCE 41-13 standard is not able to predict their deformation capacity accurately due to lack of testing data for such building components and geometries during the development of the standard.

Figure 1-2: Brutalist Architecture Examples: Inglewood City Hall, California (Left), Rainier Tower, Washington (Middle), One World Trade Center, New York (Right)

1.1.4. Sensitivity of the Building Model to Modeling Parameters

Preliminary evaluations of the building using ASCE 41-13 non-linear static procedure (NSP) and non-linear dynamic procedure (NDP) indicated that results were sensitive to the modeling parameters used for the beams and columns, which, due to their odd geometries and detailing, do not fit nicely into predefined ASCE 41-13 bins used to define modeling parameters. Per preliminary evaluations, the trapezoidal beams failed at 0.1% lateral drift, not satisfying the University of California Seismic Performance Rating (UCSPR), while based on the performance of this building and similar buildings in the 1994 Northridge Earthquake, it is expected that the building sustains about 1% of lateral drift ratio. This drift level is possible to achieve by utilizing viscous dampers throughout the building to reduce the deformation demands. Physical testing is a powerful tool to fill the knowledge gap between failure at 0.1% drift and the intuitive deformation capacity of highly redundant systems of about 1% or higher, as shown in Figure 1-3.

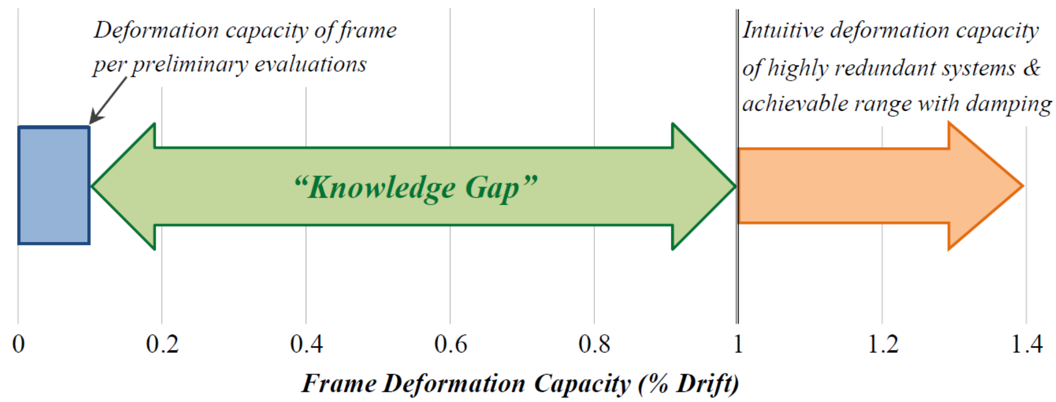

Figure 1-3: Existing Frame Lateral Deformation Capacity (% Drift)

This report includes findings related to large-scale biaxial testing of two beam-column-slab subassemblies of a non-ductile concrete moment frame building, the Franz Tower (Figure 1-4). The odd geometry and unusual shapes of the frame components, and their repetitiveness, combined with the deficiencies of ASCE 41-13 discussed above, resulted in preliminary evaluations of the building that were deemed conservative, and not fully representative of the actual performance of the building under seismic loading. Additionally, due to the geometry and orientation of the closely spaced exterior columns (Figure 3-2), it was deemed necessary to study both the in-plane and out-of-plane behavior of the frame columns under biaxial loading. There is a lack of information and test data for large-scale tests, which are expensive and more complex, especially in case of building subassembly testing as opposed to individual building component testing. There is also a lack of information on biaxial testing conducted on large scale concrete frames, especially on three-dimensional test specimens that include the slab system.

All the above, make the test unique in nature due to complexity, scale, and loading program. Hence two building subassemblies were built and tested at the UCLA Structural/ Earthquake Engineering Research Laboratory (SEERL), to better establish likely performance of the building in case of a ground shaking, and potentially lead to a less costly retrofit.

Figure 1-4: UCLA Franz Tower

The primary objective of the test was to identify the deformation capacity of the top six stories to reduce costly and disruptive retrofit at these levels. Preliminary studies by consulting engineers showed that if the exterior frame beams and columns could achieve lateral deformation ratio of about 1.5% before strength loss, a cost-effective retrofit, with no disruption to the building characteristics can be done by using viscous dampers to reduce the deformation demand. Eliminating the need to retrofit the exterior frame beams and/or columns was essential to preserve the original architectural design and integrity of the building, which is a typical brutalist concrete structure, with geometric and unusual shaped building components, common to that era.

1.1.5. Lack of Emphasis on Resiliency in the Current Building Codes

Current documents used to evaluate existing building performance and retrofit design mainly focus on performance level objectives in terms of drift ratios and deformation capacity of building components, and how it relates to the life safety of building occupants. Those matrices indirectly affect the level of damage to building components, hence the extent of repair or repair cost and repair time, however, there are not clearly defined parameters to address cost of repair and time to regain function of the building in case of a major ground shaking. Nonetheless, these two parameters are incredibly important to the public as they bear the financial impacts of such incidents.

1.2. Research Significance

Research and testing have shown that concrete frame buildings can perform desirably in an earthquake if columns of the seismic force-resisting systems are adequately designed (strong column-weak beam), and properly detailed (adequate transverse reinforcement provides concrete confinement, prevents immature bar buckling, and provides shear strength).

Many frame structures built prior to 1977 are considered non-ductile due to the lack of proper detailing in the columns and, therefore, lack of displacement capability in the columns prior to losing gravity load bearing capacity and collapse of the components, which can lead to partial or complete collapse of the building. Due to the prevalence of brutalist architecture in the 50s through the late 70s, many of the non-ductile concrete frame buildings have unusual geometries and building component shapes.

Proper means of analyzing seismic performance of an existing non-ductile concrete frame building is essential to providing an optimal and economical rehabilitation program. That, coupled with a resiliency analysis can culminate in a retrofit program that both enhances the performance of the building while optimizes cost of repair and time to regain function.

This report addresses the need to provide better information for seismic retrofit in cases where 1- unusual structural systems and building components are used, when ASC41-13 lacks the capacity to predict performance of a structure under seismic loading, as a whole or building component level; and 2- where complex loading exists, when the frame columns can undergo biaxial loading.

In this report, some deficiencies of ASCE 41-13 in predicting performance of a structure under seismic loading, as a whole or building component level are highlighted, which stemmed from the lack of test data at the time. This deficiency coupled with the special characteristics and features of the building that make it unconventional, result in conservative, and in part inaccurate, prediction of existing building performance especially when the building components fall under the “non-conforming (NC)” category. An accurate estimate of the existing building performance is paramount to an economical retrofit design, especially due to the LADBS Ordinance 183893 which mandates Earthquake Hazard Reduction of hazardous buildings. Hence the need to revisit some of the ASCE 41-13 modeling parameters and contributors to the behavior of building components is apparent. This report also discusses the cost implications and time to regain function as two important dimensions in a given retrofit program and how those should be considered in conjunction with performance enhancement of a building.

1.3. Objectives

The primary objective of this study is to identify the lateral drift capacity of the upper six stories of the building to reduce costly and disruptive retrofit at these levels. The test results can determine if and how implementing viscous dampers to reduce seismic response can amount to a more cost-effective retrofit, without disturbing the exterior façade of the building which is a part of its architectural character and representative of the era in which it was built.

To obtain overall experimental lateral-load versus displacement relations (or backbone curves), as well as to assess the damage states at each lateral drift ratio, two non-ductile concrete frame subassemblies were subjected to in-plane and out-of-plane loading. The overall backbone curves were obtained for the critical level of an eight-story building with unusual geometric conditions under biaxial loading.

Obtaining the overall backbone curve of the building subassembly, in conjunction with observed damage at each lateral displacement level, at each building components, and at each loading direction, provided valuable information on how the practicing engineers can utilize the test data in modeling building components in similar buildings, using Perform-3D and analyzing the building as a whole.

Finally, this report provides information on the functional recovery (resiliency) of prescriptive retrofit schemes and compares them with the selected retrofit scheme based on the test results. It discusses why resiliency study should be coupled with seismic performance analysis when selecting a retrofit program and shows the impact of the selected retrofit program in the resiliency of the building.

1.4. Report Outline

This document presents details of an experimental program on two subassemblies of a non-ductile concrete frame building. Chapter 1 provides an introduction to the project and research motivation, followed by Chapter 2 which includes summary of relevant background research. Chapter 3 discusses an overview of the biaxial physical testing on a subassembly physical testing on two subassemblies from the Franz Tower, building characteristics, geometry and material testing, and the test program. The experimental test results, observed damage, and discussion of the test results are presented in Chapter 4. It also outlines the contributing factors to the observed damage of the building components at each stage of the test. Chapter 5 is on functional recovery and resiliency analysis. It discusses performance vs resilience-based earthquake design, and compares the cost and downtime components of resiliency obtained by prescriptive methods and test data. Chapter 6 provides general findings from the observed test results, suggests means of using the experimental data in non-linear modeling of buildings with similar characteristics, and proposes future steps on addressing other deficiencies that were observed during the course of this research. It also discusses the importance and effect of resilience-based earthquake design. The Appendix provides additional information and details on the development and design of test specimens, identifying modes of failure, material testing, construction plans, pictures from construction and testing, Perform-3D modeling parameters, as well as detailed information about SP3 analysis.

Chapter 2. Literature Review

In this chapter, current provisions for seismic evaluation of non-ductile concrete frame buildings and their background are discussed, followed by scientific literature review of observations to non-ductile concrete frame buildings following the 1971 San Fernando earthquake which made the problems with non-ductile concrete more apparent. Previous experimental work conducted on lightly reinforced concrete columns, unreinforced beam-column joints, column lap-splice failures, and retrofit methods are discussed. A summary and research objectives are included at the end of the chapter.

2.1. Background: Seismic Evaluation and Retrofit of Buildings Code ASCE 41

ASCE 41-13, with the 2017 version published for public review and comment, is the current document providing provisions for the analysis and retrofit of existing buildings. To better understand the underlying basis and limitations of this document, it is necessary to know the process and original documents that culminated in ASCE 41-13. See Figure 2-1.

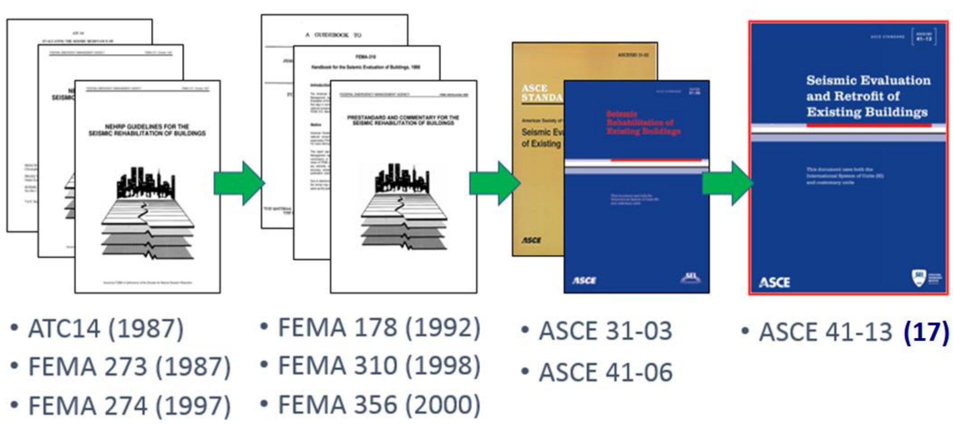

Figure 2-1: Evolution of ASCE 41

The Applied Technology Counsel (ATC) published the ATC-3 project, Tentative Provisions for the Development of Seismic Regulations for Buildings, in 1974, and final document in 1978 (ATC, 1978), with funding from the National Science Foundation (NSF) and the National Bureau of Standards (NBS). This document introduced a new seismic design approach including response reduction factors (R Factors) and new ground motion maps among other innovative features. (Rojahn, 2008)

In 1985, FEMA funded the ATC-13 Report, Earthquake Damage Evaluation Data for California (ATC, 1985), to estimate economic impacts of a major earthquake in California and nationwide.

In 1989, ATC published the ATC-14 Report, Evaluating the Seismic Resistance of Existing Buildings, which was funded by the NSF. The documents include practical approaches for evaluating existing buildings and identifying hazardous buildings and provided a methodology and checklists for field data collection. This was the foundation of FEMA 178 (NEHRP Handbook for the Seismic Evaluation of Existing Buildings, 1992). Prior to the late 90's, the seismic rehabilitation was based on the use of linear-elastic methods similar to the prescriptive new building design guidelines which tend to be overly conservative. Use of non-linear analysis methods in the late 90's allowed for more realistic and cost-effective seismic rehabilitation approaches that were presented in the FEMA 273 & 274 (NEHRP Guidelines for the Seismic Rehabilitation of Buildings) guidelines which were developed in 1997, and along with ATC-14 Report, were major breakthroughs in how engineers evaluate existing buildings. These documents were revised by ASCE in 1998 and published as FEMA 310 (Handbook for the Seismic Evaluation of Buildings – A Pre-standard) in 1998 and FEMA 356 (Pre-standard and Commentary for the Seismic Rehabilitation of Buildings, 2000) pre-standards. One of the most popular and widely used approaches introduced in these documents was the Non-linear Static Procedure (NDP) that relies on monotonic backbone curves to characterize force-deformation behavior of building components. (Lang & Wallace, 2008; Rojahn, 2008; Abdullah & Wallace, 2019)

Subsequently, these pre-standard documents were refined and expanded into ASCE/SEI 31-03 ASCE Standard for Seismic Evaluation of Existing Buildings and ASCE/SEI 41-06 Seismic Rehabilitation of Existing Buildings. (Massone & Wallace, 2006) (Lang & Wallace, 2008) These two documents were combined into ASCE/SEI 41-13 Seismic Evaluation and Retrofit of Existing Buildings, to eliminate some inconsistencies between the two previous documents and the need to go back and forth between the two. (Rojahn, 2008)

It is important to note that the modeling parameters in ASCE 41-13, are essentially the same as FEMA 356 (and ATC-14), which tend to be conservative due to lack of available data and testing at the time to establish modeling parameter to cover a wide range of loading conditions, geometry, and detailing. Additionally, there are other inherent limitations stemming from the assumptions and limitations of the basis documents of ASCE 41-13, as listed below:

- The modeling parameters in the code are provided for hinge type models while in many cases a fiber model better captures the performance of an existing building.
- The document is intended for existing buildings evaluation and analysis, but it is also used in performance-based design of new buildings.
- ASCE 41-13 is intended for non-linear static analysis of buildings, and not non-linear dynamic analysis which is widely used both in evaluation of existing buildings and in performance-based design of new buildings. The document does not capture energy dissipation in cyclic and dynamic loading and most design engineers use academic research papers as reference to estimate reduction in area under curves.
- ASCE 41-13 is shown to be conservative and at times provides inaccurate modeling parameters due to limited data available at the time its original documents were developed. This is more apparent in buildings with unusual geometry or building components with

irregular geometry. (Massone & Wallace, 2006) (Lang & Wallace, 2008) The UCLA Franz Tower has trapezoidal exterior columns with trapezoidal short beams, which are connected to a thickened slab edge beam, spanning along the length of the interior waffle slab.

2.2. History of Earthquake Performance of Non-Ductile Concrete Frame Buildings

Research and testing have shown concrete frame building can perform desirably in an earthquake if columns of the seismic force-resisting systems are adequately reinforced (adequately strong), and properly detailed (confined). It is also important that the gravity system columns are adequately detailed to withstand collapse under large lateral deformations. Many frame structures built prior to the mid 70's are deemed non-ductile due to lack of detailing in the columns, therefore lack of displacement capacity in the columns before losing gravity load bearing capacity and collapse.

Numerous tests have been conducted on non-ductile columns with varying axial forces, and there are a few tests on non-ductile beam-column joints, but due to laboratory constraints in size and capacity, there are very few tests on large scale frames. Furthermore, due to the complexity of biaxial tests, there are even fewer tests with biaxial loading conducted on non-ductile columns or frames. In the following sections, several tests that capture areas relevant to this study are discussed.

2.2.1. Non-Ductile Columns

The ability of columns to continue to deform with reduced capacity depends on the ability of the floor system to re-distribute some of the axial load to adjacent members, and of the lateral load system to prevent the collapse of the structure when that happens. Physical testing of columns even though does not fully capture the behavior of the building as a system but is the closest approach to mimic behavior of columns that undergo higher axial forces or varying axial forces, by choosing appropriate boundary conditions that are representative of actual conditions, as accurately of possible. Three research papers that are relevant to the current study are selected and discussed in this section, and they include static testing of lightly reinforced columns by Sezen and Moehle (Sezen & Moehle, 2006), dynamic testing of lightly reinforced columns by Elwood and Moehle (Elwood & Moehle, 2008), and axial failure of shear critical columns by Matamoros, Matchulat and Woods (Matamoros, Matchulat, & Woods, 2008).

2.2.1.1 Sezen and Moehle (ACI Structural Journal Nov-Dec 2006)

Sezen and Moehle (Sezen & Moehle, 2006) conducted simulated seismic loading tests to collapse on four full-scale concrete columns with nominally identical geometries and light transverse reinforcement typical of buildings not designed for seismic loading, as shown in Figure 2-2. The column geometry and properties were selected to represent a class of columns in older buildings in which flexural yielding would occur prior to shear failure. The columns were tested quasi-statically under unidirectional lateral load with various magnitude constant axial loads or varying axial loads as shown in Figure 2-3 and Table 2-1.

The columns had a cross section of 18 in. by 18 in. (457 mm by 457 mm) with eight (8) continuous No. 9 (29 mm) deformed longitudinal reinforcement, and No. 3 (10 mm) deformed hoop sets were placed at every 12 inches (305 mm) within the column clear height as transverse reinforcement, providing the longitudinal reinforcement ratio (total reinforcement area divided by gross section area) equal to 0.025, and transverse reinforcement ratio (area of transverse reinforcement in one horizontal direction divided by the product of section width and hoop spacing) equal to 0.0017. The column clear height was 9 ft. 8 in. (2946 mm) as shown in Figure 2-2. Two long, heavily reinforced beams 30 in. (762 mm) deep, 8 ft. (2438 mm) long were located at the top and bottom, post-tensioned to the loading frame and strong floor to simulate floor elements or stiff foundation, respectively. The specimens were loaded the specified axial load through the loading frame using two 400-kip (1780 kN) capacity vertical hydraulic actuators. A 500-kip (2220 kN) capacity horizontal hydraulic actuator, under displacement control, imposed the unidirectional lateral deformations in the plane of the beam-column specimen. To minimize overturning force demands on the vertical actuators, the horizontal actuator acted at the mid-height of the column as shown in Figure 2-3.

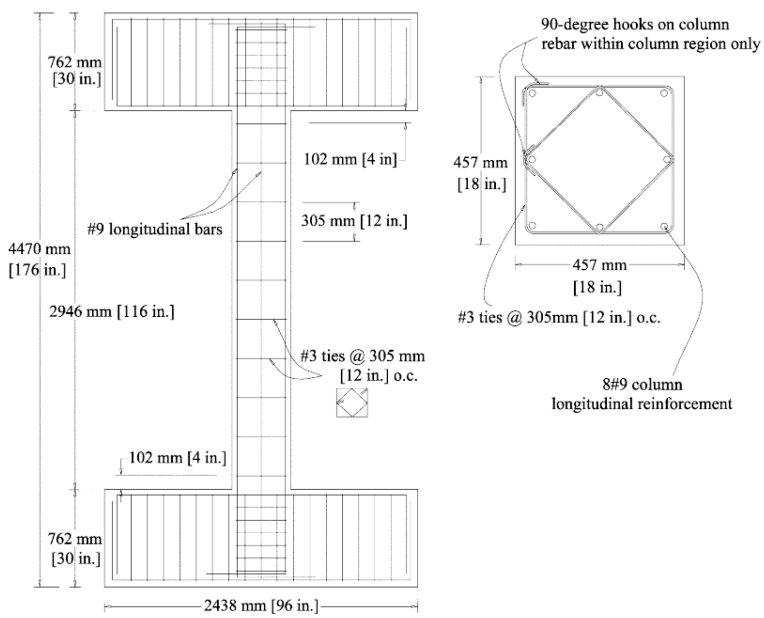

Figure 2-2: Specimen Elevation and Cross Section Details

The specified concrete type was normal weight with compressive strength of 3000 psi (20.7 MPa) at 28 days, with mean strengths between 3030 to 3160 psi (20.9 to 21.8 MPa) on the day of testing. Mean yield strengths of the No. 9 (29 mm) longitudinal bars and No. 3 (10 mm) transverse bars were 63 and 69 ksi (438 and 476 MPa), and mean ultimate strengths were 93.5 and 105 ksi (645 and 724 MPa) respectively.

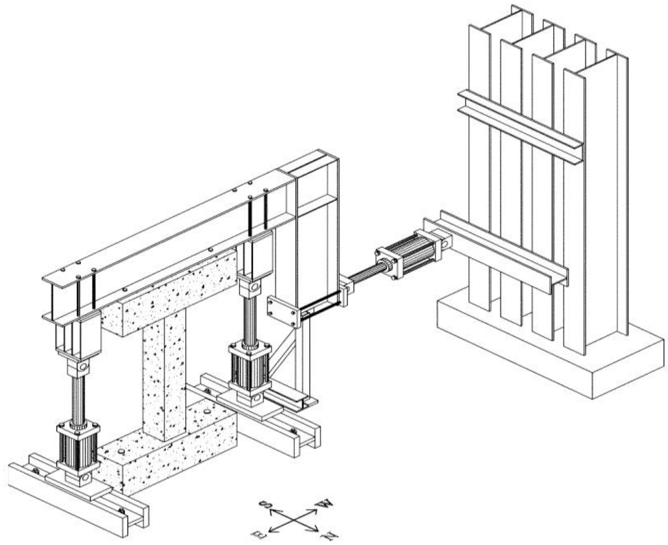

Figure 2-3: Test Setup

The reference specimen was specimen 1 with constant compressive axial load of 150 kips (667 kN), or $0.15 f_c^{'} A_g$ ($f_c^{'}$ is measured concrete compressive strength on the day of each test, and A_g is gross cross-sectional area), which is representative of a typical gravity column. The lateral displacement history had three cycles each at amplitude of $\Delta_y/4$, $\Delta_y/2$, Δ_y, $2\Delta_y$, $3\Delta_y$, until failure, (Δ_y is the nominal yield displacement), which is referred to as the standard displacement history. Specimen 2 is representative of a column with high axial (gravity) load of about $0.40 f_c^{'} A_g$ equal to axial load of 600 kips (2670 kN), with the standard displacement history. Specimen 3 is representative of an exterior column going through cyclic tension and compression axial loads varying from -56 to 600 kips (-250 to 2670 kN), with the standard displacement history. These loads correspond to the same flexural strength on the axial load-moment (P-M) interaction diagram, which means the columns have the same theoretical shear demand at flexural failure. Specimen 4 had an axial load of 150 kips (667 kN) with standard displacement history until Δ_y followed by monotonic lateral displacement to failure. Table 2-1 summarizes the details of the four specimens.

Table 2-1: Test Parameters and Results

	Test Age (Days)	f_c' ksi (MPa)	Displacement History	P_u kip (kN)	δ_y in. (mm)	δ_u in. (mm)	δ_{ug} in. (mm)	V_{test} kip (kN)	M_{test} kip-in. (kN-m)
Specimen 1	146	3.06 (21.1)	Standard	150 (667)	1.03 (26)	2.97 (75)	5.76 (146)	70.8 (315)	4320 (488)
Specimen 2	166	3.06 (21.1)	Standard	600 (2670)	0.79 (20)	1.02 (26)	2.18 (55)	80.7 (359)	5100 (576)
Specimen 3	222	3.03 (20.9)	Standard	600 (2670)	0.82 (21)	2.23 (57)	3.42 (87)	67.6 (301)	4740 (536)
				-56 (-250)	1.13 (29)	3.41 (87)	3.40 (86)	55.5 (247)	3340 (377)
Specimen 4	244	3.16 (21.8)	Monotonic	150 (667)	1.06 (27)	3.33 (85)	6.35 (161)	66.2 (294)	464 (4110)

Test observations: Due to different axial forces or displacement protocol on the four specimens, details of damage after yield displacement cycles were different and discussed below for each specimen. However similar behaviors were observed in smaller displacement cycles in all specimens: horizontal cracks of less than 0.005 in. (0.1 mm) wide formed during the initial loading cycles up to one half of the nominal yield displacement near the column ends, and vertical cracks within the joints on the faces of top and bottom beams during cycles to half the yield displacement. Vertical cracks along column longitudinal reinforcement were observed during cycles beyond the nominal yield displacement, suggesting bond failure.

Figure 2-4 shows the load-displacement history for each test and Figure 2-5 demonstrates the damage at each of the specimens after each test was completed.

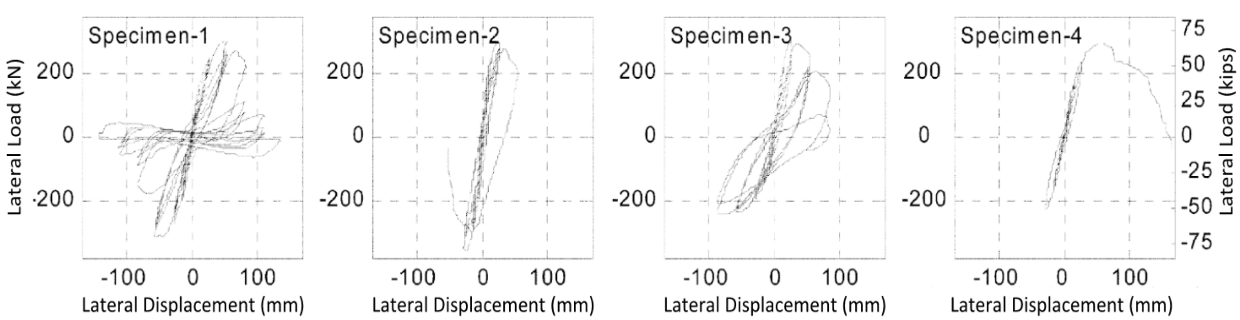

Figure 2-4: Relations between Lateral Load and Lateral Displacement (1 in. = 25.4 mm)

Specimen 1: at the first cycle of $2\Delta_y$, spalling of cover concrete followed by wide inclined cracks near mid-height were observed with lateral resistance beginning to degrade in the subsequent cycles. The column continued to support axial load until the end of the test in spite of additional damage to the column and loss of lateral resistance at that point.

Specimen 2: initial lateral stiffness was higher than specimen 1 due to higher axial load. The specimen underwent a brittle shear compression and immediately lost axial load bearing capacity. Both lateral and axial failures occurred suddenly with a steep diagonal crack at the top of the column. The longitudinal bars did not yield on the tension face, but yielding was observed in the bars was in the compression face just before peak strength was achieved.

Specimen 3: lateral stiffness and strength varied with the varying axial load, with more apparent strength degradation during the increasing compression load cycles. This specimen sustained more lateral deformation before formation of inclined and vertical cracks followed by concrete spalling before the column failed during the cycle reaching to 600 kips (2670 kN) in compression. The longitudinal reinforcement buckled in the compression face at the base of the column.

Specimen 4: this specimen is similar to specimen 1 except it was essentially loaded monotonically vs cyclic. Specimen 4 sustained failure when a large cracked at the base of the column opened up. This test demonstrated the same lateral resistance as seen in specimen 1, however, failure happened at a larger displacement. The rate of lateral force degradation was also smaller.

A comparison of the test results with available seismic models at the time (FEMA Report No. 356) was conducted for the four tests as shown in Figure 2-6, where FEMA 365 flexure is obtained per the report's guidelines on the force-deformation relationships, and FEMA 365 shear is calculated using expected material strengths and FEMA 356 equations. The strengths obtained from the test are relatively close to the calculated strengths, however the deformations measured at the test exceeded deformation capacities predicted by FEMA 356 Report. Also, the model stiffness is higher than the actual stiffness, therefore estimated yield displacement was smaller than shown by test as presented in Table 2-1.

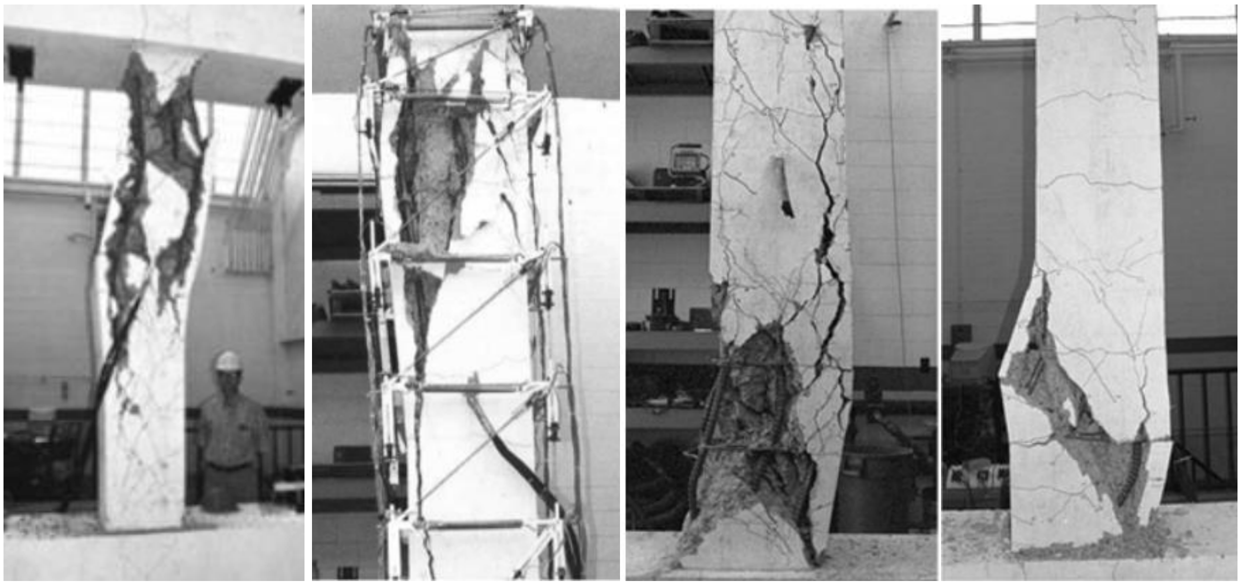

Figure 2-5: Damage after Failure in Specimens 1 to 4 (Left to Right)

It is worth noting that the lateral stiffness was strongly influenced by slip of longitudinal reinforcement from the beam-column connections, which should be considered to accurately model column stiffness in analytical models. As discussed above, modeling parameters in FEMA 365 Report are conservative in predicting deformation capacity, even though they closely estimate column strength. Other studies also recommended modeling parameter improvements, and the research conducted by Elwood and Moehle (Elwood & Moehle, 2008), is selected and discussed in section 2.2.1.2.

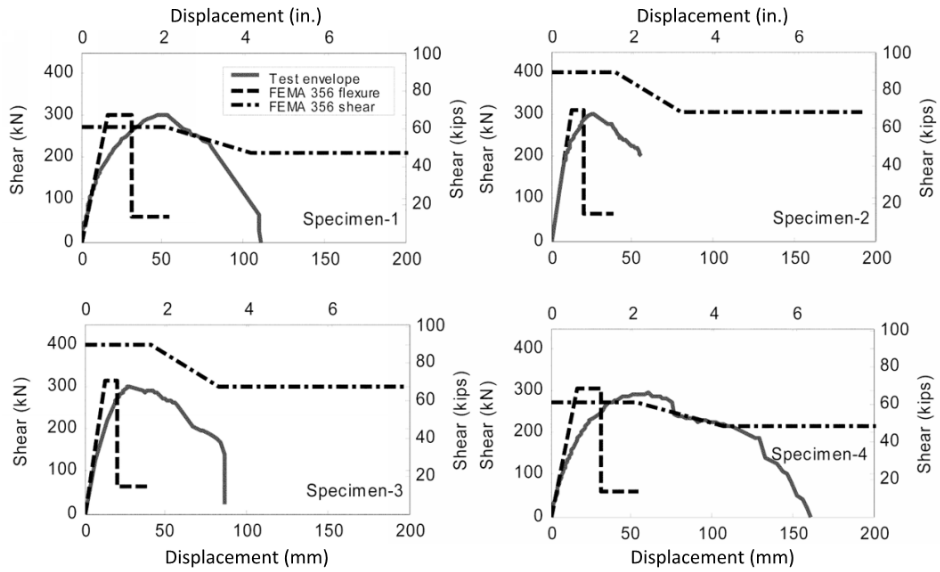

Figure 2-6: Comparison of Measured Envelope Relations and FEMA 365 Relations

2.2.1.2 Elwood and Moehle (ASCE Journal of Structural Engineering, 2008)

As discussed in the previous chapter, reinforced concrete columns constructed prior to 1977 are susceptible to shear damage, due to light transverse reinforcement, in case of a strong ground shaking. Since gravity loads can never be dissipated through yielding and damage to the structure, in the event of shear damage and therefore the axial failure of a column, the gravity loads initially supported by the column must be redistributed to neighboring elements, which can lead to collapse of the building frame (Elwood & Moehle, 2008).

Two half-scaled one-story two-dimensional frames were subjected to unidirectional loads on a shake table to evaluate behavior of such columns. The axial load applied represented the approximate expected load in the lower story columns of a seven-story building. The authors note that the out-of-plane frames and the slab systems contribute to the capacity of a building to resist gravity load collapse, but this is not considered at this time due to the level of complexity it introduces to the test. This study is further limited to reinforced concrete frames with columns that initially yield in flexure, but whose deformation capacity is limited by the subsequent onset of shear failure. The shear failure is accompanied by significant lateral strength degradation and may be followed by a loss of axial-load capacity. Columns primarily characterized by a shear failure prior to yielding of the longitudinal reinforcement are not directly considered in this study.

The center column was designed as a one-half scale reproduction of the 9 ft. 8 in. (2946 mm) tall, 18 in. by 18 in. (457 mm by 457 mm) square columns tested by Lynn and Sezen, which was expected to yield in flexure prior to failing in shear (Lynn, 2001; Sezen, 2002). Axial load failure was expected to be more gradual for the first specimen with low axial load on the center column, and more sudden for the second specimen column with higher axial load as discussed below. The rest of the frame system (base blocks, top beam, and side columns) were sufficiently designed to achieve the desired response.

The test specimens were composed of a three-column frame fixed at the base and connected at the top through a beam as shown in Figure 2-7. The center column had a square cross section of 9 in. by 9 in. (230 mm by 230 mm) with continuous four (4) No. 4 (13 mm) deformed longitudinal reinforcement at the corners and four (4) No. 5 (16 mm) deformed longitudinal reinforcement at the centers of each side, and W2.9 wire spaced at every 6 inches (152 mm) as transverse reinforcement. The light transverse reinforcement makes the center column susceptible to shear failure leading to axial load failure, while the side circular columns were designed with closely spaced spiral reinforcement to ensure columns were able to resist large ductility demands without axial failure. The top beams and footings were capacity-designed based on the capacity of the outside columns. Axial load applied to the first specimen represented the axial forces in a column at the base level of a seven-story building and was equal to while the load applied to the center column was increased to by using a pneumatic jack as shown in Figure 2-8.

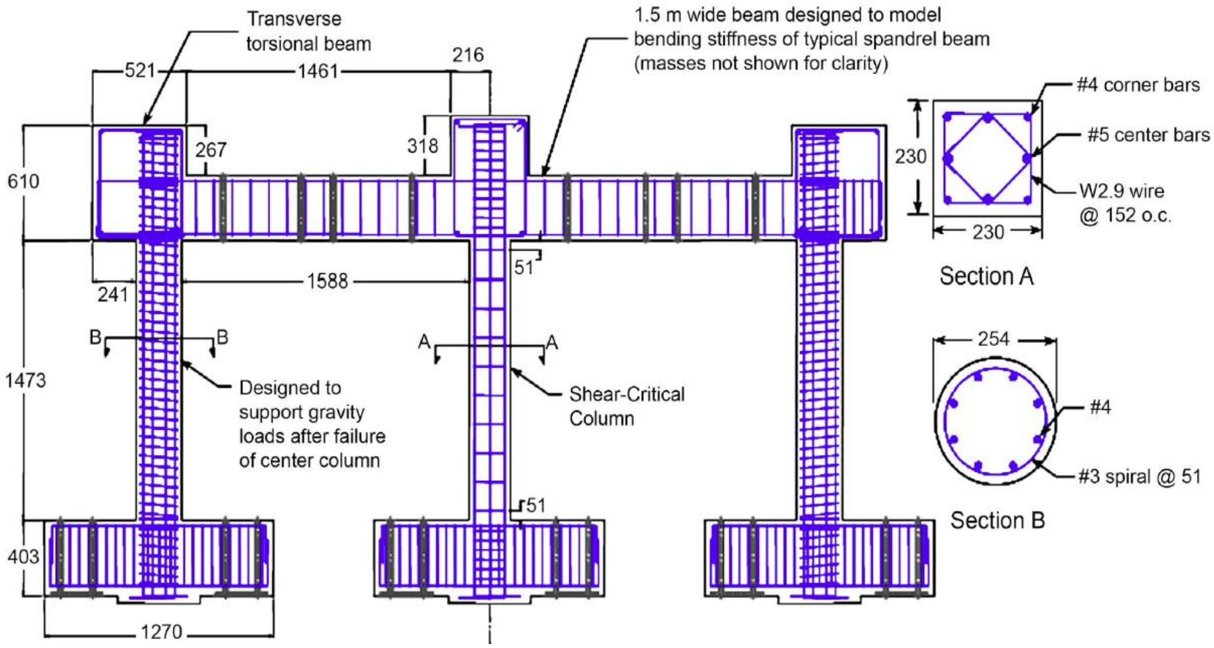

Figure 2-7: Shaking Table Test Specimen (1 in. = 25.4 mm)

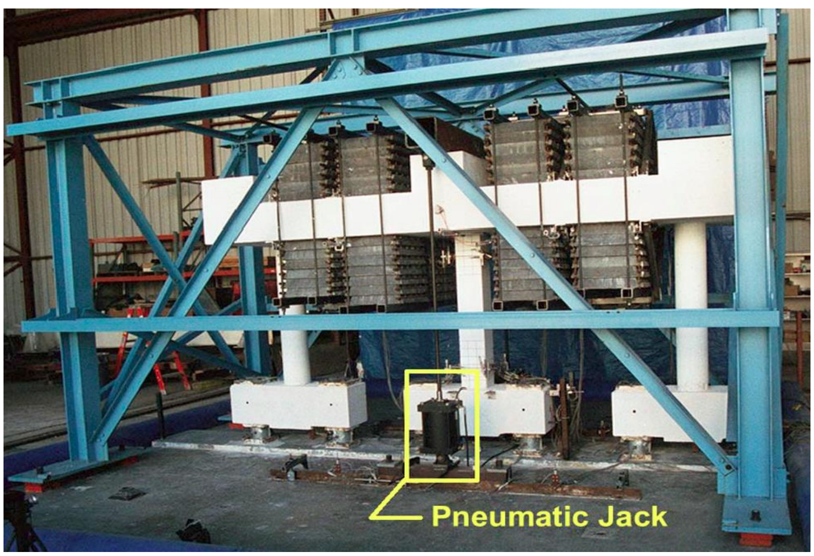

Figure 2-8: Loaded Test Specimen on Shaking Table

The test specimens were to be subjected to unidirectional horizontal base motions. Therefore, an out-of-plane bracing system was provided to restrain them from out-of-plane motion. The bracing system did not provide any horizontal or vertical motion restraint in the in-plane direction. Both specimens were subjected to one horizontal component from a scaled ground motion recorded at

Viña del Mar during the 1985 Chile earthquake (Figure 2-9). The global response histories of both specimens are drawn on one diagram in Figure 2-10 for comparison.

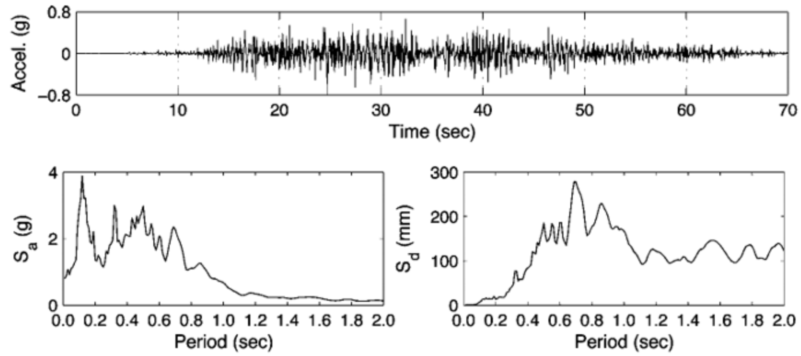

Scaled Chile, 1985 Ground Motion (S_a Pseudospectral Acceleration; S_d Spectral Displacement)

Figure 2-9: Acceleration Record and Response Spectra for 2% Damping

Markers are placed at significant times in each test: first drop in the center column shear for specimen 2 relative to specimen 1 at 16.7 seconds, initiation of axial failure of center column of specimen 2 at 24.9 seconds, end of the sudden drop in the center column axial load in specimen 2 at 29.8 seconds. The base shear at specimen 2 drops relative to that of specimen 1 at first marker, which is when wide shear cracks are developed in the center column of specimen 2 (see Figure 2-11). At this point the axial load at both columns drops by approximately 10 kips (44.5 kN) which occurs with the development of significant cracks in the outside and center columns and, hence, is thought to be caused by redistribution of gravity loads as the lengths of the columns change due to flexural response. The diagonal shear cracks appear wider and steeper for specimen 2. The drift ratio of the two specimens remains close after t=12 s with similar vibration periods, until t=24.9 s where the drift ratios for specimen 2 increase relative to specimen 1. The drift ratios are further offset from the origin prior to t=29.8 s, resulting in a permanent offset of approximately 2.0% for specimen 1 and 3.2% for specimen 2 at the end of the test.

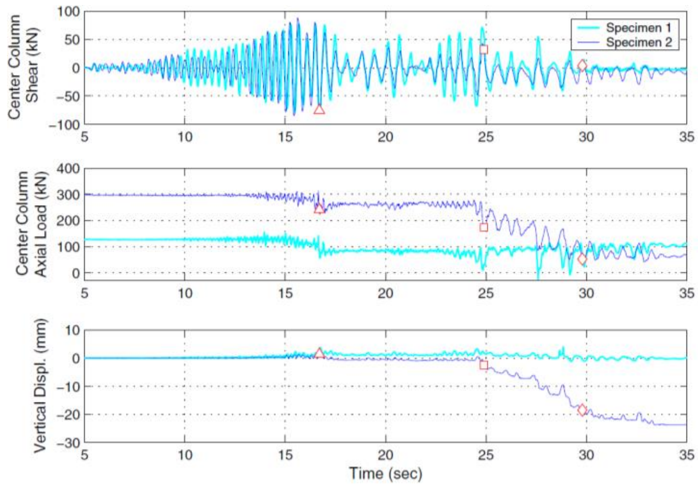

Figure 2-10: Center Column Response History

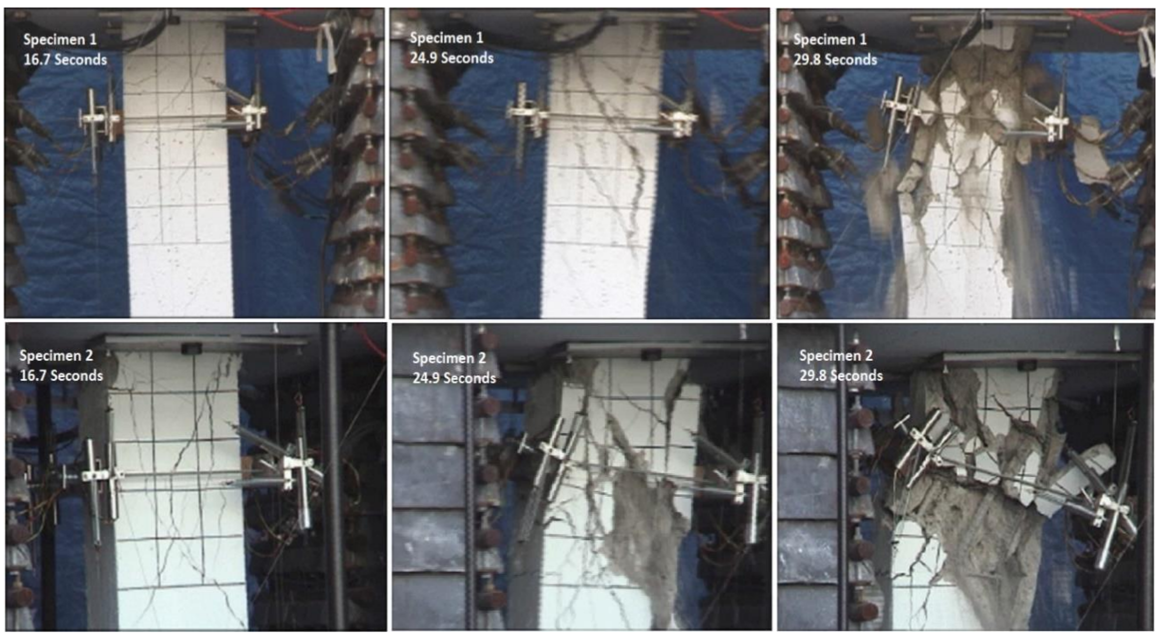

Figure 2-11: Damage at Top of Center Column in Top: Specimen 1, Bottom: Specimen 2

Figure 2-12 shows both the base shear hysteretic response (recorded by the force transducers at the base of the columns) and the inertia forces (based on the measured acceleration of the applied mass). The overall behavior of the two frames is not significantly different except there is a clear drop in the shear capacity of the center column for specimen 2.

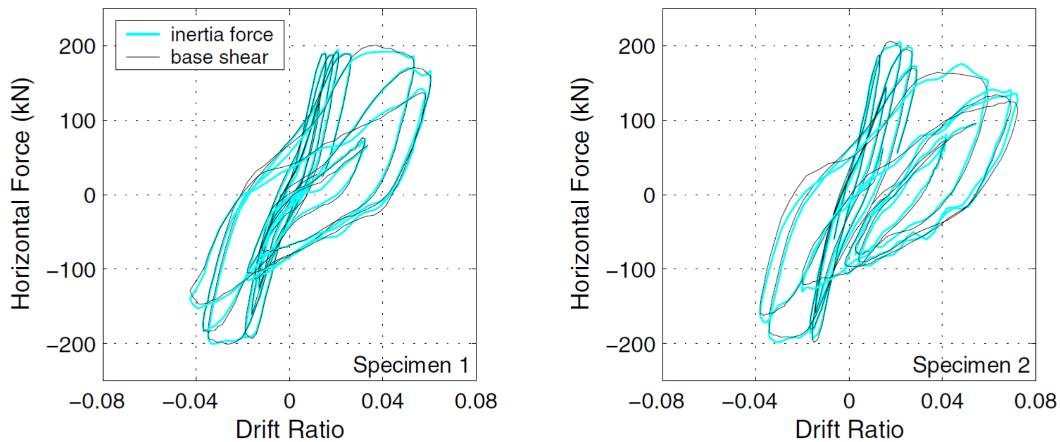

Figure 2-12: Hysteretic Response for Specimens 1 and 2

The behavior of the center column during axial failure for specimen 2 are due to two mechanisms: first, large pulses that cause a sudden increase in vertical displacement after a critical drift is attained which suggests if the ground motion impose a large lateral drift during a single pulse, the column is likely to lose axial-load capacity at a fast rate; and second, smaller oscillations that cause gradual increases in the vertical displacement, which suggest the duration of ground shaking determines the ultimate damage in the column.

At the end of the test, the specimen 1 center column was supporting 84% of its initial axial load (24.1 kips (107 kN)) while the center column of Specimen 2 was supporting only 18% of its initial axial load (11.9 kips (53 kN)) as shown in Figure 2-10, while Figure 2-13 shows the history of redistribution of gravity loads during axial failure of the specimen 2 center column. Figure 2-14 illustrates damage level to specimens 1 and 2 at the end of the test.

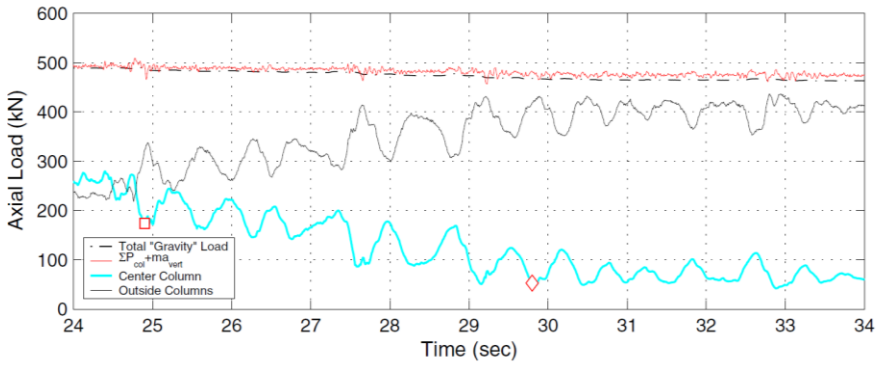

Figure 2-13: Redistribution of Axial Loads in Specimen 2

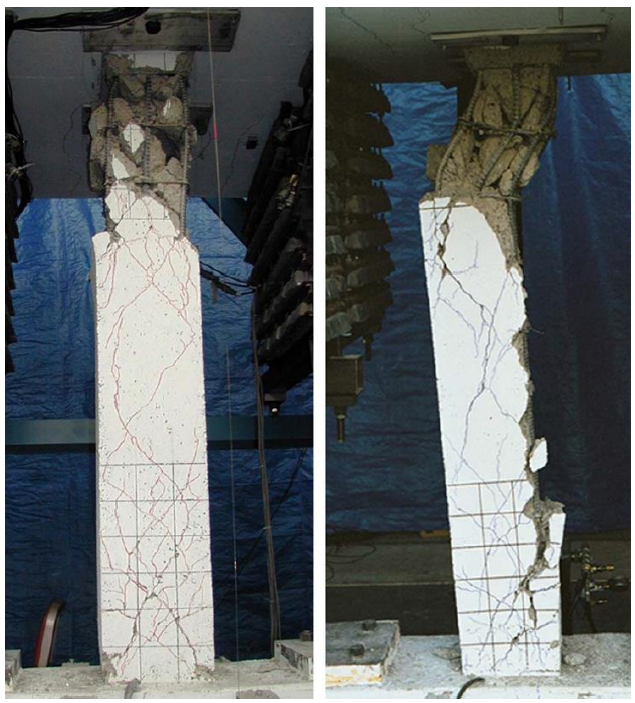

Figure 2-14: Specimens 1 (Left) and 2 (Right) at End of Tests

These tests demonstrated that the behavior of the frame is dependent on the initial axial stress on the center column. The specimen with lower axial load failed in shear but maintained most of its initial axial load. For the specimen with higher axial load, shear failure of the center column occurred at lower drifts and was followed by relatively abrupt axial failure.

2.2.1.3 Matamoros, Matchulat and Woods (14 WCEE, 2008)

As discussed in previous sections, behavior of shear critical columns subjected to high levels of axial (and lateral) loads is significantly important since it exemplifies columns that are part of the seismic force resisting system in an older building where they lack proper reinforcement detailing and confinement and are highly vulnerable to sudden collapse due to high axial forces. Such columns can experience axial forces by more than a factor of two, as a result of partial collapse of neighboring gravity force resisting system due to large lateral deformations and redistribution of vertical loads between the remaining columns. This paper discusses the experimental behavior of two columns that are lightly reinforced and are subjected to high levels of axial load. (Matamoros, Matchulat, & Woods, 2008)

The two full-scale experiments were performed to evaluate behavior of columns with ratios of nominal shear strength to plastic shear demand of about 85 percent. Both columns were 9 ft. and 8 in. (2945 mm) long and had a square cross section of 18 in. by 18 in. (457 mm by 457 mm), for a shear-span to depth ratio of 3.75. See Figure 2-15. The longitudinal reinforcement ratio was 2.5% and consisted of eight (8) No. 9 (29 mm) bars made of ASTM A706 steel with a measured yield strength of 64.5 ksi (445 MPa), and the transverse reinforcement was No. 3 bars (10mm) hoops with 90-degree bends spaced at 18 in. (457 mm), made of ASTM A615 steel with a yield strength of 54 ksi (372 MPa), for both specimens. Compressive strength of the concrete was measured on the day of the test for the two specimens and equaled 4.79 ksi (33 MPa). The axial force applied however differed between the two and was equal to 500 kips (2225 kN) or 340 kips (1510 kN). The columns were subjected to sets of three cycles with increasing maximum lateral displacement under constant axial load. The first set of cycles had an amplitude of 0.25% drift ratio, with 0.25% increments subsequently until 1.5% drift ratio, and 0.50% increments until end of the tests. To obtain an estimate of the residual capacity of the columns, the loading protocol changed when damage to the columns was deemed too severe, with the lateral deformation remaining constant while only the vertical deformation was increased.

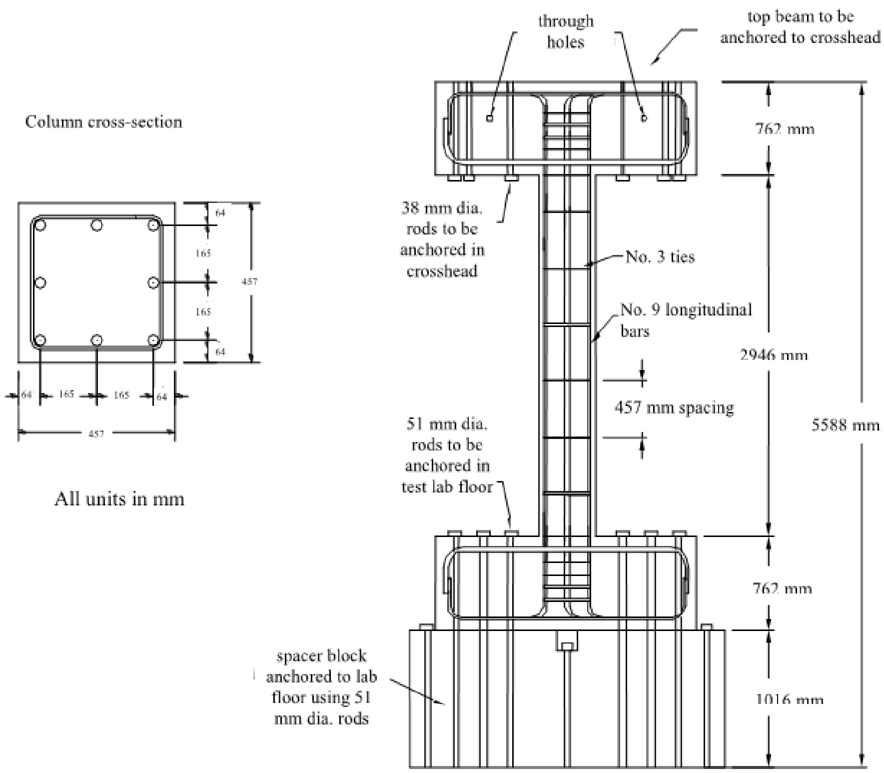

Figure 2-15: Test Setup and Dimensions (Matamoros, Matchulat, & Woods, 2008)

The axial failure event was defined by when a reduction of 10% or greater was detected in the axial load capacity. In that case the system maintained the lateral and vertical deformation constant, applied the reduced axial load recorded at the end of the failure event, and only after the axial load in the column was stabilized, the displacement protocol for the lateral deformation was continued. Equations 11-10 and 11-4 of ACI 318-08 Building Code were used to measure shear strength of the specimens were from ACI 318-08, and the nominal strength was calculated based on the Modified Compression Field Theory, per Bentz and Collins analysis program Response 2000. The nominal shear force expected to cause yielding of the flexural reinforcement, V_y, was obtained from a moment curvature analysis. As seen in Table 2-2, all methods indicate the specimens are expected to fail in shear prior to flexural yielding of the longitudinal reinforcement, and the test results were consistent with this expectation.

Table 2-2: Nominal Shear Strength of Test Specimens and Comparisons

	P kip (kN)	$V_{ci\_ACI11-10}$ kip (kN)	$V_{c\_ACI11-4}$ kip (kN)	V_S kip (kN)	$V_{n\_ACI11-10}$ kip (kN)	$V_{n\_ACI11-4}$ kip (kN)	V_{n_MCFT} kip (kN)	V_y kip (kN)	Ratio of V_n/V_y ACI 11-10	ACI 11-4	MCFT
Specimen 1	340 (1510)	44.7 (199)	68.6 (305)	10.3 (46)	78.9 (351)	55.1 (245)	63.8 (284)	92.2 (410)	0.86	0.60	0.69
Specimen 2	500 (2225)	34.6 (154)	59.4 (264)	10.3 (46)	69.9 (311)	45.2 (201)	57.1 (254)	80.9 (360)	0.86	0.56	0.71

Both specimens were loaded cyclically until two failure events occurred, and after that monotonically to get a measure of the residual capacity of the column after failure. Although both specimens had a brittle mode of failure, they had significantly different behaviors at drift demands higher than the drift at axial failure as shown in Figure 2-16. The lateral stiffness and the residual axial load capacity of the columns seem to be related to the axial load prior to axial failure.

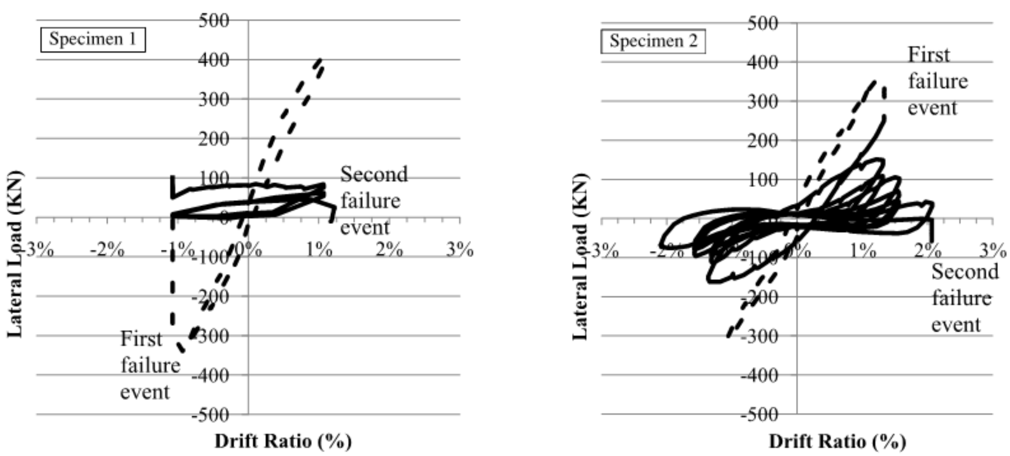

Figure 2-16: Load-Deformation Relations for Specimens 1 and 2 beyond Axial Failure

Specimen 1 had negligible residual stiffness after the brittle failure event which happened at about 1% drift, and there was a relatively small increase in lateral drift ratio (to 1.2%) of the specimen before it lost ability to carry the reduced axial load. It also was able to carry a lower level of axial force after the failure events occurred, as shown in Figure 2-17. While specimen 2 experienced some reduction in lateral stiffness after the first failure event at about 1.4% drift ratio, it was still able to undergo a significantly higher lateral drift ratio (more than 2%) before it lost the ability to carry the reduced axial load. Specimen 2 was able to sustain 88% of the initial axial force after the first failure event.

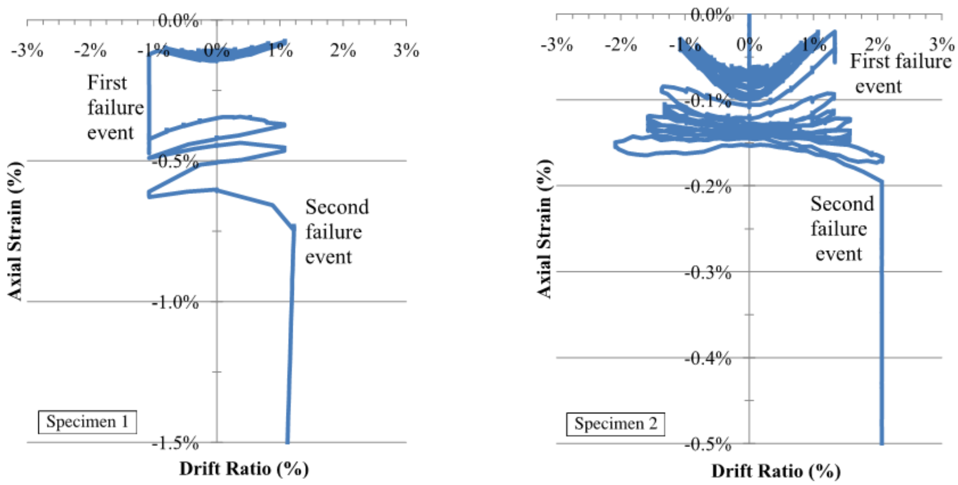

Figure 2-17: Axial Strain vs. Drift Ratio for Specimens 1 and 2

The two tests confirmed that the behavior of columns under large lateral deformations, lateral stiffness, and residual axial load capacity of the columns depended on the initial axial load applied to the columns.

2.2.2. Lap-splice Failure in Columns

2.2.2.1 Melek and Wallace (13 WCEE, 2004)

Splices in reinforced concrete columns of older buildings pre-1977 were designed for compression only, with lap-splice length of typically only 20 to 24 bar diameters (d_b), and light transverse reinforcement enclosing the lap. It should be noted that the required lap length for tension significantly exceeds the required lap length for compression, and in case of a ground shaking, the moment frame columns undergo large magnitude moments at the base level, therefore large magnitude tension and compression forces. To better understand the load-deformation response of such columns, and failure observations and poor performance of such columns after earthquakes, a program was developed to conduct tests on six (6) full-scale cantilever columns with $20d_b$ lap-splice length and light transverse reinforcement. Constant axial load with reversed cyclic uniaxial lateral displacement was applied at the top of the columns. The results indicated that: 1) lateral load vs. lateral drift relations were insensitive to change in axial load and shear demands less than V_n. However, strength degradation was sensitive to loading history beyond V_n, and 2) ACI 318-02 underestimated the bond stresses, hence actual moments and shears developed in a column with non-code compliant splices; especially for the base columns where a factor of 1.3 is applied due to all bars being spliced at one location. The test specimens consisted of 18 in. (457 mm) square cantilever columns with a foundation block connected to the strong floor as shown in Figure 2-18. (Melek & Wallace, 2004)

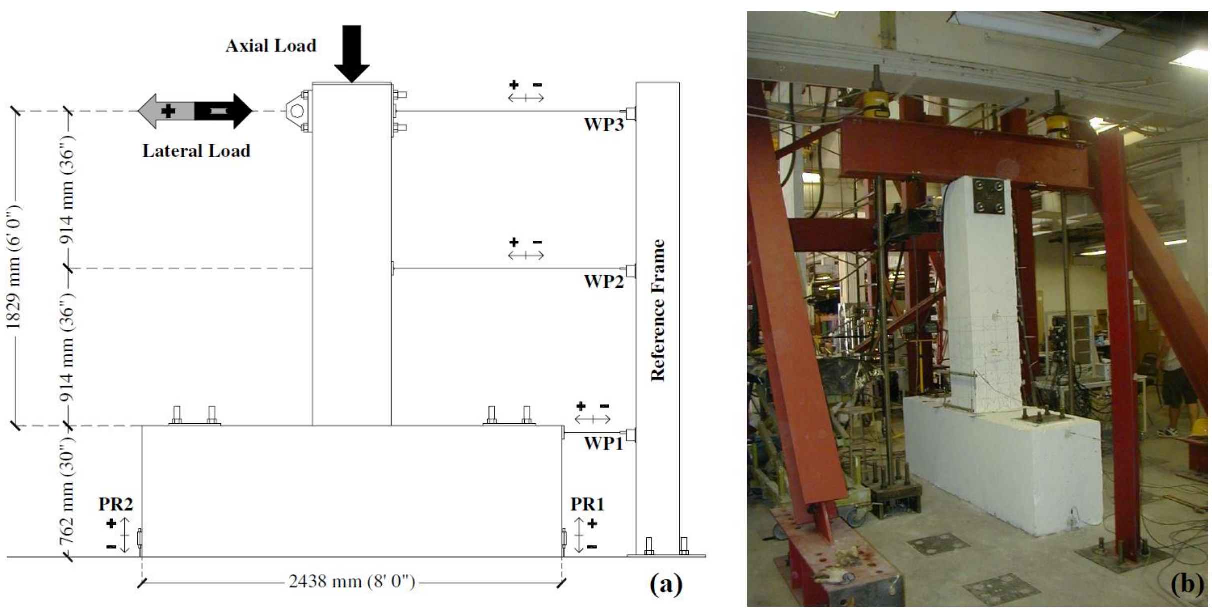

Figure 2-18: (a) Test Setup Schematic, (b) Test Setup Photo

These columns represented interior building columns from its assumed inflection point at mid-height to the column base and were of 5 ft. (1520 mm) and 6 ft. (1830 mm) in height. Column reinforcing details was based on typical reinforcing of older buildings, with eight (8) No. 8 (25 mm) vertical bars and No. 3 (10 mm) hoops with 90-degree hooks spaced at 12 inches on center (305 mm) along the column height as shown in Figure 2-19. The provided lap length is about 67% of the requirements for tension reinforcement by ACI 318-02 to reach the yield stress.

Standard lateral displacement history consisted of three cycles of increasing drift levels starting from 0.1% to 10% was applied to five specimens, and a loading history representative of the deformation demand in the near-fault region was applied to one specimen (Figure 2-20).

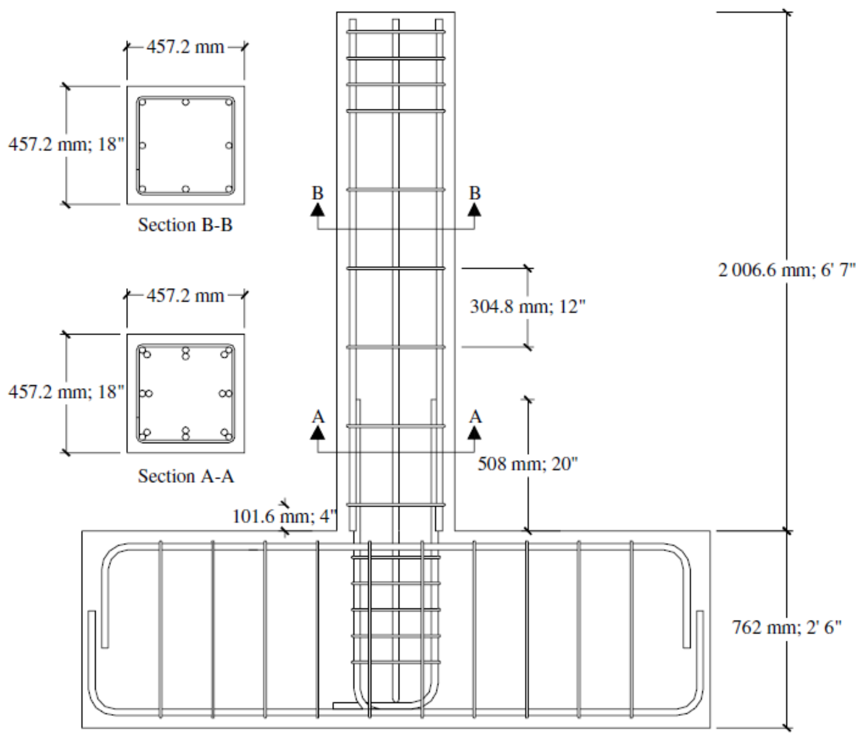

Figure 2-19: Reinforcing Detail

Test variables included the applied displacement history (Figure 2-20), the axial load ratio of 0.10, 0.20, and $0.30A_g f_c'$, and the column shear demand at maximum base moment ranging from 0.67

to 0.93 V_n. Three specimens (2S10M, 2S20M, and 2S30M) were tested under standard cyclic loading with constant axial load. Two additional specimens (2S20H and 2S20HN) were tested under higher shear demand to capacity ratios under moderate axial load ($0.20A_g f_c'$,). In the last specimen (2S30X) axial force and shear were increased to $0.30A_g f_c'$, and the calculated nominal shear capacity, respectively. Steel reinforcement properties as well as concrete compressive strengths for the two batches used, are shown in Table 2-3.

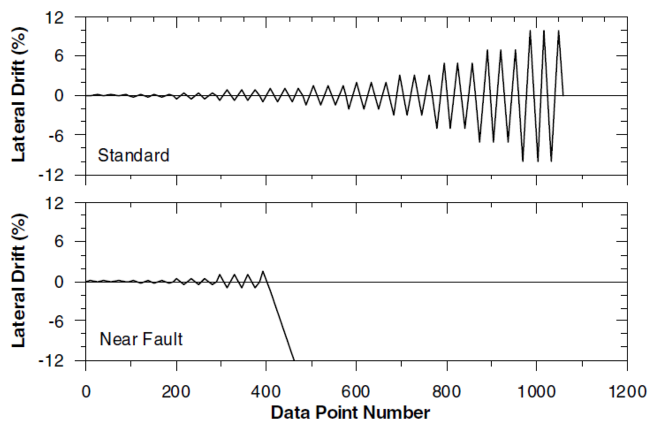

Figure 2-20: Displacement Histories

Table 2-3: Material Properties

Material	**2S10M-2S20M-2S30M**			**2S20H-2S20HN-2S30X**		
Concrete	**f'_c (MPa)**	**f_{ct} (MPa)**	**f_r (MPa)**	**f'_c (MPa)**	**f_{ct} (MPa)**	**f_r (MPa)**
	36	3.4	3.8	35	-	3.7
Steel	**d_b (mm)**	**f_y (MPa)**	**f_u (MPa)**	**d_b (mm)**	**f_y (MPa)**	**f_u (MPa)**
(Column)	25.4	510	818	25.4	510	818
(Starter)	25.4	521	746	25.4	507	807
(Ties)	9.5	481	750	9.5	481	750

Melek and Wallace reported that the maximum moments achieved in the test were 95% to 104% of the calculated yield moments as shown in Table 2-4. Average bond stress values from the tests were $10.5\sqrt{f_c'}$ psi ($0.88\sqrt{f_c'}$ MPa), with a standard deviation of $1.6\sqrt{f_c'}$ psi ($0.13\sqrt{f_c'}$ MPa), which showed actual bond stresses were higher than predicted by ACI318-02, $7.9\sqrt{f_c'}$ psi

($0.66\sqrt{f_c'}$ MPa) (Figure 2-21). This is of great importance since it can change the mode of column failure from flexure controlled to shear-controlled.

Observations showed that the rate of degradation was mainly related to the applied displacement history, and less on the axial load. Moreover, the specimen subjected to the near-fault displacement history showed less strength degradation and maintained higher lateral forces at the same displacement in comparison to the specimens subjected to standard lateral displacement history. Figure 2-22 shows damage observed in specimen 2S20M subjected to standard displacement history, and 2S20HN subjected to near fault displacement history.

Table 2-4: Test Results

Specimen	Maximum Lateral Load (kN)	Maximum Lateral Load @ Drift	Normalized Lateral Load (kN)	Analytical Yield Moment (kN-m)	Max Base Moment M_{EXP} (kN-m)	M_{EXP}/M_y
2S10M	202.7	1.50%	202.7	381.3	370.7	0.97
2S20M	233.5	1.28%	233.5	450.4	427.0	0.95
2S30M	285.3	1.45%	285.3	509.0	521.8	1.03
2S20H	269.5	1.33%	247.0	441.5	451.8	1.02
2S20HN	267.4	1.00%	245.1	441.5	448.3	1.02
2S30X	340.7	1.50%	283.9	499.5	519.2	1.04

Envelope relations of the normalized moment versus lateral drift ratios from the tests and per FEMA 356 are plotted in Figure 2-23 and show significant difference between the predicted and observed lateral strength degradations.

Melek and Wallace concluded that specimens with low, medium, and high axial loads maintained their axial load carrying capacity up to approximately 10%, 7% and 5% lateral drift ratios, respectively, maintaining about 20% (or less in medium and high axial force columns) of the axial force. It does not seem the splice failure causes collapse of the components given the columns maintained their axial load carrying capacity to large drift ratios, despite heavy damage (Figure 2-22) and significant loss of lateral-load capacity (Figure 2-23), and the system was able to remain stable after large lateral drift ratios.

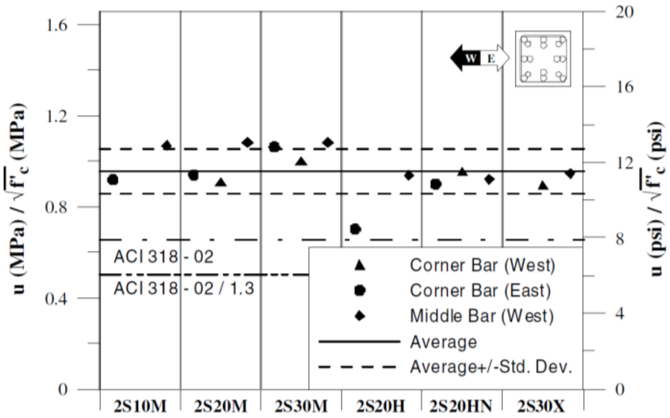

Figure 2-21: Normalized Measured Bond Strengths

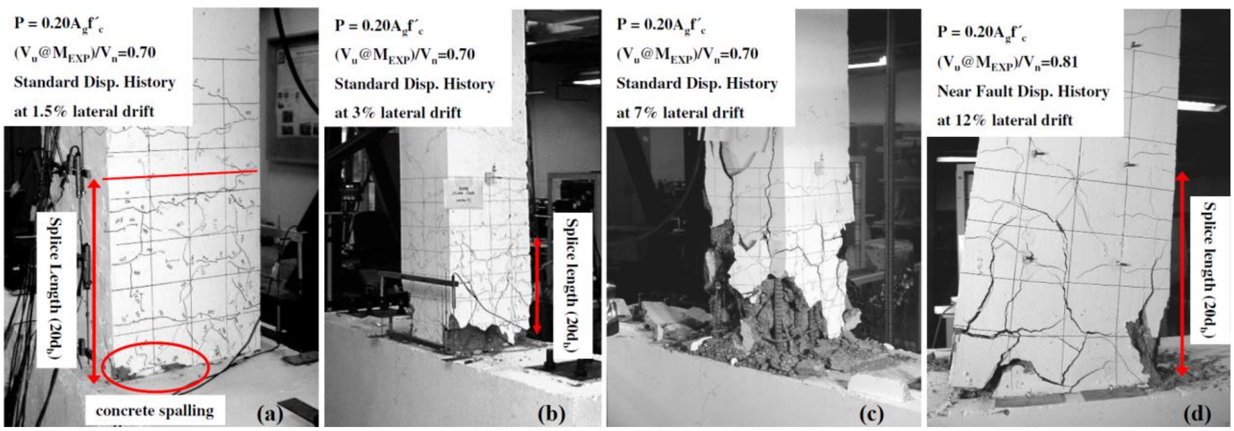

Figure 2-22: 2S20M (a) Concrete Spalling at 1.5% Lateral Drift, (b) 3% Lateral Drift, (c) 7% Lateral Drift (Loss of Axial Load Capacity), (d) 2S20HN at 12% Lateral Drift

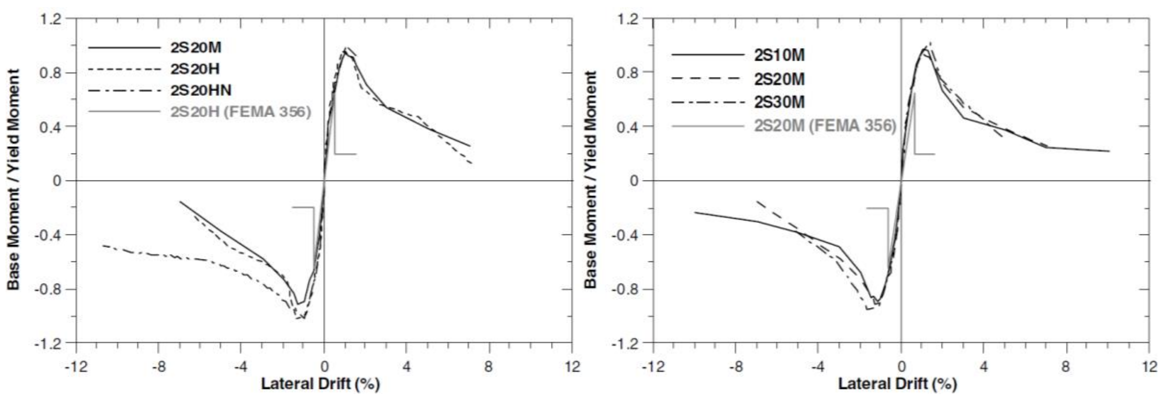

Figure 2-23: Normalzied Moment vs. Lateral Drift: 2S20M, 2S20H, 2S20HN (left), 2S10M, 2S20M, 2S30M (right)

2.2.2.2 Cho and Pincheira (ACI Structural Journal, Mar-April 2006)

As discussed in section 2.2.2.1, a common deficiency in reinforced concrete columns built prior to 1977 is the splice length. Cho and Pincheira used data obtained from 14 tests and created an analytical model to validate the test data. This model can be used to estimate the seismic response of reinforced concrete columns with short lap-splices. To estimate the bar stress and deformation at splice failure, the model uses local bond stress-slip relationship and considers degradation of stiffness and strength with increasing deformation at each cycle of the reversed cyclic lateral displacement. The model predicts the strength of short lap-splices, calculates failure mode, lateral load capacity, and lateral deformation corresponding to the splice failure very closely to the measured values. In the end, a simple equation is presented to calculate bar stress at splice failure which produced very close results to the measured strength at splice failure. (Cho & Pincheira, 2006)

Three basic deformation mechanisms, (from flexure, shear, and bond-slip) that contribute to the resistance of a reinforced concrete column were considered in the model (Figure 2-24). The model considered the principles of the lumped plasticity models and was an extension of the two-dimensional, single component model modified to include shear response (Figure 2-25). A member was defined with an elastic beam-column element with a non-linear rotational spring at the base, and a zero-length shear spring. The element length was equal to the clear height of the columns and was used to model the contributions of flexure and shear deformation mechanisms. The deformations contribution by bond-slip of the lap-splices are replicated by a non-linear rotational spring above a rigid zone at the base of the column.

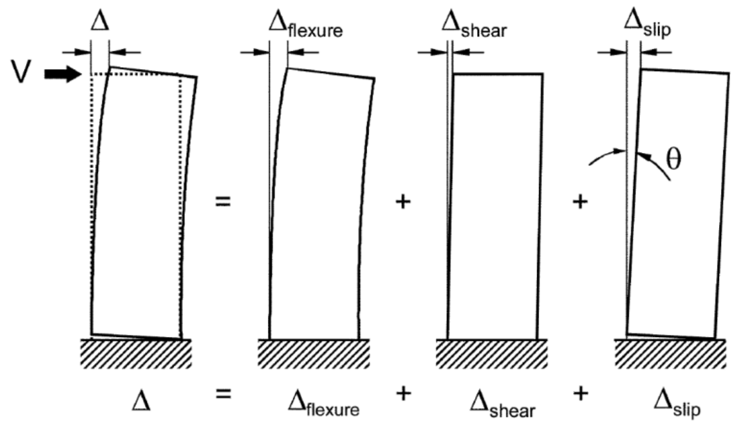

Figure 2-24: Deformation Mechanisms Considered

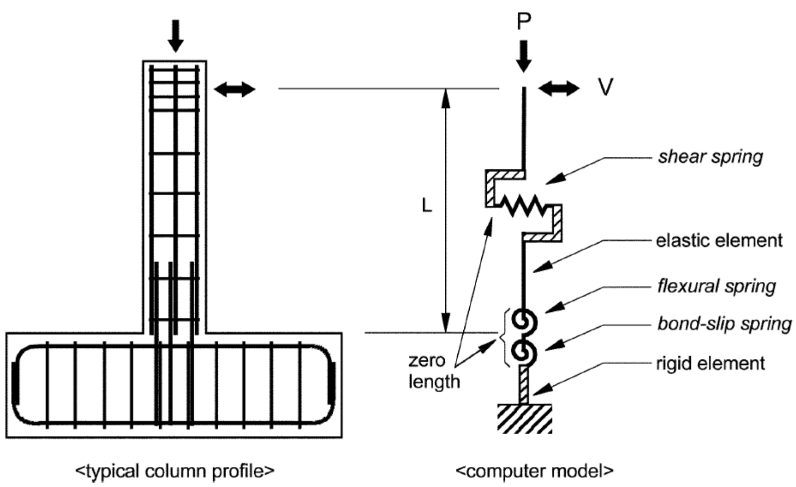

Figure 2-25: Typical Profile and Computer Model of RC Column

Data used to validate the model were from tests conducted at the University of Texas at Austin (FC1, FC4, FC5, FC14, and FC15), University of California Berkeley (2SLH18, 3SLH18, and 3SMD12), and University of California Los Angeles (S10MI, S20MI, S30MI, S20HI, S20HIN, and S30XI), with columns details and properties shown in Figure 2-26 and Table 2-5.

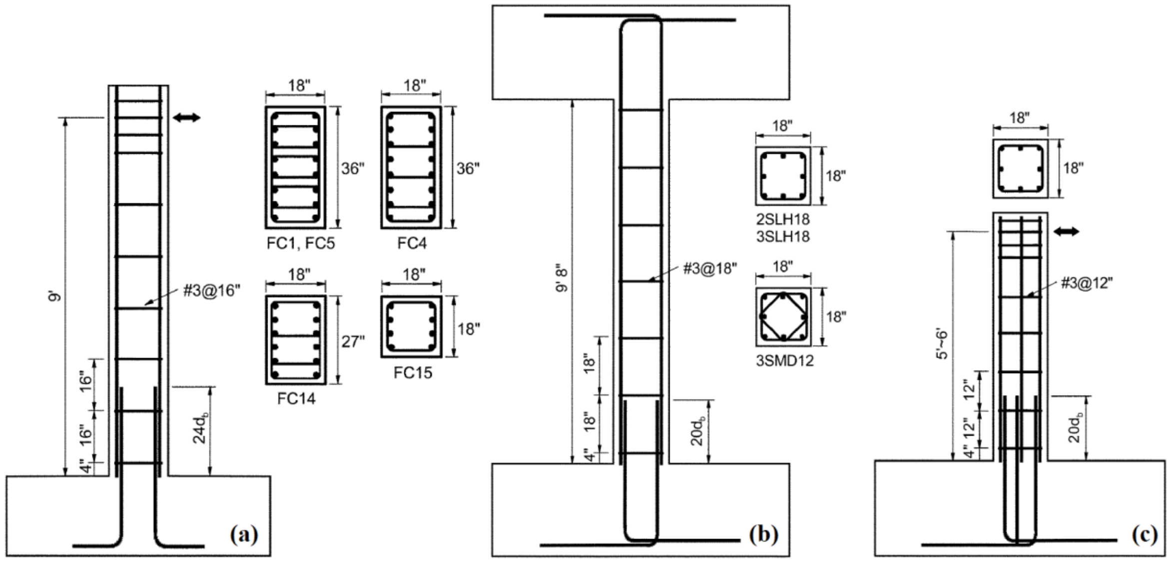

Figure 2-26: Column Details (a) UT-Austin, (b) UC-Berkeley, (c) UCLA tests

Table 2-5: Dimensions and Properties of Columns

Researcher	Column	Column dimensions			Longitudinal reinforcement			Transverse reinforcement		Concrete	Axial load
		b, in.	h, in.	l, in.	Amount	l_s, in.	f_y, ksi	Amount	f_y, ksi	f_c', ksi	
Aboutaha[3]	FC1	36	18	108	16 No. 8	24	63	No. 3 at 16	58	4.70	0
	FC4	36	18	108	16 No. 8	24	63	No. 3 at 16	58	2.85	0
	FC5	36	18	108	16 No. 8	24	63	No. 3 at 16	58	2.98	0
	FC14	27	18	108	12 No. 8	24	63	No. 3 at 16	58	4.17	0
	FC15	18	18	108	8 No. 8	24	63	No. 3 at 16	58	4.17	0
Lynn[4]	2SLH18	18	18	116	8 No. 8	20	48	No. 3 at 18	58	4.80	$0.12A_gf_c'$
	3SLH18	18	18	116	8 No. 10	25	48	No. 3 at 18	58	3.71	$0.12A_gf_c'$
	3SMD12	18	18	116	8 No. 10	25	48	No. 3 at 12	58	3.70	$0.35A_gf_c'$
Melek[6]	S10MI	18	18	72	8 No. 8	20	74	No. 3 at 12	69	5.26	$0.10A_gf_c'$
	S20MI	18	18	72	8 No. 8	20	74	No. 3 at 12	69	5.26	$0.20A_gf_c'$
	S30MI	18	18	72	8 No. 8	20	74	No. 3 at 12	69	5.26	$0.30A_gf_c'$
	S20HI	18	18	66	8 No. 8	20	74	No. 3 at 12	69	5.13	$0.20A_gf_c'$
	S20HIN	18	18	66	8 No. 8	20	74	No. 3 at 12	69	5.13	$0.20A_gf_c'$
	S30XI	18	18	60	8 No. 8	20	74	No. 3 at 12	69	5.13	$0.30A_gf_c'$

Notes: b = width of column cross section; h = height of column cross section; l = clear height of column; l_s = splice length; f_y = yield strength of reinforcing bar; f_c' = compressive strength of concrete; A_g = gross area of column cross section; 1 in. = 25.4 mm; and 1 ksi = 6.89 MPa.

The longitudinal reinforcement at the base of the columns were spliced over a length of 20 or 24 bar diameters with No. 3 (10 mm) transverse reinforcement spaced at 12, 16, or 18 in. (305, 406, or 457 mm) with 90-degree hooks (except for Column 3SMD12, with additional No. 3 (10 mm) diamond ties at 4 in. (102 mm) in the splice region). Local bond-slip relations for unconfined concrete were used in the model as the light transverse reinforcement provided little to no confinement. In the analyses, all of the columns were subjected to the same unidirectional reversed cyclic loading that corresponded to the displacement history applied during the tests, except for column 2S20HN (Figure 2-26) which was subjected to a near-fault displacement history.

Table 2-6 provides measured (by test) and calculated (by model) values for maximum lateral loads and the failure modes, and shows they are in close agreement with an average measured-to-calculated strength ratio of 1.03 and a standard deviation of 0.09.

Table 2-6: Measured and Calculated Peak Loads and Calculated Failure Modes

Column designation	Maximum lateral loads			Failure modes	
	Measured V_{meas}, kips	Calculated V_{calc}, kips	V_{meas}/V_{calc}	Observed	Calculated
FC1	51	52.6	0.97	SpF	SpF
FC4	41	43.0	0.95	SpF	SpF
FC5	40	42.7	0.94	SpF	SpF
FC14	33	38.0	0.87	SpF	SpF
FC15	24	25.2	0.95	SpF	SpF
2SLH18	53	44.8	1.18	YiR, SpD, ShF	YiR, ShF
3SLH18	61	51.6	1.18	YiR, SpD, ShF	ShF
3SMD12	83	73.9	1.12	YiR, SpD, ShF	SpF
S10MI	46	43.2	1.06	SpF	SpF
S20MI	52	52.3	0.99	SpF	SpF
S30MI	64	60.6	1.06	SpF	SpF
S20HI	61	58.3	1.05	SpF	SpF
S20HIN	60	59.1	1.02	SpF	SpF
S30XI	77	70.9	1.09	SpF	ShF
Average (SD)			1.03 (0.09)		

Notes: SpD = splice degradation; SpF = splice failure; ShF = shear failure; YiR = yielding of reinforcing bar; and 1 kip = 4.45 kN.

The calculated failure modes for columns 3SMD12 and S30XI differed from the observed failure modes mode. However, a comparison of the calculated lateral load corresponding to the measured loads at failures, revealed differences of about 3-5.5% which revealed the columns could have had either failure mode.

Table 2-7 provides measured (by test) and calculated (by model) values for maximum lateral deformations, and shows they are in relative agreement with more disparity than the peak loads, with average measured-to-calculated strength ratio of 1.30 and a standard deviation of 0.22.

Table 2-7: Measured and Calculated Displacements at Peak Loads

Column designation	Corresponding lateral displacements		
	Measured Δ_{meas}, in.	Calculated Δ_{calc}, in.	$\Delta_{meas}/\Delta_{calc}$
FC1	1.7	1.1	1.55
FC4	1.3	1.1	1.18
FC5	1.7	1.1	1.55
FC14	1.5	1.2	1.25
FC15	1.4	1.2	1.17
2SLH18	1.0	0.8	1.25
3SLH18	0.9	0.9	1.00
3SMD12	1.8	1.5	1.20
S10MI	1.1	0.7	1.57
S20MI	0.9	0.8	1.13
S30MI	1.0	0.8	1.25
S20HI	0.9	0.7	1.29
S20HIN	0.7	0.7	1.00
S30XI	0.9	0.5	1.80
Average (SD)			1.30 (0.22)

Note: 1 in. = 2.54 mm.

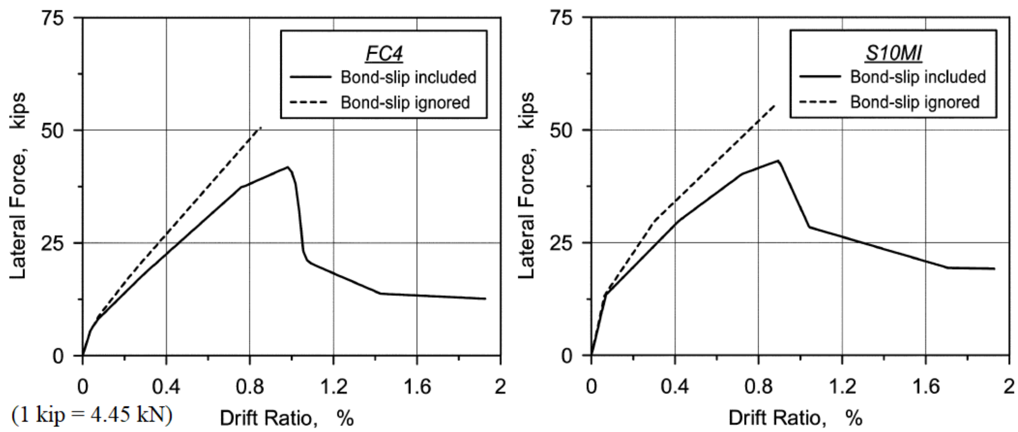

Figure 2-27: Lateral Load and Drift Computed with and without Bond-Slip Effects

Short lap-splice lengths can cause increased lateral deformations, reduce lateral resistance and deformation ductility of the column. Figure 2-27 shows the drift v. lateral load relationship calculated with the model for columns FC4 and S10MI with and without the effects of bond-slip. It is shown that the bond-slip accelerates the increase of lateral drifts as the lateral load increases, and the columns tested as cantilevers, exhibited lateral drifts at peak load of about 45% larger than when the effects of bond slip were not considered (Table 2-8). Columns 2SLH18, 3SLH18, and

3SMD12 tested in double curvature showed less influence of their lateral stiffness by the splice failure. These columns had splices at the base, and continuous reinforcement anchored with a standard hook at the top.

Table 2-8: Calculated Lateral Displacements at Peak Load with and without Bond-Slip Effects

Column designation	Lateral displacements, in.		Displacement increase, %
	Without bond-slip	With bond-slip	
FC1	0.80	1.16	45
FC4	0.74	1.06	43
FC5	0.75	1.06	41
FC14	0.83	1.18	42
FC15	0.83	1.18	42
2SLH18	0.74	0.80	8
3SLH18	0.70	0.85	21
3SMD12	1.29	1.38	7
S10MI	0.43	0.64	49
S20MI	0.46	0.69	50
S30MI	0.49	0.74	51
S20HI	0.51	0.77	51
S20HIN	0.51	0.77	51
S30 XI	0.40	0.52	30

Note: 1 in. = 2.54 mm.

As mentioned by Melek and Wallace (2004) the current FEMA356 produced very conservative stress at splice, using the equation $f_s = (\frac{l_b}{l_d^{ACI}})f_{yL}$. Based on the measured and calculated results, Cho and Pincheira proposed the following equation $f_s = (\frac{l_b}{0.8l_d^{ACI}})^{2/3}f_{yL}$ which captures the performance of the columns with great precision: average calculated peak moment to measured peak moment ratio of 0.99 and standard deviation of 0.05 (Table 2-9). This equation is now modified to $f_s = 1.25(\frac{l_b}{l_d^{ACI}})^{2/3}f_{yL}$ in ASCE 41-13.

Table 2-9: Measured and Calculated Moment at Splice Failure Using Proposed Equation

Column designation	Peak moment, kip·in.			$\frac{M_{peak}^{model}}{M_{peak}^{meas}}$	$\frac{M_{peak}^{proposed}}{M_{peak}^{meas}}$
	Measured	Uniaxial spring model	Proposed		
	M_{peak}^{meas}	M_{peak}^{model}	$M_{peak}^{proposed}$		
FC1	5508	5659	5393	1.03	0.98
FC4	4428	4505	4483	1.02	1.01
FC5	4320	4597	4559	1.06	1.06
FC14	3564	4062	3889	1.14	1.09
FC15	2592	2708	2580	1.04	1.00
S10MI	3312	3106	3130	0.94	0.95
S20MI	3744	3765	3788	1.01	1.01
S30MI	4608	4352	4386	0.94	0.95
S20HI	4026	3809	3753	0.95	0.93
S20HIN	3960	3809	3753	0.96	0.95
S30XI	4620	4390	4343	0.95	0.94
Average (SD)				1.00 (0.06)	0.99 (0.05)

Note: 1 kip·in. = 0.113 kN·m.

The analytical model calculated lateral load capacity, deformation at splice failure, and failure mode of the columns with close agreement to the test results. It also emphasized on the contribution of bond-slip in the splice region to total lateral displacements of the column. This effect should be considered as it significantly impacts the column displacement at peak lateral load. It should be noted that this effect was more pronounced in the columns tested in single curvature. Finally, the current FEMA 356 to calculate bar stress at splice failure was too conservative, and the equation proposed in the paper produced results in great agreement to the measured values.

2.2.3. Non-Ductile Concrete Frames

2.2.3.1 Islam (September 1996)

The response of a seven-story reinforced concrete moment frame building was recorded during the 1994 Northridge earthquake and is analyzed in this paper. The building was based on the 1964 Los Angeles City Building Code (Table 2-10), and therefore lacked the proper detailing for ductile performance and was severely damaged after the 1994 earthquake. Figure 2-28,Figure 2-29, and Figure 2-30 illustrate the north elevation of the damaged building, damage in the columns below level 5 spandrel beams, and the close up of the south perimeter column damage, respectively. The lateral force resisting system of the building was comprised of non-ductile concrete moment frames and interior slab-column frames. The building was unique in that it was heavily instrumented during the Northridge earthquake, and even had limited instrumentation during the 1971 San Fernando earthquake.

The instrumentation at the time of the Northridge earthquake included 16 sensors that recorded ground motion and the response of the building during the earthquake. These records were analyzed and provided valuable information including actual periods of vibration, story drift ratios, roof displacement, torsional behavior of the building, distribution of internal forces, and story shear. This data provided the opportunity to examine analytical techniques commonly used by practicing engineers and/or researchers in seismic evaluation of existing buildings and predicting their performance when subjected to seismic loading. (Islam, 1996)

Table 2-10: Building Summary

Date of construction:	1965–1966
Date of drawings:	1965–1966
Design code:	L. A. City Building Code 1964 (assumed)
Number of stories:	7
Plan dimensions:	62′8″(N–S) × 151′2″(E–W)
Building height:	$65'8\frac{1}{2}''$
Story heights:	
Ground floor:	13′6″
Second through sixth floor:	$8'8\frac{1}{2}''$
Seventh floor:	8′8″

Figure 2-28: North Elevation of the Damaged Building

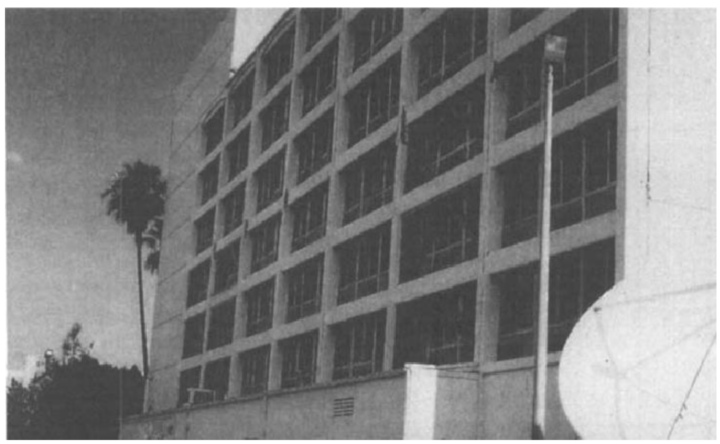

Figure 2-29: South Elevation – Damaged Columns below of the Damaged Building

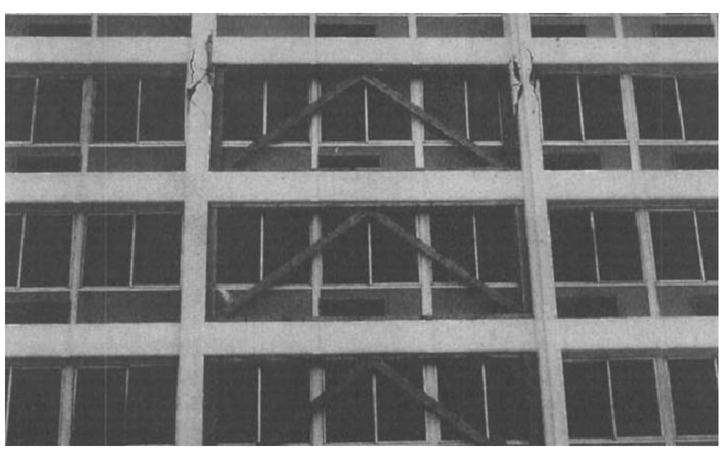

Figure 2-30: South Elevation – Typical Column Damage

The typical floor plan (Figure 2-31) consists of columns spaced at 18 ft. 9 in. (5715 mm) in the longitudinal (east-west) direction and above 20 ft. (6096 mm) in the north-south direction. Interior columns 20 in. by 20 in (508 mm by 508 mm) at level 1 and reduces to 18 in. (483 mm) square at upper levels. Column longitudinal reinforcement includes (10) No. 9 at levels 1 and 2, eight (8) No. 9 bars (29 mm) at level 3, six (6) No. 8 (25 mm) bars at level 4, and six (6) No. 7 (22 mm) bars at levels 5, 6, and 7, with No. 3 (10 mm) ties spaced at 12 in. (305 mm) on center at levels 1 to 4, and No. 2 (6 mm) at 12 in. (305 mm) on center at levels 5, 6 and 7.

Lateral force resisting system includes the perimeter frame and the interior slab column. Typical slab reinforcement in the column strip consists of (16) No. 6 (19 mm) at the top and (8) No. 6 (19 mm) at the bottom. Building material strengths are shown in Table 2-11.

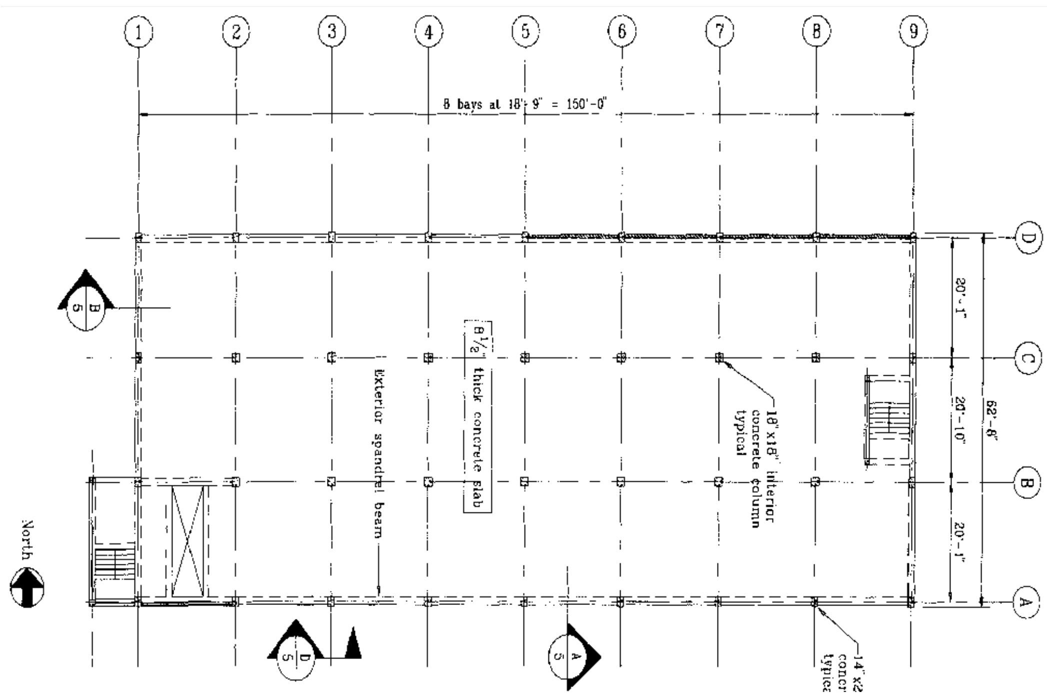

Figure 2-31: Typical Floor Plan

Table 2-11: Building Material Properties

			Specified f'_c (psi)	Assumed f'_c (psi)
Concrete	Columns, Ground–2nd floor		5000	6650
Concrete	Columns, 2nd–3rd floor		4000	5320
Concrete	Beams and slab, 2nd floor only		4000	5320
Concrete	All other concrete, 3rd–roof		3000	4000
		Grade	Minimum specified yield strength, F_y (ksi)	Assumed F_y (ksi)
Reinforcing steel	Beams and slabs	Intermediate-grade (ASTM A-15 and A-305)	40	50
Reinforcing steel	Columns bars	Deformed billet bars (ASTM A-432)	60	72

Expected material strengths are used in the calculations and include the inherent over-strength in original material strength or strength gain over time. The specified values were only used for the steel reinforcement of the beams and columns when calculating their shear capacities.

The building was instrumented with 16 accelerometers: 10 in the north-south direction, five in the east-west direction, and one measured the vertical acceleration, as shown in Figure 2-32. All sensors were triggered simultaneously at nominal 1% g vertical acceleration and recorded the response for approximately 60 seconds. The building was red tagged after the Northridge earthquake as it sustained severe structural and non-structural damage. The structural damage was primarily observed in the east-west direction, while the frames in the north-south direction sustained minor flexural cracks. Several perimeter frames up to level 5, especially between levels 4 and 5, with adjoining damaged columns were severely damaged and temporarily shored due to the loss of gravity load carrying capacity of the columns (Figure 2-33). This damage included extensive shear cracking which possibly caused buckling of vertical column reinforcement. Additionally, hairline flexural cracks and some concrete spalling were observed in several spandrel beams. Many beam-column joints below level 5 also exhibited shear cracks and some concrete spalling, with more damage observed along the south perimeter frame.

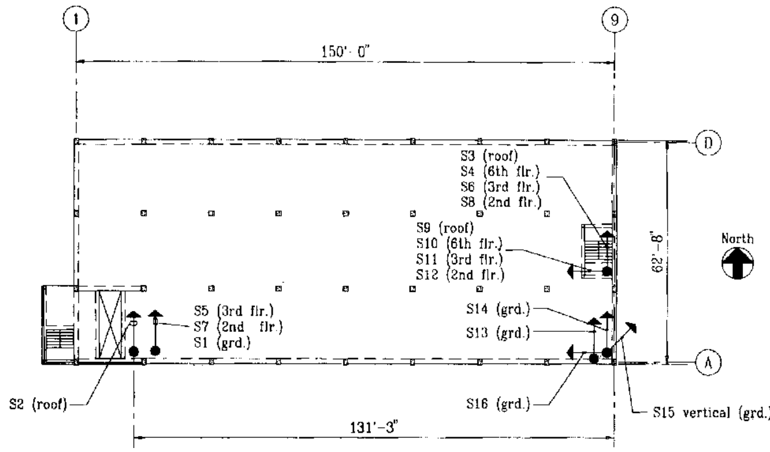

Figure 2-32: Strong Motion Instrumentation

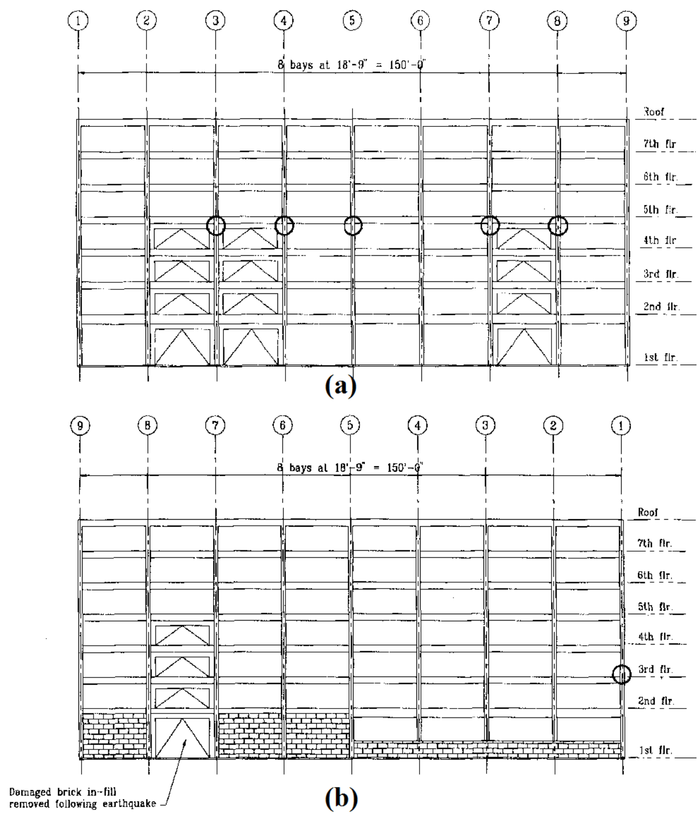

Figure 2-33: Location of Building Damage – (a) South Perimeter Frame, (b) North Perimeter Frame

Non-structural damage was limited mainly to level 4 doors, windows, and partition walls and was due to large lateral deformations at that level.

Four types of analysis were performed (analysis of recorded responses, three-dimensional elastic response history analysis, limit state analysis, and pushover analysis) to compare the actual performance of the building during the Northridge earthquake with the analytical methods commonly used by practicing engineers.

Analysis of recorded responses: The recording of the 16 sensors provided important information about the building response including periods of vibration, story drifts, roof displacement, building torsion, and distribution of internal forces and story shears. As an example, recorded peak story accelerations, and roof displacement response history are shown in Table 2-12 and Figure 2-34 respectively.

Table 2-12: Recorded Peak Accelerations and Time of Occurrence

		E–W direction (longitudinal)	N–S direction (transverse)
Northridge earthquake, 1994	Grd Fl:	S16: 0·45g @ 8·86 s	S13: 0·42g @ 5·54 s S1: 0·39g @ 5·58 s
	2nd Fl:	S12: 0·33g @ 8·44 s	S8: 0·40g @ 4·58 s S7: 0·38g @ 4·12 s
	3rd Fl:	S11: 0·36g @ 10·06 s	S6: 0·45g @ 4·44 s S5: 0·41g @ 4·84 s
	6th Fl:	S10: 0·46g @ 9·12 s	S4: 0·33g @ 7·28 s
	Roof	S9: 0·58g @ 9·22 s	S3: 0·57g @ 7·36 s S2: 0·56g @ 4·64 s
	Vertical Accel Grd Fl:	S15: 0·27g	
San Fernando earthquake, 1971	Grd Fl:	0·13g	0·25g
	4th Fl:	0·252g @ 7·9 s	0·203g @ 9·1 s
	Roof:	0·327g @ 9·2 s	0·406g @ 9·9 s
	Vertical Accel Grd Fl:	0·18g	

Three-dimensional elastic response history analysis was performed by subjecting the building to ground motions, simultaneously applied in both orthogonal directions. Member stiffness was calculated from the moment-curvature analysis at the point of first yield of the longitudinal bars. Building was considered fixed at the base with viscous damping of 5%. The analysis output is plotted with the sensor recordings as shown in Figure 2-35 to compare the validity of the elastic analysis.

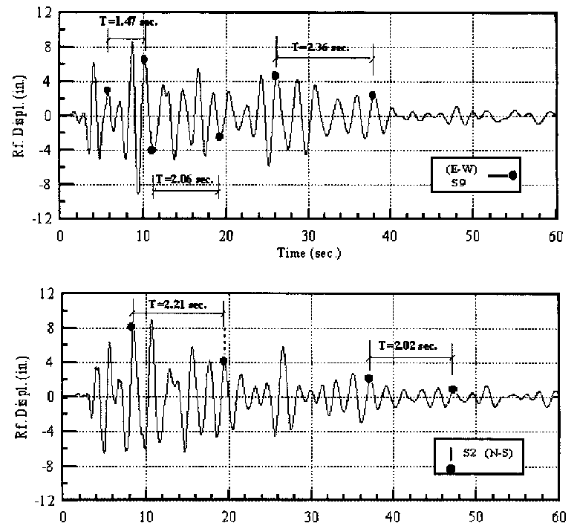

Figure 2-34: Roof Displacement Response History

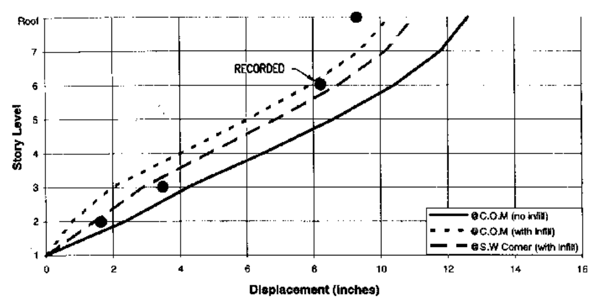

(a)

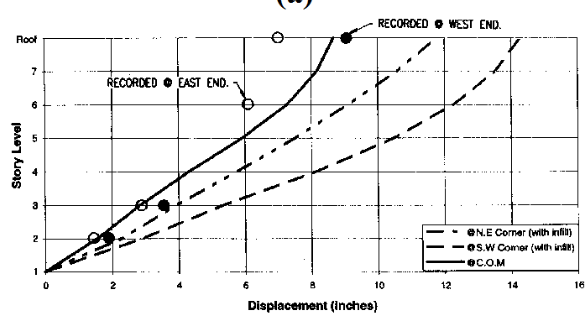

(b)

Figure 2-35: Story Displacements – 3-D Elastic Response History Analysis, (a) East-West direction, (b) North-South direction

Limit state analysis: to establish strength and deformation limit states, building structural components and sub-assemblies were analyzed. At the component level, the beams are flexure controlled (controlled by flexural limit state), and columns are shear-controlled (controlled by shear limit state). Based on probable demand calculations excessive cracks and damage were not expected at the joints but the observed damage contracted this prediction. The probable seismic story forces were calculated per DAlembert's principle, by multiplying the mass at that level by the maximum acceleration. Probably shear capacity is shown shaded in Figure 2-36 over actual response of the building from sensor recordings.

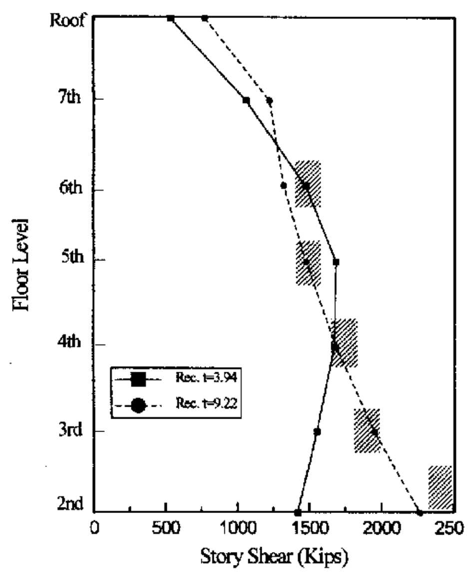

Figure 2-36: Shear Demand during Northridge Earthquake (Shear Capacity: Shaded)

Push-over analysis: A two-dimensional static non-linear analysis was performed on the south perimeter frame to determine if this method could predict the observed response of the building. Figure 2-37 shows the base shear plotted vs. roof displacement with major events (first beam yielding in flexure, first column yielding in shear, and formation of mechanism) shown on the figure. The sequence of yielding in the model is shown in Figure 2-38. Based on these flexural positive and negative cracks are expected at beam ends, while the actual building sustained minor positive flexural cracks. Also, in the actual building no flexural cracks were observed at column bases, and shear failure (not flexural failure) occurred below level 5. This inconsistency is mainly due to the difference in the assumed and actual load distribution patterns.

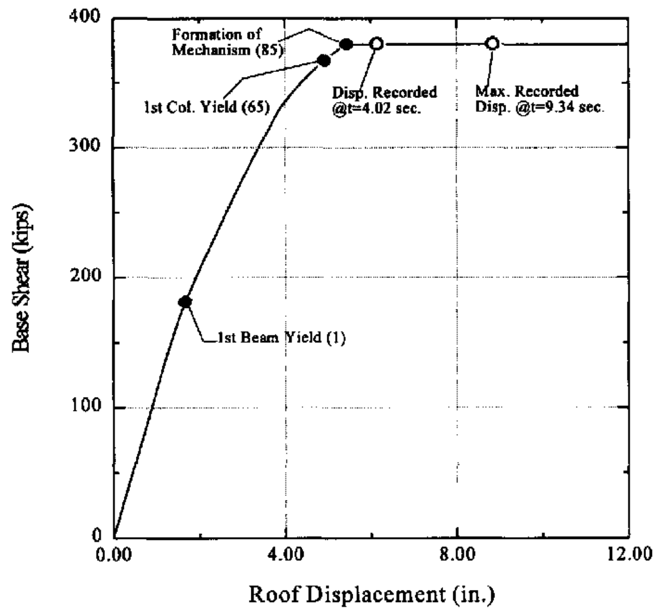

Figure 2-37: Result of Pushover Analysis

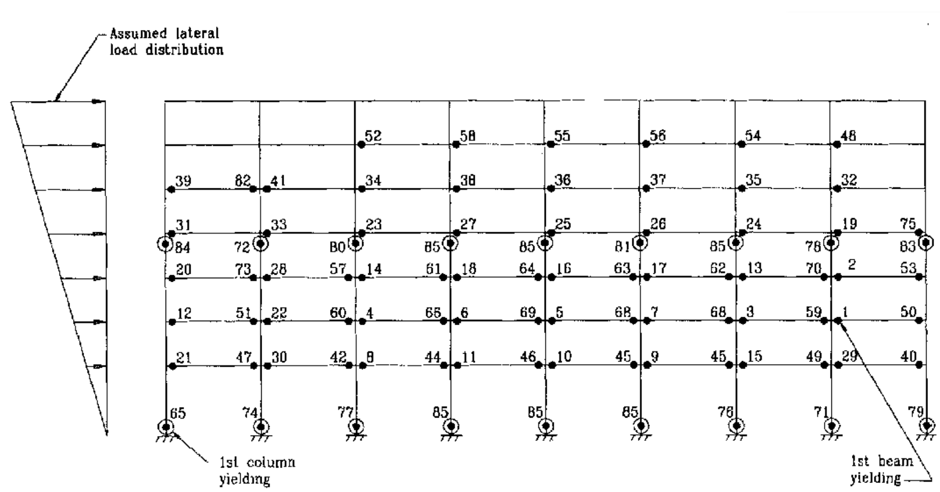

Figure 2-38: Pushover Analysis – Yielding Sequence

The building sustained more damage than anticipated especially in the south elevation, where it is believed had the earthquake gone for a few seconds longer, the columns would have completely lost their gravity load carrying capacity. The damage was also mainly in the east-west direction and the most severe damage was at level 4, below level 5. Several reasons are considered to be the contributors to the discrepancy in the predicted and actual performance of the building.

The brick filler walls at the north elevation introduced asymmetry in the east-west direction and led to higher displacement demands in the south frame. The building appeared to have experienced 20-25% larger story shear which was attributed to the participation of the slab-column system and the over-strength of building materials. Higher modes seem to have contributed more significantly to the performance of the building why analytical methods are typically dominated by higher modes. This is also the reason for almost the highest shear demand being experienced below level 5. The maximum joint shear demand was estimated to be lower than the building experienced. This seems to have been due to the beams not being centered on the columns which created a complicated load path and increased the load in the unconfined joints. The elastic analysis seems to overestimate the inelastic deformation and it is suggested to use the *equal displacement rule* for buildings with long periods. The beam-columns seem to have been designed for the weak beam-strong column condition. However, the effect of the slab in increasing the beam flexural capacity was not considered, hence changed the limit state from flexural yielding of the beams, to shear failure of the columns. Lastly the push-over analysis seems to be sensitive to the assumed load distribution and certain simplifying assumptions can result in a significantly different failure sequence that the damage observed.

2.2.3.2 Yavari and Elwood (October 2008) and Wu et al (October 2008)

During the past four decades, several severe earthquakes have caused tremendous damage to urban regions including the collapse of many older reinforced concrete buildings. Given the generally low probability of collapse of such buildings (<7%), it is prudent to focus resources on in-situ and inexpensive retrofit schemes to provide resilience in the community. A major contributor in proposing a cost-effective retrofit plan is accurate evaluation and estimation of performance of the existing conditions. This study focuses on reinforced concrete (RC) frames constructed before the late 1970s, which were mainly designed for gravity forces and lack proper detailing (transverse reinforcement) to provide sufficient shear strength and confinement. As a result, these buildings lack the strength and ductility to withstand a major ground shaking, and post-earthquake reconnaissance has identified such buildings vulnerable and hazardous. Due to lack of experimental data at the point of collapse, information available to study concrete buildings at this extreme performance level is limited. This research features a test conducted on a two-dimensional three-bay beam-column frame, composed of two non-ductile and two ductile columns. This is common in many buildings in Taiwan where a new addition was constructed and connected to an existing old building. The specimen was subjected to a uniaxial motion on a shaking table until global collapse was observed. The test data was then compared with simplified commonly used assessment methods by practicing engineers and suggested that ASCE 41-06 provided conservative estimate of the load-deformation relations for flexure-shear columns, while the code updates correlate better with the test results. (Yavari, Elwood, & Wu, 2008) (Wu, et al., 2008)

The main objective of this paper is to present additional data from shaking table tests resulting in 1) flexure-shear (where shear failure is expected to occur after flexural yielding) failure, and 2) flexural failure in a multi-column test frame and to evaluate the accuracy of existing assessment methods offered by FEMA 356 and ASCE 41-06 in identifying the observed structural collapse. Previous studies have shown these documents provide conservative estimates of drift capacity for non-ductile columns. (Sezen & Moehle, 2006) (Yavari, Elwood, & Wu, 2008) (Wu, et al., 2008)

The test specimen included a single-story, four-column frame test specimen with two ductile columns and two non-ductile columns as shown in Figure 2-39 which is a representation of the common construction practice for school buildings and other structures in Taiwan. The columns were built to one-third scale, fixed at the base, and connected by a strong beam at the top to provide double curvature bending in the columns. The columns had a square cross section of 5.9 in. by 5.9 in. (150 mm by 150 mm) with a clear height of 39.4 in. (1000 mm). The top beam carried lead packets to represent the weight of a low-rise building at about $0.10 A_g f_c'$ for each column. The longitudinal reinforcement ratio 2.54% was for non-ductile columns (C1 and C2), and 1.39% for ductile columns (C3 and C4), with continuous longitudinal reinforcement at the base. Transverse reinforcement with 135-degree bends and 90-degree/135-degree ties consisted of 1/8 in. (3.2 mm) diameter hoops and ties at approximately 4 in. (100 mm) on center for C1 and C2, and 0.20 in. (5 mm) diameter hoops and ties at 1.3 in. (33 mm) on center for C3 and C4. See Figure 2-39. Results of material testing conducted on the concrete and steel reinforcement are shown in Table 2-13.

Assessment of load redistribution during structural collapse is of significant engineering interest, hence studied in this experiment. The test confirmed that the phenomenon existed, especially for vertical load distribution. To support the frame from unfavorable out-of-plane movement, a supporting steel frame system was placed on the table. Another frame was placed outside the table connected by cables to the specimen to catch it when collapse happened. See Figure 2-40 for experimental setup and location of load cells, lead packets, and linear displacement transducers or temposonics.

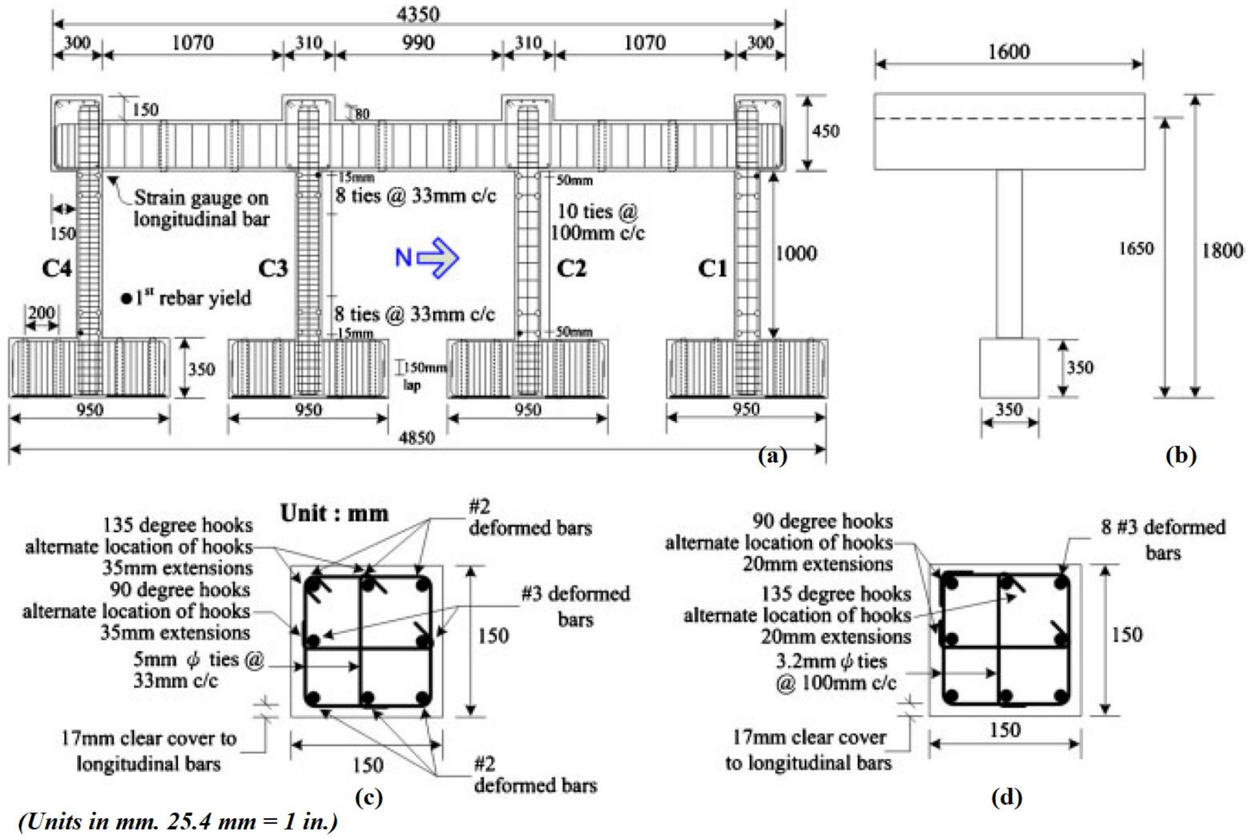

Figure 2-39: Reinforcement Details of Specimen Frame: (a) Elevation, (b) Side View, (c) Ductile Columns C3 and C4, (d) Non-Ductile Columns C1 and C2

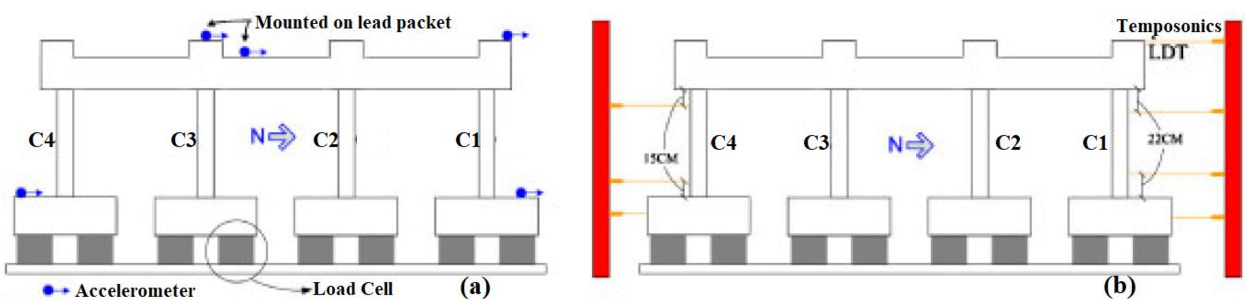

Figure 2-40: Test Setup, (a) Accelerometer and Load Cell, (b) Temposonics

Calculated shear and flexural strengths of the columns are shown in Table 2-14 and the ratios of shear demand to shear strength are also provided. Columns C1 and C2 are expected to exhibit flexure-shear failure while columns C3 and C4 are expected to fail in flexure.

Table 2-13: Materaial Properties of Concrete and Steel Reinforcement

Concrete					
Columns and footings			Beam		
	f'_c			f'_c	
Age (Day)	Mean (MPa)	COV (%)	Age (Day)	Mean (MPa)	COV (%)
28	29.7	3.4	Test day (54)	35.4	2.6
Test day (89)	32.2	4.1			

Steel				
Bar code	#2	#3	D5	D3.2
Diameter (mm)	6.0	9.5	5.0	3.2
f_y (MPa)	232	471	662	549
f_u (MPa)	284	708	692	578
Fracture strain (%)	16.4	13.6	2.9	2.7

Table 2-14: Calculated Shear and Flexural Strengths of Columns

Column no.	V_{ACI} (kN)	V_{Mp} (kN)	V_{Mp}/V_{ACI}
C1	37.9	34.6	0.91
C2	39.4	38.5	0.98
C3	93.3	20.0	0.21
C4	93.9	20.5	0.22

The base-shear history of the frame can be obtained from the accelerometers (located on the top beam) or the load cells (located underneath column footings) (Figure 2-40). To ensure the functionality of the frictionless sliders on the steel supporting frame, the data obtained from the accelerometer and load cells are compared in Figure 2-41. The readings have close agreement until 18.8 seconds which is correlated to an instant collapse of columns C1 and C2. The columns shortened by 6.7 and 1.3 in. (170 and 32 mm) respectively, causing the frame to tilt over to the north, disrupting the readings from the accelerometers.

The selected ground motion was scaled to two levels of PGAs, 1.55g (Test 1) and 1.85g (Test 2) are shown in Figure 2-42, and the recorded response spectra are shown in Figure 2-43.

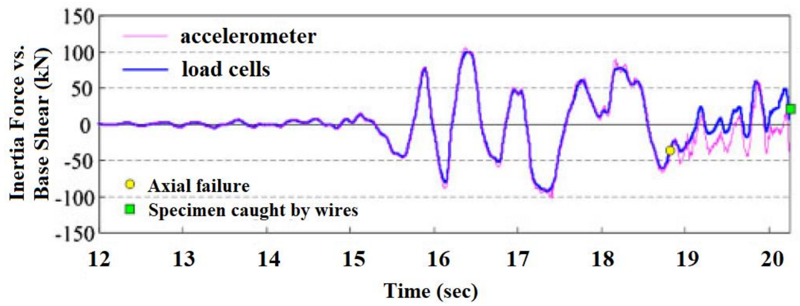

Figure 2-41: Comparison of Frame Base-Shear Histories from Accelerometers and Load Cells

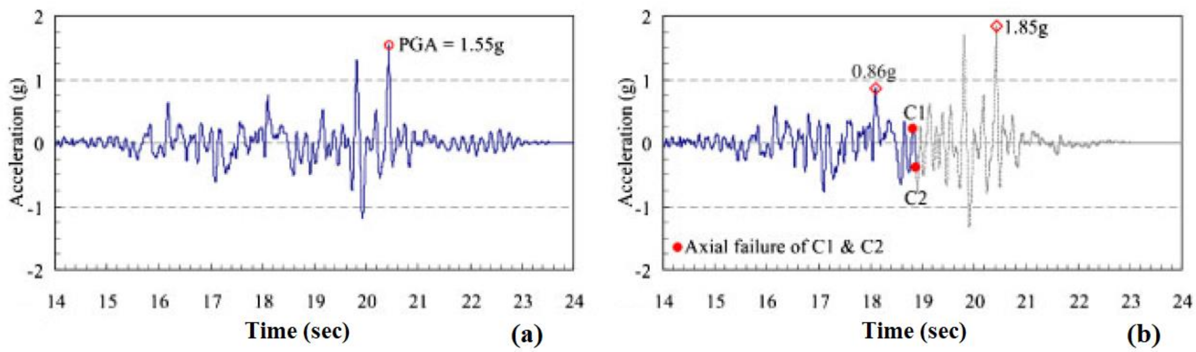

Figure 2-42: Acceleration Records of (a) Test 1, and (b) Test 2

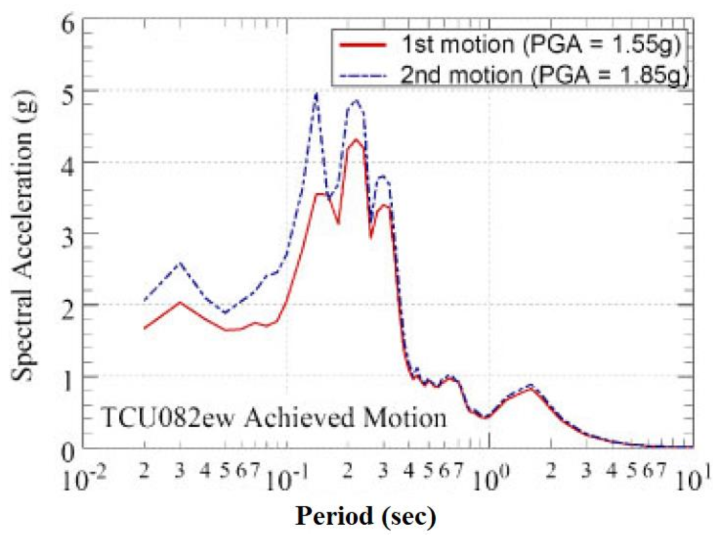

Figure 2-43: Response Spectra of Test 1 and Test 2

After Test 1, the frame underwent peak lateral drift ratio of 4.37%, but did not collapse. Non-ductile columns C1 and C2 exhibited some crushing of the concrete cover and significant flexural (horizontal) and shear (diagonal) cracks, while ductile columns C3 and C4 experienced flexural cracking and light concrete cover spalling at the column tops, as shown in Figure 2-44.

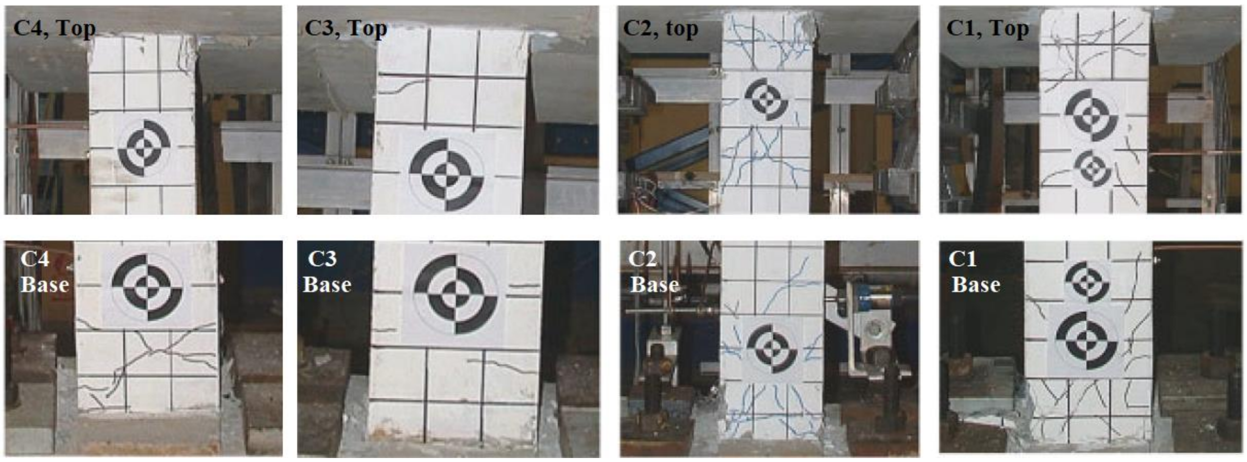

Figure 2-44: Test 1: Damage at Column Tops and Bases

Test 2 resulted in severe shear cracking and eventually axial failure of C1 and C2, and flexural failure of C3 and C4 as indicated in Figure 2-45. As the non-ductile columns failed, the vertical load was distributed to the ductile columns, which in turn caused the overload of the columns and global collapse of the frame.

To be able to assess the accuracy of analytical models, these test data can be checked by various models. In this research models by FEMA 356, ASCE 41-06, Elwood et al. 2007 which was later modified by Zhu et al. 2007 were chosen. (Elwood, et al., 2007) (Zhu, Elwood, & Haukaas, 2007) The experimental hysteresis is compared with these assessment models as shown in Figure 2-46.

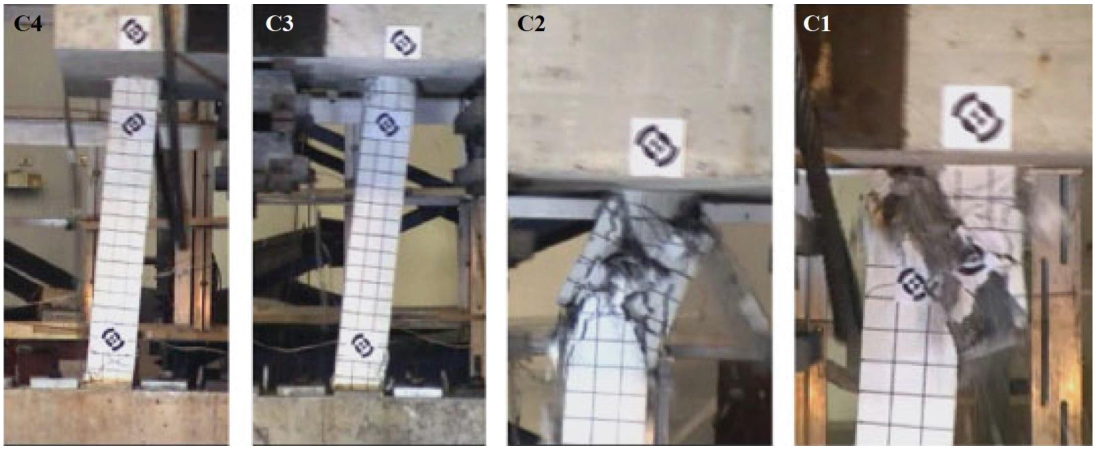

Figure 2-45: Test 2: Failure of Columns

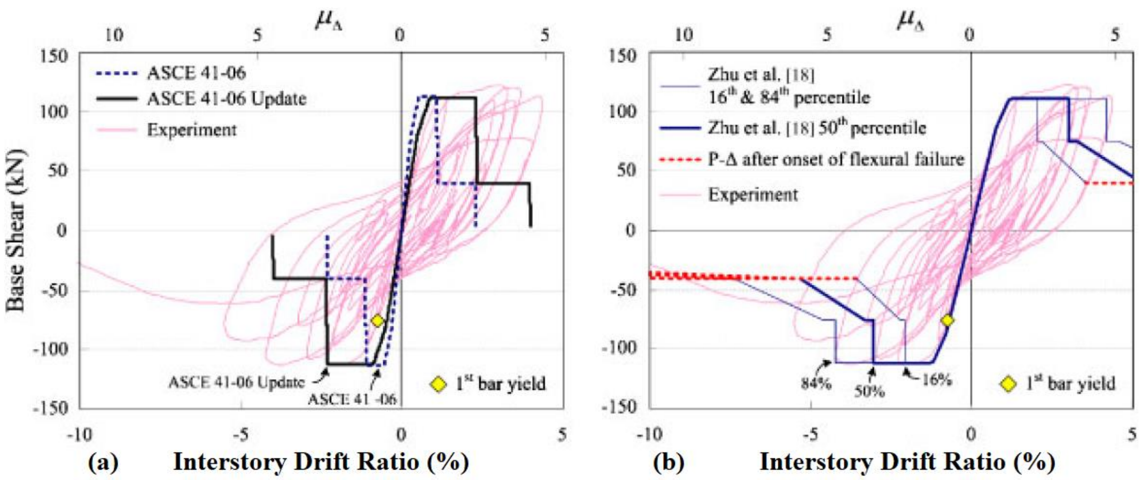

Figure 2-46: Comparison of Experimental Hysteresis with Existing Assessment Models

In conclusion, the strengths and lateral deformation capacities of the test specimen were compared with values obtained from analytical models and standards. ASCE 41-06 standard predicted the strength very closely but was very conservative in predicting the lateral deformation capacity of the frame. However, the ASCE 41-06 updates provided improved prediction od lateral deformation capacity. The model by Zhu et al. provided the closest estimation of the strength and deformation capacity when the 16th and 84th percentiles were considered (mean plus and minus one standard deviation). See Figure 2-46.

2.2.3.3 Baradaran S. (August 2013) and Baradaran S., Yang and Elwood (June 2012)

Existing reinforced concrete frame buildings that lack proper detailing to have ductile response during an earthquake are very prevalent in high seismic areas around the world. Seismic rehabilitation of these existing buildings is essential to the resiliency of the society in case of a major ground shaking. The motivation behind this study is the large number of such buildings and the high cost of seismic retrofit; hence, a reliable procedure to identify the most vulnerable buildings and the main contributors to the poor performance of such buildings is of great public interest. This research has identified three dominant deficiencies that can lead to collapse: 1- shear-critical columns, 2- unconfined beam-column joints, and 3- slab-column connections, or deficiencies A, B, and C per Figure 2-47. (NIST GCR 14-917-28, 2013) It then introduces component modeling techniques for existing frame columns, develops system-level collapse criteria, and application of collapse fragility curves to define collapse indicators and distinguish the expected performance of an existing concrete frame building at as-built condition and retrofitted. (Baradaran S., Elwood, & Yang, 2012) (Baradaran S., 2013)

The first objective is to develop a macro model that simulates the lateral load-deformation response of shear-critical concrete columns and may also be vulnerable to axial load failure. To confirm the total lateral load-deformation prediction of the model, the analysis results are compared with test results performed by Sezen and Moehle (2006) as discussed in section 2.2.1.1.

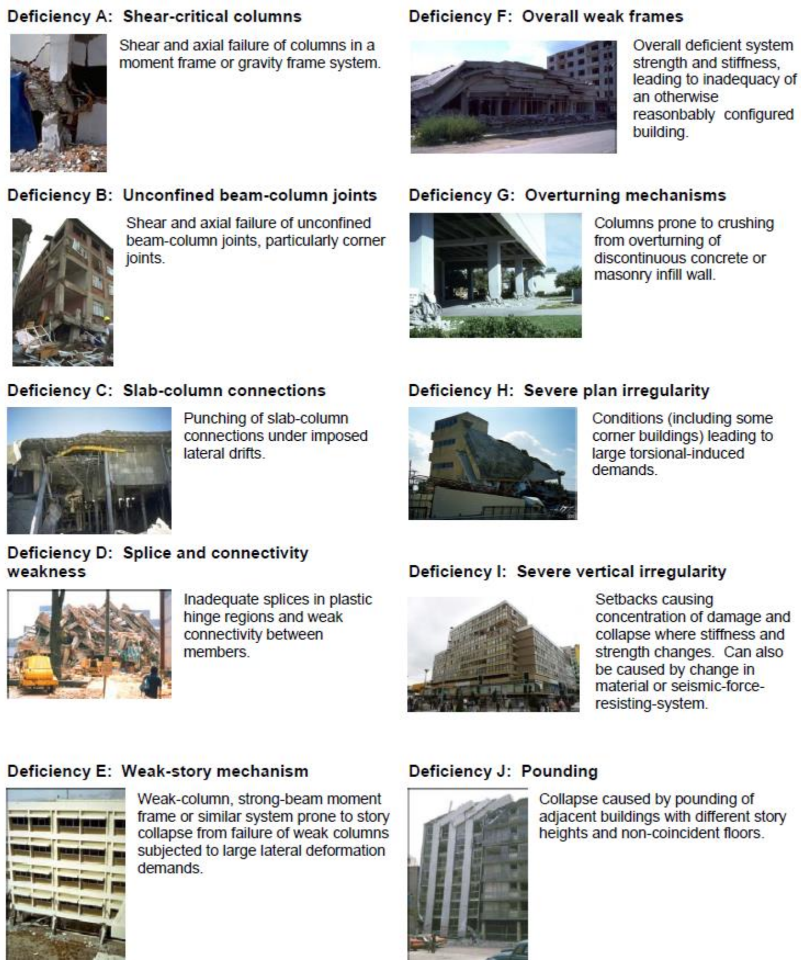

Figure 2-47: Component and System-Level Seismic Deficiencies Found in Pre-1980 Reinforced Concrete Buildings (Based on Moehle, 2007 and NIST, 2010b)

The flexural response of the column is estimated by a moment–curvature analysis using a fiber model using uniaxial stress-strain relationships for both concrete and steel reinforcement as shown in Figure 2-48 (Baradaran S., 2013) (PEER, 2009).

The bar slip was modeled per Sezen and Setzler (2008) and the column rotational deformation due to bar slip is obtained from their model and shown in Figure 2-49. Sezen and Setzler determine moment vs. bar slip rotation relationship based on column geometry, longitudinal and transverse reinforcement ratio and location, material properties, and axial forces.

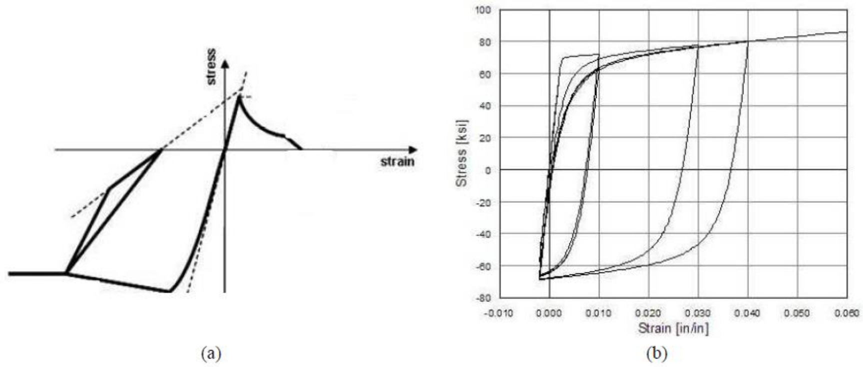

Figure 2-48: Concrete and Steel Material Models (a) Concrete (Non-linear Tension Softening), (b) Steel (Giuffré-Menegotto-Pinto Model with Isotropic Strain Hardening)

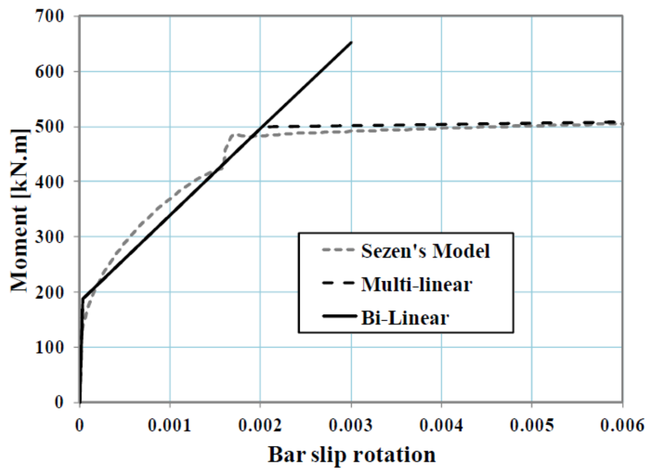

Figure 2-49: Reinforcement Slip Response

The shear response is based on three mechanical models that are attributed to three performance states of a column: pre-peak response, point of shear failure, and post-peak response. To determine shear failure, a step-by-step flow chart procedure is used as illustrated in Figure 2-50. The shear failure modes in the algorithm are the diagonal tension and diagonal compression failure, and they have been implemented in the OpenSees (PEER, 2009) source code and used with the Limit State material model to detect shear failure. (Baradaran S., 2013)

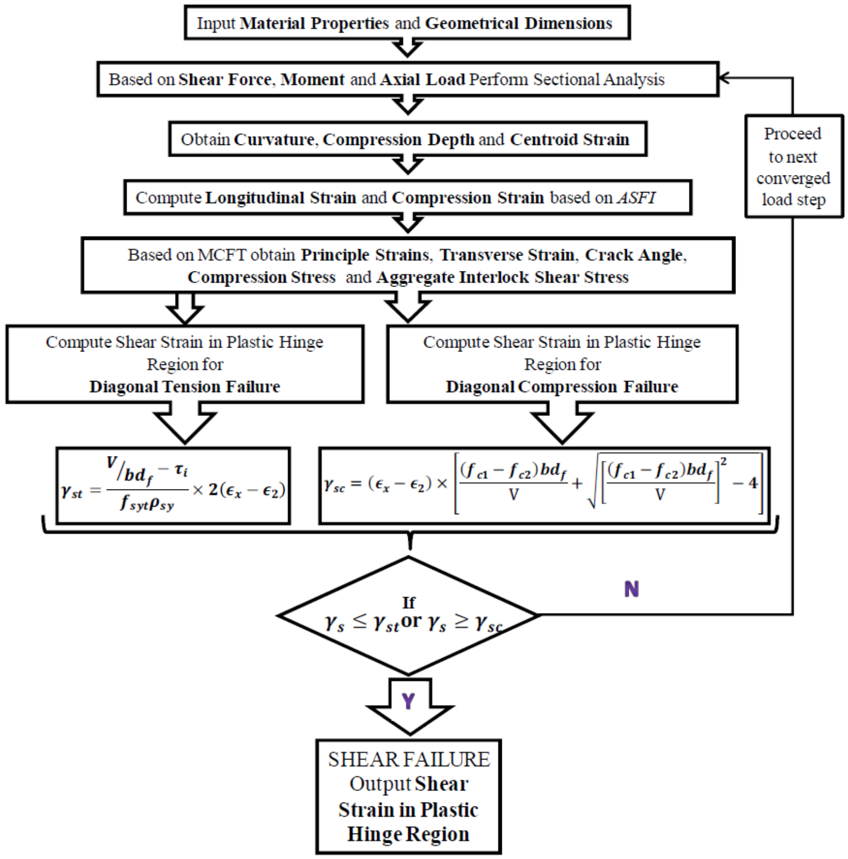

Figure 2-50: Shear Failure Detection Algorithm

The cyclic shear response model proposed is based on the hysteretic uniaxial material presented in OpenSees and captures strength and stiffness degradation with pinching of hysteresis loops. Figure 2-51 illustrates the comparison between the cyclic shear response of the proposed model and experimental results from Sezen's specimen No. 1 (Sezen & Moehle, 2006).

The proposed model adequately captures the collapse in non-ductile moment frames, and the pre-peak response, point of shear failure and post-peak response.

It should be noted that this model has been verified for test data where the columns are subjected to shear and compressive axial forces and have not been verified for cases where the columns undergo shear and tension forces. However, the concept can be applied to the latter loading too.

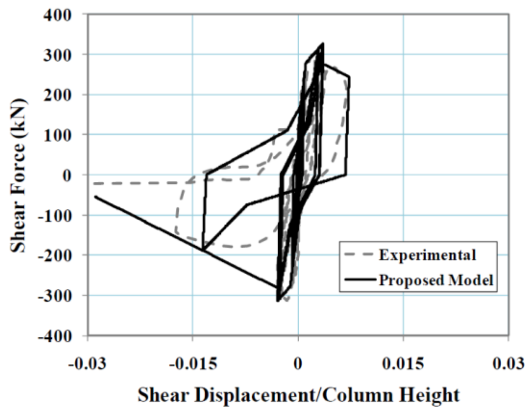

Figure 2-51: Proposed Shear Model Compared with Test Data

The proposed model is based on the mechanics of shear, flexure, and bar slip, and was not calibrated to any experimental testing prior to conducting comparisons between various test data and the model output, two of which are shown in Figure 2-52 and show the model generates results with acceptable agreement to the test data.

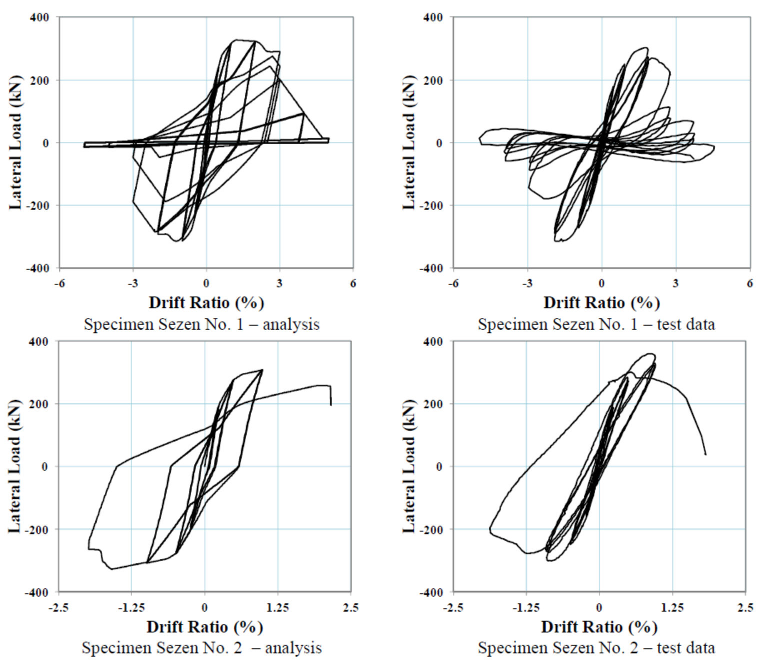

Figure 2-52: Comparisons between the Proposed Model and Experimental Data

The proposed model represents the behavior of the columns at the pre-peak and point of shear failure, before experiencing degradation of lateral load resistance. For columns experiencing diagonal compression failures the model represents the shear degradation reasonably well while it underestimates the rate of shear degradation for columns undergoing diagonal tension failure. This is due to the assumption in the post-peak model that sliding occurs on one principal crack, while multiple cracks are expected in case of diagonal tension failures. The model also has limitations in predicting the cyclic pinching especially for the specimens which experience a diagonal tension failure but generate reasonably close overall failure drift ratios as shown in Figure 2-52.

2.3. Performance-Based Earthquake Design vs Resilience-Based Earthquake Design

2.3.1. Current Practice: Performance-Based Earthquake Design (PBED)

The current performance-based earthquake design practice per ASCE 41-13, and in the case of the Franz Tower, UC seismic rating system (UCSRS), are used to establish the expected seismic performance level of a building as shown in Table 2-15. Per UCSRS all buildings on any UC campus should be rated with performance level IV at a minimum. The objective of these evaluations and performance ratings, and the subsequent improvements to improve the rating, is to reduce the threats to the lives of occupants, and discreetly meeting certain seismic performance ratings as shown below. Table 2-15 provides the definition of seismic performance level ratings mentioned above. The approximate relationship between UC's historic seismic performance rating and current expected seismic performance levels, which are understandable for non-technical audiences, is shown in Table 2-16. (UCP, 2017)

Table 2-15: Definition of Expected Seismic Performance Level Based on CBC

Definitions based upon California Building Code (CBC) requirements for seismic evaluation of buildings using Risk Categories of CBC Table 1604A.5, depending on which applies, and performance criteria in CBC Table 317.5[2]	Expected Seismic Performance Level
A building evaluated as meeting or exceeding the requirements of CBC Part 10 Chapter 3 for Risk Category IV performance criteria with BSE-1N and BSE-2N hazard levels replacing BSE-R and BSE-C as given in Chapter 3.	**I**
A building evaluated as meeting or exceeding the requirements of CBC Part 10 Chapter 3 for Risk Category IV performance criteria.	**II**
A building evaluated as meeting or exceeding the requirements of CBC Part 10 Chapter 3 for Risk Category I-III performance criteria with BSE- 1N and BSE-2N hazard levels replacing BSE-R and BSE-C respectively as given in Chapter 3; alternatively, a building meeting CBC requirements for a new building.	**III**
A building evaluated as meeting or exceeding the requirements of CBC Part 10 Chapter 3 for Risk Category I-III performance criteria.	**IV**
A building evaluated as meeting or exceeding the requirements of CBC Part 10 Chapter 3 for Risk Category I-III performance criteria only if the BSE-R and BSE-C values are reduced to 2/3 of those specified for the site.	**V**
A building evaluated as not meeting the minimum requirements for Level V designation and not requiring a Level VII designation.	**VI**
A building evaluated as posing an immediate life-safety hazard to its occupants under gravity loads. The building should be evacuated and posted as dangerous until remedial actions are taken to assure the building can support CBC prescribed dead and live loads.	**VII**

Table 2-16: Approximate Relationship between UC's Historic Seismic Performance Rating and Current Expected Seismic Performance Levels

Expected Seismic Performance Level[1]	UC's Historic Ratings[5]	Implied Risk to Life[3]	Implied Seismic Damageability[4]
I	Good	Negligible	0% to 10%
II	Good	Insignificant	0% to 15%
III	Good	Slight	5% to 20%
IV	Fair	Small	10% to 30%
V	Poor	Serious	20% to 50%
VI	Very Poor	Severe	40% to 100%
VII	Very Poor	Dangerous	100%

Meeting the life safety or collapse prevention requirements of the governing building codes, reduces the risk to the lives of the building occupants, however, does not assess other aspects that are of extreme importance to the building owners, and are essential to the resiliency of the community to resume normal activity after a major ground shaking. These aspects include but are not limited to the extent of the damage to building components structural and otherwise, cost of repair and/if repair is possible and/or feasible, downtime to address and perform the repair, and the cost associated with that. All these add more dimensions to the one-dimensional PBED with the sole goal of reducing hazard to the life of occupants, and that is how a new generation of PBED, also known as the Resilience-Based Earthquake Design (RBED) was developed.

2.3.2. Next Generation: Resilience-Based Earthquake Design (RBED)

Resilience-based earthquake design was developed by FEMA P-58 through which the performance of a building and the threat to the lives of occupants is assessed in conjunction with the repair cost of the building and time to regain basic function. (Boston & Mitrani-Reiser, 2018)

Various resilience rating systems have been developed by different agencies to assess building performance and resilience to an earthquake. Some of the more prominent rating systems are discussed below.

2.3.2.1 United States Resiliency Council (USCR)

With the goal to become the vehicle to establish and implement a building rating system that is meaningful to non-technical audiences, the United States Resiliency Council (USRC) was established in 2011. The idea originated from the Structural Engineers Association of Northern California (SEAONC) and input obtained from the FEMA-funded *Workshop on a Rating System for the Earthquake Performance of Buildings* and is applicable to all types of buildings when subjected to a major ground shaking. To receive a rating a building needs to be assessed based on methods approved by the USRC, in the three categories: safety, loss, and recovery time. The buildings receive any number from one star which corresponds to low resilience (unsafe, high damage, long recovery time) to five stars which corresponds to high resilience (safe, low damage, fast recovery time) in each category. (USRC, 2020) (Mayes & Reis, 2015) (ATC & FEMA P-58, FEMA P-58, 2012)

Safety (Table 2-17) corresponds to probability of collapse and likelihood of injury or death, and the ability of occupants to safely exit the building. (ATC & FEMA P-58, FEMA P-58, 2012) (Mayes & Reis, 2015)

Table 2-17: USRC Safety Rating

*****	**Injuries and blocking of exit paths unlikely** Expected performance results in conditions that are unlikely to cause injuries or to keep people from exiting the building.
****	**Serious injuries unlikely** Expected performance results in conditions that are unlikely to cause serious injuries.
***	**Loss of life unlikely** Expected performance results in conditions that are unlikely to cause loss of life.
**	**Loss of life possible in isolated locations** Expected performance results in conditions associated with partial collapse or falling objects, which have a potential to cause loss of life at some locations within or around the building.
*	**Loss of life likely in the building** Expected performance results in conditions associated with building collapse, which has a high potential to cause death within or collapse, which has a high potential to cause death within or around the building.

The second category, cost of repair (Table 2-18), includes structural, architectural, mechanical, electrical and, plumbing components of a building, but excludes damage to the contents of a building, cost of business interruption, cost associated with loss of use or occupancy restrictions, damage caused by breakage or leakage of water and/or gas pipes that may occur due to the ground shaking, and typically do not include costs associated with historic preservation or mandatory updates per governing code. (Mayes & Reis, 2015)

Time to regain basic function (Table 2-19) focuses on the repair time to achieve basic function and includes removing major safety hazards and providing sufficient repairs to achieve that, and not getting the building to its intended full function prior to the ground shaking. Other factors not included in this rating are external infrastructure and access to the building, building contents, delays in delivery of material and other items, lack of availability of design professionals and contractors to perform the job, and possible delays at the offices of Building and Safety due to large demand, due to the level of uncertainty in predicting each of these contributors.

Table 2-18: USRC Repair Cost Rating

*****	**Minimal Damage** Repair Cost likely less than 5% of building replacement cost.
****	**Moderate Damage** Repair Cost likely less than 10% of building replacement cost.
***	**Significant Damage** Repair Cost likely less than 20% of building replacement cost.
**	**Substantial Damage** Repair Cost likely less than 40% of building replacement cost.
*	**Severe Damage** Repair Cost likely greater than 40% of building replacement cost.
NE	**Not Evaluated** Repair Cost has not been evaluated.

Table 2-19: USRC: Time to Regain Basic Function Rating

*****	**Within hours to days** Expected performance will likely result in people being able to quickly re-enter and resume use of the building from immediately to a few days, excluding external factors.
****	**Within days to weeks** Expected performance may result in delay of minimum operational use for days to weeks, excluding external factors.
***	**Within weeks to months** Expected performance may result in delay of minimum operational use for weeks to months, excluding external factors.
**	**Within months to a year** Expected performance may result in delay of minimum operational use for months to a year.
*	**More than one year** Expected performance may result in delay of minimum operational use for at least one year or more.
NE	**Not Evaluated** Time to regain basic function has not been evaluated.

It is expected that an average building designed to modern building codes, achieve a safety rating of three to four stars, damage rating of two to three stars, and recovery rating of two to three stars. (USRC, 2020) See Figure 2-53. USRC awards the following designations to buildings that have been evaluated by the USRC and rated as shown in Figure 2-54.

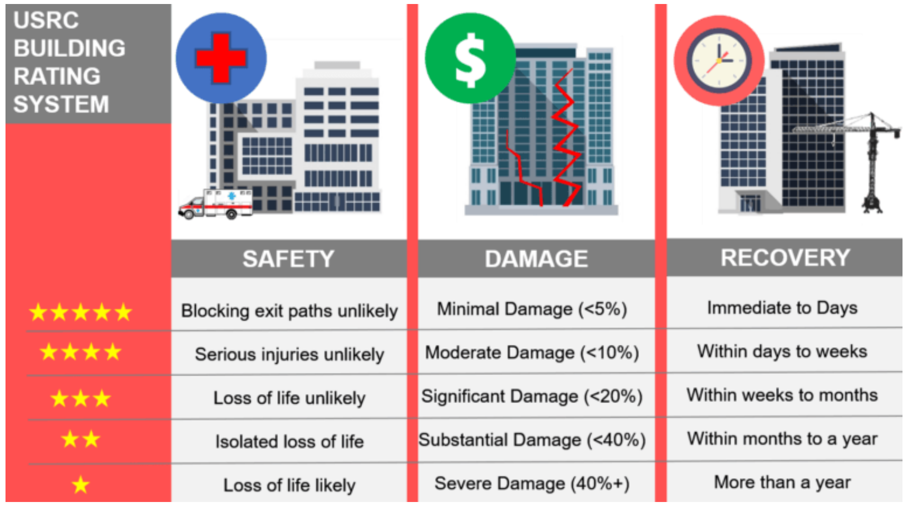

Figure 2-53: USRC Rating System Requirements – Summary

Safety	5 stars	4 stars	3 stars	3 stars
Damage	5 stars	4 stars	3 stars	2 stars
Recovery	5 stars	4 stars	3 stars	2 stars

Figure 2-54: USRC Rating Designations

2.3.2.2 OSHPD Seismic Performance Rating (for Hospitals)

OSHPD Seismic Performance Rating is another rating system that is used for hospitals, and since hospitals are essential buildings, it is prudent to discuss it in this chapter. This rating system consists of two rating categories: Structural Performance Category (SPC) and Non-structural Performance Categories (NPC) as shown in Table 2-20. The performance for each category needs to be determined by professional engineers and approved by the Office of Statewide Health Planning and Development

(OSHPD). (OSHPD, 2001)

The SPC and NPC categories each have five rating levels. A building with SPC1 rating has the highest risk of collapse and damage to the public and with SPC5 rating is expected to resume function after the ground shaking event. The NPC1 rating for the non-structural components means that they are not well anchored or braced. The next NPC categories build up on the previous category and demonstrate how well the non-structural components are secured. (ATC & FEMA P-58, FEMA P-58, 2012)

Table 2-20: OSHPD Structural and Non-Structural Performance Categories

Structural Performance Categories		*Non-structural Performance Categories*	
SPC 1	Building poses significant risk of collapse, danger to the public	NPC 1	Equipment does not meet anchoring or bracing requirements
SPC 2	Compliance with pre-1973 building code. Meets life safety requirements but unlikely to be repairable or functional.	NPC 2	Bracing and anchoring of key systems such as: communication, emergency power, medical gases
SPC 3	Compliance with HSSA prior to 1994. Meets life safety requirements but unlikely to be repairable or functional.	NPC 3	NPC 2 and bracing and anchoring of nonstructural elements in critical care, clinical labs, pharmaceutical, radiology, and sterilization areas.
SPC 4	Compliance with HSSA after 1994, may have structural damage that will hinder hospital services	NPC 4	NPC 3 plus proper anchoring and bracing of all architectural, mechanical, electrical, and medical equipment
SPC 5	Compliance with HSSA after 1994, reasonably capable of providing services after a major event	NPC 5	NCP 4 plus 72 hours of onsite water and holding tanks.

2.3.2.3 Resilience-Based Earthquake Design Initiative (REDi™)

Resilience-Based Earthquake Design Initiative (REDi) is another rating system developed by the research team at the engineering firm Arup, building on the platform of FEMA P-58. REDi provides a comprehensive guideline to ensure new buildings meet expected performance levels and considers factors beyond the USRC. To qualify for a REDi rating, mandatory criteria for two main areas need to be checked: 1- resilient design and planning, which consists of three categories: Organizational Resilience, Building Resilience, and Ambient Resilience, and 2- loss assessment. REDi has a three-tier rating system (platinum, gold, and silver), and certifies buildings based on downtime (re-occupancy and regaining function), direct financial loss, and occupant safety as shown in Figure 2-55 and Table 2-21. (ATC & FEMA P-58, FEMA P-58, 2012) (Almufti & Willford, 2013)

Figure 2-55: REDi Resilience Objectives

Table 2-21: REDi Certification Requirements

Certification	*Downtime*		*Direct Financial Loss*	*Occupant Safety*
	Re-occupancy	*Functional*		
Platinum	Immediate (Green Tag)	< 72 hours	< 1%	Injury is unlikely
Gold	Immediate (Green Tag)	< 1 month	< 5%	Injury is unlikely
Silver	< 6 months (Yellow Tag)	< 6 months	< 10%	Injury is possible but structural collapse is unlikely

2.3.3. Tools for Building Resilience Assessment per FEMA P-58

Looking at a new building built per modern building codes through the lens of FEMA P-58 and resilience-based earthquake design, the code compliant building (meeting safety requirement), may not necessarily be categorized as resilient due to extent of damage or repair cost, and/or downtime. (TWH Press, 2016; ICC, 2017)

Performance Assessment Calculation Tool (PACT) is an electronic calculation tool to provide fragility curves for extent of damage, building loss, and safety. It was developed by the Applied Technology Council (ATC) and funded by the Federal Emergency Management Agency (FEMA) to develop Next-Generation Performance-Based Seismic Design Procedures for New and Existing Buildings and is the original implementer of FEMA P-58. (ATC & FEMA P-58, 2012; Fisher, Stringer, & Horiuchi, 2017)

Repair costs include the required construction to bring the building to its pre-earthquake state and do not include any upgrading of non-conforming components. The repair costs are calculated based on the repair required at each damage state and include all the construction cost associated with performing each particular repair. This includes but is not limited to any and all of the following if necessary: contractor mobilization, removal of debris, protection of the surrounding area and shoring, removal of architectural and/or MEP systems, and cost and transportation of material. It also includes the scale and efficiency in construction when large quantity of the same repair is required. The repaired cost in this methodology does not include escalation of construction cost due to the hazard, securing financial resources to perform the repair. (ATC & FEMA P-58-1, 2018)

The time to regain function of the building vary and depends on many factors including who (owner or tenant) is responsible for the repairs, availability of financial resources, availability of design professionals and contractors, time to prepare the site, procure material, and obtain the permit. Since there are many uncertainties in the above factors, FEMA P-58 time to regain function prediction is limited to the number of labor-hours to perform a repair (actual repair time).

It also considers a factor “maximum worker per square foot” that can be adjusted for the case the building is occupied, as well as the availability of workers in the region. (ATC & FEMA P-58-1, 2018)

Casualties associated with the damage of the building are considered in the methodology. The building gets subjected to a set of ground motions to assess the extent of hazard. Environmental factors are also assessed in this methodology which is beyond the scope of this research.

SP3 (Seismic Performance Prediction Platform) is another tool developed by Haselton-Baker Risk Group. It is an online could-based tool that provides a more streamlined way to implement FEMA P-58 methodology by providing soil and hazard curves, cost estimates, and damage estimates pre-defined in the tool. SP3 cuts the analysis time and simplifies the procedure significantly and is widely used for building assessments in practice. Other capabilities of SP3 include probable maximum loss (PML) calculation, REDi rating, and USRC rating. (SP3, 2021; Fisher, Stringer, & Horiuchi, 2017)

The SP3 analysis relies on tens of thousands of building data and can be performed for a building with as little as five (5) points of input (coordinates, main structural system, year of construction, occupancy type, and number of stories). More level of details can be input for more accurate and building specific results. SP3 assess the building performance after subjecting the building to a suite of ground shakings ranging from 90% probability of exceedance in 50 years (22-year return period) to BSE-2N level and use statistical data to provide fragility curves for cost of repair and time of repair to achieve full functionality.

Chapter 3. Experimental Program

3.1. Building description

The subject building is the Franz Tower as shown in Figure 3-1, a non-ductile concrete moment frame building located on the UCLA campus. The building consists of six levels of closely spaced trapezoidal perimeter columns (fin columns) supported on a deep transfer girder, with two open lower levels supported on wider spaced column grid (Figure 3-2 and Figure 3-3). The lateral force resisting system at the upper six levels consists of a combination of exterior the fin columns, spaced at 4 ft. (1219 mm) on center around the parameter of the building, with trapezoidal beams (ledge beams) spanning between the fin columns, and the interior columns spaced at 20 ft (6096 mm) on center throughout the floor plan in both directions. (See Figure 3-2)

The floor system consists of 18 in. (457 mm) wide by 30 in. (762 mm) deep beams at 20 ft (6096 mm) on center, which align with every fifth fin column at the perimeter of the building, with five joists in between the deeper beams in both directions. The joists are 6 in. (152 mm) wide by 16 in. (406 mm) deep joists at the third level, and 18 in. (457 mm) deep at levels four through eight. The floor system is supported by 26-inch square columns, at 20 ft (6096 mm) on center. (See Figure 3-2)

The lower two levels are supported on 30-inch (762 mm) square exterior columns, and 26-inch (660 mm) square interior columns, spaced at 20 ft (6096 mm) on center throughout the floor plan in both directions and a flat slab floor system with beams also spaced 20 ft (6096 mm) on center in both directions.

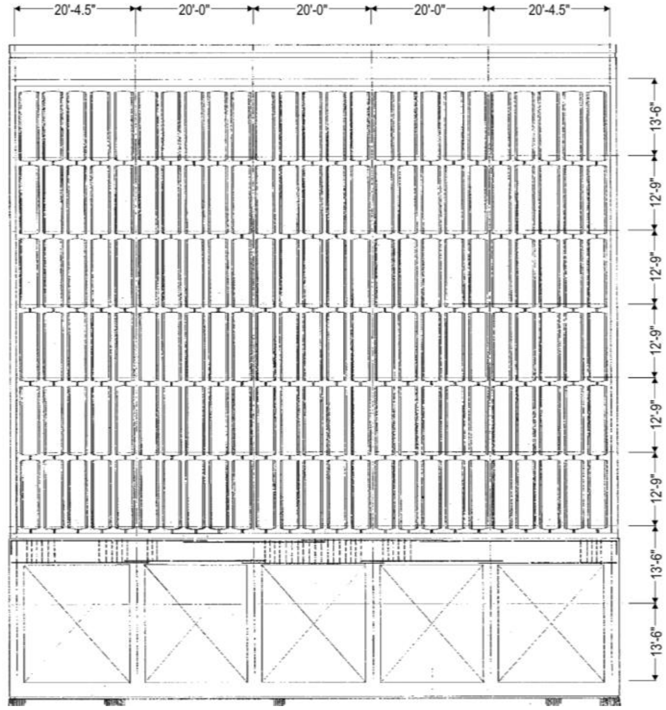

Figure 3-1: UCLA Franz Tower Elevation

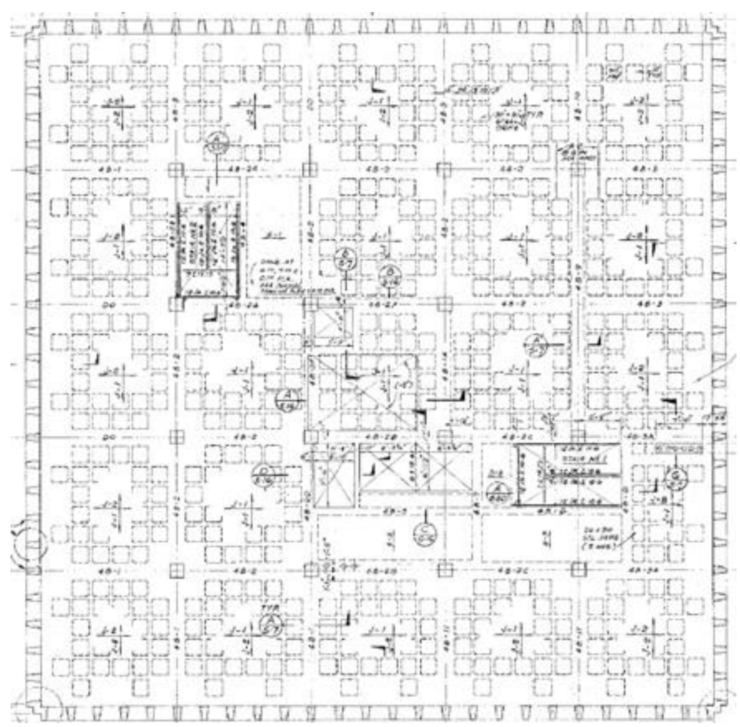

Figure 3-2: UCLA Franz Tower – Typical Floor Plan (Level 3)

The beam-column frame system is symmetrical and repetitive around the perimeter of the building, and due to the layout of the columns, all of the columns will simultaneously be engaged, and contribute to resisting of the lateral forces regardless of the direction of the load. This means that, if the lateral force is applied to the building in the east-west direction, the perimeter columns located on the east and west sides of the building are resisting the applied forces in their in-plane direction, and the perimeter columns located on the north and south sides of the building are resisting the lateral forces in their out-of-plane direction. This further clarifies why the columns need to be evaluated for both in-plane and out-of-plane directions, and hence, the biaxial test program.

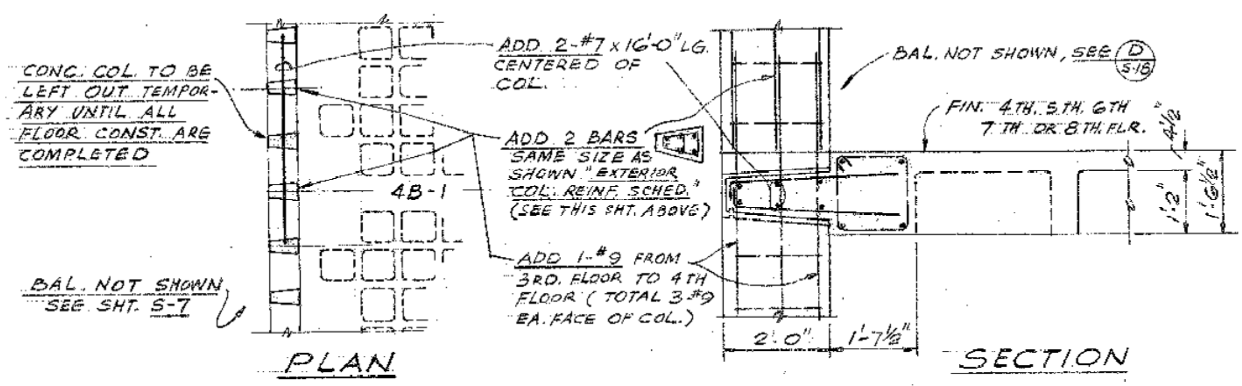

Figure 3-3: UCLA Franz Tower – Typical Section at an Exterior Column

3.2. Design of Test Specimens

Due to the repetitiveness of the perimeter framing, a subassembly module that is representative of the building, was selected to be constructed and tested in the lab. Since a large slab beam frames into every fifth perimeter moment frame column, and this slab beam will impact stiffness and the distribution of demands to the perimeter framing, this slab beam was included in the building subassembly, and since the beam repeats every fifth column, a subassembly with five columns was selected as a module that repeats around the perimeter of the building. (See Figure 3-4) All of the perimeter columns are subjected to concurrent in-plane or out-of-plane loading when the building is subjected to earthquake forces. The behavior of the columns in the in-plane direction is different from their behavior in the out-of-plane direction (flexure-shear controlled vs shear controlled, respectively as shown in Appendix A). Hence it was important to capture and study the out-of-plane behavior of the columns in addition to the in-plane behavior. This also highlights the importance of the biaxial testing which will be discussed in section 3.4.

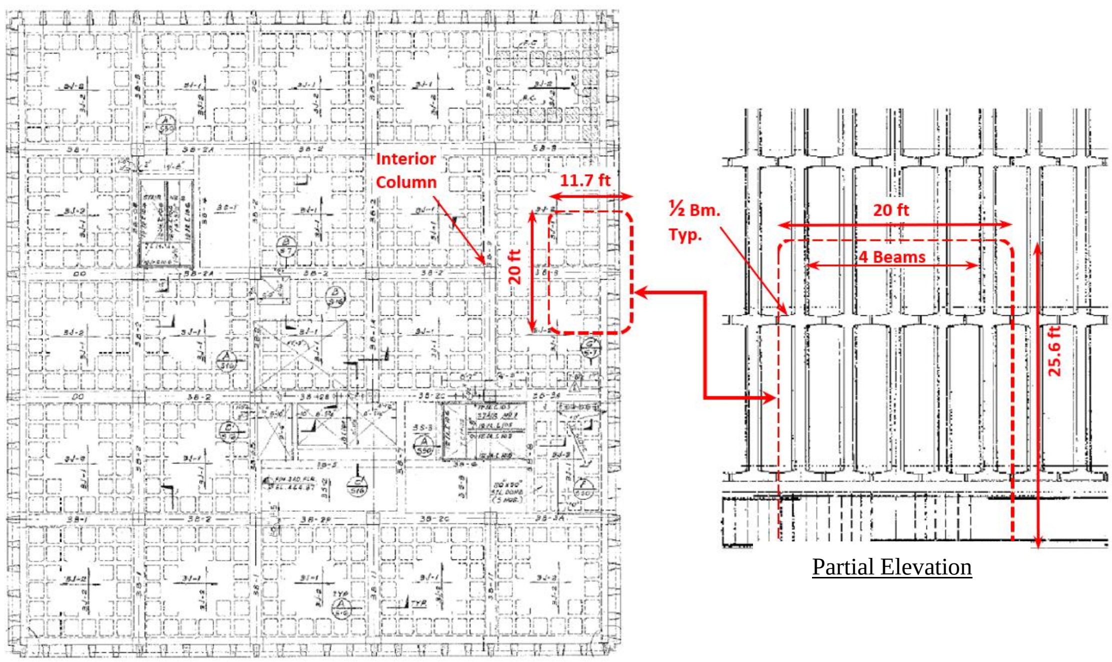

Figure 3-4: UCLA Franz Tower: Typical Floor Plan and Selection of Test Subassembly.

Two, three-dimensional test specimens (denoted as S1 and S2), were constructed and tested. The test specimens were one-bay wide, one and one-half story tall, and consisted of 5 fin columns (level three columns, which were the lowest of the top six levels of the moment frame system, and one-half of level four columns). Four beams spanned between the fin columns, along with one-half span beams at each outer column along the perimeter. One-half of the floor slab system spanning between the perimeter frame and the first interior column was also included in the specimen. The slab system was considered in the test specimen because it included features expected to impact both the in-plane and out-of-plane behavior of the test specimens. The slab was built up to an assumed inflection point halfway between the exterior fin columns and the interior columns (which were not a part of the test specimen) as shown in Figure 3-4. This would cause a reduction in the moment from the slab system at the face of the exterior frame columns due to reduced span length, and lower self-weight of the slab. Also, design live loads were not present. Preliminary calculations determined that the impact of moment at the face of the column due to slab gravity forces, was insignificant and no additional load on the slab was considered to account for lack of presence of live loads, reduced span, and reduced self-weight of the slab. To validate the preliminary calculations, dead weights were added approximately 2 ft. (610 mm) away from the interior face of the columns to produce the same moment at the face of the columns as it would be in the full span slab with live loads (see Figure 3-8, Figure 3-22 and Figure 3-23).

The specimens were subjected to biaxial lateral loading (in-plane and out-of-plane), and axial gravity loading (Figure 3-22). Axial load ratio was approximately $0.07A_g f_c'$, which was applied by two vertical actuators, one at each side of the test specimen.

The two test specimens are two-thirds scale representations of a portion of the building discussed previously and shown in Figure 3-5 and Figure 3-6. Further details about the specimen design, construction plans, and construction details can be found in Appendix C and Appendix D, respectively.

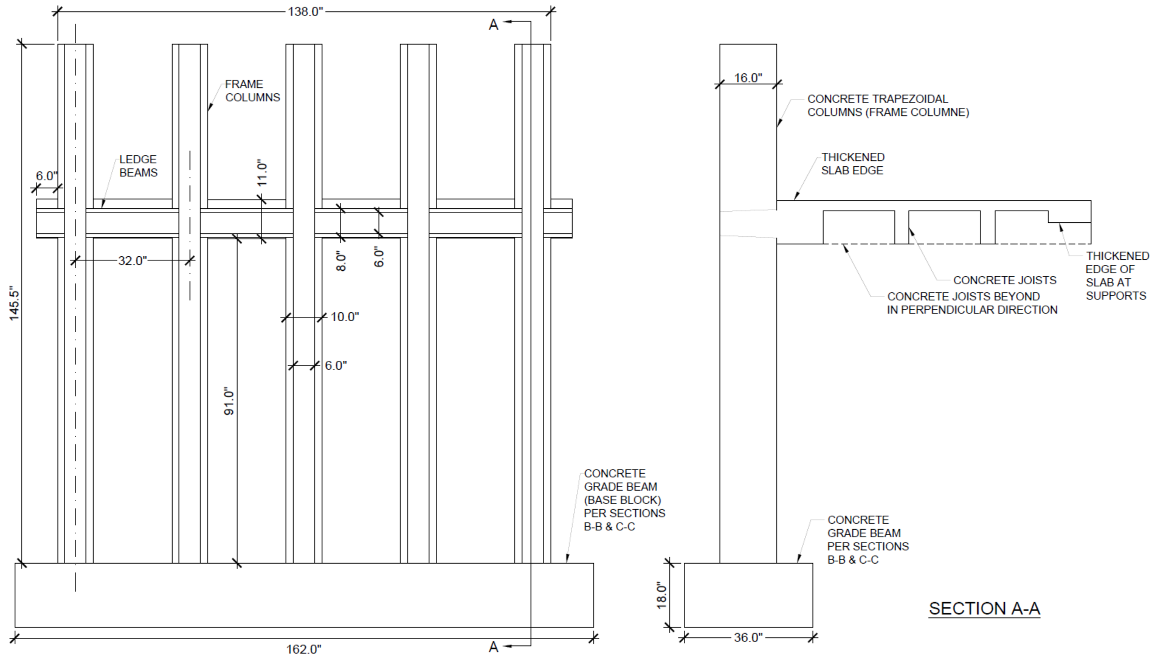

Figure 3-5: Front Elevation of the Test Specimen and Section A-A

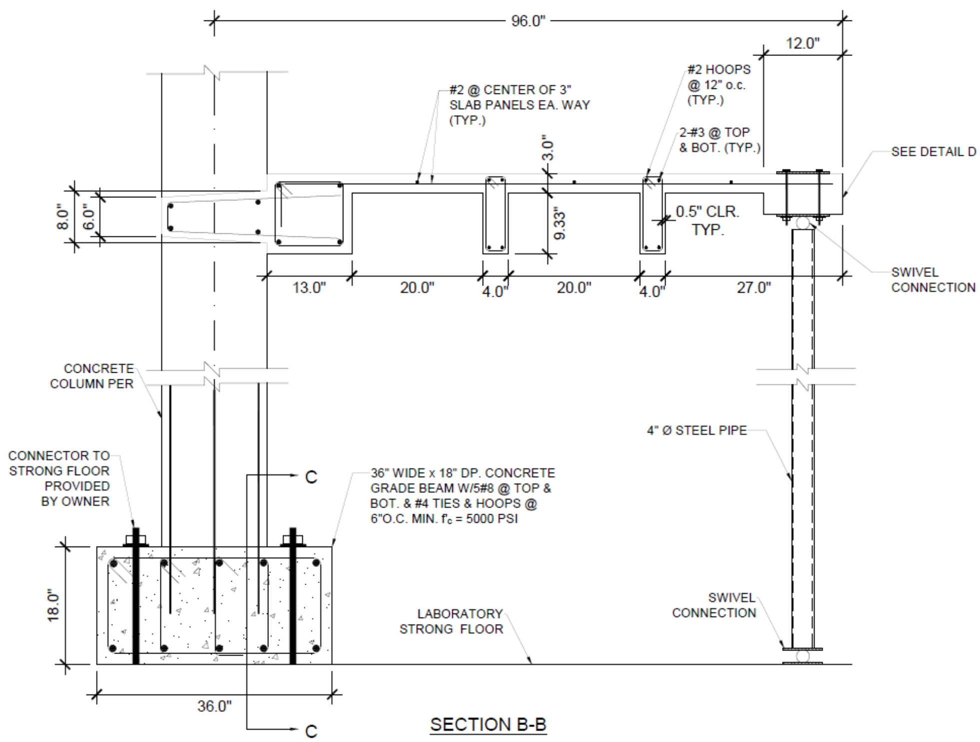

Figure 3-6: Section Through the Specimen (Section B-B)

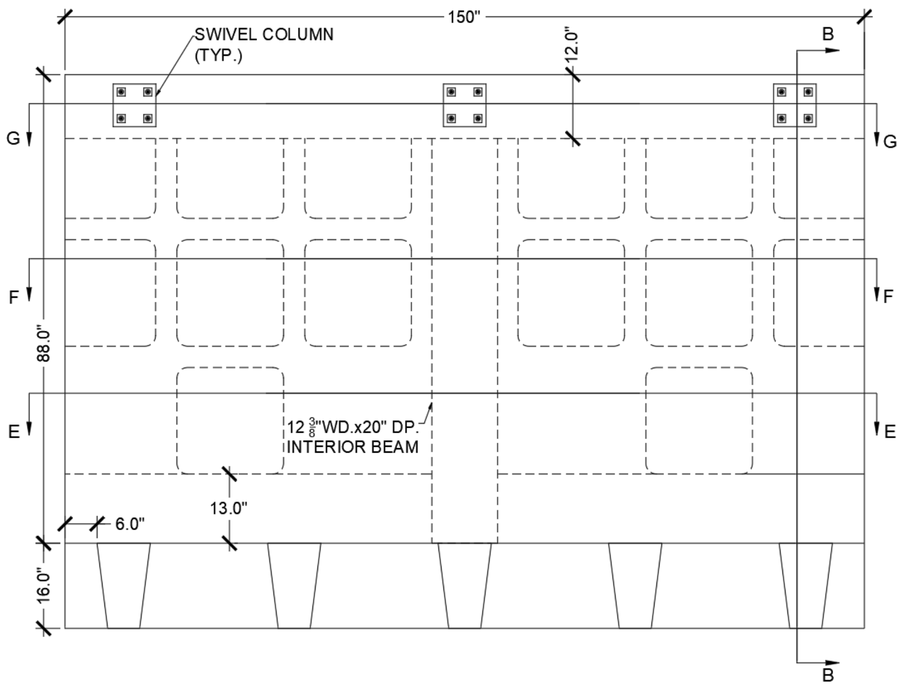

Figure 3-7: Plan View of the Specimen

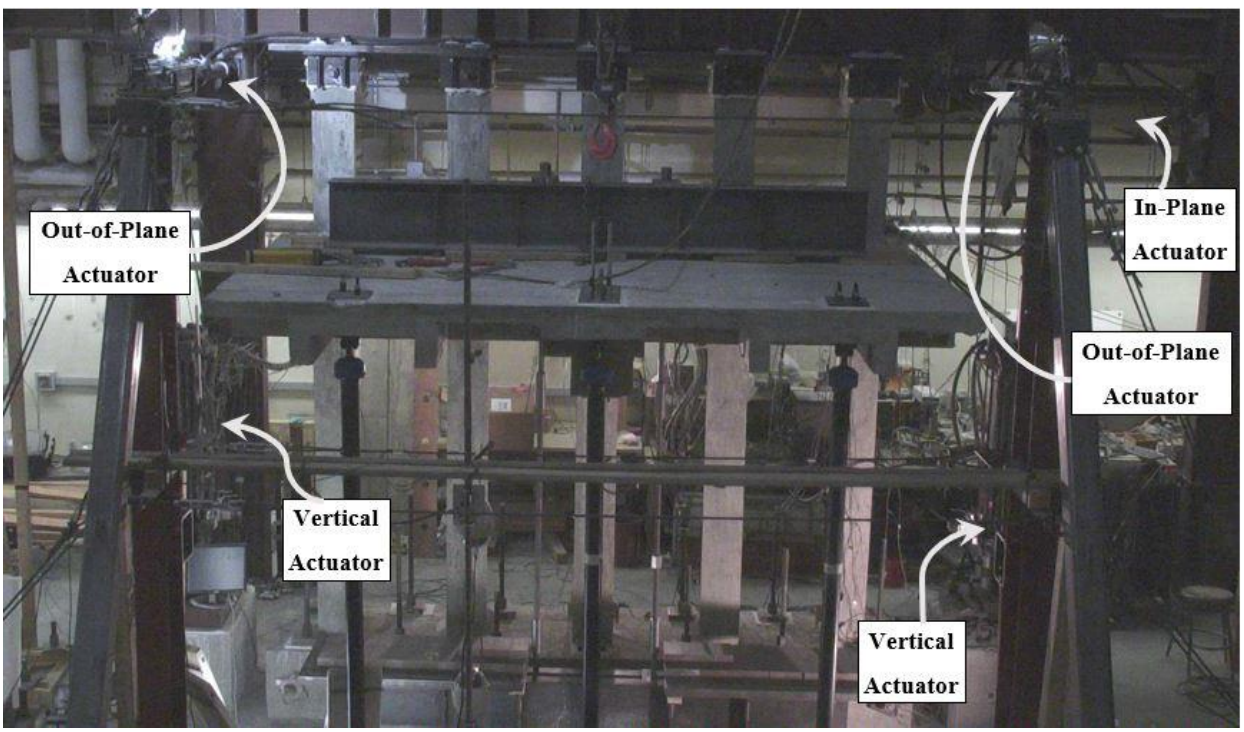

Figure 3-8: View of the Overall Test Specimen

Scaling down is performed such that the test specimen proportions and capacities accurately represent the components of the actual building. In some cases, modest compromises were made to address differences in material strengths or available rebar sizes.

3.2.1. Columns

Based on preliminary calculations (Appendix A), the columns were flexure-shear controlled in the in-plane direction, and shear-controlled in the out-of-plane direction, and the beams were flexure-shear-controlled. The lap lengths provided at the base of the columns were less than the required length per ACI 318-14 section 25.4.2.2, but the expected yield strength of the bars per equation 10-1 of ASCE 41-13 was close to f_y.

Since the performance of the frame depended on the behavior of the frame components, it was critical to scale both the shear and flexural behavior of the columns and beams as accurately as possible. Because the columns are the main contributors to resisting the lateral forces in the out-of-plane direction, scaling the columns such that both their flexural and shear behaviors are closely replicated was extremely important. The cross sections of the building columns and specimen columns are shown in Figure 3-9.

The building columns are trapezoidal shape 9 in. (229 mm) to 15 in. (381 mm) wide by 24 in. (610 mm) deep with six (6) No. 9 (29 mm) longitudinal bars and No. 3 (10 mm) hoop and ties at 12 in. (305 mm) on center. The hoops and ties had 135-degree bends.

Given the available bar sizes to use for the vertical reinforcement of the columns, and the results of material testing for the yield strength of the reinforcement bars, adjustments are made to provide a test specimen that accurately represents the expected building performance. Vertical No. 9 (29 mm) bars used in the building, translate to No. 6 (19 mm) vertical bars in a two-thirds scale specimen. However, only No. 6 (19 mm) bars with nominal yield strength of 60 ksi were available, instead of 40 ksi. In order to achieve the flexural performance in the specimen columns that are representative of the flexural performance of the columns in the building, the $A_{sL}.f_{yL}$ value needed to be scaled accurately. With the increased yield strength of the bars, a smaller bar size was used: No. 5 (16 mm) bars instead of No. 6 (19 mm). As shown in Table 3-1, this modification helped achieve $A_{sL}.f_{yL}$ value in the specimens that is 99% of the target value for $A_{sL}.f_{yL}$ in a two-thirds scale specimen.

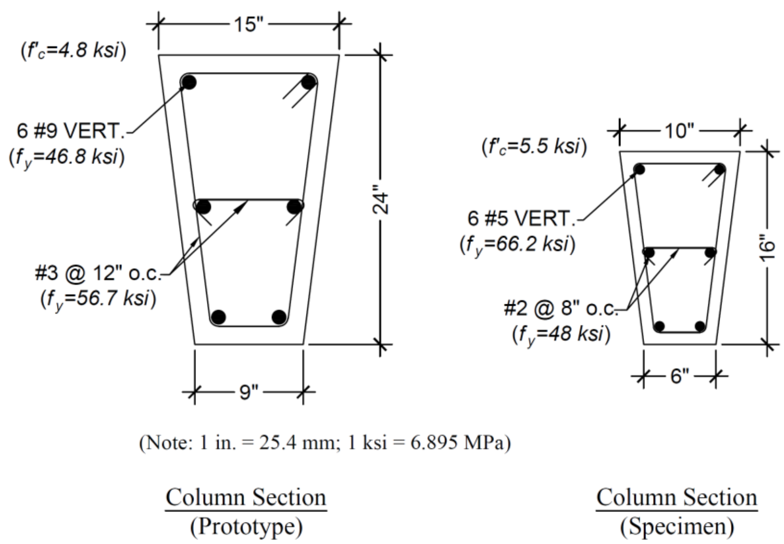

Figure 3-9: Frame columns: Franz Tower vs Test Specimen

Another value that impacts the flexural behavior of the columns is the s/d_{bL} ratio, which is commonly used as a measure of resistance to rebar buckling. Using tie spacing (s) of 8 in. (203 mm) on center, (which is the two-thirds scale of 12 in. (305 mm) on center in the building), the s/d_{bL} ratio would be 1.2 times larger than this ratio in the building. This is due to the reduced bar diameter, d_{bL}, (No. 5 (16 mm) bars instead of No. 6 (19 mm) bars) to achieve the target $A_{sL}.f_{yL}$ value. Larger s/d_{bL} ratio means the vertical bars in the specimen columns would be more susceptible to buckling under flexural loading than the vertical bars in the building columns. To mitigate this, s is reduced to 6.75 in. (171 mm) on center to achieve the desired s/d_{bL} ratio in the specimen that is almost equal to this ratio in the building (1.01 times).

Table 3-1: Sizing Columns

Element	Component	Unit	Full Scale (1)	Required (0.67-scale) (2)	Actual (0.67-scale) (3)	Actual Value (4) = (3)/(1)	Target Value (5)	Ratio (6) = (5)/(4)
Column	$b_{(min)}$	Inch	9.00	6.00	6.00	0.67	0.67	**1.00**
	$b_{(max)}$	Inch	15.0	10.0	10.0	0.67	0.67	**1.00**
	$b_{(average)}$	Inch	12.0	8.00	8.00	0.67	0.67	**1.00**
	h	Inch	24.0	16.0	16.0	0.67	0.67	**1.00**
	Cover to CL of Long. Bar	Inch	2.94	1.96	1.90	0.65	0.67	**0.97**
	$d_{bar,L\ (\#9:\#5)}$	Inch	1.127	0.75	0.625	0.55	0.67	**0.83**
	$A_{bar,L\ (\#9:\#5)}$	$Inch^2$	1.00	0.444	0.310	0.31	0.44	**0.70**
	Number of Bars	-	6	6	6	1.00	1.00	**1.00**
	$A_{Total,L}$	$Inch^2$	6.00	2.67	1.86	0.31	0.44	**0.70**
	$A_{Total,L}/(b_{ave}h)$	-	0.021	0.021	0.015	0.70	1.00	**0.70**
	$f_{y,L\ (\#9:\#5)}$	ksi	46.8	46.8	66.2	1.41	1.00	**1.41**
	$A_L.f_{y,L}$	kips	280.8	124.8	123.1	0.44	0.44	**0.99**
	$d_{bar,T\ (\#3:\#2)}$	Inch	0.375	0.250	1/4	0.67	0.67	**1.00**
	$A_{T\ (\#3:\#2)}$	$Inch^2$	0.11	0.049	0.049	0.45	0.44	**1.00**
	$f_{y,T}$	ksi	56.7	56.7	48.0	0.85	1.00	**0.85**
	$A_T.f_{y,T}/s$	kips	0.520	0.347	0.349	0.67	0.67	**1.01**
	s	Inch	12.00	8.00	6.75	0.56	0.67	**0.84**
	$s / b_{(ave)}$	-	1.000	1.000	0.844	0.84	1.00	**0.84**
	s/d_b	-	10.6	10.6	10.8	1.01	1.00	**1.01**
	f'_c	ksi	4.81	4.81	5.50	1.14	1.00	**1.14**
	$\sqrt{f'_c}$	psi	69.4	69.4	74.2	1.07	1.00	**1.07**

In order to capture the shear behavior of the columns, the goal was to scale the value of $A_{sT}f_{yT}/s$, which is an indicator of shear strength and behavior, as closely as possible. With the reduced tie spacing and use of No. 2 (6 mm) bars that have slightly lower yield strength than the No. 3 (10 mm) bars in the building, this ratio is scaled to 1.01 times of its target value.

Lastly, compressive strength of the concrete, f_c', is another factor that contributes to the capacity of the columns. Due to limitations in the material available, especially lightweight gravel with the desired size of less than 3/8" (9.5 mm), and lack of certainty in strength gain of concrete over time (between placement and testing), achieving the target value for f_c' is challenging. From various concrete mixes and test data, the closest one to provide the desirable strength at 28 days was chosen. Given the lack of control to achieve the exact compressive strength, the achieved ratio of 1.07 times the target value of square root of f_c' was deemed acceptable.

3.2.2. Beam/Thickened Slab Assembly

The trapezoidal ledge beams between the columns are 24 in. (610 mm) wide and 9 in. (229 mm) to 12 in. (305 mm) deep with four (4) No. 8 (25 mm) longitudinal bars. The ledge beams are anchored to a thickened slab edge with No. 4 (13 mm) bars spaced at 12 inches (305 mm) on center, as shown in Figure 3-10, providing shear transfer between the two sections. As a result, the two were considered the *beam assembly*. The thickened slab is almost a square section, 19 ½ in. wide by 18 ½ in. deep, with four (4) No. 8 (25 mm) longitudinal bars and No. 3 (10 mm) hoops at 12 inches (305 mm) on center with 135-degree bends.

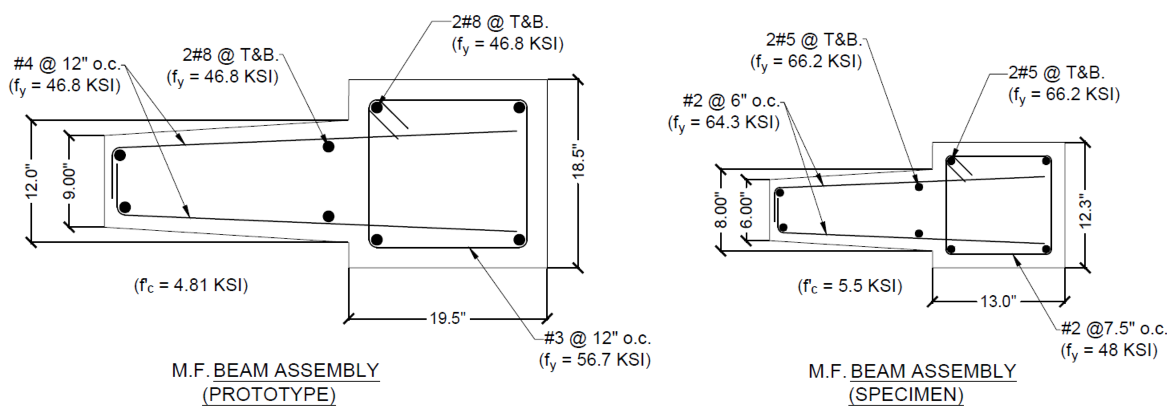

Figure 3-10: Frame Beam/Thickened Slab: Franz Tower vs Test Specimen

The beam assembly was shear-controlled in the in-plane direction; therefore, scaling the $A_{st}F_{yt}d/s$ ratio, as a measure of the shear capacity and performance of the beam assembly, as closely as possible to the target ratio was critical. This was done separately for the ledge beam and the thickened slab edge as shown in Table 3-2 and Table 3-3.

Table 3-2: Sizing Ledge Beam

Element	Component	Unit	Full Scale (1)	Required (0.67-scale) (2)	Actual (0.67-scale) (3)	Actual Value (4) = (3)/(1)	Target Value (5)	Ratio (6) = (5)/(4)
Trapezoidal Ledge Beam	b	Inch	24.0	16.0	16.0	0.67	0.67	**1.00**
	h_{short}	Inch	9.00	6.00	6.00	0.67	0.67	**1.00**
	h_{long}	Inch	12.0	8.00	8.00	0.67	0.67	**1.00**
	$h_{average}$	Inch	10.5	7.00	7.00	0.67	0.67	**1.00**
	Cover to CL of Long. Bar	Inch	1.625	1.08	1.125	0.69	0.67	**1.04**
	$d_{bar,L\ (\#8:\#5\&\#4)}$	Inch	1.00	0.67	0.56	0.56	0.67	**0.84**
	$A_{bar,L\ (\#8:\#5\&\#4)}$	$Inch^2$	0.79	0.35	0.25	0.32	0.44	**0.71**
	Number of Bars	-	4	4	4	1.00	1.00	**1.00**
	$A_{Total,L\ (\#8:\#5\&\#4)}$	$Inch^2$	3.16	1.40	1.00	0.32	0.44	**0.71**
	$A_{Total,L\ (\#8:\#5\&\#4)}/(bh_{ave})$	-	0.013	0.013	0.009	0.71	1.00	**0.71**
	$f_{y,L}$	ksi	46.8	46.8	66.2	1.41	1.00	**1.41**
	$A_L.f_{y,L}$	kips	147.9	65.7	60.2	0.41	0.44	**0.92**
	$d_{bar,T(\#4:\#2)}$	Inch	0.50	0.33	0.25	0.50	0.67	**0.75**
	$A_{bar,T(\#4:\#2)}$	$Inch^2$	0.20	0.09	0.05	0.25	0.44	**0.55**
	$f_{y,T(\#4:\#2)}$	ksi	46.8	46.8	64.3	1.37	1.00	**1.37**
	$A_T.f_{y,T}/s_{\ (\#4:\#2)}$	kips	0.78	0.52	0.53	0.67	0.67	**1.01**
	s	Inch	12.0	8.00	6.00	0.50	0.67	**0.75**
	s / h_{ave}	-	1.14	1.14	0.86	0.75	1.00	**0.75**
	$s / d_{b\ (\#8)}$	-	12.0	12.0	10.7	0.89	1.00	**0.89**
	f'_c	ksi	4.81	4.81	5.50	1.14	1.00	**1.14**
	$\sqrt{f'_c}$	psi	69.4	69.4	74.2	1.07	1.00	**1.07**

The tie between the two sections of the beam assembly is by No. 4 (13 mm) bars at 12 inches (305 mm) on center. To scale the No. 4 (13 mm) ties with cross sectional area of 0.20 in^2 (129 mm^2) to two-thirds scale, the required cross-sectional area would be 0.087 in^2 (58 mm^2), which is between the cross-sectional area of No. 3 (10 mm) bars, 0.11 in^2 (71 mm^2), and No. 2 (6 mm) bars, 0.05 in^2 (30 mm^2). The bar chosen was No. 2 (6 mm) with higher yield strength so what it lacked in cross sectional area, it made up for in yield strength. In order to uniformly space the cross ties along the length of the trapezoidal beam, the tie spacing was dictated by the beam span and they were spaced at 6 inches (152 mm) on center (Figure 3-10). All the above factors combined, the $A_{st}F_{yt}d/s$ ratio achieved in the test specimen is almost equal to the target ratio.

Table 3-3: Sizing Thickened Slab

Element	Component	Unit	Full Scale (1)	Required (0.67-scale) (2)	Actual (0.67-scale) (3)	Actual Value (4) = (3)/(1)	Target Value (5)	Ratio (6) = (5)/(4)
Thickened Slab	b	Inch	19.5	13.0	13.0	0.67	0.67	**1.00**
	h	Inch	16.5	11.0	11.0	0.67	0.67	**1.00**
	Cover to CL of Long. Bar	Inch	1.625	1.08	1.13	0.69	0.67	**1.04**
	$d_{bar,L\ (\#8:\#5)}$	Inch	1.00	0.67	0.625	0.63	0.67	**0.94**
	$A_{bar,L\ (\#8:\#5)}$	$Inch^2$	0.79	0.35	0.31	0.39	0.44	**0.88**
	Number of Bars	-	4	4	4	1.00	1.00	**1.00**
	$A_{Total,L\ (\#8:\#5)}$	$Inch^2$	3.16	1.40	1.24	0.39	0.44	**0.88**
	$A_{Total,L\ (\#8:\#5)}/bh$	-	0.010	0.010	0.009	0.88	1.00	**0.88**
	$f_{y,L}$	ksi	46.8	46.8	66.2	1.41	1.00	**1.41**
	$A_{Total,L}.f_{y,L(\#5)}$	kips	147.9	65.7	82.1	0.56	0.44	**1.25**
	$d_{Tie\ (\#3:\#2)}$	Inch	0.375	0.25	0.25	0.67	0.67	**1.00**
	$A_{T\ (\#3:\#2)}$	$Inch^2$	0.11	0.05	0.05	0.45	0.44	**1.00**
	$A_T.f_{y,T}/s$	kips	0.477	0.318	0.314	0.66	0.67	**0.99**
	$f_{y,T}$	ksi	52.0	52.0	48.0	0.92	1.00	**0.92**
	s	Inch	12.0	8.00	7.50	0.63	0.67	**0.94**
	s / h	-	0.73	0.73	0.68	0.94	1.00	**0.94**
	s/d_b	-	12.0	12.0	12.0	1.00	1.00	**1.00**
	f'_c	ksi	4.81	4.81	5.50	1.14	1.00	**1.14**
	$\sqrt{f'_c}$	psi	69.4	69.4	74.2	1.07	1.00	**1.07**

The reduced tie spacing, reduced the s/d_{bL} ratio in the specimen to be 89% of this ratio in the building. Since the reduced s/d_{bL} ratio mainly enhanced the flexural performance of the section, which in this case was not the governing mode of failure, and given lack of alternatives, the design was considered acceptable. The ledge beam was shear-controlled by a factor of two, therefore the lower value achieved for the $A_{sL}.f_{yL}$ ratio in the specimen did not change its mode of failure and therefore was deemed acceptable.

The tie spacing in the thickened slab was adjusted to be 7.5 in. (191 mm), instead of 8 in. (203 mm) in the specimen, to achieve the desired $A_{st}F_{yt}d/s$ ratio as well as the s/d_{bL} ratio. While the

$A_{sL}.f_{yL}$ value achieved was 25% higher than the target value, since the performance of the thickened slab was governed by shear, this increased flexural capacity did not impact the behavior of the section.

It should be noted that the boundary conditions are different at the ledge beams and the thickened slab, as the ledge beams frame between the columns and the thickened slab is off-center from the column centerline. This added to the complexity and ambiguity of what constitutes a beam in this assembly, and one of the reasons that justified conducting a test to determine the performance of the frame.

3.2.3. Slab Joists and Interior Beam

The slab system is waffle-slab consisted of 6 in. (152 mm) wide by 14 in. (356 mm) deep joists at levels 4 to 7, and 6 in. (152 mm) wide by 12 in. (305 mm) deep joists at levels 3 and 8, spaced at 3 ft. (914 mm) on center, with interior deep beams, 18 ½ in. (470 mm) wide by 30 in. (762 mm), spaced at 20 ft. (6096 mm) on center, as shown in Figure 3-11 and Figure 3-12.

These beams are repetitive supporting the slab system and are supported on the interior columns spaced at 20 ft. (6096 mm) on center. They are also similar in terms of size and vary slightly in terms of longitudinal reinforcement. The reinforcement pattern chosen as shown in Figure 3-11 is typical to the beams that connect to the exterior frame.

The beam had four (4) No. 10 (32 mm) bars at the bottom and two (2) No. 9 (29 mm) bars at the top corners in addition to two (2) No. 10 (32 mm) bars in between. The No. 9 (29 mm) corner bars at the top, and the No. 10 (32 mm) corner bars at the bottom were anchored in the exterior column with a standard hook. The rest of the bars stopped at the face of the column, as shown in Figure 3-12. No. 3 (10 mm) ties with 135-degree hooks are provided at 12 in. (305 mm) on center as transverse reinforcement.

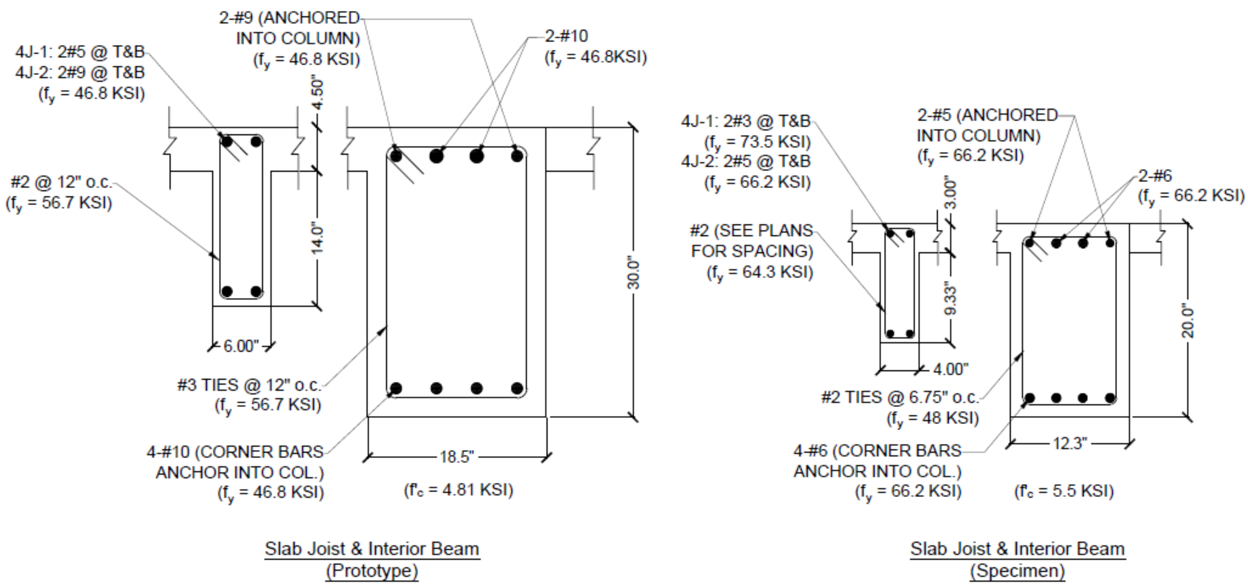

Figure 3-11: Slab Joist and Interior Beam: Franz Tower vs Test Specimen

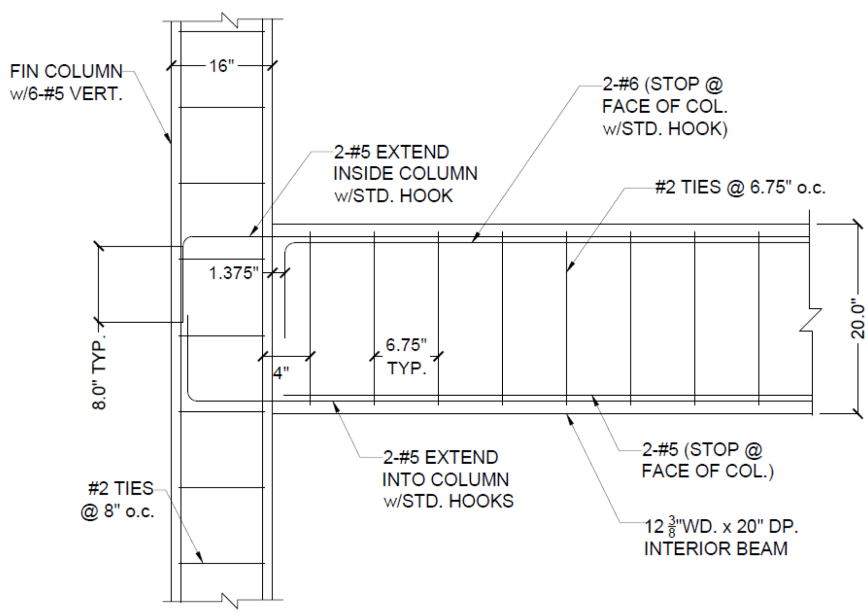

Figure 3-12: Interior Beam at Face of Fin Column (Specimen)

Table 3-4: Interior Beam Sizing

Element	Component	Unit	Full Scale (1)	Required (0.67-scale) (2)	Actual (0.67-scale) (3)	Actual Value (4) = (3)/(1)	Target Value (5)	Ratio (6) = (5)/(4)
Interior Slab Beam	b	Inch	18.5	12.3	12.3	0.66	0.67	**1.00**
	h	Inch	30.0	20.0	20.0	0.67	0.67	**1.00**
	Cover to CL of Long. Bar	Inch	2.94	1.96	2.00	0.68	0.67	**1.02**
	$d_{bar,L,top\ (\#10:\#6)\ @\ face\ of\ col.}$	Inch	1.27	0.85	0.75	0.59	0.67	**0.89**
	$d_{bar,L,top\ (\#9:\#5)\ anchored}$	Inch	1.128	0.75	0.625	0.55	0.67	**0.83**
	$d_{bar,L,bot\ (\#10:\#6)\ anchored}$	Inch	1.27	0.85	0.44	0.35	0.44	**0.79**
	$d_{bar,T\ (\#3:\#2)}$	Inch	0.375	0.25	0.25	0.67	0.67	**1.00**
	$A_{bar,L,top\ (\#10:\#6)\ @\ F.O.C.}$	$Inch^2$	1.27	0.56	0.44	0.35	0.44	**0.78**
	$A_{bar,L,top\ (\#9:\#5)\ anchored}$	$Inch^2$	1.00	0.44	0.31	0.31	0.44	**0.70**
	$A_{bar,L,bot}$	$Inch^2$	1.27	0.56	0.44	0.35	0.44	**0.78**
	$A_{bar,T\ (\#3:\#2)}$	$Inch^2$	0.11	0.05	0.05	0.45	0.44	**1.00**
	No. of Top Bars F.O.C.	-	2	2	2	1.00	1.00	**1.00**
	No. of Top Bars Anchored	-	2	2	2	1.00	1.00	**1.00**
	Number of Bot Bars	-	4	4	4	1.00	1.00	**1.00**
	$A_{L,Top\ (2\#10:2\#6)}$	$Inch^2$	2.54	1.13	0.88	0.35	0.44	**0.78**
	$A_{L,Top\ (2\#9:2\#5)}$	$Inch^2$	2.00	0.89	0.62	0.31	0.44	**0.70**
	$A_{Total,L,Top}/(bh)$	-	0.008	0.008	0.006	0.75	1.00	**0.75**
	$A_{Total,L,Bot}$	$Inch^2$	5.08	2.26	1.76	0.35	0.44	**0.78**
	$A_{Total,L,Bot}/(bh)$	$Inch^2$	0.009	0.009	0.007	0.78	1.00	**0.78**
	$A_{L,top}.f_{y,L}$	kips	212.5	94.4	99.3	0.47	0.44	**1.05**
	$A_{L,bot}.f_{y,L}$	kips	237.7	105.7	116.5	0.49	0.44	**1.10**
	$f_{y,L(\#9)}$	ksi	46.8	46.8	66.2	1.41	1.00	**1.41**
	$f_{y,L(\#10)}$	ksi	46.8	46.8	66.2	1.41	1.00	**1.41**
	$d_{Tie\ (\#3:\#2)}$	Inch	0.375	0.25	0.25	0.67	0.67	**1.00**
	$A_{T\ (\#3:\#2)}$	$Inch^2$	0.11	0.05	0.05	0.45	0.44	**1.00**
	$A_T.f_{y,T}/s$	kips	0.5	0.3	0.3	0.73	0.67	**1.10**
	$f_{y,T}$	ksi	52.0	52.0	48.0	0.92	1.00	**0.92**
	s	Inch	12.0	8.00	6.75	0.56	0.67	**0.84**
	$s\ /d_{b\ (\#9)}$	-	10.6	10.6	10.8	1.02	1.00	**1.02**
	$s\ /d_{b\ (\#10)}$	-	9.45	9.45	9.00	0.95	1.00	**0.95**
	f'_c	ksi	4.81	4.81	5.50	1.14	1.00	**1.14**
	$\sqrt{f'_c}$	ksi	69.4	69.4	74.2	1.07	1.00	**1.07**

The beam was flexure-controlled both in negative and positive directions and exerted demands on the middle column of the test specimen in the out-of-plane direction. The shear demand to the shear capacity ratio was about 2 in both the negative and positive directions. Hence, the goal was to achieve $A_{sL}.f_{yL}$ value similar to that of the Franz Tower.

No. 6 (19 mm) bars were used at the top, and a combination of No. 5 (16 mm) bars (to anchor into the column) and No. 6 (19 mm) bars (to stop at the face of the column) were used with yield strength of 66.2 ksi (456 MPa) at the bottom. This resulted in $A_{sL}.f_{yL}$ value in the test specimen to be 1.05 times larger than its desired value at the top bars (negative direction bending), and 1.10 times the desired value at the bottom bars (positive direction bending) as shown in Table 3-4, which were deemed acceptable. Given that the shear capacity was approximately twice the shear demand, the slight increase in flexural capacity of the beam did not change its mode of failure.

In the building, the joists parallel to the frame (4J-1) have two No. 5 (16 mm) bars at the top and bottom, and the joists perpendicular to the frame (4J-2) have two No. 9 (29 mm) bars at the top and bottom. Both 4J-1 and 4J -2 have No. 2 (6 mm) ties with 135-degree bend at 12 in. (305 mm) on center (Appendix A).

The joists parallel to the frame (4J-1), did not have a significant contribution in the performance of the frame when subjected to seismic loading. As a result, the tie spacing at those joists was such to accommodate the geometry. Details of the slab reinforcement layout are provided in Appendix C

3.3. Material Properties

Material testing performed on the existing building included compressive strength test and tensile strength test for concrete samples obtained from interior and exterior beams and columns, and reinforcing bar yield and ultimate strength tests, as shown in Table 3-5 and Table 3-6. The bars collected from the building, and tested, were No. 3 (10 mm) bars used as transverse reinforcement in the beams and columns. Since collecting samples from the column longitudinal reinforcement involved larger samples which impacted the integrity and load bearing capacity of the columns, the engineer of record decided against collecting samples of column or beam longitudinal bars for material testing. The expected material strengths used for building component modeling in Perform-3D for NSP and NDP are obtained from the material testing results below. Where test results were not available, provisions of ASCE 41-13 were used. Details of the material test results are presented in Appendix B.

3.3.1. Concrete

Lightweight concrete, with specified unit weight of maximum 110 pcf (17.3 kN/m^3) and mean test value of 107 pcf (16.8 kN/m^3), was used for the perimeter frames in Franz Tower with destructive material testing results for the concrete compressive strength. If the specified design strength of the concrete is known, section 10.2.2.4 of ASCE 41-13 requires at least one core to be taken from samples of each different concrete strength used in the construction of the building with a minimum of three cores taken for the entire building. Concrete core samples were obtained from interior and exterior beams and columns and slabs. Material testing performed on the existing building consisted of four-inch diameter cores from the interior beams (total of six), interior columns (total of seven), exterior columns (total of five), and three-inch diameter cores from the waffle slab system (total of six). See Table 3-5 and Figure 3-13.

Section 7.5.1.4 of ASCE 41-13 allows using the mean value of tested material properties as expected material properties. The test results were separated for the perimeter moment frame (exterior system) and the interior slab-beam-column (interior system). Measured concrete compressive strengths were approximately equal to 4.81 ksi (33.2 MPa) and 4.63 ksi (31.9 MPa) for the exterior frame system and interior system respectively, as shown in Figure 3-14. Since these values were close, and the main structural elements resisting seismic forces were the exterior frame, a single concrete mix with target compressive strength of 4.81 ksi (33.2 MPa) was used for both exterior and interior systems for the test specimens.

Table 3-5: Concrete Compressive Strength Test Results for Franz Tower

STATISTICS FOR CONCRETE COMPRESSIVE STRENGTH							
Element Type	Mean psi (MPa)	Median psi (MPa)	St. Dev. psi (MPa)	COV	Min. psi (MPa)	Max. psi (MPa)	No of Samples
Interior Beam Core through Floor	3,443 (23.7)	3,505 (24.2)	565 (3.90)	0.164	2,490 (17.2)	4,210 (29.0)	6
Exterior Balcony Waffle Slab	4,215 (29.1)	4,215 (29.2)	257 (1.77)	0.061	3,800 (26.2)	4,570 (31.5)	6
Interior Concrete Column	4,487 (30.9)	4,540 (31.3)	687 (4.74)	0.153	3,280 (22.6)	5,400 (37.2)	7
Exterior Balcony Concrete Fin Column	4,802 (33.1)	4,930 (34.0)	393 (2.71)	0.082	4,120 (28.4)	5,120 (35.3)	5

Figure 3-13: Concrete Compressive Strength Test

Due to limitations on the availability of maximum aggregate size of 3/8 in. (9.5 mm) required to ensure proper concrete placement for the two-thirds scale test specimens, the average unit weight of the concrete used for construction was modestly higher at 125 pcf (19.6 kN/m^3). Given the lack of alternatives, this difference was deemed acceptable for the testing program.

Concrete for the specimens was placed in three stages: pour 1) the foundation and lower columns of S1, pour 2) the top columns and slab system of S1 along with the foundation and lower columns of S2, and pour 3) the top columns and slab system of S2. Figure 3-15 presents the relation between concrete compressive strength and age for S1 and S2.

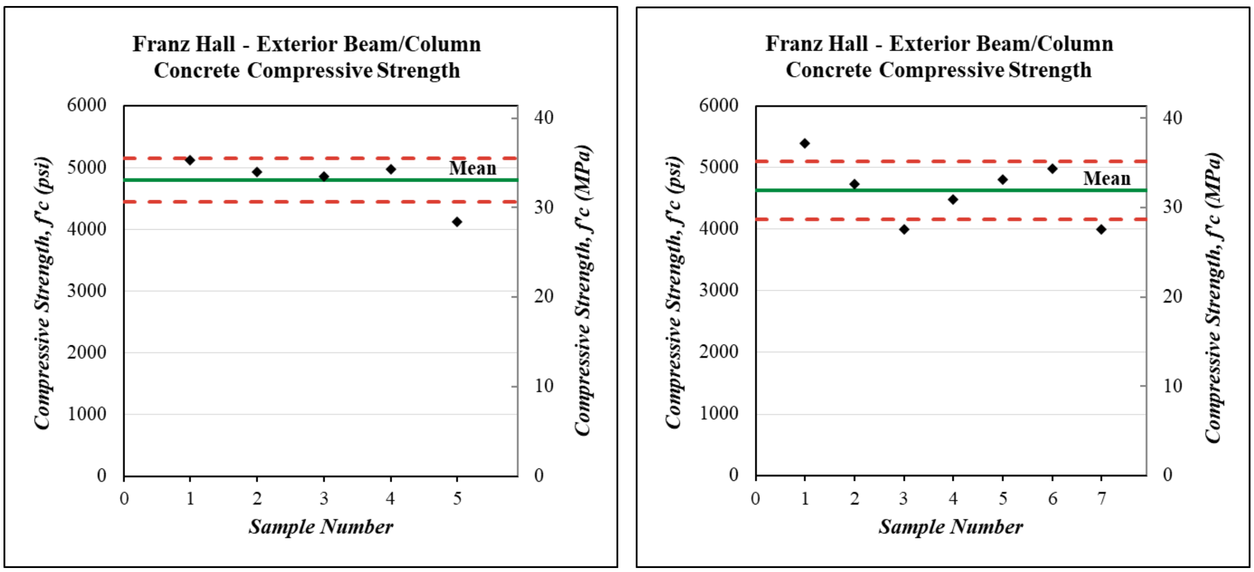

Figure 3-14: Franz Tower Concrete Compressive Strength Test Results for Exterior System (Left), and Interior System (Right)

Average concrete compressive strengths achieved for S1 was 5.4 ksi (37.2 MPa) and for S2 was 5.6 ksi (38.6 MPa) at test-day age. The slightly higher average compressive strength for the test specimens ($5.5/4.81 = 1.15$) was deemed acceptable given that this difference had slight impact on the flexural strength of the components and only modestly impacted on the contribution of concrete the shear strength of the members. Since the concrete shear strength is related to the square root of the concrete compressive strength (i.e., $\sqrt{1.15} = 1.07$), and since the contribution of concrete to shear strength of different building components was less than 50%, the impact of this higher strength concrete was considered acceptable.

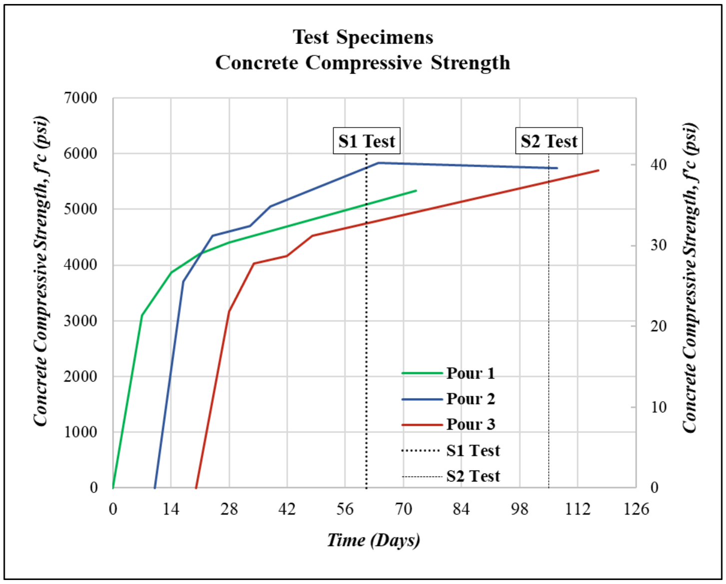

Figure 3-15: Concrete Compressive Strength Test Results for Test Specimens 1 and 2

3.3.2. Steel Reinforcement

The steel bar collected and tested were No. 3 (10 mm) bars used as tie reinforcement in the beams and columns. Since collecting samples from the column longitudinal reinforcement involved larger samples which would have impacted the integrity and load carrying capacity of the columns, the Engineer of Record decided not to collect samples of column or beam longitudinal bars for material testing. Tensile tests on reinforcement coupons from Franz Tower were only available for No. 3 (10 mm) reinforcement used for moment frame beam stirrups, columns hoops and crossties, gravity beam stirrups, and longitudinal reinforcement of slab joists. The tests indicated average yield strength of 56.7 ksi (391 MPa) for the No. 3 (10 mm) bars (Table 3-6). Where no material testing results for reinforcement were available (beam and column longitudinal reinforcement), provisions of ASCE 41-13 for the expected strengths were used. The building drawings specified Grade 40 reinforcement, for all other sizes, hence, the actual reinforcement yield strengths were assumed to be the expected yield strengths per ASCE 41-13, i.e., $f_{ye} = 1.17 f_y = 1.17\ (40\ \text{ksi}) = \ 46.8\ \text{ksi}\ (323\ \text{MPa})$.

In S1 and S2, both Grade 40 (275 MPa) and Grade 60 (414 MPa) reinforcement were used for No. 2 (6 mm) bars to provide the desired shear strength and the desired ratio of shear-to-flexural strength as explained in the previous sections. Tested average yield strengths were 48.0 ksi (331 MPa) and 64.3 ksi (443 MPa) for the Grade 40 (275 MPa) and Grade 60 (414 MPa) No. 2 (6 mm) reinforcement, respectively. See Figure 3-16.

Table 3-6: Reinforcing Steel Material Test Results for Franz Tower

STATISTICS FOR REINFORCEMENT TEST RESULTS (PROTOTYPE BUILDING)							
Element Type	Mean psi (MPa)	Median psi (MPa)	St. Dev. psi (MPa)	COV	Min. psi (MPa)	Max. psi (MPa)	No of Samples
No. 3 Bar Yield Strength	56,693 (391)	52,300 (361)	8,046 (55.5)	0.142	51,800 (357)	65,980 (455)	3
No. 3 Bar Yield Strength	74,522 (514)	73,789 (509)	2,050 (14.1)	0.028	72,939 (503)	76,838 (530)	3

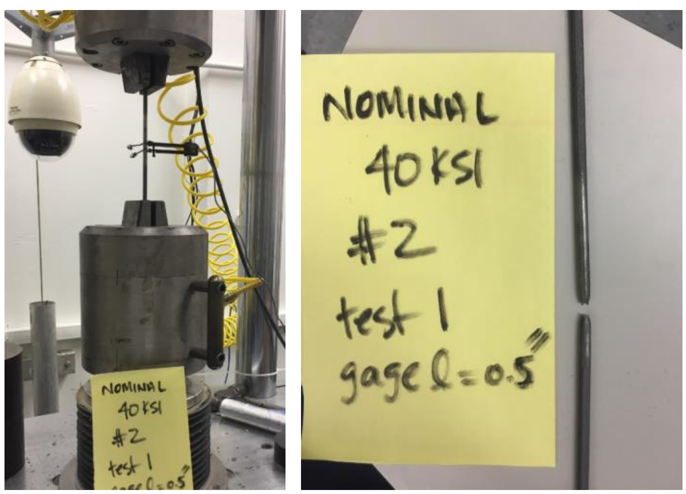

Figure 3-16: Tensile Strength Test on Grade 40 No. 2 (6 mm) Steel Reinforcement

For all other reinforcement i.e., column vertical No. 5 (16 mm) bars and beam No. 5 (16 mm) and No. 6 (19 mm) longitudinal bars, Grade 60 (414 MPa) steel was used, with average yield strength of 66.2 ksi (456 MPa). The reason to use Grade 60 (414 MPa) bars was that No. 5 (16 mm) and 6 (19 mm) bars were not available for purchase in Grade 40 (275 MPa). Other specimen design parameters were adjusted accordingly, to ensure the performance of building components in the test specimens was representative of the performance of those components in the building, as accurately as possible. Table 3-7 provides a comparison between material properties of the building and that of the test specimens.

Table 3-7: Material Strength Comparison between Franz Tower and Test Specimens

	Steel Reinforcement								***Concrete***	
Franz Tower	No. 3 (10 mm)	56.7 ksi (391 MPa)	No. 9 (29 mm)	46.8 ksi* (323 MPa)	No. 10 (32 mm)	46.8 ksi* (323 MPa)	No. 9 (29 mm)	46.8 ksi* (323 MPa)	*f'c*	4.71 ksi (32.5 MPa)
Test Specimen	No. 2 (6mm)	48.0 ksi & 64.3 ksi (331 MPa & 443 MPa)	No. 5 (16 mm)	66.2 ksi (456 MPa)	No. 5 (16 mm)	66.2 ksi (456 MPa)	No. 5 (16 mm)	66.2 ksi (456 MPa)	*f'c*	5.50 ksi (37.9 MPa)

** Material testing not provided. Expected material strength per ASCE41 provisions.*

3.4. Fabrication of Test Specimens

Two test specimens were constructed side by side with close collaboration and continuous structural observation to ensure accurate representation of the subject building. See Figure 3-17 and Figure 3-18.

First, high strength concrete (5000 psi) was poured for the base blocks at the same time. Next, due to uncertainties about concrete strength gain, and the natural delay between test 1 and test 2 (caused by test 1 set up and instrumentation, testing program, removing the instrumentation, and demolishing and hauling out the specimen, to provide space to move specimen 2 (S2) in place), pouring of the concrete was sequenced, such that the age of the concrete on the second specimen is as close to the first specimen as possible. The pouring sequence had three steps: 1- the lower columns of specimen 1 (S1), 2- the upper columns and slab level of specimen 1 (S1) and the lower columns of specimen 2 (S2), 3- the upper columns and slab level of specimen 2 (S2). Images from construction and specimen fabrication are shown in Appendix D.

Figure 3-17: Specimen Construction: (a) High Strength Concrete Pour at Both Base Blocks, (b) Side by Side Specimens prior to Pour 1, (c) Specimen 1 Top Columns and Specimen 2 Lower Columns Concrete Pour (Pour 2), (d) Specimens Prior to Testing

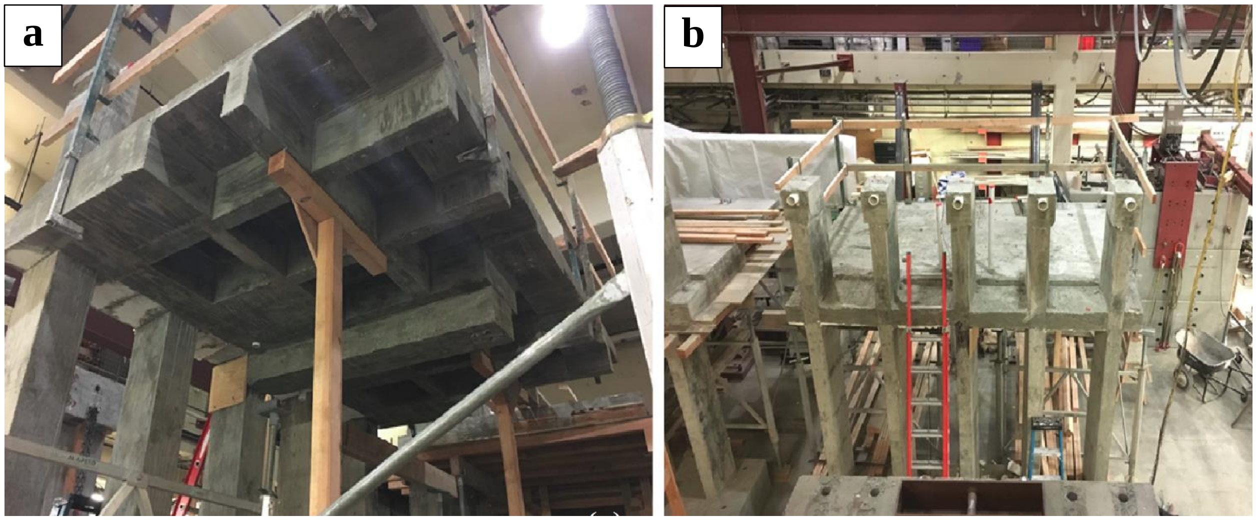

Figure 3-18: Built Specimen: (a) Slab View, (b) Overall

Figure 3-19: Top of Specimen Connection to Load Transfer Beam

Figure 3-20: Slab Gravity Load on Specimen 2

3.5. Test Setup and Instrumentation

The test subassembly was selected by extracting a portion of the frame system around the perimeter of the Franz Tower as shown in Figure 3-4, that is representative of the behavior of the perimeter framing of the building. As mentioned previously, due to the simultaneous demand on the perimeter columns in in-plane or out-of-plane direction, with loading in either orthogonal direction, it was prudent to study the out-of-plane behavior of the columns as well as the in-plane behavior of them. Therefore, having a biaxial load test setup was necessary.

The slab system consisted of large interior beams spaced every fifth perimeter column, which pose a large demand in the out-of-plane direction on the particular column they frame to. The slab also consists of joists between the interior beams that also frame into the exterior columns/frame. To study the effect of the slab system on the behavior of the frame, two three-dimensional test specimen subassemblies were designed and constructed as shown in Figure 3-21 to Figure 3-23, and tested at the UCLA Structural/Earthquake Engineering Research Laboratory (SEERL).

In order to apply the desired drift levels in in-plane and out-of-plane directions, a 100-kip (max) actuator with +/−12" stroke was used in the in-plane direction and two 60-kip (max) actuators with +/−6" stroke were used in the out-of-plane direction. The in-plane actuator was fixed to the strong wall from one side and connected to the specimen by an extension tube. The out-of-plane actuators were fixed to the top of a steel frame, which itself was tied to the laboratory strong floor by eight post tensioned bars. A connection "mechanism" was made out of steel tubes to connect the out-of-plane actuators to the specimen, along the centerline of the hinge at the top of the columns. Details of the specimen construction and test setup are provided in Appendix D.

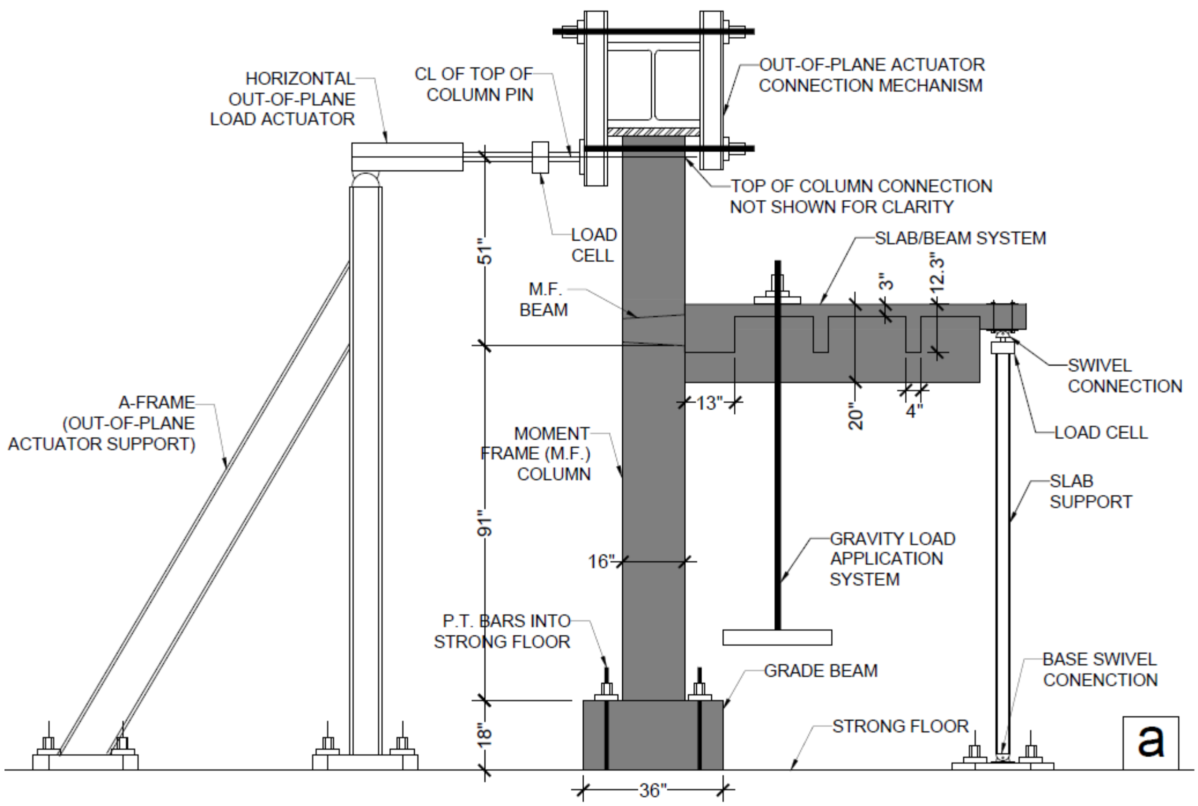

Figure 3-21: Schematic Test Setup: Out-of-Plane Direction

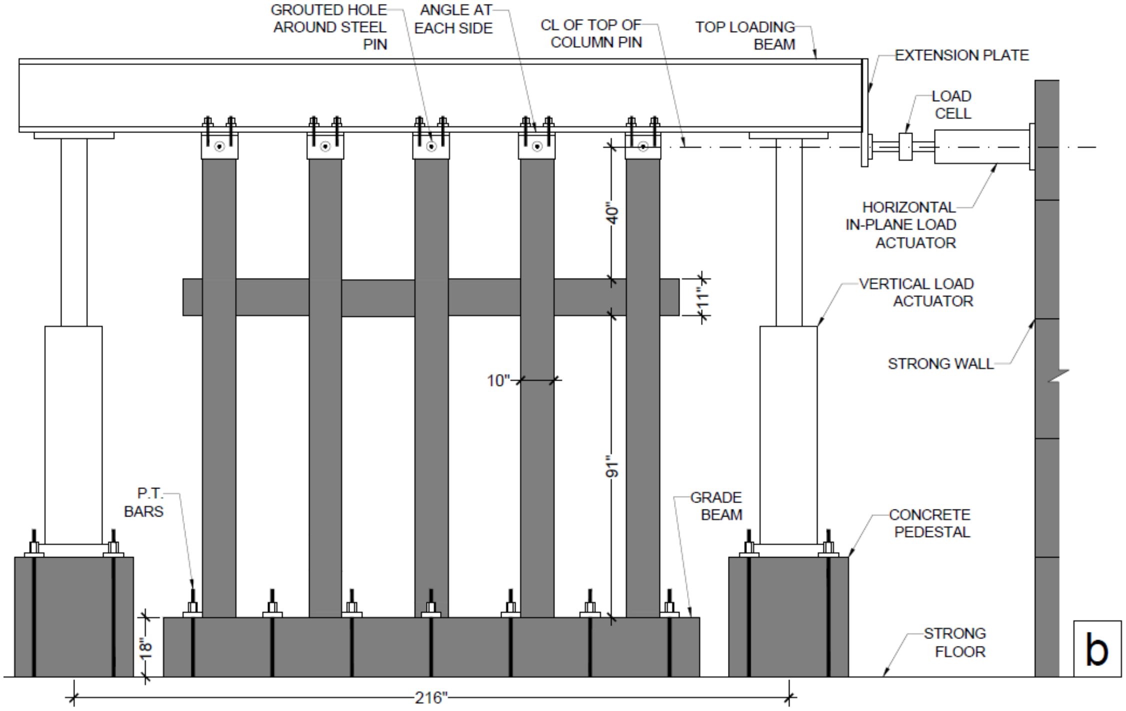

Figure 3-22: Schematic Test Setup: In-Plane Direction

Figure 3-23: Actual Test Setup

3.5.1. Connection to Loading System

Specimen 1 was moved into place 28 days after pour 2. Specimen 2 was moved into place after specimen 1 was tested and demolished, nearly two months after pour 3. The specimen base blocks were secured to the laboratory strong floor using 1.25 in. (32 mm) diameter high-strength post-tensioning rods spaced at 24 in. (610 mm) in both directions. Two horizontal post-tensioning rods were used at each end of the base block, to increase the confinement (Figure 3-23). Top of the columns were connected to the top steel transfer, the slab swivel columns were attached to the slab edge, and the specimens were connected to the in-plane and out-of-plane actuators, and vertical actuators. Once the specimens were in place, the LVDTs and string pods were connected to the exterior of the specimen. The same procedure was done for specimen 2 (S2). (Figure 3-24 and Figure 3-25).

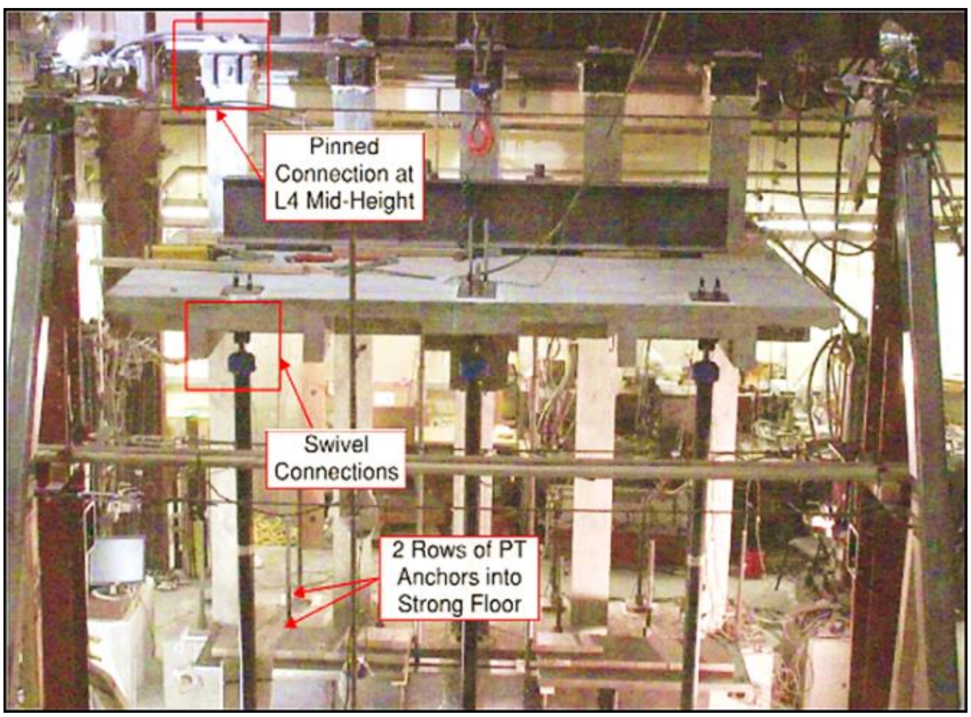

Figure 3-24: Test Setup: In-Plane Direction

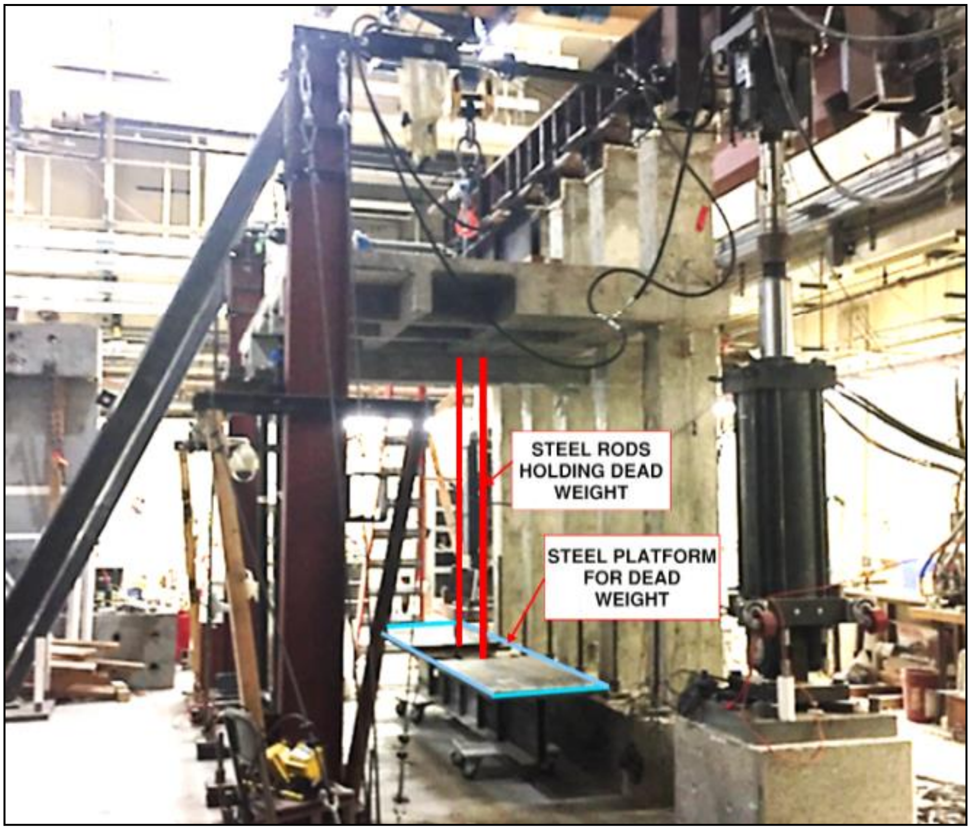

Figure 3-25: Test Setup: Out-of-Plane Direction

The loads applied by the horizontal actuators (one actuator in the in-plane direction and two in the out-of-plane direction) and two vertical actuators were measured by load cells attached to the actuator extension rods. Actuator displacements were measured by linear variable differential transducers (LVDT) attached to the outside of the actuators.

The total axial load applied by the two vertical actuators was constant throughout the tests and was equal to $0.07A_g f_c'$. The in-plane and out-of-plane actuators were displacement-controlled and were manually controlled to generate the target lateral deformation ratio at each loading cycle in each loading direction.

3.5.2. Boundary Conditions

The boundary conditions used for the test specimens were selected to reasonably represent those existing in the actual building. Selecting accurate boundary conditions is essential in obtaining similar behavior of the test specimen to the existing building when subjected to lateral loading. For the building, fixity was assumed at the base of level three perimeter columns where they anchor into the 6-ft. deep transfer girder. For the test specimen, this boundary condition was provided by using an 18 in. (457 mm) deep grade beam fixed to the laboratory strong floor with two rows of post-tensioned rods spaced at 24 inches (610 mm) on center, one on each side of the columns. The top of the test specimens was selected to be at mid-height of level four columns, which is assumed to be the inflection point for both in-plane and out-of-plane loading (portal frame assumption). To provide a pinned connection for in-plane loading at the inflection point, angles with a steel rod through the top of the column were used (Figure 3-26 and Figure 3-27). A hole centered on the smaller sides of the columns, and along their deeper side, was provided at the top of each column to allow a steel rod to pass through and be tightened to the steel angels via high strength steel nuts. This rod allowed the top of column to rotate in the in-plane direction and minimize the moment at that location. For in-plane loading, the actuator was connected to extension tubes to ensure the centerline of the actuator and the centerline of the top column mid-height hinge (or hinge at the top of the specimen) are at the same elevation, eliminating any additional and undesirable moments. To ensure the top of column was not weakened due to the hole provided to accommodate the top pin (which could lead to premature shear failure), and to ensure a load path existed from the top loading beam to the specimen, the top of column connection was strengthened by enlarging the top 12 inches (305 mm) of the column height with a 10 in. (254 mm) by 16 in. (406 mm) rectangular section (instead of the typical trapezoidal section) as illustrated in Figure 3-27. Additional No. 2 (6 mm) transverse reinforcement spaced at 3 in. (76 mm) on center also was provided in the enlarged section.

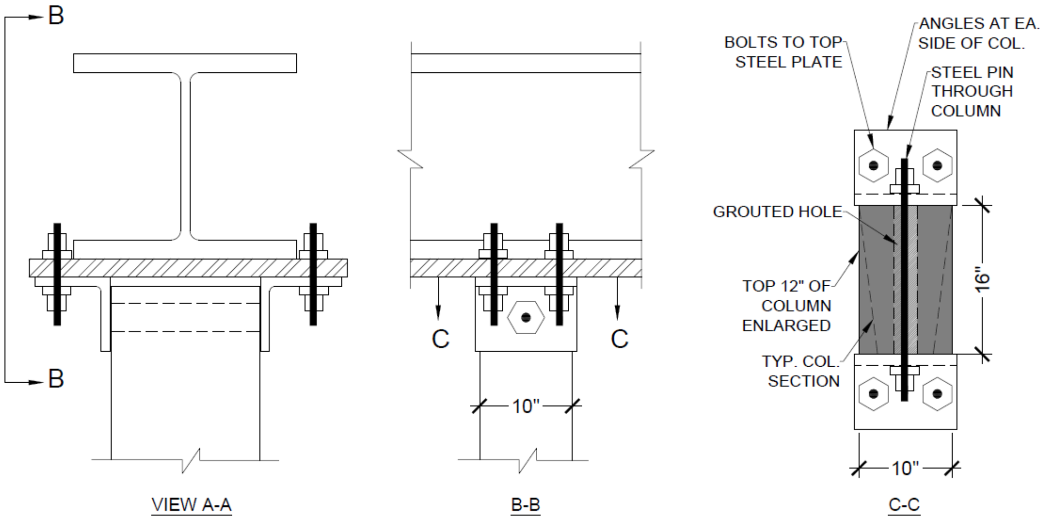

Figure 3-26: Pinned Connection at Top of Columns (Schematic View)

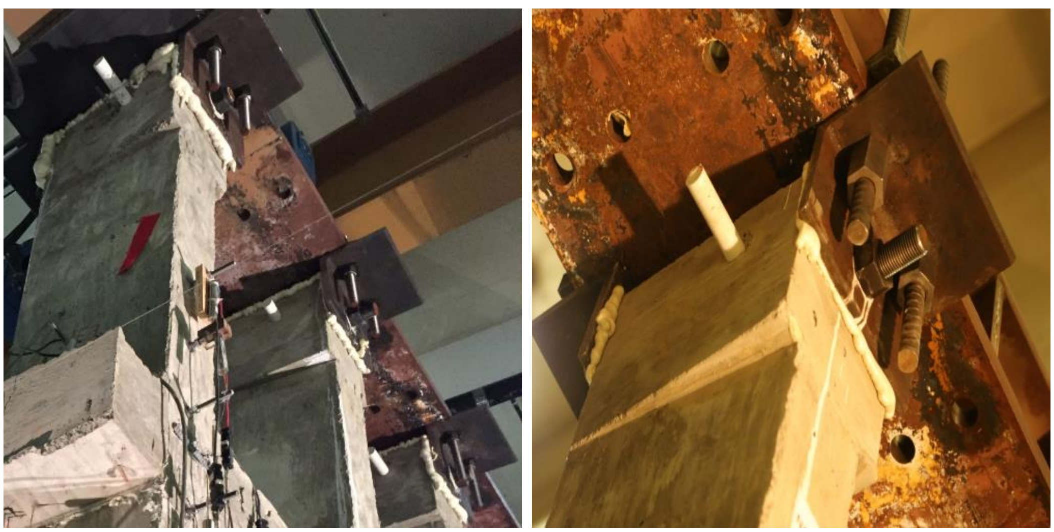

Figure 3-27: Pinned Connection at Top of Columns (Test Specimen)

At the slab edge, which is at the assumed inflection point at mid-span of level four slab (between the perimeter columns and the first interior column), three vertical rigid links with swivel connections at the top (slab) and bottom (strong floor) were used to provide vertical support while allowing in-plane and out-of-plane deformations. These connections were designed to allow in-plane and out-of-plane rotations of at least four times that expected for the maximum test target drift. Load cells were attached near the top of the truss members to measure the axial load imparted on the slab (see Figure 3-22 and Figure 3-28).

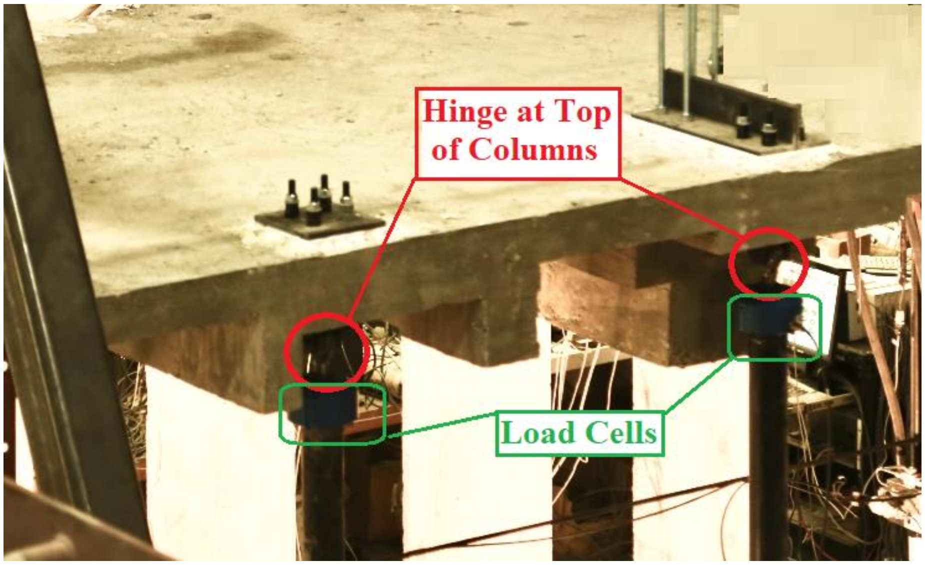

Figure 3-28: Top Connection at Swivel Columns (Test Specimen)

As previously mentioned, additional gravity load on the lower columns from the weight of the other half of the slab system that is not constructed and floor live load, was not applied to the first specimen because calculations indicated that this added gravity load have a modest impact on slab yielding due to out-of-plane loading (given the lack of negative gravity moment at the slab-column interface). These added slab gravity loads were applied to the second specimen, shown in Figure 3-25. As illustrated in the next sections, the backbone curves of the two tests were very similar; validating the expectation that added slab gravity loading had little impact on overall test specimen behavior, and the higher shear capacity of specimen 2 was believed to be attributed to overall higher compressive strength of concrete (see Figure 3-15).

3.5.3. Instrumentation

3.5.3.1 LVDTs and String Potentiometers

The primary test objective was to obtain overall lateral-load versus lateral displacement relations (or backbone curves) of the test specimens under in-plane and out-of-plane loading, as well as to assess damage states at various lateral drift ratios. Hence, linear string potentiometers (string pots) were used to measure deflections at the slab level (one story height), and at the centerline of the specimen top pin – which is the mid-height of level four columns and their assumed inflection point – as shown in Figure 3-29 and Figure 3-30. The string pots were connected to a rigid frame/support and measured the frame lateral deformations in both principal directions.

LVDTs where installed at the three assumed hinge regions along the height of columns 1 (C1), and 3 (C3): base of the columns (hinge region 1), top of the lower columns (hinge region 2), and base of the top columns (hinge region 3), as shown in Figure 3-29. C3 (the center column) was selected since it was the only column that supported an interior deep beam. This was expected to change the demand ratios and behavior of C3, and therefore that column was instrumented to study its behavior in more detail. The other four columns are expected to behave similarly with possible larger tension and compression forces on the end columns; therefore, C1 (a corner column) was selected as a typical perimeter frame column for instrumentation.

Four LVDTs were placed at each hinge zone: two (2) on the north face of the columns, one (1) on the east face, and one (1) one the west face. Research has shown various means to estimate the height of the hinge zone at the base of the columns, with an acceptable range between d (the distance from extreme compression fiber to centroid of tension reinforcement) and h_c (depth of the column). (Mortezaei, 2014) (Paulay & Priestley, 1992) (Park, Priestley, & Wayne, 1982)

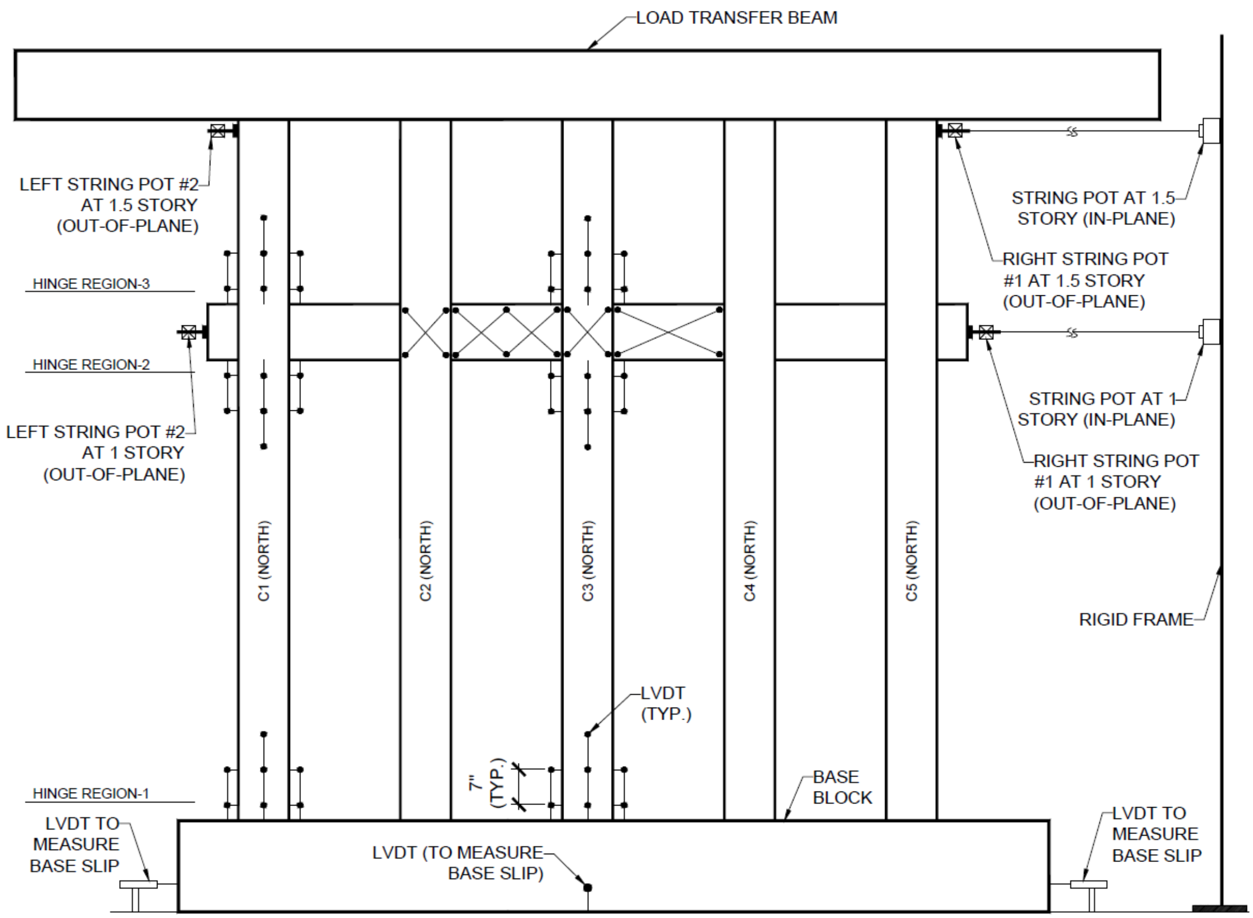

Figure 3-29: Location of LVDT and String Pots (In-Plane)

Approximating the trapezoidal column section to the nearest rectangular section (8 in. by 16 in. (203 mm by 406 mm)), $d_{in\text{-}plane}$ and $d_{out\text{-}of\text{-}plane}$ were calculated to be 6 in. (152 mm) 14 in. (356 mm) respectively. The gauge length of the LVDTs was selected to be 7 in. (178 mm) which is within the accepted range in the in-plane direction (h_c=8 in. (203 mm), and d=6 in. (152 mm)). In order to cover the hinge region in the out-of-plane direction, two LVDTs each with gauge length of 7 in. (178 mm) were used with total gauge length of 14 in. (356 mm).

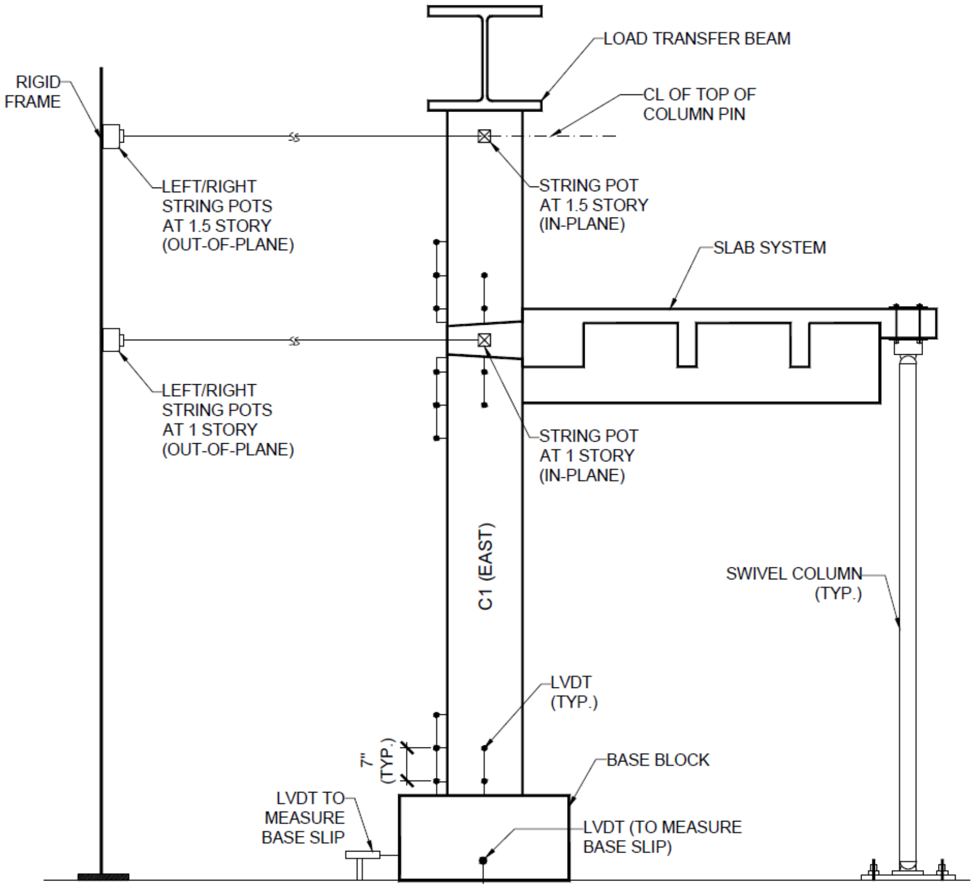

Figure 3-30: Location of LVDT and String POTS (Out-of-Plane)

The LVDTs were connected to a housing, which was attached to the specimens by extension rods mounted on the face of the columns (Figure 3-31). The cores of the LVDTs were also attached to extension rods. Only at hinge region 2 (top of the lower columns), the core was attached to the bottom of the ledge beams.

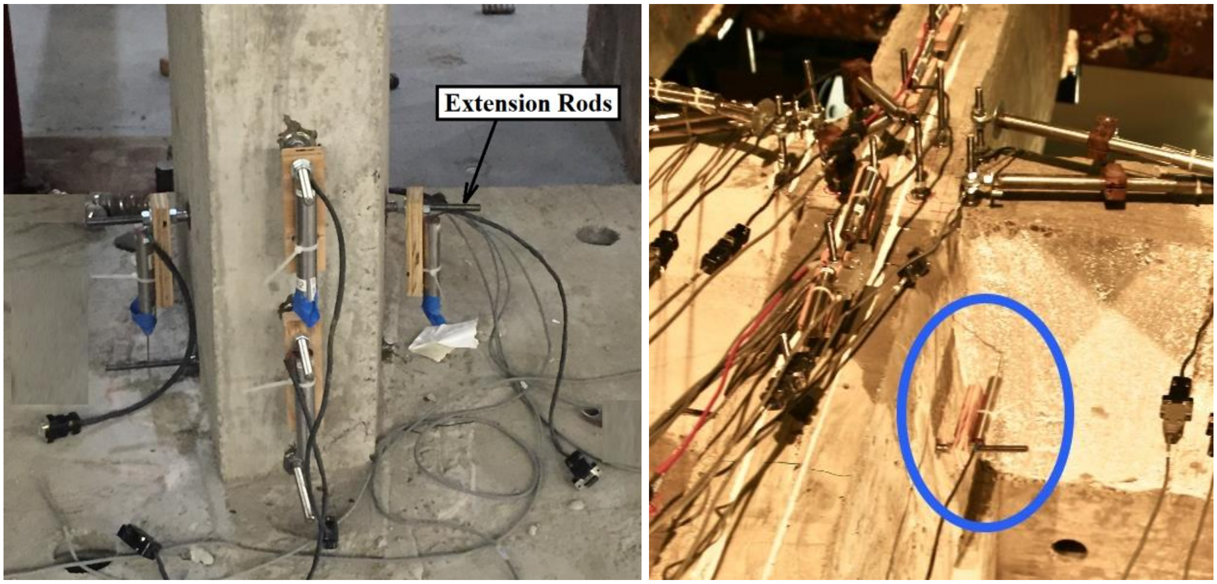

Figure 3-31: Typical Connection of LVDTs at Columns

Shear deformations at the beam-column joints, at C3 and C2, and at ledge beams at either side of C3 were measured by LVDTs arranged in X-configurations (Figure 3-32). More detail about LVDT gauge lengths and geometry can be found in Appendix C.

Figure 3-32: LVDTs Arranged in X-Configurations to Measure Shear Deformations

3.5.3.2 Strain Gauges

For each test, 28 strain gauges were used to measure strains in the column longitudinal reinforcement, column transverse hoops and cross ties, and ledge beam hoops. Strain gauges on the column vertical bars were used to identify point first yield. At each hinge region of the columns, two gauges were placed on column longitudinal bars (one corner bar at the narrow face, and one corner bar at the wide face). Two additional sensors were placed on the column tie and hoop at each hinge location, as well as two were placed on the ledge beam ties at each side of the center column (Figure 3-33).

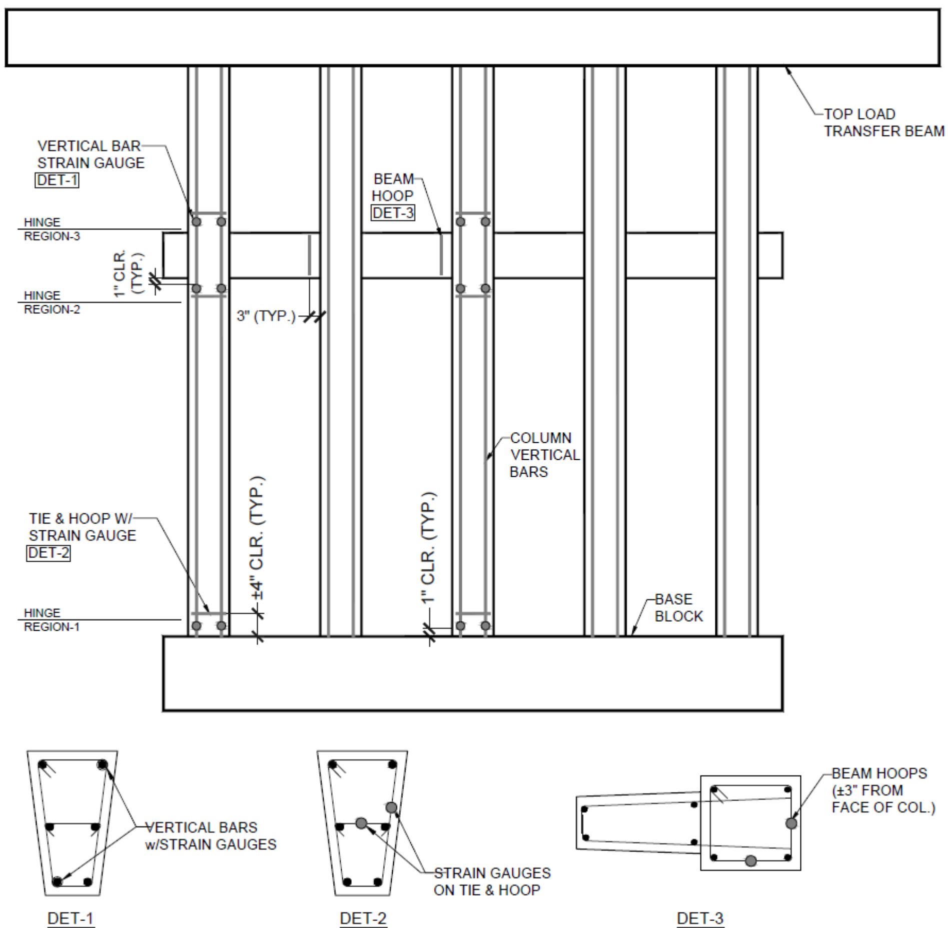

Figure 3-33: Strain Gauges at Hinge Locations

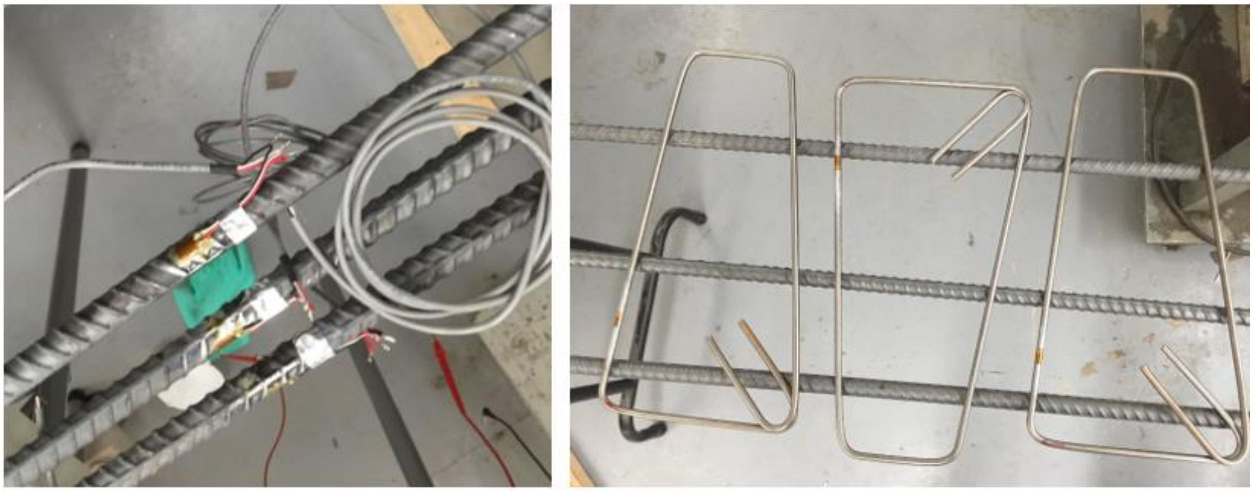

Figure 3-34: Strain Gauges on Column Vertical Bars (Left) and Ties (Right)

3.6. Loading Protocol

The test program, as discussed in detail in previous sections, included tests on two identical specimens, one-bay wide, five columns (four frames) wide, and one and one-half story tall, subjected to biaxial lateral loading and gravity loading. Due to symmetry of the building about a vertical axis at the geometric center of the building, the perimeter moment frame would be simultaneously subjected to both in-plane and out-of-plane loading. Given the biaxial loading could influence the lateral drift capacity and failure modes of the test specimens' components, a biaxial loading protocol was established and used for both tests.

Although ASCE 41-13 requires three tests to be performed on identical specimens, two identical test specimens were constructed, with an option to construct a third test specimen if the results obtained from the first two tests were inconsistent or indicated that the proposed seismic retrofit was unlikely to work given the test information. Since results obtained from the first two tests were consistent as shown later, and the information needed to support the engineer's proposed retrofit concept was obtained from the tests and accepted by the peer reviewers, a third test was not performed.

Table 3-8: Biaxial Half Clover Drift Levels

Cycle No.	1	2	3	4	5	6	7	8	9	10
Drift Level	0.125%	0.25%	0.375%	0.50%	0.750%	1.00%	1.50%	2.00%	2.50%	3.00%

The test conducted under displacement control with the specimen pushed in both orthogonal directions in a half cloverleaf pattern as shown in Figure 3-35 to peak lateral drift values shown in Table 3-8. Since preliminary evaluations of the building showed significant damage to building components at low level drifts (about 0.50%), the drift levels were incrementally increased by 0.125% up to 0.50%, to be able to observe any sudden failure. After 0.50% drift level, the incremental increase was 0.25% up to 1% drift, and 0.50% until the end of the test. Each drift cycle was performed twice before moving to the next drift cycle.

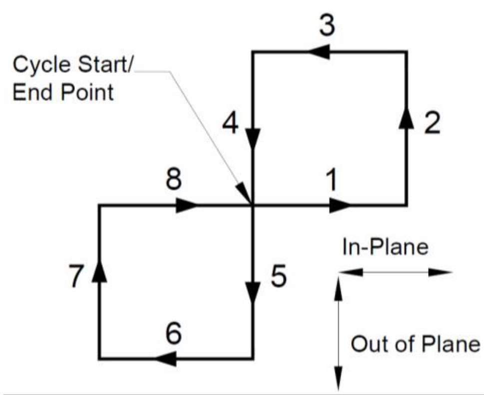

Figure 3-35: Biaxial Half Clover Loading Protocol

For test 1, gravity load was applied with vertical actuators to account for the self-weight and the live load from stories above. For test 2, as noted previously, additional gravity load was applied on the slab to account for the self-weight of a one-half slab, and level-four live load.

Rate of Loading

To evaluate performance of the subassemblies, quasi-static cyclic testing was performed at a very slow rate. For out-of-plane loading, the target drift values were generally achieved using a loading rate of 0.0002 inch/second (0.00508 mm/sec) and 0.001 inch/sec (0.0254 mm/sec) for in-plane loading. This was due to the governing mode of failure for the columns in each direction: shear-controlled in the out-of-plane direction and flexure-shear controlled in the in-plane direction. To prevent sudden shear failure of the columns in the out-of-plane direction, lower rate of loading was used when the pushing the specimen in that direction.

Testing was stopped during each half-cycle just after peak deformation was achieved to document test results by recording observations and taking photos.

Chapter 4. Experimental Test Results and Discussion

4.1. General

In this chapter, the observed level of damage of the specimens, overall and at component level, is discussed at different lateral drift levels with correlating images. Additional figures presenting progression of damage and sensor readings are presented in Appendix E and Appendix F respectively.

In both specimens, prior to a lateral drift level of approximately 1%, no significant damage was observed other than surficial hairline cracks at the base and top of the first level columns (plastic hinge regions). These cracks were horizontal and due to concrete cracking, mainly present at the corners of the column sections prior to point of first yield at about 0.25% drift (Figure 4-5). The crack widths were about 0.004 to 0.006 inches (0.10 to 0.15 mm) and they were highlighted by markers for visibility as shown in Figure 4-1.

Figure 4-1: Cracks on the Columns at Drift Levels Lower than 1%

The specimens maintained their ability to carry the applied gravity load ($0.07A_g f_c'$) until the end of the test. Gradual loss of lateral load capacity initiated at drift levels exceeding 1.8%.

As discussed in section 3.6, the specimens were tested under bi-directional loading protocol, where the specimens were first pushed in the in-plane direction, and while maintaining the in-plane deformation, it was pushed in the out-of-plane direction. The red point in Figure 4-2 at each loading cycle is the point of maximum in-plane and out-of-plane deformation of the tests. The drift ratios referred to in the subsequent section correspond to the diagonal drift ratios as shown in Figure 4-2.

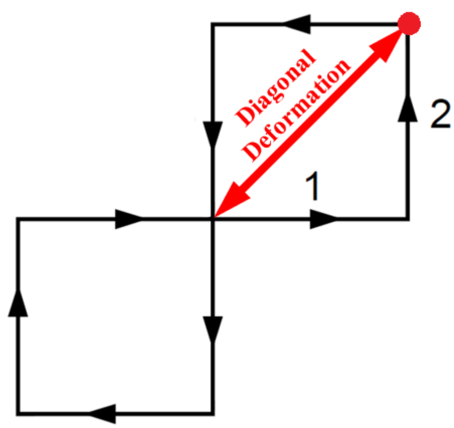

Figure 4-2: Visual Description of Diagonal Lateral Deformation

4.2. Observed Damage and Cracking

4.2.1. Up to 1% Drift Ratio

Fin Columns

No significant damage was observed until diagonal drift level of 1%. Prior to that, only hairline cracks (crack widths of approximately 0.006 to 0.010 inches (0.15 to 0.25 mm)) appeared mainly at the base or top of the first level (lower) columns which closed when the specimen was at zero lateral deformation (Figure 4-1). The hairline cracks were mainly horizontal along the height of the column and grew in number as the lateral deformation ratio increased, without concrete spalling (Figure 4-3-a and b, and Figure 4-4-b). The correlation of the observed damage and the drift ratio on the backbone curves of Test 1 are shown in Figure 4-5 in both directions of loading. The same correlation for Test 2 is provided in Appendix F. As shown in Figure 4-5, the specimen reached the point of maximum base shear (initiation of plateau) in the out-of-plane direction, and just passed it in the in-plane direction, i.e., additional strain hardening occurred after 1% diagonal drift.

Ledge Beams

Some hairline diagonal tension (shear) cracks due to the in-plane loading were observed. This was expected as the ledge beams were determined to be flexure-shear controlled in the in-plane direction (see Appendix A). Some cracks which seemed to have been from the slab due to the out of plane loading, were also observed on the lower face of the ledge beams (Figure 4-3-c).

Slab System

Some hairline cracks on the concrete slab, and shear cracks along the south side of the columns (interior face of the columns at the interface of the thickened slab edge), started to appear during the second cycle at 0.75% drift level (Figure 4-4-a). This did not impact the load carrying capacity of the slab, or its connection to the exterior frame.

Overall

No concrete spalling was observed, and overall, the specimen did not sustain any damage other than some surficial cracks on the columns and some shear cracks on the ledge beams (Figure 4-4-b).

Figure 4-3: Observed Damage: 1.0% Drift: (a and b) Column Bases, (c) Top of Columns and Bottom of Ledge Beams – Test 1

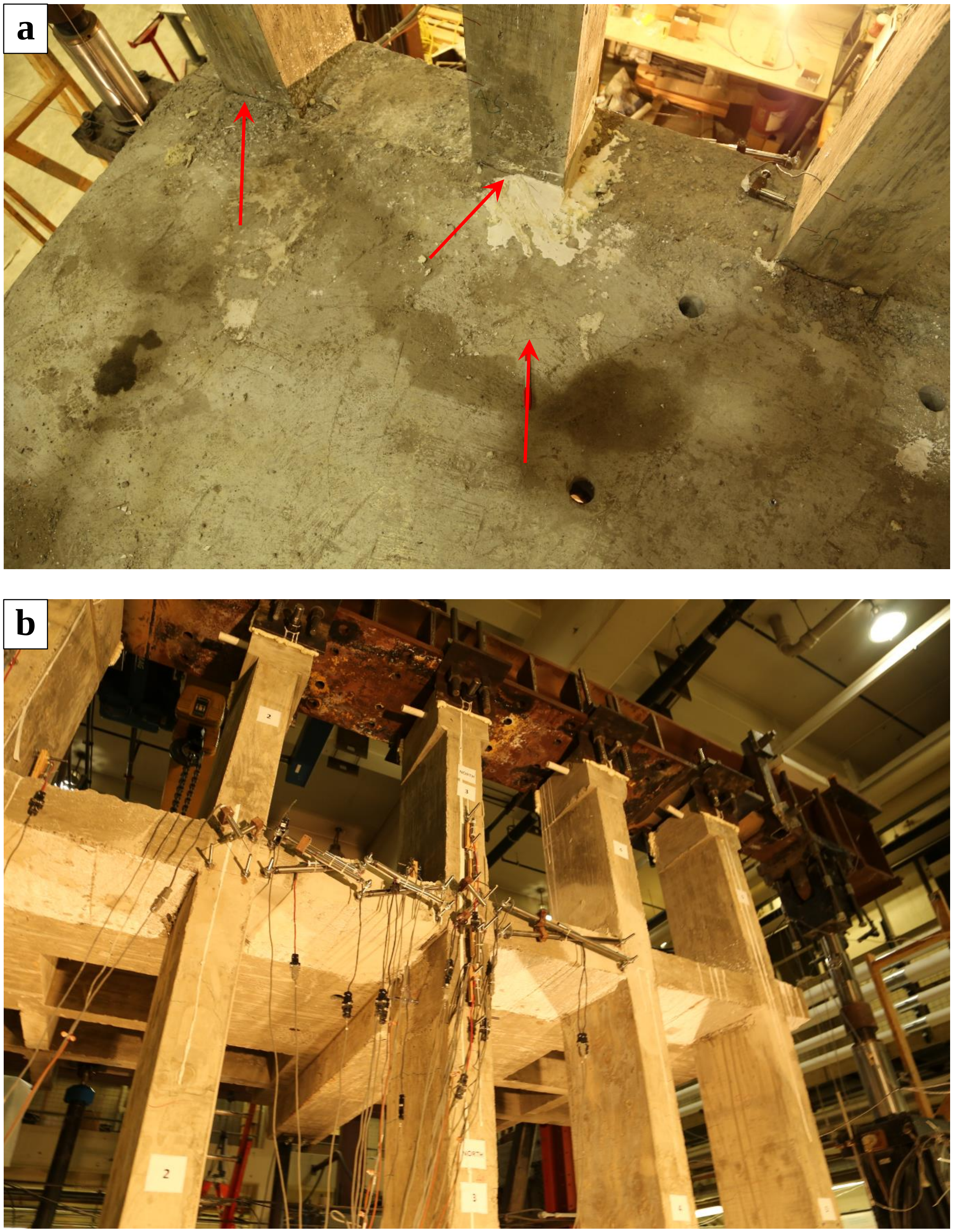

Figure 4-4: Observed Damage: 1.0% Drift: (a) Slab, (b) Overall View – Test 1

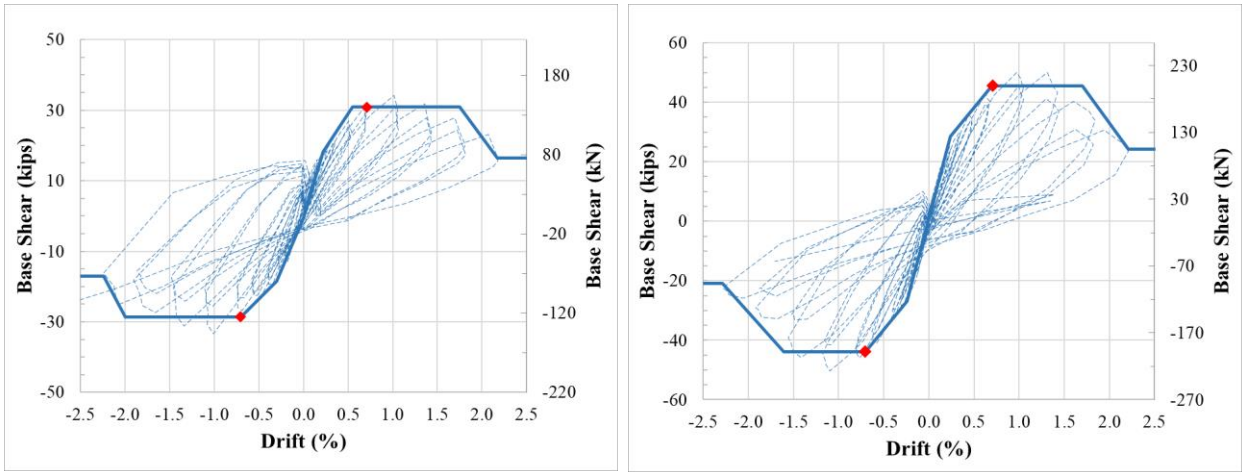

Figure 4-5: Correlation of Observed Damage at 1.0% Diagonal Drift Ratio with Load-Deformation Hyteresis of Test 1, In-Plane (Left), Out-of-Plane (Right)

4.2.2. 1.5% Drift Ratio

Fin Columns

Vertical splitting cracks at the base of the center column (C3) formed along the splice length of the longitudinal reinforcement, on the narrow face of the column (north side), which suggested slip of the column longitudinal bars at the lap-splice had occurred (Figure 4-6-a and b). The length of the crack was less than the used splice length of 16 inches (406 mm). The previously observed horizontal hairline cracks on the face of the columns grew in number and width without significant damage to the columns or any concrete cover spalling. The cracks were scattered along the mid-height of the columns and were more prominent in terms of number and size at the base of the lower columns. Based on preliminary calculations, if lap-splice failure did not occur, the columns were shear-controlled in the out-of-plane direction and flexure-shear controlled in the in-plane direction. However, diagonal cracks were not observed on any face of the columns. Towards the end of the second cycle, cracks at the top hinge location of two of the lower columns (C2 and C5) started to appear without spalling (Figure 4-6-c and d).

Ledge Beams

Some diagonal shear cracks started to appear at the beam-column interface and the shear cracks at the lower face of the ledge beams grew in depth (Figure 4-7).

Slab System

After the initial cracks along the column-slab interface during the second cycle at 0.75% drift ratio, no significant change in the level of damage in the slab system was observed. The slab system maintained its connection to the exterior frame system and did not exhibit deterioration in its gravity load carrying capacity (Figure 4-8).

Overall

No concrete spalling was observed, and overall, the specimen did not sustain any new damage other than the previously observed damages growing in size and number. Vertical cracks appeared at the base of column 3, and the cracks on the ledge beam widened.

As shown in Figure 4-9, the specimen had passed the point of initiation plateau, and reached the maximum base shear. Therefore, damage in correlation to yielding at the structural components was observed, as expected.

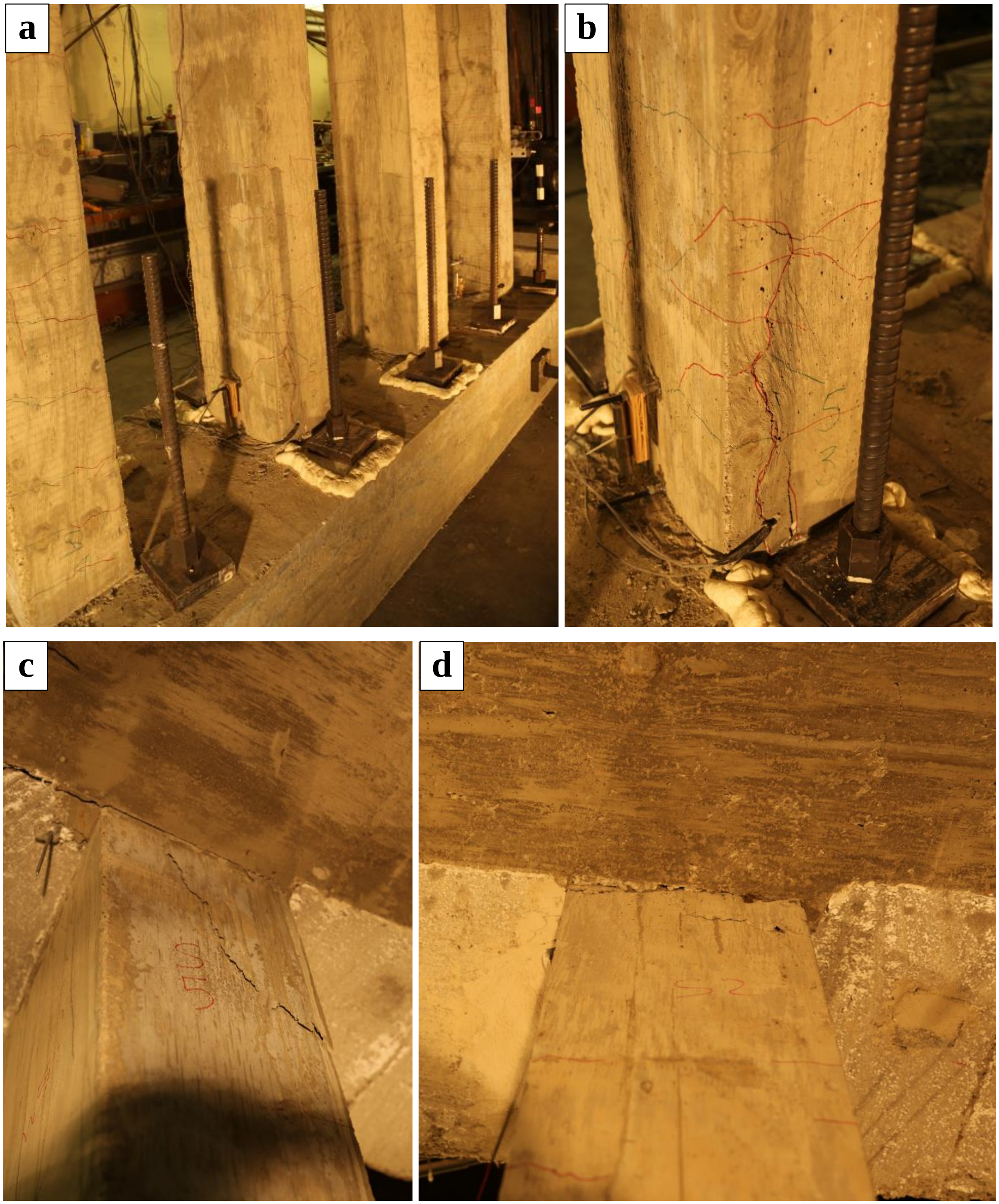

Figure 4-6: 1.5% Drift: (a) Column Bases after the 1st Cycle (South), (b) C3 Base after the 2nd Cycle (Sotuh), (c) C5 Top (South), (d) C2 Top (South) – Test 1

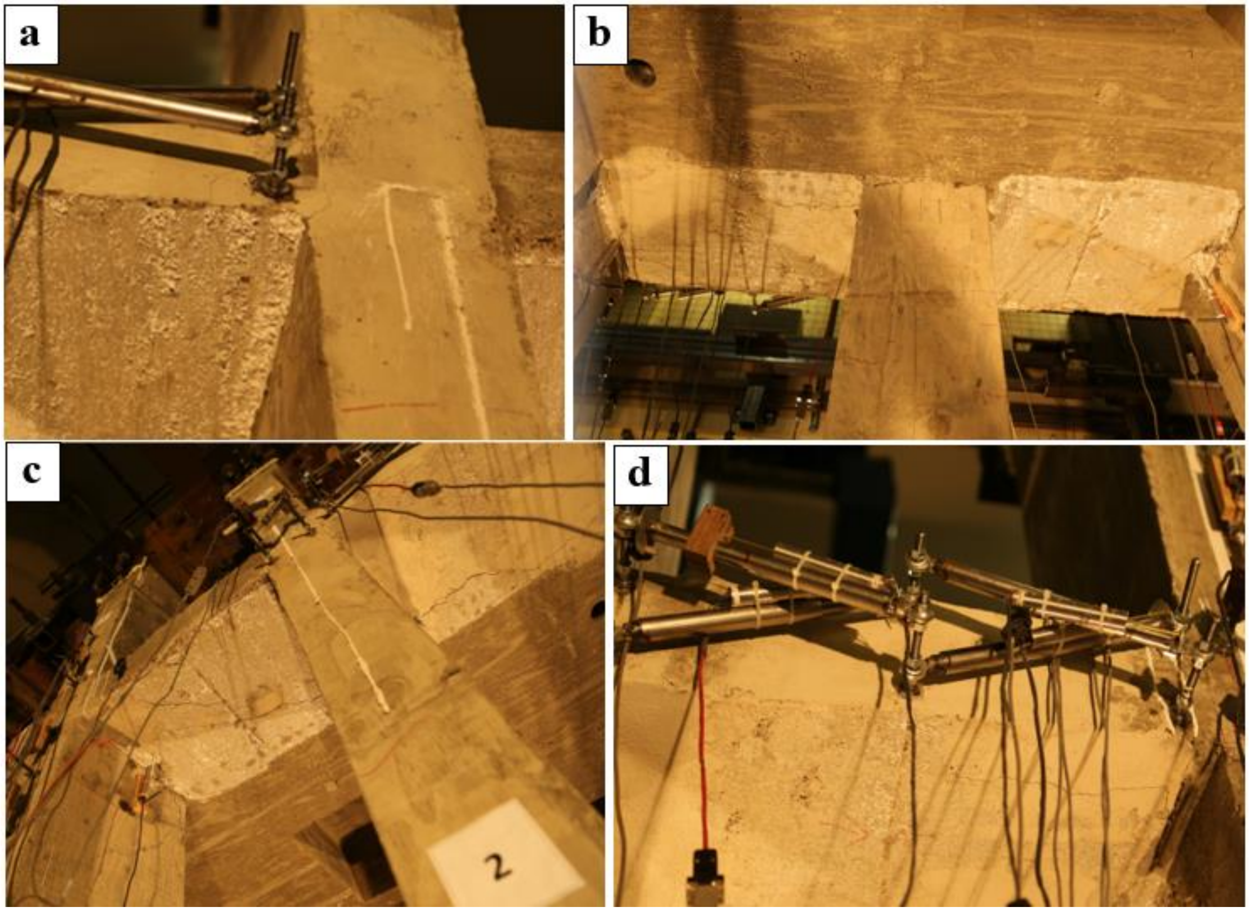

Figure 4-7: 1.5% Drift: (a) Ledge Beam Interface at C4, (b) C2 Top (South), (c) Ledge Beams at C2 Top (North), (d) Ledge Beam Between C2 and C3 – Test 1

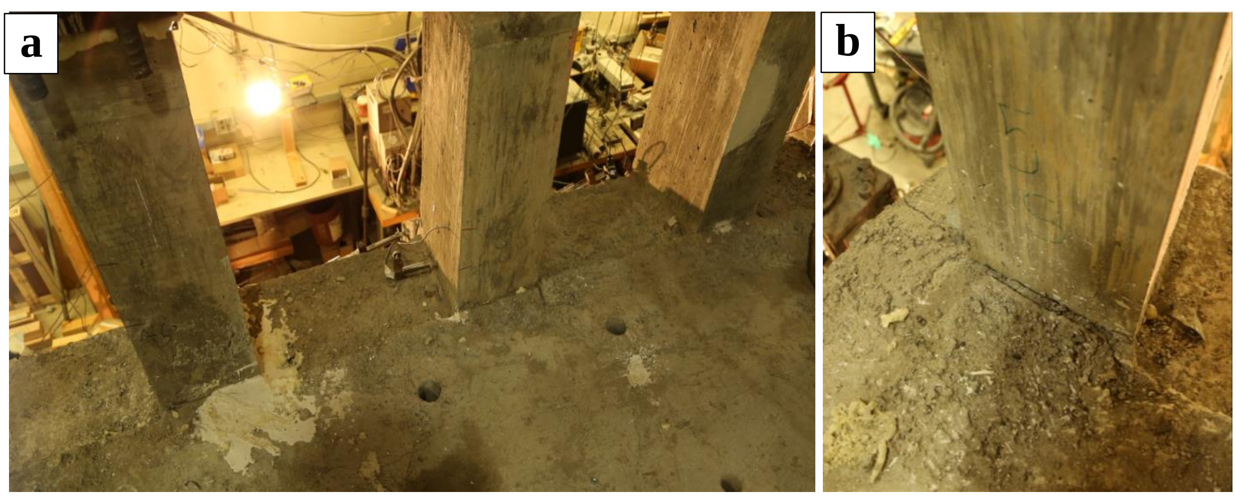

Figure 4-8: 1.5% Drift: (a) Slab Connection to Frame, (b) Crack at Slab-Column Interface – Test 1

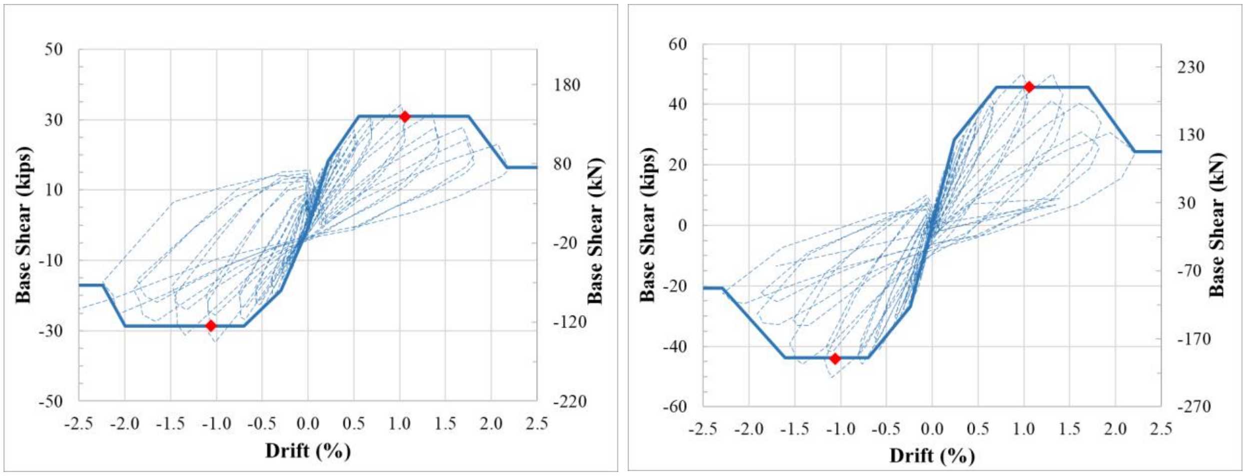

Figure 4-9: Correlation of Observed Damage at 1.5% Diagonal Drift Ratio with Load-Deformation Hyteresis of Test 1 – In-Plane (Left), Out-of-Plane (Right)

4.2.3. 2% Drift Ratio

Fin Columns

Vertical splitting cracks at the base of C3 grew and similar cracks formed at the base of the other columns (C4 and C5), on their narrow side. Previously observed damage at the top hinge of the columns deepened and widened without concrete spalling (concrete spalling initiated on C5), and similar cracks started to appear at all column tops. Additional cracks were observed at the ledge beam-column interfaces (Figure 4-11).

Ledge Beams

Shear cracks on the front face of the ledge beams and flexural cracks at their lower face grew deeper and longer without concrete spalling. Concrete spalling initiated on the face of the ledge beam, between C2 and C3, was very close to spalling (Figure 4-11).

Slab System

No change observed in the progression of damage (Figure 4-12).

Overall

The concrete cover spalling at the base of C3 and the top of C5 initiated. Growing cracks weakened the structural components, caused the stiffness of the specimen to decline, and a decline in the base shear (Figure 4-13).

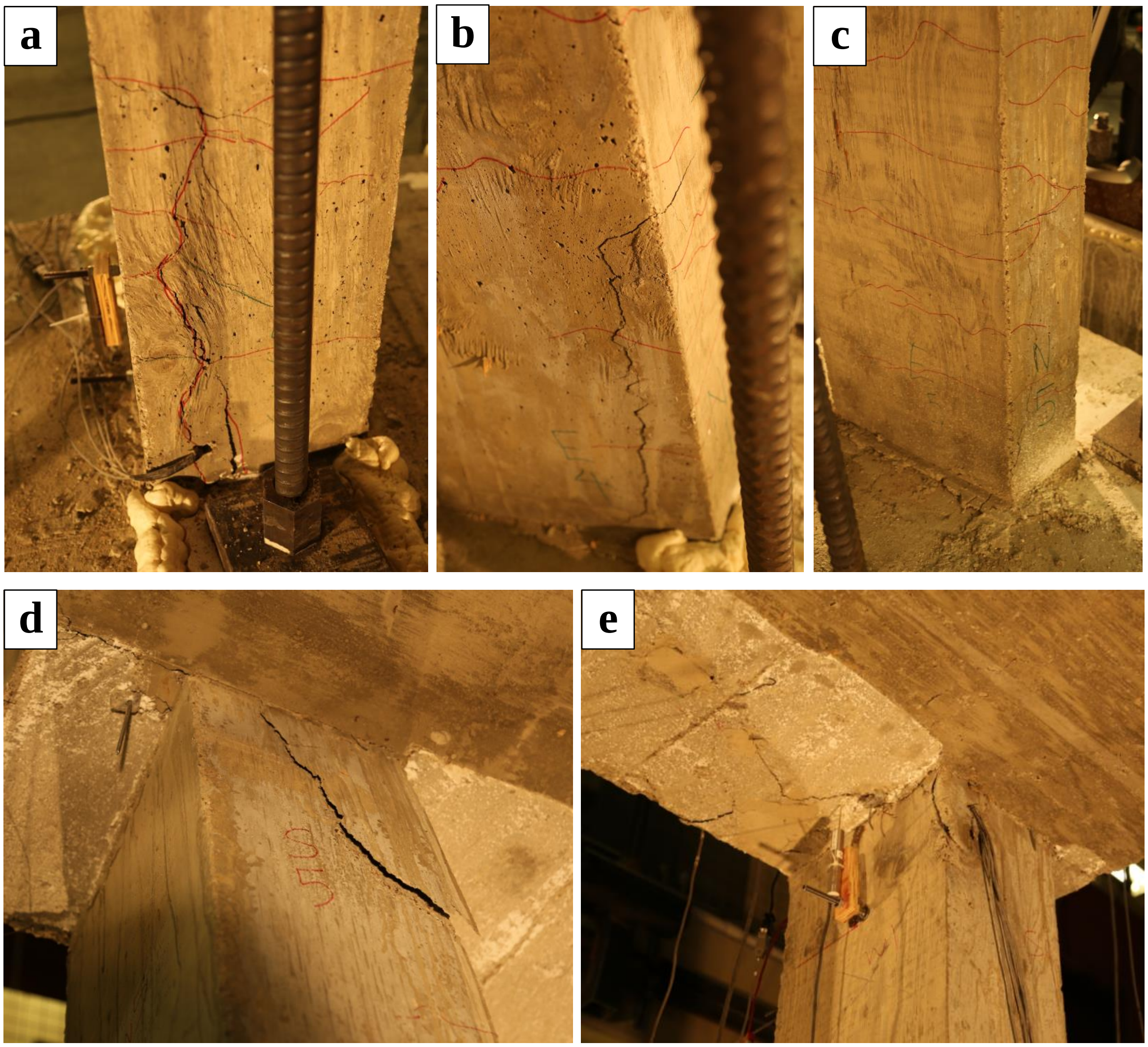

Figure 4-10: 2.0% Drift: (a) C3 Base (North), (b) C4 Base (East), (l) C5 Base (North and East), (d) C5 Top (South), (e) C1 Top (South) – Test 1

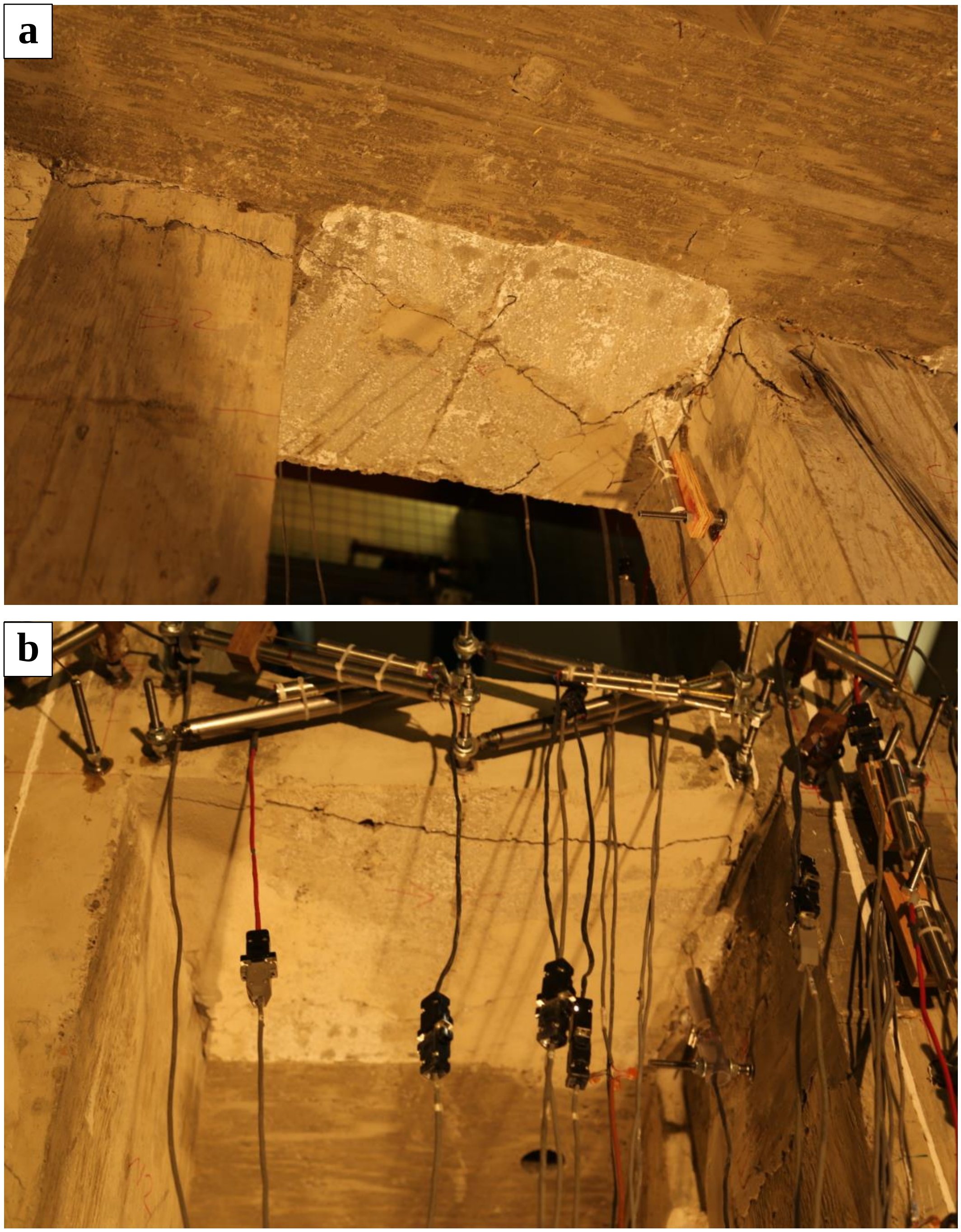

Figure 4-11: 2.0% Drift: (a) Ledge Beam between C2 and C1 (South), (b) Ledge Beam Between C3 and C2 (North) – Test 1

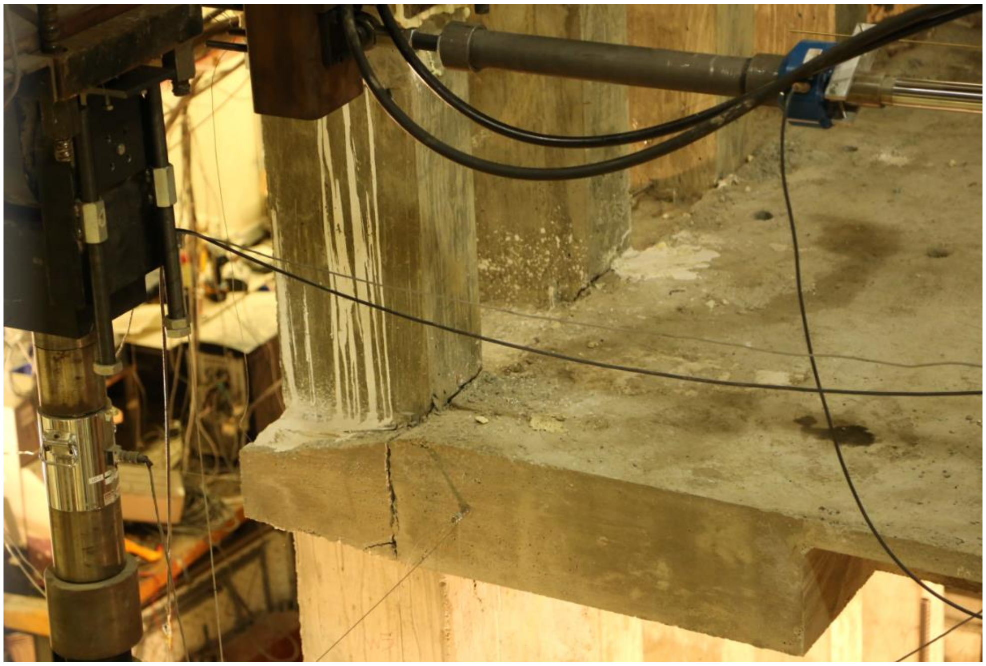

Figure 4-12: 2.0% Drift: Slab View (West) – Test 1

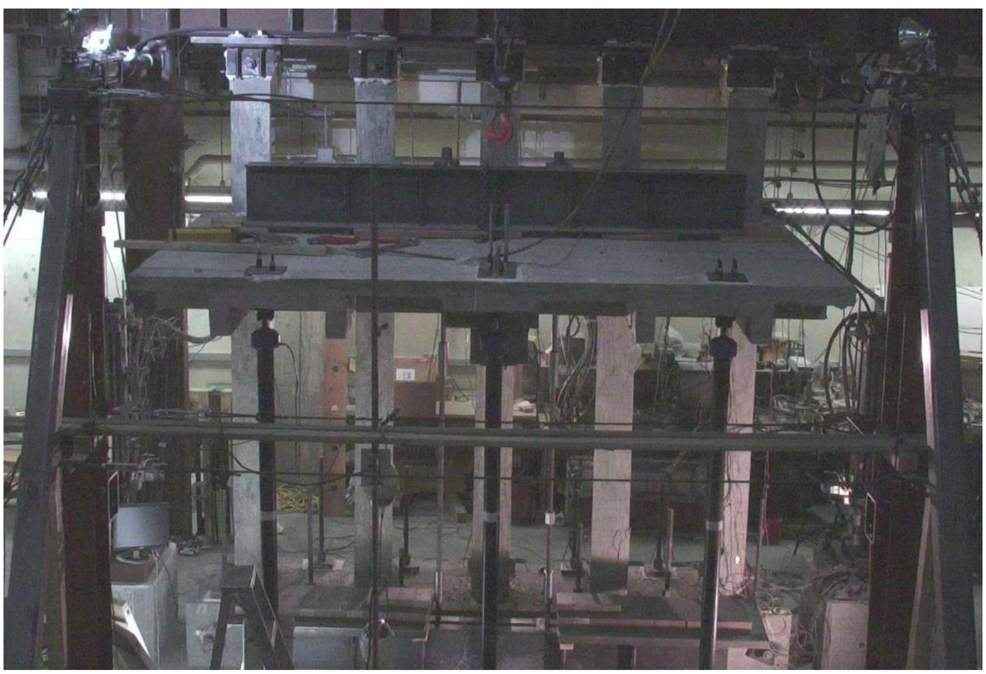

Figure 4-13: 2.0% Drift: Overall View (South) – Test 2

As shown in Figure 4-14, the specimen was experiencing plastic deformation, while it had not lost lateral load capacity yet. The observed damage at this stage was similar to the previous drift ratio, with the cracks growing in number, size, and depth.

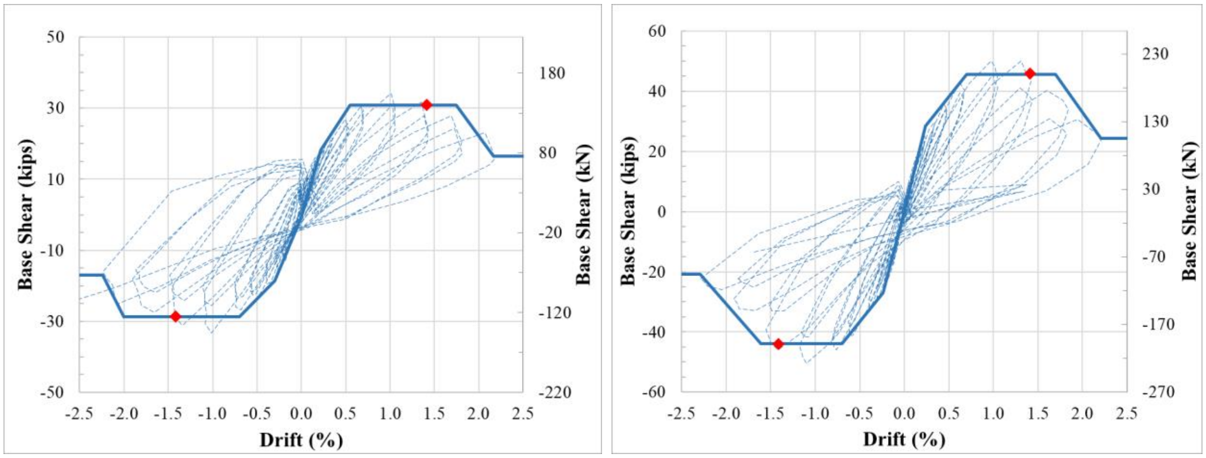

Figure 4-14: Correlation of Observed Damage at 2.0% Diagonal Drift Ratio with Load-Deformation Hyteresis of Test 1 – In-Plane (Left), Out-of-Plane (Right)

4.2.4. 2.5% Drift Ratio

Fin Columns

Vertical lap-splice failure cracks were observed, and were more pronounced at the bases of C3, C4, and C5, on their narrow face (north side), with some concrete cover spalling at C3. Due to the smaller cross section of the concrete column at their narrow face (north side), more damage was expected on that side. The cracking was more subtle at the base of the other columns. New cracks were developed at the top hinge of the specimen on C3, where it connected to the top steel transfer beam (Figure 4-15).

Ledge Beams

Concrete spalling occurred at the ledge beam connecting to C1, at the location of the interior slab joist. While some ledge beams had less severe shear cracks than others, overall wider and deeper shear cracks were observed on the beams. The beam-column connections overall did not show any damage or sign for potential failure (Figure 4-16).

Slab System

The crack along the slab at the interior face of the fin columns were observed at the lower end of the transverse beam, but the slab system had not separated from the frame. Concrete spalling occurred at the half-ledge beams at both ends of the specimen (Figure 4-17).

Overall

Concrete spalling was observed at a number of hinge locations on the narrow side (north face) of the columns, with deeper cracks. Figure 4-15 to Figure 4-18 show component damage and an overall view of the test specimen at the end of the second cycle at 2.5% drift level. The interior side of the columns (south side), which was the wider side of the columns (larger cross-sectional area) experienced less damage and no spalling.

Figure 4-19 shows the correlation of observed failure cracks and the drift ratio on the backbone curve. As observed on the hysteresis loops, the specimen had lost some of its lateral load capacity, and on the backbone, it is at the point of strength loss. The extent of damage as shown in Figure 4-15 and Figure 4-16, vertical lap-splice failure cracks and some spalling at the beams, were indicators that the specimen was reaching the point of strength loss.

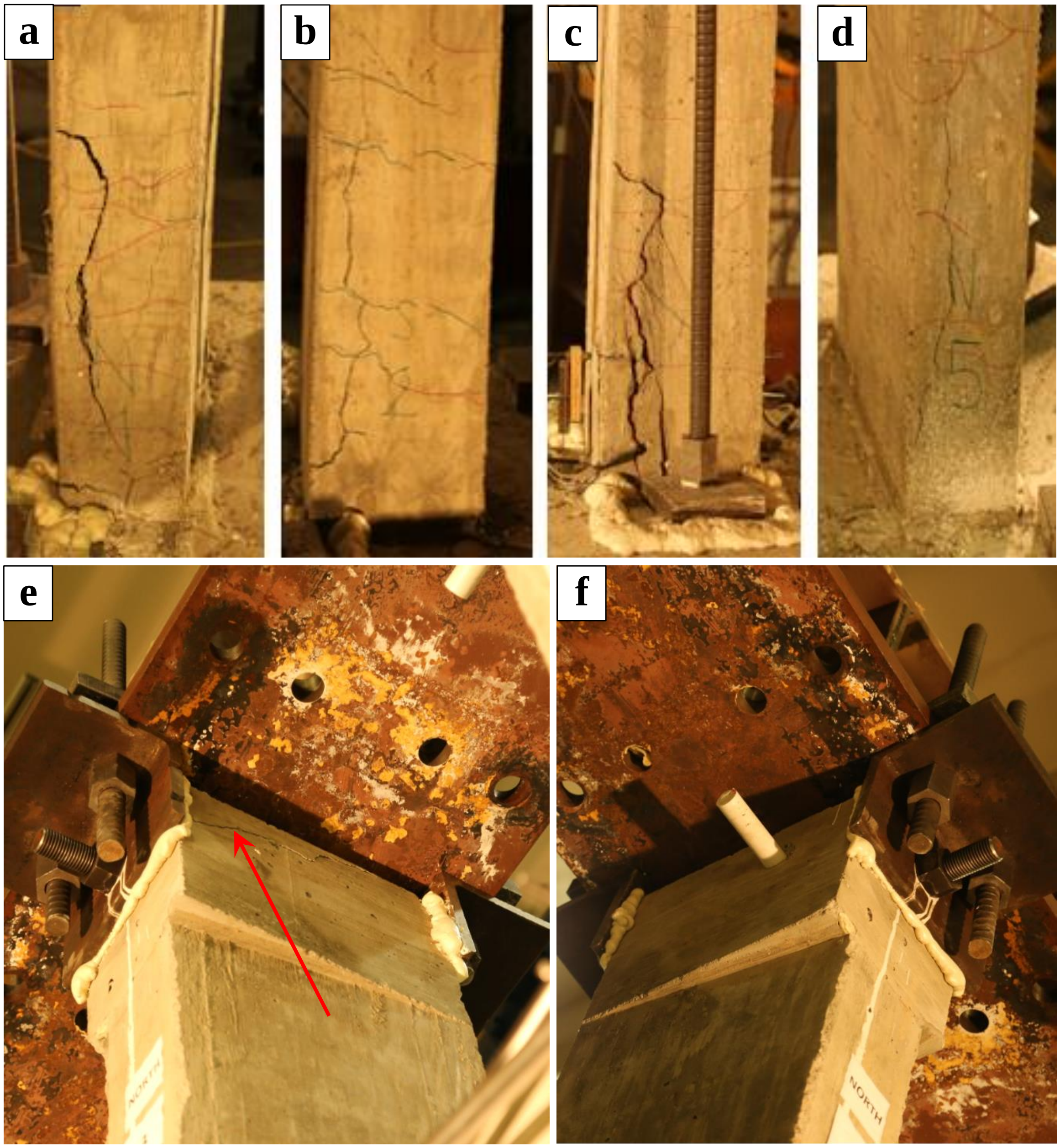

Figure 4-15: 2.5% Drift: (a) C4 Base (North), (b) C2 Base (South), (c) C3 Base (South), (d) C5 Base (North), (e) Crack at C3 Top Hinge (West), (f) C3 Top Hinge (East and North) – Test 1

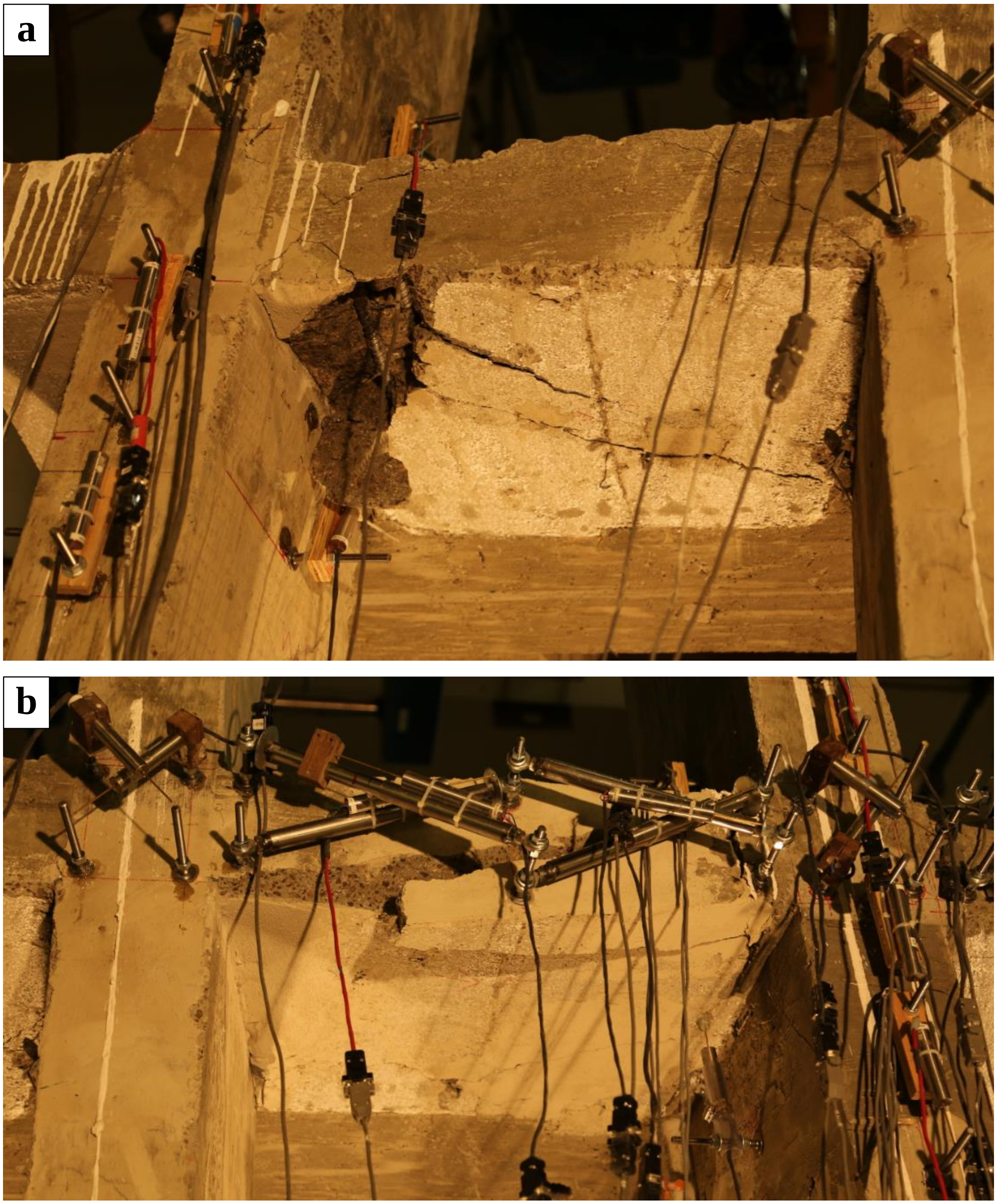

Figure 4-16: 2.5% Drift: Damage at Ledge Beams (North) between (a) C1 and C2, (b) C2 and C3, (c) C3 and C4, (d) C4 and C5 – Test 1

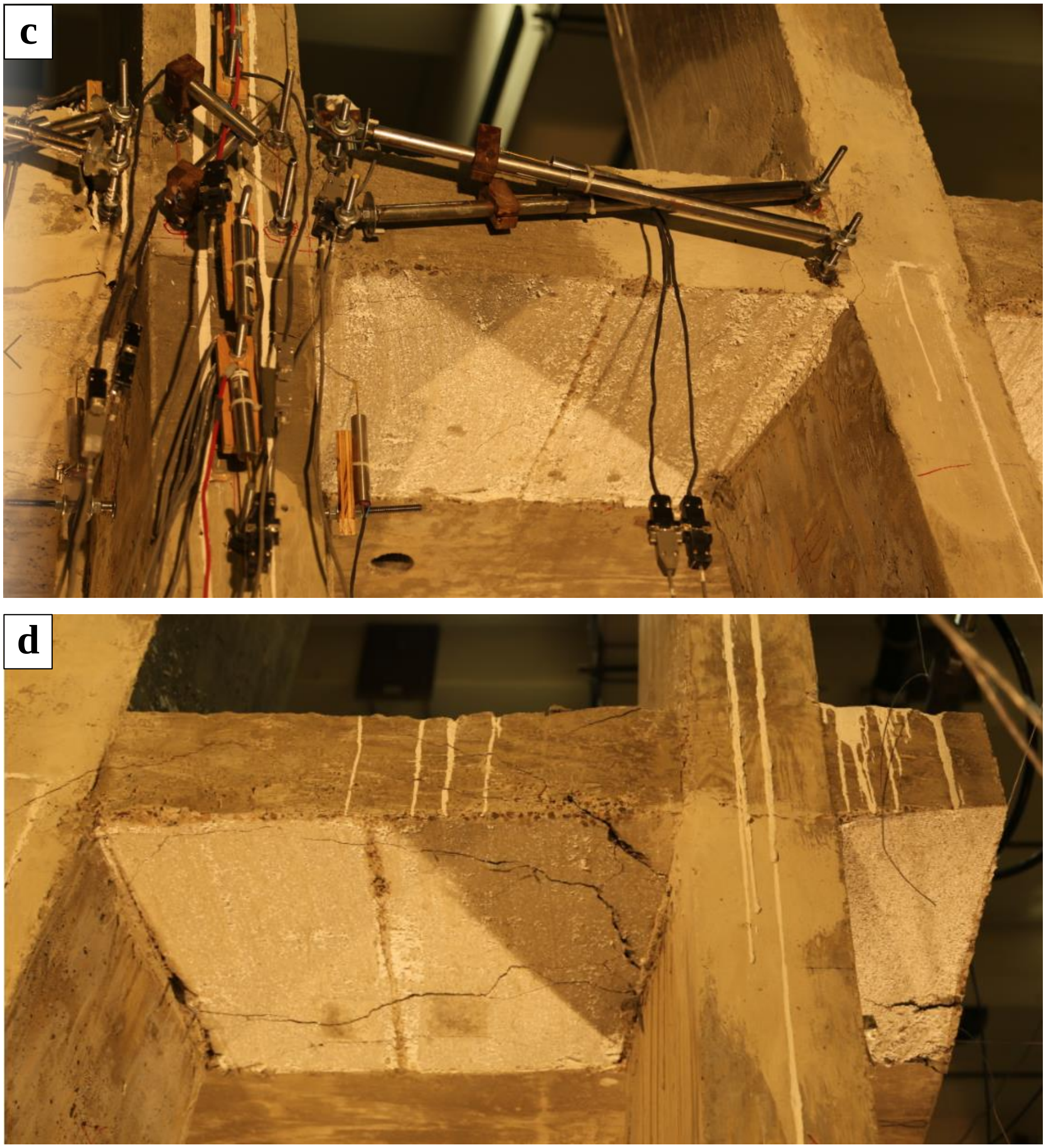

Figure 4-16: 2.5% Drift: Damage at Ledge Beams (North) between (a) C1 and C2, (b) C2 and C3, (c) C3 and C4, (d) C4 and C5 – Test 1 (Cont'd.)

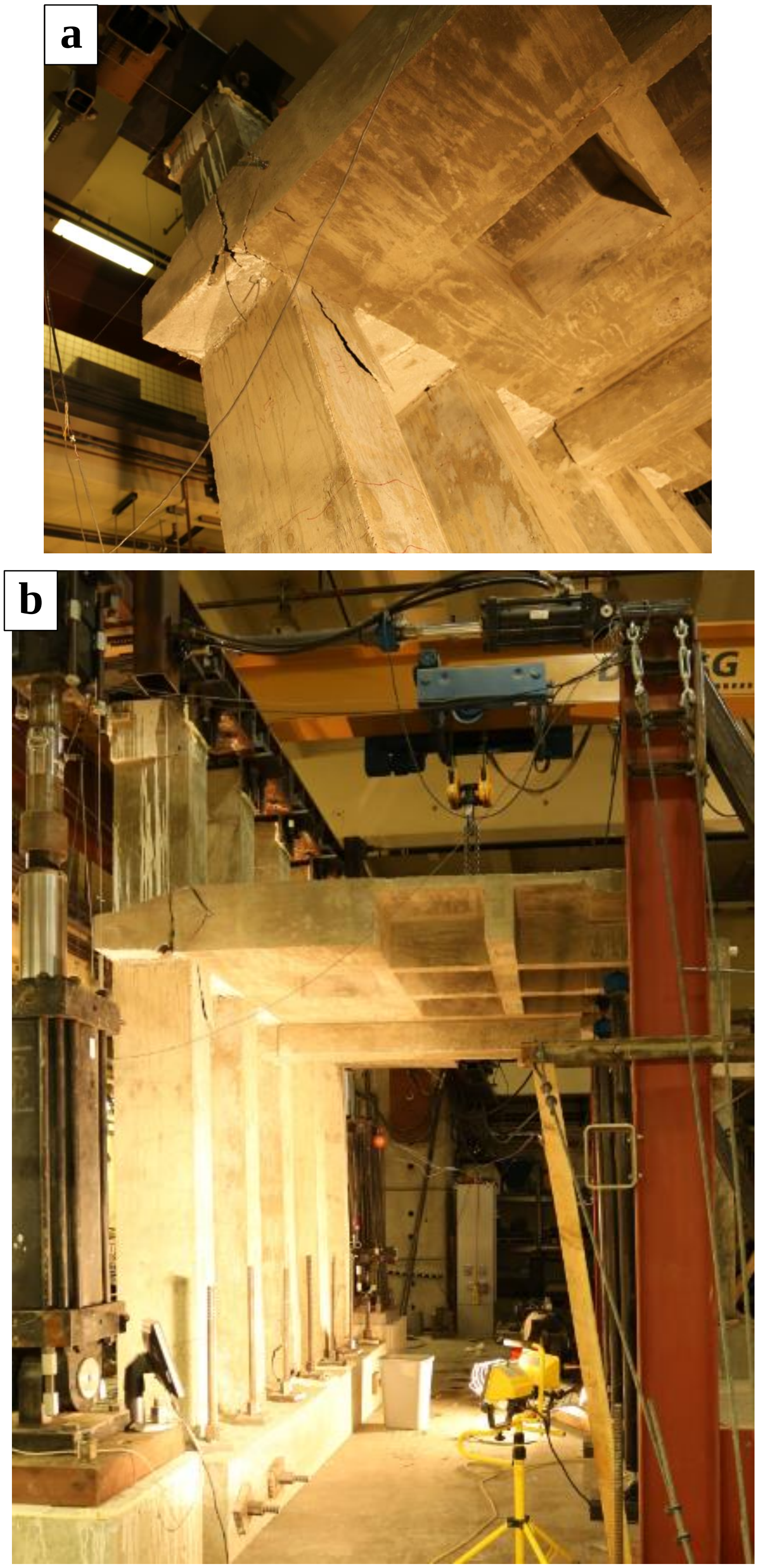

Figure 4-17: 2.5% Drift: (a) Slab Damage at Column Interface, (b) Overall View (West) – Test 1

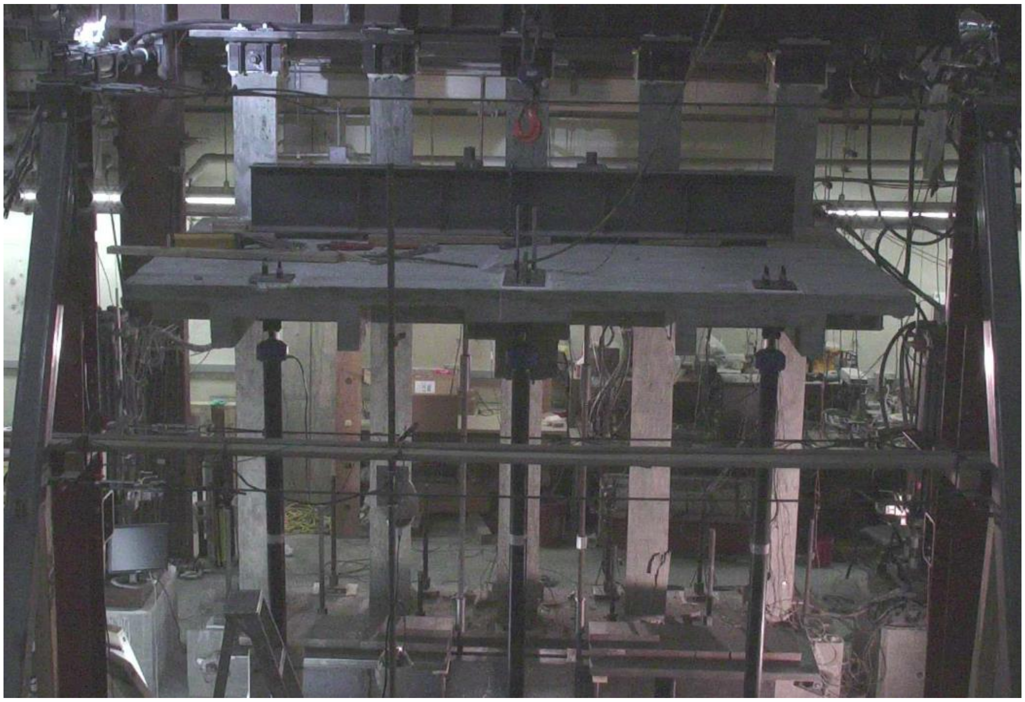

Figure 4-18: 2.5% Drift: Overall View (South) – Test 2

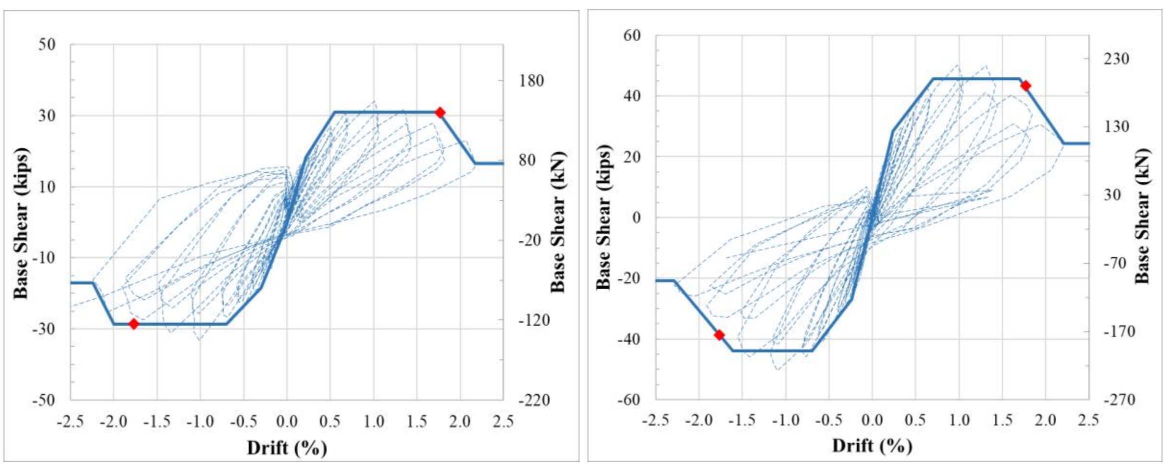

Figure 4-19: Correlation of Observed Damage at 2.5% Diagonal Drift Ratio with Load-Deformation Hyteresis of Test 1 – In-Plane (Left), Out-of-Plane (Right)

4.2.5. 3% Drift Ratio

Fin Columns

Vertical lap-splice failure was observed at the narrow side (north face) of all column bases, mostly pronounced at C3, with concrete spalling at both narrow and wide sides. This was attributed to the deep transverse beam applying large demands to this column. Top hinge of the columns sustained some damage, but they were not nearly as damaged as the bases, and concrete spalling wan not observed. Damage at the top of C3 (south side) was more pronounced as shown in Figure 4-20. See Figure 4-21 for lap splice failure at the base of the columns.

Ledge Beams

Shear cracks appeared at the ledge beams that had not sustain much damage prior to drift ratio of 3%, and some concrete spalling occurred (Figure 4-22).

Slab System

The crack along the slab at the interior face of the fin columns grew wider and more spalling was observed at the half-ledge beams at the ends of the specimen. Some crushing of the concrete core was observed at the ledge beams (Figure 4-22).

Overall

Overall, the specimen softened, lost approximately 36% of its lateral load capacity (39% in Test 1 and 34% in Test 2) but did not reach collapse nor lost its gravity load carrying capacity (Figure 4-23).

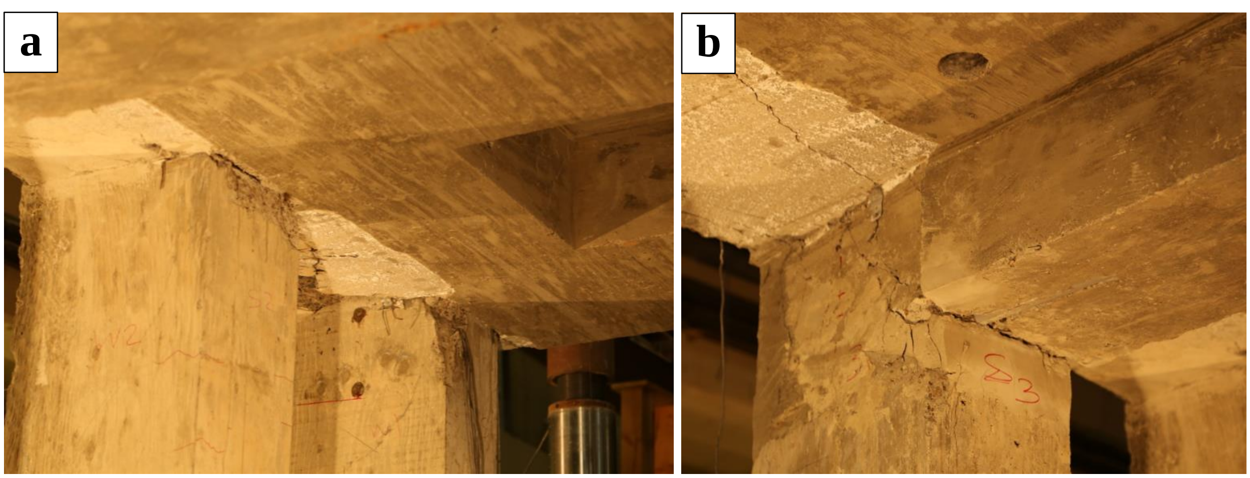

Figure 4-20: 3.0% Drift: Damage at Top of Columns (South) (a) C1 and C2, (b) C3– Test 1

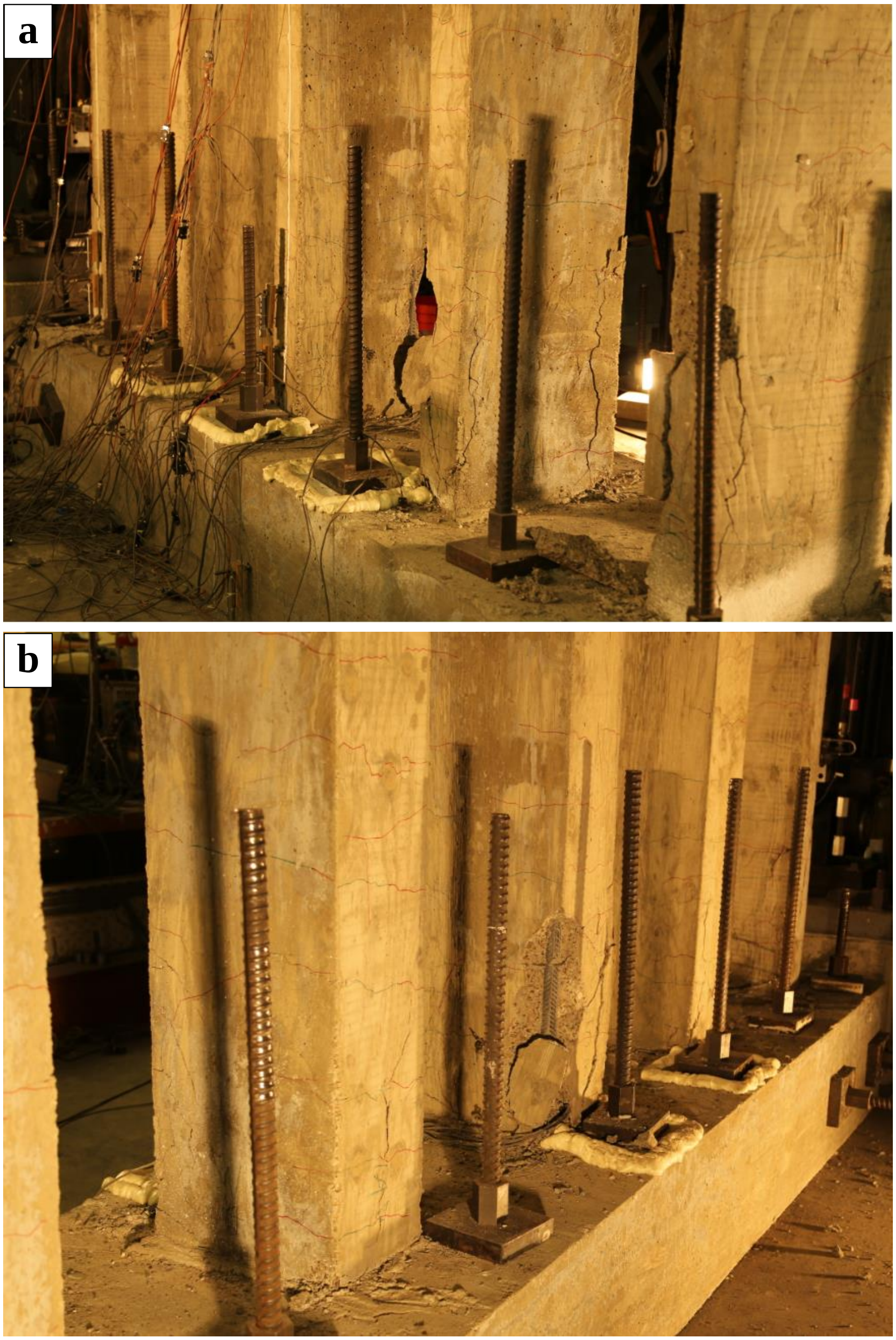

Figure 4-21: 3.0% Drift: Damage at Column Bases (a) (North), (b) (South) – Test 1

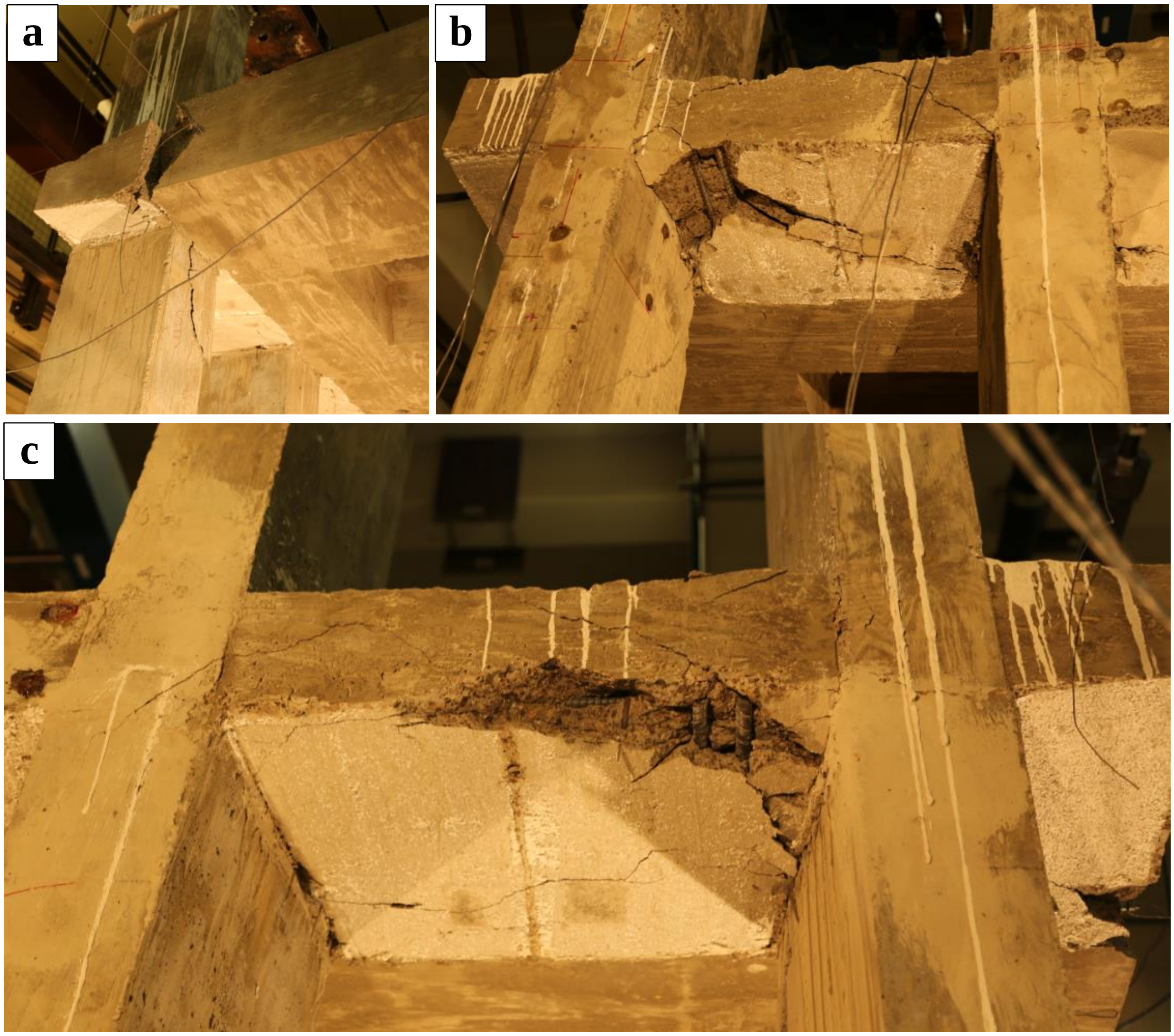

Figure 4-22: 3.0% Drift: (a) Slab Edge at C5, (b) Ledge Beam between C1 and C2 (North), (c) Ledge Beam at C4 between C5 (North) – Test 1

As shown in Figure 4-24, the specimen had lost a significant portion of its lateral load capacity (36% out-of-plane and 35% in-plane between two tests), but it had not yet reached its residual strength.

Figure 4-23: 3.0% Drift: Overall View (South) – Test 2

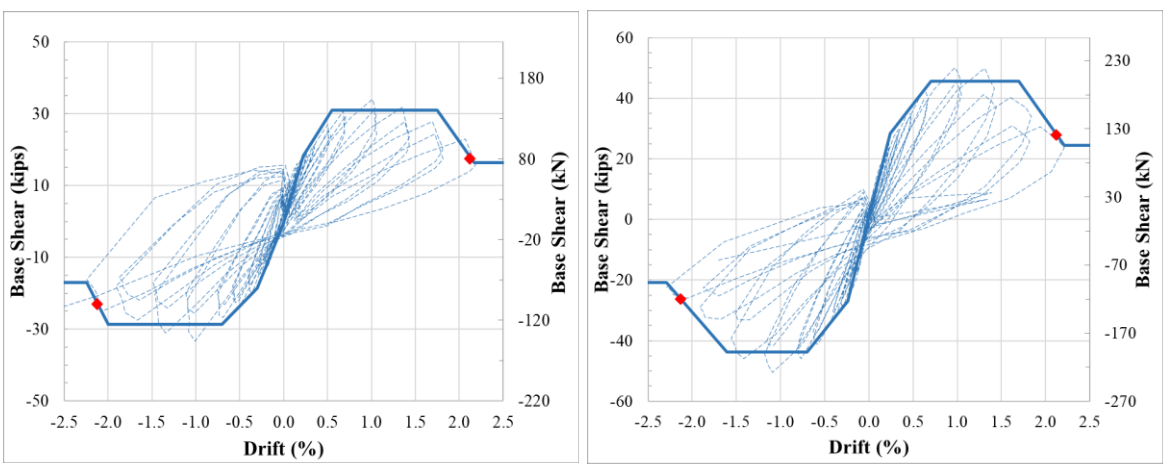

Figure 4-24: Correlation of Observed Damage at 3.0% Diagonal Drift Ratio with Load-Deformation Hyteresis of Test 1 – In-Plane (Left), Out-of-Plane (Right)

Figure 4-25 shows a comparison of the progression of damage at the ledge beams at different drift ratios. It is observed that the ledge beam and the thickened slab did not develop their full capacities at the same time and the ledge beams sustained more damage. Test pictures from both tests can be found in Appendix E.

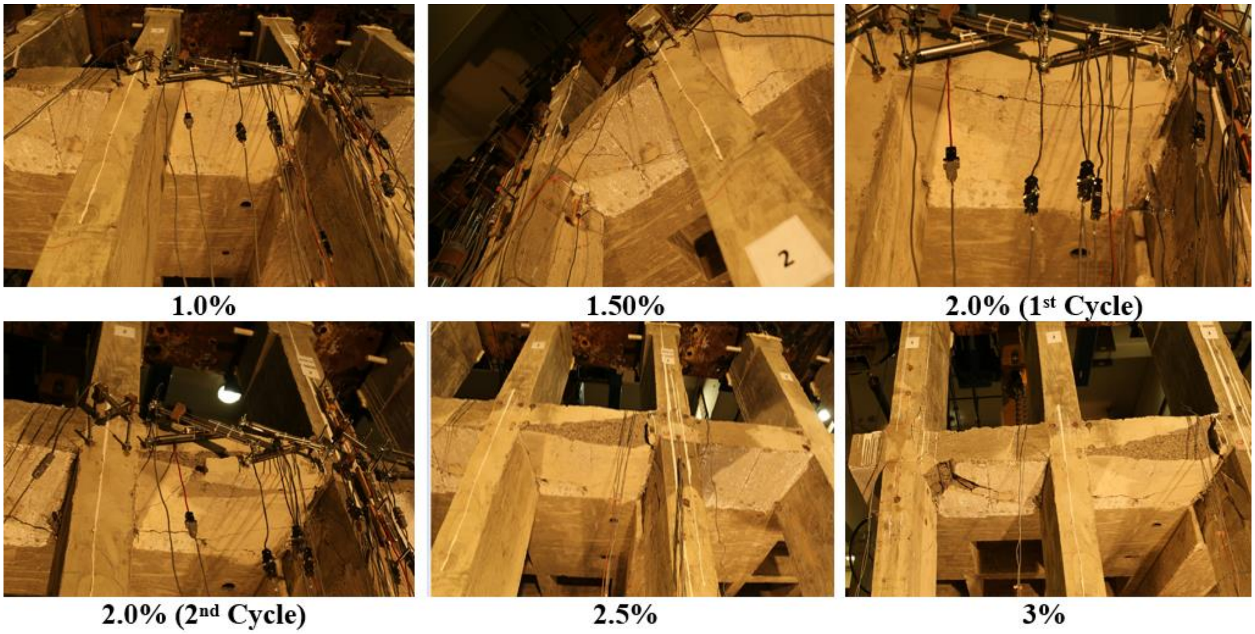

Figure 4-25: Progression of Damage in Ledge Beams – Test 1

4.2.6. 6.25% Drift Ratio

Despite the observed damage, most significantly at the base of C3, some of the ledge beams, and the slab connection to the frame, the specimens did not lose their gravity load bearing capacity, nor sustained more than 50% drop in their lateral load capacity up to lateral drift ratio of 3%. Hence, to examine the deformation capacity of the specimens, and possibly reaching collapse, Specimen-1 was pushed in the in-plane direction to lateral drift ratio of 6.25%, and to 5% drift ratio in the opposite direction (Figure 4-26). This was the maximum deformation capacity available given the actuator stroke and safety measures at the testing facility. Figure 4-27 shows the correlation of observed damage on the load-deformation hysteresis loops, and Figure 4-28 through Figure 4-29 show the extensive concrete spalling and damage at the bases of all columns, at top of the columns and the ledge beams, and the south side of the columns at the slab.

Figure 4-26: Test Specimen at 6.25% Lateral Deformation – Test 1

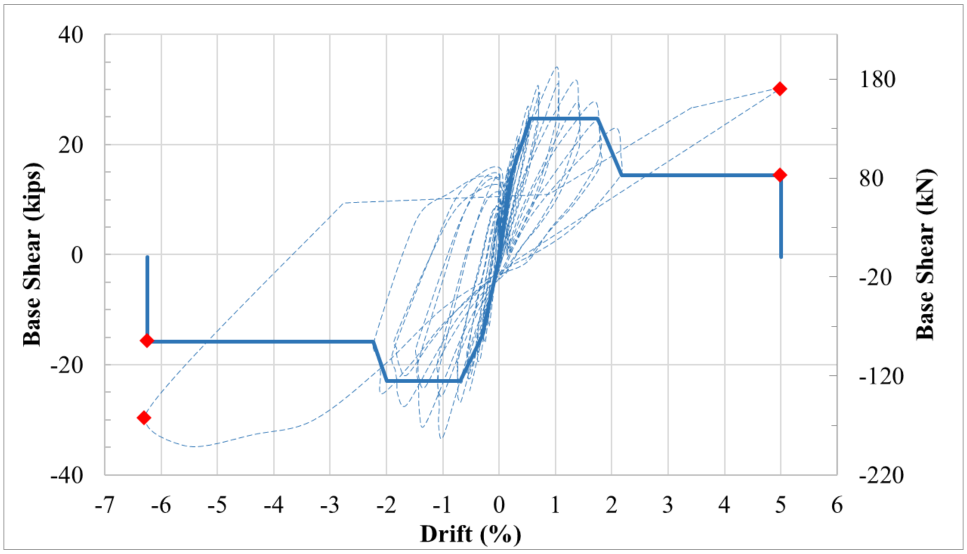

Figure 4-27: Correlation of Observed Damage at 6.25% In-Plane Drift Ratio with Load-Deformation Hyteresis of Test 1

Figure 4-28: 6.25% Drift: Overall Damage at Lower Level – Test 1

Figure 4-29: 6.25% Drift: Damage at Top of Ledge Beams and Slab – Test 1

Figure 4-30: 6.25% Drift: Close-Up Damage Condition at Column Bases (Left to Right: C1 to C5) – Test 1

As observed in Figure 4-27, the specimen maintained its residual strength until the end of the test without experiencing collapse. The hysteresis loops indicated some gain in the base shear when the specimen was pushed to 6.25% drift ratio which was attributed to four reasons: 1) the loading to this drift ratio was monotonic, which in general tends to produce higher base shears in comparison to cyclic loading as shown in Figure 4-31 (ATC, 2017), 2) the hysteresis loops of up to drift ratio of 3% were obtained by following the half clover loading protocol (biaxial loading), while this time the specimen was pushed unidirectionally in the in-plane direction, hence not degrading as fast, 3) the rigid links supporting the slab were designed to provide the desired rotations of 3 to 4%, however, while they seemed to have accommodated the 6% rotation, it is believed that they were not fully extending, hence, they provided some lateral resistance, 4) at this drift ratio the rotation limit of the test setup, specifically at the hinges supporting the out-of-plane actuators, was surpassed. This in turn resulted in some resistance at those hinges which caused the base shear to increase.

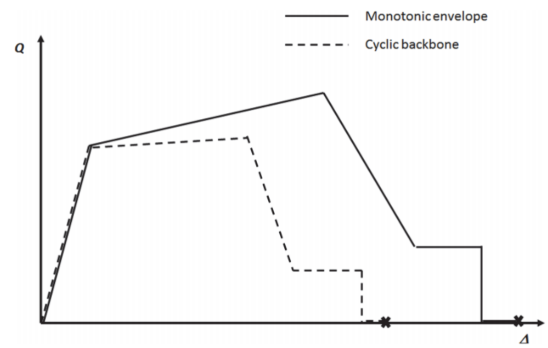

Figure 4-31: Representative Cyclic and Monotonic Backbone Curves (Figure 2-5 of ATC, 2017)

Additionally, the in-plane component of the vertical actuators load, the slab support reactions, and the out-of-plane actuators loads, were also higher due to the larger rotation. The out-of-plane actuators did not exert any force to push the specimen in the out-of-plane direction, but only to keep it in place. As shown in Figure 4-32, that force and hence its in-plane component was negligible.

Figure 4-32 shows the reading from the load cell installed on the in-plane actuator on the left axis, and the in-plane component of other forces contributing to the in-plane base shear, on the right axis. In this figure, the in-plane actuator load (solid gray line) shows an increase in the final loading cycle, which is believed to be due to the four reasons mentioned above.

The hysteresis loops in Figure 4-27, consider the in-plane component from the vertical actuators (7.6 kips), slab supports (~0.95 kips), and out-of-plane actuators (~0.65 kips) in the total in-plane base shear. The sum of these three forces caused a significant increase (~54%) to the residual strength at the end of the 3% cycle, which was approximately 17 kips.

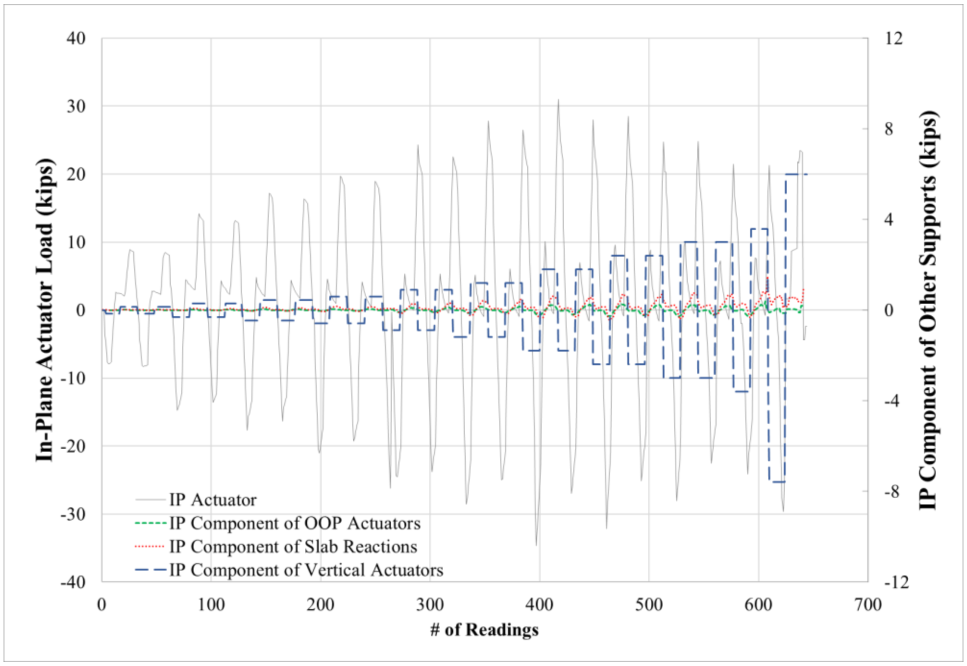

Figure 4-32: Contributing Forces to the In-Plane Base Shear

4.3. Data Processing

To process the data obtained from the test, some corrections were required to the lateral displacements recorded by the string pots and LVDTs and forces registered from the actuators.

The global displacements of the test specimens, measured by the string pots, were corrected for the base slip in both directions (any slip was considered as rigid body motion and subtracted from the slab level and top-level lateral displacements). Base slip was measured using three LVDTs located on the strong floor and attached to the base block. Two LVDTs measured the base block movements in the in-plane direction, and one in the out-of-plane direction (Figure 3-29 and Figure 3-30).

The in-plane loading history and the base slip measured by one of the LVDTs in the in-plane direction are shown versus time in Figure 4-33. See Appendix F for all base slip histories. The base slip was established to be negligible, nonetheless the global displacements of the test specimens were corrected by the base slip in both directions.

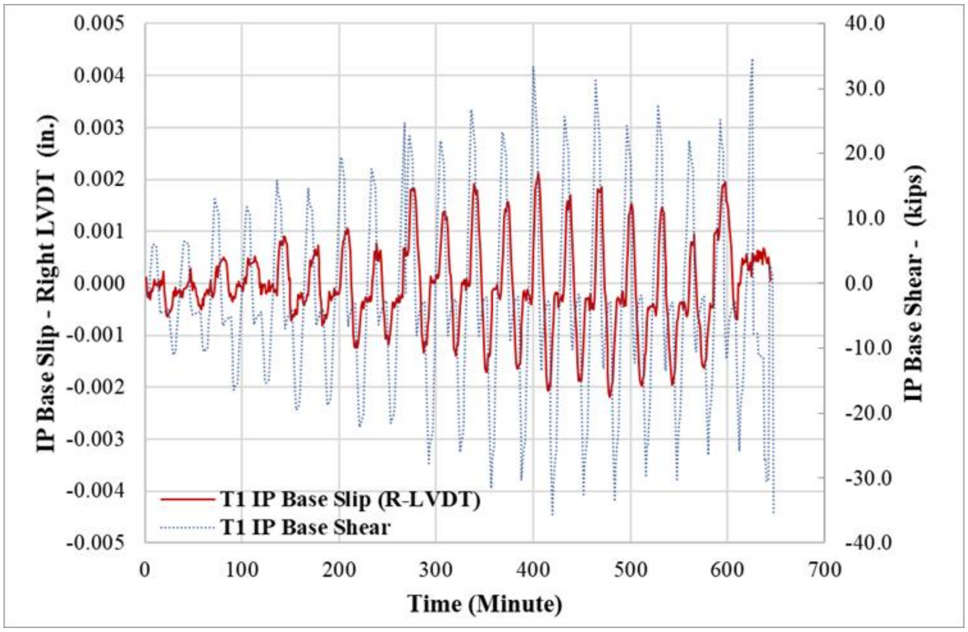

Figure 4-33: In-Plane Load History and Average In-Pnae Base Slip History versus Time (Test 1)

Since the actuators were exerting some load onto the test specimen at all times, and the actuators would rotate as the specimen was pushed in one direction, all actuators could produce load components in the vertical, in-plane, and out-of-plane directions simultaneously (Figure 4-34). Hence, the base shear in each direction was the summation of all actuator load components in that particular direction.

Figure 4-34 shows a schematic top view of the in-plane actuator, applying the in-plane force (P_{IP}) to the specimen. When the specimen was pushed (or pulled) by the out-of-plane actuators, the in-plane actuator rotated by an angle θ (or -θ). This rotation resulted in load components in the in-plane (P_{IP-IP}) and out-of-plane (P_{IP-OOP}) directions. Similarly, the out-of-plane actuator load (P_{OOP}), would have an in-plane (P_{OOP-IP}) and an out-of-plane ($P_{OOP-OOP}$) component when pushed (or pulled) by the in-plane actuator.

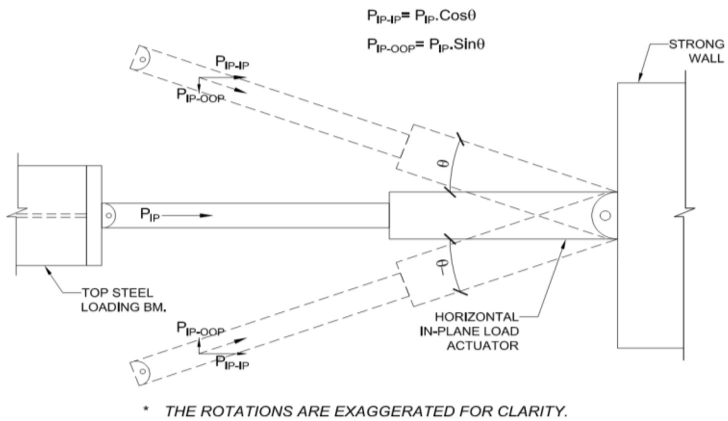

Figure 4-34: Schematic Top View of In-Plane Actuator at Rotation θ

The same is true for the vertical actuator load (P_{Grav}) that generated both in-plane ($P_{Grav-IP}$) and out-of-plane ($P_{Grav-OOP}$) loads. The in-plane and out-of-plane components of all the actuator loads were considered to provide the total base shear, for each direction of loading.

The test backbone curves were obtained with the base shear adjusted with the consideration of shear components from the actuators (<0.01 of base shear) and the displacements adjusted for base slip (<0.001 of lateral deformation at slab level) as discussed in section 4.4

4.4. Load-Deformation Responses

The lateral load versus story drift relationships at slab level for Test 1 and 2 for the in-plane and out-of-plane directions are shown in Figure 4-35 to Figure 4-37. The values for the base shear are obtained from the actuator load cells, including the adjustments mentioned in section 4.3. The story deformations were obtained from string potentiometers (pots) that measured the displacements in the in-plane and out-of-plane directions at slab level. Since two string pots were used to measure the out-of-plane displacement, the average value of the two was used to obtain lateral drift ratio in that direction. The story drifts were obtained by dividing the displacements in the in-plane and out-of-plane directions measured at slab level by the story height (8 ft. 0.5 in. (2451 mm)).

There is a slip observed in the force in both directions of loading at point of (0, 0). The slip occurred due to a mechanical switch through form positive to negative loading and it was more prominent in the in-plane direction as shown in Figure 4-34 and Figure 4-35. The in-plane actuator was taken down for observation of the valves and reinstalled after Test-1. Since the orientation of the valve was switched during installation, the direction of the slip also switched as shown below.

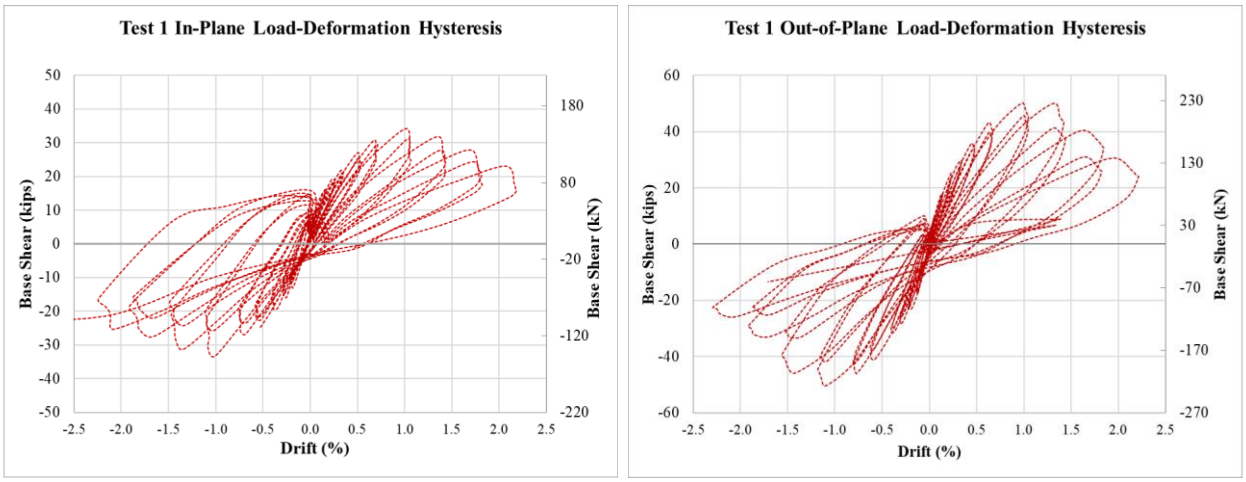

Figure 4-35: Test 1 Load-Deformation Hysteresis: In-Plane (Left), Out-of-Plane (Right)

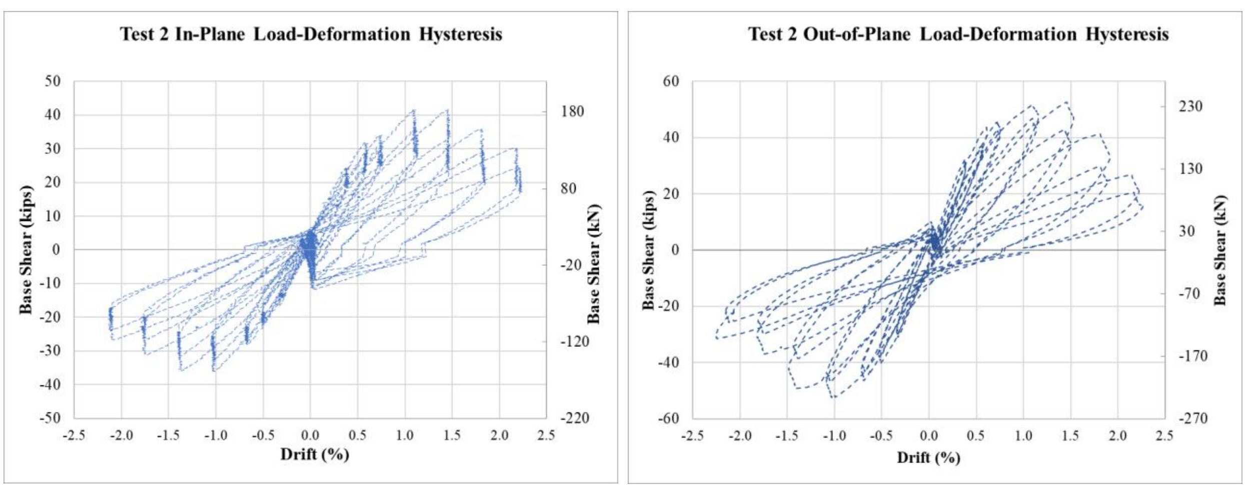

Figure 4-36: Test 2 Load-Deformation Hysteresis: In-Plane (Left), Out-of-Plane (Right)

The hysteresis relationships are in close agreement between Test 1 and Test 2, with Test 2 reaching higher maximum base shear, which was attributed to the additional gravity load applied to the columns and the higher strength of concrete at the time of the second specimen due to longer curing time. This difference was approximately 17.5% in the positive in-plane direction, 16.6% in the negative in-plane direction, 4.8% in the positive out-of-plane direction, and 4.4% in the negative out-of-plane direction.

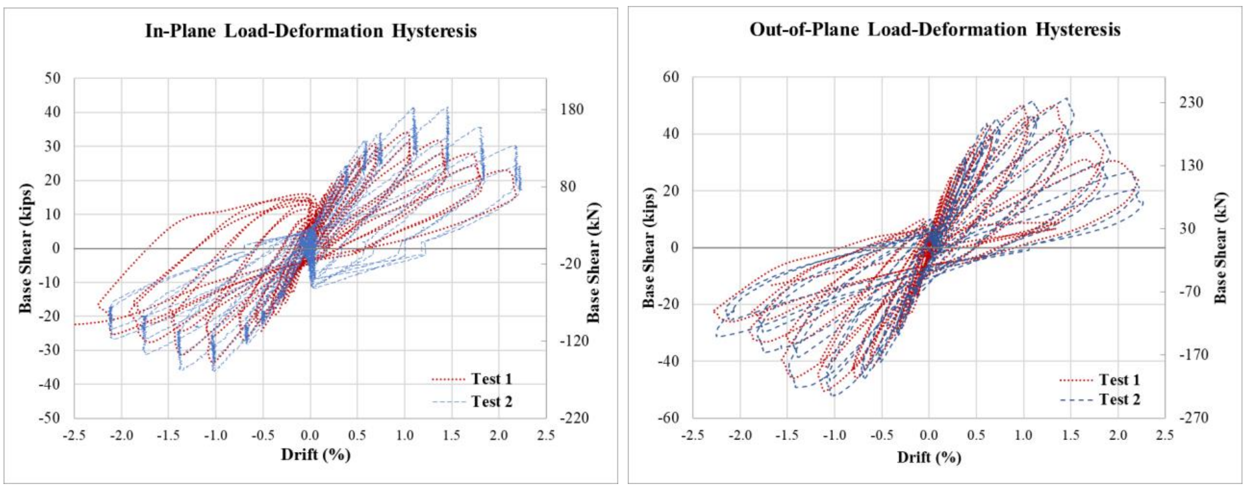

Figure 4-37: Comparison of Load-Deformation Hysteresis in Test 1 and 2: In-Plane (Left), Out-of-Plane (Right)

To obtain the corresponding backbone curve for each test and each direction of loading, provisions of ASCE 41-13, section 7.4 were used as illustrated in Figure 4-38. A fitted curve was drawn by connecting the points of maximum load-drift of the first cycle at each loading/drift level. A line from the point of zero-zero was drawn parallel to the initial slope of the test up to 0.6 of maximum shear (point A on Figure 4-38). From point A, the line was continued parallel to the fitted curve, to reach average peak shear (point B). After this point the value of shear remains constant, and the curve continues horizontally until the lateral deformation associated with 0.8 of peak shear on the fitted curve is reached (point C).

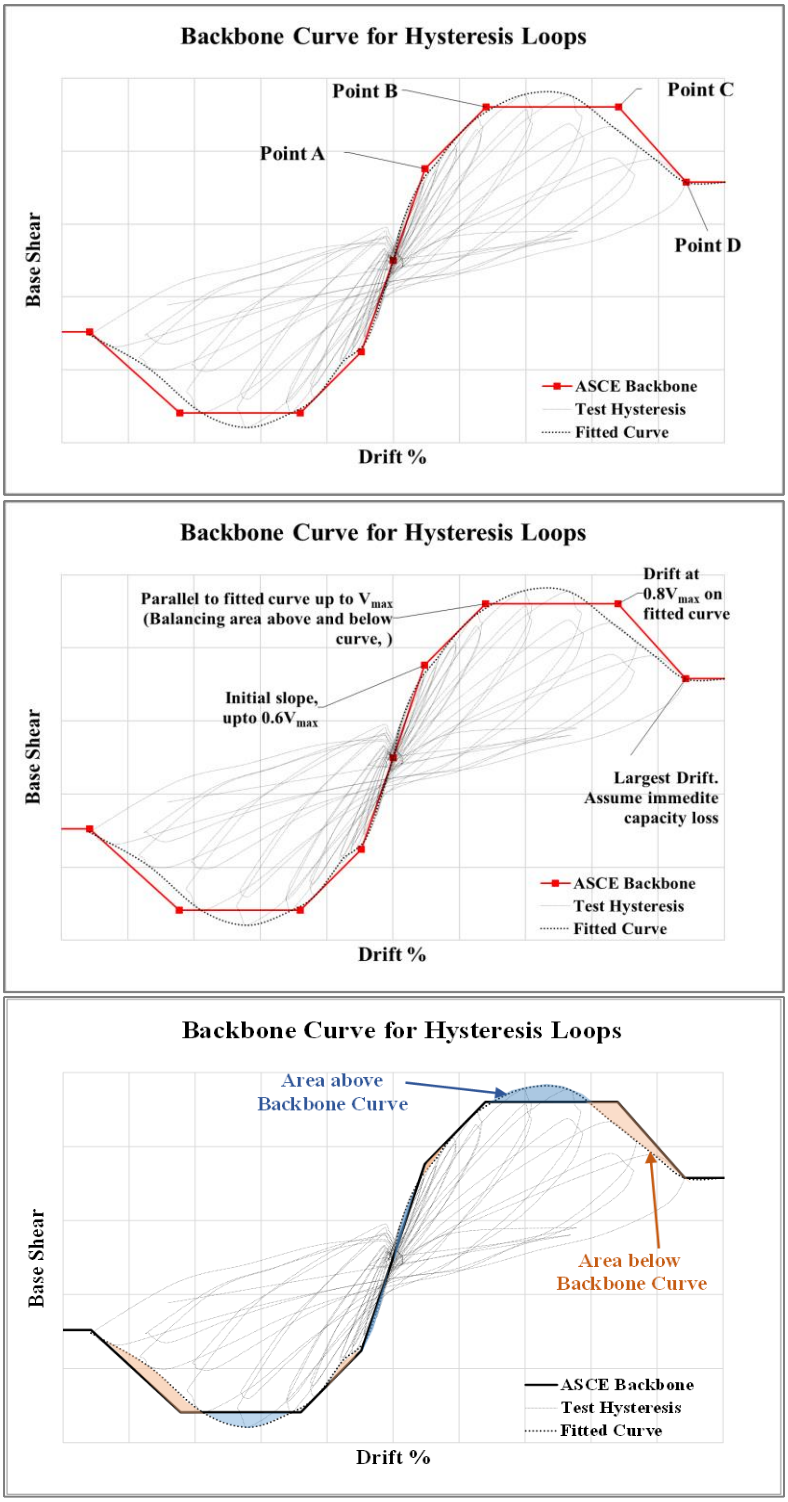

Figure 4-38: ASCE 41-13 Procedure to Obtain Backbone Curve from Test Hysteresis Data (Test 2, Out-of-Plane Direction)

Point C is then connected to point D, the last point (largest deformation) on the fitted curve where a residual plateau is extrapolated based on judgement, as immediate strength loss was not expected based on the condition of the specimens at the end of the tests. The average peak shear was selected such that the area above the backbone curve to the fitted was balanced with the area below the backbone curve, to the fitted curve. Given points A, B, and C are a function of the maximum base shear, this was an iterative process. This method was performed the force-deformation hysteresis relations obtained from Test 1 and 2 in both in-plane and out-of-plane directions, as shown in Figure 4-39 and Figure 4-40, and the average backbone curve of both tests in each direction is shown in Figure 4-41.

The average backbone curves in both loading directions show that the specimen was able to maintain lateral drift ratio of 1.8% prior to strength loss. The specimen sustained in-plane residual strength of 0.63 of the maximum base-shear in the positive direction and 0.48 in the negative direction. These ratios were 0.40 and 0.49 in the out-of-plane direction, respectively.

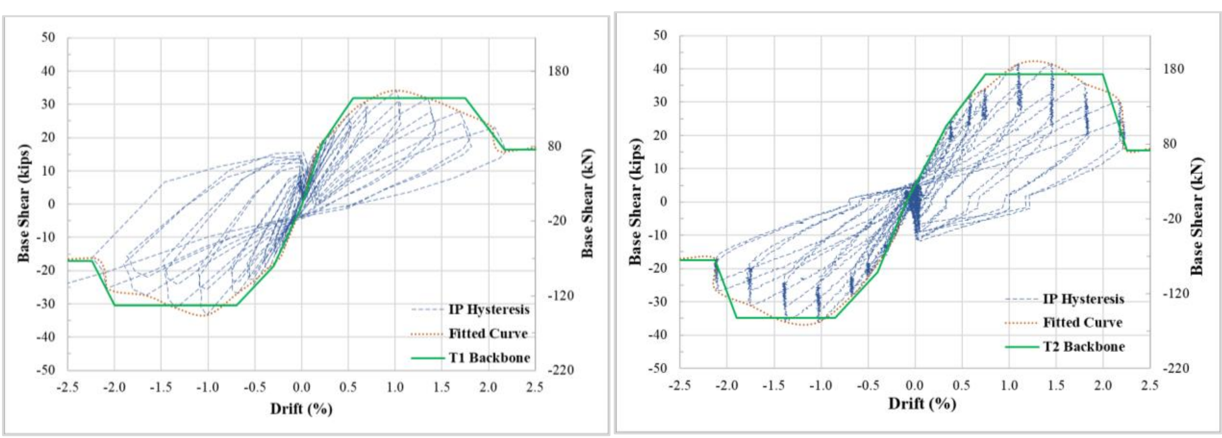

Figure 4-39: In-Plane Load-Deformation Hysteresis and ASCE 41-13 Backbone: Test 1 (Left), Test 2 (Right)

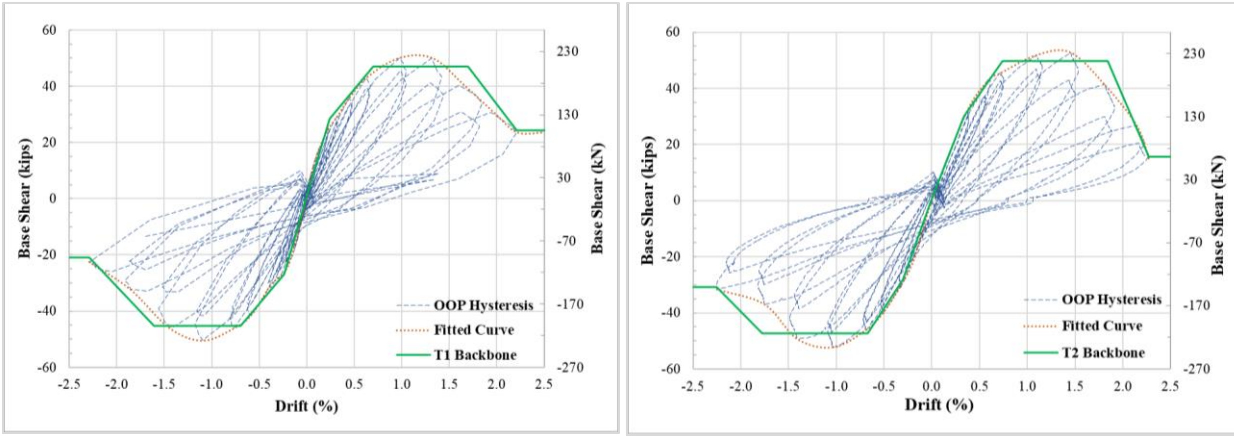

Figure 4-40: Out-of-Plane Load-Deformation Hysteresis and ASCE 41-13 Backbone: Test 1 (Left), Test 2 (Right)

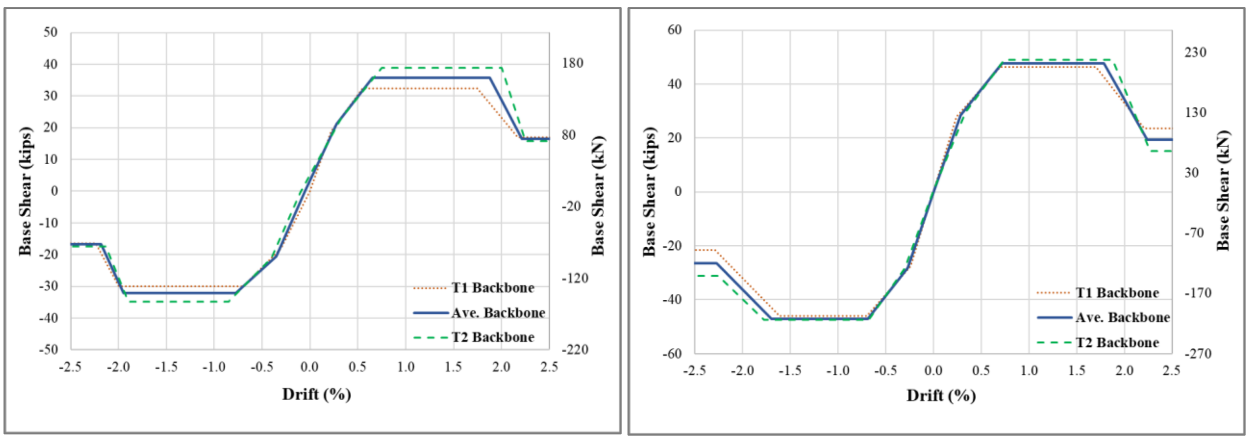

Figure 4-41: Average Backbone Curves: In-Plane (Left), Out-of-Plane (Right)

4.5. Lateral Stiffness

In the in-plane direction, the average elastic range slope is 8800 K-in/in and in the out-of-plane direction it is 12900 K-in/in (see Figure 4-41).

The backbone relations for the two tests were reasonably close, and an average backbone curve is obtained as illustrated in Figure 4-41, for each direction of loading. The initial stiffness in both directions was higher than obtained per ASCE 41 as discussed in section 4.6.

4.6. Test Backbone vs ASCE 41

The governing standard at the time of the test and retrofit program was ASCE 41-13. To further discuss the impact of the testing program on the more accurate prediction of the existing building performance when subjected to seismic forces, backbone curves for the in-plane and out-of-plane directions were generated using ASCE 41-13 Tables 10-5 (for effective stiffness), 10-7 (for non-linear modeling parameters of ledge beams, slab joists and slab beam), and 10-8 (for non-linear modeling parameters of columns). Since the columns had inadequate lap-splices at the base, the modeling parameters from condition *iv* of Table 10-8 were applicable, and the premature failure of the columns without any plastic deformation after yielding in both directions governed the overall performance of the specimens. However, the lap-splice lengths tend to be conservative and full capacity of the splice may be achieved before the bars start slipping. The lap length provided was less than required per section 25.4.2 of ACI 318-14 but the bond stress (f_s) was calculated to be approximately equal to the yield strength of the longitudinal bars (f_y) per equation 10-1 of ASCE 41-13. The flexural capacity of the columns was not reduced in the preliminary analysis but was later adjusted as discussed in section 4.7. See Appendix A and Appendix G for calculations and component non-linear modeling parameters, respectively.

Plot of the deformation backbones obtained from ASCE 41-13 and ASCE 41-17 are plotted along with the backbone curve obtained from the test for the in-plane and out-of-plane directions as shown in Figure 4-42 and Figure 4-43.

In-Plane Direction

While the initial stiffness ratio of the test backbone and the ASCE 41-13 backbone are relatively close, the deformation capacity after yielding, prior to strength loss, and overall deformation capacity before collapse, were significantly underestimated by ASCE 41-13. The strength loss after yielding occurred at drift ratio of approximately 2% and the specimen was pushed beyond 6% in-plane drift ratio without any of the structural components losing their gravity load carrying capacity. For the purpose of comparing the test results to ASCE 41, 6% drift level is assumed to be the point of collapse as shown in Figure 4-42. ASCE 41-13, however, did not allow for any post-yield deformation, and strength loss occurred at approximately 0.60% drift ratio. The building continued to deform to 2% drift before collapse.

Shear strength of the specimen was higher per ASCE 41-13 than observed in the test. This could be attributed to the cyclic bi-axial testing effect which deteriorated the building components faster. This effect was also observed in the base shear in the negative direction, as the test specimens were first pushed in the positive direction, and then in the negative direction as discussed in section 3.6. Another contributing factor was the inadequate lap-splice lengths at the base of the columns (Appendix A). While the columns did not fail in shear, they were not able to achieve full flexural capacity due to premature lap-splice failure at the base.

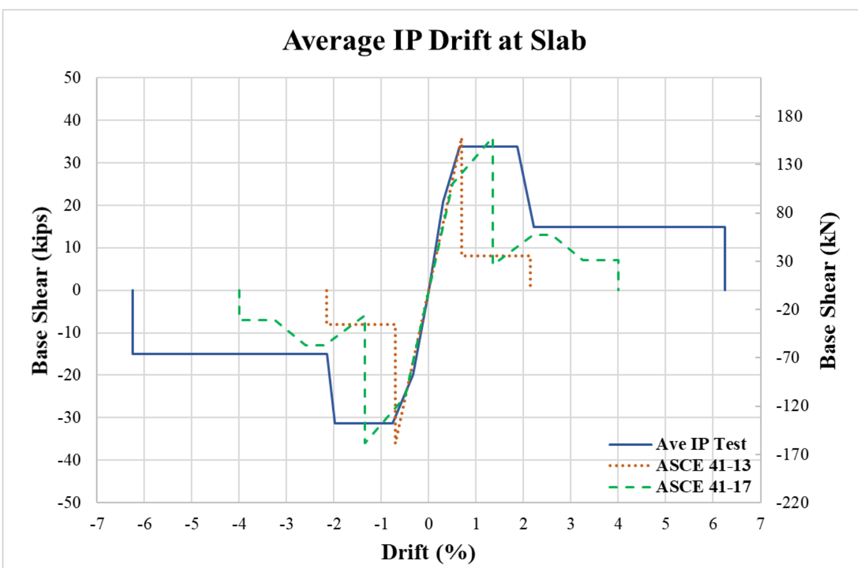

Figure 4-42: Average In-Plane Backbone from Test Compared with ASCE 41-13 and ASCE 41-17 Backbone Curves

Since the governing standard at the time of writing this manuscript was ASCE 41-17, it seemed prudent to include the backbone curves obtained from it and compare it with the test results. Tables 10-7 (for non-linear modeling parameters for beams), and 10-8 (for non-linear modeling parameters for columns) of ASCE 41-17 were used to obtain the modeling parameters (Appendix A). While Table 10-7 is essentially the same as ASCE 41-13, significant changes were made to Table 10-8 of ASCE 41-13 (see Table 4-1) resulting in column modeling parameters in the form of equations rather than the table form, which at times required triple interpolation. ASCE 41-17 generates the non-linear modeling parameters by using equations that incorporate a combination of factors based on a database of approximately 500 pseudo-static tests on reinforced concrete columns subjected to lateral loading. It is expected that it represents existing conditions and columns that lack proper shear detailing or are shear or flexure-shear controlled more accurately. (Ghannoum & Matamoros; Pekelnicky, Hagen, & Martin, 2017; Elwood, et al., 2007)

The backbone curves obtained from ASCE 41-17 non-linear modeling parameters match the experimental test results (the overall performance and deformation capacity) very closely (Figure 4-42) but it underestimates the drift ratio at which strength loss occurs (1.5% vs. approximately 1.92%). The residual strength is about 0.30 times the base shear which is lower than observed in the test (0.45 times the base shear).

Out-of-Plane Direction

The initial stiffness per ASCE 41-13 was lower than observed in the test results (Figure 4-43). Overall deformation capacity before collapse per ASCE 41-13 is close to the out-of-plane drift ratio at the end of the test (2% vs. 2.3%). In the out-of-plane direction the specimen was not pushed monolithically after the end of the test (unlike the in-plane direction), and as a result no information about the building behavior beyond this drift level is not available. In the actual building, it is expected that the building could undergo larger lateral deformation drifts in the out-of-plane direction prior to collapse. The strength loss occurred at drift ratio of approximately 1.8%, and none of the structural components lost their gravity load-carrying capacity throughout or after the test. The failure condition of the columns in this direction was determined to be adequate lap splice lengths, and in case that did not occur, they were deemed shear controlled. In either failure condition, ASCE 41-13 did not allow for any post-yield deformation capacity and strength loss occurred at approximately 0.80% drift ratio. After which the building continued to deform to 2% drift before collapse. The average residual strength ratio in the out-of-plane direction obtained from testing was 0.44 (of the maximum base shear), while the residual strength ratio per ASCE 41-13 was 0.20.

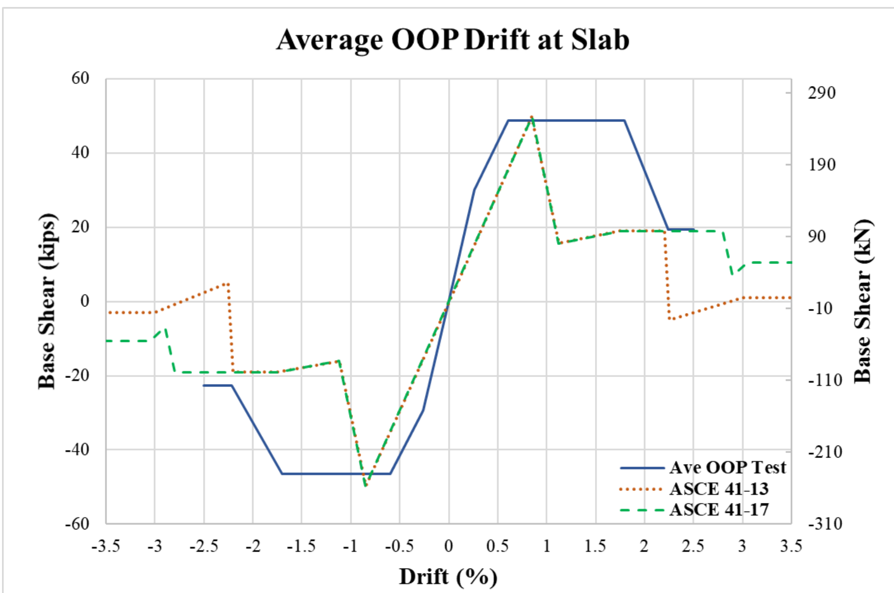

Figure 4-43: Average Out-of-Plane Backbone from Test Compared with ASCE 41-13 and ASCE 41-17 Backbone Curves

Table 4-1: Modeling Parameters and Numerical Acceptance Criteria for Non-linear Procedures – Reinforced Concrete Columns Other Than Circular with Spiral Reinforcement or Seismic Hoops as Defined in ACI 318 (Table 10-8 of ASCE 41-17)

Modeling Parameters	Acceptance Criteria		
	Plastic Rotation Angle (radians)		
	Performance Level		
Plastic Rotation Angles, *a* and *b* (radians) **Residual Strength Ratio, *c***	**IO**	**LS**	**CP**
Columns not controlled by inadequate development or splicing along the clear height[a]			
$a = \left(0.042 - 0.043\frac{N_{UD}}{A_g f'_{cE}} + 0.63\rho_t - 0.023\frac{V_{yE}}{V_{ColOE}}\right) \geq 0.0$	$0.15\,a$ ≤ 0.005	$0.5\,b^b$	$0.7\,b^b$
For $\frac{N_{UD}}{A_g f'_{cE}} \leq 0.5 \left\{ b = \frac{0.5}{5 + \frac{N_{UD}}{0.8 A_g f'_{cE}} \frac{1}{\rho_t} \frac{f'_{cE}}{f_{ytE}}} - 0.01 \geq a^a \right.$			
$c = 0.24 - 0.4\frac{N_{UD}}{A_g f'_{cE}} \geq 0.0$			
Columns controlled by inadequate development or splicing along the clear height[c]			
$a = \left(\frac{1}{8}\frac{\rho_t f_{ytE}}{\rho_l f_{ylE}}\right) \begin{matrix} \geq 0.0 \\ \leq 0.025^d \end{matrix}$	0.0	$0.5\,b$	$0.7\,b$
$b = \left(0.012 - 0.085\frac{N_{UD}}{A_g f'_{cE}} + 12\rho_t^{\,e}\right) \begin{matrix} \geq 0.0 \\ \geq a \\ \leq 0.06 \end{matrix}$			
$c = 0.15 + 36\rho_t \leq 0.4$			

Similar to the in-plane direction, backbone curve obtained from ASCE 41-17 for the out-of-plane direction is shown in Figure 4-43. Although ASCE 41-17 provides a better estimate of the building performance in comparison to ASCE 41-31 and allows for some non-linear lateral deformation before strength loss, it still significantly underestimated the deformation prior to strength loss (0.57% vs 1.75%). The residual strength per ASCE 41-17 was 0.187, which was lower than ASCE 41-13.

4.7. Perform-3D Model – Incorporating Test Results

A series of Perform-3D models of the test specimens were created in order to replicate the test results in the building subassembly. See Figure 4-44 and Appendix G.

Non-linear modeling parameters and stiffness multipliers were obtained from ASCE 41-13 with some adjustments to calibrate the Perform-3D model based on the test observations and recreate the test backbone in Perform-3D (Figure 4-45 and Figure 4-46). These adjustments included the following:

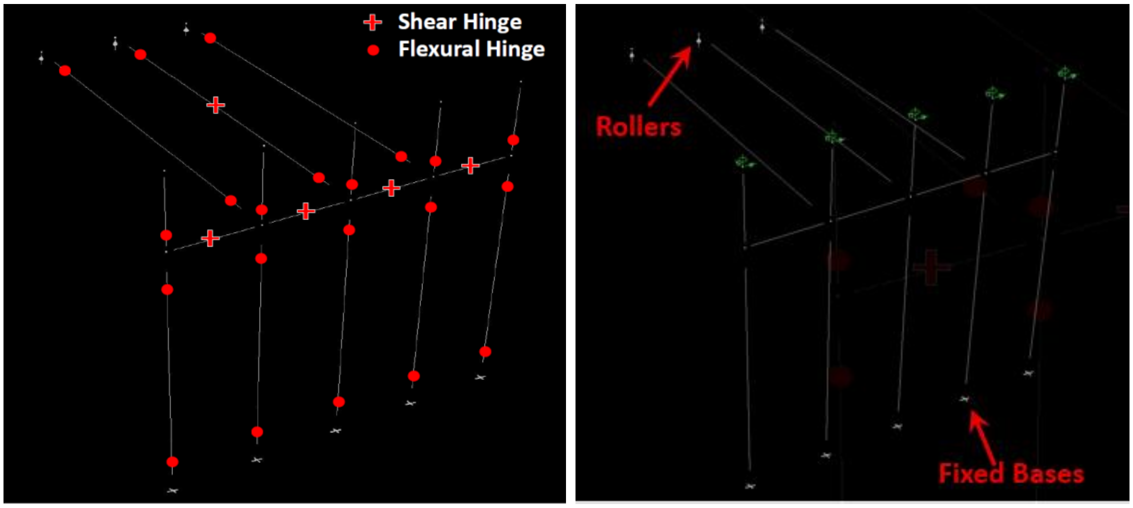

Figure 4-44: Perform-3D Model of Test Specimens

- Based on the calculations, the columns longitudinal bars did not have the required lap length at the base, and while this mode of failure was being observed, the columns were expected to be shear-controlled in the out-of-plane direction and flexure-shear controlled in the in-plane direction. The observed behavior in both directions was governed by lap-splice slip which limited the stresses in the bars but the columns did not experience a brittle failure with rapid strength loss as suggested by ASCE 41-13 and in fact the moment capacity of the specimen remained rather constant for a while before strength loss (Figure 4-41). Hence the columns were not modeled with a shear hinge, and just flexural hinges at each end. The behavior of the columns was fairly ductile failure, maintaining the and allowing for some plastic rotation prior to strength loss. As a result, a backbone curve for lap-splice controlled condition was developed based on the test observations, that did not have rapid strength loss. The observed rotation post slip (length of the plateau or plastic rotation) was about 1.15% in the out-of-plane direction and 1.24% in the in-plane direction. To match the observed performance, the non-linear modeling parameter “a” was chosen to be 0.0065 in the in-plane direction (about half of the “a” parameter of a flexure-shear column per ASCE 41-13) and 0.012 in the out-of-plane direction (approximately three quarters of the “a” parameter for a flexure-shear controlled element per ASCE 41-13).

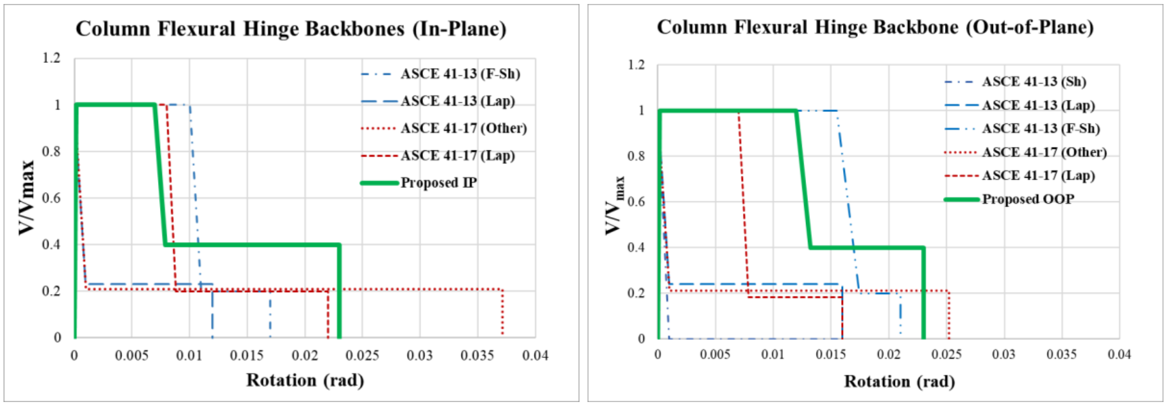

Figure 4-45: Comparison of ASCE 41-13 and ASCE 41-17 Backbone Relations with Proposed Backbone Relation for Fin Columns

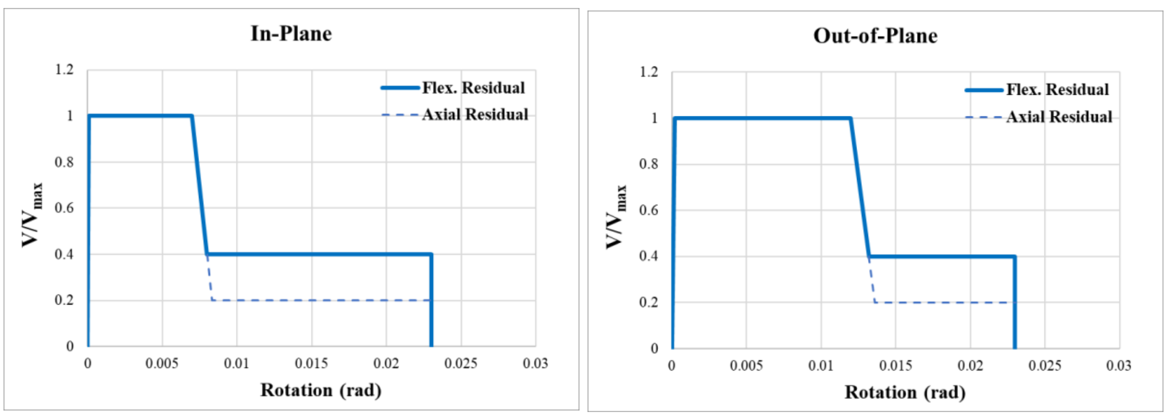

Figure 4-46: Backbone Relations Used for Column Modeling

The obtained backbone is conceptually similar to a flexure-shear controlled column where some deformation strength is maintained prior to strength loss, and the values for the “b” parameter are obtained from condition ii of Table 10-8 of ASCE 41-13. See Appendix G for information about Perform-3D input values.

- The residual strength ratio, “c” parameter, for the fin column moment hinges was 0.20 in axial compression, but this value was increased to 0.40 for flexure to obtain similar residual strength as the test (Figure 4-46). The "c" parameter for the ledge beam shear hinge was 0.20 per Table 10-8 of ASCE41-13. As illustrated in section 4.4, the residual strength at the end of the tests was approximately 0.46 in the in-plane and 0.44 in the out-of-plane direction.

- The beam assembly consisted of the ledge beam and the thickened slab edge (Figure 3-10). ACI 318-14 allows projection of the beam beyond the width of the supporting column per section 18.6.2.1 as long as it is the lesser of c_2 and $0.75c_1$, which in the case of the ledge beams, was 8 inches (203 mm), which was less than the full width of the thickened slab edge, 13 in. (330 mm). However, this provision does not allow to consider the shear strength of the projected section in the shear capacity of the beam. As a result, the shear capacity of the thickened slab was not considered in modeling the beam assembly in Perform-3D (lower bound analysis). To assess the effect of including the shear capacity of the whole beam assembly (ledge beams and the thickened slab), an upper bound analysis was performed as shown in Appendix G. It determined that the lower bound analysis, per ACI 318-14 is the more accurate representation of the condition observed in the test, and the thickened slab was not very effective in increasing the frame beam shear capacity. As observed in Figure 4-25, the ledge beam and the thickened slab did not develop their full capacity at the same time. Due to the flexure-shear controlled behavior of the ledge beams, they were modeled both by flexural hinges at each end, and a shear hinge at midspan.
- The flexural strength of the fin columns was reduced to 0.89 in the in-plane direction and 0.81 in the out-of-plane direction (Figure 4-47 and Figure 4-48). This reduction was to account for the failure of the column longitudinal bars prior to yield due to inadequate lap-splice lengths. The peak shear strengths obtained from Perform-3D analyses in the out-of-

plane direction were higher than observed in the tests (Figure 4-48 and Figure 4-50). To match the peak strength of the test, the flexural strength of the columns in the out-of-plane direction was reduced by approximately 8% (Figure 4-51). This reduction was believed to be attributed to the cyclic damage. Pushing the columns beyond the splice strength in the in-plane direction prevented the columns to achieve the expected strength in the out-of-plane direction.

- The transverse beam was flexure-shear controlled too, therefore modeled by both flexural and shear hinges. The joists were flexure-controlled and modeled by flexural hinges.
- The 3 in. (76 mm) slab was not modeled in Perform-3D since it was too far from the frame to impact the behavior of the frame due to the presence of the thickened slab edge, which was considered in the model. The connection of the slab to the frame was only through the longitudinal reinforcement of the transverse beam and the joists, which were also considered in the model.
- Stiffness modifiers to obtain effective stiffness values for the columns, beam assembly and the transverse beams were obtained from ASCE41-13 (and 17), a moment-curvature analysis, and per a research by Elwood and Eberhard (Table 4-2). The results of the analyses are plotted with the test backbone curve in Figure 4-47 to Figure 4-51.

The effective stiffness of the frame beams and fin columns per ASCE 41-13 Table 10-5 was $0.3EI_g$. However, this value has been studied extensively to assess its accuracy. When the columns undergo flexural and shear yielding as well as bar slip extension, experimental data have shown the values from ASCE 41-13 tend to be inaccurate. To account for flexural, shear and slip deformations, Elwood and Eberhard suggested equations 1 to 3 (EQ.1 to 3) to obtain customized estimates of EI_{eff} based on loading conditions and geometry. EQ.1 is the simplified equation suggested for practicing engineers, and equations 4 to 6 (EQ.4 to 6) provide parameters to be used in EQ. 1 to 3. (Elwood & Eberhard, 2009)

$$\frac{EI_{eff,calc}}{EI_g} = \frac{0.45 + 2.5P/A_g f_c'}{1 + 110(\frac{d_b}{D})(\frac{D}{a})} \leq 1.0 \text{ and } \geq 0.2 \qquad (\mathbf{EQ.\,1})$$

$$\frac{EI_{eff,calc}}{EI_g} = \frac{1.5\alpha_{approx\ (Eq.13)}}{[1 + 110\left(\frac{d_b}{D}\right)\left(\frac{D}{a}\right)\left(\frac{f_s}{f_{y\ approx\ (Eq.15)}}\right)]} \leq 1.0 \text{ and } \geq 0.2 \qquad (\mathbf{EQ.\,2})$$

$$\frac{EI_{eff,calc}}{EI_g} = \frac{\alpha}{[1 + \frac{3}{8}\frac{d_b}{D}\frac{D}{a}\frac{f_s}{f_y}\frac{f_y}{u} + \frac{18}{5}\alpha(\frac{r_v}{D})^2(\frac{D}{a})^2\left(\frac{E_c}{G_{eff}}\right)]} \qquad (\mathbf{EQ.\,3})$$

$$\alpha_{approx\ (Eq.13)} = 0.2 + 1.3\left(\frac{P/A_g E_C}{\varepsilon_0}\right) + \rho n \leq 1.0 \qquad (\mathbf{EQ.\,4})$$

$$\alpha_{approx\ (Eq.14)} = 0.35 + 1.3\left(\frac{P/A_g E_C}{\varepsilon_0}\right) \leq 1.0 \qquad (\mathbf{EQ.\,5})$$

$$0.0 \leq f_s/f_{y\ approx\ (Eq.15)} = \frac{4}{3} - \frac{10}{3}\left(\frac{P/A_g E_C}{\varepsilon_0}\right) \leq 1.0 \qquad (\mathbf{EQ.\,6})$$

Table 4-2: Effective Stiffness to Gross Stiffness Ratio by Different Methods

	Column (IP)	Column (OOP)	Beam Assembley	Transvese Beam
EQ.1	0.28	0.28	0.36	0.35
EQ.2	0.29	0.29	0.39	0.27
EQ.3 & EQ.4	0.29	0.29	0.33	0.24
EQ.3 & EQ.5	0.30	0.31	0.33	0.33
Elwood & Eberhrad Average Ratio	**0.29**	**0.29**	**0.35**	**0.30**
Moment-Curvature Calculations	**0.30**	**0.38**	**0.42**	**0.43**
ASCE 41-13 (Table 10-5)	**0.30**	**0.30**	**0.30**	**0.30**

P is the axial force on the column, *D* is the column depth in the direction of loading or h_c, a is the shear span, u is the average bar stress for elastic response equal to $9.6\sqrt{f_c'}$ psi ($0.8\sqrt{f_c'}$ MPa) in this research, r_v is the radius of gyration using shear area where $r_v^2 = I_g/A_v$, G_{eff} is the effective shear modulus equal to one half of the elastic value, and ε_o is considered 0.002 and is the nominal strain at which concrete is assumed to yield.

A moment-curvature analysis was also performed on the sections to obtain the initial stiffness ratio at the point of first yield in the tension reinforcement. The effective stiffness ratio to the gross stiffness ratio of the fin columns was 0.38 in the out-of-plane direction, 0.30 in the in-plane direction, and 0.42 for the beam assembly. The fin column was approximated by an equivalent rectangular section of 8 in. (203 mm) wide by 16 in (406 mm) deep. The ledge beam portion of the beam assembly was also approximated by a 7 in. (178 mm) by 16 in. (406 mm) rectangular section for these calculations.

All the pushover curves from Perform-3D analyses follow the test backbones closely in both directions, especially in the out-of-plane direction. There are some differences in the non-linear portion of the in-plane backbone curves before strength loss, and the models with effective stiffness ratios per ASCE 41-13 and moment-curvature analysis overestimate the deformation at which stress loss occurs. However, the overall shape, and ultimate drift relations are very close in the model with effective stiffness ratios per Elwood and Eberhard (2009). The in-plane residual strength values are about half of those observed in the tests, while they were very close to the test observations in the out-of-plane direction.

As shown in Figure 4-47 to Figure 4-51, the initial stiffness of the pushover curve in the in-plane direction, using effective stiffness ratios by Elwood and Eberhard (2009) provided the closest match in the negative and positive direction of loading. The initial stiffness of the pushover curves using moment-curvature analysis and Table 10-5 of ASCE41-13 (and 17), matched the stiffness of the test in the negative direction closely, but were significantly lower in the positive direction. Since the positive in-plane direction is the first direction that the specimen was pushed in, it represented the stiffness of the specimen prior to sustaining any damage at each loading cycle. The effective stiffness in the negative direction was expected to be lower than in the positive direction, as the specimen had already gone through deformations in the positive in-plane direction and in the out-of-plane direction, prior to be being pushed in the negative in-plane direction. In the out-of-plane direction the pushover curves obtained from Perform-3D analyses show close agreement with the observations in the tests. The initial stiffness of the pushover curve using effective stiffness ratios per Table 10-5 of ASCE41-13 and 17 resulted in the lowest initial stiffness (Figure 4-47 and Figure 4-48).

The models per moment-curvature analysis were the closest to the observed initial stiffness in the tests followed closely by the moment-curvature analysis. However, it should be noted that the moment-curvature analysis does not account for yield penetration (bar slip) and crack opening as Elwood and Eberhard's model does. The reason these two models are not vastly different in the case of this building was attributed to the fact that the structural elements did not go through flexural yielding (especially at the beams), hence no to little yield penetration and crack openings occurred which would normally result in lower effective stiffnesses.

The residual strength of all the Perform-3D analyses matched the test results very closely up to the stopping point of the test.

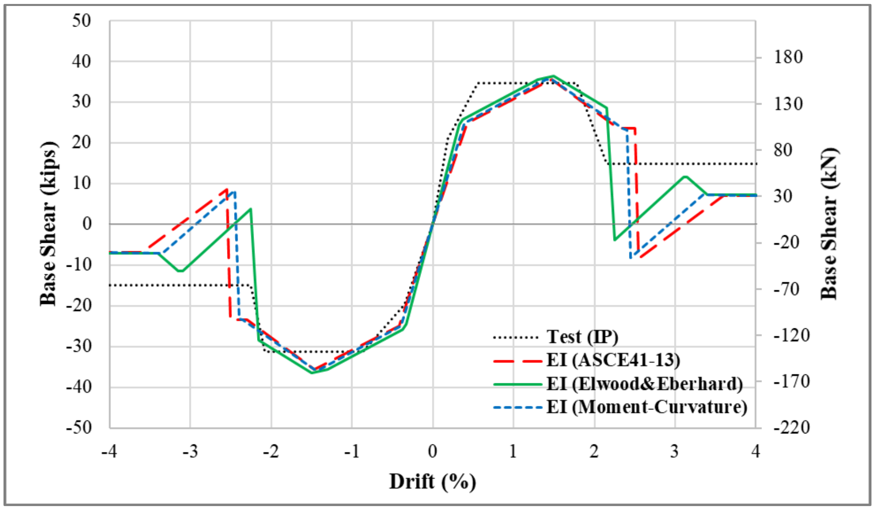

Figure 4-47: Test Average In-Plane Drift Compared with Perform-3D Pushover Curves

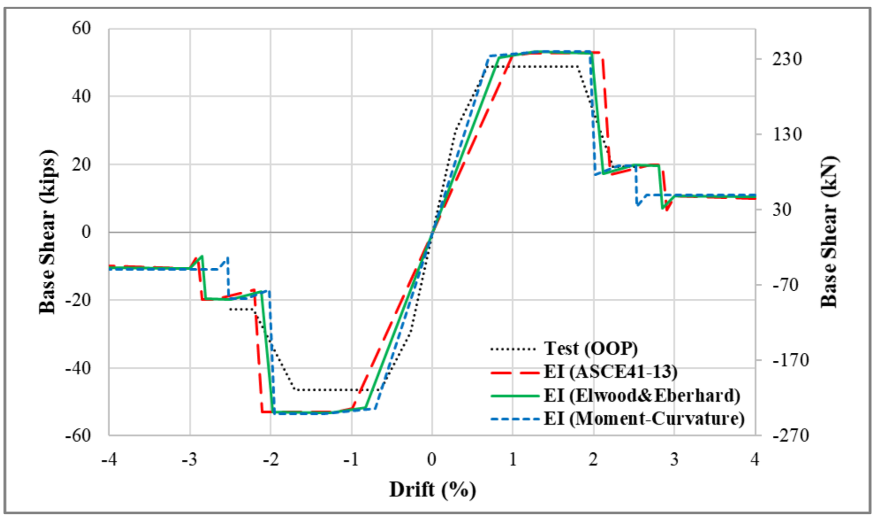

Figure 4-48: Test Average Out-of-Plane Drift Compared with Perform-3D Pushover Curves

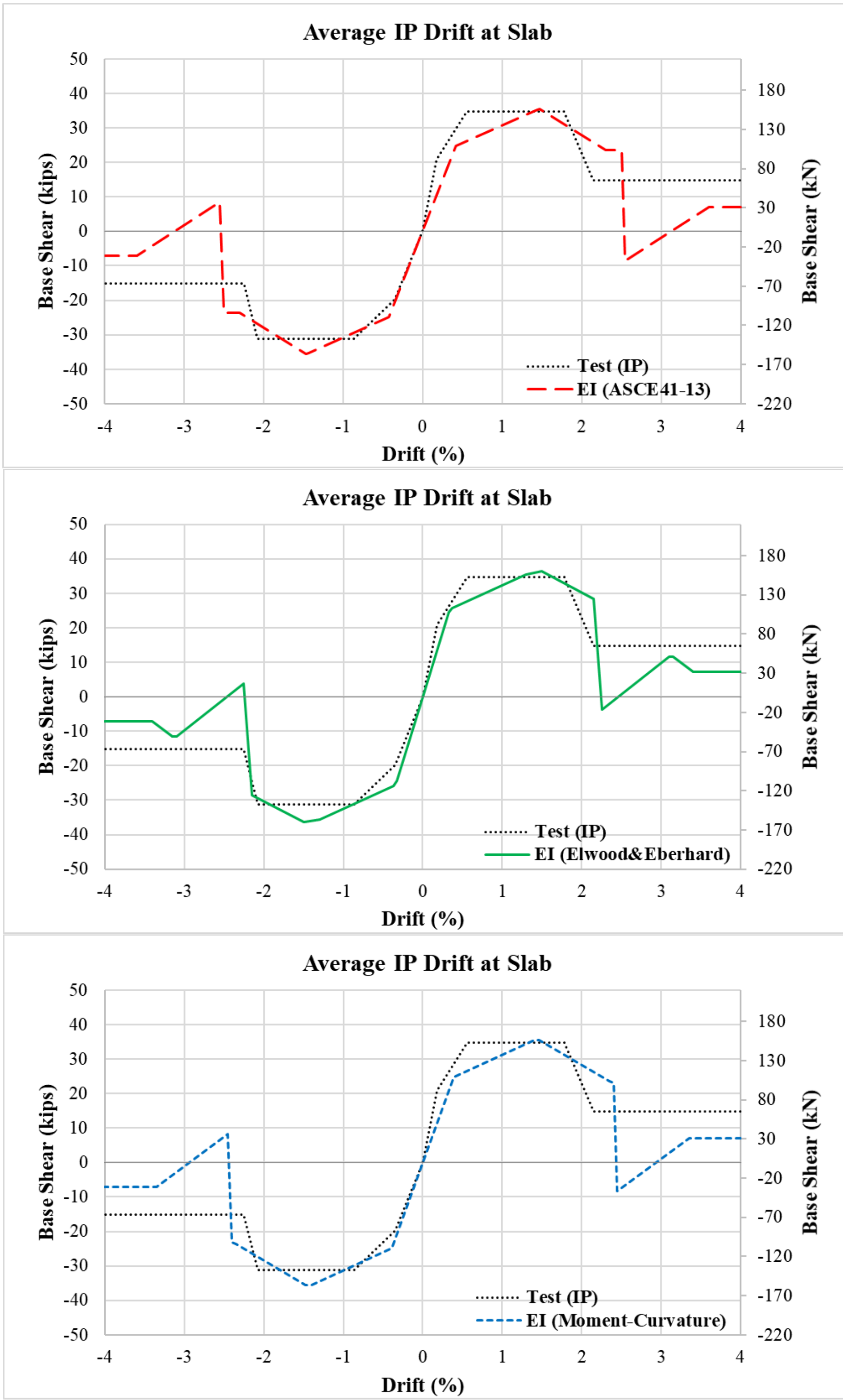

Figure 4-49: Comparison of In-Plane Test Results and Perform-3D Pushover Curves (EI_{eff} Obtained from ASCE41-13, Elwood & Eberhard, and Moment-Curvature Analysis)

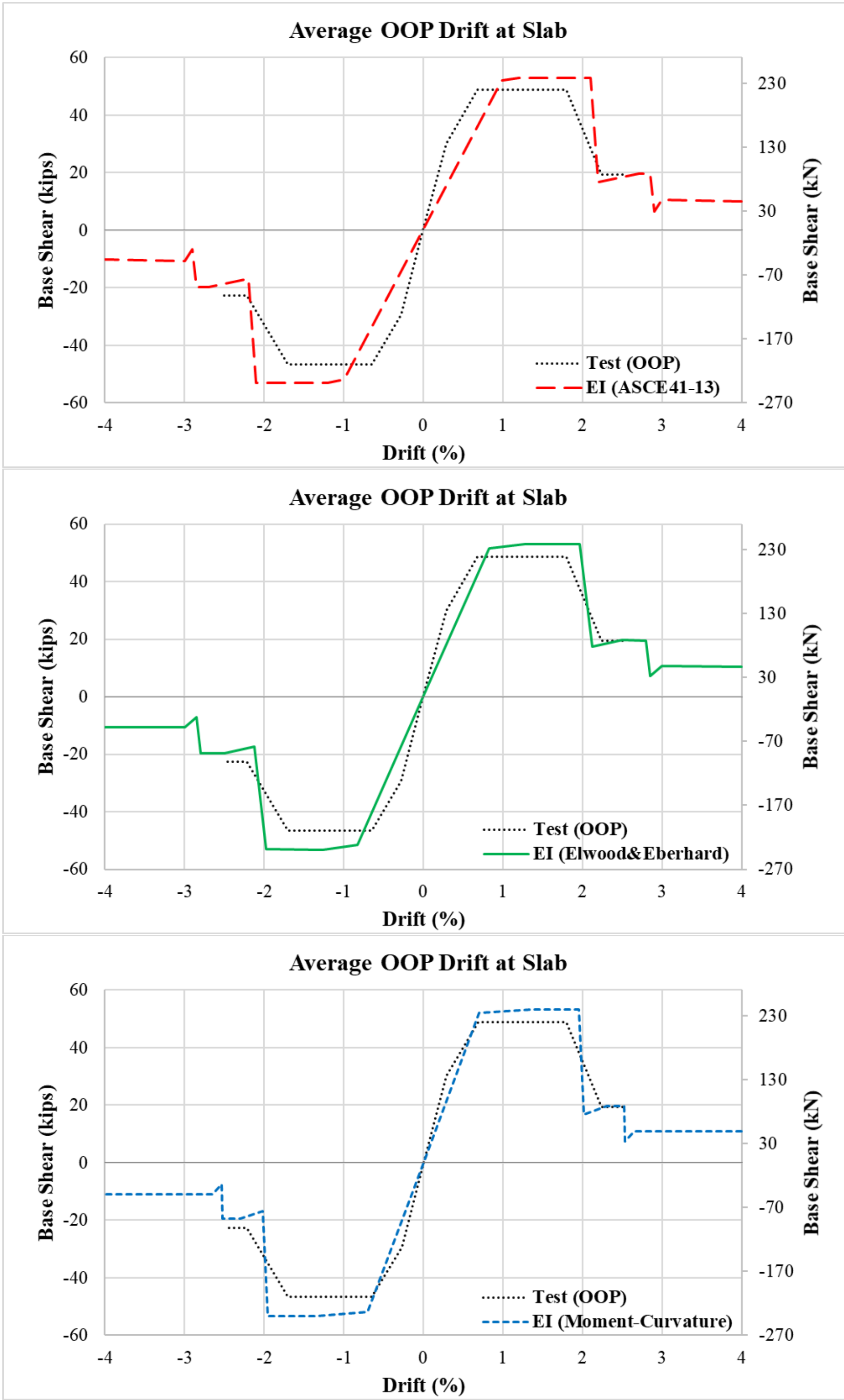

Figure 4-50: Comparison of Out-of-Plane Test Results and Perform-3D Pushover Curves (EI_{eff} Obtained from ASCE41-13, Elwood & Eberhard, and Moment-Curvature Analysis)

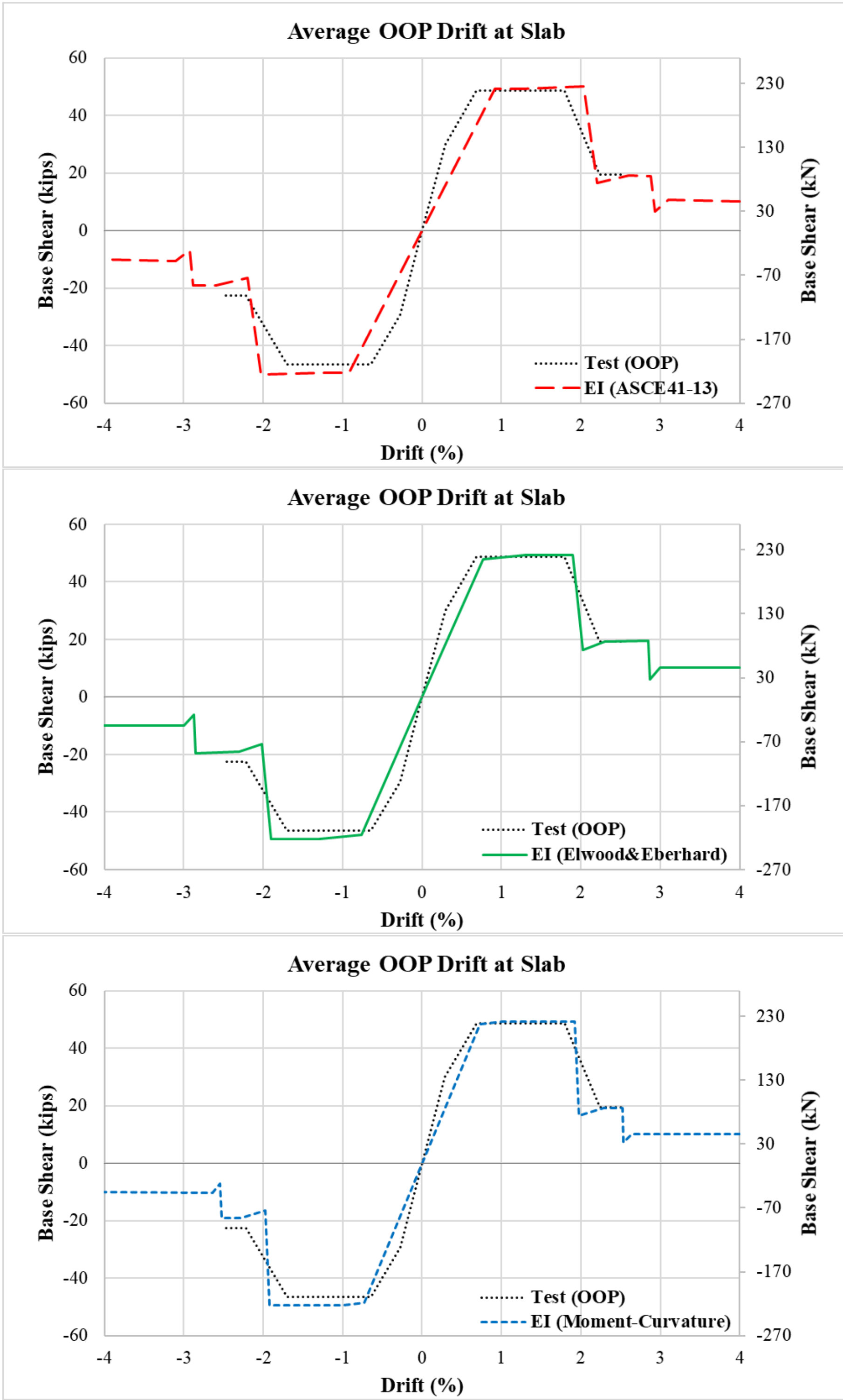

Figure 4-51: Comparison of Out-of-Plane Test Results and Perform-3D Pushover Curves (Reduced Out-of-Plane Flexural Capacity of Columns by ~8%)

The abovementioned parameters and adjustments were used to analyze the Franz Tower and assess the proposed retrofit scheme. Since the existing building components performed better than expected in the experimental testing, the final Perform-3D analysis determined that viscous dampers at levels 7 and 8 were not required, and they were only installed at levels one through six. This resulted in material and construction cost savings, reduced disruption to the top two floors, and allowed budget for interior renovation of the building.

Chapter 5. Functional Recovery Analysis

5.1. Background on the Performance-Based Earthquake Design for Franz Tower

As discussed in Chapter 2, current performance-based earthquake design practice per ASCE 41-13, and in the case of the Franz Tower, UC seismic rating system (UCSRS), primarily focus on performance rating improvements to reduce the threats to the lives of occupants, and meeting seismic performance ratings as shown in Table 2-15. These performance levels relate to the life safety of the occupants, when subjected to major ground shakings, and not as much to the downtime and cost to repair.

Prior to performing the physical testing, ASCE 41-13 and UCSRS were used to establish the expected seismic performance level of the building. The seismic rating was done per the CBC Part 10, Chapter 3 (Provisions for All Compliance Methods), for buildings in risk categories I-III, which is also shown in Table 2-15. The building was initially rated Performance Level V with two retrofit schemes proposed to improve it to Performance Level IV: exterior concrete moment frame (CMF) scheme, and exterior buckling-restrained brace (BRB) scheme.

Using the data obtained from the physical testing and viscous dampers (VD retrofit scheme), a third retrofit scheme was proposed per which the building was retrofitted to meet Performance Level III. As defined in Table 2-15, a building with Performance Level III indicates that the building should meet Life Safety requirements when subjected to BSE-1N hazard level, and Collapse Prevention when subjected to BSE-2N hazard level.

The building rated with Performance Level IV is expected to meet or exceed the abovementioned requirements for BSE-R and BSE-C hazard levels, and Level V is when the requirements are met when the BSE-R and BSE-C hazard levels values are reduced to two thirds of those specified for the site.

BSE-2N is the 2,475-year return period earthquake ground motion, or the Maximum Considered Earthquake (MCE_R) ground motion for the site, and BSE-1N is two-thirds of the BSE-2N, nominally the 475-year return period earthquake ground motion. BSE-R and BSE-C are the 225-year and 975-year return period earthquake ground motions, respectively.

All the above has the main objective of meeting building performance requirements without any direct focus and emphasis on cost or downtime. Since these parameters are extremely important to the building owners and the general public who would be directly affected by them, in the next sections the resilience-based analysis of Franz Tower in SP3 is discussed.

5.2. Resilience-Based Earthquake Design Analysis for Franz Tower

In the next sections of this chapter the results SP3 analyses performed on the existing building and the retrofitted buildings are presented.

The analyses on the existing building are performed to assess the performance of Franz Tower under site specific seismic loading in conjunction with the estimated annual repair cost and downtime. These analyses are different in terms of level of building specific details inputted in SP3 and are called 1- express analysis (minimum input), 2- standard analysis (some building specific input), and 3- detailed analysis (building component level of input). This was to compare the sensitivity of SP3 predictions to the level of input.

Since the experimental testing revealed that the building performed better than ASCE 41-13 predicted, a fourth analysis was performed by modifying structural component level properties (of the columns, and beam-column joints mainly), to assess the impact of accurate modeling of structural components on the performance of the building, level of damage, and downtime.

In the next section the results of three analyses performed on the retrofitted building are presented. First, the two traditional retrofit schemes (CMF and BRB) that were originally proposed to the

UCLA Capital Programs, were analyzed to obtain cost of repair and time to regain function. Next, the VD retrofit program was analyzed using the experimental test data, with modified structural component properties according to their observed performance in the tests.

Lastly, the third analysis was repeated, this time by inputting engineering design parameters (maximum story drift ratio, peak floor acceleration, and maximum story residual drift ratio) obtained from a Perform-3D dynamic non-linear analysis conducted on the building by the design team to evaluate the VD retrofit scheme, instead of using the SP3 database. This non-linear analysis was performed by subjecting the retrofitted building to seven pairs of ground motions provided by a geotechnical consultant and approved by the peer review committee. The purpose to perform this fourth analysis was to assess the similarity of the default site-specific ground motions in SP3 to the set of site-specific ground motions provided by geotechnical professionals, as it is common practice. SP3 results are found in Appendix H.

5.2.1. Evaluation of Existing Building

5.2.1.1 SP3 Express Evaluation

Express level analysis is performed by inputting five (5) primary information about the building as shown in Figure 5-1: 1- location (coordinates per street address of the building), 2- structural system, 3- year built, 4- number of stories (which is a measure of building height), and 5- occupancy type.

This information can be inputted in SP3 very quickly and the expected loss and median repair time can be obtained in minutes. This is especially helpful for practicing engineers to have a general idea of what to expect in terms of loss assessment.

The structural system for this building was considered to be reinforced concrete space frames, due to the participation of the interior beam-column frames in resisting seismic forces.

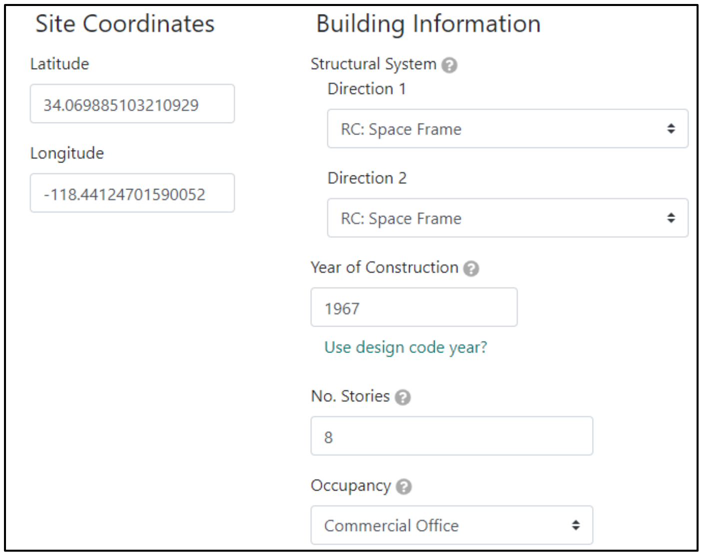

Figure 5-1: Franz Tower – SP3 Express Analysis (5 Points of Input) – Input Parmeters

SP3 uses a database of building types and deficiencies based on the year of construction and known deficiencies and characteristic unique to that time and uses an "average building" representative of the construction type and time. The average building was then subjected to a suite of 11 ground shakings with various intensities (return periods) and had an expected loss of 30% for an earthquake with return period of 475 years (as highlighted in Table 5-1) based on $21.2 M building value. This translates to $84,909 in annual expected loss. The loss breakdown is shown in Table 5-2 and Figure 5-2 for clarity.

Table 5-1: Franz Tower – SP3 Express Analysis: Expected Loss (% of Total Building Value)

Shaking Intensity	Return Period	SEL (%)	SUL (%)
90% in 50 years	22 Years	2	4
50% in 30 years	43 Years	4	8
50% in 50 years	72 Years	7	14
50% in 75 years	108 Years	10	19
50% in 100 years	144 Years	13	23
20% in 50 years	224 Years	18	31
DE	411 Years	26	44
10% in 50 years	475 Years	30	50
MCE_R	938 Years	47	77
5% in 50 years	975 Years	48	79
2% in 50 years	2475 Years	72	100

Table 5-2: Expected Mean Loss Breakdown – SP3 Express Analysis

Intensity	Total	Structural	Collapse	Exterior	Residual	Partitions	HVAC	Other	Interior
90% in 50 years	2.0	0.0	0.0	0.4	0.0	0.0	1.3	0.1	0.1
50% in 30 years	4.4	0.1	0.0	1.7	0.0	0.1	1.9	0.4	0.2
50% in 50 years	7.3	0.5	0.0	3.2	0.0	0.3	2.1	0.7	0.4
50% in 75 years	10	1.5	0.1	4.5	0.0	0.5	2.2	0.9	0.5
50% in 100 years	13	2.6	0.3	5.3	0.0	0.7	2.2	1.0	0.6
20% in 50 years	18	5.0	0.9	6.9	0.0	1.0	2.3	1.3	0.8
DE	26	8.6	3.1	8.7	0.1	1.3	2.2	1.4	1.0
10% in 50 years	30	10	4.0	9.3	0.0	1.4	2.3	1.5	1.1
MCE_R	47	18	10.0	11	0.6	1.8	2.1	1.7	1.4
5% in 50 years	47	18	10	12	0.6	1.8	2.1	1.7	1.4
2% in 50 years	73	25	25	13	3.3	1.9	1.8	1.7	1.6

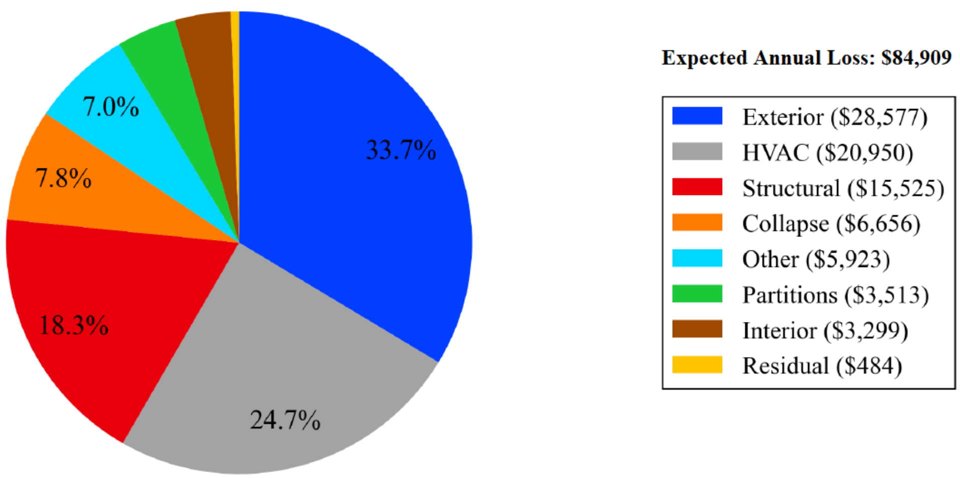

Figure 5-2: Annualized Loss Breakdown – SP3 Express Analysis

Peak story demands are shown in Figure 5-3, and the median repair time is presented in Table 5-3. The median repair time per FEMA-P58 is 2 months and per REDi Re-Occupancy is 3.5 months. (Appendix H)

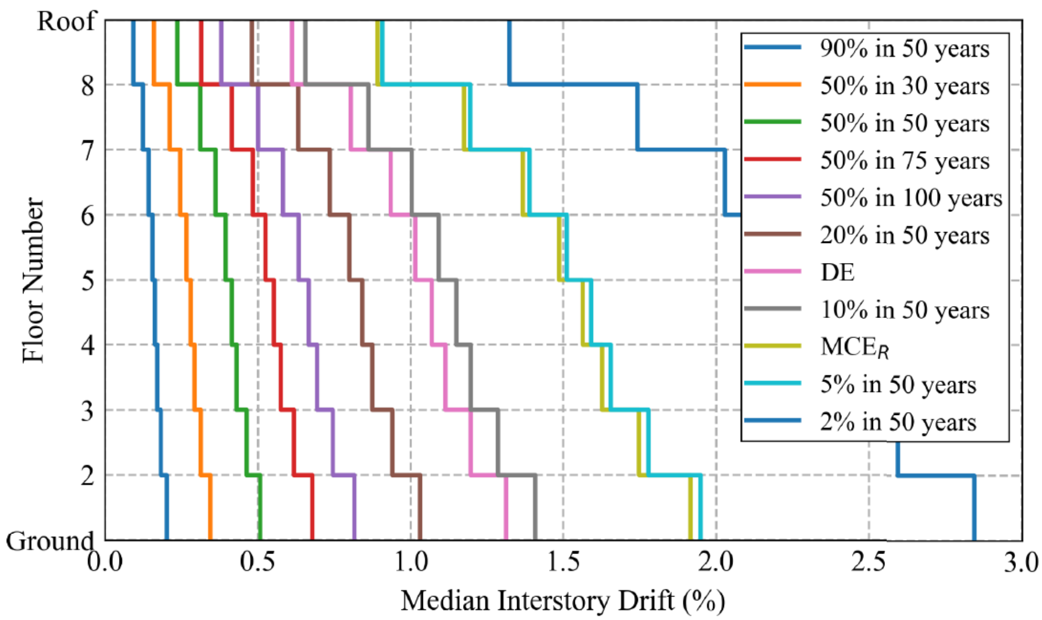

Figure 5-3: Peak Strory Drift Demands – SP3 Express Analysis

Table 5-3: Franz Tower – SP3 Express Analysis: Median Repair Time

Intensity	FEMA P-58 Parallel	FEMA P-58 Series	REDi Re-Occupancy	REDi Functional Recovery	REDi Full Recovery
90% in 50 years	5 days	7 days	0 days	14 days	14 days
50% in 30 years	9 days	2.4 weeks	4 days	3.1 weeks	3.2 weeks
50% in 50 years	14 days	4.8 weeks	11 days	4.2 weeks	4.2 weeks
50% in 75 years	2.8 weeks	7.5 weeks	3.6 weeks	5.3 weeks	5.3 weeks
50% in 100 years	3.5 weeks	2.4 months	5.3 weeks	6.6 weeks	6.6 weeks
20% in 50 years	5.1 weeks	3.8 months	2.0 months	2.1 months	2.1 months
DE	7.4 weeks	6.0 months	3.0 months	3.1 months	3.1 months
10% in 50 years	2.0 months	7.2 months	3.5 months	3.7 months	3.7 months
MCE$_R$	3.1 months	13 months	6.3 months	6.4 months	6.4 months
5% in 50 years	3.2 months	14 months	6.7 months	6.7 months	6.7 months
2% in 50 years	4.7 months	19 months	12 months	12 months	12 months

5.2.1.2 SP3 Standard Analysis

In the standard analysis, additional details about the building geometry are inputted, but not component level details, for more accurate estimate of the building performance. These input information include: 1- building square footage, 2- building aspect ratio, 3- first and upper story heights, 4- building irregularities (vertical strength and stiffness, and plan torsion), 5- level of detailing (ordinary, intermediate, or special), 6- seismic risk category, 7- seismic importance factor, 8- drift limit in both directions, 9- site class (soil) information, and 10- general component information (seismic bracing of electrical, piping, and HVAC systems, or seismic joints at stairs). These parameters allow for a more building specific assessment without the need to get into component level detailing which is a more time-consuming process. Input parameters for the standard level of analysis are shown in Figure 5-4.

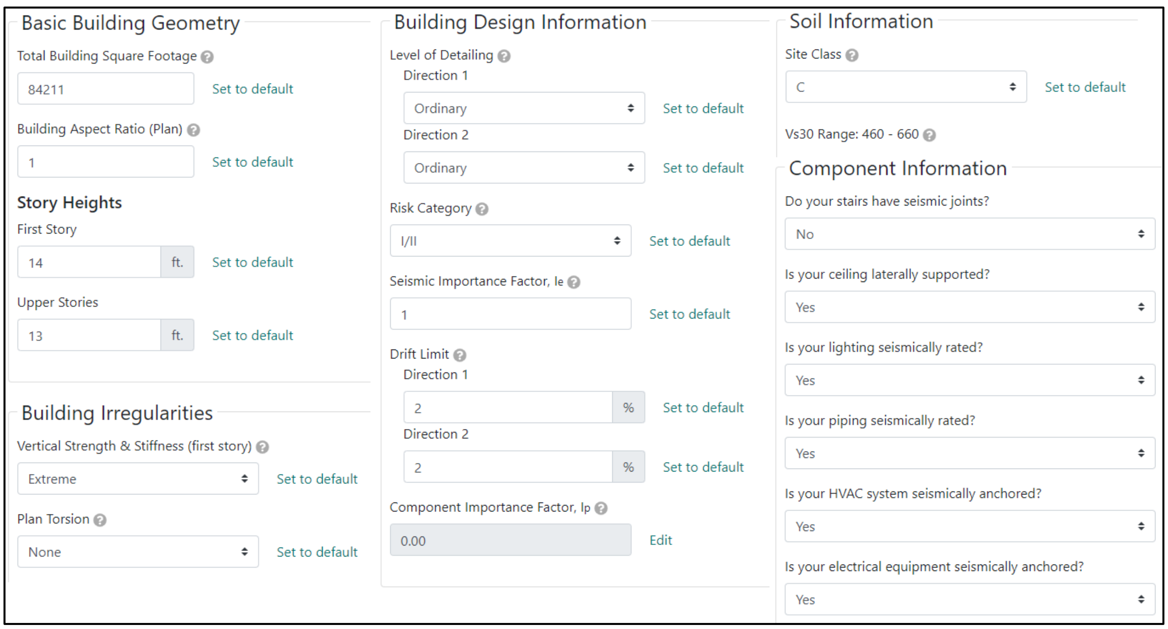

Figure 5-4: Franz Tower – SP3 Standard Analysis – Input Parameters

The building was subjected to the same suite of ground shakings as in the express analysis, and the SEL for each ground shaking is shown in Table 5-4. SEL for an earthquake with return period of 475 years is increased from 30% to 39% for the highlighted hazard level. This increase is mainly attributed to extreme vertical irregularity (vs. none) and ordinary level of detailing (vs. default which is intermediate). The former causes 10% increase in the SEL and the latter 5% if all other parameters remain constant.

The breakdown of expected mean loss is shown in Table 5-5 and Figure 5-5.

Table 5-4: Franz Tower – SP3 Standard Analysis: Expected Loss (% of Building Value)

Shaking Intensity	Return Period	SEL (%)	SUL (%)
90% in 50 years	22 Years	3	5
50% in 30 years	43 Years	5	8
50% in 50 years	72 Years	8	13
50% in 75 years	108 Years	11	18
50% in 100 years	144 Years	15	23
20% in 50 years	224 Years	22	36
10% in 50 years	475 Years	39	66
DE	791 Years	53	86
5% in 50 years	975 Years	60	96
MCE_R	1956 Years	78	100
2% in 50 years	2475 Years	83	100

Table 5-5: Expected Mean Loss Breakdown – SP3 Standard Analysis

Intensity	Total	Collapse	Structural	Exterior	Residual	Other	Partitions	HVAC	Interior
90% in 50 years	2.9	0.0	0.0	0.2	0.0	1.5	0.0	1.1	0.0
50% in 30 years	4.6	0.1	0.3	1.1	0.0	1.8	0.1	1.3	0.0
50% in 50 years	7.6	0.4	1.0	2.4	0.0	2.0	0.1	1.5	0.1
50% in 75 years	11	1.4	2.2	3.6	0.0	2.1	0.2	1.5	0.2
50% in 100 years	15	2.6	3.7	4.4	0.0	2.2	0.3	1.5	0.2
20% in 50 years	23	6.2	6.5	5.4	0.0	2.3	0.5	1.5	0.3
10% in 50 years	39	18	11	6.6	0.0	2.1	0.7	1.3	0.4
DE	54	28	14	6.9	0.3	1.9	0.7	1.2	0.5
5% in 50 years	61	33	16	6.9	0.7	1.8	0.8	1.1	0.5
MCE_R	79	50	18	6.3	1.3	1.4	0.8	0.8	0.5
2% in 50 years	83	56	17	5.9	2.0	1.2	0.7	0.7	0.5

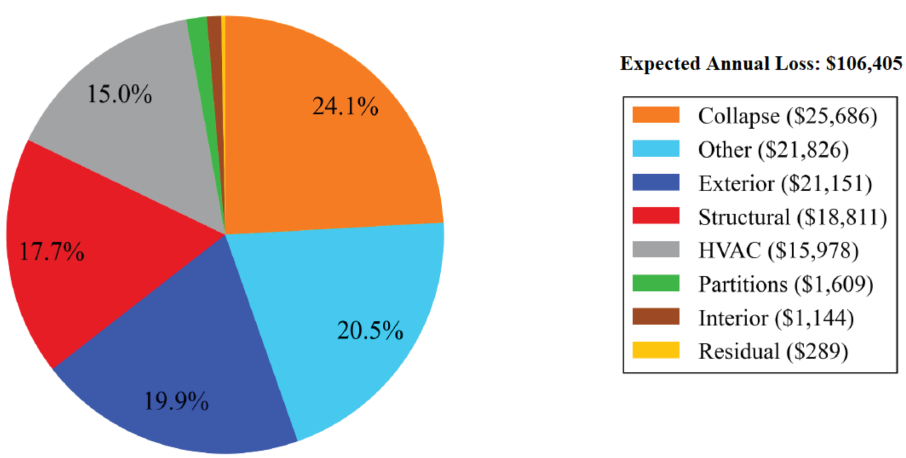

Figure 5-5: Annualized Loss Breakdown – SP3 Standard Analysis

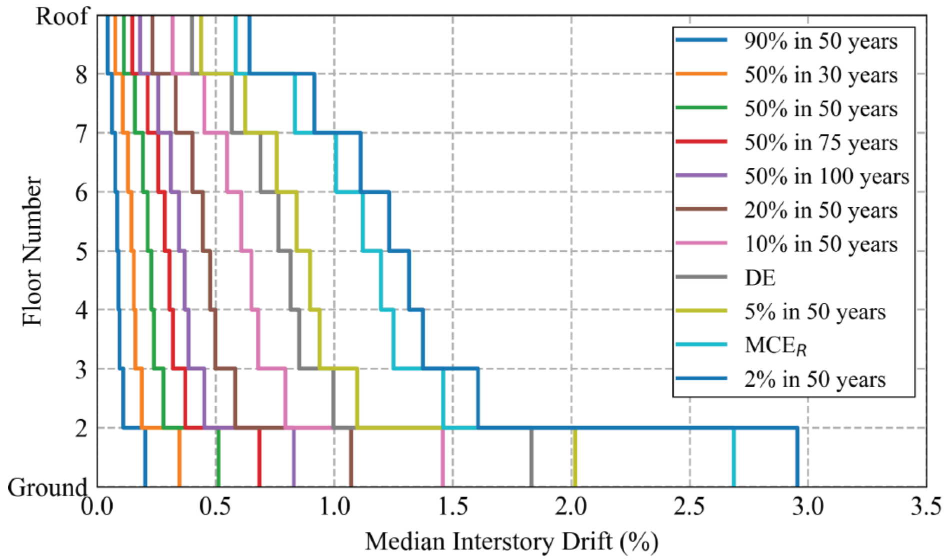

Figure 5-6: Peak Story Drift Demands – SP3 Standard Analysis

Peak story drift demands are shown in Figure 5-6. This value increased from 1.41% in the express analysis to 1.46% in the standard analysis for the ground motion with 475-year return period. The former is based on an "average" building representing the building type and era, while the latter is closer to the actual building behavior due to the customizations shown in Figure 5-4.

The median repair time for the same hazard level is increased for parallel repair per FEMA P-58, from 2 months to 4.0 months. However, no significant change in the repair time is observed per REDi Re-Occupancy as shown in Table 5-6.

Table 5-6: Franz Tower – SP3 Standard Analysis: Median Repair Time

Median repair time, without impeding factors

Intensity	FEMA P-58 Parallel	FEMA P-58 Series	REDi Re-Occupancy	REDi Functional Recovery	REDi Full Recovery
90% in 50 years	4 days	6 days	0 days	9 days	9 days
50% in 30 years	7 days	13 days	1 days	2.2 weeks	2.2 weeks
50% in 50 years	14 days	4.0 weeks	6 days	3.2 weeks	3.2 weeks
50% in 75 years	4.1 weeks	7.2 weeks	2.2 weeks	4.5 weeks	4.5 weeks
50% in 100 years	6.6 weeks	2.6 months	3.9 weeks	6.1 weeks	6.1 weeks
20% in 50 years	2.5 months	4.1 months	6.9 weeks	2.1 months	2.1 months
10% in 50 years	4.0 months	8.0 months	3.4 months	3.8 months	3.8 months
DE	5.6 months	14 months	6.1 months	6.5 months	6.5 months
5% in 50 years	6.4 months	18 months	7.8 months	8.2 months	8.2 months
MCE_R	19 months	19 months	19 months	19 months	19 months
2% in 50 years	19 months	19 months	19 months	19 months	19 months

5.2.1.3 SP3 Detailed (Building Specific) Analysis (Not Considering Test Data)

In the detailed analysis component level information were inputted. SP3 has a large database of architectural, MEP, HVAC, and structural components to choose from. Since the focus of this research is the structural retrofit of Franz Tower, more effort was spent in accurately modeling the structural building components (beams, columns, and joints). Capacity of the structural components, their mode of failure, and joint capacities are shown in Appendix A.

Since the predetermined sizes of the structural components in SP3 did not exactly match the sizes of the structural components in the actual building, capacity modifiers were used to account for this difference. This was mostly prominent in the fin columns and ledge beams.

The cost associated with the repair of these components were not changed due to the difference in size of the joints. This was due to a number of reasons: the structural components at the Franz Tower have unusual shapes and geometry, and repair of an odd-shaped component is more costly due to increased labor cost, even though material (concrete and steel reinforcement) cost may be less.

Another modification that seemed necessary was to adjust the number of joints at the top six levels of the building. The columns were spaced at 4 ft. on center (1219 mm) and the joints are much closer to each other than a typical moment frame where the columns could be 20 ft. (6096 mm) apart, based on which the default cost to repair a joint is established in SP3. It is reasonably assumed that repairing two joints that are 4 ft. (1219 mm) apart requires less movement of the workers, equipment, scaffolding and material. As a result, the cost of repairing two adjacent joints is not twice the cost of repairing one joint. To incorporate all the nuances associated with the odd shape and geometry of this building, it was decided to keep the cost multiplier factor for each joint 1 but reduce the number of joints by half to account for the lower labor costs due to the proximity of the joints.

Due to the lack of proper detailing and confinements in the columns, and the behavior of the columns to be shear/flexure-shear controlled, the expected loss increased to 55% as shown in Table 5-7 with cost breakdowns shown in Table 5-8 and Figure 5-7. The building had a rating of V per UCSPR which is associated with estimated repair cost of 20-50%. (See Table 2-15 and Table 2-16).

Table 5-7: Franz Tower – SP3 Detailed Analysis (No Test Data): Expected Loss (% of Total Building Value)

Shaking Intensity	Return Period	SEL (%)	SUL (%)
90% in 50 years	22 Years	5.0	9.1
50% in 30 years	43 Years	11	20
50% in 50 years	72 Years	17	29
50% in 75 years	108 Years	25	37
50% in 100 years	144 Years	30	43
20% in 50 years	224 Years	39	58
10% in 50 years	475 Years	55	89
DE	791 Years	68	100
5% in 50 years	975 Years	73	100
MCE_R	1956 Years	87	100
2% in 50 years	2475 Years	90	100

Table 5-8: Expected Mean Loss Breakdown – SP3 Detailed Analysis (No Test Data)

Intensity	Total	Collapse	Structural	Exterior	Residual	Other	HVAC	Partitions	Interior
90% in 50 years	5.0	0.0	1.8	0.3	0.0	1.5	1.5	0.0	0.0
50% in 30 years	11	0.1	5.8	1.3	0.0	1.8	1.7	0.1	0.1
50% in 50 years	17	0.4	10	2.6	0.0	2.0	1.8	0.1	0.1
50% in 75 years	25	1.4	15	3.9	0.0	2.1	1.8	0.2	0.2
50% in 100 years	30	2.7	18	4.6	0.0	2.2	1.8	0.3	0.3
20% in 50 years	39	6.2	22	6.0	0.0	2.3	1.8	0.4	0.4
10% in 50 years	55	18	26	6.9	0.0	2.1	1.6	0.6	0.5
DE	68	28	28	7.5	0.1	1.9	1.4	0.7	0.6
5% in 50 years	73	33	28	7.4	0.4	1.8	1.3	0.7	0.6
MCE_R	87	50	26	6.6	1.7	1.3	1.0	0.7	0.6
2% in 50 years	90	56	24	6.2	2.4	1.2	0.8	0.7	0.5

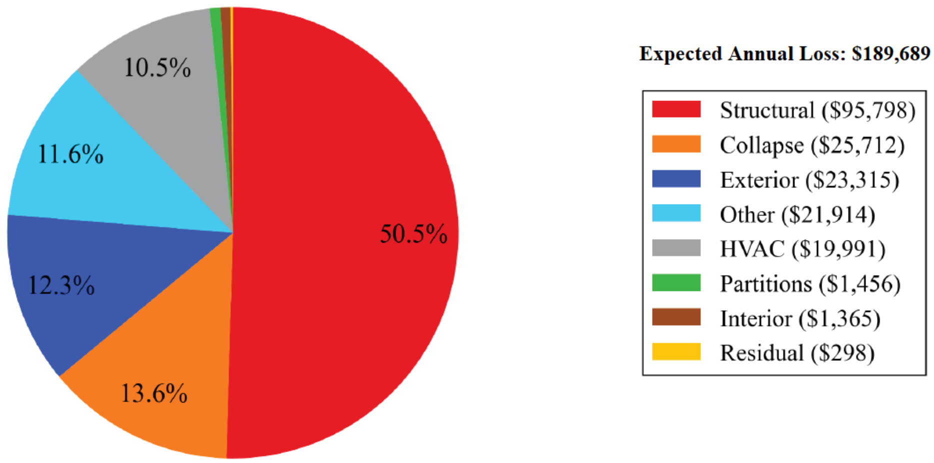

Figure 5-7: Annualized Loss Breakdown – SP3 Detailed Analysis (No Test Data)

Peak story demands are shown in Figure 5-8, with maximum drift of 1.37% at level 1 and 0.75% at level 2, which is attributed to the extreme vertical irregularity.

The median repair time for the same hazard level is increased for parallel repair per FEMA P-58, is 3.5 month which is about the same as the standard analysis. However, the repair time per REDi Re-Occupancy almost doubled as shown in Table 5-9.

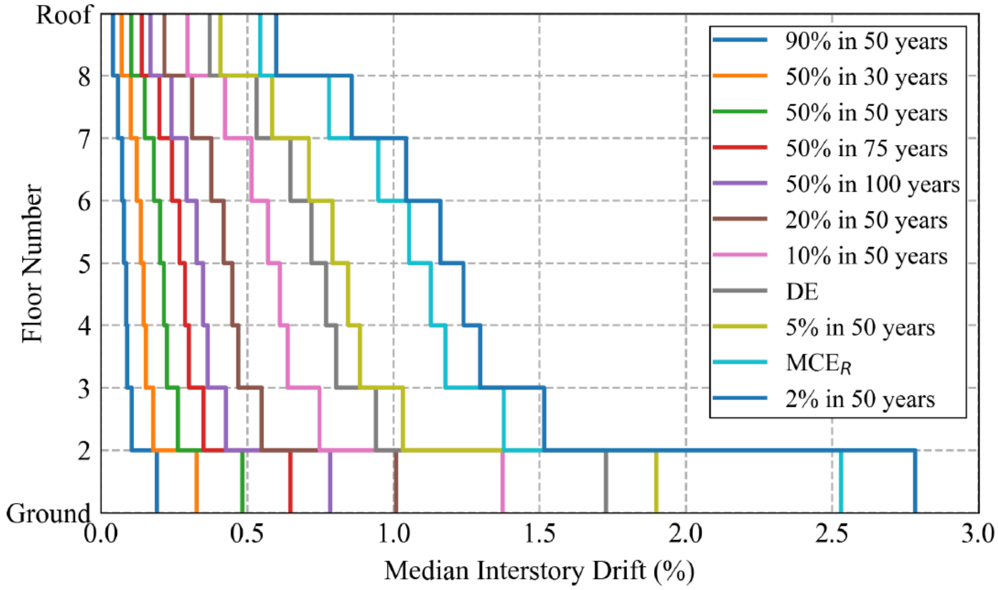

Figure 5-8: Peak Story Drift Demands – SP3 Detailed Analysis (No Test Data)

Table 5-9: Franz Tower – SP3 Detailed Analysis (No Test Data): Median Repair Time

Intensity	FEMA P-58 Parallel	FEMA P-58 Series	REDi Re-Occupancy	REDi Functional Recovery	REDi Full Recovery
90% in 50 years	8 days	2.4 weeks	0 days	14 days	14 days
50% in 30 years	3.2 weeks	2.2 months	3.7 weeks	5.7 weeks	5.7 weeks
50% in 50 years	5.8 weeks	5.0 months	2.2 months	2.6 months	2.6 months
50% in 75 years	7.9 weeks	7.9 months	3.5 months	3.9 months	3.9 months
50% in 100 years	2.1 months	9.5 months	4.3 months	4.7 months	4.7 months
20% in 50 years	2.6 months	12 months	5.6 months	6.0 months	6.0 months
10% in 50 years	3.5 months	17 months	7.8 months	8.2 months	8.2 months
DE	4.8 months	19 months	11 months	11 months	11 months
5% in 50 years	5.4 months	19 months	12 months	13 months	13 months
MCE$_R$	19 months	19 months	19 months	19 months	19 months
2% in 50 years	19 months	19 months	19 months	19 months	19 months

5.2.1.4 SP3 Detailed (Building Specific) Analysis, Incorporating Test Data

After the physical testing, and the observed behavior of the building components, particularly the ledge beams, fin columns and the joints, it seemed prudent to modify the structural components in SP3 based on the test observations. The columns did not exhibit non-ductile shear failure, and the joints did not sustain any significant damage. Therefore, components to match this behavior were selected.

Upgrading the structural components to match the testing observations, not only shows a reduction in the expected loss as shown in Table 5-10, but it also provided a more accurate estimate for this specific building. The Cost breakdowns shown in Table 5-11 and Figure 5-9, was 41% of the building replacement cost of $22.1 M.

In comparison to the model without considering the test data SEL dropped from 55% to 41%, and time to regain basic function dropped from 3.5 months and 7.8 months per FEMA-P58 and REDi Re-Occupancy, respectively, to 2.9 months and 4.7 months.

Table 5-10: Franz Tower – SP3 Detailed Analysis (With Test Data): Expected Loss (% of Total Building Value)

Shaking Intensity	Return Period	SEL (%)	SUL (%)
90% in 50 years	22 Years	3.3	5.4
50% in 30 years	43 Years	5.1	8.7
50% in 50 years	72 Years	7.9	14
50% in 75 years	108 Years	11	20
50% in 100 years	144 Years	15	28
20% in 50 years	224 Years	23	43
10% in 50 years	475 Years	41	69
DE	791 Years	57	92
5% in 50 years	975 Years	64	100
MCE_R	1956 Years	83	100
2% in 50 years	2475 Years	88	100

Table 5-11: Expected Mean Loss Breakdown – SP3 Detailed Analysis (With Test Data): Expected Loss

Intensity	Total	Structural	Collapse	Exterior	Other	HVAC	Partitions	Interior	Residual
90% in 50 years	3.3	0.0	0.0	0.3	1.5	1.5	0.0	0.0	0.0
50% in 30 years	5.1	0.2	0.0	1.3	1.8	1.7	0.0	0.1	0.0
50% in 50 years	7.9	0.9	0.1	2.9	2.0	1.8	0.1	0.2	0.0
50% in 75 years	11	2.7	0.2	4.1	2.2	1.8	0.2	0.2	0.0
50% in 100 years	15	4.9	0.5	5.0	2.3	1.9	0.3	0.4	0.0
20% in 50 years	23	10	1.4	6.4	2.4	1.9	0.5	0.4	0.0
10% in 50 years	41	22	5.4	8.3	2.4	1.9	0.7	0.6	0.0
DE	57	32	11	9.7	2.4	1.8	0.9	0.8	0.0
5% in 50 years	64	37	13	10.0	2.3	1.7	1.0	0.8	0.2
MCE_R	83	49	25	11	2.1	1.5	1.2	1.0	0.5
2% in 50 years	88	52	30	11	2.0	1.4	1.2	1.1	0.8

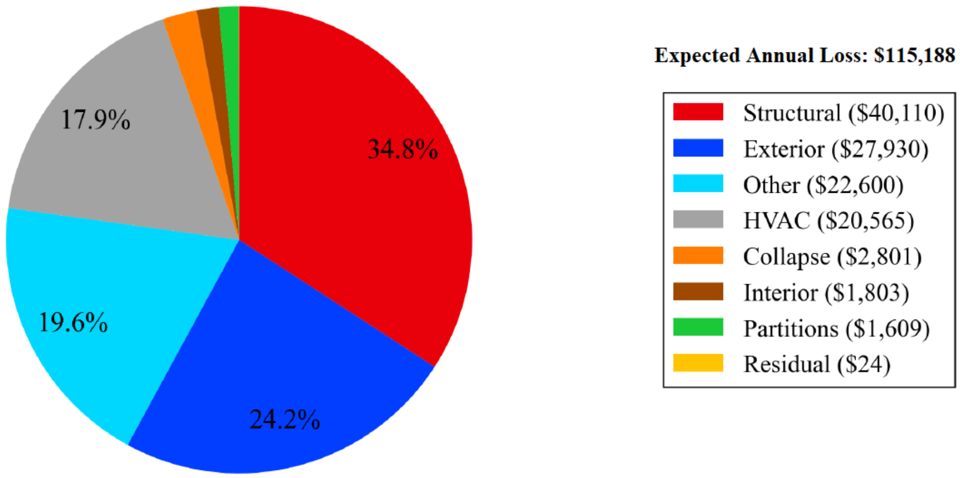

Figure 5-9: Annualized Loss Breakdown – SP3 Detailed Analysis (With Test Data): Expected Loss

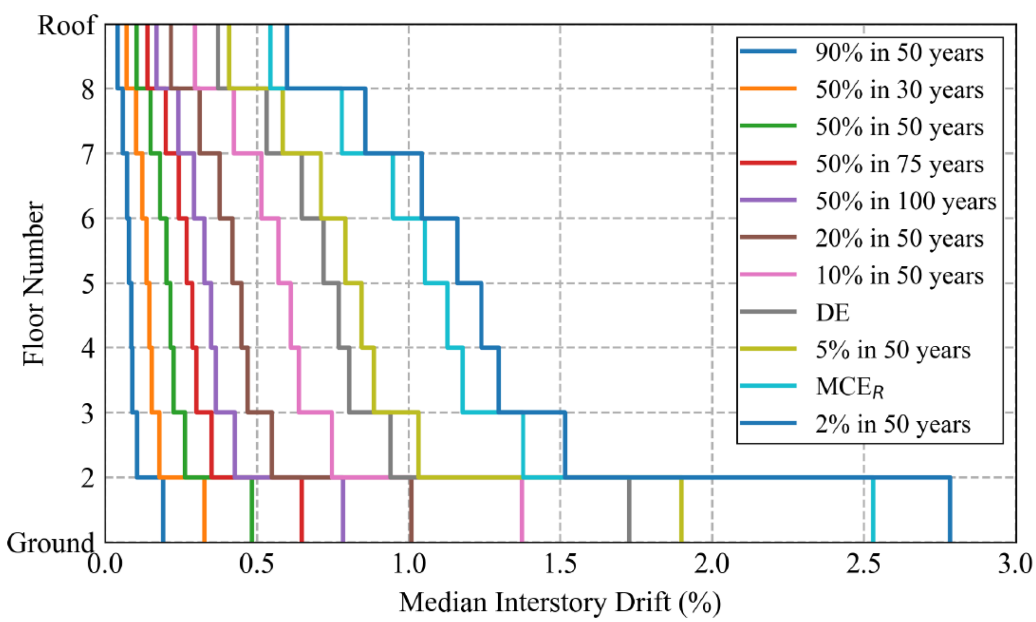

Figure 5-10: Peak Story Drift Demands – SP3 Detailed Analysis (With Test Data)

Table 5-12: Franz Tower – SP3 Detailed Analysis (With Test Data): Median Repair Time

Intensity	FEMA P-58 Parallel	FEMA P-58 Series	REDi Re-Occupancy	REDi Functional Recovery	REDi Full Recovery
90% in 50 years	5 days	6 days	0 days	8 days	8 days
50% in 30 years	7 days	12 days	1 days	13 days	13 days
50% in 50 years	11 days	3.5 weeks	5 days	2.8 weeks	2.8 weeks
50% in 75 years	2.7 weeks	6.5 weeks	13 days	4.0 weeks	4.0 weeks
50% in 100 years	3.8 weeks	2.3 months	3.3 weeks	5.3 weeks	5.3 weeks
20% in 50 years	6.2 weeks	4.3 months	7.2 weeks	2.1 months	2.1 months
10% in 50 years	2.9 months	11 months	4.7 months	5.1 months	5.1 months
DE	4.9 months	19 months	9.2 months	9.6 months	9.6 months
5% in 50 years	6.0 months	19 months	12 months	12 months	12 months
MCE_R	19 months	19 months	19 months	19 months	19 months
2% in 50 years	19 months	19 months	19 months	19 months	19 months

5.2.2. Evaluation of Retrofit Schemes

To compare the resiliency of the CMF, BRB, and VD retrofit schemes, building information and component data were obtained from the plans and calculations presented in Appendix A. All three scenarios were subjected to the same suite of 11 site specific ground motions from the US Geological Survey (USGS) database. The detailed reports from the analyses presented in this chapter are provided in Appendix H.

Later, a comparison is done for the VD retrofit scheme using engineering design parameters (EDP) such as maximum story drift ratios, residual story drift ratios, and peak story accelerations from the Perform-3D dynamic non-linear analyses formerly done to validate the VD retrofit scheme. The suite of ground motions used were provided by a geotechnical firm and approved by the peer review committee.

5.2.2.1 Exterior Concrete Moment Frames (CMF)

One of the first retrofit schemes proposed to the UCLA Capital Programs Group was to add 3-bay exterior special moment frames to all four exterior sides of the building as shown in Figure 5-11. The moment frame columns were spaced at 20 ft. (6096 mm) on center, aligned with the existing

24 in. (610 mm) square columns at levels 1 and 2. The first moment frame beam was placed at the same elevation of the level 3 slab framing 27 ft. (8230 mm) above ground, and the next beams were placed at each story slab level, every 12 ft. 9 in. (3886 mm).

In this retrofit scheme the new moment frame beam jacketed 15 existing shear-controlled ledge beams and 16 existing beam-column joints, on each exterior side of the building (see Figure 5-11). The jacket provided a connection between the existing frame and the new moment frame, and also reduced the number of vulnerable joints in each direction.

Since detailed retrofit design was not available to assess the extent of the proposed work, to model structural components in SP3, it was assumed this retrofit program included enhancing the performance of shear-controlled and flexure-shear-controlled interior columns by FRP wrapping too. Since shear deficiency in columns is a critical concern in seismic performance of buildings, and FRP wrapping is a very common means of addressing this issue, assuming the deficient columns would be repaired along with adding exterior moment frames, is a reasonable assumption.

A detailed SP3 analysis was run for this retrofit scheme. The average repair cost of the building normalized by total replacement cost, or Scenario Expected Loss (SEL), is 25% ($5.5 M) for a ground shaking with 475-year return period as highlighted in Table 5-13, with breakdown of the repair cost shown in Table 5-14 and Figure 5-12. It was expected that the retrofit brought the building to UCSPR level IV, with estimated 10-30% replacement cost.

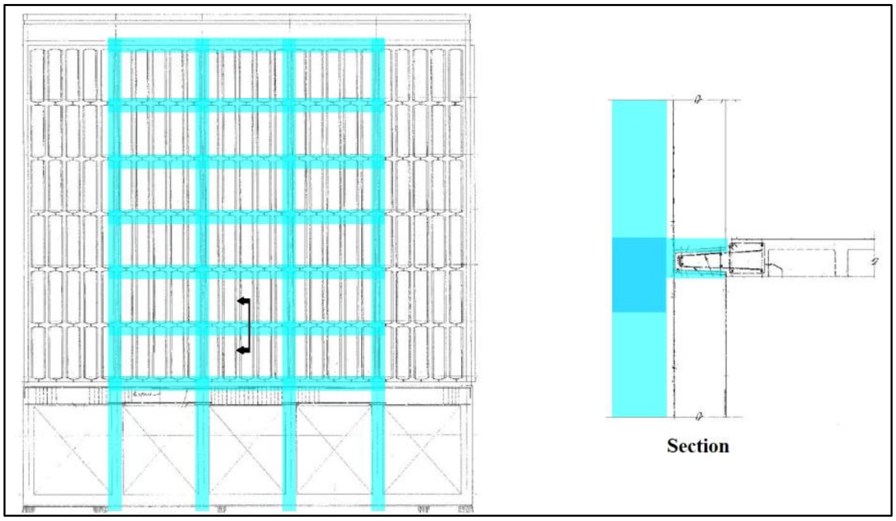

Figure 5-11: CMF Retrofit Scheme

Peak story drift demands are shown in Figure 5-13, with maximum drift ratio occurring at level 2 which is expected given the building geometry.

Repair time is calculated based on FEMA P-58 methodology, for both parallel and series repair, as well as different repair levels per REDi. Table 5-15 shows the median repair time with the values highlighted for the same level of ground shaking as before. Minimum repair time is 2.0 months per FEMA P-58, parallel sequence of repair, and 3.9 month per REDi for Re-Occupancy.

Table 5-13: Expected Loss – Exterior CMF Retrofit (% of Total Building Value)

Shaking Intensity	Return Period	SEL (%)	SUL (%)
90% in 50 years	22 Years	3.0	4.7
50% in 30 years	43 Years	3.8	5.8
50% in 50 years	72 Years	5.0	7.6
50% in 75 years	108 Years	7.1	12
50% in 100 years	144 Years	9.1	15
20% in 50 years	224 Years	14	25
10% in 50 years	475 Years	25	41
DE	791 Years	34	54
5% in 50 years	975 Years	39	62
MCE_R	1956 Years	54	87
2% in 50 years	2475 Years	59	94

Table 5-14: Expected Mean Loss Breakdown – Exterior CMF Retrofit

Intensity	PGA (g)	Mean (SEL) (%)	Fitted SUL (%)	Median (%)	Counted 90^{th} Percentile (%)
90% in 50 years	0.08	3.0	4.7	2.9	4.6
50% in 30 years	0.13	3.8	5.8	3.6	5.7
50% in 50 years	0.18	5.0	7.6	4.5	7.6
50% in 75 years	0.23	7.1	12	6.1	12
50% in 100 years	0.28	9.1	15	7.7	15
20% in 50 years	0.35	14	25	12	25
10% in 50 years	0.50	25	41	22	41
DE	0.62	34	54	31	54
5% in 50 years	0.68	39	62	36	62
MCE_R	0.87	54	87	50	100
2% in 50 years	0.95	59	94	56	100

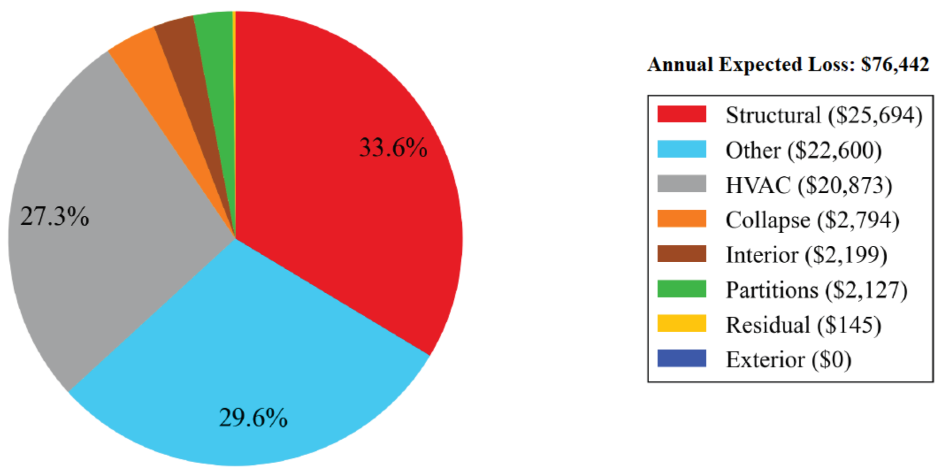

Figure 5-12: Annualized Loss Breakdown – Exterior CMF Retrofit

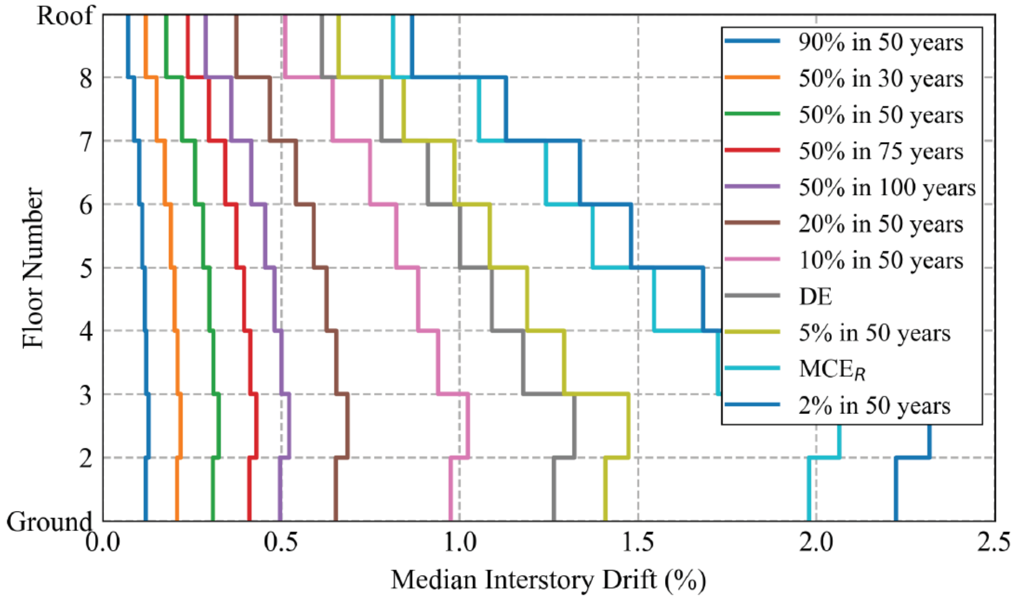

Figure 5-13: Peal Story Drift Demands – Exterior CMF Retrofit

Table 5-15: Median Repair Time – Exterior CMF Retrofit

Intensity	FEMA P-58 Parallel	FEMA P-58 Series	REDi Re-Occupancy	REDi Functional Recovery	REDi Full Recovery
90% in 50 years	5 days	6 days	0 days	8 days	8 days
50% in 30 years	7 days	11 days	0 days	13 days	13 days
50% in 50 years	10 days	3.1 weeks	3 days	2.7 weeks	2.7 weeks
50% in 75 years	2.2 weeks	5.6 weeks	12 days	3.9 weeks	3.9 weeks
50% in 100 years	2.8 weeks	2.1 months	3.3 weeks	5.3 weeks	5.3 weeks
20% in 50 years	4.5 weeks	3.9 months	6.8 weeks	2.0 months	2.0 months
10% in 50 years	2.0 months	8.7 months	3.9 months	4.2 months	4.2 months
DE	2.6 months	13 months	5.7 months	6.0 months	6.0 months
5% in 50 years	3.0 months	15 months	6.8 months	7.0 months	7.0 months
MCE$_R$	4.0 months	19 months	9.8 months	10 months	10 months
2% in 50 years	4.3 months	19 months	11 months	11 months	11 months

5.2.2.2 Exterior Buckling-Restrained Brace (BRB) Frames

Another proposed retrofit scheme was to add 3-bay exterior steel buckling restrained braced (BRB) frames. The schematic design as shown in Figure 5-14 provides braces at all levels above level 1, to provide open access to the building. The frame columns line up with the existing concrete columns spaced at 20 ft. (6096 mm) on center.

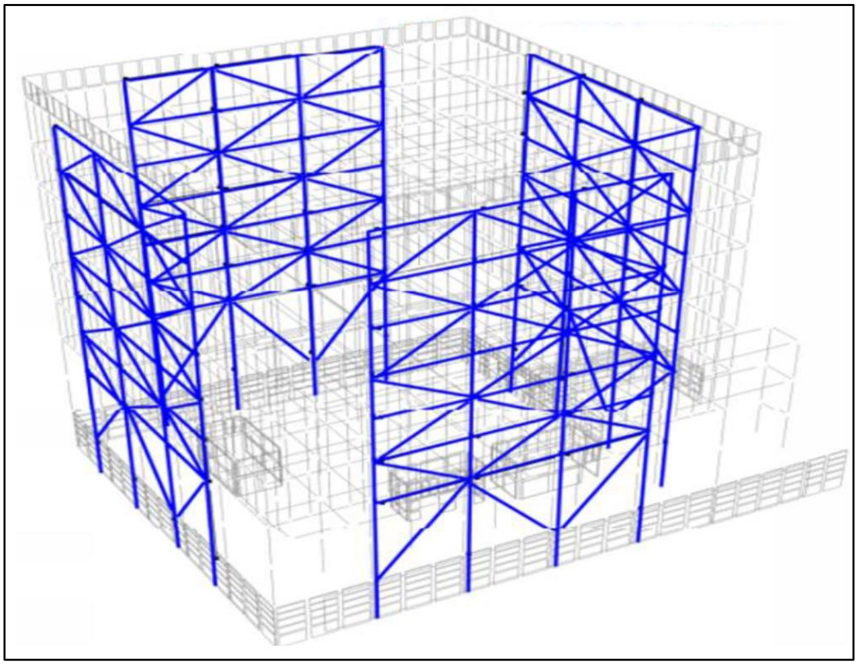

Figure 5-14: BRB Retrofit Scheme, 3D Schematic

Details on how the BRB frames connected to the existing building were not available. However, in order for the BRB frames help the existing building to perform desirably under seismic loading, it was assumed that the existing beams and fin columns to which the BRB frames connected, where enhanced to have adequate capacity and desirable performance. (Mahrenholtz, et al., 2015)

The analysis showed the SEL to be 20% ($4.4 M) as highlighted in Table 5-16, with breakdown of the repair cost shown in Table 5-15 and Figure 5-15. It was expected that the retrofit brought the building to UCSPR level IV, with estimated 10-30% replacement cost (Table 2-16).

Table 5-16: Expected Loss – Exterior BRB Retrofit

Shaking Intensity	Return Period	SEL (%)	SUL (%)
90% in 50 years	22 Years	3.1	4.8
50% in 30 years	43 Years	3.7	5.7
50% in 50 years	72 Years	4.7	7.1
50% in 75 years	108 Years	6.4	10
50% in 100 years	144 Years	8.1	13
20% in 50 years	224 Years	12	22
10% in 50 years	475 Years	20	37
DE	791 Years	28	49
5% in 50 years	975 Years	34	59
MCE_R	1956 Years	61	97
2% in 50 years	2475 Years	68	100

Table 5-17: Expected Mean Loss Breakdown – Exterior BRB Retrofit

Intensity	Total	Residual	Structural	Collapse	Interior	Other	HVAC	Partitions	Exterior
90% in 50 years	3.1	0.0	0.0	0.0	0.0	1.5	1.6	0.0	0.0
50% in 30 years	3.7	0.0	0.1	0.0	0.1	1.8	1.8	0.0	0.0
50% in 50 years	4.7	0.0	0.5	0.0	0.2	2.0	1.9	0.1	0.0
50% in 75 years	6.4	0.0	1.7	0.0	0.4	2.1	1.9	0.1	0.0
50% in 100 years	8.1	0.0	2.8	0.0	0.7	2.3	2.0	0.2	0.0
20% in 50 years	12	0.0	5.7	0.1	1.1	2.4	2.1	0.3	0.0
10% in 50 years	20	0.2	12	0.6	1.6	2.5	2.1	0.6	0.0
DE	28	0.7	18	1.8	2.0	2.6	2.1	0.8	0.0
5% in 50 years	34	3.0	21	2.7	2.1	2.5	2.0	0.8	0.0
MCE_R	61	30	17	8.0	1.8	1.7	1.3	0.7	0.0
2% in 50 years	68	37	15	11	1.6	1.4	1.1	0.6	0.0

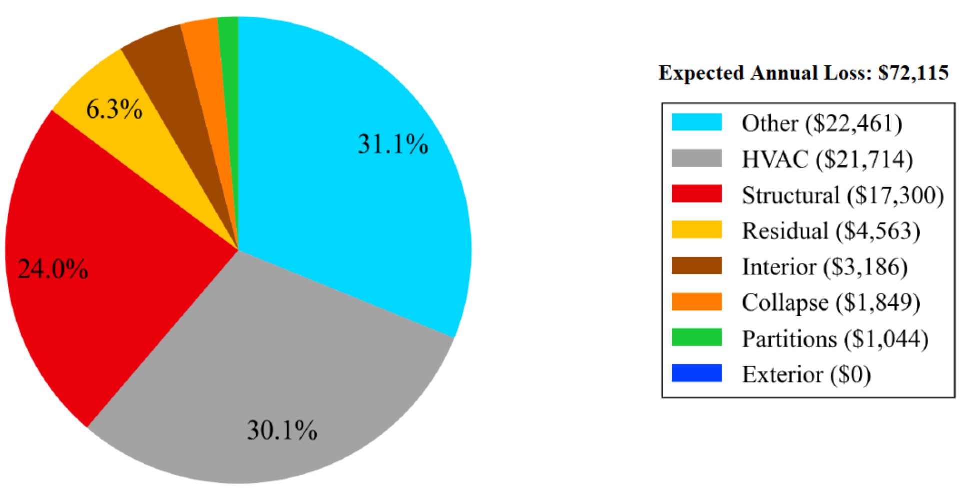

Figure 5-15: Annualized Loss Breakdown – Exterior BRB Retrofit

Figure 5-16 shows the maximum story drift demands, with the highest demand at levels 2 and 3, with smaller drift ratios in comparison to the CMF retrofit scenario. This explains the lower retrofit cost of this scheme, even though the CMF scheme had less vulnerable joints due to the CMF beam jacketing the joints.

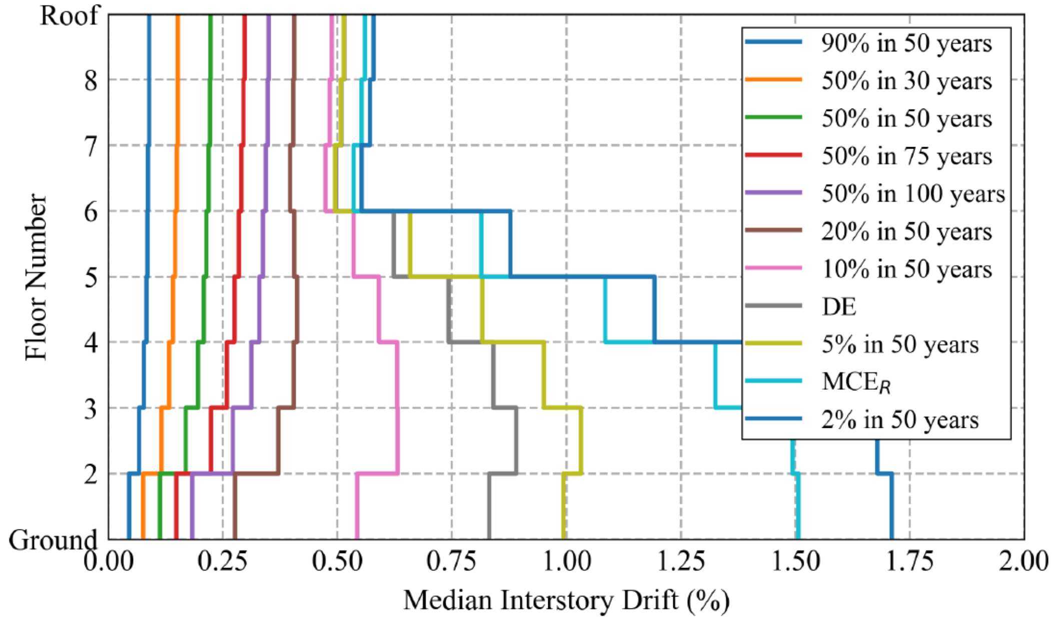

Figure 5-16: Peak Story Drift Demands – Exterior BRB Retrofit

Table 5-18: Median Repair Time – Exterior BRB Retrofit

Intensity	FEMA P-58 Parallel	FEMA P-58 Series	REDi Re-Occupancy	REDi Functional Recovery	REDi Full Recovery
90% in 50 years	5 days	6 days	0 days	8 days	8 days
50% in 30 years	7 days	10 days	0 days	13 days	13 days
50% in 50 years	10 days	2.6 weeks	1 days	2.6 weeks	2.6 weeks
50% in 75 years	14 days	4.5 weeks	7 days	3.5 weeks	3.5 weeks
50% in 100 years	2.8 weeks	7.2 weeks	2.5 weeks	4.5 weeks	4.5 weeks
20% in 50 years	3.9 weeks	2.8 months	4.8 weeks	6.6 weeks	6.6 weeks
10% in 50 years	6.8 weeks	5.7 months	2.4 months	2.8 months	2.8 months
DE	2.4 months	9.0 months	4.0 months	4.3 months	4.3 months
5% in 50 years	3.1 months	11 months	5.1 months	5.3 months	5.3 months
MCE$_R$	5.7 months	19 months	10 months	10 months	10 months
2% in 50 years	7.6 months	19 months	14 months	14 months	14 months

Table 5-18 shows the median repair time, with the values highlighted for the same level of ground shaking. Minimum repair time for the BRB retrofit is 6.8 weeks per FEMA P-58, parallel sequence of repair and 2.4 months for REDi Re-Occupancy.

5.2.2.3 Viscous Dampers (VD), Using Test Data and SP3 Default Ground Motions

The final retrofit scheme was to utilize the physical test data (from section 4.7) to predict the performance of structural components individually and building as a whole more accurately. In order to reduce the seismic demand on the building, 40 viscous dampers (eight at levels 1 to 6) were used as shown schematically in Figure 5-17.

Figure 5-18 is an example of an interior section showing the dampers. It should be noted that preliminary calculations required the use of viscous dampers at all eight levels of the building, however due to the desirable performance of the test specimens, viscous dampers were used at the lower six levels of the building.

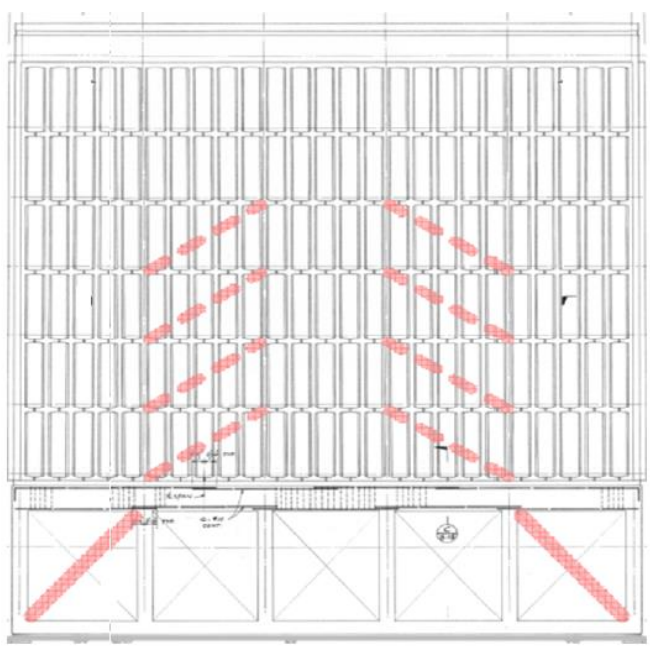

Figure 5-17: Location of Viscous Dampers

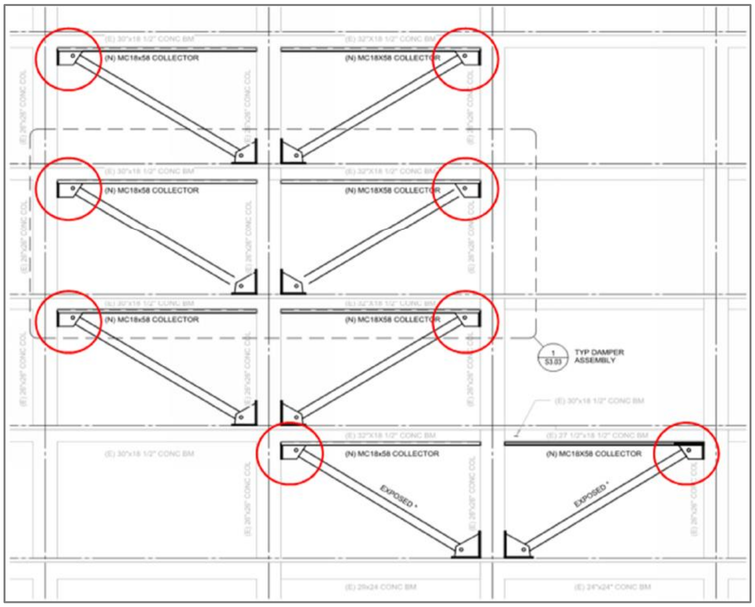

Figure 5-18: Interior Section – Location of Viscous Dampers

The analysis showed the SEL was 14% ($3.1 M) for the highlighted ground motion in Table 5-19, with the breakdown of cost shown in Table 5-20 and Figure 5-19.

Table 5-19: Expected Loss – VD Retrofit + Test Data

Shaking Intensity	Return Period	SEL (%)	SUL (%)
90% in 50 years	22 Years	3.0	4.7
50% in 30 years	43 Years	3.6	5.5
50% in 50 years	72 Years	4.3	6.5
50% in 75 years	108 Years	5.2	7.8
50% in 100 years	144 Years	6.3	9.9
20% in 50 years	224 Years	8.6	14
10% in 50 years	475 Years	14	25
DE	791 Years	21	38
5% in 50 years	975 Years	25	46
MCE_R	1956 Years	41	69
2% in 50 years	2475 Years	46	77

This retrofit scheme enhanced the performance of the building from UCSPR level V to level III. The approximate relationship between the UC seismic performance rating and the expected seismic performance level (in terms of repair cost and level of damage), is shown in Table 2-16.

A building with UCSPR of level III is expected to incur damages approximately 5-20% of its replacement cost.

Table 5-20: Expected Mean Loss Breakdown – VD Retrofit + Test Data

Intensity	Total	Structural	Collapse	Other	HVAC	Partitions	Interior	Residual	Exterior
90% in 50 years	3.0	0.0	0.0	1.5	1.5	0.0	0.0	0.0	0.0
50% in 30 years	3.6	0.0	0.0	1.8	1.7	0.0	0.1	0.0	0.0
50% in 50 years	4.3	0.2	0.0	2.0	1.8	0.1	0.2	0.0	0.0
50% in 75 years	5.2	0.7	0.0	2.2	1.9	0.2	0.3	0.0	0.0
50% in 100 years	6.3	1.3	0.1	2.3	1.9	0.3	0.4	0.0	0.0
20% in 50 years	8.6	3.0	0.2	2.4	2.0	0.5	0.5	0.0	0.0
10% in 50 years	14	7.0	1.3	2.5	2.0	0.8	0.7	0.0	0.0
DE	21	12	3.1	2.6	1.9	1.0	0.9	0.0	0.0
5% in 50 years	25	14	4.3	2.6	1.9	1.1	1.0	0.0	0.0
MCE_R	41	24	10	2.5	1.9	1.4	1.2	0.3	0.0
2% in 50 years	46	26	13	2.5	1.8	1.5	1.3	0.3	0.0

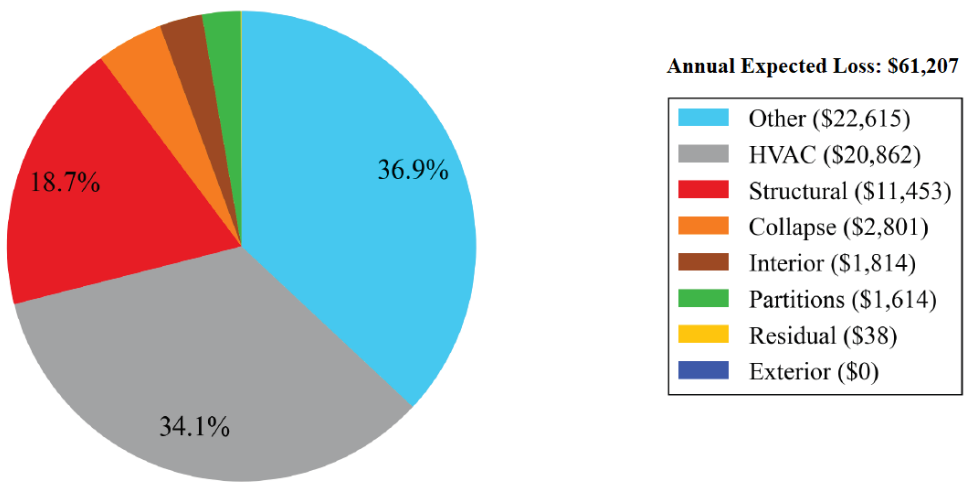

Figure 5-19: Annualized Expected Loss – VD Retrofit + Test Data

Figure 5-20 shows the peak story drift demands for the earthquake with return period of 475 years, was reduced to under 1%, with the highest drift demand ratio of 0.83% at level 1.

Table 5-21 shows the minimum repair time for the VD retrofit scenario is 4.3 weeks per FEMA P-58, parallel sequence of repair for the same level of ground shaking, and 6.3 weeks per REDi Re-Occupancy.

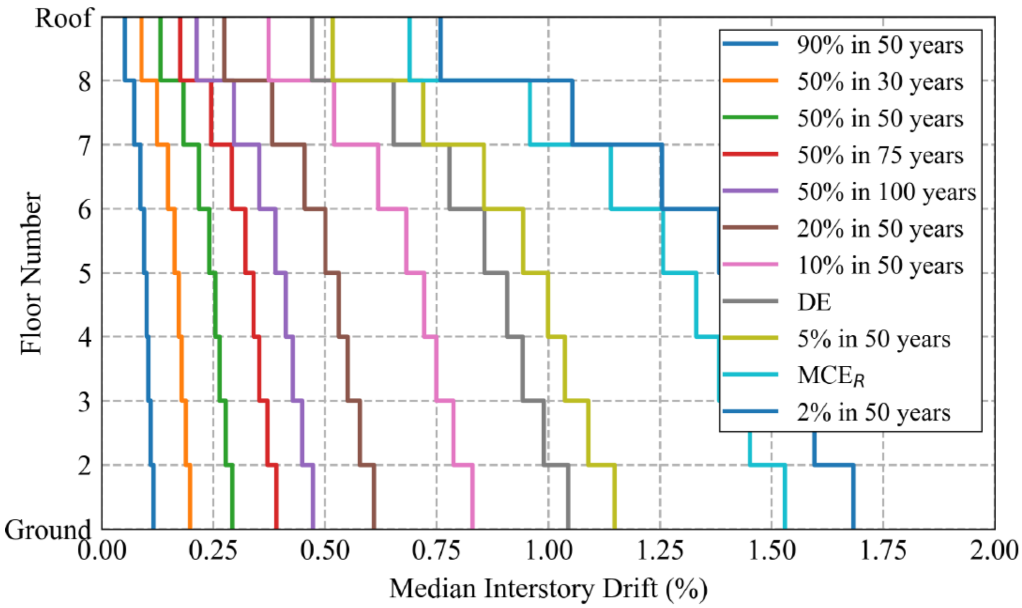

Figure 5-20: Peak Story Drift Demands – VD Retrofit + Test Data

Table 5-21: Median Repair Time – VD Retrofit + Test Data

Intensity	FEMA P-58 Parallel	FEMA P-58 Series	REDi Re-Occupancy	REDi Functional Recovery	REDi Full Recovery
90% in 50 years	5 days	6 days	0 days	8 days	8 days
50% in 30 years	6 days	10 days	0 days	12 days	12 days
50% in 50 years	9 days	2.3 weeks	1 days	2.4 weeks	2.4 weeks
50% in 75 years	11 days	3.5 weeks	3 days	2.9 weeks	2.9 weeks
50% in 100 years	2.1 weeks	4.9 weeks	8 days	3.4 weeks	3.4 weeks
20% in 50 years	2.8 weeks	1.9 months	2.7 weeks	4.7 weeks	4.7 weeks
10% in 50 years	4.3 weeks	3.7 months	6.3 weeks	7.9 weeks	7.9 weeks
DE	6.8 weeks	5.9 months	2.6 months	2.9 months	2.9 months
5% in 50 years	2.0 months	7.7 months	3.4 months	3.7 months	3.7 months
MCE$_R$	3.3 months	14 months	6.6 months	6.8 months	6.8 months
2% in 50 years	3.7 months	17 months	7.8 months	8.0 months	8.0 months

5.2.2.4 Viscous Dampers (VD), Using Test Data and Ground Motions Provided by Geotechnical Consultants

This final run used the ground motions obtained from the geotechnical consultant for the analysis of the building. Seven pairs of ground motions were run for four intensity levels (return periods of 225, 475, 975, and 2475 years), and the ground motion information was inputted in SP3 to analyze the building. Engineering design parameters (EDPs) from the dynamic analyses performed for residual story drift ratio were not available since the analyses had not been run long enough to establish that.

As shown in Figure 5-21 and Figure 5-22, and Table 5-22 to Table 5-24, the Expected loss for the 475-year earthquake is 21% which is 50% higher than the value obtained for the model that used the SP3 default ground motions of 11 intensity levels, and the annualized repair cost ($27,483) was significantly lower. Table 5-22 and Figure 5-21 do not seem to be consistent. The increase in the SEL was due to the increase in the mean spectral acceleration value, S_a, for 1 and 1.4 seconds, but the decrease in the annualized loss was due to insufficient number of hazard intensities provided to compute it accurately. Annualized losses are determined by integrating the loss curves (or vulnerability curves) with the hazard curve over the range of hazard intensities provided. Since the user-defined hazard only goes down to a return period of 225 years, smaller seismic events than that event were not accounted for properly in the numerical integration; as a result, the annualized loss calculation was inaccurate. The inter-story drift ratios and the repair times were also higher than the model with SP3 default ground motions.

Table 5-22: Expected Loss – VD Retrofit + Test Data

Shaking Intensity	Return Period	SEL (%)	SUL (%)
20% in 50 years	225 Years	12	21
10% in 50 years	475 Years	21	39
5% in 50 years	975 Years	35	60
2% in 50 years	2475 Years	59	95

Table 5-23: Expected Mean Loss Breakdown – VD Retrofit + Test Data and Input Ground Motions

Intensity	Total	Structural	Collapse	Other	Partitions	HVAC	Residual	Interior	Exterior
20% in 50 years	12	5.3	1.0	2.4	0.7	1.9	0.0	0.4	0.0
10% in 50 years	21	12	3.9	2.5	1.0	1.9	0.0	0.6	0.0
5% in 50 years	35	19	9.0	2.5	1.3	1.8	0.0	0.8	0.0
2% in 50 years	59	29	23	2.2	1.6	1.6	1.1	1.1	0.0

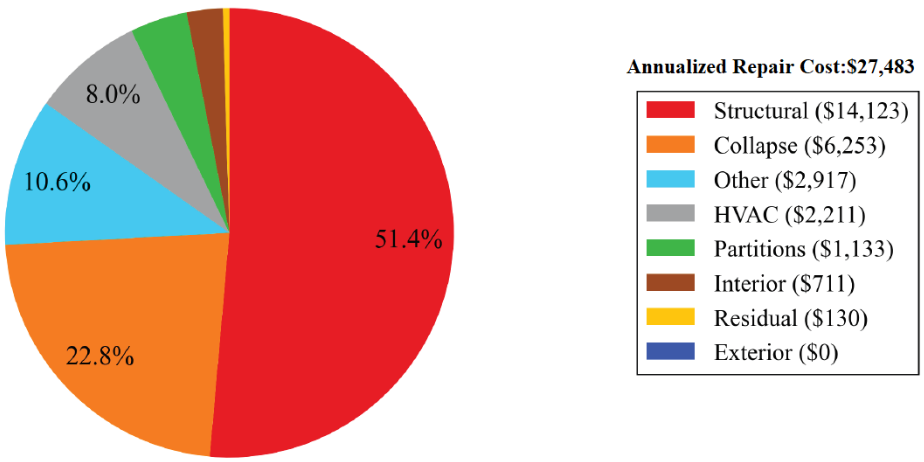

Figure 5-21: Annualized Expected Loss – VD Retrofit + Test Data and Input Ground Motions

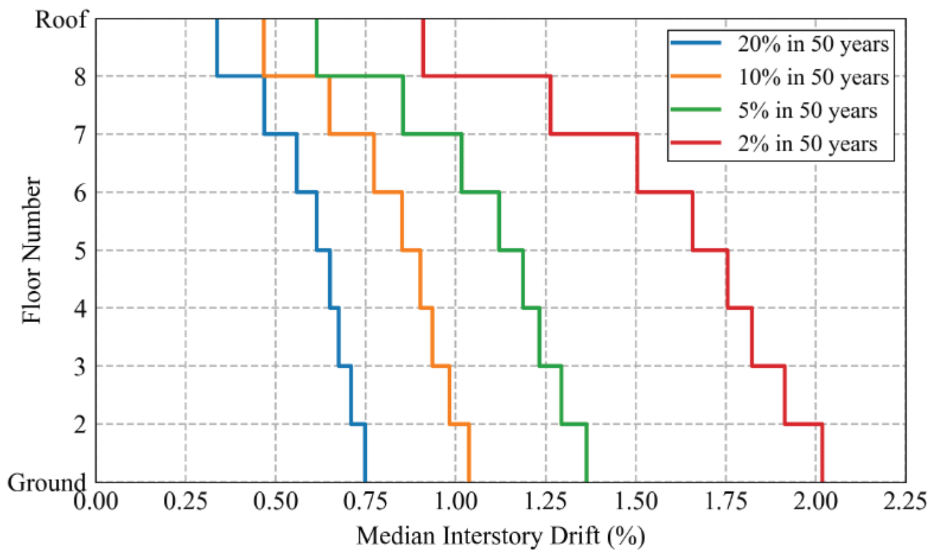

Figure 5-22: Peak Story Drift Demands – VD Retrofit + Test Data and Input Ground Motions

Table 5-24: Median Repair Time – VD Retrofit + Test Data and Input Ground Motions

Intensity	FEMA P-58 Parallel	FEMA P-58 Series	REDi Re-Occupancy	REDi Functional Recovery	REDi Full Recovery
20% in 50 years	3.6 weeks	2.8 months	4.4 weeks	6.4 weeks	6.4 weeks
10% in 50 years	6.6 weeks	5.8 months	2.5 months	2.9 months	2.9 months
5% in 50 years	2.7 months	11 months	5.0 months	5.3 months	5.3 months
2% in 50 years	4.9 months	19 months	11 months	11 months	11 months

It is concluded that if sufficient ground motion intensities are not provided, the site-specific default values by SP3 are expected to provide more reliable results.

Chapter 6. Conclusions and Recommendations

6.1. Conclusions

The objectives of this project were to use test results to provide accurate backbone relations for critical levels of an eight-story building with unusual geometric conditions subjected biaxial loading, instead of using ASCE 41-13 backbone relations which were deemed inappropriate and conservative.

The test results indicated that lateral drift ratios of greater than 1.0% were required to produce significant damage to the structural components, and that lateral drift levels of approximately 2% could be achieved prior to significant loss in the lateral load capacity of the test subassembly, while at no point during the test did the subassembly loss its capability to carry gravity loads.

The test results indicated substantially higher drift capacity than would be predicted based on backbone relations derived from Tables10-7 and 10-8 of ASCE 41-13 and ASCE 41-17. ASCE 41-13 indicated that lateral drift capacities of 0.50% (in-plane) and 0.80% (out-of-plane), and ASCE 41-17 predicted lateral drift capacities 1.49% (in-plane) and 1.28% (out of plane), prior to lateral strength loss. The deformation capacities for the in-plane direction at collapse per ASCE 41-13 and ASCE 41-17 were 2% and 4%, which were lower than demonstrated in the test, as the specimen did not reach collapse even after being subjected to a lateral drift ratio of 6%.

In the out-of-plane direction collapse per ASCE 41-13 and ASCE 41-17 occurred at drift ratios of 1.8% and 2% respectively. These values are relatively close to the stopping point of the experimental testing at 2.3% drift ratio for the out-of-plane direction. However, based on the observed behavior of the test specimens, and since the columns did not actually collapse at that drift ratio, it was expected that the building sustained larger lateral deformations than 2.3% prior to collapse.

The residual strengths based on ASCE 41-13 were 20%, whereas values of 27% for the in-plane and 19% for the out-of-plane direction were obtained using ASCE 41-17. The tests demonstrated higher residual strengths, 45% and 56% for the in-plane and out-of-plane directions, respectively. Even though backbone relations obtained from ASCE 41-17 were closer to those obtained from the test results. with some post-yield lateral deformations, they still underestimated the deformation capacity of the test structure, especially in the out-of-plane direction where the frame columns were determined to be shear-controlled.

Whereas the initial stiffness ratios of the test backbone and backbones from ASCE 41-13 and ASCE 41-17 were relatively close to that observed in the test in the positive in-plane direction, they were lower than the test results in the negative direction. This difference was attributed to the rapid softening of the test specimens due to the simultaneous in-plane and out-of-plane (biaxial) loading.

In the out-of-plane direction, the initial stiffnesses per ASCE 41-13 and 17, and the test observations were vastly different. The effective stiffness of the beams and fin columns per ASCE 41-13 (and ASCE41-17) Table 10-5 were $0.3EI_g$. Approaches to determine effective stiffness have been studied extensively; therefore, the more appropriate equations proposed by Elwood and Eberhard (2009) and a moment-curvature analysis were performed to obtain EI_{eff} were used and found to produce results more consistent with test results as shown in Chapter 4.

Shear strength of the building was estimated to be higher per ASCE 41-13 and 17 than observed in the tests. The main contributing factor to the lower base shear was the inadequate lap-splice length at column bases (see Appendix A). While the columns did not fail in shear (as expected by preliminary calculations in the out-of-plane direction), they were not able to achieve probable moment strength due to the premature lap-splice failure at the base. Another contributing factor was believed to be the biaxial loading which led to more rapid deterioration of the building components, and hence, resulting in an overall lower base shear. This reduction was also observed when comparing the base shear in the negative direction for both in-plane and out-of-plane loading, to the base shear in the positive direction for that same direction of loading. As the test specimens were first pushed in the positive direction (as discussed in section 3.6), the base shear in the positive direction was slightly higher than that in the negative direction.

Overall, the experimental results provided an accurate force-deformation relation for the building subassembly to be used in the final retrofit design with modeling parameters that represented the building performance more closely than using relationships from available standards. It should also be noted that the observed responses of the test specimens were for bi-axial loading at simultaneous maximum drift ratios for both in-plane and out-of-plane directions. Hence, it could be expected that the test result represented a lower-bound estimate of the deformation capacity of the building when subjected to bi-directional ground shaking.

Lastly, the test results produced information that led to a less disruptive retrofit (no viscous dampers on levels 7 and 8), resulting in savings in material and construction costs, as well as a less disruptive retrofit that preserved the exterior and architectural character of the building (the exterior frame system remained intact).

To assess the effect of the experimental results on the resilience-based earthquake design analysis of the building, SP3 analysis both with and without incorporating the test results was conducted. For the existing building analysis without the test data, the Seismic Expected Loss (SEL) was 55% of the total building value with annualized repair cost of $190,000, and repair time to regain function of 3.5 months per FEMA P-58 Parallel (and 7.8 months per REDi Re-Occupancy). Incorporating the experimental data and observations, those values reduced to 41%, $113,000 and

3.0 months (and 4.8 months), respectively. This estimate is especially important in determining whether it is financially and otherwise justified to retrofit an existing building (Appendix H).

It should be noted that, although resiliency was not originally considered as a factor in selecting a retrofit method for the Franz Tower, the final retrofit scheme based on the experimental testing and the use of viscous dampers, resulted in an efficient solution (if not an optimal solution). As summarized in Appendix H, the selected retrofit method had lower repair cost in comparison to the Buckling Restrained Brace (BRB) and Concrete Moment Frame (CMF) retrofit schemes (based on ASCE 41-13). Total repair costs were 14% of the total building cost for the Viscous Damper (VD) + test data retrofit versus 20% for the BRB and 25% for the CMF retrofit schemes. It also significantly reduced the time to repair and regain basic function: 4.3 weeks vs. 6.8 weeks and 2 months, respectively, improving the UCSPR of the building from rating level IV for BRB or CMF, to level III for the selected retrofit method.

6.2. Recommendations

In order to incorporate the test results into the non-linear computer modeling of the Franz Tower, several modifications to the modeling parameters or capacities of the structural components were made. These recommended adjustments are listed below and discussed in detailed in section 4.7:

- Based on the calculations, the lap length of the longitudinal reinforcement was insufficient at the column base, but it the bond stress was expected to be equal to the yield stress per equation 10-1 of ASCE 41-13. Therefore, the columns were expected to be shear-controlled in the out-of-plane direction and flexure-shear controlled in the in-plane direction. The observed behavior in both directions was governed by lap-splice slip, which limited the stresses in the bars such that the columns did not experience the brittle failures with rapid strength loss as suggested by ASCE41-13. Thus, the moment capacity of the specimen remained approximately constant (due to slip of longitudinal reinforcement) over a modest deformation range before strength loss was observed (Figure 4-41). To model this behavior, a backbone curve for the splice failure was developed that allowed plastic deformation as observed in the tests, prior to strength loss, with non-linear modeling parameter “a” of 0.0065 in the in-plane direction and 0.012 in the out-of-plane direction. The obtained backbone is conceptually similar to a flexure-shear controlled column, with modest non-linear deformation prior to strength loss (Appendix G).

- The residual strength ratio, “c” parameter, for the fin column moment hinges was 0.20 in axial compression, but this value was increased to 0.40 for flexure to obtain similar residual strength as the test (Figure 4-46).
- The beam assembly consisted of the ledge beam and the thickened slab edge (Figure 3-10). Although ACI 318-14 allows projection of the beam beyond the width of the supporting column, it does not allow the beam shear strength to be increased to account for the projected section (e.g., slab). As a result, the shear capacity of the thickened slab was not considered in modeling of the beam assembly in Perform-3D. Considering the analysis per the ACI 318-14 provision as a lower-bound analysis, an upper bound analysis was performed by considering the shear capacity of the ledge beams and the thickened slab, as shown in Appendix G. The test results suggested that the lower-bound analysis was a better representation of the actual performance of the specimen and the thickened slab edge was not effective in increasing the shear capacity of the frame beam.
- The flexural strength of the fin columns was reduced by a factor of 0.89 in the in-plane direction and 0.81 in the out-of-plane direction (Appendix A). The reduction for the in-plane direction is due to the inadequate lap lengths, while the lower reduction factor in the

out-of-plane direction was attributed to the cyclic damage of the columns. Pushing the columns beyond the splice strength in the in-plane direction prevented the columns from achieving their expected strength in the out-of-plane direction.

- Stiffness modifiers to obtain effective stiffness values for the columns, beam assembly and the transverse beams were obtained from ASCE41-13 (and 17), a moment-curvature analysis, and as proposed by Elwood and Eberhard (2009), see Table 4-2. The ratios obtained per Elwood and Eberhard (2009) best represented the test results for both directions of loading.

These adjustments captured the actual performance of the test specimens and produced pushover curves in close agreement with the test results (see section 4.7).

Although the geometry of this building is unique, it is similar to brutalist design and architecture that was common prior to about 1977. The findings of this experimental program can be used for non-linear modeling of other non-ductile concrete frame buildings having similar geometry and characteristics, with engineering judgment and peer review.

Lastly, most of the tests and research reported in the literature, and hence the building codes and standards, are based on tests of isolated test specimens. However, for highly redundant buildings, there is likely to be substantial benefit in performing building-specific testing of key components or subassemblies. This building was highly redundant, resulting in load redistribution, such that the observed strength loss was not as abrupt as for the isolated test specimens. Such buildings can benefit significantly from building specific testing for a more economical retrofit strategy.

6.3. Future Work

There are several areas related to non-ductile concrete frame buildings that can be topics of future research:

1. Based on the tests observations, one reason that may have contributed to the superior performance of the test specimen over prescriptive evaluation methods, was the high degree of redundancy of the frame system. The influence of redundancy has been studied in frame buildings, but the level of redundancy and how this degree of redundancy influences building performance requires further research. Other than the geometry of Franz Tower and short span between the fin columns, which is observed in many other buildings built in the same era, many of the non-ductile concrete frame buildings do not have a clearly identified lateral force resisting system. Even if they do, the detailing of these elements and of the gravity carrying elements are fairly similar (and inadequate compared to modern codes), resulting in almost equal participation of the identified lateral system and gravity system in resisting the lateral forces. As a result, many of such buildings have a high level of redundancy.
2. The lap splice failure was not expected to occur, but it was the governing mode of failure for the columns. Current non-linear modeling parameters per ASCE 41-13 and 17 do not take into account the ratio of the splice length provided to the splice length required. Whereas the failure, and non-linear modeling parameters for columns, are likely influenced by the degree to which the lap splice length is deficiency.
3. The joints in this building did not sustain major damage, but many non-ductile concrete frames with weak joints, are expected to sustain major damage. Repair of joints can be complicated and costly, and currently there is insufficient guideline to categorize joints based on observed performance in experimental testing, level of damage, and suggested effective retrofit method for each category of damage.

Appendix A. Building Component Capacity Calculations

A1. Franz Tower

Table A-1: Franz Tower Fin Column Moment Hinge Calculation

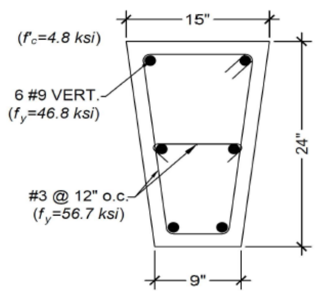

d (OOP) = 21.125 in
d (IP) = 9.125 in

6√fc.Ag = 119.7 kips
Lambda = 0.75

M/Vd = 4 (Conservatively assumed)
Ag = 288 in2

$$\frac{6\sqrt{fc}}{M/Vd} = 103.9 \quad \text{psi}$$

Steel Strength

Av.fy.d/s = 22.0 kips OOP
14.2 kips IP

Concrete Strength (ASCE 41-13 EQ 10.3)

$$V_n = kV_o = k\left[\frac{A_v f_y d}{s} + \lambda\left(\frac{6\sqrt{f'_c}}{M/Vd}\sqrt{1+\frac{N_u}{6\sqrt{f'_c}A_g}}\right)0.8A_g\right]$$

(lb/in.^{2} units)

Vc = 0.75 (103.9 x sqrt(1 + 20.3/120) (0.8 x 288 in2)
Vc = 25.5 kips

Shear Strength

Vs = 22 kips (OOP)
14.2 kips (IP)

Vc = 25.5 kips

Vn = 47.5 kips (OOP)
Vn = 39.7 kips (IP)

Mn @ Pn = 329 k.ft OOP
152 k.ft IP

Vp = 2Mn/h_c = 57.7 kips OOP
26.7 kips IP

h_c = (12 ft 9 in) - (16.5 in)
h_c = 11.4 ft

Vp/Vn = 1.21 OOP (shear)
0.67 OOP (flexure-shear)

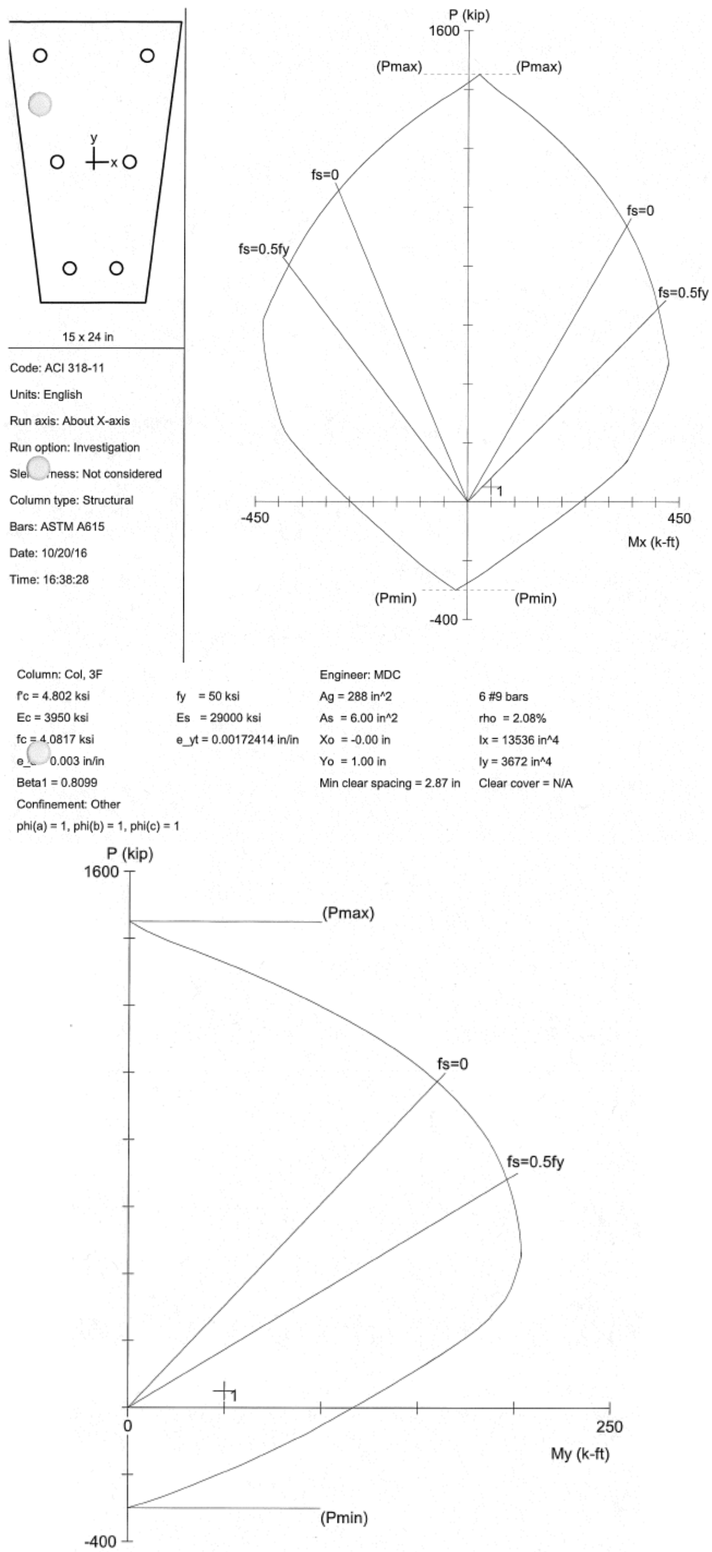

Figure A-1: Third Level Column P-M Diagram

Table A-2: Franz Tower 4th Level Beam Capacity and Governing Condition

ID	L [ft]	M_y [k-ft]	M_p [k-ft]	V_p [k]	V_n [k]	Governing Conditions	Moment Hinge Rotation Angles a	b	c	LS	CP
3B-2D N POS	17.8	257.6	317.4	45.4	57.3	i	0.017	0.025	0.200	0.017	0.025
3B-2D N NEG	17.8	70.8	82.8	22.1	57.1	i	0.020	0.030	0.200	0.020	0.030
3B-2D S POS	17.8	252.4	310.9	22.1	45.7	i	0.020	0.030	0.200	0.020	0.030
3B-2D S NEG	17.8	399.5	492.2	45.4	46.8	i	0.017	0.025	0.200	0.017	0.025
3B-11 N POS	19.3	491.6	606.9	62.9	58.6	i	0.020	0.030	0.200	0.020	0.030
3B-11 N NEG	19.3	491.6	606.9	62.9	58.6	i	0.020	0.030	0.200	0.020	0.030
3B-11 S POS	19.3	491.6	606.9	62.9	58.6	i	0.020	0.030	0.200	0.020	0.030
3B-11 S NEG	19.3	491.6	606.9	62.9	58.6	i	0.020	0.030	0.200	0.020	0.030
3B-1A N POS	17.8	439.3	542.1	64.4	58.8	i	0.020	0.030	0.200	0.020	0.030
3B-1A N NEG	17.8	491.6	606.9	68.1	58.8	ii	0.003	0.010	0.200	0.005	0.010
3B-1A S POS	17.8	491.6	606.9	68.1	58.8	ii	0.003	0.010	0.200	0.005	0.010
3B-1A S NEG	17.8	491.6	606.9	64.4	58.8	i	0.020	0.030	0.200	0.020	0.030
4B-1 E/N POS	19.3	268.4	328.3	39.6	51.4	i	0.019	0.029	0.200	0.019	0.029
4B-1 E/N NEG	19.3	241.2	294.2	32.2	51.4	i	0.020	0.030	0.200	0.020	0.030
4B-1 W/S POS	19.3	268.6	327.9	32.2	51.4	i	0.020	0.030	0.200	0.020	0.030
4B-1 W/S NEG	19.3	355.8	436.0	39.6	51.7	i	0.018	0.027	0.200	0.018	0.027
4B-2A E POS	17.8	238.6	292.2	40.7	48.0	i	0.015	0.022	0.200	0.015	0.022
4B-2A E NEG	17.8	58.3	66.8	20.1	47.5	i	0.020	0.030	0.200	0.020	0.030
4B-2A W POS	17.8	239.0	291.5	20.1	48.0	i	0.020	0.030	0.200	0.020	0.030
4B-2A W NEG	17.8	353.4	433.3	40.7	48.3	i	0.017	0.025	0.200	0.017	0.025
4B-2 E/N POS	17.8	240.4	294.6	41.0	51.6	i	0.015	0.023	0.200	0.015	0.023
4B-2 E/N NEG	17.8	60.3	68.8	20.4	51.1	i	0.020	0.030	0.200	0.020	0.030
4B-2 W/S POS	17.8	241.6	294.2	20.4	51.6	i	0.020	0.030	0.200	0.020	0.030
4B-2 W/S NEG	17.8	356.1	436.5	41.0	51.9	i	0.017	0.025	0.200	0.017	0.025
4B-3 E/N POS	19.3	301.0	367.7	34.3	51.8	i	0.014	0.021	0.200	0.014	0.021
4B-3 E/N NEG	19.3	61.0	69.5	22.7	51.1	i	0.020	0.030	0.200	0.020	0.030
4B-3 W/S POS	19.3	300.6	368.2	22.7	51.8	i	0.018	0.028	0.200	0.018	0.028
4B-3 W/S NEG	19.3	241.0	294.2	34.3	51.4	i	0.020	0.030	0.200	0.020	0.030
4B-2F E/N POS	17.8	273.7	336.3	47.0	58.2	i	0.016	0.024	0.200	0.016	0.024
4B-2F E/N NEG	17.8	65.5	75.2	23.1	57.6	i	0.020	0.030	0.200	0.020	0.030
4B-2F W/S POS	17.8	274.9	335.8	23.1	58.2	i	0.020	0.030	0.200	0.020	0.030
4B-2F W/S NEG	17.8	408.1	501.5	47.0	58.6	i	0.017	0.026	0.200	0.017	0.026
4B-2B E POS	17.8	273.7	336.3	47.0	58.2	i	0.016	0.024	0.200	0.016	0.024
4B-2B E NEG	17.8	65.5	75.2	23.1	57.6	i	0.020	0.030	0.200	0.020	0.030
4B-2B W POS	17.8	274.9	335.8	23.1	58.2	i	0.020	0.030	0.200	0.020	0.030
4B-2B W NEG	17.8	408.1	501.5	47.0	58.6	i	0.017	0.026	0.200	0.017	0.026
4B-2C E POS	17.8	240.4	294.6	46.2	51.6	i	0.015	0.023	0.200	0.015	0.023
4B-2C E NEG	17.8	60.3	68.8	20.2	51.1	i	0.020	0.030	0.200	0.020	0.030
4B-2C W POS	17.8	239.0	291.4	20.2	48.0	i	0.020	0.030	0.200	0.020	0.030
4B-2C W NEG	17.8	433.3	530.1	46.2	48.9	i	0.014	0.021	0.200	0.014	0.021

Table A-1: Franz Tower 4th Level Beam Capacity and Governing Condition (Cont'd.)

ID	L [ft]	M_y [k-ft]	M_p [k-ft]	V_p [k]	V_n [k]	Governing Conditions	Moment Hinge Rotation Angles a	b	c	LS	CP
4B-3A E POS	19.3	301.0	367.7	34.3	51.8	i	0.014	0.021	0.200	0.014	0.021
4B-3A E NEG	19.3	61.0	69.5	22.7	51.1	i	0.020	0.030	0.200	0.020	0.030
4B-3A W POS	19.3	300.6	368.2	22.7	51.8	i	0.018	0.028	0.200	0.018	0.028
4B-3A W NEG	19.3	241.0	294.2	34.3	51.4	i	0.020	0.030	0.200	0.020	0.030
4B-2G E POS	17.8	241.7	296.4	41.2	54.4	i	0.016	0.024	0.200	0.016	0.024
4B-2G E NEG	17.8	61.8	70.3	20.6	54.1	i	0.020	0.030	0.200	0.020	0.030
4B-2G W POS	17.8	243.6	296.3	20.6	54.4	i	0.020	0.030	0.200	0.020	0.030
4B-2G W NEG	17.8	358.2	438.9	41.2	54.7	i	0.017	0.026	0.200	0.017	0.026
4B-10 N POS	19.3	193.4	234.0	27.4	50.7	i	0.020	0.030	0.200	0.020	0.030
4B-10 N NEG	19.3	355.5	434.8	30.9	51.7	i	0.016	0.024	0.200	0.016	0.024
4B-10 S POS	19.3	133.8	160.6	30.9	50.8	i	0.020	0.030	0.200	0.020	0.030
4B-10 S NEG	19.3	240.8	294.3	27.4	51.4	i	0.017	0.026	0.200	0.017	0.026
4B-2E N POS	17.8	227.6	279.7	39.1	32.9	ii	0.003	0.010	0.200	0.005	0.010
4B-2E N NEG	17.8	340.8	417.7	39.1	33.4	ii	0.003	0.010	0.200	0.005	0.010
4B-2E S POS	17.8	227.6	279.7	39.1	32.9	ii	0.003	0.010	0.200	0.005	0.010
4B-2E S NEG	17.8	340.8	417.7	39.1	33.4	ii	0.003	0.010	0.200	0.005	0.010
4B-9 N POS	37.8	850.1	1054.7	54.2	85.7	i	0.019	0.028	0.200	0.019	0.028
4B-9 N NEG	37.8	802.5	995.5	50.6	85.1	i	0.020	0.030	0.200	0.020	0.030
4B-9 S POS	37.8	741.5	919.6	50.6	85.7	i	0.019	0.028	0.200	0.019	0.028
4B-9 S NEG	37.8	802.5	995.5	54.2	85.1	i	0.020	0.030	0.200	0.020	0.030
4B-1A N POS	17.8	407.4	500.7	56.1	58.6	i	0.020	0.030	0.200	0.020	0.030
4B-1A N NEG	17.8	407.4	500.7	53.9	58.6	i	0.020	0.030	0.200	0.020	0.030
4B-1A S POS	17.8	375.2	460.7	53.9	58.6	i	0.020	0.030	0.200	0.020	0.030
4B-1A S NEG	17.8	407.4	500.7	56.1	58.6	i	0.020	0.030	0.200	0.020	0.030
4B-2D N POS	17.8	240.4	294.6	40.3	51.6	i	0.015	0.023	0.200	0.015	0.023
4B-2D N NEG	17.8	60.3	68.8	19.8	51.1	i	0.020	0.030	0.200	0.020	0.030
4B-2D S POS	17.8	232.1	284.3	19.8	38.6	i	0.020	0.030	0.200	0.020	0.030
4B-2D S NEG	17.8	345.9	424.2	40.3	39.1	i	0.016	0.023	0.200	0.016	0.023
4B-11 N POS	19.3	356.1	436.9	45.2	51.7	i	0.018	0.028	0.200	0.018	0.028
4B-11 N NEG	19.3	300.5	367.5	41.6	51.8	i	0.020	0.030	0.200	0.020	0.030
4B-11 S POS	19.3	355.4	435.7	41.6	51.7	i	0.020	0.030	0.200	0.020	0.030
4B-11 S NEG	19.3	355.4	435.7	45.2	51.7	i	0.020	0.030	0.200	0.020	0.030

Table A-3: Franz Tower Ledge Beam Capacity and Governing Condition

ID	L [ft]	M_y [k-ft]	M_p [k-ft]	V_p [k]	V_n [k]	Governing Conditions	a	b	c	LS	CP
3rd FLOOR LEDGE BEAM	17.5	2855.2	3527.7	402.5	411.4	i	0.020	0.030	0.200	0.020	0.030
3rd FLOOR LEDGE BEAM	17.5	2822.7	3516.8	402.5	411.4	i	0.020	0.030	0.200	0.020	0.030
3rd FLOOR LEDGE BEAM	17.5	2855.2	3527.7	402.5	411.4	i	0.020	0.030	0.200	0.020	0.030
3rd FLOOR LEDGE BEAM	17.5	2822.7	3516.8	402.5	411.4	i	0.020	0.030	0.200	0.020	0.030
L4 BEAM AT FIN COLUMN BOTTOM (H/S-20)	2.8	1364.4	1784.4	1272.0	759.9	ii	0.003	0.020	0.200	0.010	0.020
L4 BEAM AT FIN COLUMN BOTTOM (H/S-20)	2.8	1311.3	1713.6	1272.0	761.5	ii	0.003	0.020	0.200	0.010	0.020
L4 BEAM AT FIN COLUMN BOTTOM (H/S-20)	2.8	1364.4	1784.4	1272.0	759.9	ii	0.003	0.020	0.200	0.010	0.020
L4 BEAM AT FIN COLUMN BOTTOM (H/S-20)	2.8	1311.3	1713.6	1272.0	761.5	ii	0.003	0.020	0.200	0.010	0.020
LEDGE BEAM 8th FLOOR	2.8	170.2	206.0	149.8	74.7	ii	0.003	0.010	0.200	0.005	0.010
LEDGE BEAM 8th FLOOR	2.8	170.2	206.0	149.8	74.7	ii	0.003	0.010	0.200	0.005	0.010
LEDGE BEAM 8th FLOOR	2.8	170.2	206.0	149.8	74.7	ii	0.003	0.010	0.200	0.005	0.010
LEDGE BEAM 8th FLOOR	2.8	170.2	206.0	149.8	74.7	ii	0.003	0.010	0.200	0.005	0.010
LEDGE BEAM 6th-7th FLOOR	2.8	190.6	231.2	168.1	75.5	ii	0.003	0.010	0.200	0.005	0.010
LEDGE BEAM 6th-7th FLOOR	2.8	190.6	231.2	168.1	75.5	ii	0.003	0.010	0.200	0.005	0.010
LEDGE BEAM 6th-7th FLOOR	2.8	190.6	231.2	168.1	75.5	ii	0.003	0.010	0.200	0.005	0.010
LEDGE BEAM 6th-7th FLOOR	2.8	190.6	231.2	168.1	75.5	ii	0.003	0.010	0.200	0.005	0.010
LEDGE BEAM 4th-5th FLOOR	2.8	214.6	260.6	189.5	76.4	ii	0.003	0.010	0.200	0.005	0.010
LEDGE BEAM 4th-5th FLOOR	2.8	214.6	260.6	189.5	76.4	ii	0.003	0.010	0.200	0.005	0.010
LEDGE BEAM 4th-5th FLOOR	2.8	214.6	260.6	189.5	76.4	ii	0.003	0.010	0.200	0.005	0.010
LEDGE BEAM 4th-5th FLOOR	2.8	214.6	260.6	189.5	76.4	ii	0.003	0.010	0.200	0.005	0.010

Table A-4: Franz Tower Beam-Column Joint Calculation - Example

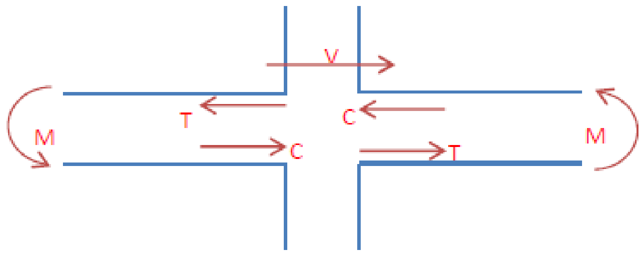

$V_{jh} = T + C - V_{col}$

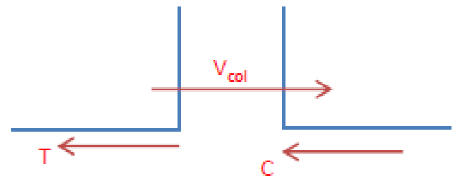

Joint: B5, North-South (4th story)

Column: C26x26, LWC, 8#10, #3@16" (3rd-3rd)

$V_{n,\ column}$ = 68.3 k

Beams connected to joint: 4B-1 W/S, 4B-2 E/N

Top rebar on 4B-1 W/S:	A_s =	6.24	in^2	f_y =	40.0	ksi
Bottom rebar on 4B-1 W/S:	A_s =	4.54	in^2			
Top rebar on 4B-2 E/N:	A_s =	0.62	in^2	f_y =	40.0	ksi
Bottom rebar on 4B-2 E/N:	A_s =	4.00	in^2			

The magnitude of (T+C) must be considered with seismic forces in either direction:

$$(T+C) = \text{Maximum of} \begin{cases} [6.24 \times 40.0 + 4.00 \times 40.0\ ]\ k = & 409.6\ k \\ [4.54 \times 40.0 + 0.62 \times 40.0\ ]\ k = & 206.4\ k \end{cases}$$

= 409.6 k

$V_{jh} = T + C - V_{col}$

= 341.3 k

h_c =	26	in	Joint Geometry:	a	Interior joint with transverse beams
b_c =	26	in	s_v =	16	in
A_j =	676	in^2	γ =	12	
f'_c =	4487	psi	$V_{n,\ joint}$ =	$\gamma\lambda A_j sqrt(f'_c)$	
λ =	0.75		=	407.5	k

DCR = 0.84 OK

A2. Test Specimens

Table A-5: Specimen Sizing – Exterior Columns

Element	Component	Unit	Full Scale (1)	Required (0.67-scale) (2)	Actual (0.67-scale) (3)	Actual Value (4) = (3)/(1)	Target Value (5)	Ratio (6) = (5)/(4)
Column	$b_{(min)}$	Inch	9.00	6.00	6.00	0.67	0.67	**1.00**
	$b_{(max)}$	Inch	15.0	10.0	10.0	0.67	0.67	**1.00**
	$b_{(average)}$	Inch	12.0	8.00	8.00	0.67	0.67	**1.00**
	h	Inch	24.0	16.0	16.0	0.67	0.67	**1.00**
	Cover to CL of Long. Bar	Inch	2.94	1.96	1.90	0.65	0.67	**0.97**
	$d_{bar,L\ (\#9:\#5)}$	Inch	1.127	0.75	0.625	0.55	0.67	**0.83**
	$A_{bar,L\ (\#9:\#5)}$	$Inch^2$	1.00	0.444	0.310	0.31	0.44	**0.70**
	Number of Bars	-	6	6	6	1.00	1.00	**1.00**
	$A_{Total,L}$	$Inch^2$	6.00	2.67	1.86	0.31	0.44	**0.70**
	$A_{Total,L}/(b_{ave}h)$	-	0.021	0.021	0.015	0.70	1.00	**0.70**
	$f_{y,L\ (\#9:\#5)}$	ksi	46.8	46.8	66.2	1.41	1.00	**1.41**
	$A_L.f_{y,L}$	kips	280.8	124.8	123.1	0.44	0.44	**0.99**
	$d_{bar,T\ (\#3:\#2)}$	Inch	0.375	0.250	1/4	0.67	0.67	**1.00**
	$A_{T\ (\#3:\#2)}$	$Inch^2$	0.11	0.049	0.049	0.45	0.44	**1.00**
	$f_{y,T}$	ksi	56.7	56.7	48.0	0.85	1.00	**0.85**
	$A_T.f_{y,T}/s$	kips	0.520	0.347	0.349	0.67	0.67	**1.01**
	s	Inch	12.00	8.00	6.75	0.56	0.67	**0.84**
	$s / b_{(ave)}$	-	1.000	1.000	0.844	0.84	1.00	**0.84**
	s / d_b	-	10.6	10.6	10.8	1.01	1.00	**1.01**
	f'_c	ksi	4.81	4.81	5.50	1.14	1.00	**1.14**
	$\sqrt{f'_c}$	psi	69.4	69.4	74.2	1.07	1.00	**1.07**

Table A-6: Specimen Sizing – Exterior Beams

Element	Component	Unit	Full Scale (1)	Required (0.67-scale) (2)	Actual (0.67-scale) (3)	Actual Value (4) = (3)/(1)	Target Value (5)	Ratio (6) = (5)/(4)
Trapezoidal Ledge Beam	b	Inch	24.0	16.0	16.0	0.67	0.67	**1.00**
	h_{short}	Inch	9.00	6.00	6.00	0.67	0.67	**1.00**
	h_{long}	Inch	12.0	8.00	8.00	0.67	0.67	**1.00**
	$h_{average}$	Inch	10.5	7.00	7.00	0.67	0.67	**1.00**
	Cover to CL of Long. Bar	Inch	1.625	1.08	1.125	0.69	0.67	**1.04**
	$d_{bar,L\ (\#8:\#5\&\#4)}$	Inch	1.00	0.67	0.56	0.56	0.67	**0.84**
	$A_{bar,L\ (\#8:\#5\&\#4)}$	$Inch^2$	0.79	0.35	0.25	0.32	0.44	**0.71**
	Number of Bars	-	4	4	4	1.00	1.00	**1.00**
	$A_{Total,L\ (\#8:\#5\&\#4)}$	$Inch^2$	3.16	1.40	1.00	0.32	0.44	**0.71**
	$A_{Total,L\ (\#8:\#5\&\#4)}/(bh_{ave})$	-	0.013	0.013	0.009	0.71	1.00	**0.71**
	$f_{y,L}$	ksi	46.8	46.8	66.2	1.41	1.00	**1.41**
	$A_L.f_{y,L}$	kips	147.9	65.7	60.2	0.41	0.44	**0.92**
	$d_{bar,T(\#4:\#2)}$	Inch	0.50	0.33	0.25	0.50	0.67	**0.75**
	$A_{bar,T(\#4:\#2)}$	$Inch^2$	0.20	0.09	0.05	0.25	0.44	**0.55**
	$f_{y,T(\#4:\#2)}$	ksi	46.8	46.8	64.3	1.37	1.00	**1.37**
	$A_T.f_{y,T}/s_{\ (\#4:\#2)}$	kips	0.78	0.52	0.53	0.67	0.67	**1.01**
	s	Inch	12.0	8.00	6.00	0.50	0.67	**0.75**
	s / h_{ave}	-	1.14	1.14	0.86	0.75	1.00	**0.75**
	$s / d_{b\ (\#8)}$	-	12.0	12.0	10.7	0.89	1.00	**0.89**
	f'_c	ksi	4.81	4.81	5.50	1.14	1.00	**1.14**
	$\sqrt{f'_c}$	psi	69.4	69.4	74.2	1.07	1.00	**1.07**

Table A-7: Specimen Sizing – Interior Beam

Element	Component	Unit	Full Scale (1)	Required (0.67-scale) (2)	Actual (0.67-scale) (3)	Actual Value (4) = (3)/(1)	Target Value (5)	Ratio (6) = (5)/(4)
Interior Slab Beam	b	Inch	18.5	12.3	12.3	0.66	0.67	**1.00**
	h	Inch	30.0	20.0	20.0	0.67	0.67	**1.00**
	Cover to CL of Long. Bar	Inch	2.94	1.96	2.00	0.68	0.67	**1.02**
	$d_{bar,L,top\ (\#10:\#6)\ @\ face\ of\ col.}$	Inch	1.27	0.85	0.75	0.59	0.67	**0.89**
	$d_{bar,L,top\ (\#9:\#5)\ anchored}$	Inch	1.128	0.75	0.625	0.55	0.67	**0.83**
	$d_{bar,L,bot\ (\#10:\#6)\ anchored}$	Inch	1.27	0.85	0.44	0.35	0.44	**0.79**
	$d_{bar,T\ (\#3:\#2)}$	Inch	0.375	0.25	0.25	0.67	0.67	**1.00**
	$A_{bar,L,top\ (\#10:\#6)\ @\ F.O.C.}$	$Inch^2$	1.27	0.56	0.44	0.35	0.44	**0.78**
	$A_{bar,L,top\ (\#9:\#5)\ anchored}$	$Inch^2$	1.00	0.44	0.31	0.31	0.44	**0.70**
	$A_{bar,L,bot}$	$Inch^2$	1.27	0.56	0.44	0.35	0.44	**0.78**
	$A_{bar,T\ (\#3:\#2)}$	$Inch^2$	0.11	0.05	0.05	0.45	0.44	**1.00**
	No. of Top Bars F.O.C.	-	2	2	2	1.00	1.00	**1.00**
	No. of Top Bars Anchored	-	2	2	2	1.00	1.00	**1.00**
	Number of Bot Bars	-	4	4	4	1.00	1.00	**1.00**
	$A_{L,Top\ (2\#10:2\#6)}$	$Inch^2$	2.54	1.13	0.88	0.35	0.44	**0.78**
	$A_{L,Top\ (2\#9:2\#5)}$	$Inch^2$	2.00	0.89	0.62	0.31	0.44	**0.70**
	$A_{Total,L,Top}/(bh)$	-	0.008	0.008	0.006	0.75	1.00	**0.75**
	$A_{Total,L,Bot}$	$Inch^2$	5.08	2.26	1.76	0.35	0.44	**0.78**
	$A_{Total,L,Bot}/(bh)$	$Inch^2$	0.009	0.009	0.007	0.78	1.00	**0.78**
	$A_{L,top}.f_{y,L}$	kips	212.5	94.4	99.3	0.47	0.44	**1.05**
	$A_{L,bot}.f_{y,L}$	kips	237.7	105.7	116.5	0.49	0.44	**1.10**
	$f_{y,L(\#9)}$	ksi	46.8	46.8	66.2	1.41	1.00	**1.41**
	$f_{y,L(\#10)}$	ksi	46.8	46.8	66.2	1.41	1.00	**1.41**
	$d_{Tie\ (\#3:\#2)}$	Inch	0.375	0.25	0.25	0.67	0.67	**1.00**
	$A_{T\ (\#3:\#2)}$	$Inch^2$	0.11	0.05	0.05	0.45	0.44	**1.00**
	$A_T.f_{y,T}/s$	kips	0.5	0.3	0.3	0.73	0.67	**1.10**
	$f_{y,T}$	ksi	52.0	52.0	48.0	0.92	1.00	**0.92**
	s	Inch	12.0	8.00	6.75	0.56	0.67	**0.84**
	$s\ /d_{b\ (\#9)}$	-	10.6	10.6	10.8	1.02	1.00	**1.02**
	$s\ /d_{b\ (\#10)}$	-	9.4	9.4	9.0	0.95	1.00	**0.95**
	f'_c	ksi	4.81	4.81	5.50	1.14	1.00	**1.14**
	$\sqrt{f'_c}$	ksi	69.4	69.4	74.2	1.07	1.00	**1.07**

Table A-8: Specimen Sizing – Thickened Slab

Element	Component	Unit	Full Scale (1)	Required (0.67-scale) (2)	Actual (0.67-scale) (3)	Actual Value (4) = (3)/(1)	Target Value (5)	Ratio (6) = (5)/(4)
Thickened Slab	b	Inch	19.5	13.0	13.0	0.67	0.67	**1.00**
	h	Inch	16.5	11.0	11.0	0.67	0.67	**1.00**
	Cover to CL of Long. Bar	Inch	1.625	1.08	1.13	0.69	0.67	**1.04**
	$d_{bar,L\ (\#8:\#5)}$	Inch	1.00	0.67	0.625	0.63	0.67	**0.94**
	$A_{bar,L\ (\#8:\#5)}$	$Inch^2$	0.79	0.35	0.31	0.39	0.44	**0.88**
	Number of Bars	-	4	4	4	1.00	1.00	**1.00**
	$A_{Total,L\ (\#8:\#5)}$	$Inch^2$	3.16	1.40	1.24	0.39	0.44	**0.88**
	$A_{Total,L\ (\#8:\#5)}/bh$	-	0.010	0.010	0.009	0.88	1.00	**0.88**
	$f_{y,L}$	ksi	46.8	46.8	66.2	1.41	1.00	**1.41**
	$A_{Total,L} \cdot f_{y,L(\#5)}$	kips	147.9	65.7	82.1	0.56	0.44	**1.25**
	$d_{Tie\ (\#3:\#2)}$	Inch	0.375	0.25	0.25	0.67	0.67	**1.00**
	$A_{T\ (\#3:\#2)}$	$Inch^2$	0.11	0.05	0.05	0.45	0.44	**1.00**
	$A_T.f_{y,T} / s$	kips	0.477	0.318	0.314	0.66	0.67	**0.99**
	$f_{y,T}$	ksi	52.0	52.0	48.0	0.92	1.00	**0.92**
	s	Inch	12.0	8.00	7.50	0.63	0.67	**0.94**
	s / h	-	0.73	0.73	0.68	0.94	1.00	**0.94**
	s / d_b	-	12.0	12.0	12.0	1.00	1.00	**1.00**
	f'_c	ksi	4.81	4.81	5.50	1.14	1.00	**1.14**
	$\sqrt{f'_c}$	psi	69.4	69.4	74.2	1.07	1.00	**1.07**

Table A-9: Specimen Sizing – Slab Joists

Element		Component	Unit	Full Scale (1)	Required (0.67-scale) (2)	Actual (0.67-scale) (3)	Actual Value (4) = (3)/(1)	Target Value (5)	Ratio (6) = (5)/(4)
Slab		t_{slab}	Inch	4.5	3.0	3.0	0.67	0.67	1.00
		b_{joist}	Inch	6.0	4.0	4.0	0.67	0.67	1.00
		$h_{joist\ (from\ bot.\ of\ slab)}$	Inch	14.0	9.3	9.4	0.67	0.67	1.00
	4J-1 (Parallel to Frame)	Cover to CL of Long. Bar	Inch	1.31	0.875	0.875	0.67	0.67	1.00
		$d_{bar\ L,Top\ Bar\ A\ (2\#5:\#3)}$	Inch	0.625	0.42	0.38	0.60	0.67	0.90
		$d_{bar\ L,Top\ Bar\ B\ (2\#5:\#3)}$	Inch	0.625	0.42	0.38	0.60	0.67	0.90
		$d_{bar\ L,Bot\ Bar\ C\ (2\#5:\#3)}$	Inch	0.625	0.42	0.38	0.60	0.67	0.90
		$A_{bar,L\ (\#5:\#3)}$	$Inch^2$	0.31	0.14	0.11	0.35	0.44	0.80
		Number of Bars	-	2	2	2	1.00	1.00	1.00
		$A_{Total,L\ (\#5:\#3)}/b_{joist}$	Inch	0.0517	0.0344	0.0275	0.53	0.67	0.80
		$f_{y,L(\#5:\#3)}$	KSI	46.8	46.8	48	1.03	1.00	1.03
		$A_{bar,L}\,f_{y,L(\#5:\#3)}$	KIPS	14.5	6.4	5.3	0.36	0.44	**0.82**
		$d_{bar,T\ (\#2@12":\#2)}$	Inch	0.25	0.17	0.25	1.00	0.67	1.49
		$A_{bar,T\ (\#2:\#2)}$	$Inch^2$	0.049	0.022	0.050	1.02	0.44	2.30
		s	Inch	12.00	8.00	11.50	0.96	0.67	1.44
		$s\ /\ d_b$	-	19.2	19.2	30.7	1.60	1.00	**1.60**
		$f_{y,T(\#2)}$	KSI	52	52	48	0.92	1.00	0.92
		$A_{bar,T}\,f_{y,T}/s$	KIPS	0.21	0.14	0.21	0.98	0.67	**1.47**
	4J-2 (Perpendicular to Frame)	Cover to CL of Long. Bar	Inch	1.56	1.04	1	0.64	0.67	0.96
		$d_{bar\ L,Top\ Bar\ A\ (2\#9:\#5)}$	Inch	1.128	0.75	5/8	0.55	0.67	0.83
		$d_{bar\ L,Top\ Bar\ B\ (2\#9:\#5)}$	Inch	1.128	0.75	5/8	0.55	0.67	0.83
		$d_{bar\ L,Bot\ Bar\ C\ (2\#9:\#5)}$	Inch	1.128	0.75	5/8	0.55	0.67	0.83
		$A_{bar,L\ (\#9:\#5)}$	$Inch^2$	1.0	0.44	0.31	0.31	0.44	0.70
		Number of Bars	-	2	2	2	1.00	1.00	1.00
		$A_{bar,L\ (\#9:\#5)}/(h+t)$	Inch	0.0541	0.0360	0.0251	0.46	0.67	0.70
		$A_{Total,L\ (\#9:\#5)}$	Inch	2.0	0.89	0.62	0.31	0.44	0.70
		$A_{Total,L\ (\#9:\#5)}/b_{joist}$	Inch	0.333	0.222	0.155	0.47	0.67	0.70
		$f_{y,L(\#9:\#5)}$	KSI	46.8	46.8	72.0	1.54	1.00	1.54
		$A_{bar,L}\,f_{y,L(\#9:\#5)}$	KIPS	93.6	41.6	44.6	0.48	0.44	**1.07**
		$d_{bar,T\ (\#2@12":\#2)}$	Inch	0.25	0.17	0.162	0.65	0.67	0.97
		$A_{bar,T\ (\#2:\#2)}$	$Inch^2$	0.049	0.022	0.021	0.42	0.44	0.95
		s	Inch	12.00	8.00	7.00	0.58	0.67	0.88
		$s\ /\ d_b$	-	10.6	10.6	11.2	1.05	1.00	**1.05**
		$f_{y,T(\#2)}$	KSI	52	52	48	0.92	1.00	0.92
		$A_{bar,T}\,f_{y,T}/s$	KIPS	0.21	0.14	0.14	0.67	0.67	**1.00**
		f'_c	ksi	4.81	4.81	5.50	1.14	1.00	**1.14**
		$\sqrt{f'_c}$	psi	69.4	69.4	74.2	1.07	1.00	**1.07**

Table A-10: Franz Tower Column (In-Plane) Yield

Actual: Column | Weak Axis									
Calculating M_{yeild}:									
cover=	2.939	Inch		f_y =	40,000	psi			
f'_c =	3000	psi		$f_{y(expected)}$ =	46,800	psi	$\varepsilon_{y(expected)}$ =	0.00161	
$f'_{c(expected)}$ =	4802	psi		$f_{u(expected)}$ =	46,800	psi	ε_u =	0.00161	
E_s=	29,000,000	psi		β=	0.810				
d_{min}=	6.06	Inch					$h_{col,clear}$=	11.21	ft
d_{max}=	12.06	Inch	c_{yield} =	2.72	Inch		h_{col}=	135	Inch
d_{ave}=	9.06	Inch							
b =	24.0	Inch							
(#9) A_s (longitudenal) =		1.00	$Inch^2$						
No. of #9 Rows (1st Level) =		3							
(#3) A_{st} (transverese)=		0.11	$Inch^2$	S=	12.00	Inch			
Calculating Tension & Comp. Forces:									
$C_c = 0.85\,\lambda f'_c\, ba = 0.85\,(0.75)\, f'_c\, b\,(\beta\, c)$				C_c =	162	KIPS			
$C'_s = A_s\, f_s$									
$f_s = E.\varepsilon_s = E\,(0.003)(c\text{-cover})/c$			ε' =	0.0002	Tension				
f_s =	7.1	KIPS							
A_s =	3.00	$Inch^2$							
C'_s =	-21	KIPS							
$T_s = A_s\, f_s$									
$f_s = E.\varepsilon_s = E\,(0.003)(d - c)/c$			ε_s =	0.0070	Tension				
f_s =	46.8	KIPS							
A_s =	3.00	$Inch^2$							
T_s =	-140	KIPS							
Calculating M_{yeild} (about weak axis) at c:									
$M_n = C_c\,(c - 0.84c/2) + C'_s\,(c\text{-cover}) + T_s\,(d\text{-}c)$									
C_c =	162	KIPS							
C'_s =	21	KIPS							
T_s =	140.4	KIPS							
(c - 0.84c/2) =	1.58	Inch	(Moment Arm to Nuetral Axis for C_c)						
(cover-c) =	0.22	Inch	(Moment Arm to Nuetral Axis for C'_s)						
(d-c) =	6.34	Inch	(Moment Arm to Nuetral Axis for T_s)						
$M_{n\text{-}y,actual(weak)}$ =	1150	K.Inch							
$V@M_{n\text{-}y,actual(weak)}$ =	17.1	KIPS							

Table A-11: Franz Tower Column (In-Plane) Balanced Point

Actual: Column | Weak Axis									
Calculating M_{bal}:									
cover=	**2.939**	**Inch**		**f_y =**	**40,000**	**psi**			
f'_c =	**3000**	**psi**		**$f_{y(expected)}$ =**	**46,800**	**psi**	**$\varepsilon_{y(expected)}$ =**	**0.00161**	
$f'_{c(expected)}$ =	**4802**	**psi**		**$f_{u(expected)}$ =**	**46,800**	**psi**	**ε_u =**	**0.00161**	
E_s=	**29,000,000**	**psi**		**β=**	**0.810**				
d_{min}=	**6.06**	**Inch**					**$h_{col,clear}$=**	**11.21**	**ft**
d_{max}=	**12.06**	**Inch**	**c_{bal} =**	**3.98**	**Inch**		**h_{col}=**	**135**	**Inch**
d_{ave}=	**9.06**	**Inch**							
b =	**24.0**	**Inch**							
(#9) A_s (longitudenal) =		**1.00**	**$Inch^2$**						
No. of #9 Rows (1st Level) =		**3**							
(#3) A_{st} (transverese)=		**0.11**	**$Inch^2$**	**S=**	**12.00**	**Inch**			
Calculating Tension & Comp. Forces:									
$C_c = 0.85\,\lambda f'_c\, ba = 0.85\,(0.75)\, f'_c\, b\, (\beta\, c)$				**C_c =**	**237**	**KIPS**			
$C'_s = A_s\, f_s$									
$f_s = E.\varepsilon_s = E\,(0.003)(c\text{-cover})/c$			**ε' =**	**-0.0008**	**Compression**				
f_s =	-22.8	KIPS							
A_s =	3.00	$Inch^2$							
C'_s =	**68**	**KIPS**							
$T_s = A_s\, f_y$									
			ε_s =	**0.0016**	**Tension**				
f_s =	46.8	KIPS							
A_s =	3.00	$Inch^2$							
T_s =	**-140**	**KIPS**							
Calculating M_{yeild} (about weak axis) at c:									
$M_n = C_c\,(c - 0.84c/2) + C'_s\,(c\text{-cover}) + T_s\,(d\text{-c})$									
C_c =	237	KIPS							
C'_s =	68	KIPS							
T_s =	140.4	KIPS							
(c - 0.84c/2) =	2.31	Inch	(Moment Arm to Nuetral Axis for C_c)						
(cover-c) =	1.04	Inch	(Moment Arm to Nuetral Axis for C'_s)						
(d-c) =	5.08	Inch	(Moment Arm to Nuetral Axis for T_s)						
$M_{n\text{-}y,actual(weak)}$ =	**1331**	**K.Inch**		**111**	K.ft				
V@$M_{n\text{-}y,actual(weak)}$ =	**19.8**	**KIPS**							
$P_{balanced(weak)}$ =	**164.8**	**KIPS**							

Table A-12: Test Specimen Column (In-Plane) Yield

Specimen: Column | Weak Axis									
Calculating M_{veild}:									
cover=	1.96	Inch		f_y =	60,000	psi			
f'_c =	3,000	psi		$f_{y(expected)}$ =	66,200	psi	$\varepsilon_{y(expected)}$ =	0.00228	
$f'_{c(expected)}$ =	5,500	psi		f_u =	95,000	psi	ε_u =	0.00328	
E_s=	29,000,000	psi		β=	0.775				
d_{min}=	4.04	Inch					$h_{col,clear}$=	7.50	ft
d_{max}=	8.04	Inch	c_{yield} =	1.70	Inch		h_{col}=	90	Inch
d_{ave}=	6.04	Inch							
b =	16.0	Inch							
(#5) As (longitudenal) =		0.31	$Inch^2$						
No. of #5 Rows =		3							
(#2) A_{st} (transverese)=		0.05	$Inch^2$	S=	6.750	Inch			
Calculating Tension & Comp. Forces:									
$C_c = 0.85\,\lambda f'_c\,ba = 0.85\,(0.75)\,f'_c\,b\,(\beta\,c)$				C_c =	73.9	KIPS			
$C'_s = A_s\,f_s$									
$f_s = E.\varepsilon_s = E\,(0.003)(c\text{-cover})/c$			ε' =	0.0005	Tension				
f_s =	13.3	KIPS							
A_s =	0.93	$Inch^2$							
C'_s =	-12.3	KIPS							
$T_s = A_s\,f_s$									
$f_s = E.\varepsilon_s = E\,(0.003)(d - c)/c$			ε_s =	0.0077	Tension				
f_s =	66.2	KIPS							
A_s =	0.93	$Inch^2$							
T_s =	-62	KIPS							
Calculating M_{veild} (about weak axis):									
$M_n = C_c\,(c - 0.84c/2) + C'_s\,(c\text{-cover}) + T_s\,(d\text{-}c)$									
C_c =	73.9	KIPS							
C'_s =	12.3	KIPS							
T_s =	61.6	KIPS							
(c - 0.84c/2) =	0.99	Inch	(Moment Arm to Nuetral Axis for C_c)						
(cover-c) =	0.26	Inch	(Moment Arm to Nuetral Axis for C'_s)						
(d-c) =	4.34	Inch	(Moment Arm to Nuetral Axis for T_s)						
$M_{n\text{-}y,SP,(weak)}$ =	343	K.Inch		$M_{y,full,w}$ =	1159	K.Inch			
$V@M_{n\text{-}y,SP(weak)}$ =	7.6	KIPS							
$M_{n\text{-}y,act(weak)}$ =	1150	K.Inch			$M_{SP(w)}/M_{actual(w)}$=	0.30	$(2/3)^3$=	0.30	
$V@M_{n\text{-}y,act(weak)}$ =	17.1	KIPS			$V@M_{SP(w)}/V@M_{actual(w)}$=	0.45	$(2/3)^2$=	0.44	

Table A-13: Test Specimen Column (In-Plane) Balanced Point

Specimen: Column | Weak Axis									
Calculating M_{bal}:									
cover=	1.96	Inch		f_y =	60,000	psi			
f'_c =	3,000	psi		$f_{y(expected)}$ =	66,200	psi	$\varepsilon_{y(expected)}$ =	0.00228	
$f'_{c(expected)}$ =	5,500	psi		f_u =	95,000	psi	ε_u =	0.00328	
E_s=	29,000,000	psi		β=	0.775				
d_{min}=	4.04	Inch					$h_{col,clear}$=	7.50	ft
d_{max}=	8.04	Inch	c_{bal} =	2.32	Inch		h_{col}=	90	Inch
d_{ave}=	6.04	Inch							
b =	16.0	Inch							
(#5) As (longitudenal) =		0.31	$Inch^2$						
No. of #5 Rows =		3							
(#2) A_{st} (transverese)=		0.05	$Inch^2$	S=	6.750	Inch			
Calculating Tension & Comp. Forces:									
$C_c = 0.85\ \lambda f'_c\ ba = 0.85\ (0.75)\ f'_c\ b\ (\beta\ c)$				C_c =	101	KIPS			
$C'_s = A_s\ f_s$									
$f_s = E.\varepsilon_s = E\ (0.003)(c\text{-cover})/c$			ε' =	-0.00047	Compression				
f_s =	-13.5	KIPS							
A_s =	0.93	$Inch^2$							
C'_s =	13	KIPS							
$T_s = A_s\ f_y$									
			ε_s =	0.0023	Tension				
f_s =	66.2	KIPS							
A_s =	0.93	$Inch^2$							
T_s =	-61.6	KIPS							
Calculating M_{yeild} (about weak axis) at c:									
$M_n = C_c\ (c - 0.84c/2) + C'_s\ (c\text{-cover}) + T_s\ (d\text{-c})$									
C_c =	101	KIPS							
C'_s =	13	KIPS							
T_s =	62	KIPS							
(c - 0.84c/2) =	1.34	Inch	(Moment Arm to Nuetral Axis for C_c)						
(cover-c) =	0.36	Inch	(Moment Arm to Nuetral Axis for C'_s)						
(d-c) =	3.72	Inch	(Moment Arm to Nuetral Axis for T_s)						
$M_{b,actual(weak)}$ =	369	K.Inch							
$V@M_{b,actual(weak)}$ =	8.2	KIPS							
$P_{balanced(weak)}$ =	51.8	KIPS							

Table A-14: Franz Tower Column (In-Plane) Shear Capacity

Actual: Column | Weak Axis									
Calculating V_n :							P =	60.75	K
cover=	2.939	Inch					$P/A_g f'_c$ =	0.044	
f'_c =	3000	psi					A_v/sb_w =	0.0011	
$f'_{c(expected)}$ =	4,802	psi		$f_{yt(expected)}$ =	56,693	psi			
E_s=	29,000,000	psi		β=	0.810				
d_{min}=	6.06	Inch					$h_{col,clear}$=	11.21	ft
d_{max}=	12.06	Inch					h_{col}=	134.5	Inch
d_{ave}=	9.06	Inch							
b =	24.0	Inch							
(#9) A_s (longitudenal) =		1.0	$Inch^2$						
(#3) A_{st} (transverese)=		0.11	$Inch^2$	S=	12	Inch			
No. of #9 Rows =		3							
$V_n = V_c + V_s$									
$V_c = 2\lambda\sqrt{f'_c} \, . \, b_w \, d$	V_c =	22.6	KIPS						
$V_s = A_{st} \, .f_{yt} \, d/s$	V_s =	14.1	KIPS					V_s/V_c =	0.62
	V_n =	36.7	KIPS					V_s/V_n =	0.38
From before:	V @ M_b =	19.8	KIPS						
	$V@M_b/V_n$ =	0.54	KIPS	Flexural failure before shear failure					
Assuming 150% V_n	$V@M_u/1.5V_n$ =	0.36	KIPS	Flexural failure before shear failure					

Table A-15: Test Specimen Column (In-Plane) Shear Capacity

Specimen: Column | Weak Axis									
Calculating V_n :							P =	27	K
cover=	1.958	Inch					$P/A_g f'_c$ =	0.038	
f'_c =	3,000	psi					A_v/sb_w =	0.0014	
$f'_{c(expected)}$ =	5,500	psi		$f_{yt(expected)}$ =	48,000	psi			
E_s=	29,000,000	psi		β=	0.775				
d_{min}=	4.04	Inch					$h_{col,clear}$=	7.50	ft
d_{max}=	8.04	Inch					h_{col}=	90.0	Inch
d_{ave}=	6.04	Inch							
b =	16.00	Inch							
(#5) A_s (longitudenal) =		0.31	$Inch^2$						
No. of #5 Rows =		3		S=	6.750	Inch			
(#2) A_{st} (transverese)=		0.05	$Inch^2$						
$V_n = V_c + V_s$									
$V_c = 2\lambda\sqrt{f'_c} \cdot b_w d$	V_c =	10.8	KIPS				$V_{c,spec(w)}/V_{c,actual(w)}$=		0.48
$V_s = A_{st} \cdot f_{yt} d/s$	V_s =	6.4	KIPS				$V_{s,spec(w)}/V_{s,actual(w)}$=		0.46
	V_n =	17.2	KIPS	$V_{n,full,s}$ =	38.7	KIPS	$V_{n,spec(w)}/V_{n,actual(w)}$=		0.47
From before:	V @ M_y =	7.6	KIPS	$V@M_{n-y,SP(w)}/V@M_{n-y,act}$=			0.45		
	V @ M_u =	7.6	KIPS	V_{demand} =	1.1	$bd\sqrt{f'c}$			
	$V@M_y/V_n$ =	0.44		Flexural failure before shear failure					
Assuming 150% V_n	$V@M_y/1.5V_n$ =	0.30		Flexural failure before shear failure					

Table A-16: Franz Tower Column (Out-of-Plane) Yield

Actual: Column | Strong Axis									
Calculating M_{yeild}:									
cover=	**2.939**	**Inch**		**f_y =**	**40,000**	**psi**			
f'_c =	**3000**	**psi**		**$f_{y(expected)}$ =**	**46,800**	**psi**	**$\varepsilon_{y(expected)}$ =**	**0.00161**	
$f'_{c(expected)}$ =	**4,802**	**psi**		**f_u =**	**46,800**	**psi**	**ε_u =**	**0.00161**	
E_s=	**29,000,000**	**psi**		**β=**	**0.810**				
h=	**24.00**	**Inch**							
d =	**21.06**	**Inch**	**c_{yield} =**	**4.37**	**Inch**		**$h_{col,clear}$=**	**11.21**	**ft**
b_{ave} =	**12.0**	**Inch**					**h_{col}=**	**134.5**	**Inch**
(#9) A_s (longitudenal) =		**1.00**	**$Inch^2$**						
(#3) A_{st} (transverese)=		**0.11**	**$Inch^2$**	**s =**	**12**	**Inch**			
No. of Middle #9 (1st Level) =		**2**							
Calculating Tension & Comp. Forces:									
$C_c = 0.85\ \lambda f'_c\ ba = 0.85\ (0.75)\ f'_c\ b\ (\beta\ c)$				**C_c =**	**130**	**KIPS**			
$C'_{s(top)} = A_{s(top)}\ f_{s(top)}$									
$f_{s(top)} = E.\varepsilon_{s(top)} = E\ (0.003)(cover - c)/c$			**$\varepsilon_{s(top)}$ =**	**-0.0010**	**Compression**				
$f_{s(top)}$ =	28.5	KIPS							
A_s =	2.00	$Inch^2$							
$C'_{s(top)}$ =	**57**	**KIPS**							
$C'_{s(mid)} = A_{s(mid)}\ f_{s(mid)}$									
$f_{s(mid)} = E.\varepsilon_{s(mid)} = E\ (0.003)(h/2-c)/c$			**$\varepsilon_{s(mid)}$ =**	**0.0052**	**Tension**				
$f_{s(mid)}$ =	46.8	KIPS							
A_s =	2.00	$Inch^2$							
$C'_{s(mid)}$ =	**-93.6**	**KIPS**							
$T_s = A_s\ f_s$									
$f_s = E.\varepsilon_s = E\ (0.003)(d - c)/c$			**ε_s =**	**0.0114**	**Tension**				
f_s =	46.8	KIPS							
A_s =	2.00	$Inch^2$							
T_s =	**-93.6**	**KIPS**							
								Mn = V*L/2	
Calculating M_{yeild} (about strong axis):								V = 2 Mn/L	
$M_n = C_c\ (c - 0.84c/2) + C'_{s(top)}\ (c\text{-}cover) + C'_{s(mid)}\ (h/2\text{-}c) + T_s\ (d\text{-}c)$									
C_c =	130	KIPS							
$C'_{s(top)}$ =	57	KIPS							
$C'_{s(mid)}$ =	94	KIPS							
T_s =	94	KIPS							
(c - 0.84c/2) =	2.54	Inch							
(c-cover) =	1.43	Inch							
(h/2-c) =	7.63	Inch							
(d-c) =	16.69	Inch							
M_y =	**2688**	**K.Inch**							
V @ $M_{y(strong)}$ =	**40.0**	**KIPS**							

Table A-17: Franz Tower Column (Out-of-Plane) Balanced Point

Actual: Column | Strong Axis									
Calculating M_{bal}:									
cover=	2.939	Inch		f_y =	40,000	psi			
f'_c =	3000	psi		$f_{y(expected)}$ =	46,800	psi	$\varepsilon_{y(expected)}$ =	0.00161	
$f'_{c(expected)}$ =	4,802	psi		f_u =	46,800	psi	ε_u =	0.00161	
E_s=	29,000,000	psi		β=	0.810				
h=	24.00	Inch							
d =	21.06	Inch	c_{bal} =	13.69	Inch		$h_{col,clear}$=	11.21	ft
b_{ave} =	12.0	Inch					h_{col}=	134.5	Inch
(#9) A_s (longitudenal) =		1.00	$Inch^2$						
(#3) A_{st} (transverese)=		0.11	$Inch^2$	s =	12	Inch			
No. of Middle #9 (1st Level) =		2							
Calculating Tension & Comp. Forces:									
$C_c = 0.85\ \lambda f'_c\ ba = 0.85\ (0.75)\ f'_c\ b\ (\beta\ c)$				C_c =	407	KIPS			
$C'_{s(top)} = A_{s(top)}\ f_{s(top)}$									
$f_{s(top)} = E.\varepsilon_{s(top)} = E\ (0.003)(cover - c)/c$			$\varepsilon_{s(top)}$ =	-0.0024	Compression				
$f_{s(top)}$ =	46.8	KIPS							
A_s =	2.00	$Inch^2$							
$C'_{s(top)}$ =	94	KIPS							
$C'_{s(mid)} = A_{s(mid)}\ f_{s(mid)}$									
$f_{s(mid)} = E.\varepsilon_{s(mid)} = E\ (0.003)(h/2-c)/c$			$\varepsilon_{s(mid)}$ =	-0.0004	Compression				
$f_{s(mid)}$ =	10.8	KIPS							
A_s =	2.00	$Inch^2$							
$C'_{s(mid)}$ =	21.5	KIPS							
$T_s = A_s\ f_s$									
			ε_s =	0.0016	Tension				
f_s =	46.8	KIPS							
A_s =	2.00	$Inch^2$							
T_s =	-93.6	KIPS							
Calculating M_{yeild} (about strong axis):									
$M_n = C_c\ (c - 0.84c/2) + C'_{s(top)}\ (c\text{-cover}) + C'_{s(mid)}\ (h/2\text{-}c) + T_s\ (d\text{-}c)$									
C_c =	407	KIPS							
$C'_{s(top)}$ =	94	KIPS							
$C'_{s(mid)}$ =	22	KIPS	Compression						
T_s =	94	KIPS							
(c - 0.84c/2) =	7.94	Inch							
(c-cover) =	10.76	Inch							
(h/2-c) =	1.69	Inch							
(d-c) =	7.37	Inch							
$M_{balanced,\ st}$ =	4969	K.Inch		414.1	K.ft				
V @ $M_{y(strong)}$ =	73.9	KIPS							
$P_{balanced,\ strong}$ =	429	KIPS							

Table A-18: Test Specimen Column (Out-of-Plane) Yield

Specimen: Column | Strong Axis Calculating M_{yield}:									
cover=	1.96	Inch		f_y =	60,000	psi			
f'_c =	3,000	psi		$f_{y(expected)}$ =	66,200	psi	$\varepsilon_{y(expected)}$ =	0.002283	
$f'_{c(expected)}$ =	5,500	psi		f_u =	95,000	psi	ε_u =	0.001614	
E_s=	29,000,000	psi		β=	0.775				
h=	16.00	Inch							
d =	14.04	Inch	c_{yield} =	2.94	Inch		$h_{col,clear}$=	7.50	ft
b_{ave} =	8.0	Inch					h_{col}=	90.0	Inch
(#5) A_s (longitudenal) =		0.31	$Inch^2$						
No. of #5 Rows =		2		S=	6.750	Inch			
(#2) Ast (transverese)=		0.05	$Inch^2$						

Calculating Tension & Comp. Forces:						
$C_c = 0.85\,\lambda f'_c\, ba = 0.85\,(0.75)\, f'_c\, b\,(\beta\, c)$				C_c =	64	KIPS
$C'_{s(top)} = A_{s(top)}\, f_{s(top)}$						
$f_{s(top)} = E.\varepsilon_{s(top)} = E\,(0.003)(c - cover)/c$			$\varepsilon_{s(mid)}$ =	0.0010	Compression	
$f_{s(top)}$ =	29.1	KIPS				
A_s =	0.62	$Inch^2$				
$C'_{s(top)}$ =	18.1	KIPS				
$C'_{s(mid)} = A_{s(mid)}\, f_{s(mid)}$						
$f_{s(mid)} = E.\varepsilon_{s(mid)} = E\,(0.003)(h/2\text{-}c)/c$			$\varepsilon_{s(mid)}$ =	0.0051	Tension	
$f_{s(mid)}$ =	66.2	KIPS				
A_s =	0.62	$Inch^2$				
$C'_{s(mid)}$ =	-41.0	KIPS				
$T_s = A_s\, f_s$						
$f_s = E.\varepsilon_s = E\,(0.003)(d - c)/c$			ε_s =	0.0113	Tension	
f_s =	66.2	KIPS				
A_s =	0.62	$Inch^2$				
T_s =	-41.0	KIPS				

Calculating M_{yeild} (about strong axis):						
$M_b = C_c\,(c - 0.84c/2) + C'_{s(top)}\,(c\text{-}cover) + C'_{s(mid)}\,(c\text{-}cover\text{-}2/3x10") + T_s\,(d\text{-}c)$						
C_c =	64.0	KIPS				
$C'_{s(top)}$ =	18.1	KIPS				
$C'_{s(mid)}$ =	41.0	KIPS				
T_s =	41.0	KIPS				
(c - 0.84c/2) =	1.71	Inch				
(c-cover) =	0.99	Inch				
(h/2-c)=	5.06	Inch				
(d-c) =	11.10	Inch				
M_y =	790	K.Inch	$M_{spec(s)}/\, M_{actual(s)}$=	0.29	$(2/3)^3$=	0.30
V @ $M_{y(strong)}$ =	17.6	KIPS	$V@M_{spec(s)}/\, V@M_{actual(s)}$=	0.44	$(2/3)^2$=	0.44

Table A-19: Test Specimen Column (Out-of-Plane) Balanced Point

Specimen: Column | Strong Axis									
Calculating M_{bal}:									
cover=	1.96	Inch		f_y =	60,000	psi			
f'_c =	3,000	psi		$f_{y(expected)}$ =	66,200	psi	$\varepsilon_{y(expected)}$ =	0.002283	
$f'_{c(expected)}$ =	5,500	psi		f_u =	95,000	psi			
E_s=	29,000,000	psi		β=	0.775				
h=	16.00	Inch							
d =	14.04	Inch	c_{bal} =	7.97	Inch		$h_{col,clear}$=	7.50	ft
b_{ave} =	8.0	Inch					h_{col}=	90.0	Inch
(#5) A_s (longitudenal) =		0.31	$Inch^2$						
No. of #5 Rows =		2		S=	6.750	Inch			
(#2) Ast (transverese)=		0.05	$Inch^2$						
Calculating Tension & Comp. Forces:									
$C_c = 0.85\ \lambda f'_c\ ba = 0.85\ (0.75)\ f'_c\ b\ (\beta\ c)$				C_c =	173	KIPS			
$C'_{s(top)} = A_{s(top)}\ f_{s(top)}$									
$f_{s(top)} = E.\varepsilon_{s(top)} = E\ (0.003)(c - cover)/c$			$\varepsilon_{s(mid)}$ =	0.0023	Compression				
$f_{s(top)}$ =	65.6	KIPS							
A_s =	0.62	$Inch^2$							
$C'_{s(top)}$ =	40.7	KIPS							
$C'_{s(mid)} = A_{s(mid)}\ f_{s(mid)}$									
$f_{s(mid)} = E.\varepsilon_{s(mid)} = E\ (0.003)(h/2-c)/c$			$\varepsilon_{s(mid)}$ =	0.0000	Tension				
$f_{s(mid)}$ =	0.3	KIPS							
A_s =	0.62	$Inch^2$							
$C'_{s(mid)}$ =	-0.2	KIPS							
$T_s = A_s\ f_s$									
$f_s = E.\varepsilon_s = E\ (0.003)(d - c)/c$			ε_s =	0.0023	Tension				
f_s =	66.2	KIPS							
A_s =	0.62	$Inch^2$							
T_s =	-41.0	KIPS							
Calculating M_{yeild} (about strong axis):									
$M_b = C_c\ (c - 0.84c/2) + C'_{s(top)}\ (c\text{-}cover) + C'_{s(mid)}\ (c\text{-}cover\text{-}2/3x10") + T_s\ (d\text{-}c)$									
C_c =	173.3	KIPS							
$C'_{s(top)}$ =	40.7	KIPS							
$C'_{s(mid)}$ =	0.2	KIPS							
T_s =	41.0	KIPS							
(c - 0.84c/2) =	4.62	Inch							
(c-cover) =	6.02	Inch							
(h/2-c)=	0.03	Inch							
(d-c) =	6.07	Inch							
M_b =	1296	K.Inch	$M_{spec(s)}/\ M_{actual(s)}$=			0.26	$(2/3)^3$=	0.30	
V @ $M_{y(strong)}$ =	28.8	KIPS	$V@M_{spec(s)}/\ V@M_{actual(s)}$=			0.39	$(2/3)^2$=	0.44	
$P_{balanced,\ strong}$ =	173	KIPS					$(2/3)^2$=	0.44	

Table A-20: Franz Tower Column (Out-of-Plane) Shear Capacity

Actual: Column | Strong Axis									
Calculating V_n:							P =	60.75	K
cover=	2.939	Inch					$P/A_g f'_c$ =	0.044	
f'_c =	3,000	psi					A_v/sb_w =	0.0015	
$f'_{c(expected)}$ =	4,802	psi		$f_{y(tensile)}$ =	56,693	psi			
E_s=	29,000,000	psi		β=	0.810				
h=	24.0	Inch							
d =	21.1	Inch					$h_{col,clear}$=	11.21	ft
b_{ave} =	12.0	Inch					h_{col}=	134.5	Inch
(#3) A_{st} (transverese)=		0.11	$Inch^2$	S=	12.0	Inch			
No. of Middle #9 =		2							
$V_n = V_c + V_s$									
$V_c = 2\lambda\sqrt{f'_c} . b_w d$	V_c =	26.3	KIPS						
$V_s = A_{st} .f_{yt} d/s$	V_s =	21.9	KIPS						
	V_n =	48.2	KIPS						
From before:	V @ M_b =	73.9	KIPS						
	$V@M_b/V_n$ =	1.53	KIPS	Shear failure before felxural failure					
Assuming 150% V_n	$V@M_b/1.5V_n$ =	1.02	KIPS	Shear failure before felxural failure					

Table A-21: Test Specimen Column (Out-of-Plane) Shear Capacity

Specimen: Column | Strong Axis									
Calculating V_n :							P =	27	K
cover=	1.96	Inch					$P/A_g f'_c$ =	0.038	
f'_c =	3,000	psi					A_v/sb_w =	0.0019	
$f'_{c(expected)}$ =	5,500	psi		$f_{yt(expected)}$ =	48,000	psi			
E_s=	29,000,000	psi		β=	0.775				
h=	16.00	Inch							
d =	14.04	Inch					$h_{col,clear}$=	7.5	ft
b_{ave}=	8.00	Inch					h_{col}=	90.0	Inch
(#2) A_{st} (transverese)=		0.05	$Inch^2$	S=	6.75	Inch			
No. of Middle #6 =		2							
$V_n = V_c + V_s$									
$V_c = 2\lambda\sqrt{f'_c} \cdot b_w d$	V_c =	12.5	KIPS				$V_{c,spec(w)}/V_{c,actual(w)}$=		0.48
$V_s = A_{st} .f_{yt}\ d/s$	V_s =	10.0	KIPS				$V_{s,spec(w)}/V_{s,actual(w)}$=		0.46
	V_n =	22.5	KIPS	$V_{n,full,s}$ =	50.6	KIPS	$V_{n,spec(w)}/V_{n,actual(w)}$=		0.47
From before:	V @ M_b =	28.8	KIPS	V_{demand} =	3.5	bd√f'c			
	$V@M_b/V_n$ =	1.28		Shear failure before felxural failure					
Assuming 150% V_n	$V@M_b/1.5V_n$ =	0.85		Flexural failure before shear failure					

Table A-22: Lap-Splice Check

Lap Splice

b, ave	12	in	As,v =	0.049	in2	As =	0.310	in2
h	24	in	Fy,v =	48	ksi	Fy,L =	66.2	ksi
CC	2	in	s =	6.75	in			
cover	2.81	in	tie dia =	0.25				
f'c	5400	psi						
Lambda	0.75		wc =	106	pcf (unit wgt of concrete)			
Nu	0	lbs						
fy	66.2	ksi						
bar dia	0.625							
As	0.31							

cb =	2.5625	in			
Ktr =	0.097	OOP	(cb+ktr)/db=	4.25	use 2.5
Ktr =	0.145	IP	(cb+ktr)/db=	4.33	use 2.5

fs =	0.796	x fy	OOP
fs =	0.796	x fy	IP

			Lap Length Ratio			
Ld (#5) =	47.6	in (Table 12.2.2)	34%		0.60	x fu(test)
Ld (#5) =	**22.5**	**in (EQ 12-1) OOP**	**71%**	fs (10-1a) =	0.99	x fu(test)
Ld (#5) =	**22.5**	**in (EQ 12-1) IP**	**71%**	fs (10-1a) =	0.99	x fu(test)
$Ld_{provided}$ =	**16.0**	**in**			99%	x fu(test)

Table A-23: Effective Stiffness Calculation per Elwood & Eberhard (2009)

	Columns	Beams	Beam Assembly	
Ag	128	117	274	gross cross-sectional area of column (8*16)
d (D-cover)	14	6	10	
Asl	1.81	1.2	2.4	total area of longitudinal reinforcement (6#5)
rho	1.61%	1.37%	1.79%	
Av	107	98	228	effective shear area of column cross section =5/6 of Ag
a	102	32	160	shear span
b	8	16	13	width of rectangular column section
D	16	7.5	12.33	column depth in direction of loading (rectangular column)
db	0.625	0.625	0.625	nominal diameter of longitudinal bars
Ec	3420	3420	3420	concrete modulus of elasticity
Es	29000	29000	29000	reinforcing steel modulus of elasticity
f'c	5.4	5.4	5.4	concrete compressive strength
fs	66.2	66.2	66.2	longitudinal reinforcement steel stress at column fixed end
fy	66.2	66.2	66.2	longitudinal reinforcement yield stress
G eff	684.1	684.1	684.1	effective shear modulus (half of G_{gross})
n	8.48	8.48	8.48	modular ratio (Es/Ec)
P	34	40	50	axial load (positive is compression)
u	0.71	0.71	0.71	constant bond stress
alpha (eq13)	0.387	0.381	0.387	
alpha (eq14)	0.400	0.415	0.385	
epsilon.o	0.002	0.002	0.002	
I (gross) IP	683	2560	2257	
I (gross) OOP	2731	563	2031	
r_v IP	2.53	5.12	3.15	
r_v OOP	5.06	2.40	2.98	
fs/fy.app	1	1	1	

Table A-25: Effective Stiffness Calculation per Elwood & Eberhard (2009) (Cont'd.)

Elwood & Eberhard's Paper 2009

$$\frac{EI_{eff\ calc}}{EI_g} = \frac{0.45 + 2.5P/A_g f_c'}{1 + 110\left(\frac{d_b}{D}\right)\left(\frac{D}{a}\right)} \leq 1.0 \text{ and } \geq 0.2 \qquad (18)$$

Col IP $EI_{(eff,calc)}$	Col OOP $EI_{(eff,calc)}$	Bm $EI_{(eff,calc}$	Bm Assembly $EI_{(eff,calc)}$
0.341	**0.341**	**0.200**	**0.374**

$$\frac{EI_{eff\ calc}}{EI_g} = \frac{\alpha}{\left[1 + \frac{3 d_b D f_s f_y}{8 D a f_y u} + \frac{18}{5}\alpha\left(\frac{r_v}{D}\right)^2\left(\frac{D}{a}\right)^2 \frac{E_c}{G_{eff}}\right]} \qquad (12)$$

	Col IP $EI_{(eff,calc)}$	Col OOP $EI_{(eff,calc)}$	Bm $EI_{(eff,calc}$	Bm Assembly $EI_{(eff,calc)}$
using alpha 13	**0.317**	**0.309**	**0.204**	**0.339**
using alpha 14	**0.328**	**0.336**	**0.223**	**0.337**

alpha 13	0.216	0.216	0.69	0.14
	0.004	0.017	0.18	0.00
	1.220	1.233	1.86	1.14
alpha 14	0.008	0.008	0.027	0.005
	0.004	0.018	0.191	0.003
	1.013	1.026	1.218	1.008

$$\alpha_{approx} = 0.2 + 1.3\left(\frac{P/A_g E_c}{\varepsilon_o}\right) + \rho n \leq 1.0 \qquad (13)$$

$$\alpha_{approx} = 0.35 + 1.3\left(\frac{P/A_g E_c}{\varepsilon_o}\right) \leq 1.0 \qquad (14)$$

$$\frac{EI_{eff\ calc}}{EI_g} = \frac{1.5\alpha_{approx\_Eq.\ 13}}{\left[1 + 110\left(\frac{d_b}{D}\right)\left(\frac{D}{a}\right)\left(\frac{f_s}{f_{y\ approx\_Eq.\ 15}}\right)\right]} \leq 1.0 \text{ and } \geq 0.2 \qquad (16)$$

$$0.0 \leq f_s/f_{y\ approx} = \frac{4}{3} - \frac{10}{3}\left(\frac{P/A_g E_c}{\varepsilon_o}\right) \leq 1.0$$

Col IP $EI_{(eff,calc)}$	Col OOP $EI_{(eff,calc)}$	Bm $EI_{(eff,calc}$	Bm Assembly $EI_{(eff,calc)}$
0.346	**0.346**	**0.200**	**0.406**

Table A-24: Column Modeling Parameters per ASCE 41-17 (Columns Not Controlled by Inadequate Splicing)

Nud / Ag.f'c	0.075		
pt = Av/db	0.0008	OOP	
pt = Av/db	0.0014	IP	
Vy / Vcol	2.08	OOP	
Vy / Vcol	5.96	IP	
Knl	1	Conservatively	
Vcol =	15.8		OOP
Vcol =	3.0		IP
alpha col=	0.47		1 OOP
alpha col=	1.00		0 IP
a	0.000	OOP	
a	0.000	IP	
b	0.025	OOP	
b	0.037	IP	
c	0.21	OOP	
c	0.21	IP	

$V_{Col} =$

$+ \lambda$

EQ. 10.3

$$V_{Col} = k_{nl} V_{Col0} = k_{nl} \left[\alpha_{Col} \left(\frac{A_v f_{ytL/E} d}{s} \right) + \lambda \left(\frac{6 \sqrt{f'_{cL/E}}}{M_{UD}/V_{UD}\, d} \sqrt{1 + \frac{N_{UG}}{6A_g \sqrt{f'_{cL/E}}}} \right) 0.8 A_g \right]$$

From Table 10-8

Columns not controlled by inadequate development or splicing along the clear height[a]

$$a = \left(0.042 - 0.043 \frac{N_{UD}}{A_g f'_{cE}} + 0.63\rho_t - 0.023 \frac{V_{yE}}{V_{ColOE}} \right) \geq 0.0 \qquad \begin{matrix} 0.15\, a \\ \leq 0.005 \end{matrix}$$

$$For \; \frac{N_{UD}}{A_g f'_{cE}} \leq 0.5 \left\{ b = \frac{0.5}{5 + \frac{N_{UD}}{0.8 A_g f'_{cE}} \frac{1}{\rho_t} \frac{f'_{cE}}{f_{ytE}}} - 0.01 \geq a^a \right.$$

$$c = 0.24 - 0.4 \frac{N_{UD}}{A_g f'_{cE}} \geq 0.0$$

A3. References Used

Table A-25: Effective Stiffness Values (Table 10-5 of ASCE 41-13)

Component	Flexural Rigidity	Shear Rigidity	Axial Rigidity
Beams—nonprestressed[a]	$0.3E_cI_g$	$0.4E_cA_w$	—
Beams—prestressed[a]	E_cI_g	$0.4E_cA_w$	—
Columns with compression caused by design gravity loads $\geq 0.5A_gf_c'$	$0.7E_cI_g$	$0.4E_cA_w$	E_cA_g
Columns with compression caused by design gravity loads $\leq 0.1A_gf_c'$ or with tension	$0.3E_cI_g$	$0.4E_cA_w$	E_cA_g (compression) E_sA_s (tension)
Beam–column joints	Refer to Section 10.4.2.2.1		E_cA_g
Flat slabs—nonprestressed	Refer to Section 10.4.4.2	$0.4E_cA_g$	—
Flat slabs—prestressed	Refer to Section 10.4.4.2	$0.4E_cA_g$	—
Walls-cracked[b]	$0.5E_cA_g$	$0.4E_cA_w$	E_cA_g (compression) E_sA_s (tension)

[a]For T-beams, I_g can be taken as twice the value of I_g of the web alone. Otherwise, I_g should be based on the effective width as defined in Section 10.3.1.3. For columns with axial compression falling between the limits provided, flexural rigidity should be determined by linear interpolation. If interpolation is not performed, the more conservative effective stiffnesses should be used.
[b]See Section 10.7.2.2.

Table A-26: Modeling Parameters and Numerical Acceptance Criteria for Non-linear Procedures – Reinforced Concrete Beams (Table 10-7 of ASCE 41-13)

Conditions			Modeling Parameters[a]: Plastic Rotations Angle (radians) a	b	Residual Strength Ratio c	Acceptance Criteria[a]: Plastic Rotations Angle (radians), Performance Level IO	LS	CP
Condition i. Beams controlled by flexure[b]								
$\frac{\rho-\rho'}{\rho_{bal}}$	Transverse reinforcement[c]	$\frac{V}{b_wd\sqrt{f_c'}}$ [d]						
≤0.0	C	≤3 (0.25)	0.025	0.05	0.2	0.010	0.025	0.05
≤0.0	C	≥6 (0.5)	0.02	0.04	0.2	0.005	0.02	0.04
≥0.5	C	≤3 (0.25)	0.02	0.03	0.2	0.005	0.02	0.03
≥0.5	C	≥6 (0.5)	0.015	0.02	0.2	0.005	0.015	0.02
≤0.0	NC	≤3 (0.25)	0.02	0.03	0.2	0.005	0.02	0.03
≤0.0	NC	≥6 (0.5)	0.01	0.015	0.2	0.0015	0.01	0.015
≥0.5	NC	≤3 (0.25)	0.01	0.015	0.2	0.005	0.01	0.015
≥0.5	NC	≥6 (0.5)	0.005	0.01	0.2	0.0015	0.005	0.01
Condition ii. Beams controlled by shear[b]								
Stirrup spacing ≤ $d/2$			0.0030	0.02	0.2	0.0015	0.01	0.02
Stirrup spacing > $d/2$			0.0030	0.01	0.2	0.0015	0.005	0.01
Condition iii. Beams controlled by inadequate development or splicing along the span[b]								
Stirrup spacing ≤ $d/2$			0.0030	0.02	0.0	0.0015	0.01	0.02
Stirrup spacing > $d/2$			0.0030	0.01	0.0	0.0015	0.005	0.01
Condition iv. Beams controlled by inadequate embedment into beam–column joint[b]								
			0.015	0.03	0.2	0.01	0.02	0.03

NOTE: f_c' in lb/in.^{2} (MPa) units.
[a]Values between those listed in the table should be determined by linear interpolation.
[b]Where more than one of conditions i, ii, iii, and iv occur for a given component, use the minimum appropriate numerical value from the table.
[c]"C" and "NC" are abbreviations for conforming and nonconforming transverse reinforcement, respectively. Transverse reinforcement is conforming if, within the flexural plastic hinge region, hoops are spaced at ≤ $d/3$, and if, for components of moderate and high ductility demand, the strength provided by the hoops (V_s) is at least 3/4 of the design shear. Otherwise, the transverse reinforcement is considered nonconforming.
[d]V is the design shear force from NSP or NDP.

Table A-27: Modeling Parameters and Numerical Acceptance Criteria for Non-linear Procedures – Reinforced Concrete Columns (Table 10-8 of ASCE 41-13)

Conditions			Modeling Parameters[a]			Acceptance Criteria[a]		
			Plastic Rotations Angle (radians)		Residual Strength Ratio	Plastic Rotations Angle (radians)		
						Performance Level		
			a	*b*	*c*	IO	LS	CP
Condition i.[b]								
$\frac{P}{A_g f_c'}$ [c]	$\rho = \frac{A_v}{b_w s}$							
≤0.1	≥0.006		0.035	0.060	0.2	0.005	0.045	0.060
≥0.6	≥0.006		0.010	0.010	0.0	0.003	0.009	0.010
≤0.1	=0.002		0.027	0.034	0.2	0.005	0.027	0.034
≥0.6	=0.002		0.005	0.005	0.0	0.002	0.004	0.005
Condition ii.[b]								
$\frac{P}{A_g f_c'}$ [c]	$\rho = \frac{A_v}{b_w s}$	$\frac{V}{b_w d\sqrt{f_c'}}$ [d]						
≤0.1	≥0.006	≤3 (0.25)	0.032	0.060	0.2	0.005	0.045	0.060
≤0.1	≥0.006	≥6 (0.5)	0.025	0.060	0.2	0.005	0.045	0.060
≥0.6	≥0.006	≤3 (0.25)	0.010	0.010	0.0	0.003	0.009	0.010
≥0.6	≥0.006	≥6 (0.5)	0.008	0.008	0.0	0.003	0.007	0.008
≤0.1	≤0.0005	≤3 (0.25)	0.012	0.012	0.2	0.005	0.010	0.012
≤0.1	≤0.0005	≥6 (0.5)	0.006	0.006	0.2	0.004	0.005	0.006
≥0.6	≤0.0005	≤3 (0.25)	0.004	0.004	0.0	0.002	0.003	0.004
≥0.6	≤0.0005	≥6 (0.5)	0.0	0.0	0.0	0.0	0.0	0.0
Condition iii.[b]								
$\frac{P}{A_g f_c'}$ [c]	$\rho = \frac{A_v}{b_w s}$							
≤0.1	≥0.006		0.0	0.060	0.0	0.0	0.045	0.060
≥0.6	≥0.006		0.0	0.008	0.0	0.0	0.007	0.008
≤0.1	≤0.0005		0.0	0.006	0.0	0.0	0.005	0.006
≥0.6	≤0.0005		0.0	0.0	0.0	0.0	0.0	0.0
Condition iv. Columns controlled by inadequate development or splicing along the clear height[b]								
$\frac{P}{A_g f_c'}$ [c]	$\rho = \frac{A_v}{b_w s}$							
≤0.1	≥0.006		0.0	0.060	0.4	0.0	0.045	0.060
≥0.6	≥0.006		0.0	0.008	0.4	0.0	0.007	0.008
≤0.1	≤0.0005		0.0	0.006	0.2	0.0	0.005	0.006
≥0.6	≤0.0005		0.0	0.0	0.0	0.0	0.0	0.0

NOTE: f_c' is in lb/in.^{2} (MPa) units.
[a]Values between those listed in the table should be determined by linear interpolation.
[b]Refer to Section 10.4.2.2.2 for definition of conditions i, ii, and iii. Columns are considered to be controlled by inadequate development or splices where the calculated steel stress at the splice exceeds the steel stress specified by Eq. (10-2). Where more than one of conditions i, ii, iii, and iv occurs for a given component, use the minimum appropriate numerical value from the table.
[c]Where $P > 0.7A_g f_c'$, the plastic rotation angles should be taken as zero for all performance levels unless the column has transverse reinforcement consisting of hoops with 135-degree hooks spaced at $\leq d/3$ and the strength provided by the hoops (V_s) is at least 3/4 of the design shear. Axial load P should be based on the maximum expected axial loads caused by gravity and earthquake loads.
[d]V is the design shear force from NSP or NDP.

Appendix B. Material Test Results

B1. Concrete

Table B-1: Franz Tower Concrete Core Compressive Strength Test

UNITED INSPECTION & TESTING
An EIS Company

Client: University of Calif. Capital Programs
1060 Veterans Ave. #125 Box 951365
Los Angeles, CA. 90095-1365

UIT JOB # 10-08889PW
UIT LAB # 10C151217-1-2

CONCRETE CORE TEST REPORT

Project Name: UCLA Franz Hall Investigative Study
Location: 502 Portola Plaza
Sampled By: Fidel Eviota **Tested By:** Mark Tabb **Test Date:** 12/18/15

COMPRESSIVE STRENGTH – ASTM C-42

Core Number:	7WC	7FC	6BC	6CC	6FC
Location:	Ext. Balcony Waffle Slab	Ext. Balcony Conc. Fin	Int. Beam Core through Floor	Int. Conc. Column	Ext. Balcony Conc. Fin
Diameter (in.):	2.98	3.94	3.94	3.94	3.94
Area, Sq. in:	6.97	12.19	12.19	12.19	12.19
Height (Rec'd), (in.):	4.63	8.75	7.00	11.25	10.25
Height in capped:	4.82	7.73	6.36	8.14	8.13
Weight (g):	939.7	2558.1	2077.6	2761.0	2775.6
Density (pcf):	111.0	103.0	102.0	106.0	107.0
Ultimate Load (lbs.):	32,870	50,170	41,260	48,750	59,250
Compressive Strength (psi):	4720	4120	3380	4000	4860
Corrected Compressive Strength (psi):	4570	----	----	3280	----

CONCRETE CORE TEST REPORT

Project Name: UCLA Franz Hall Investigative Study
Location: 502 Portola Plaza
Sampled By: Fidel Eviota **Tested By:** Mark Tabb **Test Date:** 12/18/15

COMPRESSIVE STRENGTH - ASTM C-42

Core Number:	5BC	5CS	5WC	5FC
Location:	Int. Beam Core through Floor	Int. Conc. Column	Ext. Balcony Waffle Slab	Ext. Balcony Conc. Fin
Diameter (in.):	3.94	3.94	2.98	3.94
Area, Sq. in:	6.97	12.19	12.19	12.19
Height (Rec'd), (in.):	10.25	9.875	4.563	9.875
Height in capped:	8.19	8.17	4.66	8.16
Weight (g):	2701.4	2743.3	872.7	2796.2
Density (pcf):	103.0	105.0	107.0	107.0
Ultimate Load (lbs.):	30,320	54,610	30,910	60,750
Compressive Strength (psi):	2490	4480	4430	4980
Corrected Compressive Strength (psi):	----	----	4270	----

Table B-1 (Cont'd.): Franz Tower Concrete Core Compressive Strength Test

UNITED INSPECTION & TESTING

An ETS Company

Client: University of Calif. Capital Programs
1060 Veterans Ave. #125 Box 951365
Los Angeles, CA. 90095-1365

UIT JOB # 10-08889PW

UIT LAB # 10C151217-1-4

CONCRETE CORE TEST REPORT

Project Name: UCLA Franz Hall Investigative Study

Location: 502 Portola Plaza

Sampled By: Fidel Eviota **Tested By:** Mark Tabb **Test Date:** 12/18/15

COMPRESSIVE STRENGTH - ASTM C-42

Core Number:	4BC	4WC	4FC	3BC	3CC	3WC
Location:	Int. Beam Core through Floor	Ext. Balcony Waffle Slab	Ext. Balcony Conc. Fin	Int. Beam Core through Floor	Int. Conc. Column	Ext. Balcony Waffle Slab
Diameter (in.):	3.94	2.98	3.94	3.94	3.94	2.98
Area, Sq. in:	12.19	6.97	12.19	12.19	12.19	6.97
Height (Rec'd), (in.):	10.125	4.75	10.25	9.875	6.500	4.875
Height in capped:	8.10	4.59	8.18	8.16	5.48	4.77
Weight (g):	2705.8	863.3	2789.7	2704.3	1842.6	879.6
Density (pcf):	104.0	106.0	107.0	103.0	105.0	104.0
Ultimate Load (lbs.):	44,460	27,550	60,050	44,260	58,460	30,350
Compressive Strength (psi):	3650	3950	4930	3630	4800	4350
Corrected Compressive Strength (psi):	----	3800	----	----	4540	4210

CONCRETE CORE TEST REPORT

Project Name: UCLA Franz Hall Investigative Study

Location: 502 Portola Plaza

Sampled By: Fidel Eviota **Tested By:** Mark Tabb **Test Date:** 12/18/15

COMPRESSIVE STRENGTH – C-42

Core Number:	2BC	2CC	2WC	1CC
Location:	Int. Beam Core through Floor	Int. Conc. Column	Ext. Balcony Waffle Slab	Int. Conc. Column
Diameter (in.):	3.94	3.94	2.98	3.94
Area, Sq. in:	12.19	12.19	6.97	12.19
Height (Rec'd), (in.):	10.25	8.50	4.5625	8.875
Height in capped:	8.08	8.10	4.59	8.10
Weight (g):	2619.0	2860.7	855.2	2725.0
Density (pcf):	101.0	110.0	105.0	105.0
Ultimate Load (lbs.):	40,250	60,760	31,410	48,750
Compressive Strength (psi):	3300	4980	4510	4000
Corrected Compressive Strength (psi):	----	----	4340	----

Table B-2: Franz Tower Concrete Core Split Tensile Test Report

UNITED INSPECTION & TESTING
An ETS Company

Client: University of Calif. Capital Programs
1060 Veterans Ave. #125 Box 951365
Los Angeles, CA. 90095-1365

UIT JOB # 10-08889PW
UIT LAB # 10C151217-1-6

CONCRETE CORE TEST REPORT

Project Name: UCLA Franz Hall Investigative Study
Location: 502 Portola Plaza
Sampled By: Fidel Eviota **Tested By:** Mark Tabb **Test Date:** 12/18/15

SPLIT TENSILE – ASTM C-42

Core Number:	8BS	8CS	7BS	6WC	4CS	3FC
Location:	Int. Beam Core through Floor	Int. Conc. Column	Int. Beam Core through Floor	Ext. Balcony Waffle Slab	Int. Conc. Column	Ext. Balcony Conc. Fin
Diameter (in.):	3.94	3.94	3.94	2.98	3.94	3.94
Height (Rec'd), (in.):	9.625	9.125	10.375	3.875	10.125	5.25
Height in capped:	8.10	8.09	8.12	3.77	8.12	4.66
Weight (g):	2702.2	2773.9	2680.4	714.7	2660.6	1539.2
Density (pcf):	104.0	107.0	103.0	104.0	102.0	103.0
Ultimate Load (lbs.):	18,770	22,440	15,390	7,790	20,120	11,530
Compressive Strength (psi):	375	450	305	440	400	400

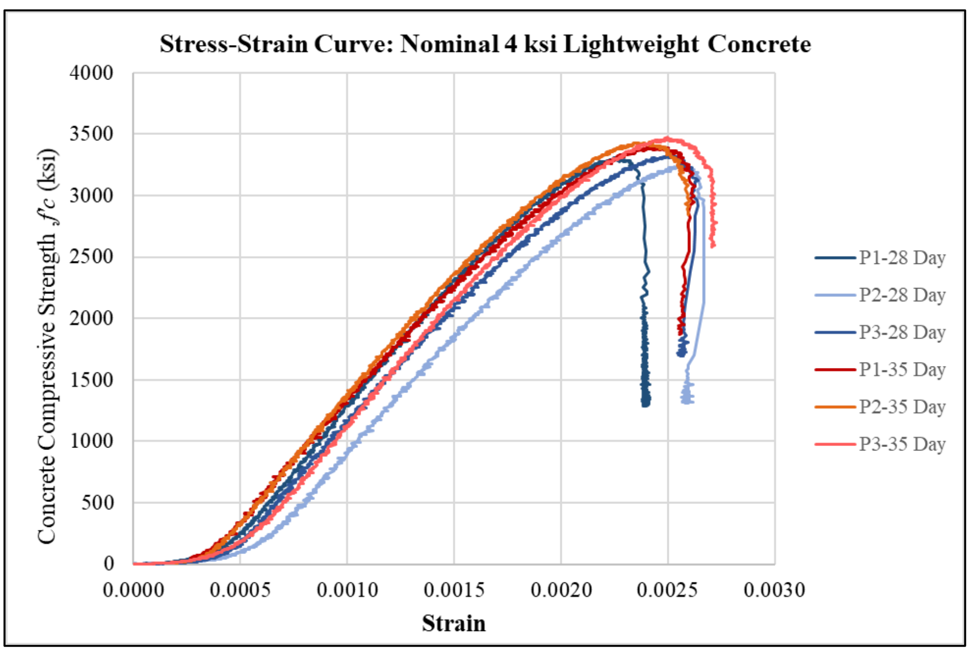

Figure B-1: Test Specimen, 4000 psi Light Weight Concrete Stress-Strain Curve

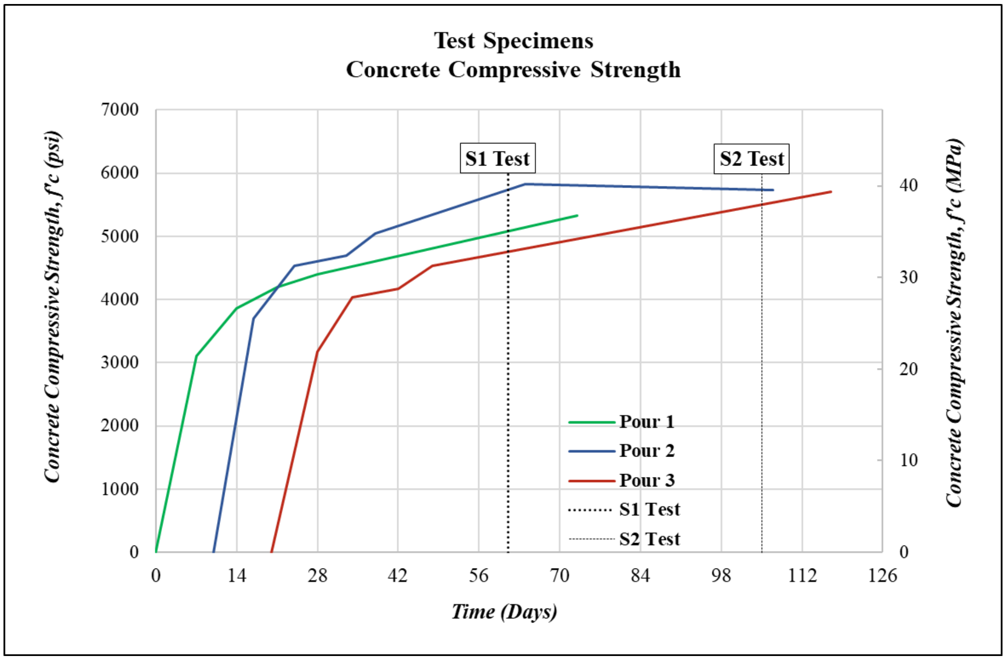

Figure B-2: Test Specimen, 4000 psi Light Weight Concrete Compressive Strength

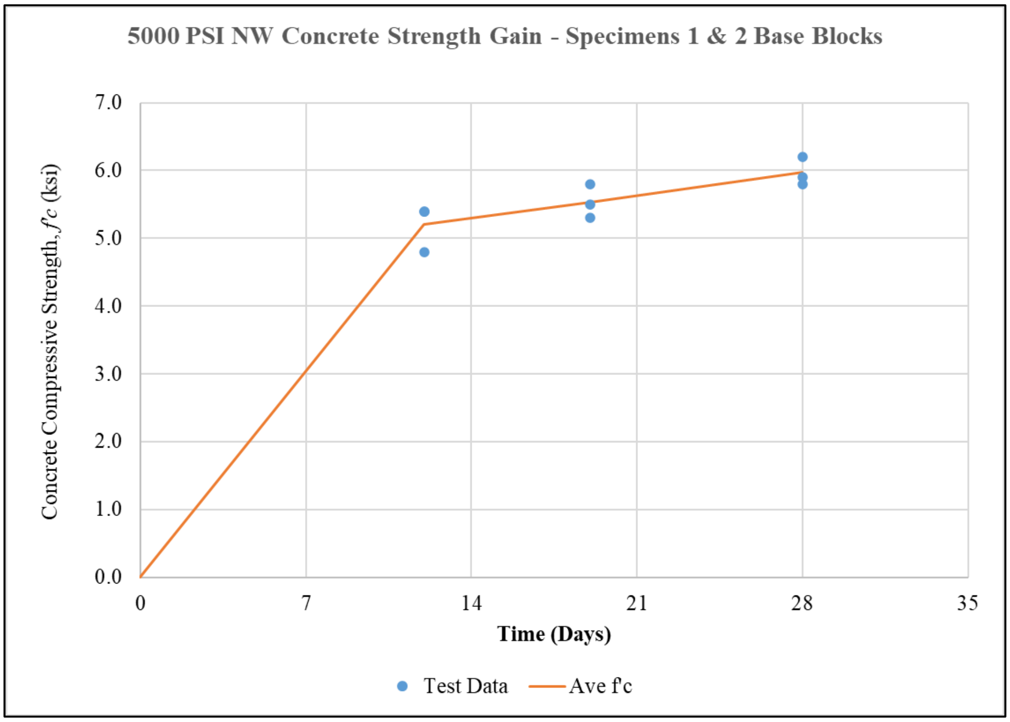

Figure B-3: Test Specimen, 5000 psi Normal Weight Concrete Compressive Strength for Base Blocks

Figure B-4: Concrete Compressive Strength Test of Specimens

Table B-3: Test Specimen, Light Weight Concrete Weight

Cylinder Specimen	Weight (kg)	Net Weight* (kg)	Average Net Weight (kg)	Average Net Weight (lbs)	Average Specific Weight (pcf)
Empty cylinder + lid	0.300	0.000	-	-	-
BB1	12.973	12.673	**12.642**	**27.87**	**141.9**
	12.998	12.698			
	12.855	12.555			
LC1	11.730	11.43	**11.365**	**25.06**	**127.6**
	11.640	11.34			
	11.625	11.325			
BC2/S1/TC1 A	11.390	11.09	**11.135**	**24.55**	**125.0**
	11.501	11.201			
	11.415	11.115			
BC2/S1/TC1 B	11.525	11.225	**11.152**	**24.59**	**125.2**
	11.447	11.147			
	11.385	11.085			
S2/TC2 A	11.412	11.112	**11.085**	**24.44**	**124.5**
	11.326	11.026			
	11.417	11.117			
S2/TC2 B	11.408	11.108	**11.138**	**24.55**	**125.1**
	11.407	11.107			
	11.498	11.198			
S1-P (9/6)	12.865	12.565	**12.566**	**27.70**	**141.1**
	12.877	12.577			
	12.855	12.555			

B2. Steel Reinforcement

CEL CONSULTING, INC

Product Evaluations · Metallurgy

Structural Investigations · Forensics

Sample ID

6CR-1

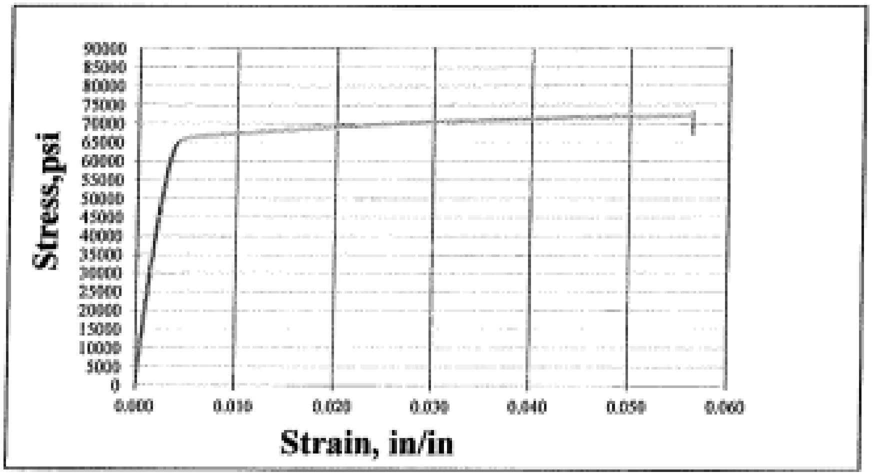

	Results	Specified Requirements		
Yield Point	65,980 psi	Not required, info only	Specification	Unknown
Ultimate Strength	72,939 psi	Not required, info only	Grade	Unknown
Elongation %, in 8"	19.0%	Not required, info only	Size	#3
Diameter, in	0.375 in			
Nominal Area	0.110 in^2			
M.O.E. (psi)	25,335,839 psi	Not required, info only		
Maximum Average Spacing, In.	0.178	0.262		
Minimum Average Height, In.	0.025	0.015		
Maximum Gap, In.	0.090	0.143		
Location in structure	6CR-1			
Project Name	UCLA Franz Hall			
Project Job #	50-53094M	Tested in accordance with ASTM A370.		
Met Lab#	J1210-3992			
Date Tested	12/15/2015	Reviewed by:		
Tested By	Jose Luis Alonso		James Powers, PE	

This report relates only to the items tested.

Page 1 of 3

Figure B-5: Franz Tower No. 3 Steel Reinforcement Tensile Strength Test (Sample 6CR-1)

CEL CONSULTING, INC

Product Evaluations · Metallurgy
Structural Investigations · Forensics

Sample ID
8CR-1

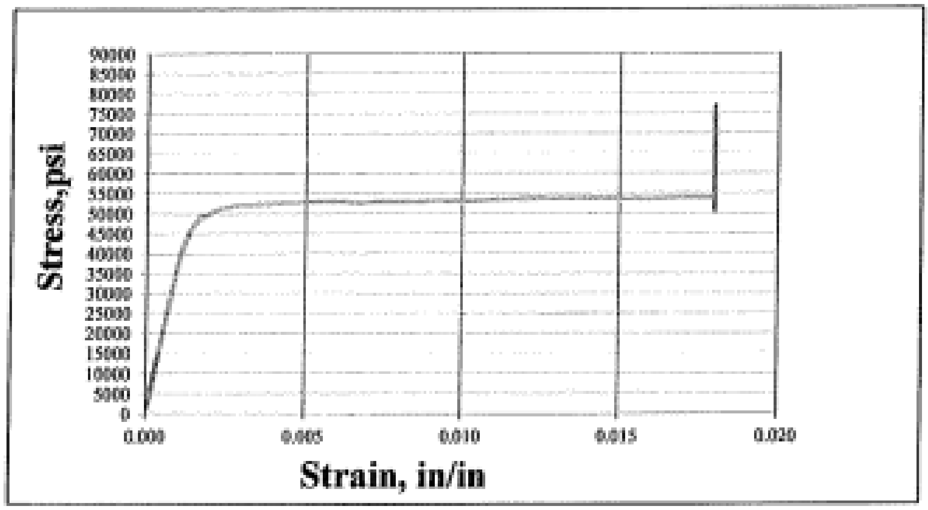

	Results	Specified Requirements		
Yield Point	52,300 psi	Not required, info only	Specification Unknown	
Ultimate Strength	76,838 psi	Not required, info only	Grade	Unknown
Elongation %, in 8"	14.0%	Not required, info only	Size	#3
Diameter, in	0.375 in			
Nominal Area	0.110 in^2			
M.O.E. (psi)	30,869,577 psi	Not required, info only		
Maximum Average Spacing, In.	176.000	0.262		
Minimum Average Height, In.	0.026	0.015		
Maximum Gap, In.	0.095	0.143		
Location in structure	8CR-1			
Project Name	UCLA Franz Hall			
Project Job #	50-53094M	Tested in accordance with ASTM A370.		
Met Lab#	J1210-3992			
Date Tested	12/15/2015	Reviewed by:		
Tested By	Jose Luis Alonso		James Powers, PE	

This report relates only to the items tested.

Page 2 of 3

Figure B-6: Franz Tower No. 3 Steel Reinforcement Tensile Strength Test (Sample 8CR-1)

CEL CONSULTING, INC

Product Evaluations - Metallurgy
Structural Investigations - Forensics

Sample ID
8CR-2

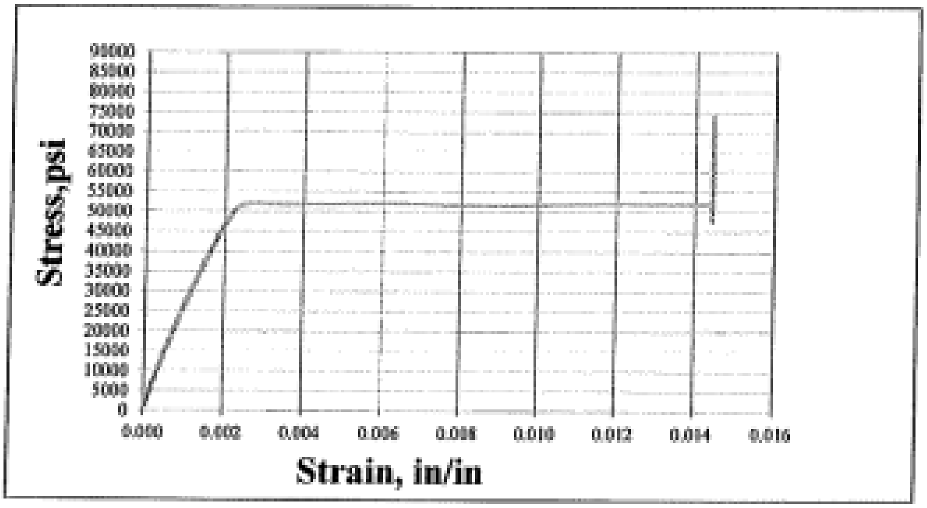

	Results	Specified Requirements		
Yield Point	51,800 psi	Not required, info only	Specification Unknown	
Ultimate Strength	73,789 psi	Not required, info only	Grade	Unknown
Elongation %, in 8"	20.0%	Not required, info only	Size	#3
Diameter, in	0.375 in			
Nominal Area	0.110 in^2			
M.O.E. (psi)	28,491,291 psi	Not required, info only		
Maximum Average Spacing, In.	0.176	0.262		
Minimum Average Height, In.	0.026	0.015		
Maximum Gap, In.	0.095	0.143		
Location in structure	8CR-2			
Project Name	UCLA Franz Hall			
Project Job #	50-53094M	Tested in accordance with ASTM A370.		
Met Lab#	J1210-3992			
Date Tested	12/15/2015	Reviewed by:		
Tested By	Jose Luis Alonso		James Powers, PE	

This report relates only to the items tested.

Page 3 of 3

Figure B-7: Franz Tower No. 3 Steel Reinforcement Tensile Strength Test (Sample 8CR-2)

element

Element Materials Technology
15062 Bolsa Chica
Huntington Beach, CA
92649-1023 USA

P 714 892 1961
F 714 892 8159
T 888 786 7555
info.hb@element.com
element.com

Contact: Steve Lindquist
United Inspection & Testing Co
22620 Goldencrest Dr., #114
MORENO VALLEY, CA 92553

TEST CERTIFICATE — EAR-CONTROLLED DATA

Date: 12/10/2015
Purchase Order Number: Lab# 0S15-071
Work Order Number UNI157-12-08-54412-1

Lab Number:	0S15-071
Description:	#3 REBAR 6CR.1 GRADE 40
Project:	UCLA FRANZ HALL
UIT Job Number:	10-08889PW

CHEMICAL ANALYSIS

Element		Result %
C	=	0.28
Mn	=	0.47
Si	=	0.06
P	=	0.004
S	=	0.052
Cr	=	0.12
Ni	=	0.15
Mo	=	0.04
Cu	=	0.34
Al	<	0.01
V	<	0.01
Cb	<	0.01
Ti	<	0.01
Fe	=	Balance

Chemical Analysis performed by Optical Emission per SOP 2.02, Revision 16
Carbon and Sulfur by Combustion per SOP 7.00, Revision 13

FOR INFORMATION ONLY

This document contains technical data whose export and re-export/ retransfer is subject to control by the U.S. Department of Commerce under the Export Administration Act and the Export Administration Regulations. The Department of Commerce's prior written approval may be required for the export or re-export/retransfer of such technical data to any foreign person, foreign entity or foreign organization whether in the United States or abroad.

Respectfully submitted

Kelly Nguyen
Senior Quality Administrator

15062 Bolsa Chica, Huntington Beach, CA 92649
(714) 892-1961 ph • (714) 892-8159 fax www.element.com

The information contained in this certification represents only the material submitted and is certified only for the quantities tested. Reproduction except in full is reserved pending written approval. The recording of false, fictitious, or fraudulent statements or entries on the certificate may be punishable as a felony under federal law. All testing was performed in a mercury free environment. **All testing performed in accordance with the latest edition of the applicable ASTM, or other Federal Test Method in effect at the time of test.**

Page 1 of 1

Figure B-8: Franz Tower No. 3 Steel Reinforcement Chemical Analysis (Sample 6CR-1)

element

Element Materials Technology
15062 Bolsa Chica
Huntington Beach, CA
92649-1023 USA

P 714 892 1961
F 714 892 8159
T 888 786 7555
info.hb@element.com
element.com

Contact: Steve Lindquist
United Inspection & Testing Co
22620 Goldencrest Dr., #114
MORENO VALLEY, CA 92553

TEST CERTIFICATE — EAR-CONTROLLED DATA

Date: 12/10/2015
Purchase Order Number: Lab# 0S15-071
Work Order Number UNI157-12-08-54412-2

Lab Number:	0S15-071
Description:	#3 REBAR 8CR.1 GRADE 40
Project:	UCLA FRANZ HALL
UIT Job Number:	10-08889PW

CHEMICAL ANALYSIS

Element		Result %
C	=	0.30
Mn	=	0.51
Si	=	0.06
P	=	0.007
S	=	0.057
Cr	=	0.18
Ni	=	0.14
Mo	=	0.03
Cu	=	0.36
Al	<	0.01
V	<	0.01
Cb	<	0.01
Ti	<	0.01
Fe	=	Balance

Chemical Analysis performed by Optical Emission per SOP 2.02, Revision 16
Carbon and Sulfur by Combustion per SOP 7.00, Revision 13

FOR INFORMATION ONLY

This document contains technical data whose export and re-export/ retransfer is subject to control by the U.S. Department of Commerce under the Export Administration Act and the Export Administration Regulations. The Department of Commerce's prior written approval may be required for the export or re-export/retransfer of such technical data to any foreign person, foreign entity or foreign organization whether in the United States or abroad.

Respectfully submitted

Kelly Nguyen
Senior Quality Administrator

15062 Bolsa Chica, Huntington Beach, CA 92649
(714) 892-1961 ph • (714) 892-8159 fax www.element.com

The information contained in this certification represents only the material submitted and is certified only for the quantities tested. Reproduction except in full is reserved pending written approval. The recording of false, fictitious, or fraudulent statements or entries on the certificate may be punishable as a felony under federal law. All testing was performed in a mercury free environment. **All testing performed in accordance with the latest edition of the applicable ASTM, or other Federal Test Method in effect at the time of test.**

Page 1 of 1

Figure B-9: Franz Tower No. 3 Steel Reinforcement Chemical Analysis (Sample 8CR-1)

element

Element Materials Technology
15062 Bolsa Chica
Huntington Beach, CA
92649-1023 USA

P 714 892 1961
F 714 892 8159
T 888 786 7555
info.hb@element.com
element.com

Contact: Steve Lindquist
United Inspection & Testing Co
22620 Goldencrest Dr., #114
MORENO VALLEY, CA 92553

TEST CERTIFICATE — EAR-CONTROLLED DATA

Date: 12/10/2015
Purchase Order Number: Lab# 0S15-071
Work Order Number UNI157-12-08-54412-3

Lab Number:	0S15-071
Description:	#3 REBAR 8CR.2 GRADE 40
Project:	UCLA FRANZ HALL
UIT Job Number:	10-08889PW

CHEMICAL ANALYSIS

Element		Result %
C	=	0.30
Mn	=	0.51
Si	=	0.06
P	=	0.007
S	=	0.056
Cr	=	0.18
Ni	=	0.14
Mo	=	0.03
Cu	=	0.36
Al	<	0.01
V	<	0.01
Cb	<	0.01
Ti	<	0.01
Fe	=	Balance

Chemical Analysis performed by Optical Emission per SOP 2.02, Revision 16
Carbon and Sulfur by Combustion per SOP 7.00, Revision 13

FOR INFORMATION ONLY

This document contains technical data whose export and re-export/ retransfer is subject to control by the U.S. Department of Commerce under the Export Administration Act and the Export Administration Regulations. The Department of Commerce's prior written approval may be required for the export or re-export/retransfer of such technical data to any foreign person, foreign entity or foreign organization whether in the United States or abroad.

Respectfully submitted -

Kelly Nguyen
Senior Quality Administrator

15062 Bolsa Chica, Huntington Beach, CA 92649
(714) 892-1961 ph • (714) 892-8159 fax www.element.com

The information contained in this certification represents only the material submitted and is certified only for the quantities tested. Reproduction except in full is reserved pending written approval. The recording of false, fictitious, or fraudulent statements or entries on the certificate may be punishable as a felony under federal law. All testing was performed in a mercury free environment. **All testing performed in accordance with the latest edition of the applicable ASTM, or other Federal Test Method in effect at the time of test.**

Page 1 of 1

Figure B-10: Franz Tower No. 3 Steel Reinforcement Chemical Analysis (Sample 8CR-2)

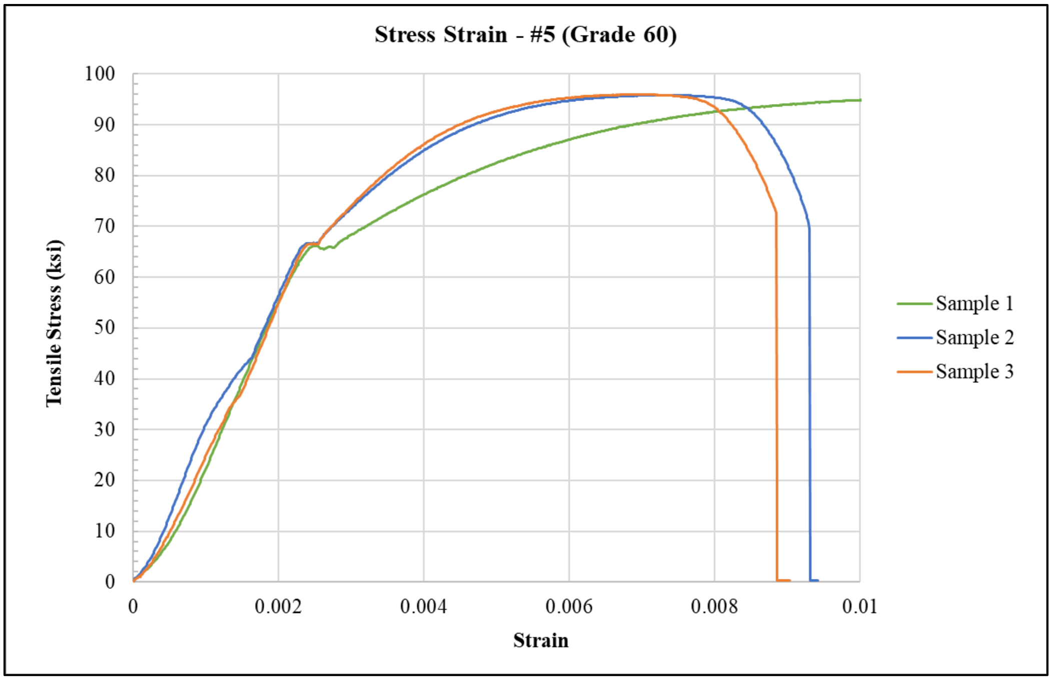

Figure B-11: Test Specimen Gr. 60 No. 5 Steel Reinforcement Tensile Stress vs Strain

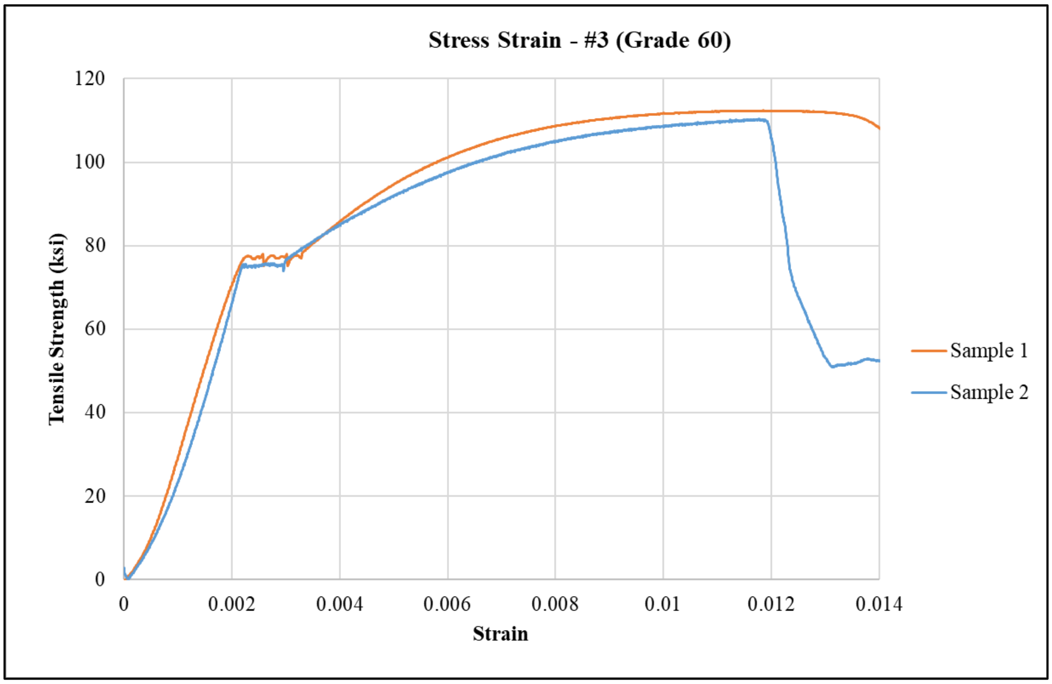

Figure B-12: Test Specimen Gr. 60 No. 3 Steel Reinforcement Tensile Stress vs Strain

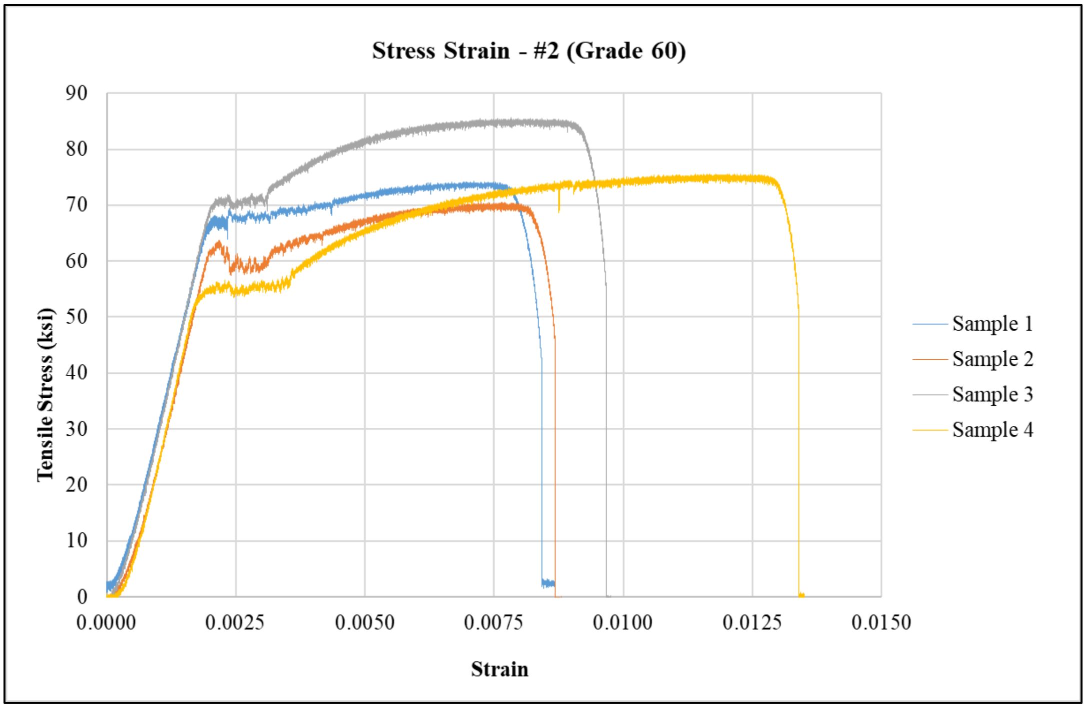

Figure B-13: Test Specimen Gr. 60 No. 2 Steel Reinforcement Tensile Stress vs Strain

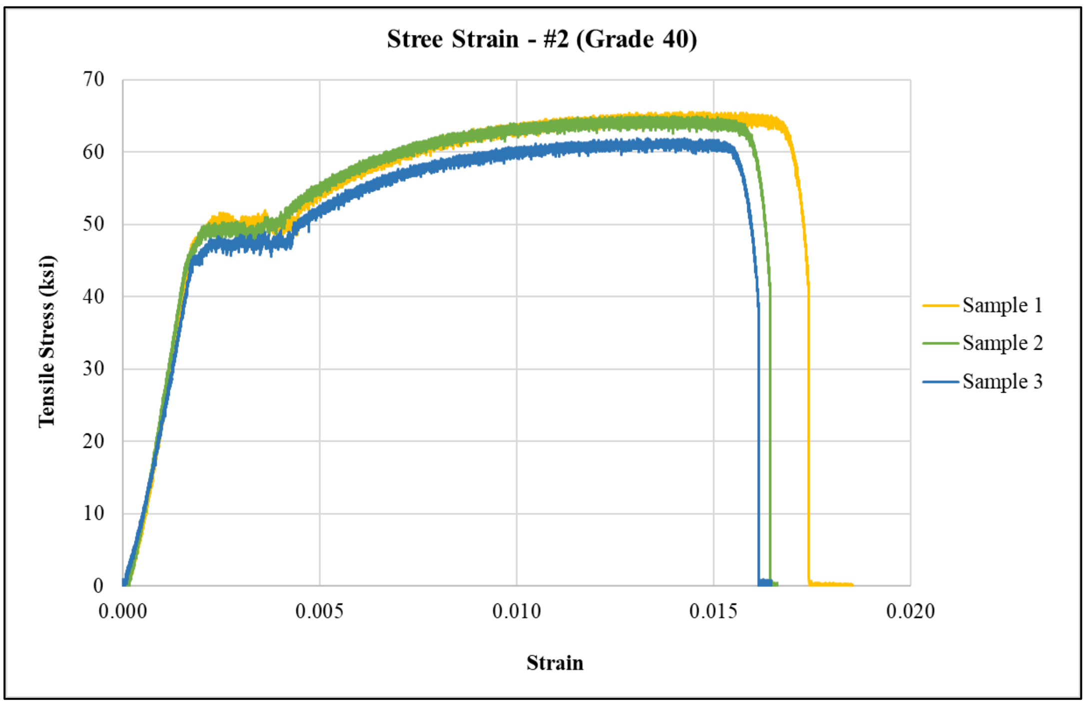

Figure B-14: Test Specimen Gr. 40 No. 2 Steel Reinforcement Tensile Stress vs Strain

Appendix C. Plans and Details

C1. Franz Tower

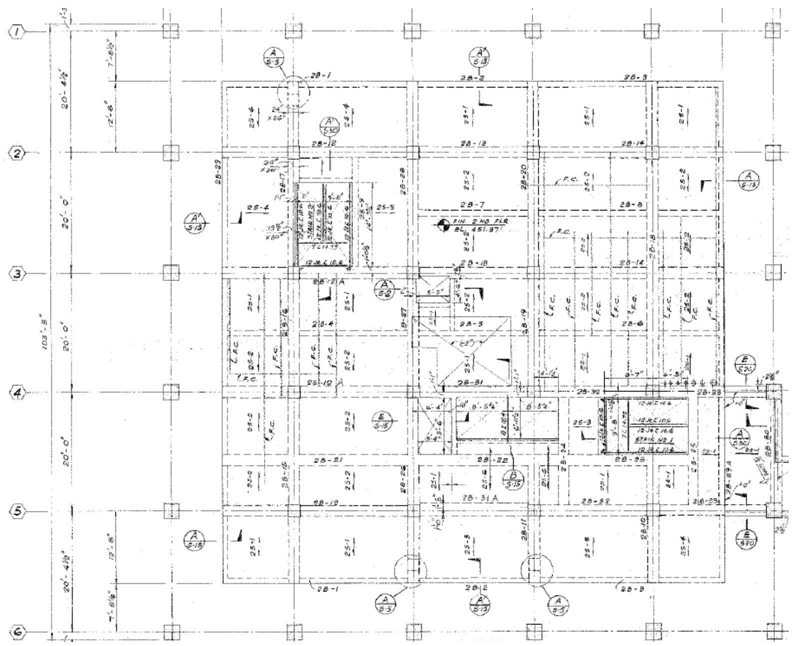

Figure C-1: Franz Tower 2nd Level Floor Plan

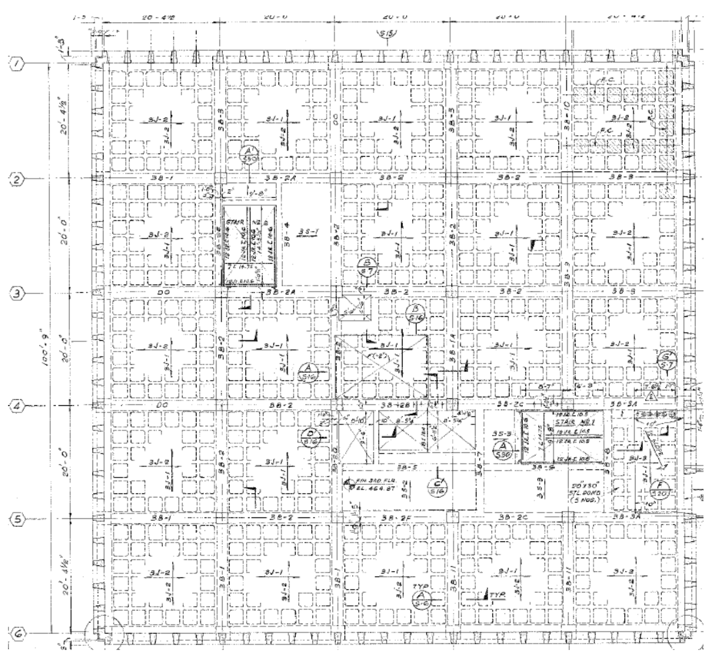

Figure C-2: Franz Tower 3rd Level Floor Plan

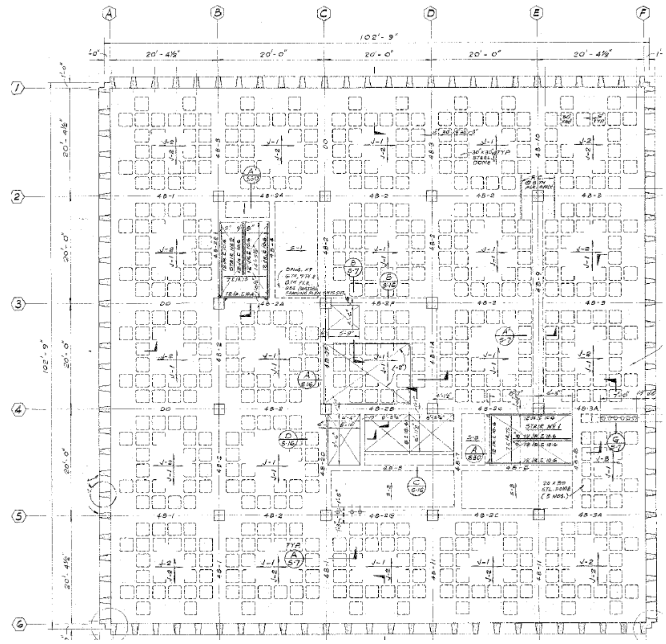

Figure C-3: Franz Tower 4th to 8th Level Floor Plan

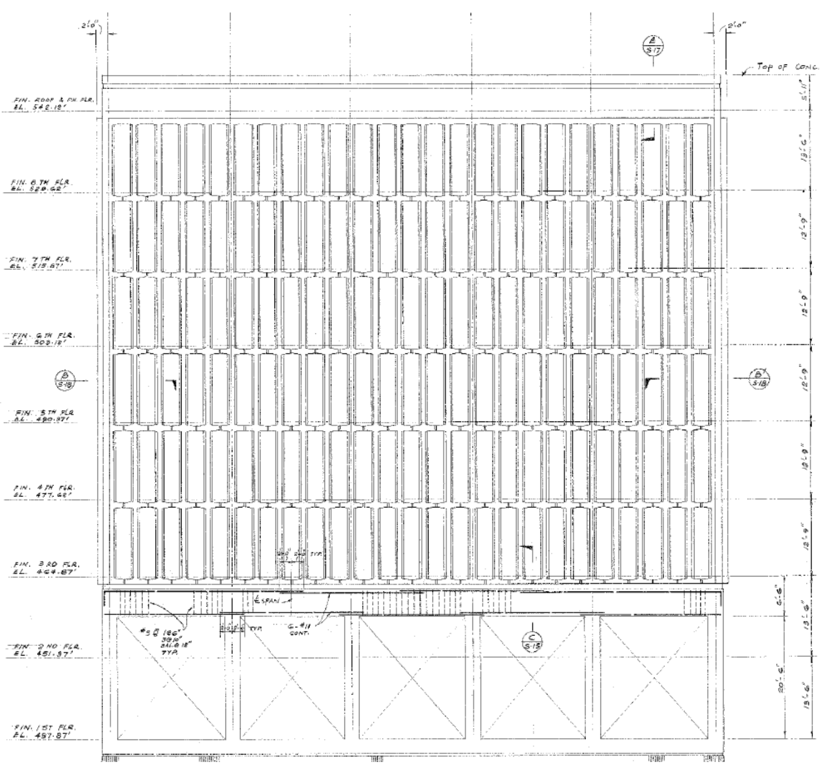

Figure C-4: Typical Franz Tower Elevation

C2. Test Specimen Construction Plans

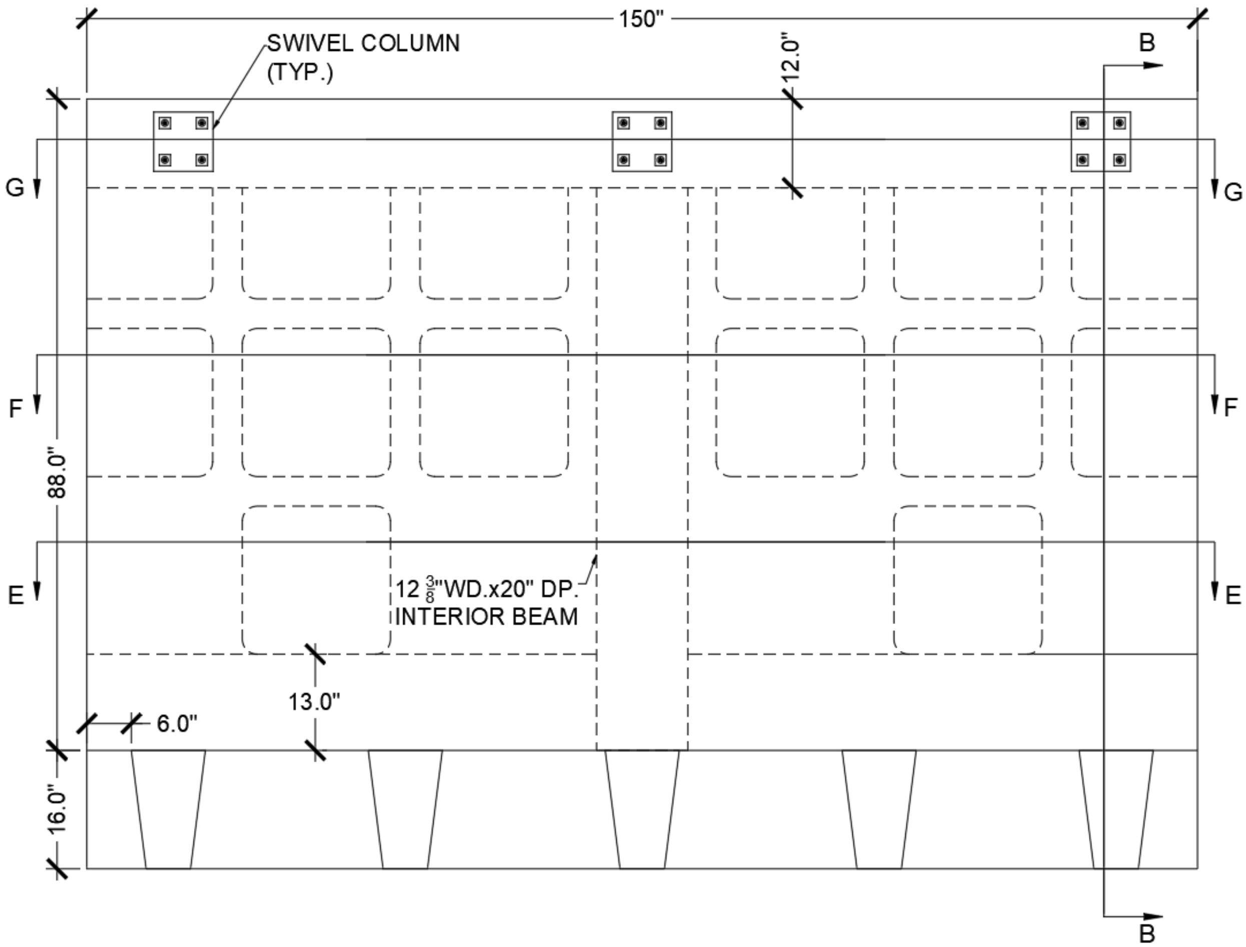

Figure C-5: Plan View of the Test Specimen

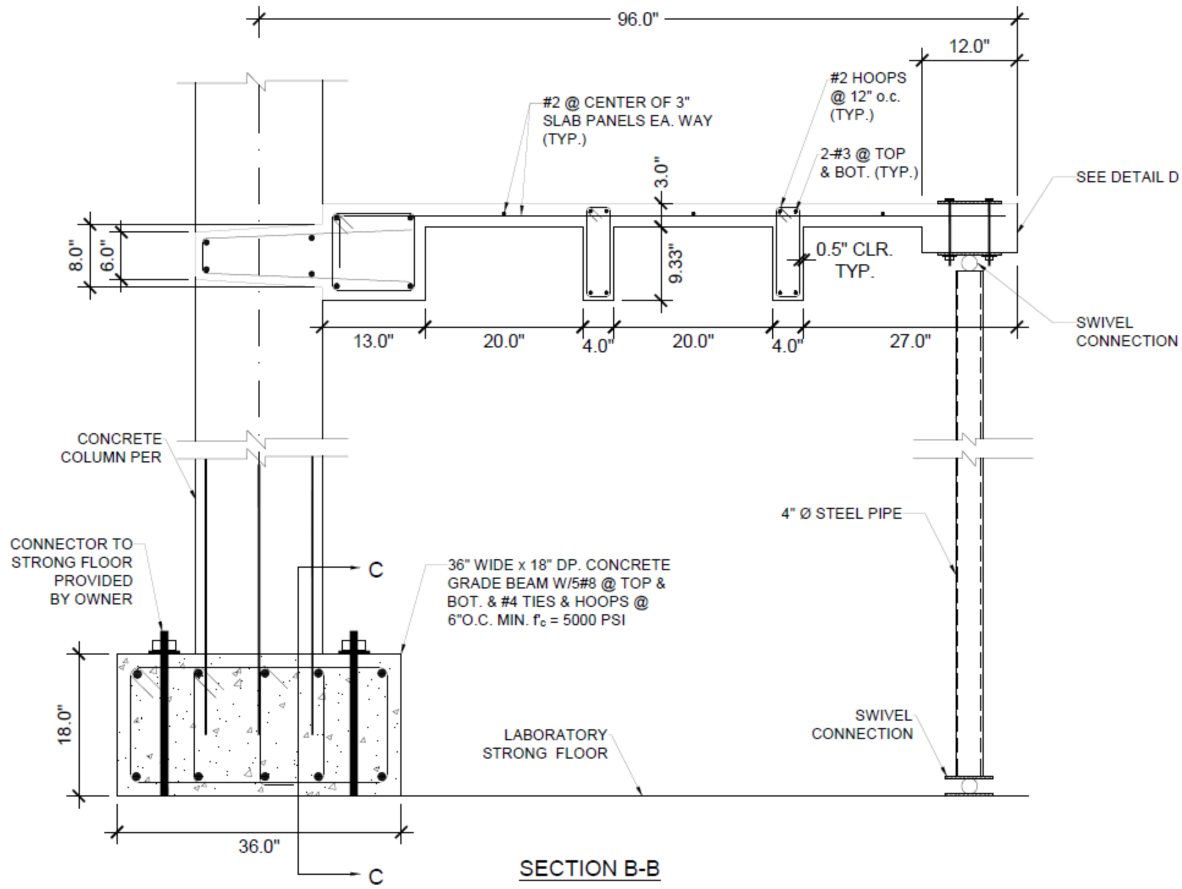

Figure C-6: Section B-B Through the Specimen

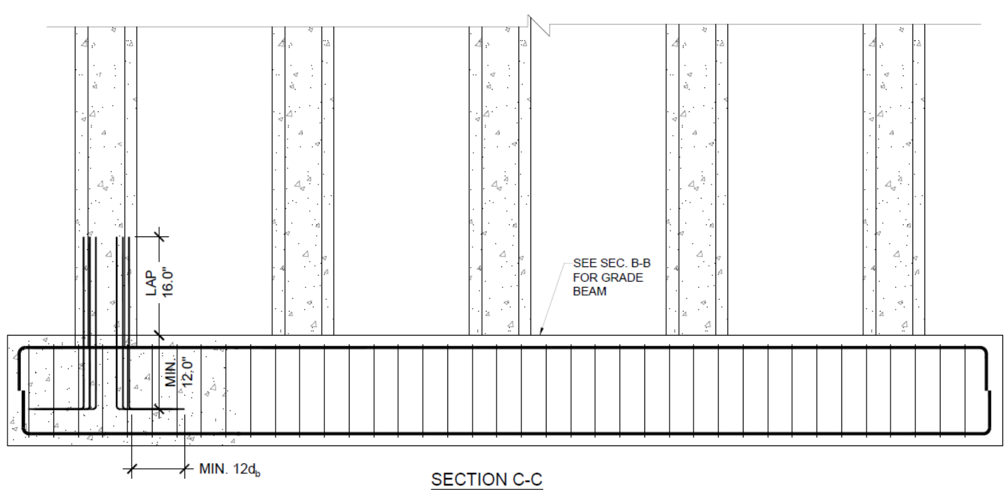

Figure C-7: Section C-C Through the Specimen at the Base Block

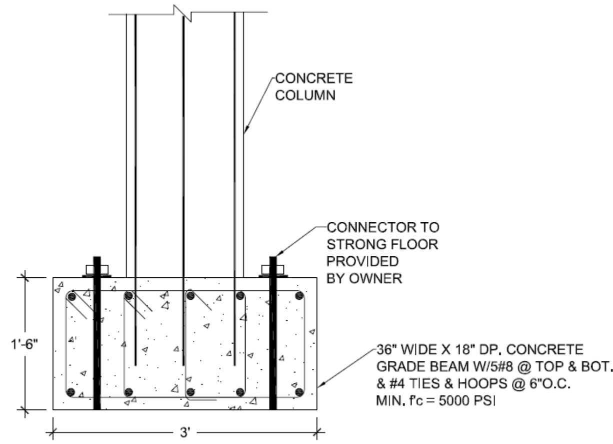

Figure C-8: Detail of Base Block Reinforcement

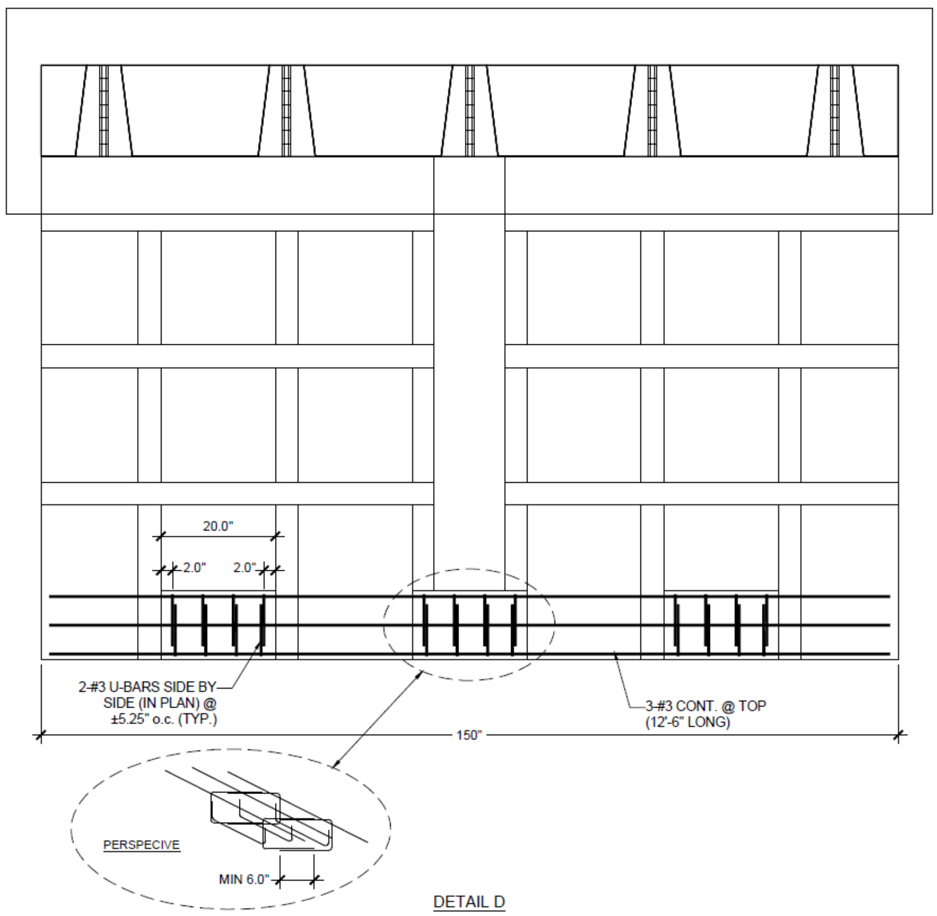

Figure C-9: Slab Section (Detail D)

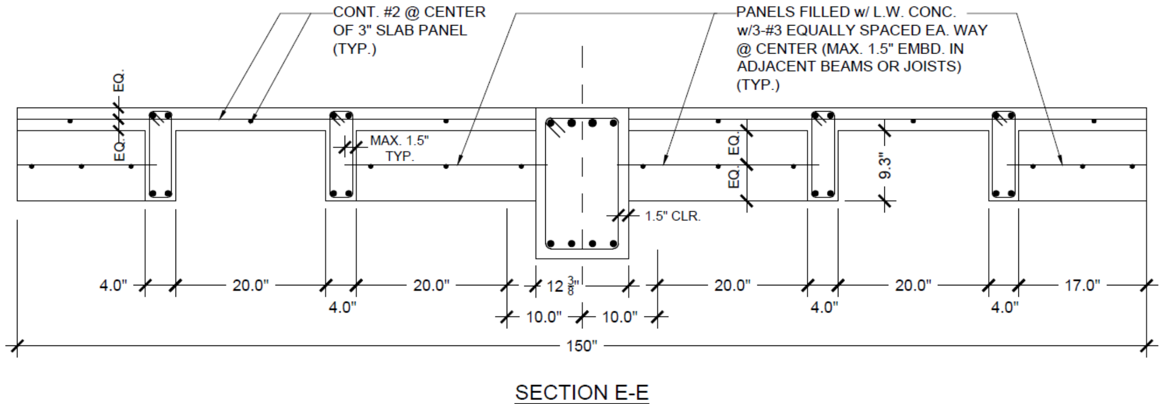

Figure C-10: Section E-E Through the Slab

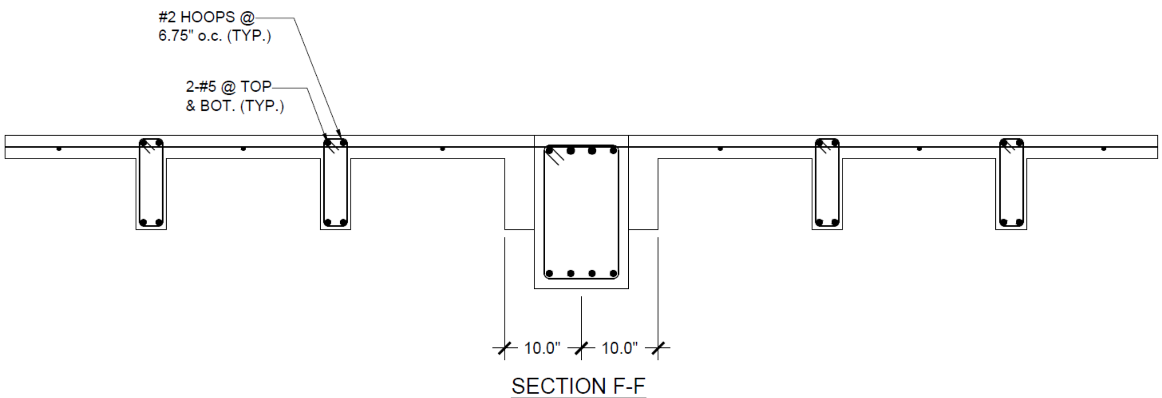

Figure C-11: Section F-F Through the Slab

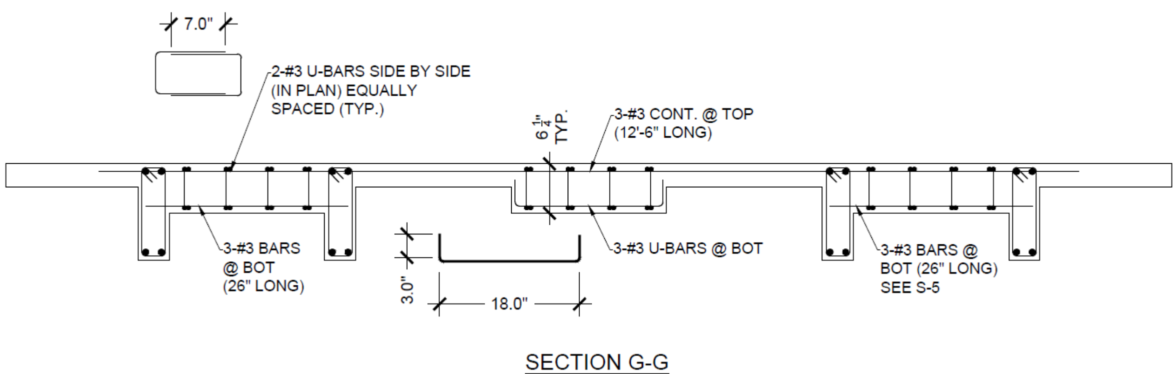

Figure C-12: Section G-G Through the Slab End at Vertical Support

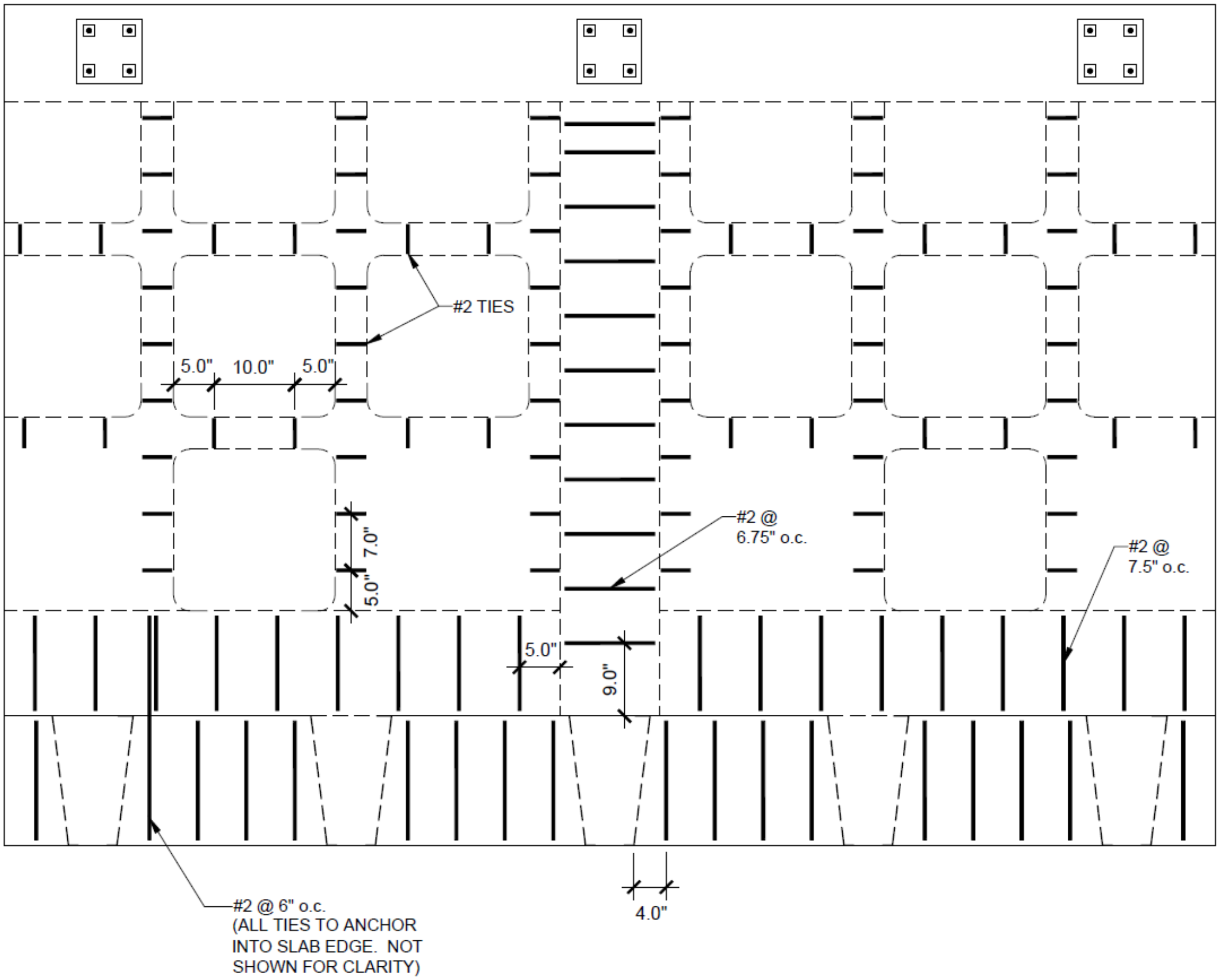

Figure C-13: Tie Layout in the Slab

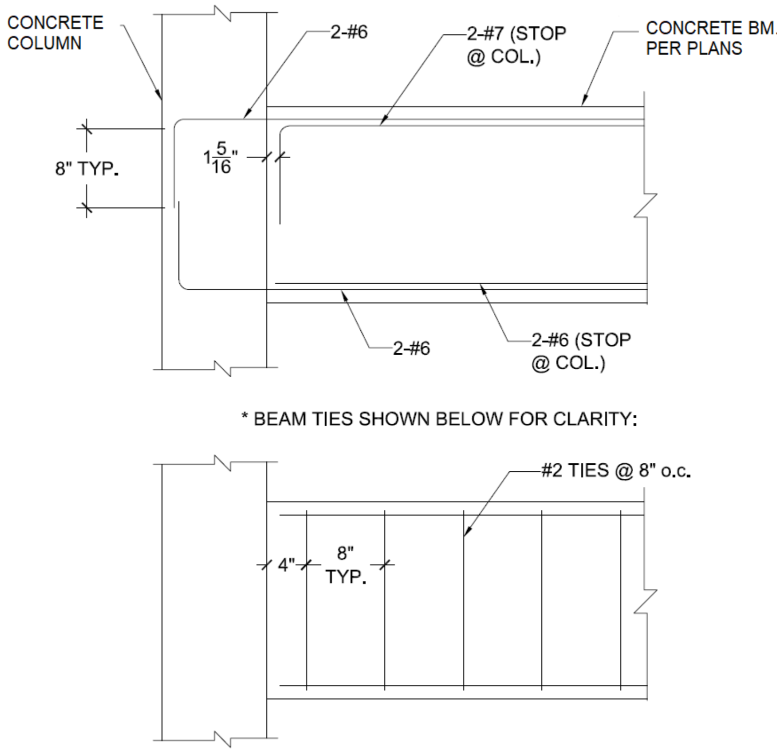

Figure C-14: Interior Beam to Fin Column Connection

C3. Test Specimen Instrumentation

Column 1	Side Column Left, Hinge 3	Side Column Front Low, Hinge 3	Side Column Right, Hinge 3	Side Column Front Upper, Hinge 3
LVDT Designation	**SCL3**	**SCFL3**	**SCR3**	**SCFU3**
Core Dist. To FOC	2.875	2.125	2.0625	2
Gage Length (rod to rod)	6.25	6.75	6.9375	7.125
Top Rod to Top of Beam	0	0	0	0
Total Gauge Length	6.25	6.75	6.9375	7.125
	Side Column Left, Hinge 2	Side Column Front Low, Hinge 2	Side Column Right, Hinge 2	Side Column Front Upper, Hinge 2
LVDT Designation	**SCL2**	**SCFU2**	**SCR2**	**SCFL2**
Core Dist. To FOC	1.125	1.625	2.125	2.125
Gage Length (rod to rod)	6.875	7.125	7.3125	7.25
Top Rod to Bot of Beam	0	0	0	0
Total Gauge Length	6.875	7.125	7.3125	7.25
	Side Column Left, Hinge 1	Side Column Front Low, Hinge 1	Side Column Right, Hinge 1	Side Column Front Upper, Hinge 1
LVDT Designation	**SCL1**	**SCFL1**	**SCR1**	**SCFU1**
Core Dist. To FOC	2	1.875	2.1875	1.75
Gage Length (rod to rod)	7	6.875	7.375	6.875
Bot Rod to Top of Base	0.875	0.75	1.5625	0
Total Gauge Length	7.875	7.625	8.9375	6.875

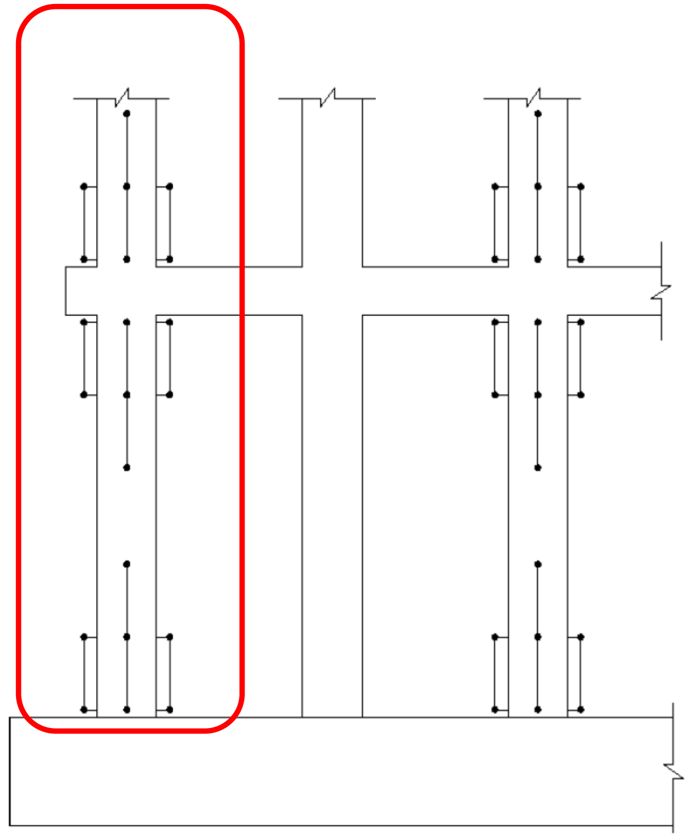

Figure C-15: Column 1 LVDT Information

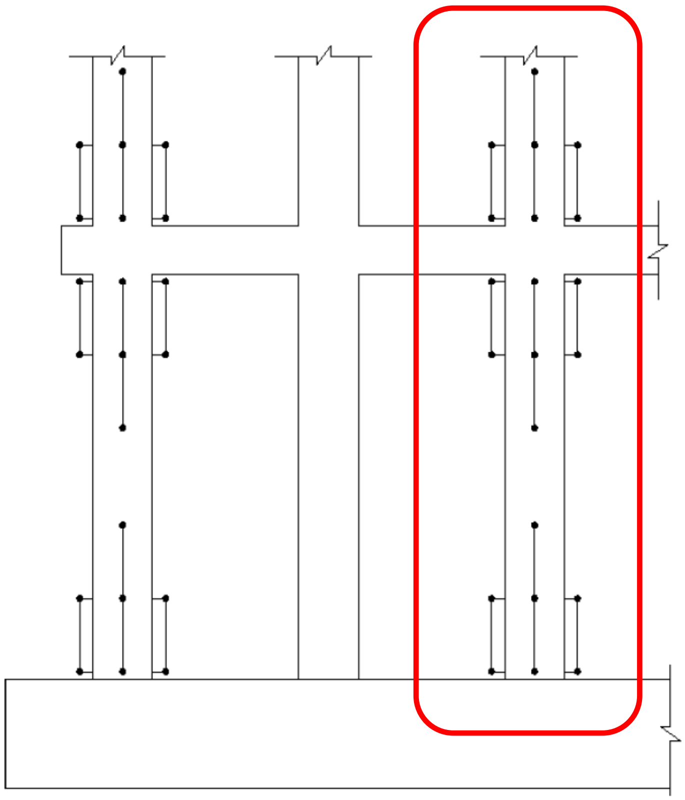

Column 3	Middle Column Left, Hinge 3	Middle Column Front Low, Hinge 3	Middle Column Right, Hinge 3	Middle Column Front Upper, Hinge 3
LVDT Designation	MCL3	MCFL3	MCR3	MCFU3
Core Dist. To FOC	2	2.0625	2.625	2.125
Gage Length (rod to rod)	7.125	7.125	4.875	6.25
Top Rod to Top of Beam	0	0	0	0
Total Gauge Length	7.125	7.125	4.875	6.25
	Side Column Left, Hinge 2	Side Column Front Low, Hinge 2	Side Column Right, Hinge 2	Side Column Front Upper, Hinge 2
LVDT Designation	MCL2	MCFU2	MCR2	MCFL2
Core Dist. To FOC	1.75	1.625	2	7.0625
Gage Length (rod to rod)	7.125	6.5	7	2
Top Rod to Bot of Beam	0	0	0	0
Total Gauge Length	7.125	6.5	7	2
	Side Column Left, Hinge 1	Side Column Front Low, Hinge 1	Side Column Right, Hinge 1	Side Column Front Upper, Hinge 1
LVDT Designation	MCL1	MCFL1	MCR1	MCFU1
Core Dist. To FOC	2.25	2	1.875	2.25
Gage Length (rod to rod)	7.125	7.0625	6.75	7.125
Bot Rod to Top of Base	1.125	0.625	1.0625	0
Total Gauge Length	8.25	7.6875	7.8125	7.125

Figure C-16: Column 3 LVDT Information

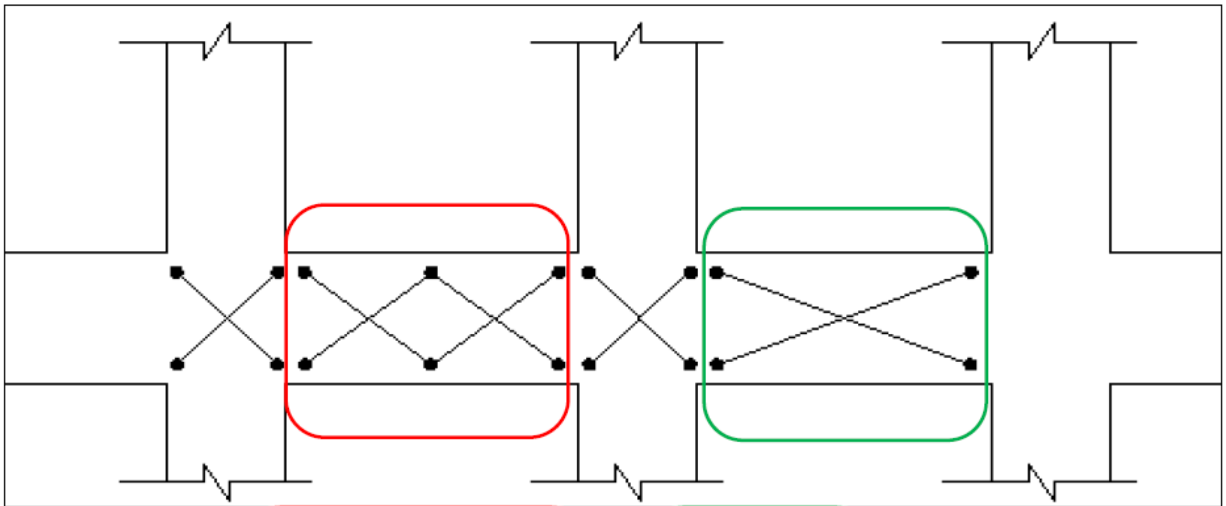

	Dbl, Left X, Top-Left, Bottom Right	Dbl, Left X, Top-Right, Bottom Left	Dbl, Rigt X, Top-Left, Bottom Right	Dbl, Right X, Top-Right, Bottom Left	One X, Top-Left, Bottom Right	One X, Top-Right, Bottom Left
	2XL-TLBR	**2XL-TRBL**	**2XR-TLBR**	**2XR-TRBL**	**X-TLBR**	**X-TRBL**
Core Dist to FOC (in)	3.25	2.25	3.25	2	2.375	1
Gage Length (in)	13	13	12.625	12.75	23.3125	23.3125

Figure C-17: Ledge Beam LVDT Information

C4. Test Setup Schematics and Shoring

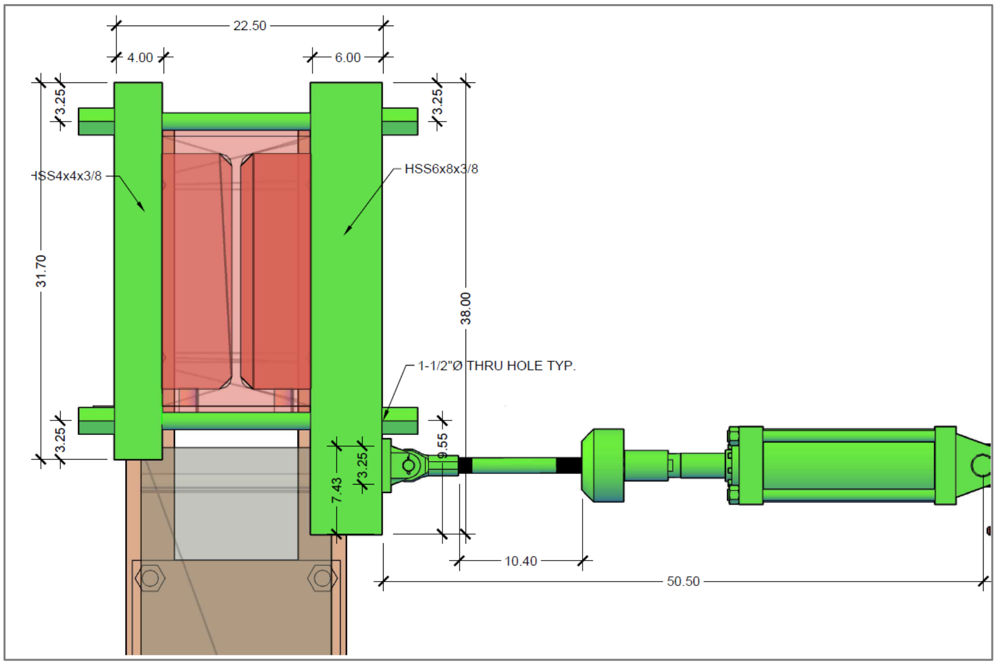

Figure C-18: Side View of the Out-of-Plane Actuators Top Attachment

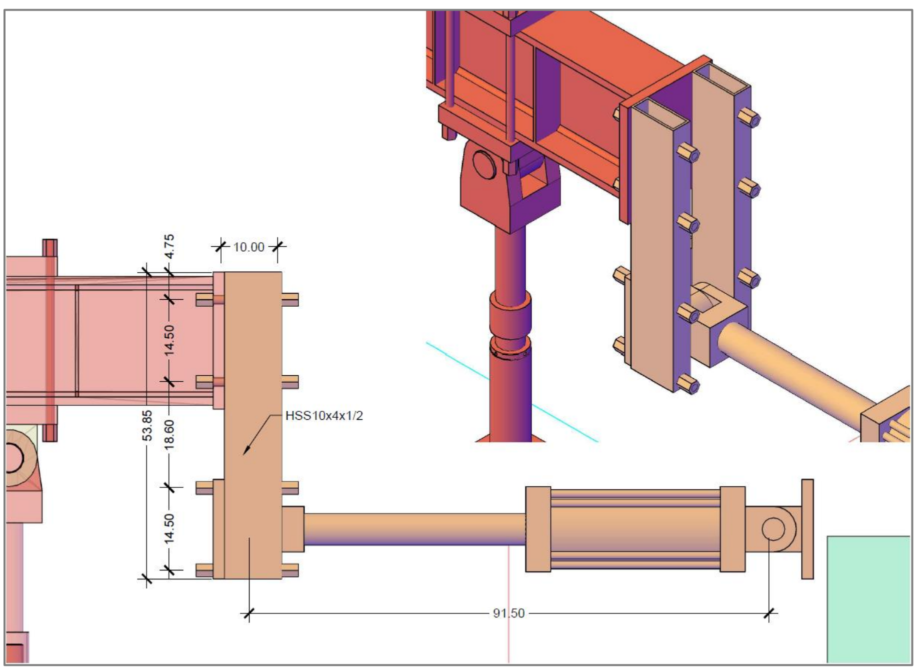

Figure C-19: Side and 3D View of the Out-of-Plane Actuators Top Attachment

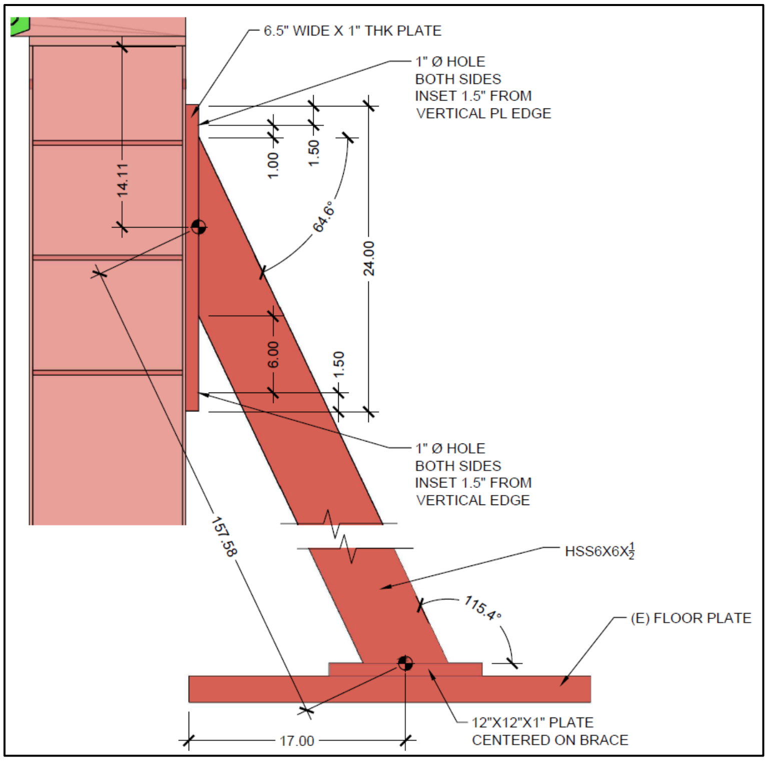

Figure C-20: A-Frame Braces (Support Structure of the Out-of-Plane Actuators)

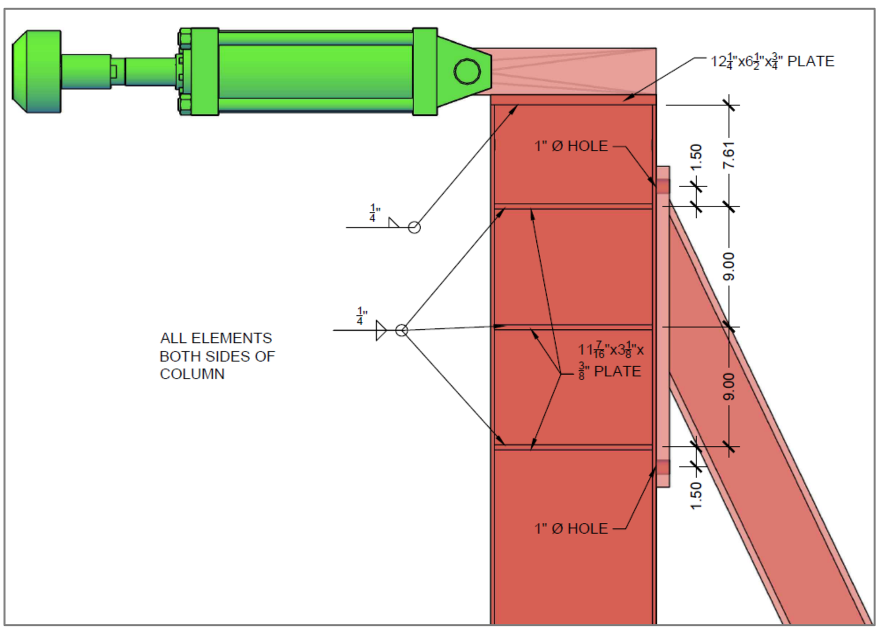

Figure C-21: A-Frame Stiffener Plates

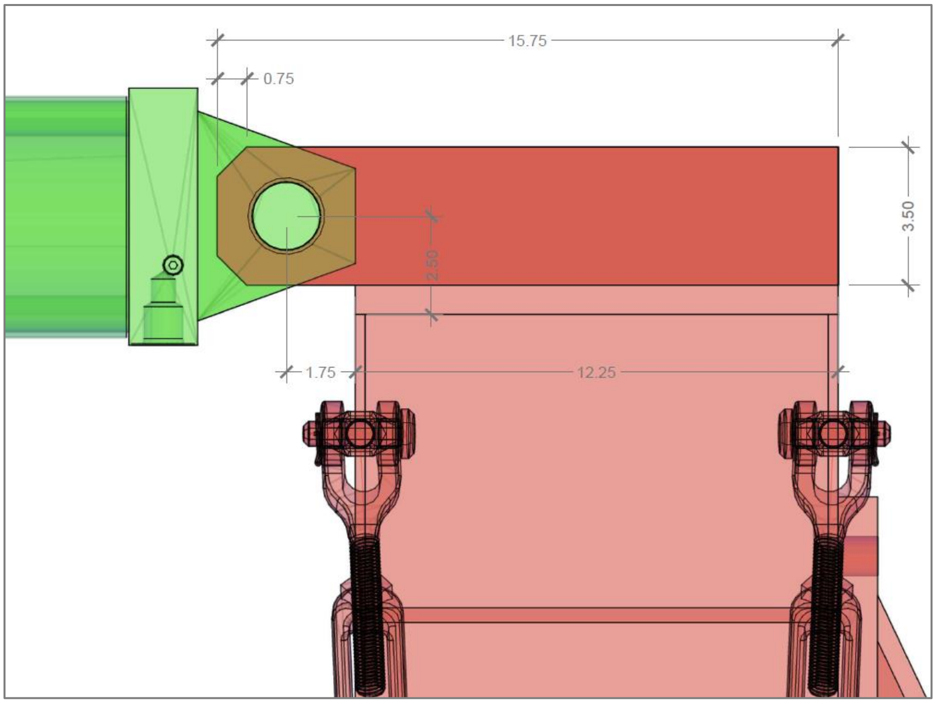

Figure C-22: Actuator Attachment

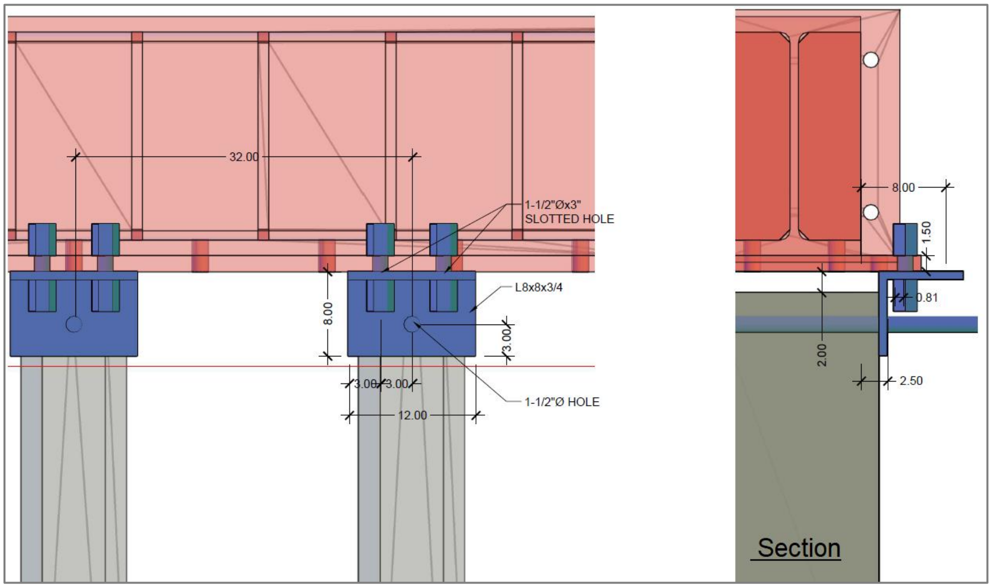

Figure C-23: Top Column Pin Attachment

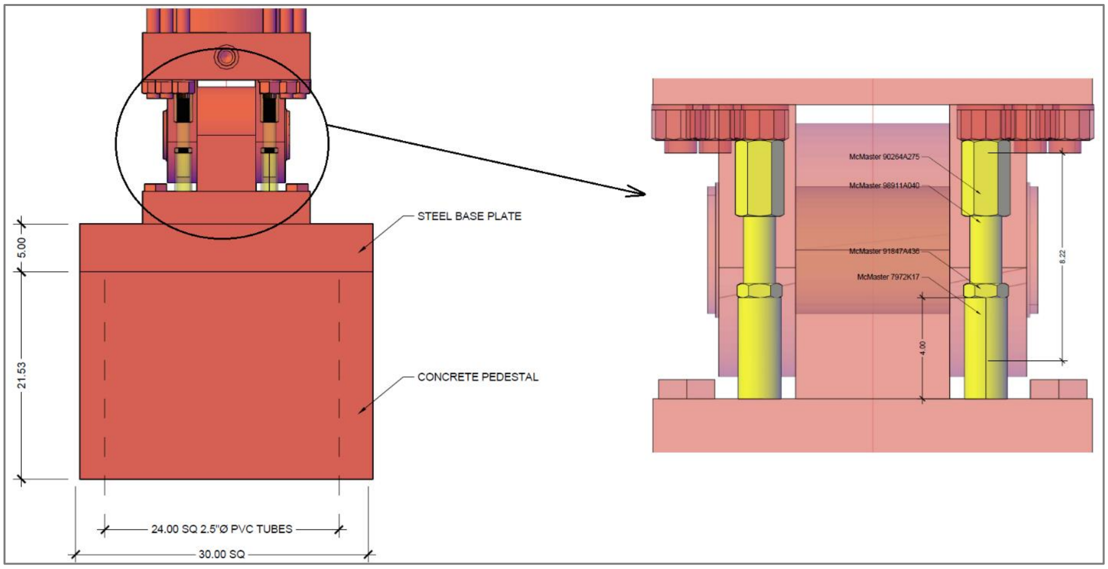

Figure C-24: Vertical Actuator Pedestal and Stabilizer

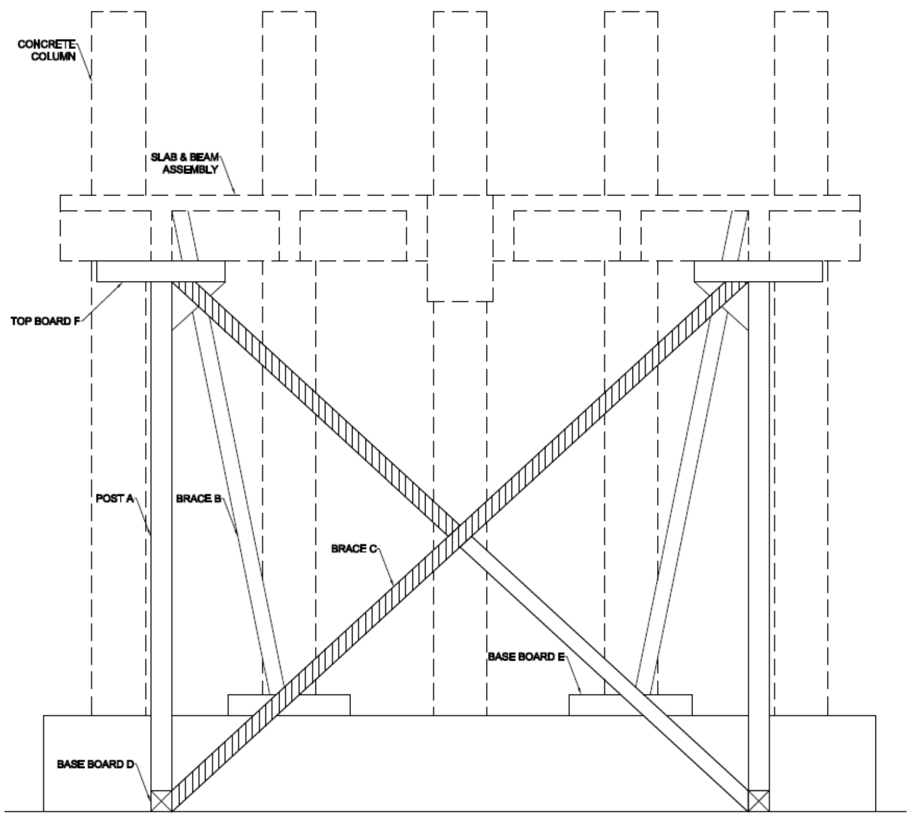

Figure C-25: Specimen Shoring – Elevation

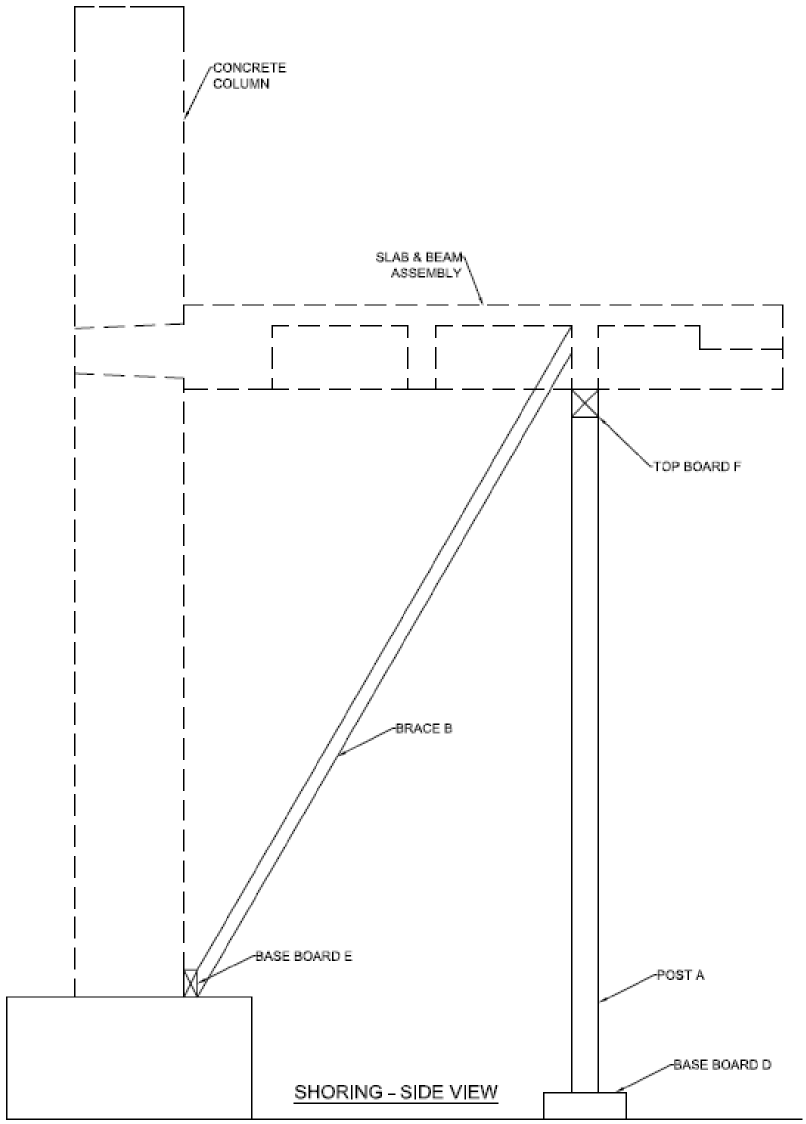

Figure C-26: Specimen Shoring – Side View

Appendix D. Construction Pictures

Figure D-1: Preparation and Attachment of Strain Gauges to Column Longitudinal Bars

Figure D-2: Strain Gauges Attached to Column Transverse Reinforcement

Figure D-3: No. 2 (6 mm) Column Ties (Left), and Beam Ties (Right)

Figure D-4: Soldering Wires to Strain Gauges

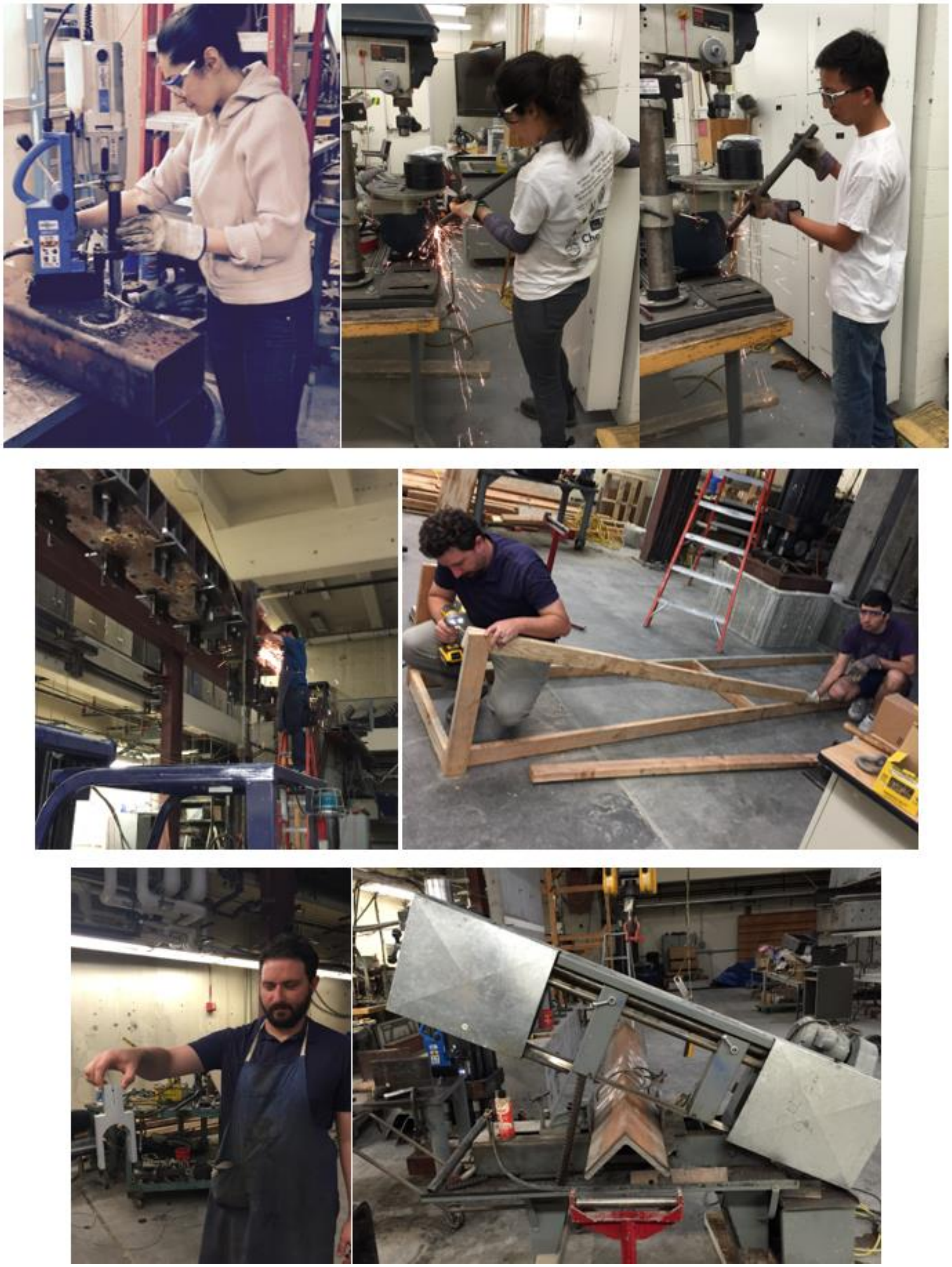

Figure D-5: Preparation of Mounting Equipment for Actuators and Test Setup Equipment

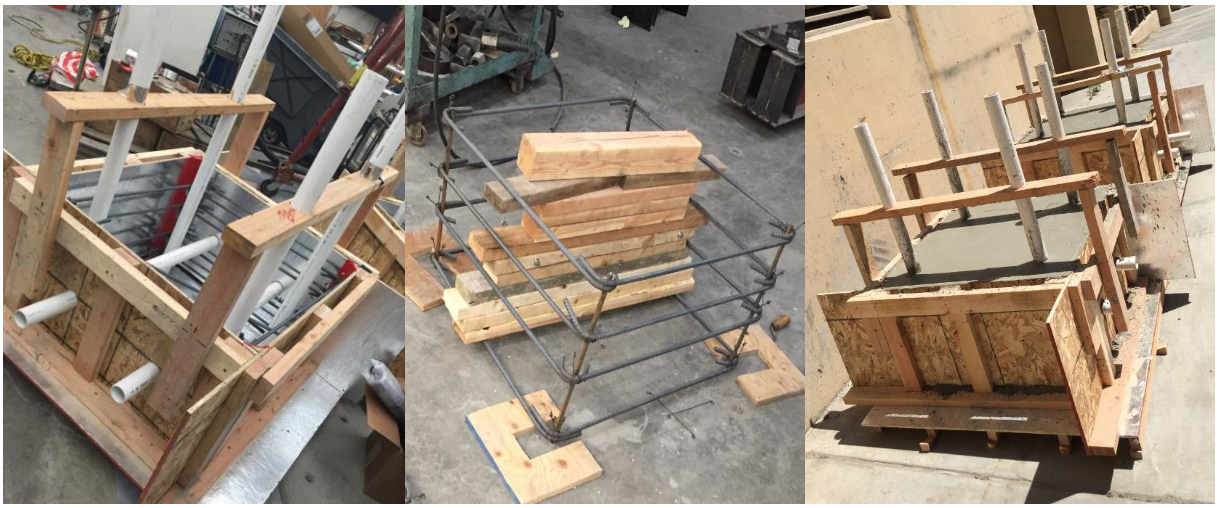

Figure D-6: Vertical Actuator Pedestals with Pipes to Allow for Post Tensioning Bars

Figure D-7: Base Block Reinforcement (Left), with Column Bars (Right)

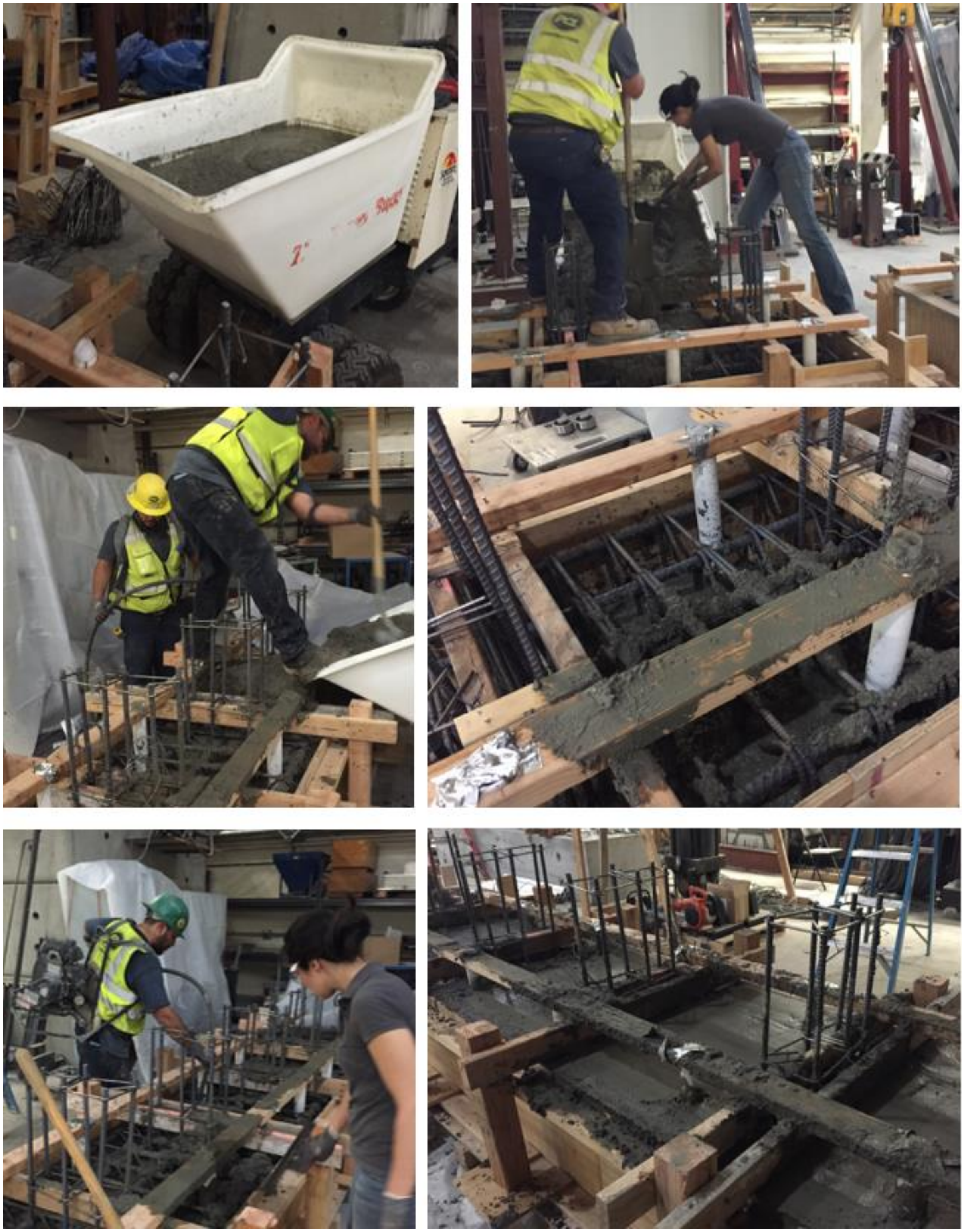

Figure D-8: Base Blocks: Concrete Pour

Figure D-9: Base Blocks: Concrete Curing

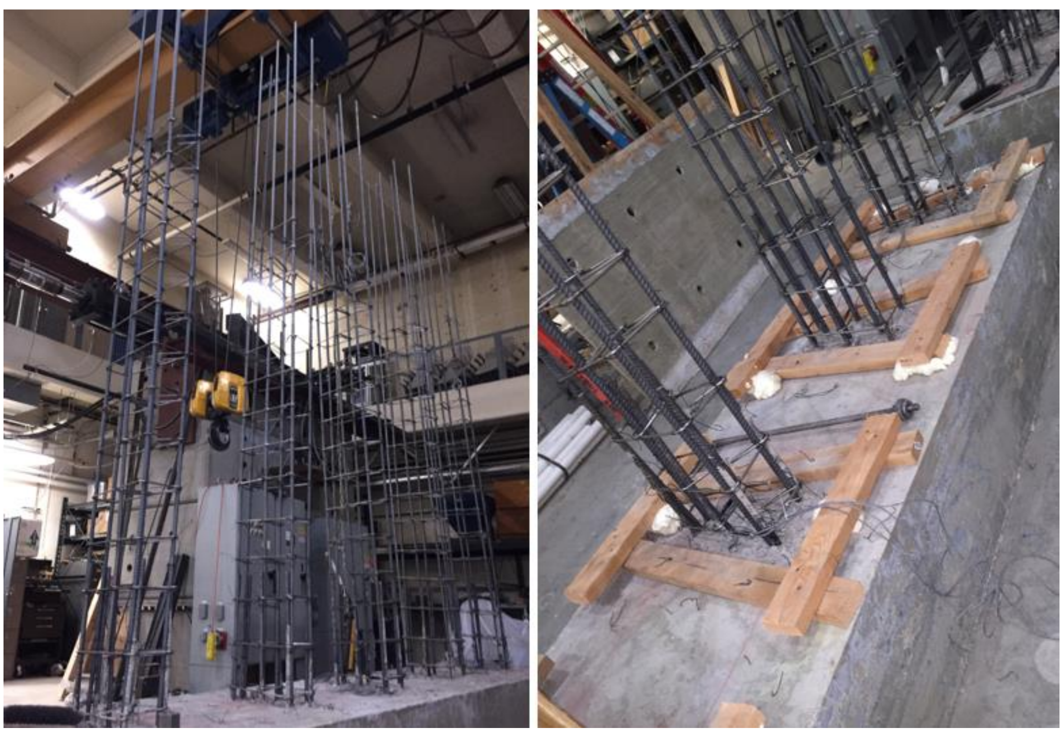

Figure D-10: Column Reinforcement (Left), Close Up of Bar Instrumentation (Right)

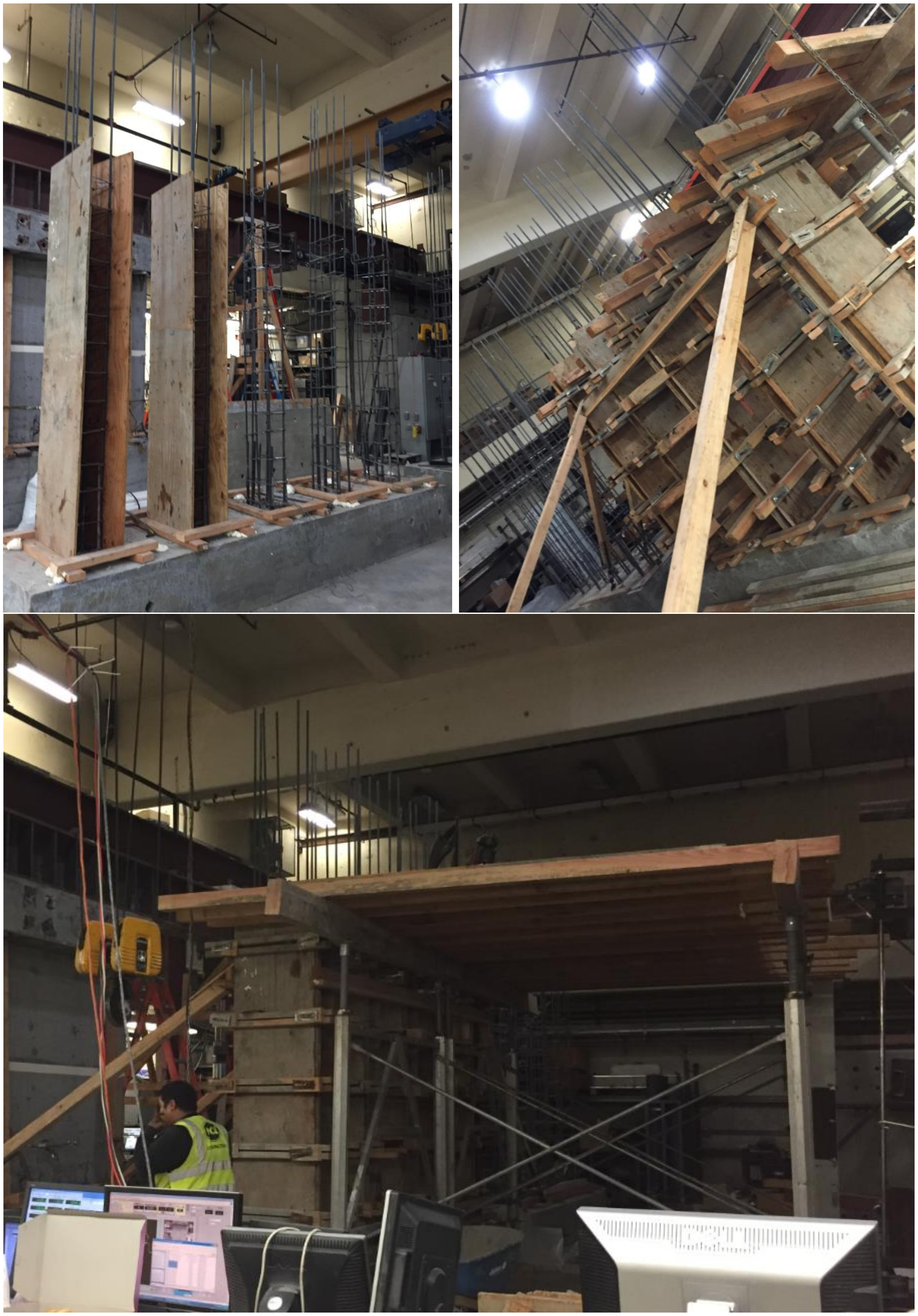

Figure D-11: Column and Slab Forms

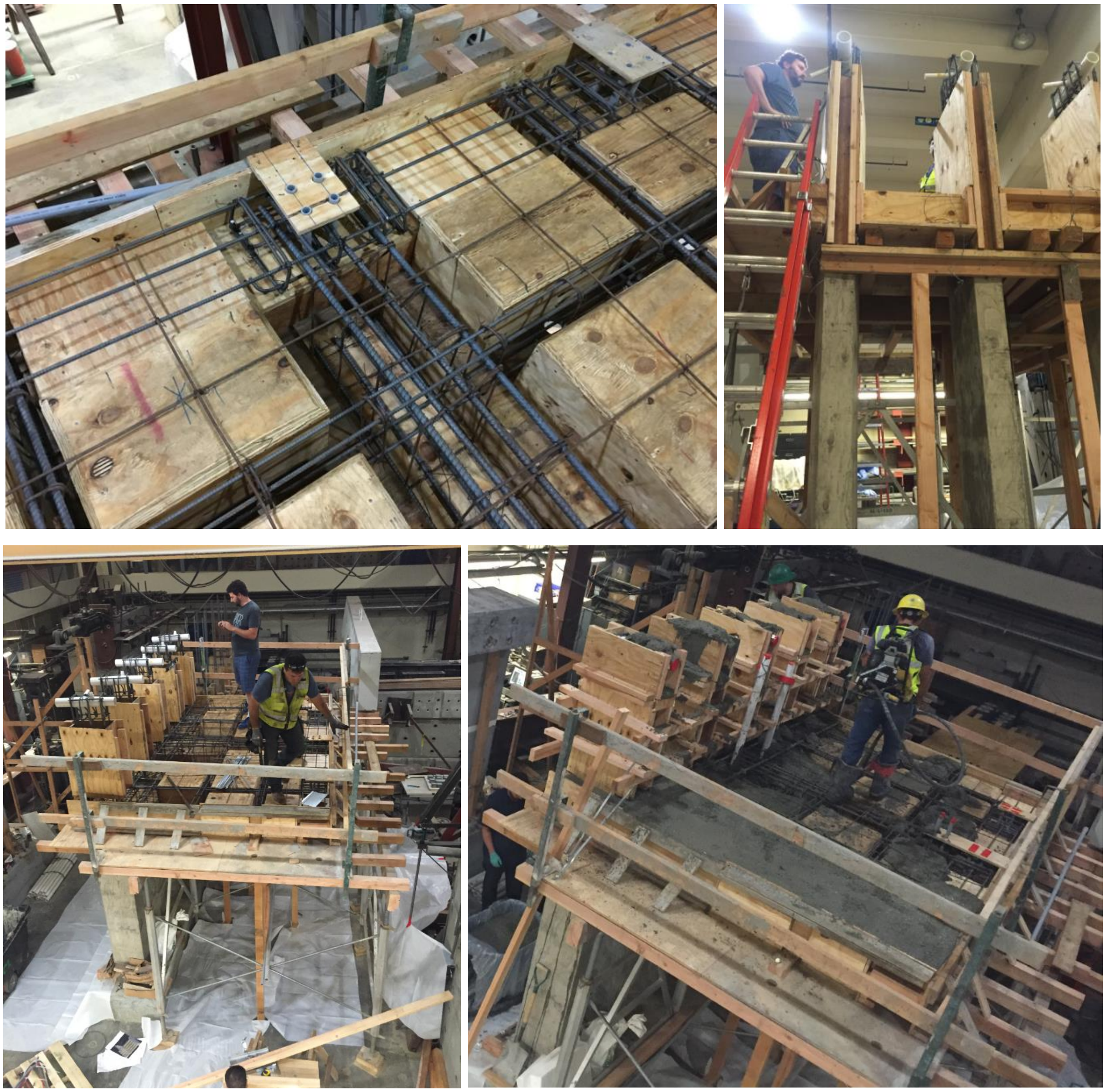

Figure D-12: Waffle Slab and Upper Column Formwork and Concrete Pour (Specimen 1)

Figure D-13: Concrete Cylinder Samples and Slump Test

Figure D-14: Removing Formwork

Figure D-15: Enlarged Top of Column to Connect to Top Load Transfer Beam

Figure D-16: Waffle Slab and Upper Column Formwork and Concrete Pour (Specimen 2)

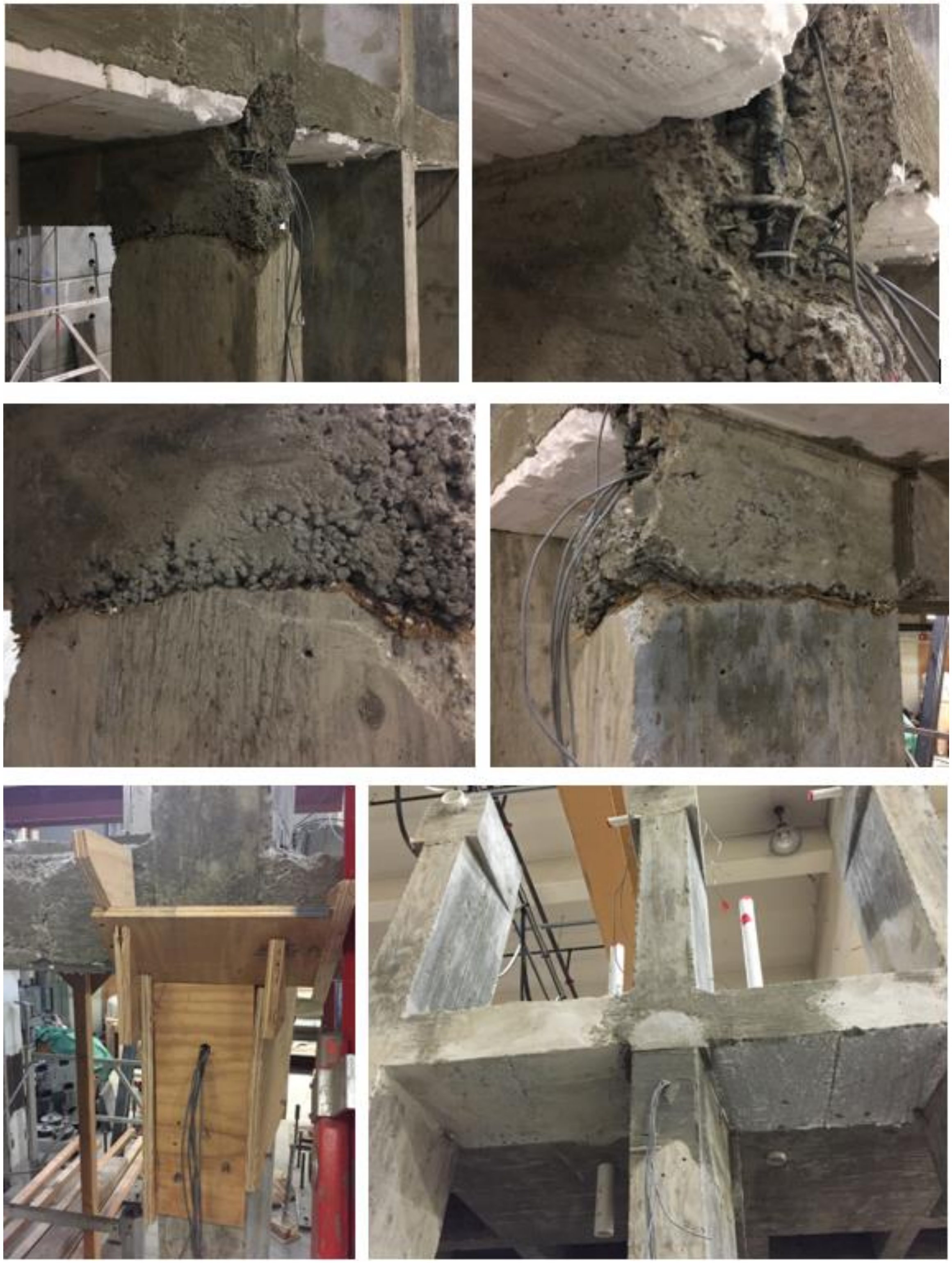

Figure D-17: Honeycombing at Column 3 and Repair (Specimen 1)

Figure D-18: Slab Shoring Before Installing Slab Edge Supports

Figure D-19: Gravity Load Application Apparatus (Specimen 2)

Figure D-20: Instrumentation and Connection of Specimen 1 to Strong Floor

Appendix E. Experimental Testing Pictures

E1. Test 1

Figure E-1: Damage at Base of Column 5 – Test 1, 0.50% Drift Ratio (W: West, S: South, N: North, E: East Faces)

Figure E-2: Damage at Base of Column 3 – Test 1, 0.50% Drift Ratio (W: West, S: South, N: North, E: East Faces)

Figure E-3: Damage at Top of Column 3 (Left) and Column 5 (Right) – Test 1, 0.50% Drift Ratio

Figure E-4: Damage at Base of Columns 1, 3, and 5 (Left to Right) – Test 1, 0.75% Drift Ratio

Figure E-5: Damage at Base of Columns 1, 2, 3 and 5 (Left to Right) – Test 1, 1.0% Drift Ratio

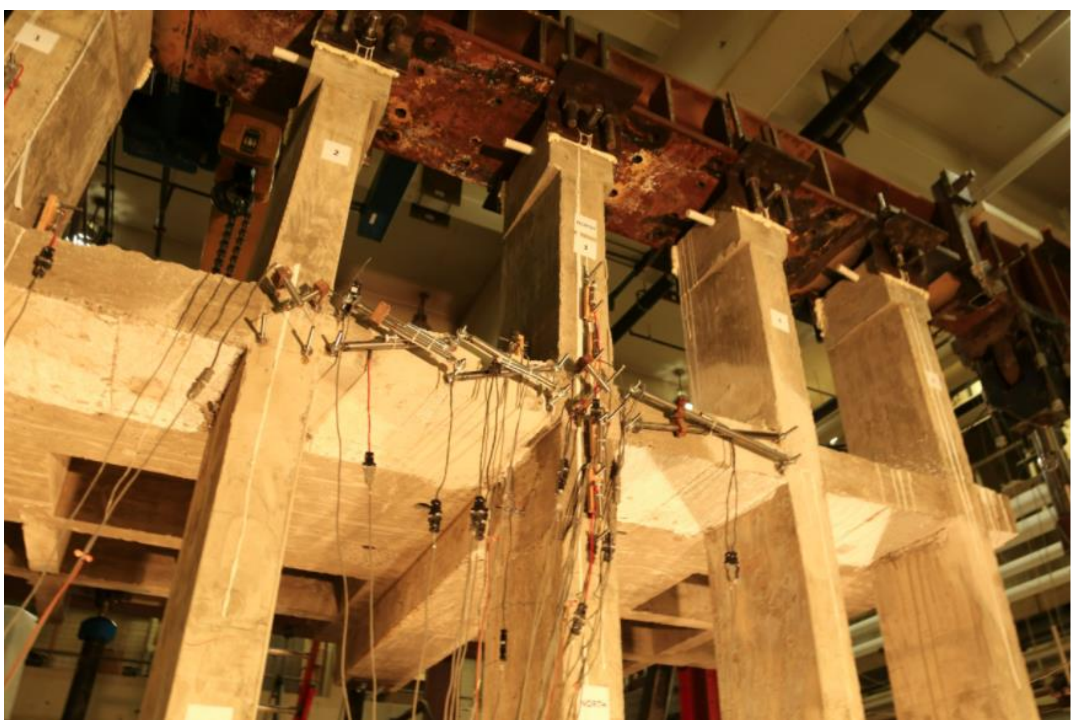

Figure E-6: Overall View of the Specimen – Test 1, 1.0% Drift Ratio

Figure E-7: Cracks at Slab-Columns Interface and across the Slab– Test 1, 1.0% Drift Ratio

Figure E-8: Damage at Slab-Column Interface (C5 (Left), C3 (Right) – Test 1, 1.0% Drift Ratio

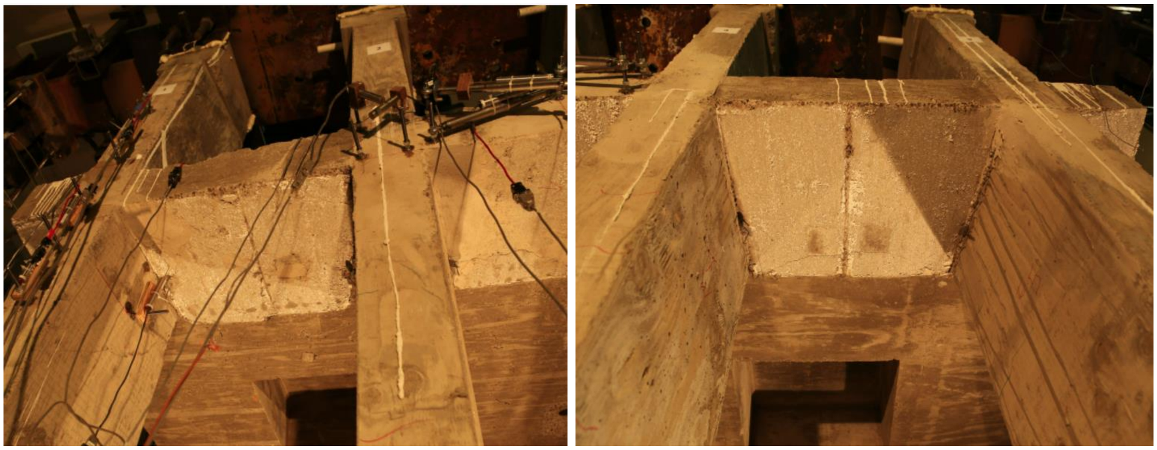

Figure E-9: Damage at Ledge Beams – Test 1, 1.0% Drift Ratio

Figure E-10: Damage at Base of Columns 1 to 5 (Left to Right) – Test 1, 1.5% Drift Ratio

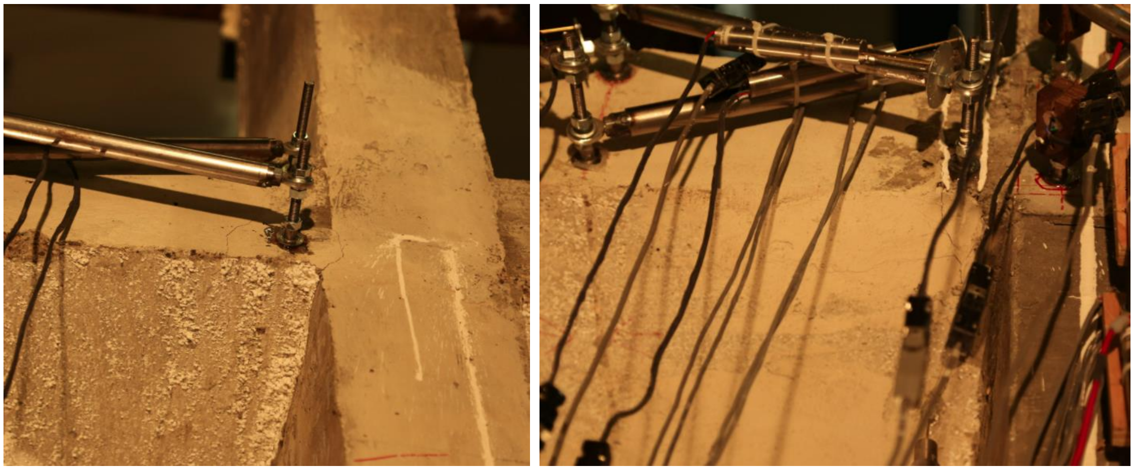

Figure E-11: Damage at Interface of Beam-Column 3 – Test 1, 1.5% Drift Ratio

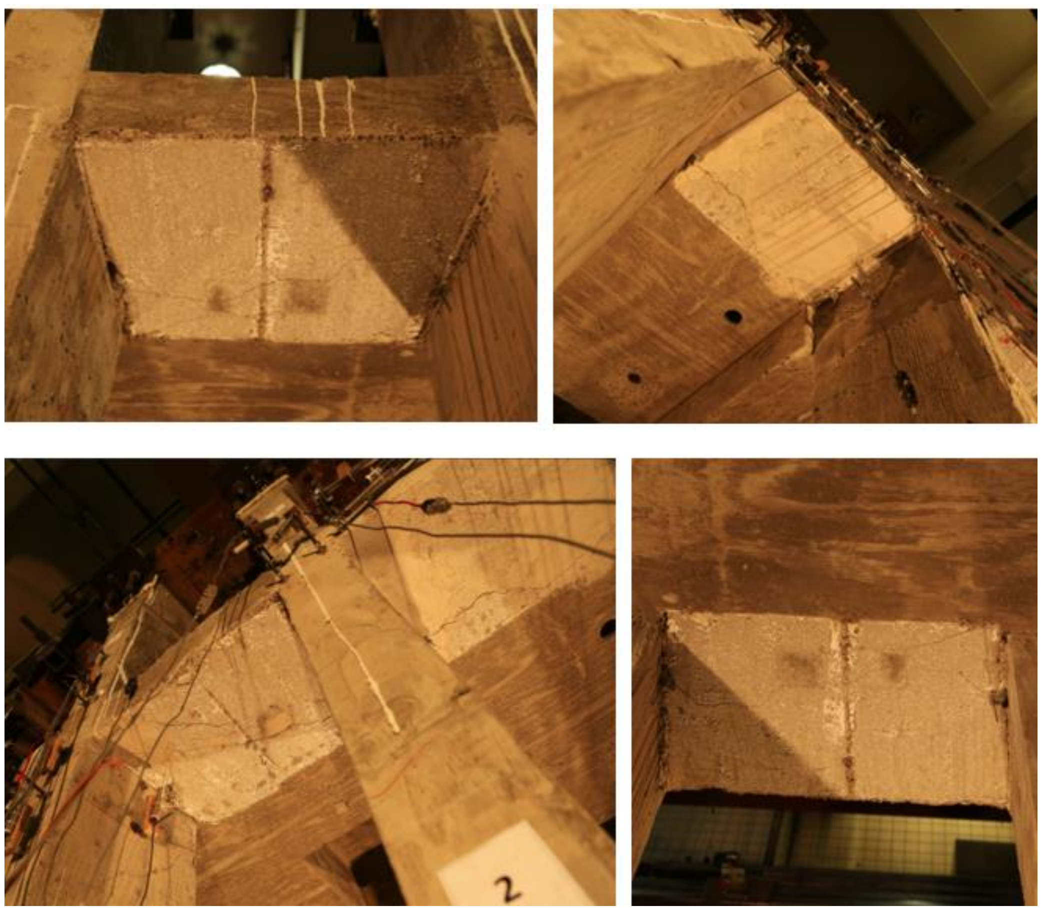

Figure E-12: Damage at Ledge Beams – Test 1, 1.5% Drift Ratio

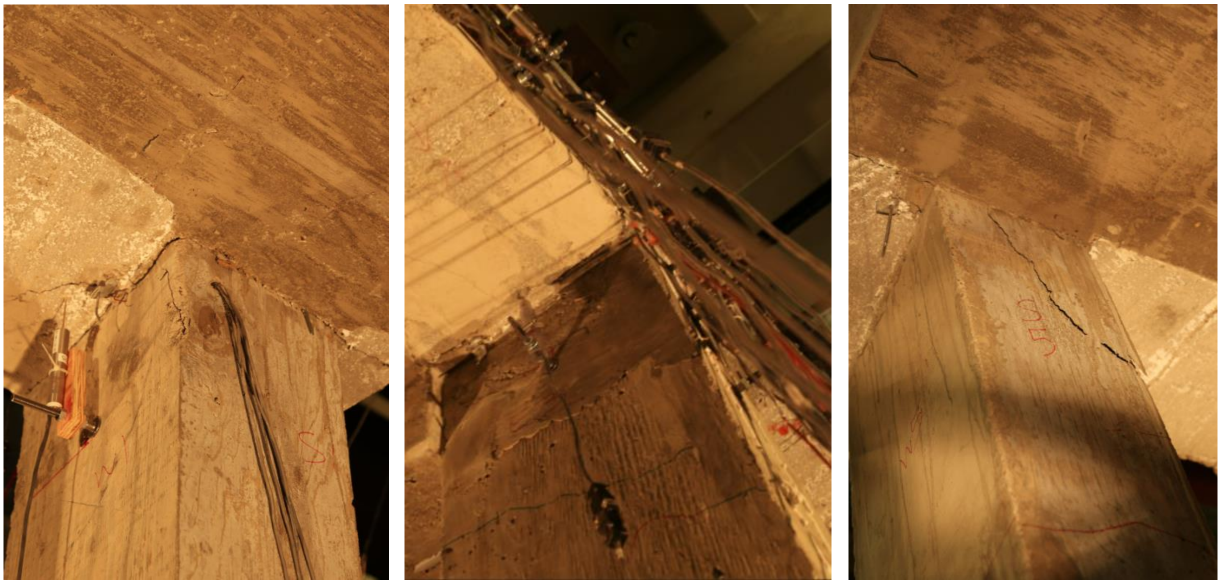

Figure E-13: Damage at Top of Columns 1, 3 and 5 (Left to Right) – Test 1, 1.5% Drift Ratio

E2. Test 2

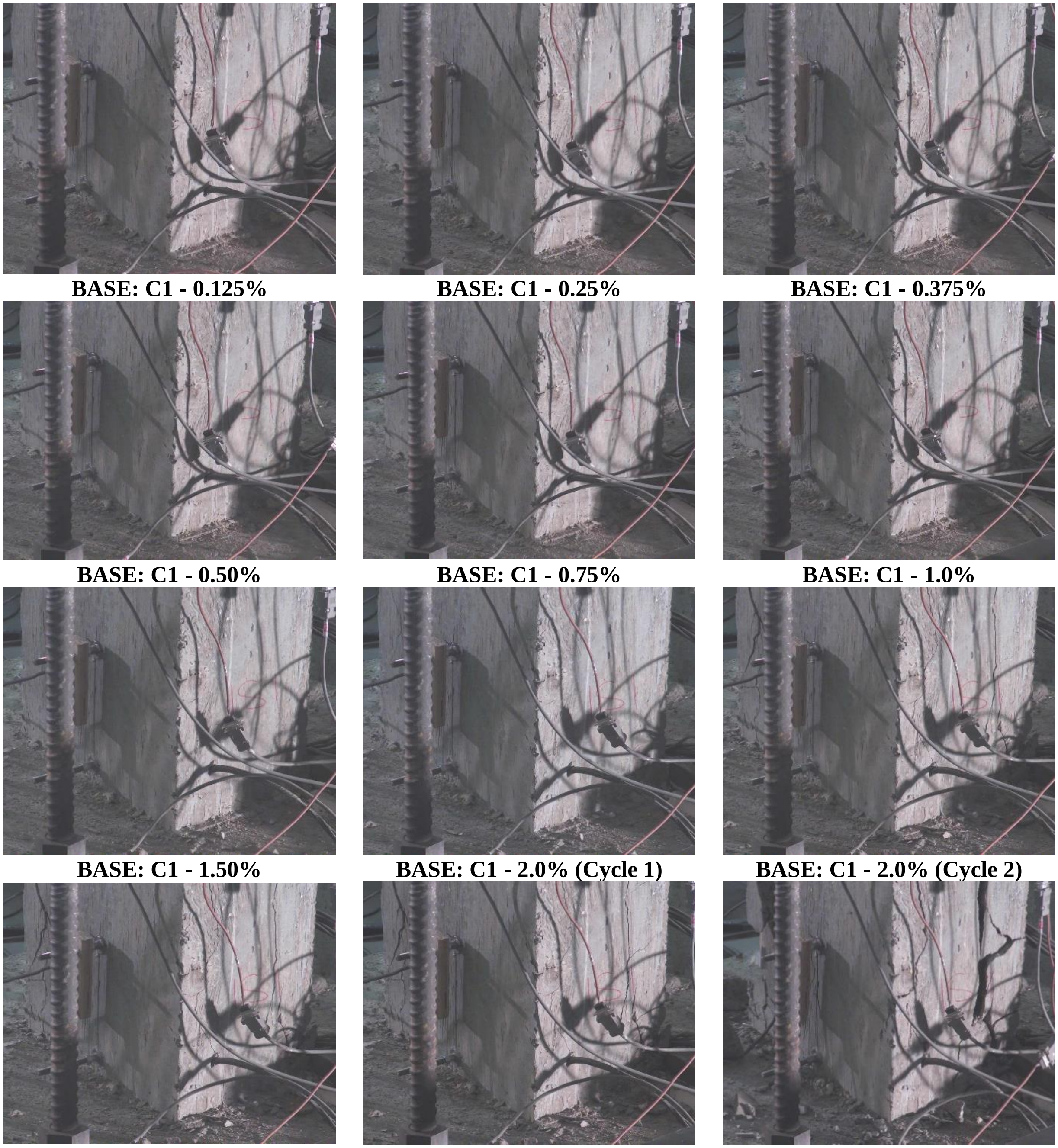

BASE: C1 - 0.125% | BASE: C1 - 0.25% | BASE: C1 - 0.375%

BASE: C1 - 0.50% | BASE: C1 - 0.75% | BASE: C1 - 1.0%

BASE: C1 - 1.50% | BASE: C1 - 2.0% (Cycle 1) | BASE: C1 - 2.0% (Cycle 2)

BASE: C1 - 2.5% (Cycle 1) | BASE: C1 - 2.5% (Cycle 2) | BASE: C1 - 3.0%

Figure E-14: Progression of Damage at Base of Column 1 – Test 2


BASE: C2 - 0.125%


BASE: C2 - 0.25%


BASE: C2 - 0.375%


BASE: C2 - 0.50%


BASE: C2 - 0.75%


BASE: C2 - 1.0%

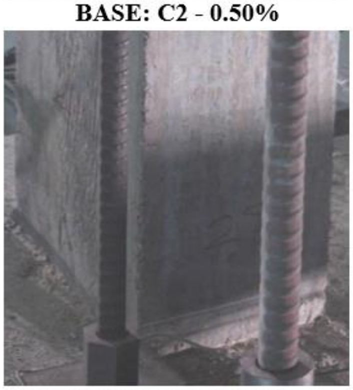
BASE: C2 - 1.50%

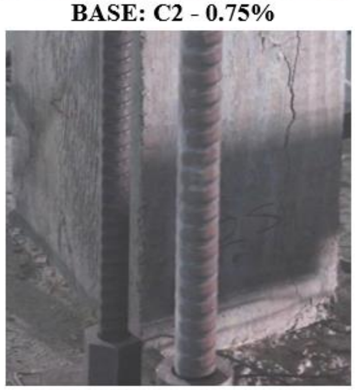
BASE: C2 - 2.0% (Cycle 1)

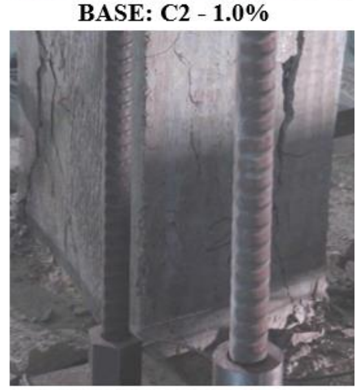
BASE: C2 - 2.0% (Cycle 2)

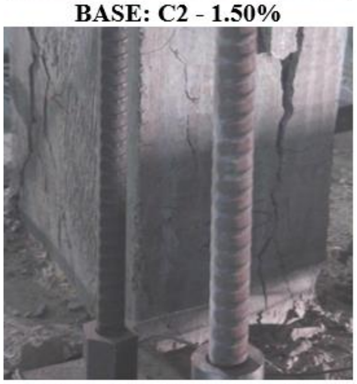
BASE: C2 - 2.5% (Cycle 1)

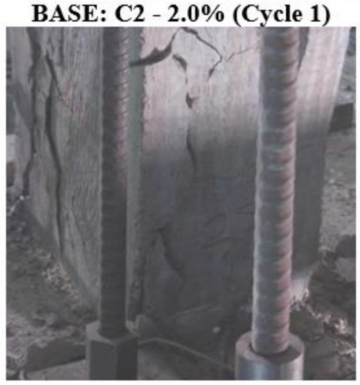
BASE: C2 - 2.5% (Cycle 2)


BASE: C2 - 3.0%

Figure E-15: Progression of Damage at Base of Column 2 – Test 2

Figure E-16: Progression of Damage at Base of Column 3 – Test 2


BASE: C3 - 0.125%


BASE: C3 - 0.25%


BASE: C3 - 0.375%


BASE: C3 - 0.50%


BASE: C3 - 0.75%


BASE: C3 - 1.0%


BASE: C3 - 1.50%


BASE: C3 - 2.0% (Cycle 1)


BASE: C3 - 2.0% (Cycle 2)


BASE: C3 - 2.5% (Cycle 1)


BASE: C3 - 2.5% (Cycle 2)


BASE: C3 - 3.0%

Figure E-17: Progression of Damage at Base of Column 4 – Test 2


BASE: C4 - 0.125%


BASE: C4 - 0.25%


BASE: C4 - 0.375%


BASE: C4 - 0.50%


BASE: C4 - 0.75%


BASE: C4 - 1.0%


BASE: C4 - 1.50%


BASE: C4 - 2.0% (Cycle 1)


BASE: C4 - 2.0% (Cycle 2)


BASE: C4 - 2.5% (Cycle 1)


BASE: C4 - 2.5% (Cycle 2)


BASE: C4 - 3.0%

Figure E-18: Progression of Damage at Base of Column 4 – Test 2


BASE: C5 - 0.125%


BASE: C5 - 0.25%


BASE: C5 - 0.375%


BASE: C5 - 0.50%


BASE: C5 - 0.75%

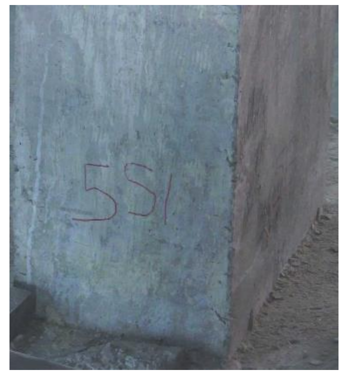
BASE: C5 - 1.0%


BASE: C5 - 1.50%


BASE: C5 - 2.0% (Cycle 1)

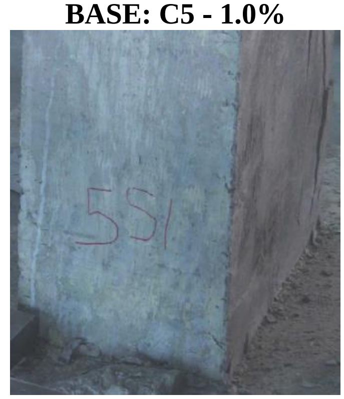
BASE: C5 - 2.0% (Cycle 2)


BASE: C5 - 2.5% (Cycle 1)

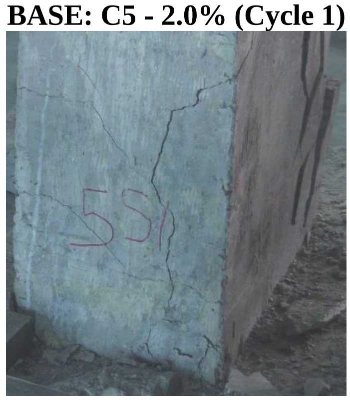
BASE: C5 - 2.5% (Cycle 2)

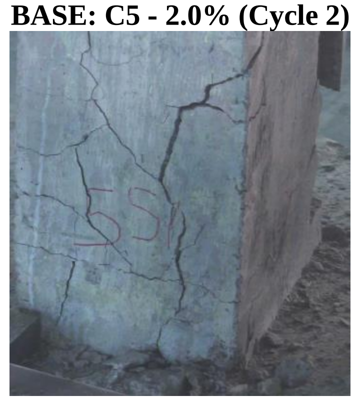
BASE: C5 - 3.0%

Figure E-19: Progression of Damage at Base of Column 5 – Test 2

Top of low C1 - 0.125%

Top of low C1 - 0.25%

Top of low C1 - 0.375%

Top of low C1 - 0.50%

Top of low C1 - 0.75%

Top of low C1 - 1.0%

Top of low C1 - 1.50%

Top of low C1 - 2.0% (Cycle 1)

Top of low C1 - 2.0% (Cycle 2)

Top of low C1 - 2.5% (Cycle 1)

Top of low C1 - 2.5% (Cycle 2)

Top of low C1 - 3.0%

Figure E-20: Progression of Damage at Top of Lower Column 1 – Test 2

Top of low C2 - 0.125%

Top of low C2 - 0.25%

Top of low C2 - 0.375%

Top of low C2 - 0.50%

Top of low C2 - 0.75%

Top of low C2 - 1.0%

Top of low C2 - 1.50%

Top of low C2 - 2.0% (Cycle 1)

Top of low C2 - 2.0% (Cycle 2)

Top of low C2 - 2.5% (Cycle 1)

Top of low C2 - 2.5% (Cycle 2)

Top of low C2 - 3.0%

Figure E-21: Progression of Damage at Top of Lower Column 2 – Test 2

Top of low C3 - 0.125%

Top of low C3 - 0.25%

Top of low C3 - 0.375%

Top of low C3 - 0.50%

Top of low C3 - 0.75%

Top of low C3 - 1.0%

Top of low C3 - 1.50%

Top of low C3 - 2.0% (Cycle 1)

Top of low C3 - 2.0% (Cycle 2)

Top of low C3 - 2.5% (Cycle 1)

Top of low C3 - 2.5% (Cycle 2)

Top of low C3 - 3.0%

Figure E-22: Progression of Damage at Top of Lower Column 3 – Test 2

Top of low C4 - 0.125%

Top of low C4 - 0.25%

Top of low C4 - 0.375%

Top of low C4 - 0.50%

Top of low C4 - 0.75%

Top of low C4 - 1.0%

Top of low C4 - 1.50%

Top of low C4 - 2.0% (Cycle 1)

Top of low C4 - 2.0% (Cycle 2)

Top of low C4 - 2.5% (Cycle 1)

Top of low C4 - 2.5% (Cycle 2)

Top of low C4 - 3.0%

Figure E-23: Progression of Damage at Top of Lower Column 4 – Test 2

Top of low C5 - 0.125%

Top of low C5 - 0.25%

Top of low C5 - 0.375%

Top of low C5 - 0.50%

Top of low C5 - 0.75%

Top of low C5 - 1.0%

Top of low C5 - 1.50%

Top of low C5 - 2.0% (Cycle 1)

Top of low C5 - 2.0% (Cycle 2)

Top of low C5 - 2.5% (Cycle 1)

Top of low C5 - 2.5% (Cycle 2)

Top of low C5 - 3.0%

Figure E-24: Progression of Damage at Top of Lower Column 5 – Test 2

OVERALL - 0.125%

OVERALL - 0.25%

OVERALL - 0.375%

OVERALL – 0.50%

OVERALL – 0.75%

OVERALL - 1.0%

Figure E-25: Overall Progression of Damage – Test 2

OVERALL - 1.5%

OVERALL - 2.0% (Cycle 1)

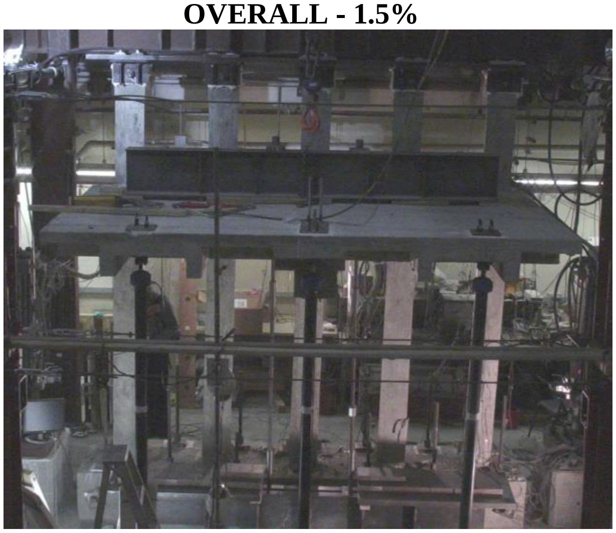

OVERALL - 2.0% (Cycle 2)

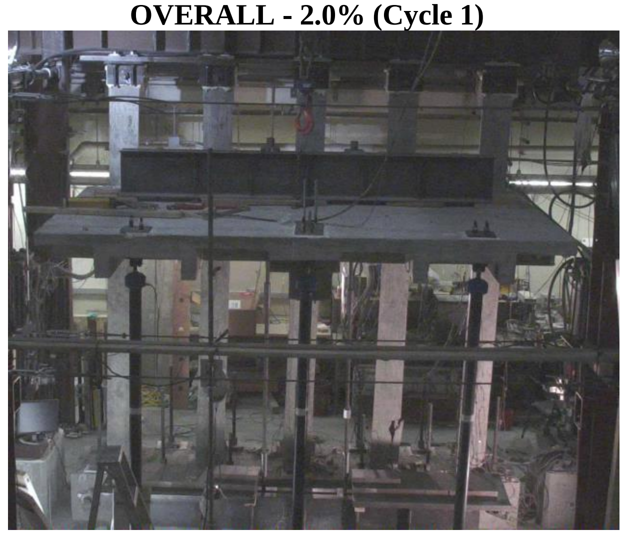

OVERALL - 2.5% (Cycle 1)

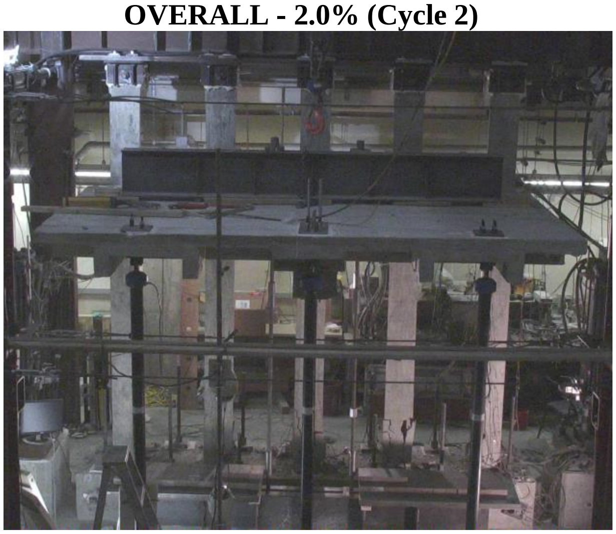

OVERALL - 2.5% (Cycle 2)

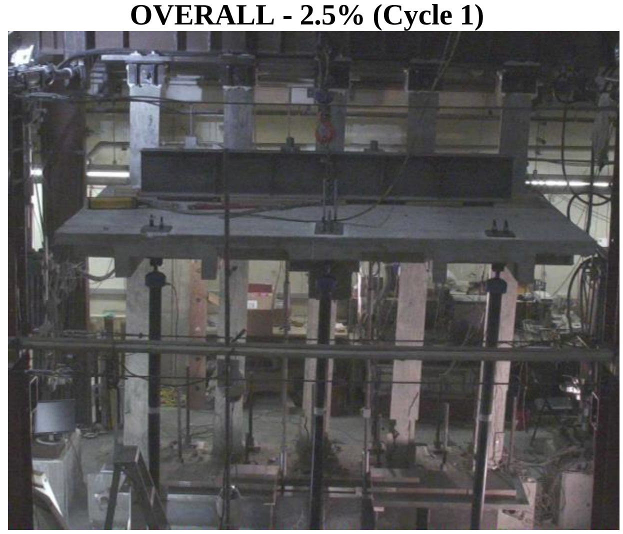

OVERALL - 3.0%

Figure E-25: Overall Progression of Damage – Test 2 (Cont'd.)

Appendix F. Experimental Testing – Sensor Readings

F1. Test 1

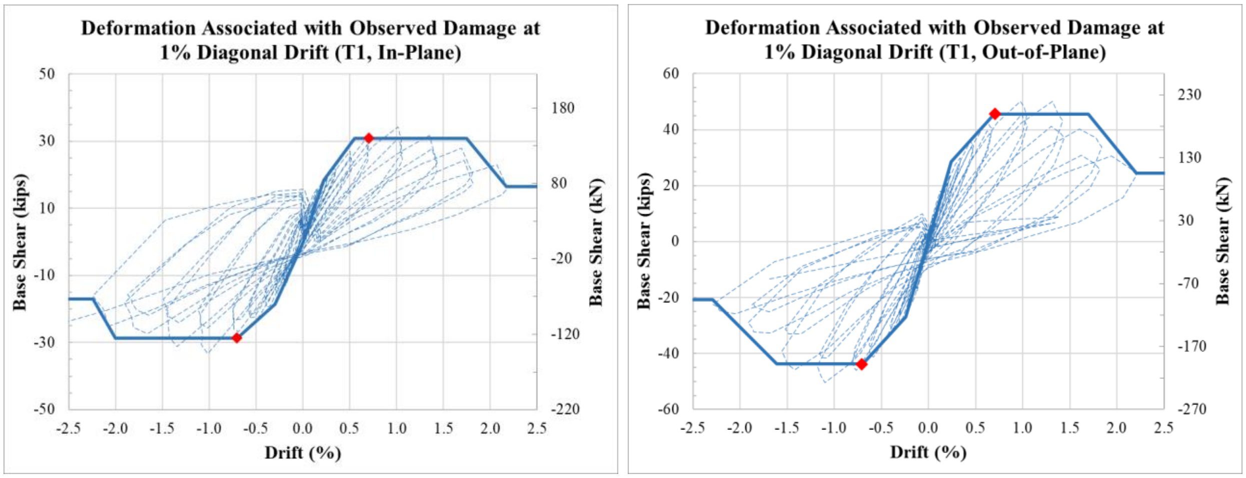

Figure F-1: Correlation of Observed Damage to 1.0% Lateral Drift Ratio (Test 1)

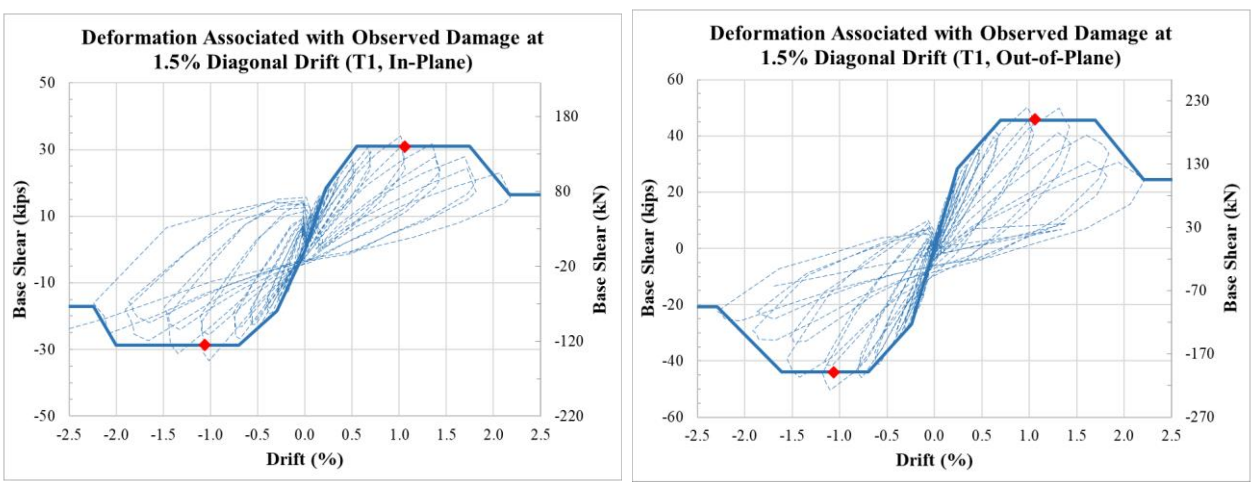

Figure F-2: Correlation of Observed Damage to 1.5% Lateral Drift Ratio (Test 1)

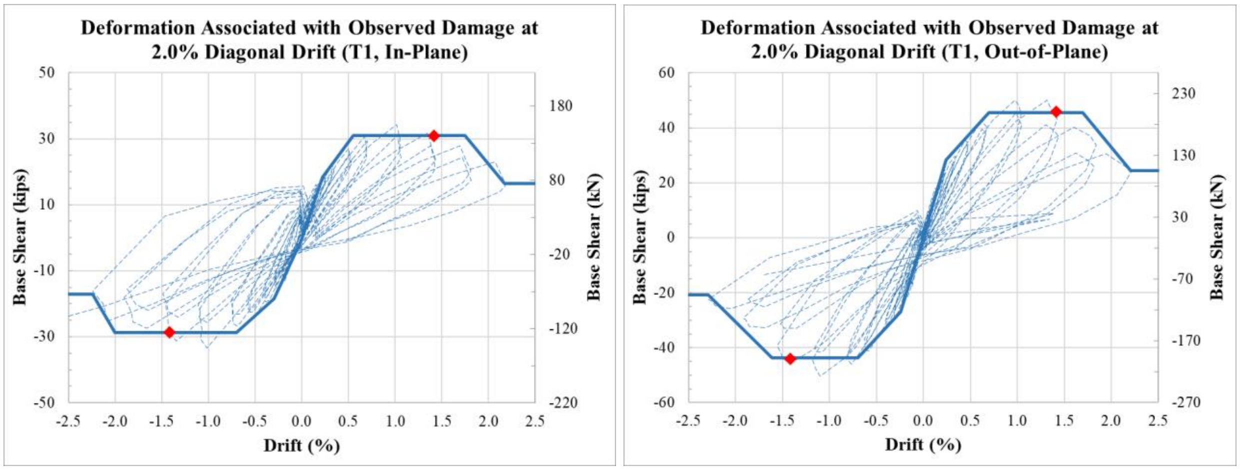

Figure F-3: Correlation of Observed Damage to 2.0% Lateral Drift Ratio (Test 1)

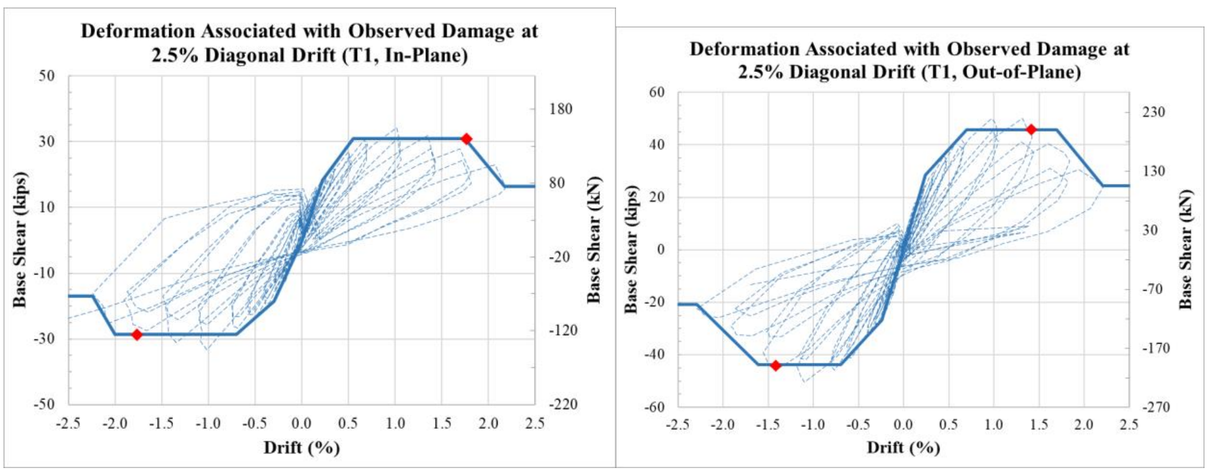

Figure F-4: Correlation of Observed Damage to 2.5% Lateral Drift Ratio (Test 1)

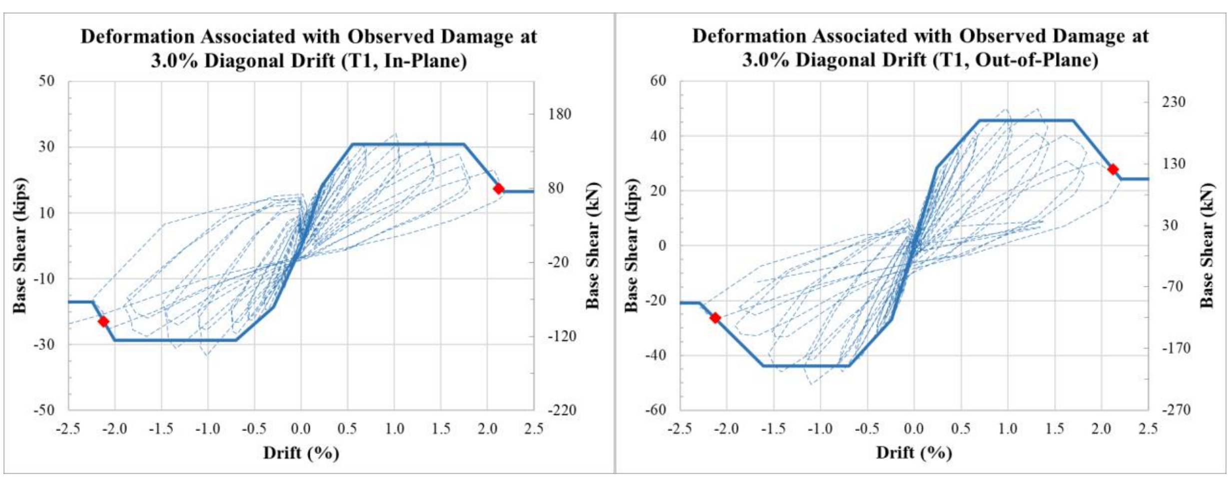

Figure F-5: Correlation of Observed Damage to 3.0% Lateral Drift Ratio (Test 1)

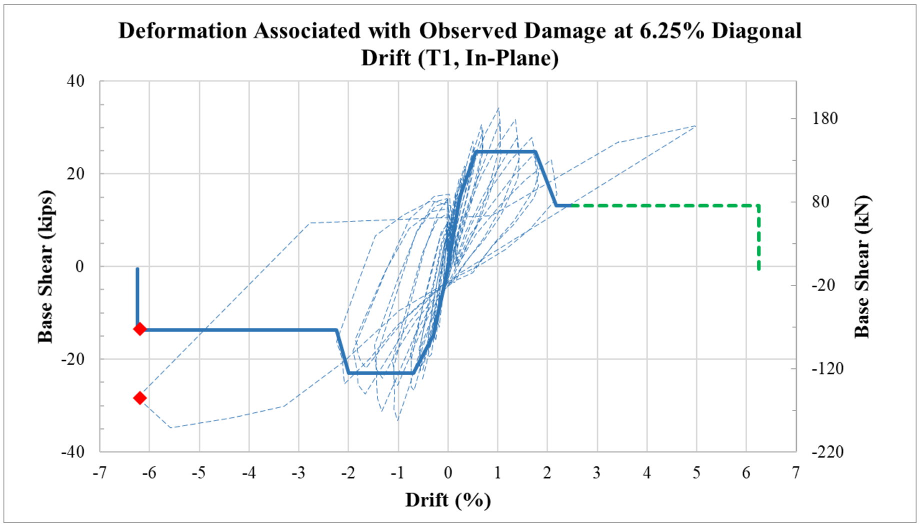

Figure F-6: Correlation of Observed Damage to 6.25% Lateral Drift Ratio (Test 1)

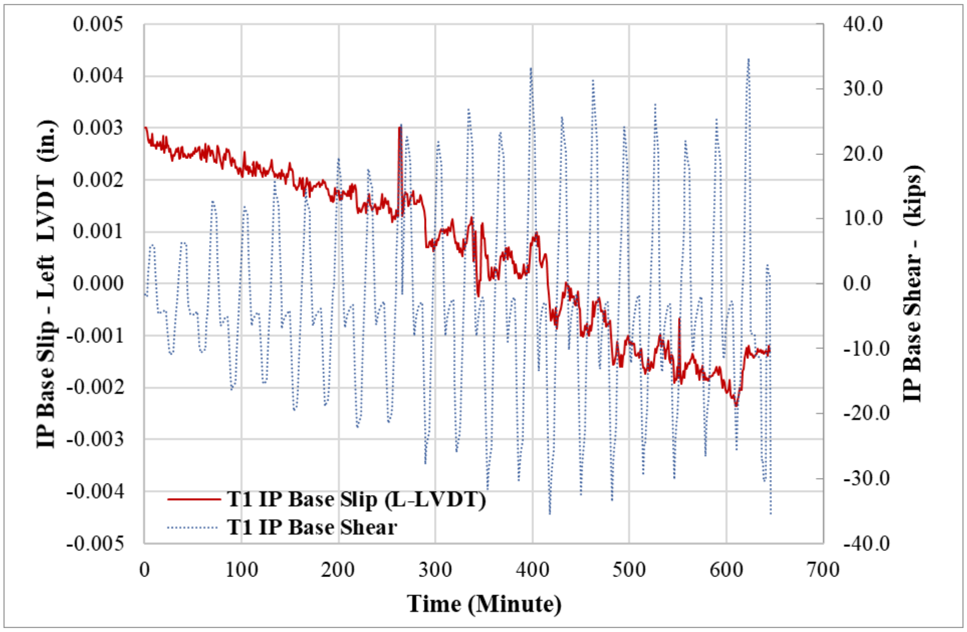

Figure F-7: In-Plane Load History and Base Slip History of the Left LVDT versus Time (Test 1)

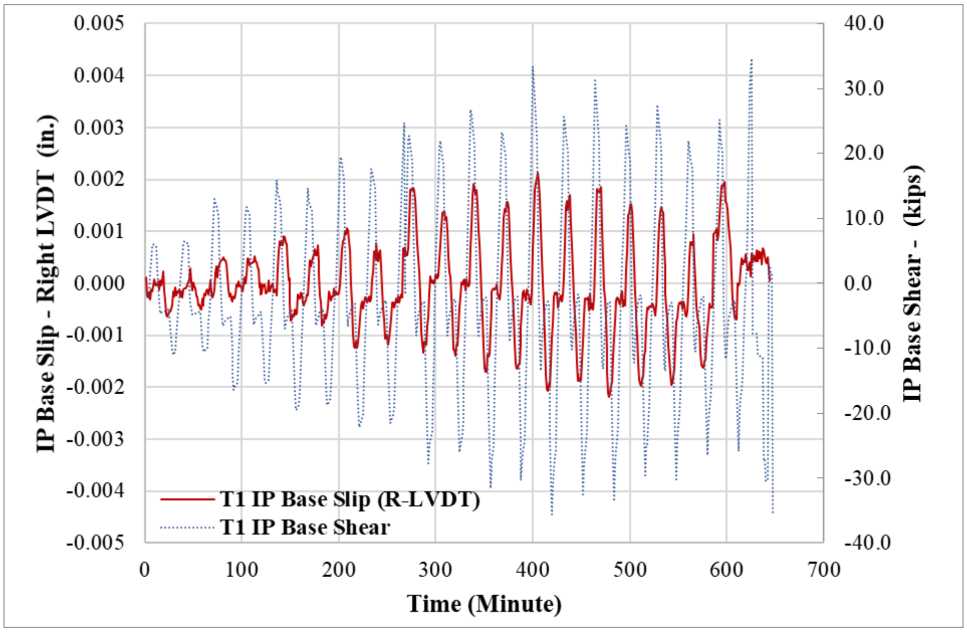

Figure F-8: In-Plane Load History and Base Slip History of the Right LVDT versus Time (Test 1)

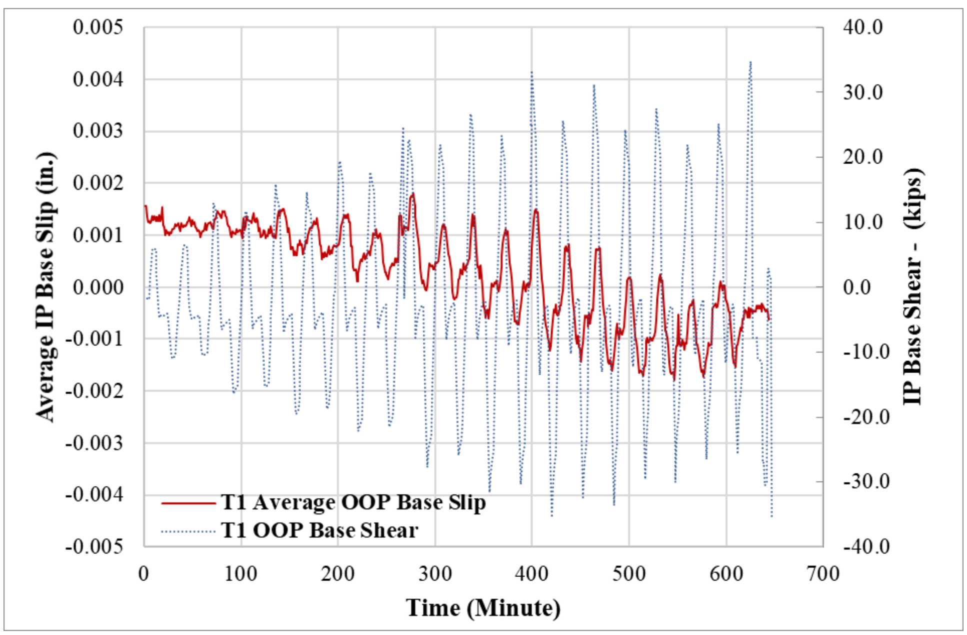

Figure F-9: In-Plane Load History and Average Base Slip History of LVDTs versus Time (Test 1)

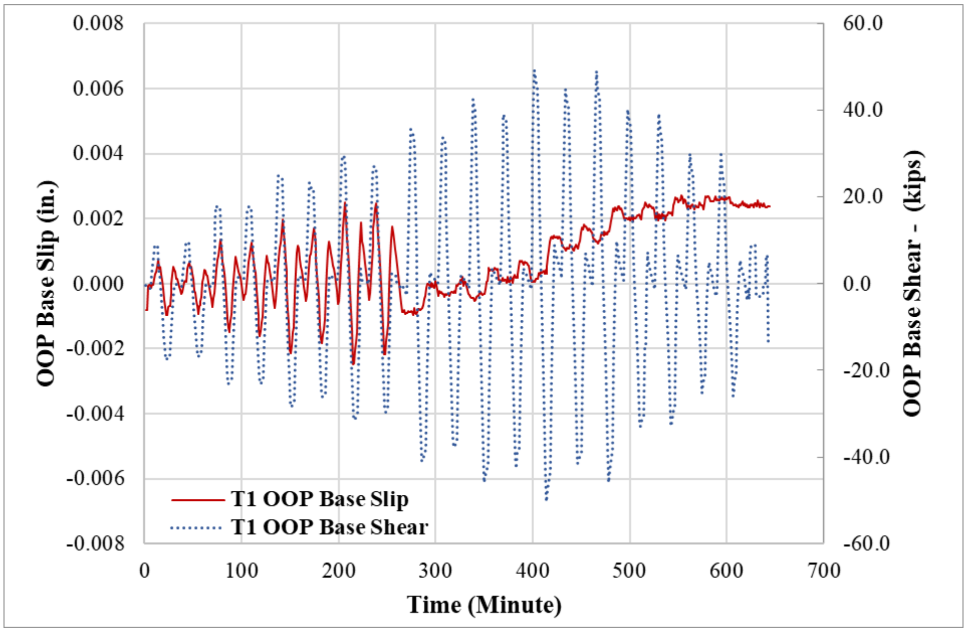

Figure F-10: Out-of-Plane Load History and Base Slip History versus Time (Test 1)

F2. Test 2

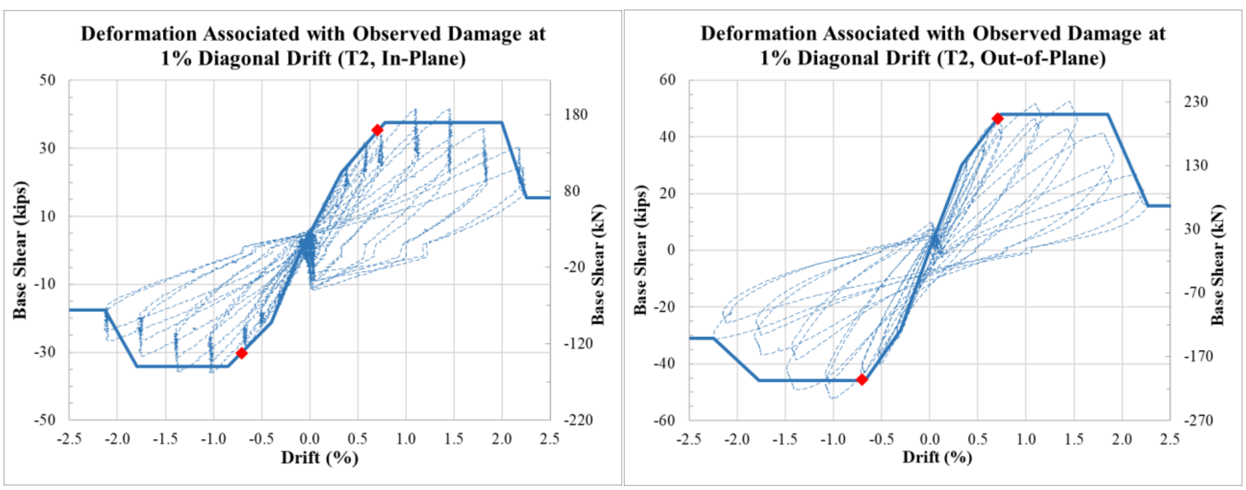

Figure F-11: Correlation of Observed Damage to 1.0% Lateral Drift Ratio (Test 2)

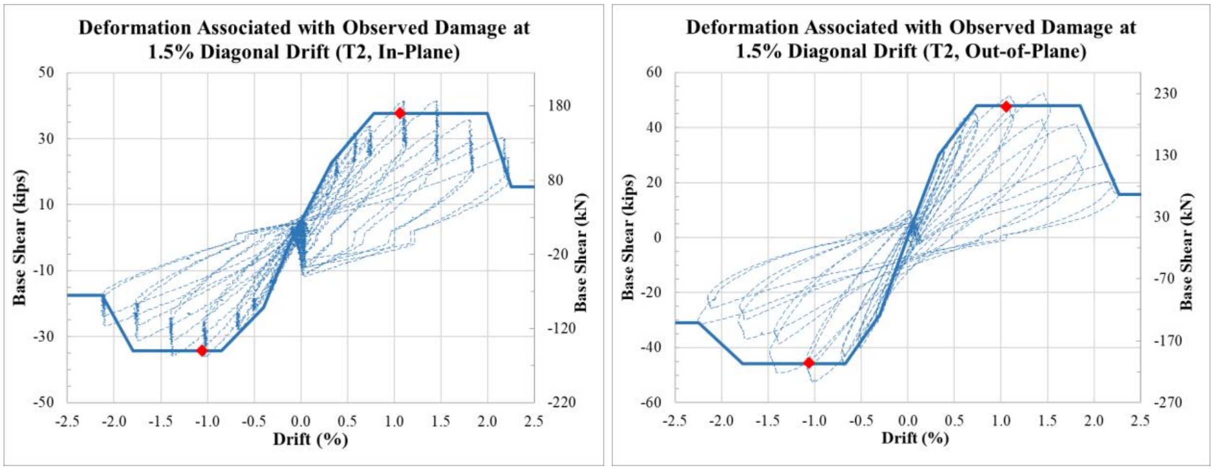

Figure F-12: Correlation of Observed Damage to 1.5% Lateral Drift Ratio (Test 2)

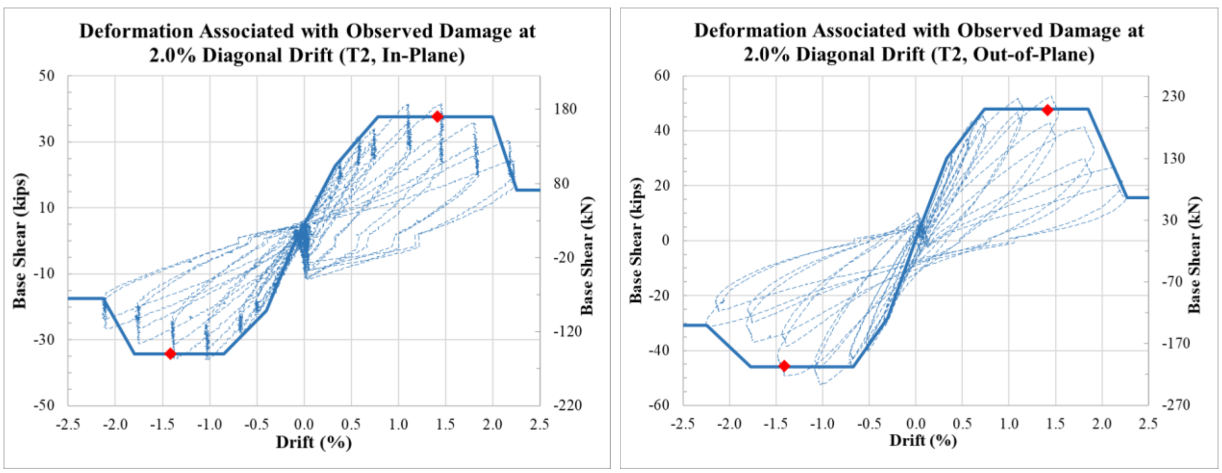

Figure F-13: Correlation of Observed Damage to 2.0% Lateral Drift Ratio (Test 2)

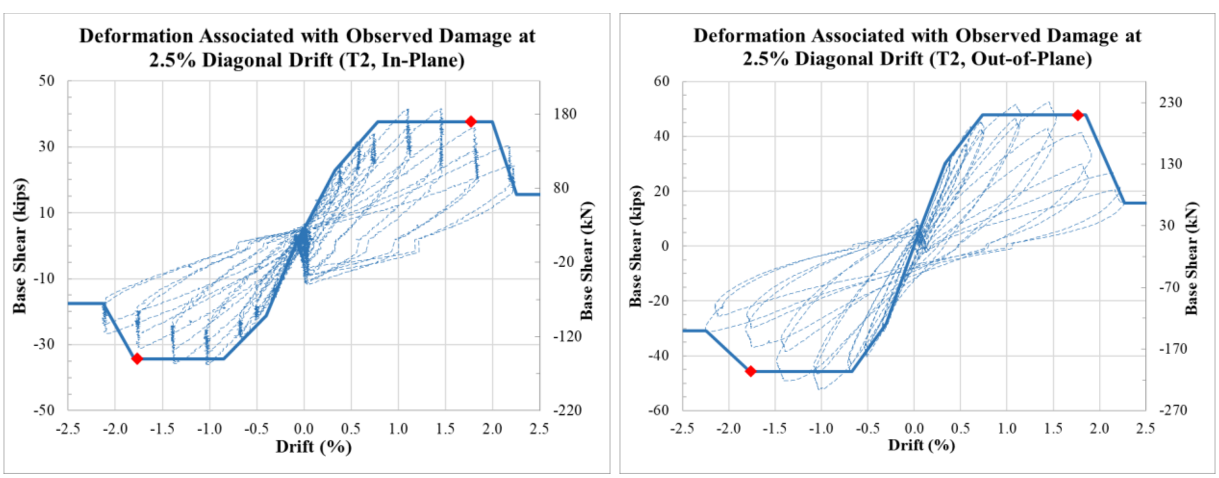

Figure F-14: Correlation of Observed Damage to 2.5% Lateral Drift Ratio (Test 2)

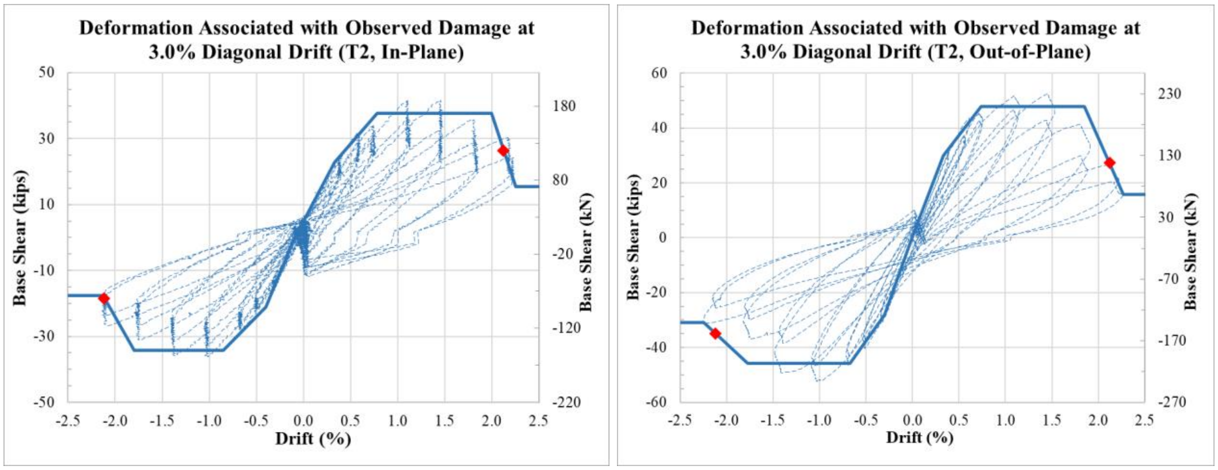

Figure F-15: Correlation of Observed Damage to 3.0% Lateral Drift Ratio (Test 2)

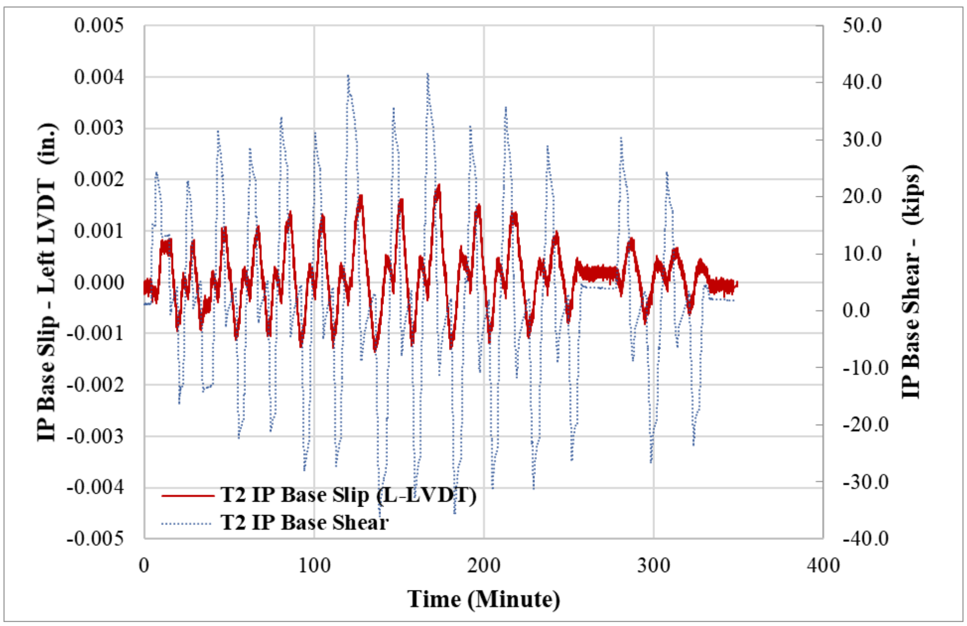

Figure F-16: In-Plane Load History and Base Slip History of the Left LVDT versus Time (Test 2)

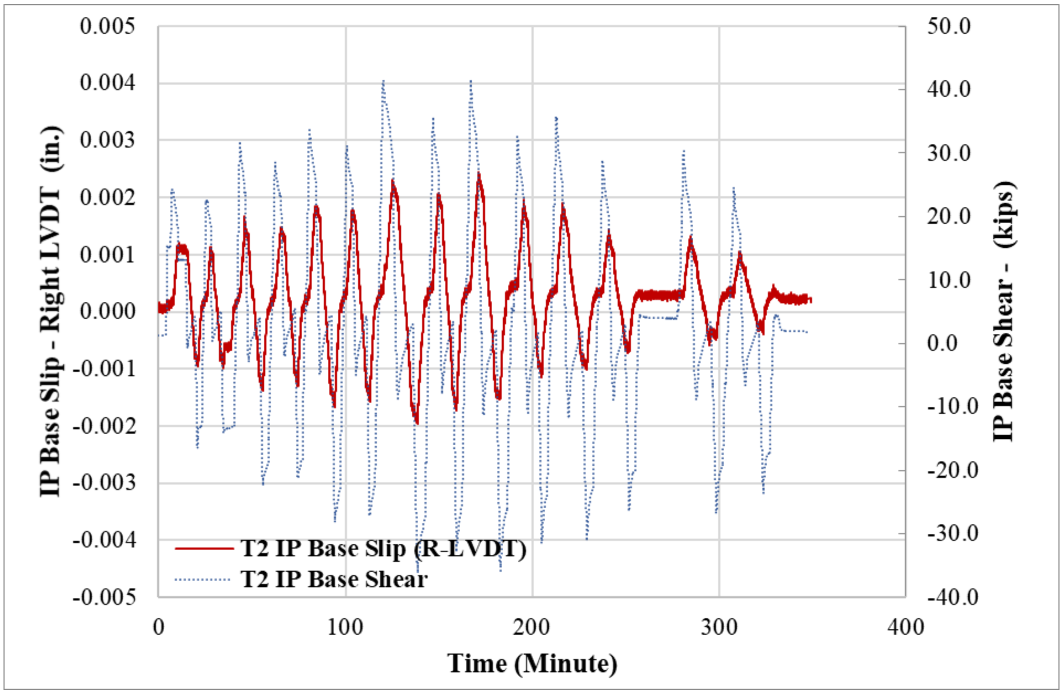

Figure F-17: In-Plane Load History and Base Slip History of the Right LVDT versus Time (Test 2)

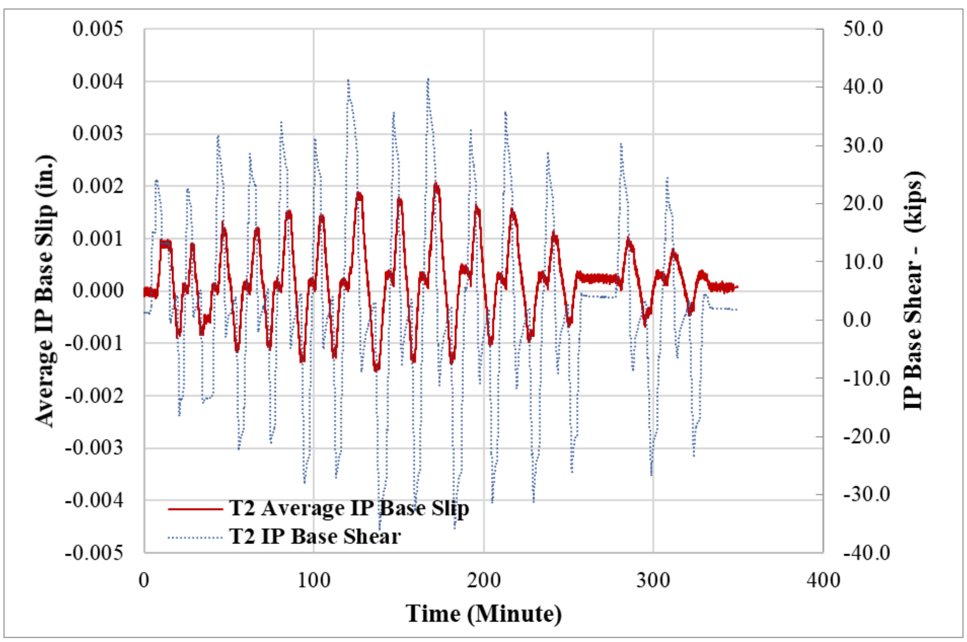

Figure F-18: In-Plane Load History and Average Base Slip History of LVDTs versus Time (Test 2)

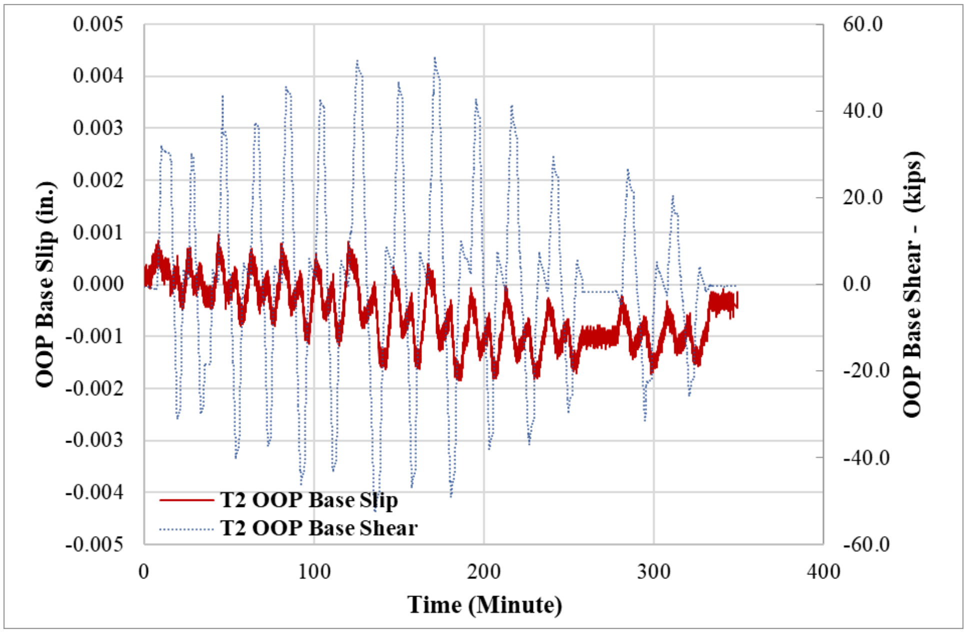

Figure F-19: Out-of-Plane Load History and Base Slip History versus Time (Test 2)

Appendix G. Perform-3D Modeling

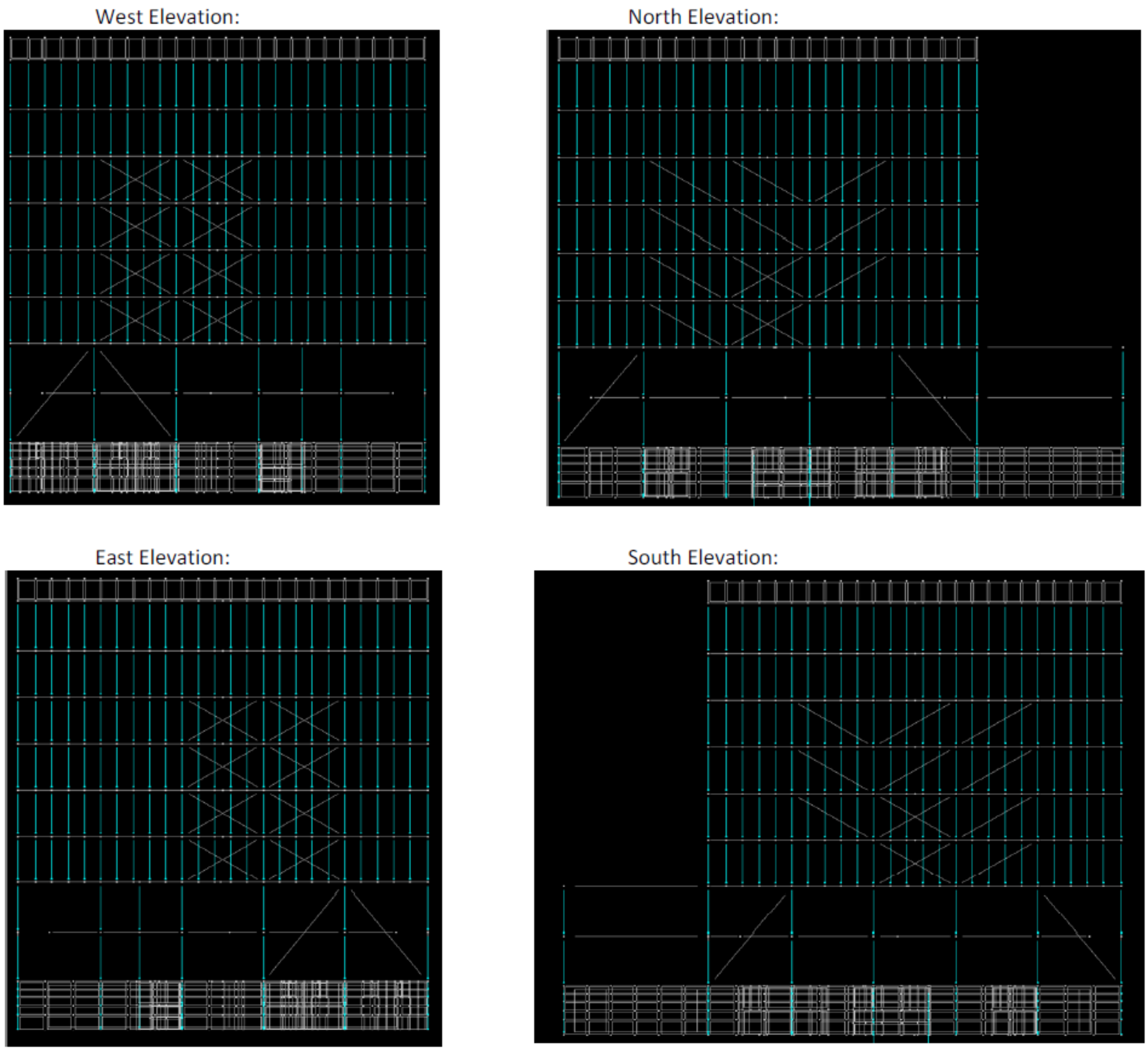

Figure G-1: Elevation Views of the Franz Tower in Perform-3D

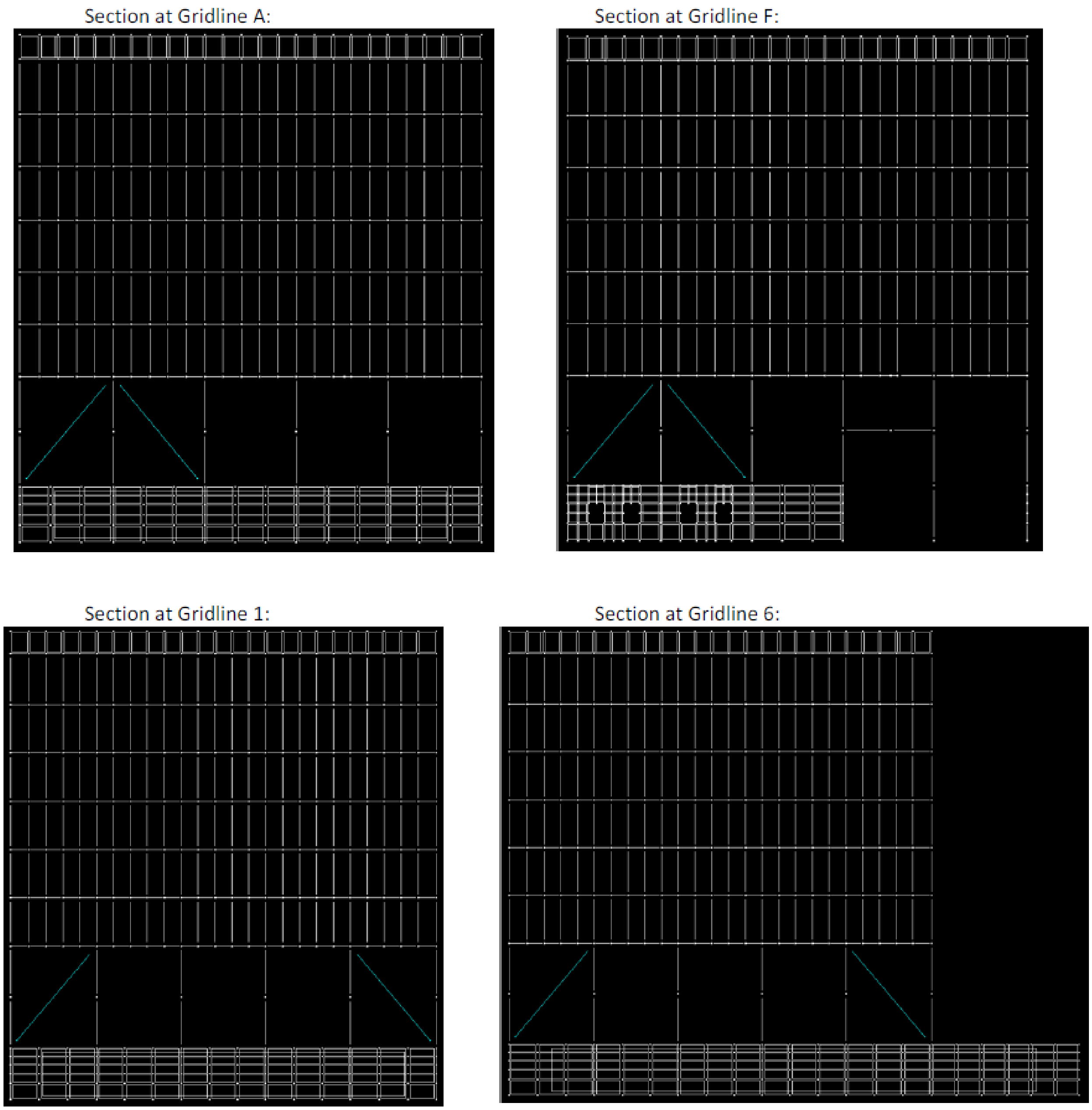

Figure G-2: Section Views of the Franz Tower in Perform-3D (Grids A, F, 1 and 6)

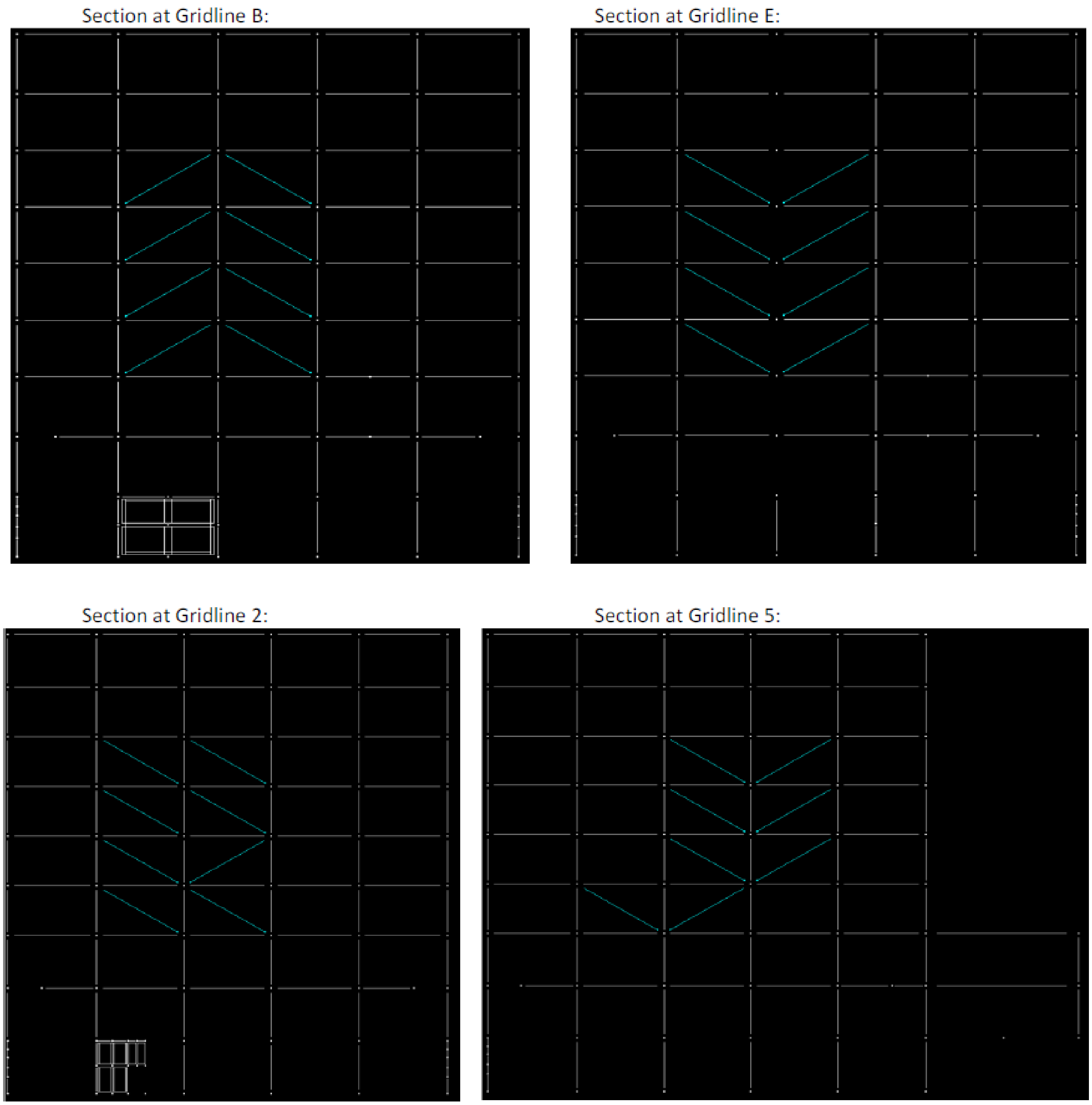

Figure G-3: Section Views of the Franz Tower in Perform-3D (Grids B, E, 2 and 5)

1st floor constraint:

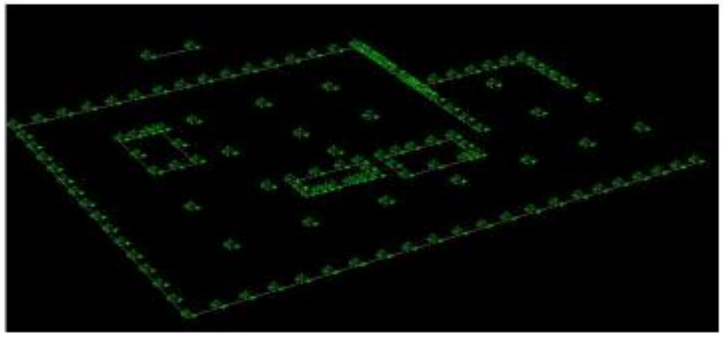

2nd floor constraint:

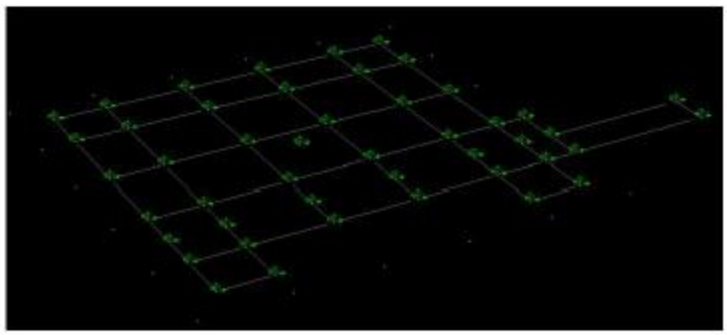

3rd floor constraint:

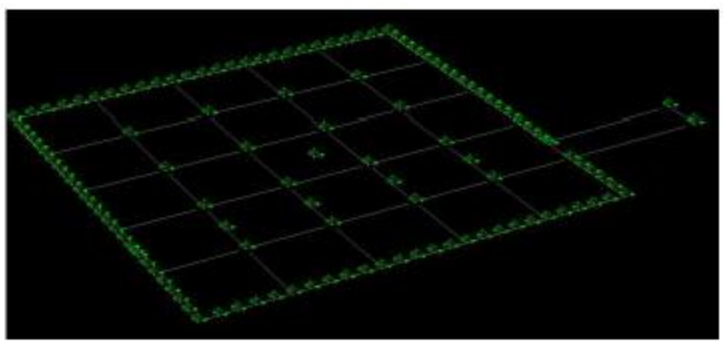

4th-Roof constraint:

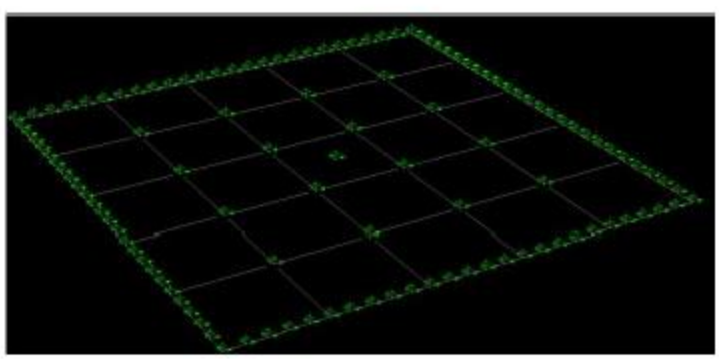

Figure G-4: Rigid Diaphragm Constraints

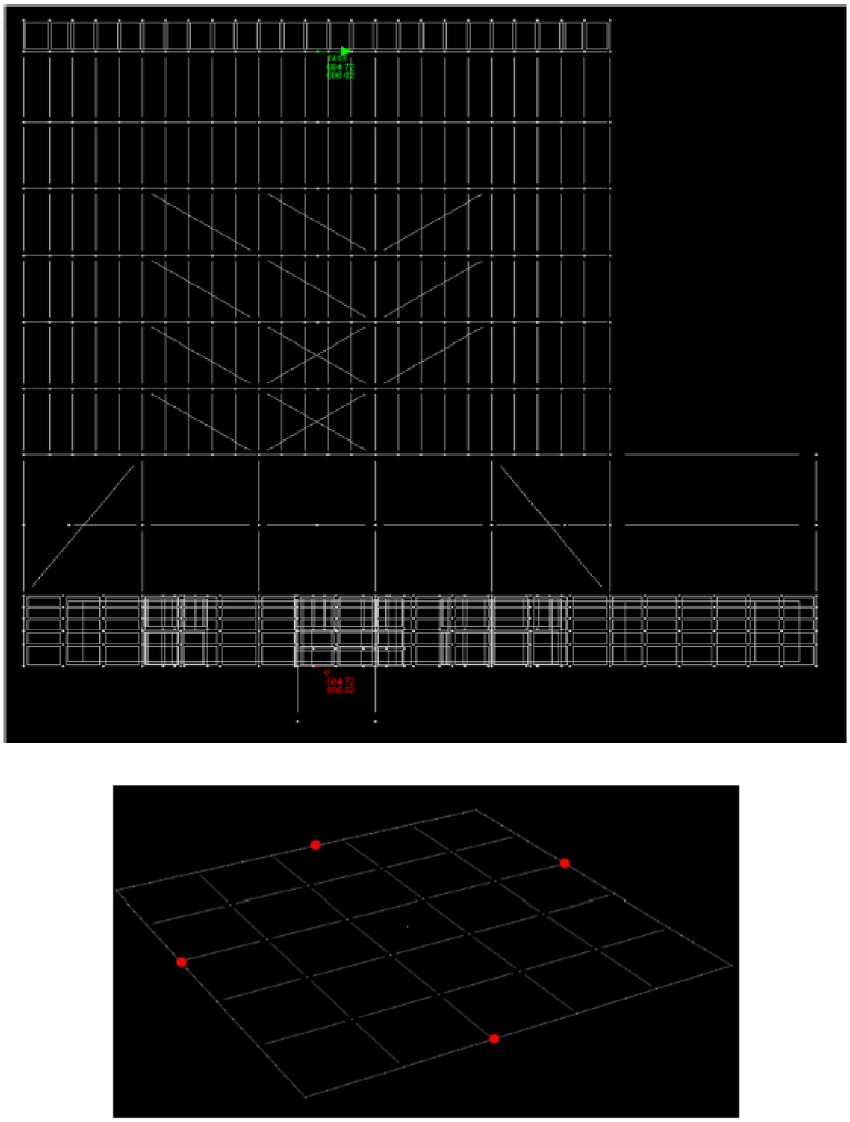

Figure G-5: Definition and Measurement of Lateral Deformation Ratio (Drift)

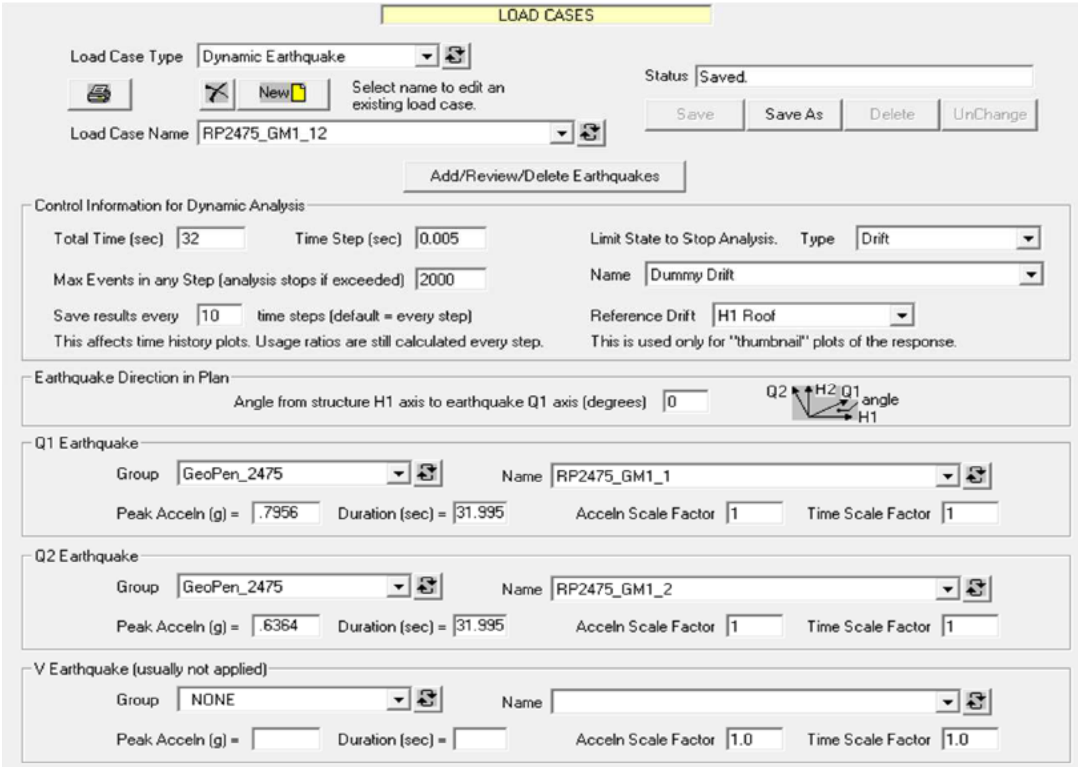

Figure G-6: Lateral Load Patterns

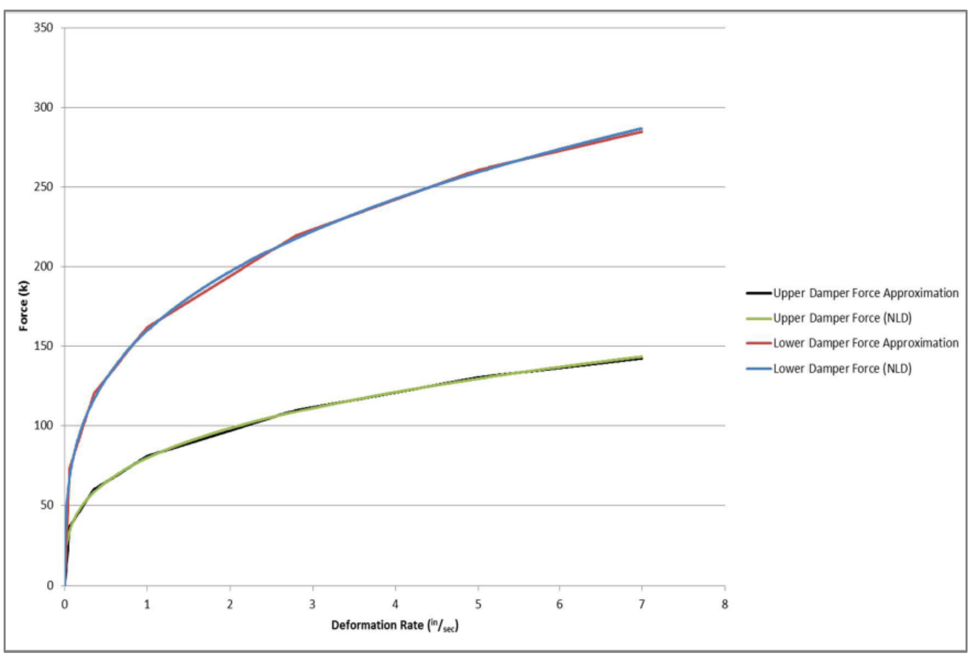

Figure G-7: Fluid Viscose Damper Force-Deformation Relationship

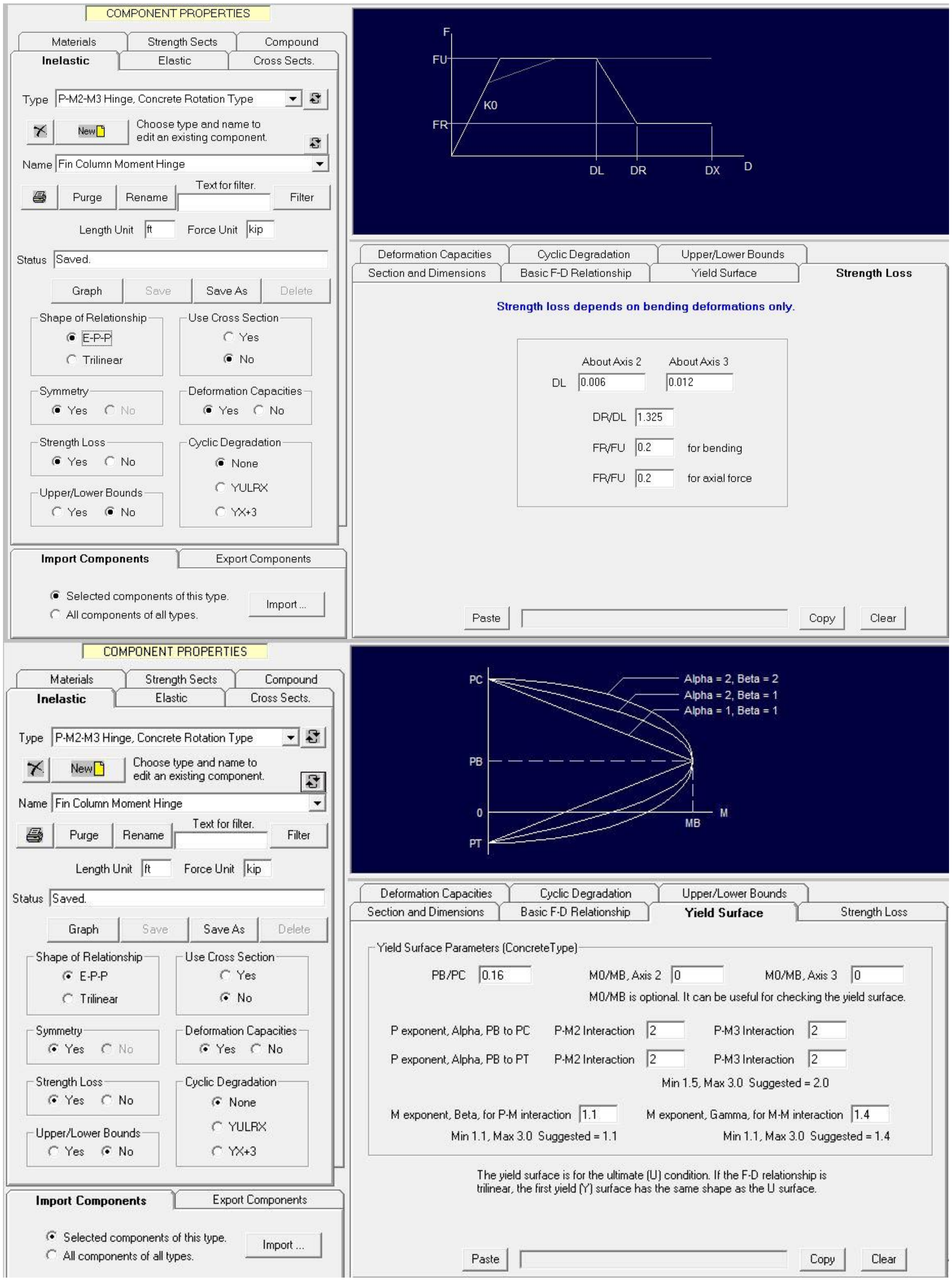

Figure G-8: Perform-3D – Moment Hinge – Fin Column

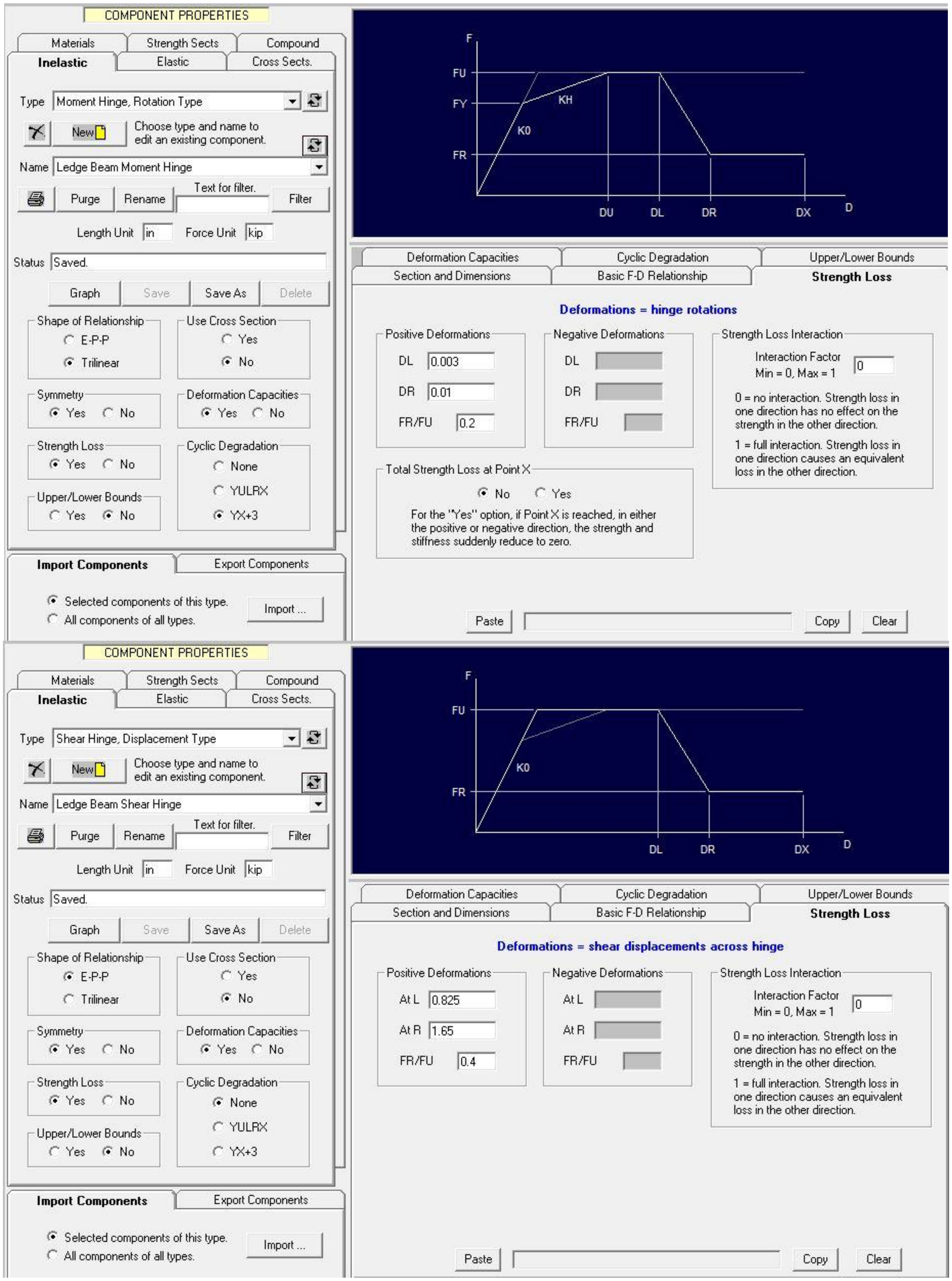

Figure G-9: Perform-3D – Moment Hinge – Beam Assembly

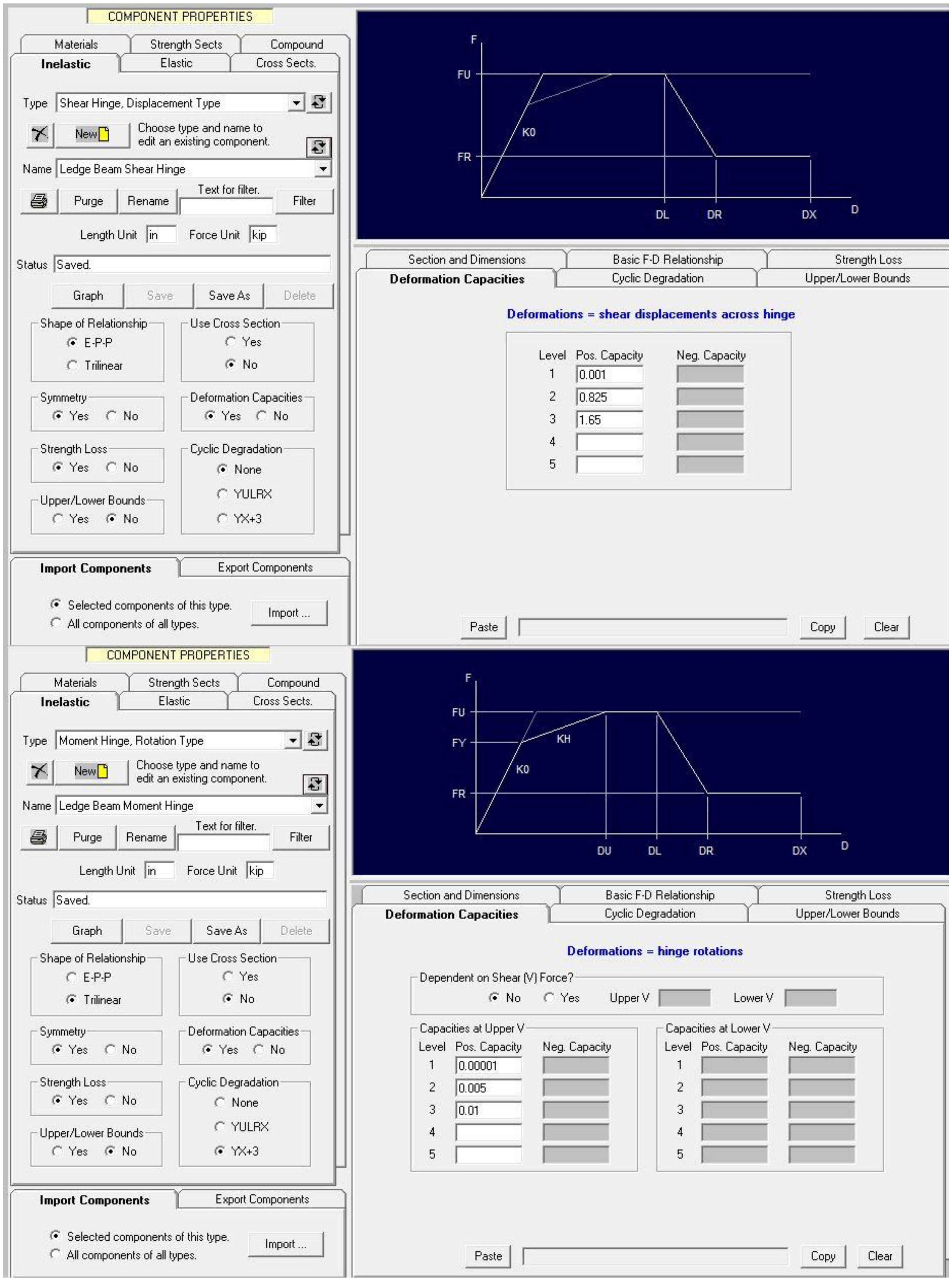

Figure G-10: Perform-3D – Deformation Capacities – Beam Assembly

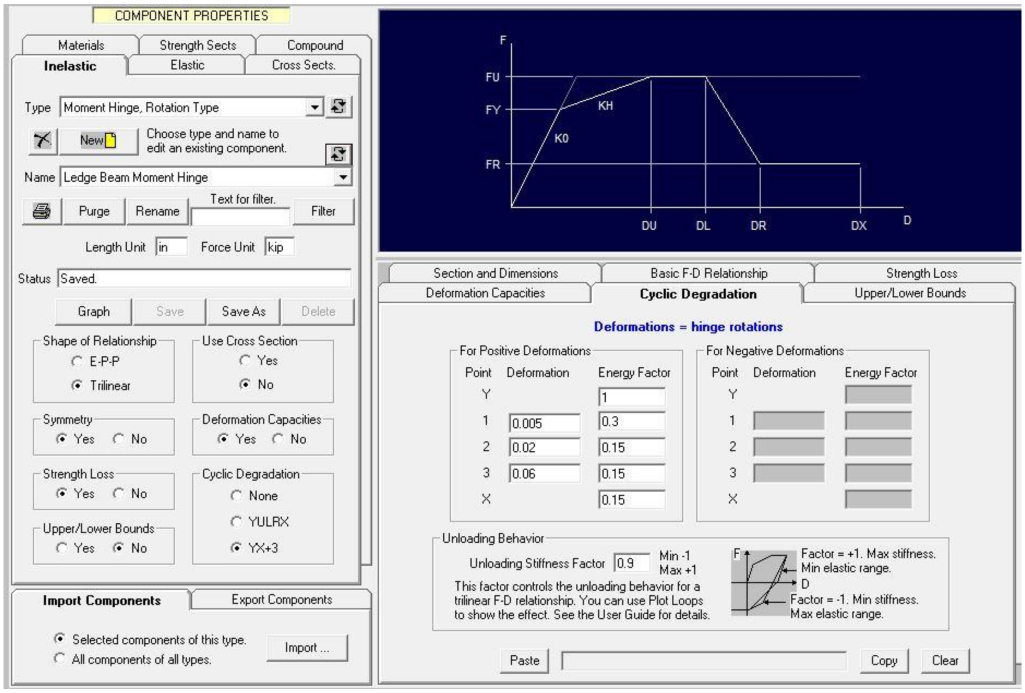

Figure G-11: Perform-3D – Shear Hinge – Cyclic Degradation

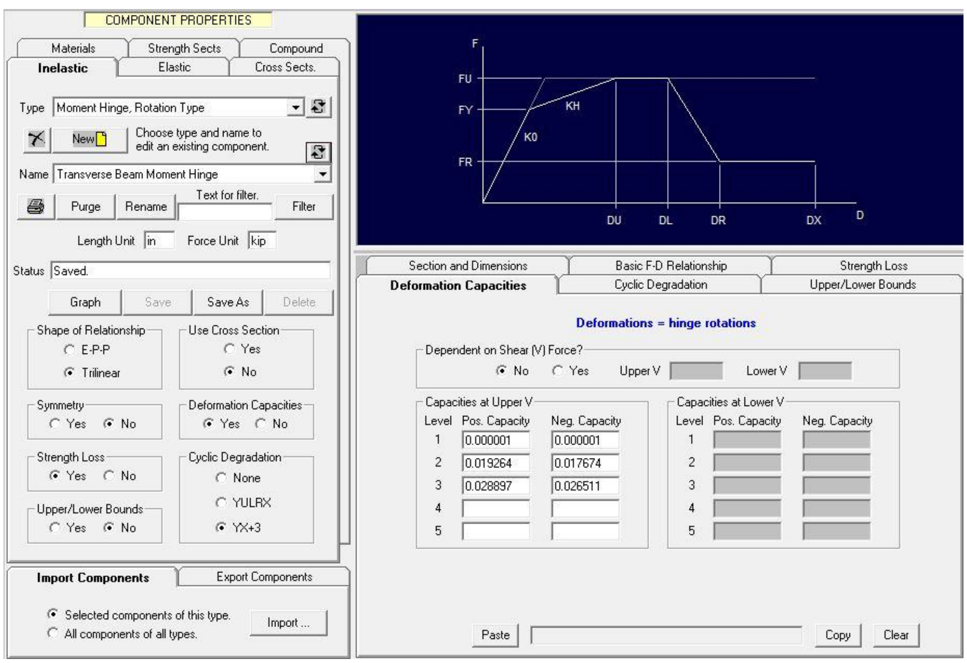

Figure G-12: Perform-3D – Deformation Capacities – Transverse Beam

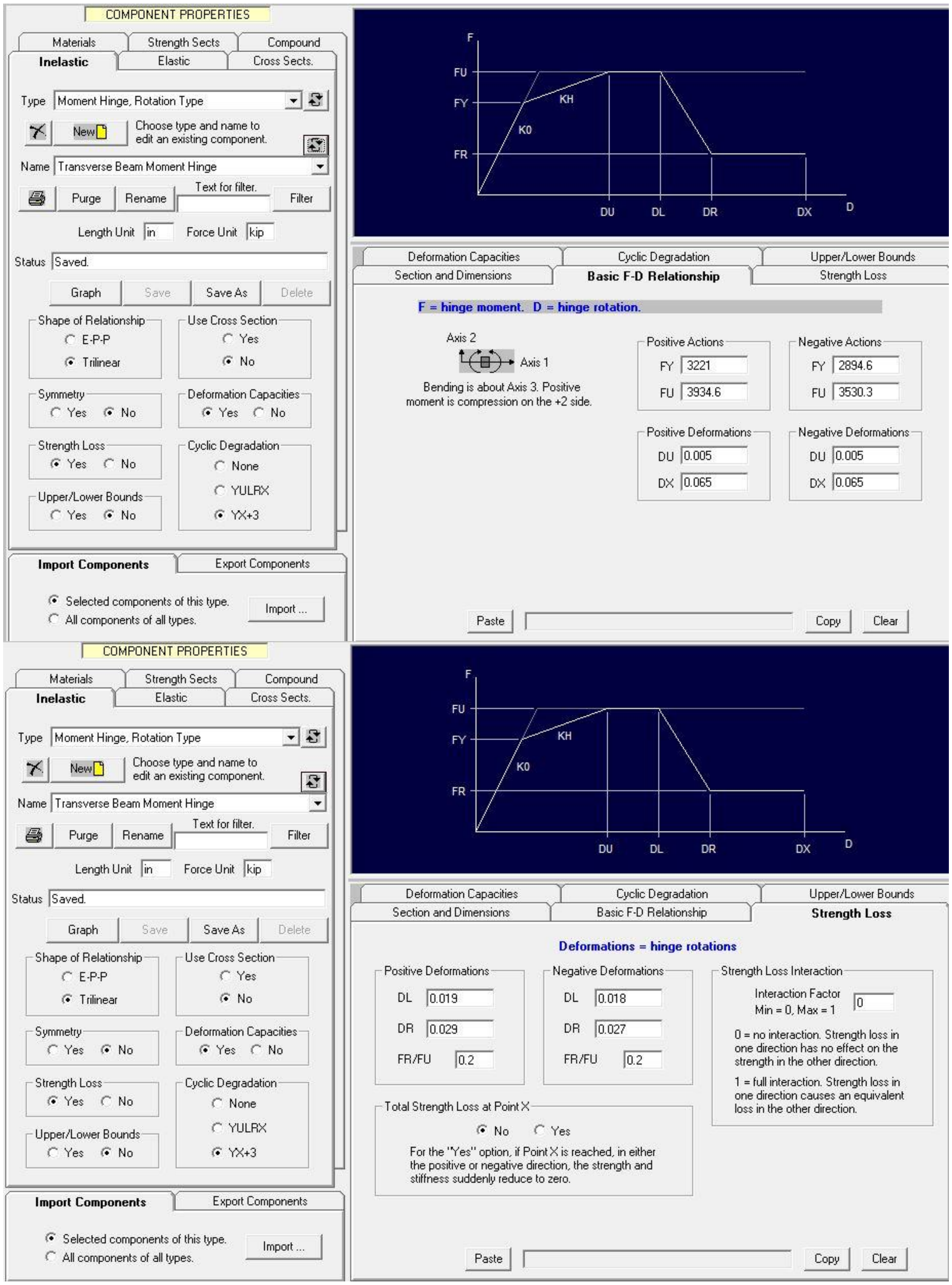

Figure G-13: Perform-3D – Moment Hinge – Transverese Beam

Appendix H. SP3

H1. General

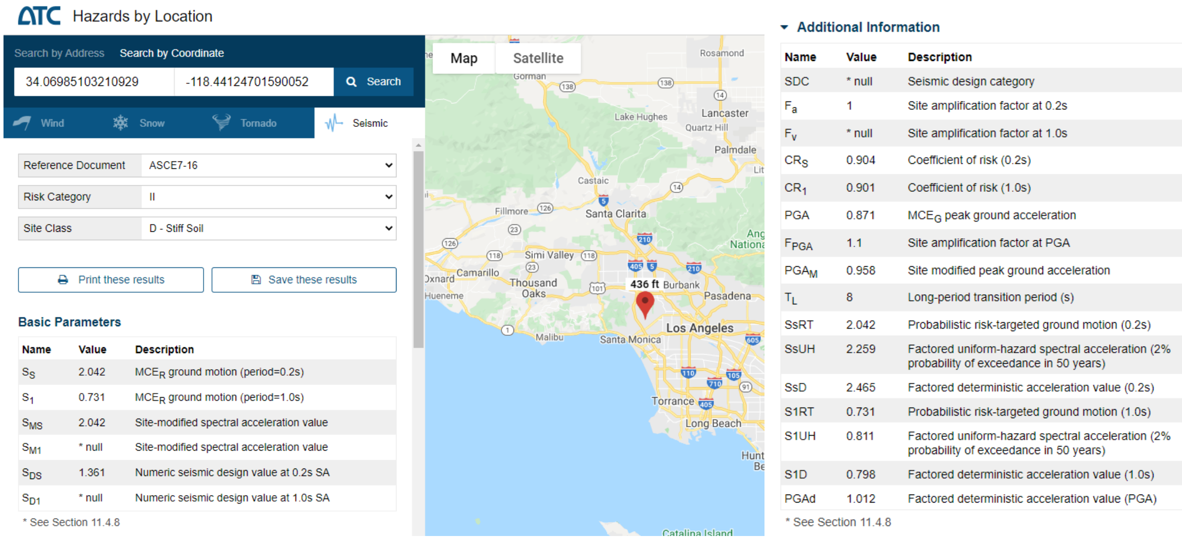

Figure H-1: Seismic Properties (https://hazards.atcouncil.org/)

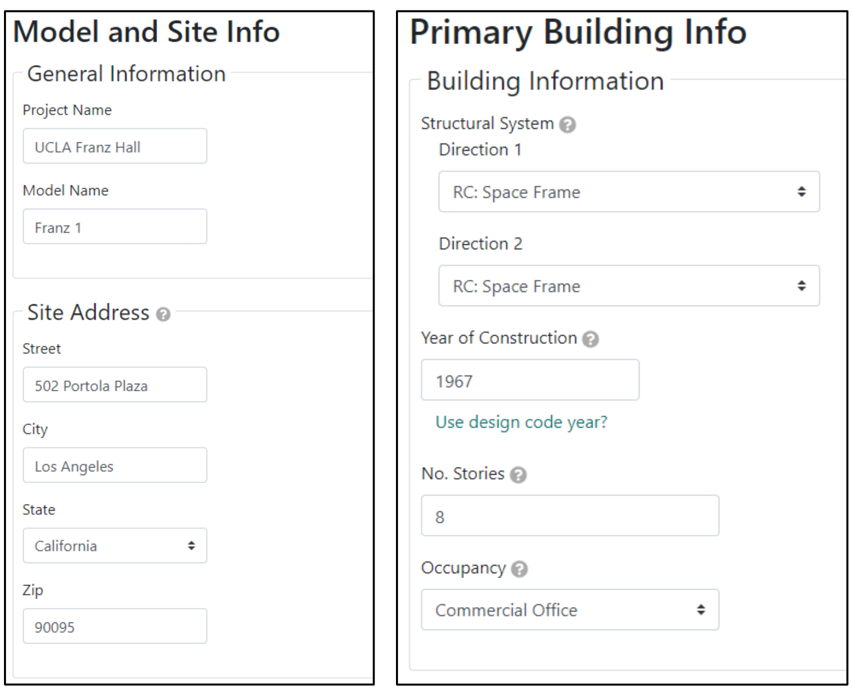

Figure H-2: SP3 – Primary Inputs

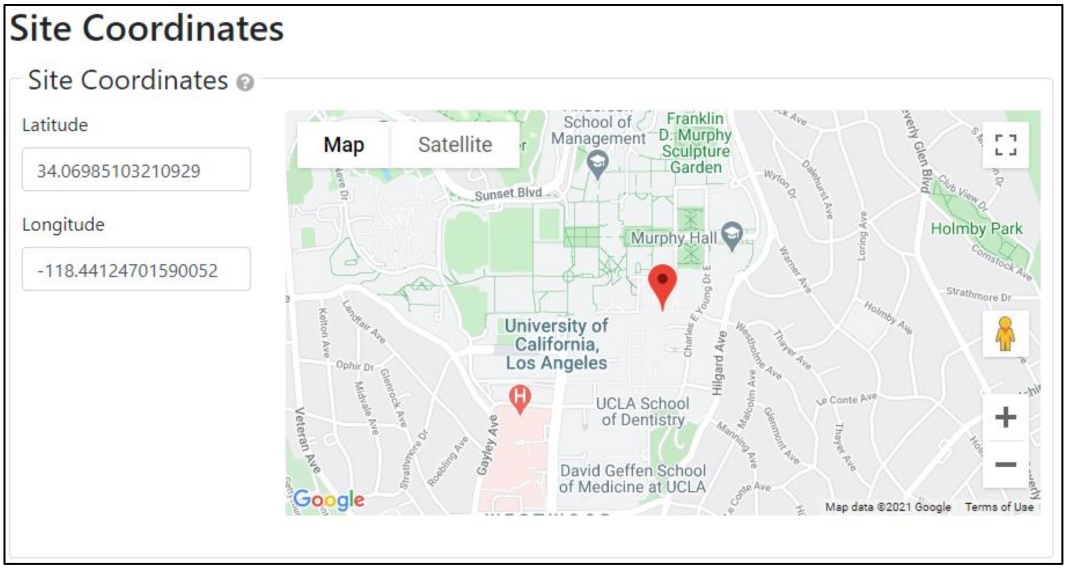

Figure H-3: SP3 – Site Coordinates

Story heights are 13 ft. 9 in. in levels 1, 2 and 8, and 12 ft. 9 in. in levels 3, 4, 5, 6, and 7, with a 5 ft. 11 in. parapet. To have the extra height of levels 2 and 8 considered in the building height, the "upper story" height input is adjusted to 13 ft. and the first level height to 14 ft.

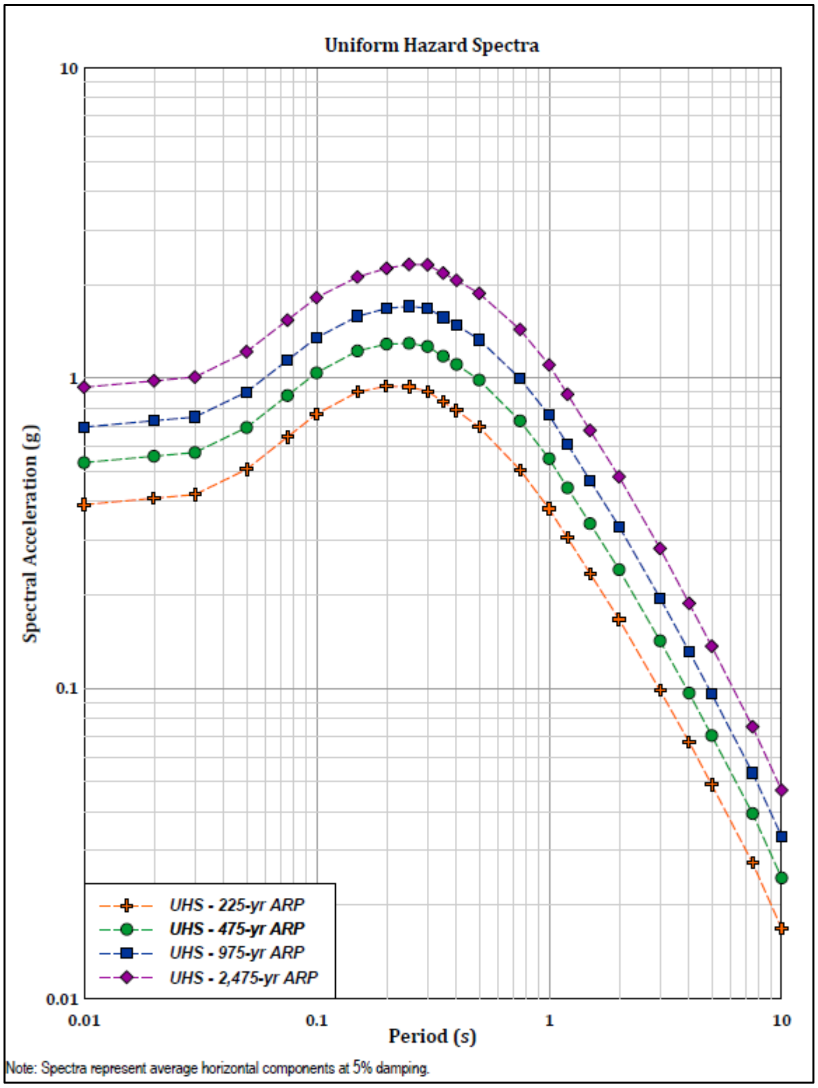

Figure H-4: Site Specific Uniform Hazard Spectra

H2. Express Analysis – Existing Franz Tower

CONTENTS

1 SUMMARY OF INPUTS AND RISK RESULTS

Risk Model Inputs

Primary

Project Name:	1 Franz-Pritzker
Model Name:	5 Level of input
Building Type:	RC: Space Frame
Year of Construction:	1967
Number of Stories:	8
Occupancy:	Commercial Office
Address:	
502 Portola Plaza	
Los Angeles, CA, 90095	
Latitude:	34.06989°
Longitude:	-118.44125°

Analysis Options

Include Collapse in Analysis:	Yes
Consider Residual Drift:	Yes

Building Layout Information

Cost per Square Foot:	–
Total Square Feet:	–
Aspect Ratio:	–
First Story Height (ft):	–
Upper Story Heights (ft):	–
Vertical Irregularity:	–
Plan Irregularity:	–

Ground Motion and Soil Information

Site Class:	–
Site Hazard:	SP3 Default

Building Design Info

Level of Detailing (Dir. 1, 2):	–, –
Drift Limit (Dir. 1, 2):	–, –
Risk Category:	–
Seismic Importance Factor, I_e:	–
Component Importance Factor, I_p:	–
Include Retrofit Information?	No

Structural Properties

Property	Dir. 1	Dir. 2
Base Shear Strength (g):	–	–
Yield Drift (%):	–	–
1^{st} Mode Period (T_1) (s):	–	–
2^{nd} Mode Period (T_2) (s):	–	–
3^{rd} Mode Period (T_3) (s):	–	–

Component Information

Do your stairs have seismic joints?	–
Is your ceiling laterally supported?	–
Is your lighting seismically rated?	–
Is your piping seismically rated?	–
Is your HVAC system seismically anchored?	–
Is your electrical equipment seismically rated?	–
Percent of Building Glazed:	–

Building Stability

Median Collapse Capacity:	–
Beta (Dispersion):	–

Responses

No responses provided

Repair Time Options

Factors Delaying Start of Repairs	
Inspection	Yes
Financing	Yes
Permitting	Yes
Engineering Mobilization	Yes
Contractor Mobilization	Yes
Mitigation Factors	
Inspector on Retainer	No
Engineer on Retainer	No
Engineer on Retainer	No
Funding Source	Private Loans

Expected Loss

Expected loss in percent of total building value

Shaking Intensity	Return Period	SEL (%)	SUL (%)
90% in 50 years	22 Years	2.0	4.5
50% in 30 years	43 Years	4.4	8.4
50% in 50 years	72 Years	7.3	14
50% in 75 years	108 Years	10	19
50% in 100 years	144 Years	13	23
20% in 50 years	224 Years	18	31
DE	411 Years	26	45
10% in 50 years	475 Years	30	50
MCE_R	938 Years	47	77
5% in 50 years	975 Years	47	78
2% in 50 years	2475 Years	73	100

Repair Time

Median repair time, without impeding factors

Intensity	FEMA P-58 Parallel	FEMA P-58 Series	REDi Re-Occupancy	REDi Functional Recovery	REDi Full Recovery
90% in 50 years	5 days	7 days	0 days	14 days	14 days
50% in 30 years	9 days	2.5 weeks	4 days	3.2 weeks	3.2 weeks
50% in 50 years	14 days	4.8 weeks	10 days	4.2 weeks	4.2 weeks
50% in 75 years	2.7 weeks	7.5 weeks	3.6 weeks	5.3 weeks	5.3 weeks
50% in 100 years	3.5 weeks	2.4 months	5.3 weeks	6.5 weeks	6.5 weeks
20% in 50 years	5.1 weeks	3.8 months	1.9 months	2.1 months	2.1 months
DE	7.4 weeks	6.0 months	3.0 months	3.1 months	3.1 months
10% in 50 years	2.0 months	7.0 months	3.5 months	3.6 months	3.6 months
MCE_R	3.1 months	13 months	6.4 months	6.5 months	6.5 months
5% in 50 years	3.2 months	14 months	6.6 months	6.7 months	6.7 months
2% in 50 years	4.8 months	19 months	12 months	12 months	12 months

2 BASIS OF ANALYSIS

This analysis is based on the SP3-RiskModel of the Seismic Performance Prediction Program (SP3) software platform. The underlying analysis methods are based on the FEMA P-58 analytical method, which is a transparent and well documented method developed through a 15 year project (Applied Technology Council, 2018). This project leveraged the previous decades of academic research, funded by a $16 million investment by the Federal Emergency Management Agency (FEMA). In contrast to many risk assessment methods based on judgment and past earthquake experience, the FEMA P-58 and SP3 analysis are based on engineering-oriented risk evaluation methods.

3 DOCUMENTATION OF SITE AND BUILDING INPUT DATA

Project Name: 1 Franz-Pritzker
Model Name: 5 Level of input

3.1 Site Information

Address: 502 Portola Plaza, Los Angeles, CA, 90095
Latitude: 34.06989°
Longitude: -118.44125°

3.2 Building Information

Material Type:	Cast-in-Place Concrete
Number of Stories:	8
Total Building Square Footage:	80,000
Occupancy Type:	Commercial Office
Total Expected Building Replacement Value:	$21,167,946

4 SITE HAZARD INFORMATION

This section presents the site's seismic hazard information. The V_{S30} value is the shear wave velocity in the soil at a depth of 30 meters. This value and the associated site class are presented in Table 1.

Table 1. Site soil information

V_{S30} (m/s):	364.0
Site Class:	C/D

Table 2 and Figure 1 present the spectral acceleration information for this site. The spectral acceleration is a measure of how much force the building will attract in an earthquake. This amount of force is dependent on the intensity of the ground shaking (e.g. 10% in 50 years), as well as a dynamic property of the building known as the "fundamental period". Shorter buildings tend to have smaller fundamental periods and taller buildings tend to have larger fundamental periods. As indicated by Figure 1, smaller fundamental periods (with the exception of very short fundamental periods) will attract more force in an earthquake.

The Design Earthquake (DE) and Maximum Considered Earthquake (MCE) are based on the modern code maximum direction spectra and are converted to geometric mean for comparison.

Table 2. Geometric mean spectral acceleration values (in g)

Shaking Intensity	Return Period	PGA	$S_a(0.2s)$	$S_a(1.0s)$	$S_a(1.6s)$
90% in 50 years	22 years	0.09	0.22	0.08	0.05
50% in 30 years	43 years	0.15	0.36	0.13	0.09
50% in 50 years	72 years	0.21	0.50	0.19	0.13
50% in 75 years	108 years	0.26	0.63	0.25	0.17
50% in 100 years	144 years	0.30	0.73	0.30	0.21
20% in 50 years	224 years	0.38	0.91	0.39	0.27
DE	411 years	0.50	1.19	0.55	0.38
10% in 50 years	475 years	0.53	1.26	0.59	0.41
MCE_R	938 years	0.69	1.63	0.82	0.58
5% in 50 years	975 years	0.70	1.65	0.84	0.59
2% in 50 years	2475 years	0.96	2.25	1.24	0.87

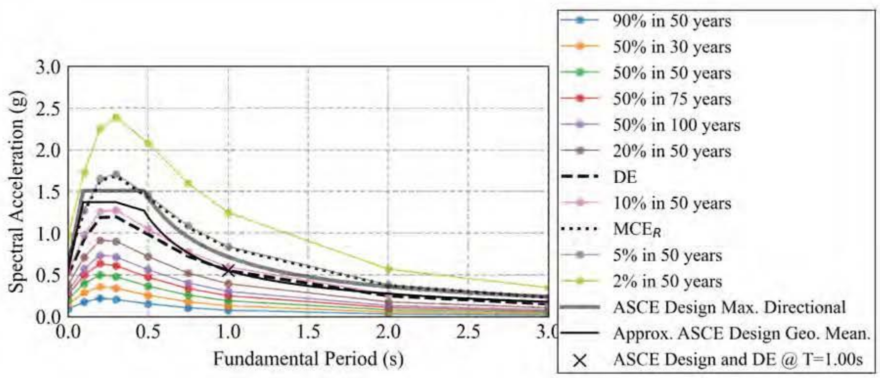

Figure 1. Hazard curves for this site. All curves are geometric mean unless otherwise stated.

5 BUILDING DESIGN SUMMARY FROM THE *SP3 BUILDING CODE DESIGN DATABASE*

5.1 Building Code Design Parameters

The seismic design parameters used to compute the seismic base shear coefficients for this building are presented in Table 3. These parameters are specific to the 1961 edition of the Uniform Building Code (International Conference of Building Officials, 1961).

Table 3. Code design parameters

(a) UBC 1961 structural system parameters

Parameter	Dir. 1	Dir. 2
C_d	1.49	1.49
k	0.67	0.67

(b) UBC 1961 site specific parameters

Parameter	Value
Z	1
Seismic Zone	3

5.2 Modern Building Code Design Parameters

For comparison to modern code, the modern code parameters are presented in Table 4.

Table 4. Modern code design parameters

(a) ASCE/SEI 7-2010 structural system parameters

Parameter	Dir. 1	Dir. 2
C_t	0.016	0.016
C_d	5.5	5.5
x	0.9	0.9
R	8	8
Ω_0	3	3

(b) ASCE/SEI 7-2010 site specific parameters

Parameter	Value
S_s	2.263
S_1	0.825
S_{ds}	1.508
S_{d1}	0.715
SDC	E
C_u	1.4
$\text{MCE}_{R,max}(g)$	0.691
$\text{MCE}_{R,geomean}(g)$	0.532
$\text{DE}_{max}(g)$	0.461
$\text{DE}_{geomean}(g)$	0.354

5.3 Structural Properties

This section summarizes the main structural properties of the building in each direction. These structural properties are used as inputs to the SP3 Structural Response Prediction Engine.

Table 5. Structural properties table

Parameter	Direction 1	Direction 2
General		
Structural System	RC: Space Frame	RC: Space Frame
Building Edge Length (ft)	100	100
Detailing Level	Intermediate	Intermediate
Strength		
Seismic Design Base Shear Ratio, C_s	0.023	0.023
Ultimate Base Shear Ratio, v_{ult}	0.140	0.140
Stiffness		
$T_{1,design}$ (s)	2.11	2.11
T_1 with structural overstiffness (s)	1.78	1.78
T_1 with gravity system (s)	1.77	1.77
T_1 with non-structural components (s)	1.65	1.65
T_1 empirical lower bound (s)	0.87	0.87
T_1 empirical upper bound (s)	1.55	1.55
T_1 Final (s)	1.55	1.55

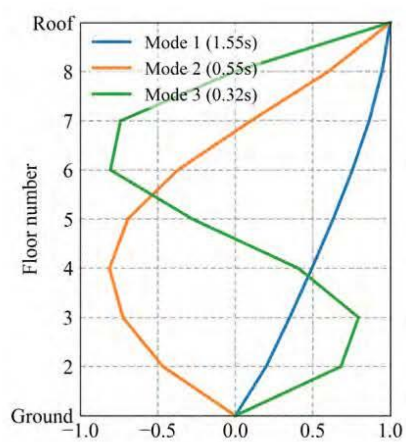

Figure 2. Mode shapes

6 BUILDING STABILITY

The FEMA P-154 collapse capacity score was calculated as follows using the "very high" seismicity level. The terminology used in this section is consistent with the FEMA P-154 methodology (Applied Technology Council, 2015a):

- P$[COL|MCE_R]_{P-154}$: the probability that the building will be in the HAZUS complete structural damage state when subjected to MCER shaking, times the collapse factor
- P$[COL|MCE_R]_{P-58}$: the probability that the building will be in the HAZUS complete structural damage state when subjected to MCER shaking, times the collapse factor
- Collapse Factor: expected ratio of collapsed area to total area given that the building is in the HAZUS Complete structural damage state

For a more in-depth explanation of "collapse," refer to Section 4.4.1.5 of FEMA P-155 Third Edition available here (Applied Technology Council, 2015b).

Table 6. Breakdown of FEMA P-154 score assignment

FEMA ID:	C1
Basic Score	1
Soil	0
Year	0
Plan Irregularity	0
Vertical Irregularity	0
Risk Category* (Cat I/II)	0
Sum:	1
Minimum Allowed:	0.3
Score:	**1**
Dispersion (β):	0.7

*Non-standard property implemented by SP3

The FEMA P-154 probability of collapse at the MCE_R level event is then calculated as:

$$\begin{aligned} \text{P}[COL|MCE_R]_{P-154} &= 10^{-\text{score}} \\ &= 10^{-1} \qquad \text{(FEMA P-155 eqn. 4-1)} \\ &= 10.0\% \end{aligned}$$

Taking into account the fraction of floor area collapsed (1 in this case), the probability of collapse is:

$$\begin{aligned} \text{P}[COL|MCE_R]_{P-58} &= \text{P}[COL|MCE_R]_{P-154} \ / \ \text{Collapse Factor} \\ &= 10.0\% \ / \ 1 \\ &= 10.0\% \end{aligned}$$

The median collapse capacity is calculated as:

$$\begin{aligned} S_{a,\ collapse\ median,\ P-58} &= \exp\left(\ln(S_{a,MCE_R}) - \text{norminv}\left(P[COL|MCE_R]_{P-58}\right) \cdot \beta\right) \\ &= \exp\left(\ln(0.576g) - \text{norminv}\left(10.0\%\right) \cdot 0.7\right) \\ &= 1.41g \end{aligned}$$

where `norminv` is the inverse of the standard normal cumulative distribution function (CDF).

Figure 3 shows the collapse capacity cumulative distribution function used in the analysis.

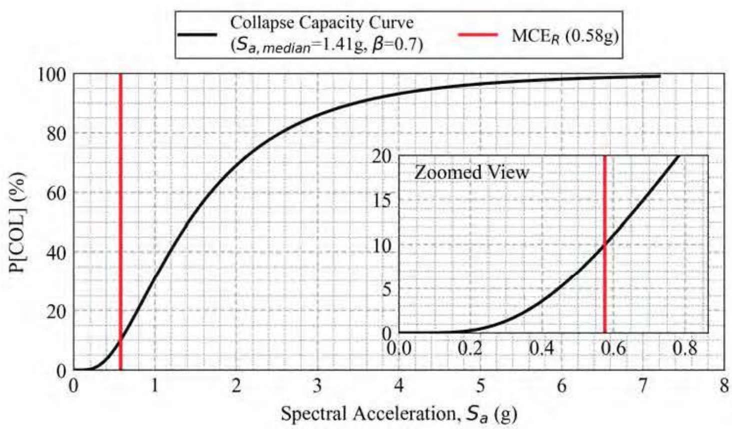

Figure 3. Cumulative distribution function for collapse capacity

7 STRUCTURAL RESPONSE PREDICTIONS FROM THE SP3 STRUCTURAL RESPONSE PREDICTION ENGINE

The SP3 Response Prediction Engine predicts the structural responses (typically providing 100 ground motions per intensity level); this is done by using a combination of three-mode elastic modal analysis, coupled with both elastic and inelastic response modifiers mined from the large SP3 Structural Responses Database (with over 4,000,000 response simulations, and growing). These response predictions track all of the important statistical information in the responses (mean, variability, and correlations); this enables a statistically robust vulnerability curve at the end of the risk assessment process.

7.1 Peak Story Drift

Peak interstory drift ratio is an important metric for both structural and non-structural components in the building. It measures how much the ceiling of a given story moves relative to the floor, normalized to the height of the story. The greater the interstory drift ratio, the greater the damage to the components on that level. Typical components that are damaged from interstory drift ratio are structural components (beams and columns), gypsum partition walls, and exterior cladding and glazing.

Table 7. Peak story drift demands are the same in both directions

Story	90% in 50 years	50% in 30 years	50% in 50 years	50% in 75 years	50% in 100 years	20% in 50 years	DE	10% in 50 years	MCE_R	5% in 50 years	2% in 50 years
8	0.09	0.16	0.24	0.32	0.38	0.48	0.61	0.66	0.89	0.91	1.32
7	0.12	0.21	0.31	0.42	0.50	0.63	0.80	0.86	1.17	1.19	1.74
6	0.14	0.25	0.36	0.48	0.58	0.73	0.93	1.00	1.37	1.39	2.03
5	0.16	0.27	0.39	0.53	0.63	0.80	1.02	1.09	1.49	1.51	2.20
4	0.16	0.28	0.41	0.55	0.67	0.84	1.07	1.15	1.56	1.59	2.32
3	0.17	0.29	0.43	0.58	0.69	0.88	1.11	1.20	1.63	1.65	2.41
2	0.18	0.31	0.46	0.62	0.74	0.94	1.20	1.29	1.75	1.78	2.59
1	0.20	0.34	0.51	0.68	0.82	1.03	1.31	1.41	1.92	1.95	2.84

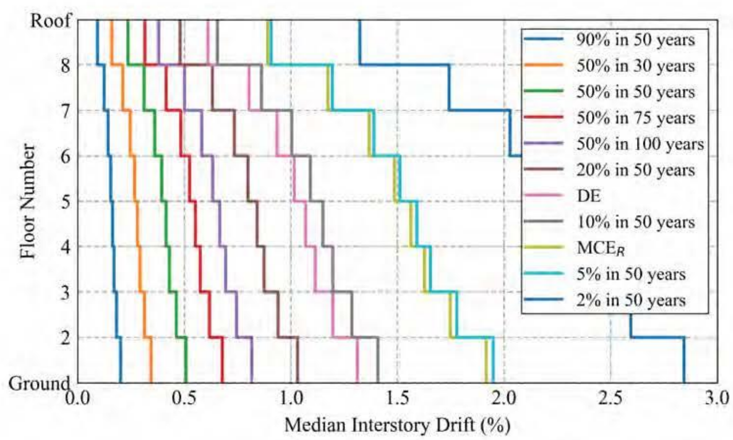

Figure 4. Peak story drift demands are the same in both directions

7.2 Peak Floor Acceleration

Peak floor acceleration is an an important metric for non-structural components in the building. Components such as piping, HVAC, and electrical switchgear are sensitive to the floor accelerations. High accelerations will typically damage a component itself or cause the component's anchorage to fail, both of which may require repair or replacement of the component.

Table 8. Peak floor acceleration demands are the same in both directions

Floor	90% in 50 years	50% in 30 years	50% in 50 years	50% in 75 years	50% in 100 years	20% in 50 years	DE	10% in 50 years	MCE_R	5% in 50 years	2% in 50 years
Roof	0.19	0.31	0.40	0.45	0.47	0.48	0.51	0.52	0.55	0.55	0.59
8	0.15	0.25	0.32	0.36	0.38	0.39	0.42	0.43	0.46	0.46	0.50
7	0.14	0.22	0.30	0.34	0.35	0.37	0.41	0.42	0.46	0.46	0.52
6	0.12	0.20	0.26	0.30	0.32	0.34	0.39	0.40	0.45	0.45	0.53
5	0.11	0.19	0.25	0.29	0.32	0.35	0.40	0.41	0.48	0.48	0.58
4	0.11	0.18	0.24	0.28	0.31	0.35	0.41	0.43	0.51	0.51	0.64
3	0.10	0.17	0.23	0.27	0.30	0.35	0.43	0.45	0.55	0.56	0.72
2	0.10	0.16	0.22	0.27	0.30	0.36	0.45	0.48	0.60	0.61	0.81
Ground	0.09	0.15	0.21	0.26	0.30	0.38	0.50	0.53	0.69	0.70	0.96

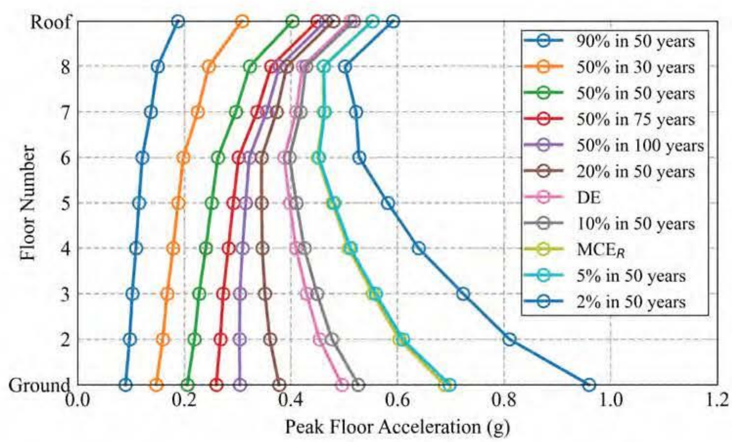

Figure 5. Peak floor acceleration demands are the same in both directions

7.3 Residual Story Drift

Residual drift is a metric that informs the need for structural repairs or building demolition (where excessive drifts are present). Residual drift ratio is a measure of how much the building is "leaning over" after the seismic event has ceased. A residual drift of 2% would indicate that the story is laterally displaced 2% of it's height, which equates to about 3.6 inches for a 15 foot tall story.

Table 9. Residual story drift demands are the same in both directions

Story	90% in 50 years	50% in 30 years	50% in 50 years	50% in 75 years	50% in 100 years	20% in 50 years	DE	10% in 50 years	MCE_R	5% in 50 years	2% in 50 years
8	0.00	0.00	0.00	0.00	0.00	0.00	0.00	0.00	0.02	0.02	0.07
7	0.00	0.00	0.00	0.00	0.00	0.00	0.01	0.01	0.05	0.06	0.12
6	0.00	0.00	0.00	0.00	0.00	0.00	0.02	0.03	0.08	0.08	0.16
5	0.00	0.00	0.00	0.00	0.00	0.01	0.03	0.04	0.09	0.10	0.18
4	0.00	0.00	0.00	0.00	0.00	0.01	0.04	0.05	0.10	0.11	0.20
3	0.00	0.00	0.00	0.00	0.00	0.02	0.05	0.06	0.11	0.11	0.21
2	0.00	0.00	0.00	0.00	0.00	0.02	0.06	0.07	0.12	0.13	0.23
1	0.00	0.00	0.00	0.00	0.01	0.04	0.07	0.08	0.15	0.15	0.26

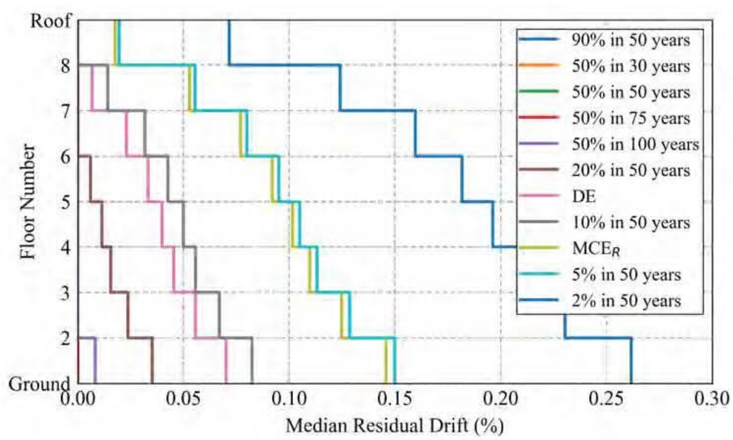

Figure 6. Residual story drift demands are the same in both directions

7.4 Maximum Residual Story Drift

Residual drift is a metric that informs the need for structural repairs or building demolition (where excessive drifts are present). A residual drift of 2% would indicate that the story is laterally displaced 2% of it's height, which equates to about 3.6 inches for a 15 foot tall story. Maximum residual drift is the maximum of the residual drifts on all levels. This is the value used to determine if the building is demolished due to excessive residual drift. Excessive drifts can be visually unsettling and prohibitively expensive (or even impossible) to "straighten" and repair the structural damage. Due to this, the building owner may decide to demolish and rebuild the building if the residual drifts are too large.

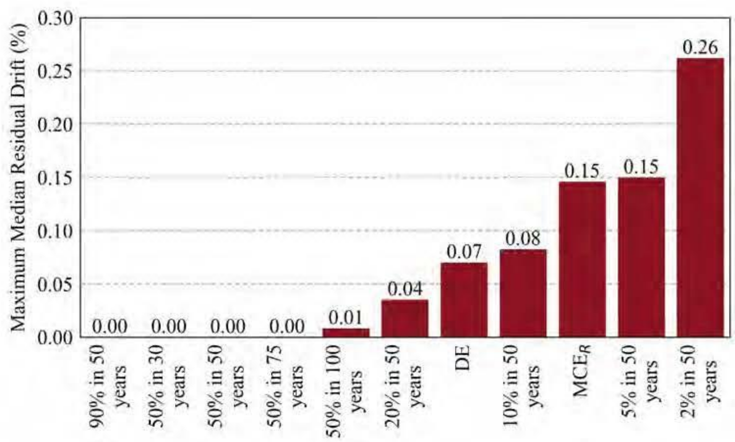

Figure 7. Maximum residual story drift demands are the same in both directions

8 REPAIR COSTS - BY LEVEL OF GROUND MOTION

8.1 Mean and 90^{th} Percentile Repair Costs (SEL and SUL)

The different metrics for repair cost are as follows:

- **Mean (SEL)**: ("Scenario Expected Loss") the average repair cost of the building repair/replacement.
- **Median**: there is a 50% probability that the repair cost will not exceed this value.
- **Fitted SUL**: Fitted value of "Scenario Upper Loss".
- **Counted 90^{th} Percentile**: there is a 90% probability that the repair cost will not exceed this value.

Table 10. Expected loss normalized by building cost

Intensity	PGA (g)	Mean (SEL) (%)	Fitted SUL (%)	Median (%)	Counted 90^{th} Percentile (%)
90% in 50 years	0.09	2.0	4.5	1.4	4.5
50% in 30 years	0.15	4.4	8.4	3.7	8.4
50% in 50 years	0.21	7.3	14	6.2	14
50% in 75 years	0.26	10	19	8.8	19
50% in 100 years	0.30	13	23	11	23
20% in 50 years	0.38	18	31	16	31
DE	0.50	26	45	22	45
10% in 50 years	0.53	30	50	25	50
MCE_R	0.69	47	77	41	100
5% in 50 years	0.70	47	78	42	100
2% in 50 years	0.96	73	100	73	100

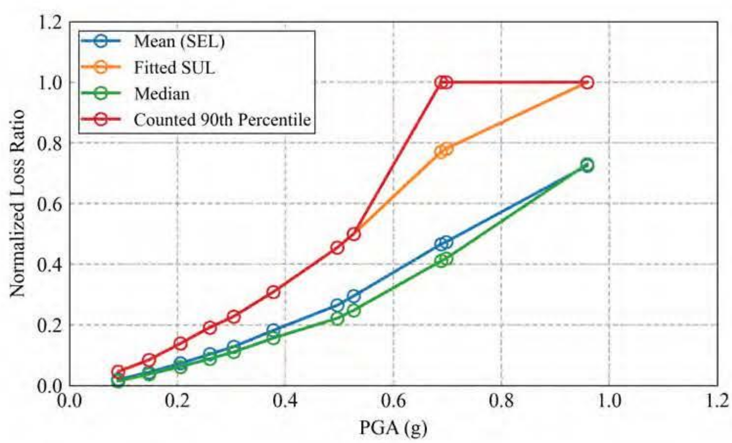

Figure 8. Loss metrics across all intensity levels analyzed

9 REPAIR COST BREAKDOWN BY BUILDING COMPONENTS

9.1 Categories for Repair Cost Breakdowns

Repair costs are binned into eight categories as follows:

- **Collapse**: building demolition and replacement following a collapse.
- **Residual**: building demolition and replacement following unacceptable residual drifts.
- **Structural**: components of the lateral force resisting system or gravity system (e.g. beam column connections, link beams, shear wall, shear tabs, etc.).
- **Partitions**: partition wall components (e.g. wood or metal stud gypsum full height partitions).
- **Exterior**: components placed on the exterior of the building (e.g. cladding, glazing, etc.).
- **Interior**: non-structural components on the interior of the building (e.g. raised access floors, ceilings, lighting).
- **HVAC**: HVAC and plumbing components (e.g. water piping and bracing, sanitary piping, ducting, boilers etc.).
- **Other**: components not included in the categories above (e.g. elevators, user defined components, fire protection components).

9.2 Repair Cost Breakdown for Various Ground Motion Levels

Table 11. Expected mean loss per component group (in percent)

Intensity	Total	Structural	Collapse	Exterior	Residual	Partitions	HVAC	Other	Interior
90% in 50 years	2.0	0.0	0.0	0.4	0.0	0.0	1.3	0.1	0.1
50% in 30 years	4.4	0.1	0.0	1.7	0.0	0.1	1.9	0.4	0.2
50% in 50 years	7.3	0.5	0.0	3.2	0.0	0.3	2.1	0.7	0.4
50% in 75 years	10	1.5	0.1	4.5	0.0	0.5	2.2	0.9	0.5
50% in 100 years	13	2.6	0.3	5.3	0.0	0.7	2.2	1.0	0.6
20% in 50 years	18	5.0	0.9	6.9	0.0	1.0	2.3	1.3	0.8
DE	26	8.6	3.1	8.7	0.1	1.3	2.2	1.4	1.0
10% in 50 years	30	10	4.0	9.3	0.0	1.4	2.3	1.5	1.1
MCE_R	47	18	10.0	11	0.6	1.8	2.1	1.7	1.4
5% in 50 years	47	18	10	12	0.6	1.8	2.1	1.7	1.4
2% in 50 years	73	25	25	13	3.3	1.9	1.8	1.7	1.6

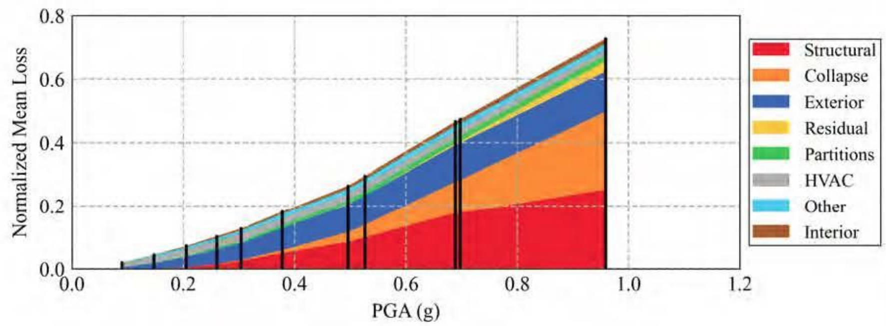

Figure 9. Contribution of building components to mean loss ratio

9.3 Repair Cost Breakdown for Expected Annual Loss

The expected annual loss for this building is $84,909.

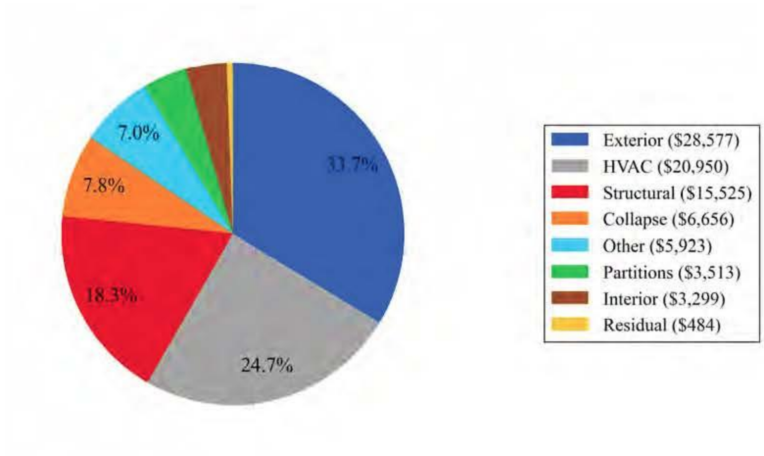

Figure 10. Annualized loss breakdown

H3. Standard Analysis – Existing Franz Tower

CONTENTS

1 SUMMARY OF INPUTS AND RISK RESULTS

Risk Model Inputs

Primary

Project Name:	2 Franz-Pritzker
Model Name:	Standard Analysis
Building Type:	RC: Space Frame
Year of Construction:	1967
Number of Stories:	8
Occupancy:	Commercial Office
Address:	
502 Portola Plaza	
Los Angeles, CA, 90095	
Latitude:	34.06989°
Longitude:	-118.44125°

Analysis Options

Include Collapse in Analysis:	Yes
Consider Residual Drift:	Yes

Building Layout Information

Cost per Square Foot:	–
Total Square Feet:	84,211
Aspect Ratio:	1
First Story Height (ft):	14
Upper Story Heights (ft):	13
Vertical Irregularity:	Extreme
Plan Irregularity:	None

Ground Motion and Soil Information

Site Class:	C
Site Hazard:	SP3 Default

Building Design Info

Level of Detailing (Dir. 1, 2):	Ordinary, Ordinary
Drift Limit (Dir. 1, 2):	–, –
Risk Category:	I/II
Seismic Importance Factor, I_e:	–
Component Importance Factor, I_p:	–
Include Retrofit Information?	No

Structural Properties

Property	Dir. 1	Dir. 2
Base Shear Strength (g):	–	–
Yield Drift (%):	–	–
1^{st} Mode Period (T_1) (s):	–	–
2^{nd} Mode Period (T_2) (s):	–	–
3^{rd} Mode Period (T_3) (s):	–	–

Component Information

Do your stairs have seismic joints?	No
Is your ceiling laterally supported?	Yes
Is your lighting seismically rated?	Yes
Is your piping seismically rated?	Yes
Is your HVAC system seismically anchored?	Yes
Is your electrical equipment seismically rated?	Yes
Percent of Building Glazed:	–

Building Stability

Median Collapse Capacity:	–
Beta (Dispersion):	–

Responses

No responses provided

Repair Time Options

Factors Delaying Start of Repairs	
Inspection	Yes
Financing	Yes
Permitting	Yes
Engineering Mobilization	Yes
Contractor Mobilization	Yes
Mitigation Factors	
Inspector on Retainer	No
Engineer on Retainer	No
Engineer on Retainer	No
Funding Source	Private Loans

Expected Loss

Expected loss in percent of total building value

Shaking Intensity	Return Period	SEL (%)	SUL (%)
90% in 50 years	22 Years	2.9	4.7
50% in 30 years	43 Years	4.6	7.8
50% in 50 years	72 Years	7.6	13
50% in 75 years	108 Years	11	18
50% in 100 years	144 Years	15	23
20% in 50 years	224 Years	23	35
10% in 50 years	475 Years	39	67
DE	791 Years	54	87
5% in 50 years	975 Years	61	97
MCE_R	1956 Years	79	100
2% in 50 years	2475 Years	83	100

Repair Time

Median repair time, without impeding factors

Intensity	FEMA P-58 Parallel	FEMA P-58 Series	REDi Re-Occupancy	REDi Functional Recovery	REDi Full Recovery
90% in 50 years	4 days	6 days	0 days	9 days	9 days
50% in 30 years	7 days	13 days	1 days	2.2 weeks	2.2 weeks
50% in 50 years	14 days	4.0 weeks	6 days	3.2 weeks	3.2 weeks
50% in 75 years	4.1 weeks	7.2 weeks	2.2 weeks	4.5 weeks	4.5 weeks
50% in 100 years	6.6 weeks	2.6 months	3.9 weeks	6.1 weeks	6.1 weeks
20% in 50 years	2.5 months	4.1 months	6.9 weeks	2.1 months	2.1 months
10% in 50 years	4.0 months	8.0 months	3.4 months	3.8 months	3.8 months
DE	5.6 months	14 months	6.1 months	6.5 months	6.5 months
5% in 50 years	6.4 months	18 months	7.8 months	8.2 months	8.2 months
MCE_R	19 months	19 months	19 months	19 months	19 months
2% in 50 years	19 months	19 months	19 months	19 months	19 months

2 BASIS OF ANALYSIS

This analysis is based on the SP3-RiskModel of the Seismic Performance Prediction Program (SP3) software platform. The underlying analysis methods are based on the FEMA P-58 analytical method, which is a transparent and well documented method developed through a 15 year project (Applied Technology Council, 2018). This project leveraged the previous decades of academic research, funded by a $16 million investment by the Federal Emergency Management Agency (FEMA). In contrast to many risk assessment methods based on judgment and past earthquake experience, the FEMA P-58 and SP3 analysis are based on engineering-oriented risk evaluation methods.

3 DOCUMENTATION OF SITE AND BUILDING INPUT DATA

Project Name: 2 Franz-Pritzker
Model Name: Standard Analysis

3.1 Site Information

Address: 502 Portola Plaza, Los Angeles, CA, 90095
Latitude: 34.06989°
Longitude: -118.44125°

3.2 Building Information

Material Type:	Cast-in-Place Concrete
Number of Stories:	8
Total Building Square Footage:	84,211
Occupancy Type:	Commercial Office
Total Expected Building Replacement Value:	$22,110,841

4 SITE HAZARD INFORMATION

This section presents the site's seismic hazard information. The V_{S30} value is the shear wave velocity in the soil at a depth of 30 meters. This value and the associated site class are presented in Table 1.

Table 1. Site soil information

V_{S30} (m/s):	537.0
Site Class:	C

Table 2 and Figure 1 present the spectral acceleration information for this site. The spectral acceleration is a measure of how much force the building will attract in an earthquake. This amount of force is dependent on the intensity of the ground shaking (e.g. 10% in 50 years), as well as a dynamic property of the building known as the "fundamental period". Shorter buildings tend to have smaller fundamental periods and taller buildings tend to have larger fundamental periods. As indicated by Figure 1, smaller fundamental periods (with the exception of very short fundamental periods) will attract more force in an earthquake.

The Design Earthquake (DE) and Maximum Considered Earthquake (MCE) are based on the modern code maximum direction spectra and are converted to geometric mean for comparison.

Table 2. Geometric mean spectral acceleration values (in g)

Shaking Intensity	Return Period	PGA	$S_a(0.2s)$	$S_a(1.0s)$	$S_a(1.4s)$
90% in 50 years	22 years	0.08	0.18	0.05	0.04
50% in 30 years	43 years	0.13	0.30	0.09	0.07
50% in 50 years	72 years	0.18	0.44	0.13	0.10
50% in 75 years	108 years	0.23	0.56	0.18	0.13
50% in 100 years	144 years	0.28	0.67	0.21	0.16
20% in 50 years	224 years	0.35	0.84	0.28	0.21
10% in 50 years	475 years	0.50	1.22	0.43	0.32
DE	791 years	0.62	1.53	0.55	0.41
5% in 50 years	975 years	0.68	1.66	0.61	0.46
MCE_R	1956 years	0.87	2.18	0.82	0.62
2% in 50 years	2475 years	0.95	2.36	0.91	0.69

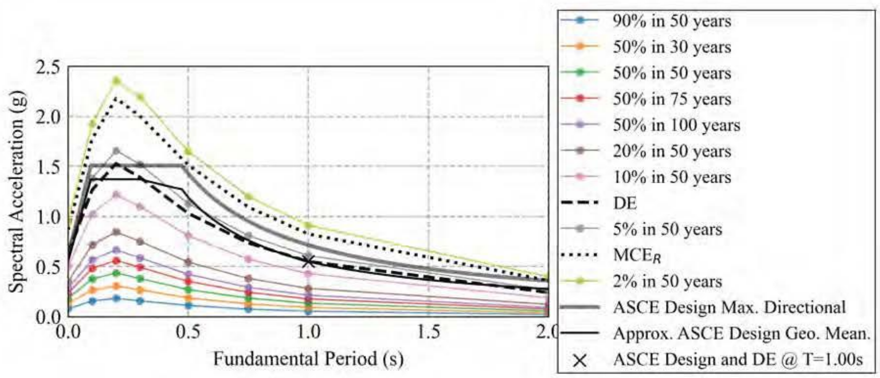

Figure 1. Hazard curves for this site. All curves are geometric mean unless otherwise stated.

5 BUILDING DESIGN SUMMARY FROM THE *SP3 BUILDING CODE DESIGN DATABASE*

5.1 Building Code Design Parameters

The seismic design parameters used to compute the seismic base shear coefficients for this building are presented in Table 3. These parameters are specific to the 1961 edition of the Uniform Building Code (International Conference of Building Officials, 1961).

Table 3. Code design parameters

(a) UBC 1961 structural system parameters

Parameter	Dir. 1	Dir. 2
C_d	1	1
k	1	1

(b) UBC 1961 site specific parameters

Parameter	Value
Z	1
Seismic Zone	3

5.2 Modern Building Code Design Parameters

For comparison to modern code, the modern code parameters are presented in Table 4.

Table 4. Modern code design parameters

(a) ASCE/SEI 7-2010 structural system parameters

Parameter	Dir. 1	Dir. 2
C_t	0.016	0.016
C_d	5.5	5.5
x	0.9	0.9
R	8	8
Ω_0	3	3

(b) ASCE/SEI 7-2010 site specific parameters

Parameter	Value
S_s	2.263
S_1	0.825
S_{ds}	1.508
S_{d1}	0.715
SDC	E
C_u	1.4
$\text{MCE}_{R,max}(g)$	0.747
$\text{MCE}_{R,geomean}(g)$	0.575
$\text{DE}_{max}(g)$	0.498
$\text{DE}_{geomean}(g)$	0.383

5.3 Structural Properties

This section summarizes the main structural properties of the building in each direction. These structural properties are used as inputs to the SP3 Structural Response Prediction Engine.

Table 5. Structural properties table

Parameter	Direction 1	Direction 2
General		
Structural System	RC: Space Frame	RC: Space Frame
Building Edge Length (ft)	102	102
Detailing Level	Ordinary	Ordinary
Strength		
Seismic Design Base Shear Ratio, C_s	0.034	0.034
Ultimate Base Shear Ratio, v_{ult}	0.121	0.121
Stiffness		
$T_{1,design}$ (s)	1.76	1.76
T_1 with structural overstiffness (s)	1.53	1.53
T_1 with gravity system (s)	1.52	1.52
T_1 with non-structural components (s)	1.44	1.44
T_1 empirical lower bound (s)	0.91	0.91
T_1 empirical upper bound (s)	1.80	1.80
T_1 Final (s)	1.44	1.44

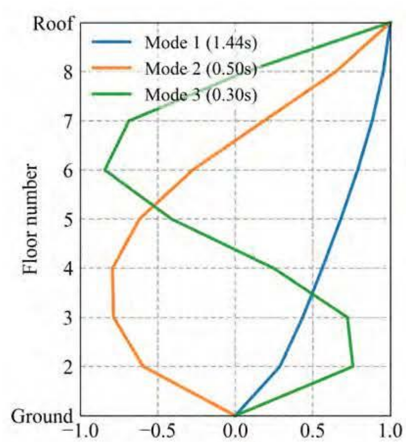

Figure 2. Mode shapes

6 BUILDING STABILITY

The FEMA P-154 collapse capacity score was calculated as follows using the "very high" seismicity level. The terminology used in this section is consistent with the FEMA P-154 methodology (Applied Technology Council, 2015a):

- P$[COL|MCE_R]_{P-154}$: the probability that the building will be in the HAZUS complete structural damage state when subjected to MCER shaking, times the collapse factor
- P$[COL|MCE_R]_{P-58}$: the probability that the building will be in the HAZUS complete structural damage state when subjected to MCER shaking, times the collapse factor
- Collapse Factor: expected ratio of collapsed area to total area given that the building is in the HAZUS Complete structural damage state

For a more in-depth explanation of "collapse," refer to Section 4.4.1.5 of FEMA P-155 Third Edition available here (Applied Technology Council, 2015b).

Table 6. Breakdown of FEMA P-154 score assignment

FEMA ID:	C1
Basic Score	1
Soil	0
Year	0
Plan Irregularity	0
Vertical Irregularity	-0.7
Risk Category* (Cat I/II)	0
Sum:	0.3
Minimum Allowed:	0.3
Score:	**0.3**
Dispersion (β):	0.7

*Non-standard property implemented by SP3

The FEMA P-154 probability of collapse at the MCE_R level event is then calculated as:

$$\begin{aligned} \text{P}[COL|MCE_R]_{P-154} &= 10^{-\text{score}} \\ &= 10^{-0.3} \qquad \text{(FEMA P-155 eqn. 4-1)} \\ &= 50.1\% \end{aligned}$$

Taking into account the fraction of floor area collapsed (1 in this case), the probability of collapse is:

$$\begin{aligned} \text{P}[COL|MCE_R]_{P-58} &= \text{P}[COL|MCE_R]_{P-154} \;/\; \text{Collapse Factor} \\ &= 50.1\% \;/\; 1 \\ &= 50.1\% \end{aligned}$$

The median collapse capacity is calculated as:

$$\begin{aligned} S_{a,\ collapse\ median,\ P-58} &= \exp\left(\ln(S_{a,MCE_R}) - \text{norminv}\left(P[COL|MCE_R]_{P-58}\right) \cdot \beta\right) \\ &= \exp\left(\ln(0.622g) - \text{norminv}\left(50.1\%\right) \cdot 0.7\right) \\ &= 0.621g \end{aligned}$$

where `norminv` is the inverse of the standard normal cumulative distribution function (CDF).

Figure 3 shows the collapse capacity cumulative distribution function used in the analysis.

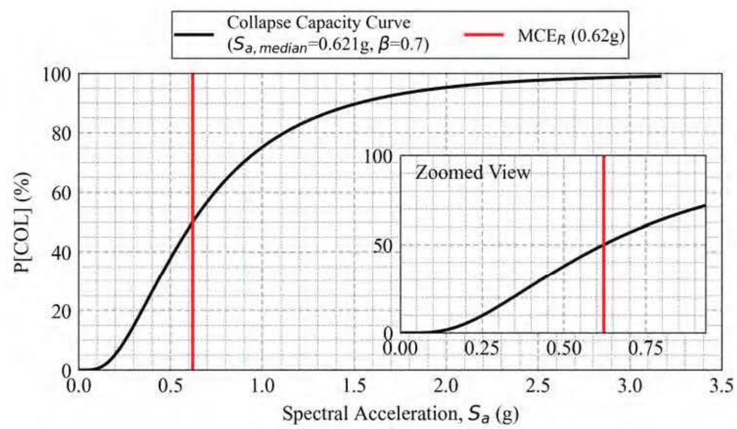

Figure 3. Cumulative distribution function for collapse capacity

7 STRUCTURAL RESPONSE PREDICTIONS FROM THE SP3 STRUCTURAL RESPONSE PREDICTION ENGINE

The SP3 Response Prediction Engine predicts the structural responses (typically providing 100 ground motions per intensity level); this is done by using a combination of three-mode elastic modal analysis, coupled with both elastic and inelastic response modifiers mined from the large SP3 Structural Responses Database (with over 4,000,000 response simulations, and growing). These response predictions track all of the important statistical information in the responses (mean, variability, and correlations); this enables a statistically robust vulnerability curve at the end of the risk assessment process.

7.1 Peak Story Drift

Peak interstory drift ratio is an important metric for both structural and non-structural components in the building. It measures how much the ceiling of a given story moves relative to the floor, normalized to the height of the story. The greater the interstory drift ratio, the greater the damage to the components on that level. Typical components that are damaged from interstory drift ratio are structural components (beams and columns), gypsum partition walls, and exterior cladding and glazing.

Table 7. Peak story drift demands are the same in both directions

Story	90% in 50 years	50% in 30 years	50% in 50 years	50% in 75 years	50% in 100 years	20% in 50 years	10% in 50 years	DE	5% in 50 years	MCE_R	2% in 50 years
8	0.04	0.08	0.11	0.15	0.18	0.23	0.32	0.40	0.44	0.58	0.64
7	0.06	0.11	0.16	0.21	0.26	0.33	0.45	0.57	0.63	0.83	0.92
6	0.08	0.13	0.19	0.26	0.31	0.40	0.55	0.69	0.76	1.01	1.11
5	0.08	0.14	0.21	0.29	0.35	0.45	0.61	0.76	0.84	1.12	1.23
4	0.09	0.15	0.23	0.31	0.37	0.48	0.65	0.82	0.90	1.20	1.32
3	0.09	0.16	0.24	0.32	0.39	0.50	0.68	0.85	0.94	1.25	1.37
2	0.11	0.19	0.28	0.37	0.45	0.58	0.79	1.00	1.10	1.46	1.61
1	0.20	0.35	0.51	0.68	0.83	1.07	1.46	1.83	2.02	2.69	2.95

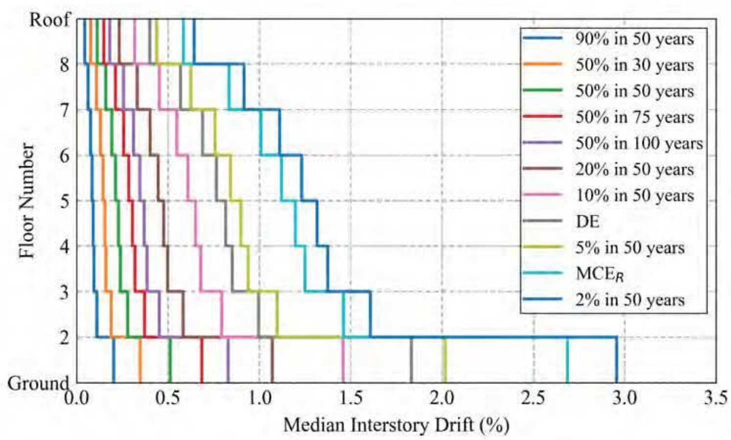

Figure 4. Peak story drift demands are the same in both directions

7.2 Peak Floor Acceleration

Peak floor acceleration is an an important metric for non-structural components in the building. Components such as piping, HVAC, and electrical switchgear are sensitive to the floor accelerations. High accelerations will typically damage a component itself or cause the component's anchorage to fail, both of which may require repair or replacement of the component.

Table 8. Peak floor acceleration demands are the same in both directions

Floor	90% in 50 years	50% in 30 years	50% in 50 years	50% in 75 years	50% in 100 years	20% in 50 years	10% in 50 years	DE	5% in 50 years	MCE_R	2% in 50 years
Roof	0.15	0.25	0.34	0.41	0.46	0.49	0.54	0.58	0.59	0.63	0.63
8	0.13	0.21	0.29	0.34	0.38	0.40	0.44	0.48	0.49	0.52	0.53
7	0.11	0.19	0.26	0.31	0.34	0.37	0.42	0.46	0.47	0.51	0.53
6	0.10	0.17	0.24	0.28	0.31	0.33	0.39	0.43	0.45	0.50	0.52
5	0.10	0.16	0.22	0.26	0.29	0.32	0.39	0.44	0.46	0.53	0.56
4	0.09	0.15	0.21	0.25	0.28	0.31	0.39	0.46	0.48	0.57	0.61
3	0.08	0.14	0.20	0.24	0.27	0.32	0.42	0.50	0.53	0.65	0.69
2	0.08	0.14	0.19	0.23	0.27	0.32	0.44	0.53	0.57	0.72	0.78
Ground	0.08	0.13	0.18	0.23	0.28	0.35	0.50	0.62	0.68	0.87	0.95

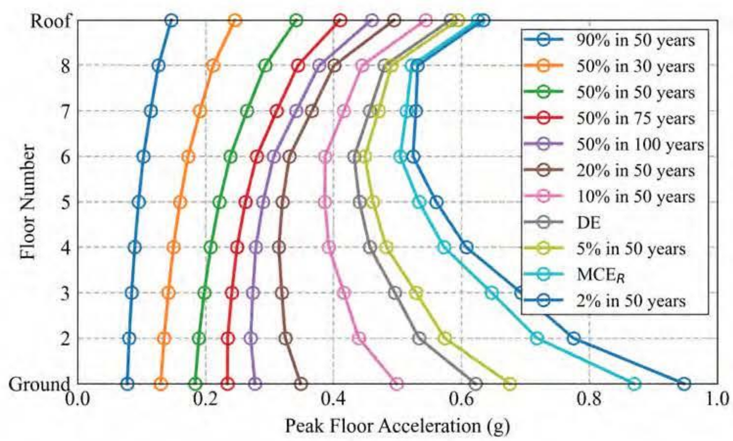

Figure 5. Peak floor acceleration demands are the same in both directions

7.3 Residual Story Drift

Residual drift is a metric that informs the need for structural repairs or building demolition (where excessive drifts are present). Residual drift ratio is a measure of how much the building is "leaning over" after the seismic event has ceased. A residual drift of 2% would indicate that the story is laterally displaced 2% of it's height, which equates to about 3.6 inches for a 15 foot tall story.

Table 9. Residual story drift demands are the same in both directions

Story	90% in 50 years	50% in 30 years	50% in 50 years	50% in 75 years	50% in 100 years	20% in 50 years	10% in 50 years	DE	5% in 50 years	MCE_R	2% in 50 years
8	0.00	0.00	0.00	0.00	0.00	0.00	0.00	0.00	0.00	0.00	0.00
7	0.00	0.00	0.00	0.00	0.00	0.00	0.00	0.00	0.00	0.01	0.02
6	0.00	0.00	0.00	0.00	0.00	0.00	0.00	0.00	0.00	0.03	0.04
5	0.00	0.00	0.00	0.00	0.00	0.00	0.00	0.00	0.01	0.05	0.06
4	0.00	0.00	0.00	0.00	0.00	0.00	0.00	0.01	0.02	0.06	0.07
3	0.00	0.00	0.00	0.00	0.00	0.00	0.00	0.01	0.02	0.06	0.08
2	0.00	0.00	0.00	0.00	0.00	0.00	0.01	0.03	0.04	0.09	0.11
1	0.00	0.00	0.00	0.00	0.01	0.04	0.09	0.14	0.16	0.24	0.28

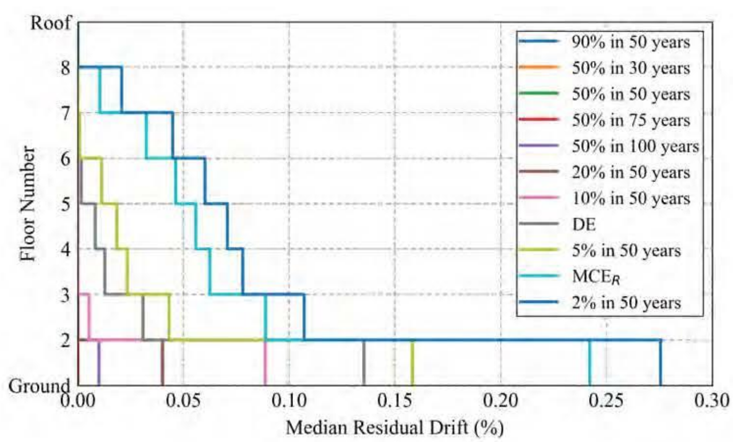

Figure 6. Residual story drift demands are the same in both directions

7.4 Maximum Residual Story Drift

Residual drift is a metric that informs the need for structural repairs or building demolition (where excessive drifts are present). A residual drift of 2% would indicate that the story is laterally displaced 2% of it's height, which equates to about 3.6 inches for a 15 foot tall story. Maximum residual drift is the maximum of the residual drifts on all levels. This is the value used to determine if the building is demolished due to excessive residual drift. Excessive drifts can be visually unsettling and prohibitively expensive (or even impossible) to "straighten" and repair the structural damage. Due to this, the building owner may decide to demolish and rebuild the building if the residual drifts are too large.

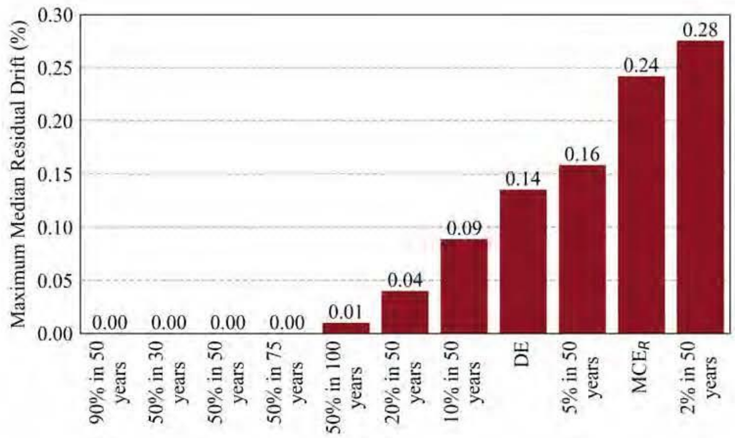

Figure 7. Maximum residual story drift demands are the same in both directions

8 REPAIR COSTS - BY LEVEL OF GROUND MOTION

8.1 Mean and 90^{th} Percentile Repair Costs (SEL and SUL)

The different metrics for repair cost are as follows:

- **Mean (SEL)**: ("Scenario Expected Loss") the average repair cost of the building repair/replacement.
- **Median**: there is a 50% probability that the repair cost will not exceed this value.
- **Fitted SUL**: Fitted value of "Scenario Upper Loss".
- **Counted 90^{th} Percentile**: there is a 90% probability that the repair cost will not exceed this value.

Table 10. Expected loss normalized by building cost

Intensity	PGA (g)	Mean (SEL) (%)	Fitted SUL (%)	Median (%)	Counted 90^{th} Percentile (%)
90% in 50 years	0.08	2.9	4.7	2.7	4.7
50% in 30 years	0.13	4.6	7.8	4.0	7.8
50% in 50 years	0.18	7.6	13	6.2	13
50% in 75 years	0.23	11	18	8.8	18
50% in 100 years	0.28	15	23	12	23
20% in 50 years	0.35	23	35	16	35
10% in 50 years	0.50	39	67	27	100
DE	0.62	54	87	42	100
5% in 50 years	0.68	61	97	53	100
MCE_R	0.87	79	100	100	100
2% in 50 years	0.95	83	100	100	100

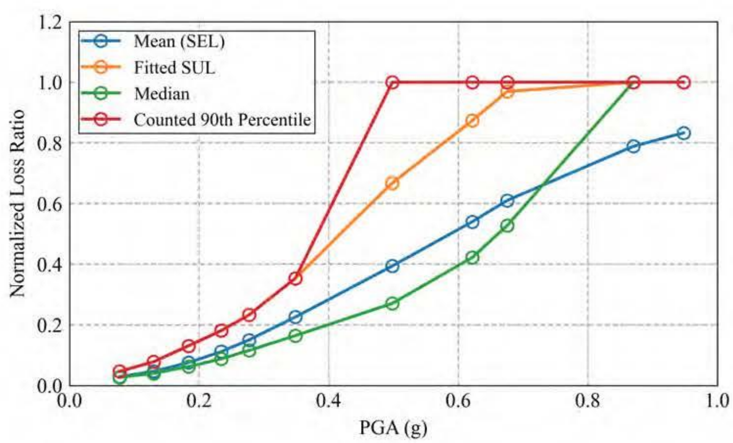

Figure 8. Loss metrics across all intensity levels analyzed

9 REPAIR COST BREAKDOWN BY BUILDING COMPONENTS

9.1 Categories for Repair Cost Breakdowns

Repair costs are binned into eight categories as follows:

- **Collapse**: building demolition and replacement following a collapse.
- **Residual**: building demolition and replacement following unacceptable residual drifts.
- **Structural**: components of the lateral force resisting system or gravity system (e.g. beam column connections, link beams, shear wall, shear tabs, etc.).
- **Partitions**: partition wall components (e.g. wood or metal stud gypsum full height partitions).
- **Exterior**: components placed on the exterior of the building (e.g. cladding, glazing, etc.).
- **Interior**: non-structural components on the interior of the building (e.g. raised access floors, ceilings, lighting).
- **HVAC**: HVAC and plumbing components (e.g. water piping and bracing, sanitary piping, ducting, boilers etc.).
- **Other**: components not included in the categories above (e.g. elevators, user defined components, fire protection components).

9.2 Repair Cost Breakdown for Various Ground Motion Levels

Table 11. Expected mean loss per component group (in percent)

Intensity	Total	Collapse	Structural	Exterior	Residual	Other	Partitions	HVAC	Interior
90% in 50 years	2.9	0.0	0.0	0.2	0.0	1.5	0.0	1.1	0.0
50% in 30 years	4.6	0.1	0.3	1.1	0.0	1.8	0.1	1.3	0.0
50% in 50 years	7.6	0.4	1.0	2.4	0.0	2.0	0.1	1.5	0.1
50% in 75 years	11	1.4	2.2	3.6	0.0	2.1	0.2	1.5	0.2
50% in 100 years	15	2.6	3.7	4.4	0.0	2.2	0.3	1.5	0.2
20% in 50 years	23	6.2	6.5	5.4	0.0	2.3	0.5	1.5	0.3
10% in 50 years	39	18	11	6.6	0.0	2.1	0.7	1.3	0.4
DE	54	28	14	6.9	0.3	1.9	0.7	1.2	0.5
5% in 50 years	61	33	16	6.9	0.7	1.8	0.8	1.1	0.5
MCE_R	79	50	18	6.3	1.3	1.4	0.8	0.8	0.5
2% in 50 years	83	56	17	5.9	2.0	1.2	0.7	0.7	0.5

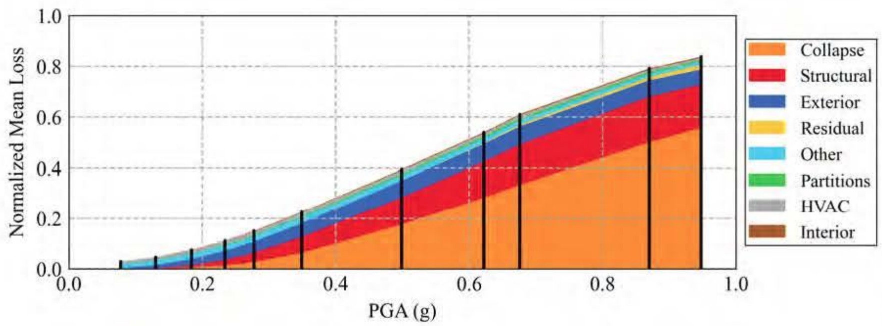

Figure 9. Contribution of building components to mean loss ratio

9.3 Repair Cost Breakdown for Expected Annual Loss

The expected annual loss for this building is $106,405.

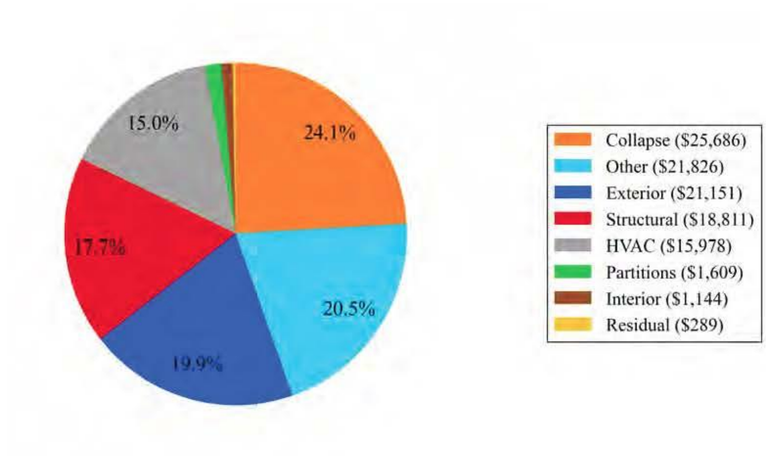

Figure 10. Annualized loss breakdown

10 REPAIR TIME AND BUILDING CLOSURE TIME

The building repair times are computed from the REDi Rating System methodology (Almufiti & Willford, 2013). These are the preferred method to compare building repair time because these include detailed repair schedules as part of the calculation process.

- **Re-Occupancy**: This is the time after which the building is deemed safe enough to be used for shelter.
- **Functional Recovery**: This is time required to establish re-occupancy and regain the facility's primary function. This is what is typically used for assessing building closure time.
- **Full Recovery**: This is the time required to restore the building to its original pre-earthquake condition.

For comparison, the methods of calculating building repair time from the FEMA P-58 methodology are as follows. These are typically not used to estimate building closure time.

- **Series**: Repair activities are limited to one floor at a time
- **Parallel**: All floors are repaired at the same time

For a design level or 10% in 50 year event, the REDi methodology is also calibrated to include "impedance factors" associated with the following processes:

- Post-earthquake Inspection
- Engineering Mobilization and Review/Re-design
- Financing
- Contractor Mobilization and Bid Process
- Permitting

These capture the time required to start the repairs, since beginning repairs immediately after an earthquake may not be realistic. **With these impedance factors, the median functional recovery time is 14 months.**

Table 12. Median repair time, without impeding factors

Intensity	FEMA P-58 Parallel	FEMA P-58 Series	REDi Re-Occupancy	REDi Functional Recovery	REDi Full Recovery
90% in 50 years	4 days	6 days	0 days	9 days	9 days
50% in 30 years	7 days	13 days	1 days	2.2 weeks	2.2 weeks
50% in 50 years	14 days	4.0 weeks	6 days	3.2 weeks	3.2 weeks
50% in 75 years	4.1 weeks	7.2 weeks	2.2 weeks	4.5 weeks	4.5 weeks
50% in 100 years	6.6 weeks	2.6 months	3.9 weeks	6.1 weeks	6.1 weeks
20% in 50 years	2.5 months	4.1 months	6.9 weeks	2.1 months	2.1 months
10% in 50 years	4.0 months	8.0 months	3.4 months	3.8 months	3.8 months
DE	5.6 months	14 months	6.1 months	6.5 months	6.5 months
5% in 50 years	6.4 months	18 months	7.8 months	8.2 months	8.2 months
MCE_R	19 months	19 months	19 months	19 months	19 months
2% in 50 years	19 months	19 months	19 months	19 months	19 months

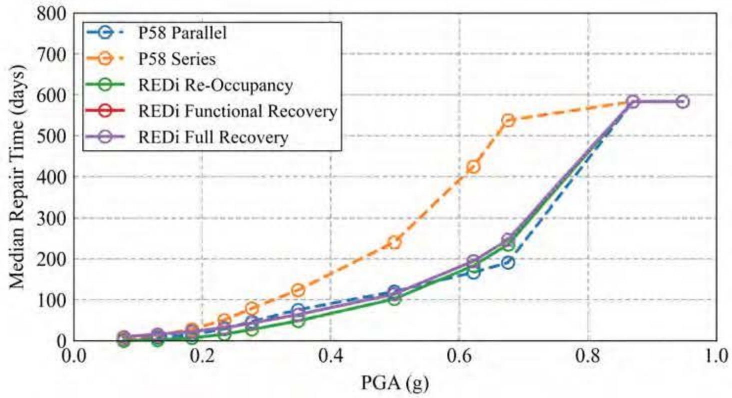

Figure 11. Median repair time, without impeding factors

11 JUSTIFICATION OF SECONDARY MODIFIERS

No justification of secondary inputs was provided.

12 DISCLAIMER

REFERENCES

Almufiti, Ibrahim, & Willford, Michael. 2013. *REDi Rating System*. Arup.

Applied Technology Council. 2015a. *FEMA P-154: Rapid Visual Screening of Buildings for Potential Seismic Hazards: A Handbook*.

Applied Technology Council. 2015b. *FEMA P-155: Rapid Visual Screening of Buildings for Potential Seismic Hazards: Supporting Documentation*.

Applied Technology Council. 2018. *FEMA P-58: Seismic Perfromance Assessment of Buildings*.

International Conference of Building Officials. 1961. *Uniform Building Code 1961 Edition*. International Conference of Building Officials.

H4. Detailed Analysis – Existing Franz (No Test Data)

CONTENTS

1 SUMMARY OF INPUTS AND RISK RESULTS

Risk Model Inputs

Primary

Project Name:	3 Franz-Pritzker
Model Name:	S.F. (w/o test data) reduced top joints
Building Type:	RC: Space Frame
Year of Construction:	1967
Number of Stories:	8
Occupancy:	Commercial Office
Address: 502 Portola Plaza Los Angeles, CA, 90095	
Latitude:	34.06985°
Longitude:	-118.44125°

Analysis Options

Include Collapse in Analysis:	Yes
Consider Residual Drift:	Yes

Building Layout Information

Cost per Square Foot:	–
Total Square Feet:	84,211
Aspect Ratio:	–
First Story Height (ft):	14
Upper Story Heights (ft):	13
Vertical Irregularity:	Extreme
Plan Irregularity:	–

Ground Motion and Soil Information

Site Class:	C
Site Hazard:	SP3 Default

Building Design Info

Level of Detailing (Dir. 1, 2):	Ordinary, Ordinary
Drift Limit (Dir. 1, 2):	2.000%, 2.000%
Risk Category:	I/II
Seismic Importance Factor, I_e:	1
Component Importance Factor, I_p:	–
Include Retrofit Information?	No

Structural Properties

Property	Dir. 1	Dir. 2
Base Shear Strength (g):	0.128	0.128
Yield Drift (%):	0.69	0.69
1^{st} Mode Period (T_1) (s):	1.35	1.35
2^{nd} Mode Period (T_2) (s):	–	–
3^{rd} Mode Period (T_3) (s):	–	–

Component Information

Do your stairs have seismic joints?	No
Is your ceiling laterally supported?	Yes
Is your lighting seismically rated?	Yes
Is your piping seismically rated?	Yes
Is your HVAC system seismically anchored?	Yes
Is your electrical equipment seismically rated?	Yes
Percent of Building Glazed:	–

Building Stability

Median Collapse Capacity:	–
Beta (Dispersion):	–

Responses

No responses provided

Repair Time Options

Factors Delaying Start of Repairs	
Inspection	Yes
Financing	Yes
Permitting	Yes
Engineering Mobilization	Yes
Contractor Mobilization	Yes
Mitigation Factors	
Inspector on Retainer	No
Engineer on Retainer	No
Engineer on Retainer	No
Funding Source	Private Loans

Expected Loss

Expected loss in percent of total building value

Shaking Intensity	Return Period	SEL (%)	SUL (%)
90% in 50 years	22 Years	5.0	9.1
50% in 30 years	43 Years	11	20
50% in 50 years	72 Years	17	29
50% in 75 years	108 Years	25	37
50% in 100 years	144 Years	30	43
20% in 50 years	224 Years	39	58
10% in 50 years	475 Years	55	89
DE	791 Years	68	100
5% in 50 years	975 Years	73	100
MCE_R	1956 Years	87	100
2% in 50 years	2475 Years	90	100

Repair Time

Median repair time, without impeding factors

Intensity	FEMA P-58 Parallel	FEMA P-58 Series	REDi Re-Occupancy	REDi Functional Recovery	REDi Full Recovery
90% in 50 years	8 days	2.4 weeks	0 days	14 days	14 days
50% in 30 years	3.2 weeks	2.2 months	3.7 weeks	5.7 weeks	5.7 weeks
50% in 50 years	5.8 weeks	5.0 months	2.2 months	2.6 months	2.6 months
50% in 75 years	7.9 weeks	7.9 months	3.5 months	3.9 months	3.9 months
50% in 100 years	2.1 months	9.5 months	4.3 months	4.7 months	4.7 months
20% in 50 years	2.6 months	12 months	5.6 months	6.0 months	6.0 months
10% in 50 years	3.5 months	17 months	7.8 months	8.2 months	8.2 months
DE	4.8 months	19 months	11 months	11 months	11 months
5% in 50 years	5.4 months	19 months	12 months	13 months	13 months
MCE_R	19 months	19 months	19 months	19 months	19 months
2% in 50 years	19 months	19 months	19 months	19 months	19 months

2 BASIS OF ANALYSIS

This analysis is based on the SP3-RiskModel of the Seismic Performance Prediction Program (SP3) software platform. The underlying analysis methods are based on the FEMA P-58 analytical method, which is a transparent and well documented method developed through a 15 year project (Applied Technology Council, 2018). This project leveraged the previous decades of academic research, funded by a $16 million investment by the Federal Emergency Management Agency (FEMA). In contrast to many risk assessment methods based on judgment and past earthquake experience, the FEMA P-58 and SP3 analysis are based on engineering-oriented risk evaluation methods.

3 DOCUMENTATION OF SITE AND BUILDING INPUT DATA

Project Name: 3 Franz-Pritzker
Model Name: S.F. (w/o test data) reduced top joints

3.1 Site Information

Address: 502 Portola Plaza, Los Angeles, CA, 90095
Latitude: 34.06985°
Longitude: -118.44125°

3.2 Building Information

Material Type:	Cast-in-Place Concrete
Number of Stories:	8
Total Building Square Footage:	84,211
Occupancy Type:	Commercial Office
Total Expected Building Replacement Value:	$22,110,841

4 SITE HAZARD INFORMATION

This section presents the site's seismic hazard information. The V_{S30} value is the shear wave velocity in the soil at a depth of 30 meters. This value and the associated site class are presented in Table 1.

Table 1. Site soil information

V_{S30} (m/s):	537.0
Site Class:	C

Table 2 and Figure 1 present the spectral acceleration information for this site. The spectral acceleration is a measure of how much force the building will attract in an earthquake. This amount of force is dependent on the intensity of the ground shaking (e.g. 10% in 50 years), as well as a dynamic property of the building known as the "fundamental period". Shorter buildings tend to have smaller fundamental periods and taller buildings tend to have larger fundamental periods. As indicated by Figure 1, smaller fundamental periods (with the exception of very short fundamental periods) will attract more force in an earthquake.

The Design Earthquake (DE) and Maximum Considered Earthquake (MCE) are based on the modern code maximum direction spectra and are converted to geometric mean for comparison.

Table 2. Geometric mean spectral acceleration values (in g)

Shaking Intensity	Return Period	PGA	$S_a(0.2s)$	$S_a(1.0s)$	$S_a(1.4s)$
90% in 50 years	22 years	0.08	0.18	0.05	0.04
50% in 30 years	43 years	0.13	0.30	0.09	0.07
50% in 50 years	72 years	0.18	0.44	0.13	0.11
50% in 75 years	108 years	0.23	0.56	0.18	0.14
50% in 100 years	144 years	0.28	0.67	0.21	0.17
20% in 50 years	224 years	0.35	0.84	0.28	0.23
10% in 50 years	475 years	0.50	1.22	0.43	0.34
DE	791 years	0.62	1.53	0.55	0.44
5% in 50 years	975 years	0.68	1.66	0.61	0.49
MCE_R	1956 years	0.87	2.18	0.82	0.66
2% in 50 years	2475 years	0.95	2.36	0.91	0.73

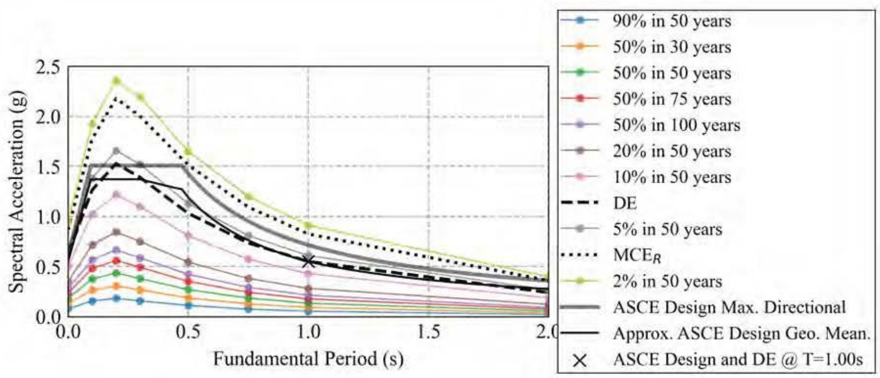

Figure 1. Hazard curves for this site. All curves are geometric mean unless otherwise stated.

5 BUILDING DESIGN SUMMARY FROM THE *SP3 BUILDING CODE DESIGN DATABASE*

5.1 Building Code Design Parameters

The seismic design parameters used to compute the seismic base shear coefficients for this building are presented in Table 3. These parameters are specific to the 1961 edition of the Uniform Building Code (International Conference of Building Officials, 1961).

Table 3. Code design parameters

(a) UBC 1961 structural system parameters

Parameter	Dir. 1	Dir. 2
C_d	1	1
k	1	1

(b) UBC 1961 site specific parameters

Parameter	Value
Z	1
Seismic Zone	3

5.2 Modern Building Code Design Parameters

For comparison to modern code, the modern code parameters are presented in Table 4.

Table 4. Modern code design parameters

(a) ASCE/SEI 7-2010 structural system parameters

Parameter	Dir. 1	Dir. 2
C_t	0.016	0.016
C_d	5.5	5.5
x	0.9	0.9
R	8	8
Ω_0	3	3

(b) ASCE/SEI 7-2010 site specific parameters

Parameter	Value
S_s	2.263
S_1	0.825
S_{ds}	1.508
S_{d1}	0.715
SDC	E
C_u	1.4
$\text{MCE}_{R,max}(g)$	0.794
$\text{MCE}_{R,geomean}(g)$	0.611
$\text{DE}_{max}(g)$	0.529
$\text{DE}_{geomean}(g)$	0.407

5.3 Structural Properties

This section summarizes the main structural properties of the building in each direction. These structural properties are used as inputs to the SP3 Structural Response Prediction Engine.

Table 5. Structural properties table

Parameter	Direction 1	Direction 2
General		
Structural System	RC: Space Frame	RC: Space Frame
Building Edge Length (ft)	102	102
Detailing Level	Ordinary	Ordinary
Strength		
Seismic Design Base Shear Ratio, C_s	0.034	0.034
Ultimate Base Shear Ratio, v_{ult}	0.128*	0.128*
Stiffness		
$T_{1,design}$ (s)	1.76	1.76
T_1 with structural overstiffness (s)	1.53	1.53
T_1 with gravity system (s)	1.52	1.52
T_1 with non-structural components (s)	1.44	1.44
T_1 empirical lower bound (s)	0.91	0.91
T_1 empirical upper bound (s)	1.80	1.80
T_1 Final (s)	1.35	1.35

*User defined, not SP3 default

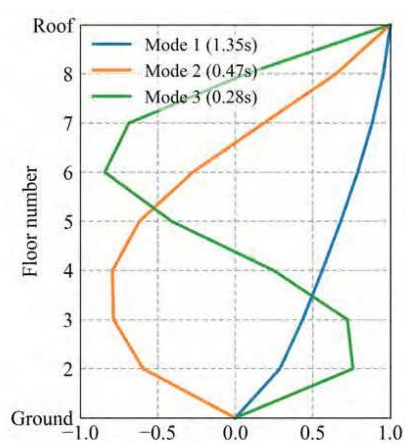

Figure 2. Mode shapes

6 BUILDING STABILITY

The FEMA P-154 collapse capacity score was calculated as follows using the "very high" seismicity level. The terminology used in this section is consistent with the FEMA P-154 methodology (Applied Technology Council, 2015a):

- P$[COL|MCE_R]_{P-154}$: the probability that the building will be in the HAZUS complete structural damage state when subjected to MCER shaking, times the collapse factor
- P$[COL|MCE_R]_{P-58}$: the probability that the building will be in the HAZUS complete structural damage state when subjected to MCER shaking, times the collapse factor
- Collapse Factor: expected ratio of collapsed area to total area given that the building is in the HAZUS Complete structural damage state

For a more in-depth explanation of "collapse," refer to Section 4.4.1.5 of FEMA P-155 Third Edition available here (Applied Technology Council, 2015b).

Table 6. Breakdown of FEMA P-154 score assignment

FEMA ID:	C1
Basic Score	1
Soil	0
Year	0
Plan Irregularity	0
Vertical Irregularity	-0.7
Risk Category* (Cat I/II)	0
Sum:	0.3
Minimum Allowed:	0.3
Score:	**0.3**
Dispersion (β):	0.7

*Non-standard property implemented by SP3

The FEMA P-154 probability of collapse at the MCE_R level event is then calculated as:

$$\begin{aligned} \text{P}[COL|MCE_R]_{P-154} &= 10^{-\text{score}} \\ &= 10^{-0.3} \\ &= 50.1\% \end{aligned} \qquad \text{(FEMA P-155 eqn. 4-1)}$$

Taking into account the fraction of floor area collapsed (1 in this case), the probability of collapse is:

$$\begin{aligned} \text{P}[COL|MCE_R]_{P-58} &= \text{P}[COL|MCE_R]_{P-154} \text{ / Collapse Factor} \\ &= 50.1\% / 1 \\ &= 50.1\% \end{aligned}$$

The median collapse capacity is calculated as:

$$\begin{aligned} S_{a,\ collapse\ median,\ P-58} &= \exp\left(\ln(S_{a,MCE_R}) - \text{norminv}\left(P[COL|MCE_R]_{P-58}\right) \cdot \beta\right) \\ &= \exp\left(\ln(0.662g) - \text{norminv}\left(50.1\%\right) \cdot 0.7\right) \\ &= 0.660g \end{aligned}$$

where `norminv` is the inverse of the standard normal cumulative distribution function (CDF).

Figure 3 shows the collapse capacity cumulative distribution function used in the analysis.

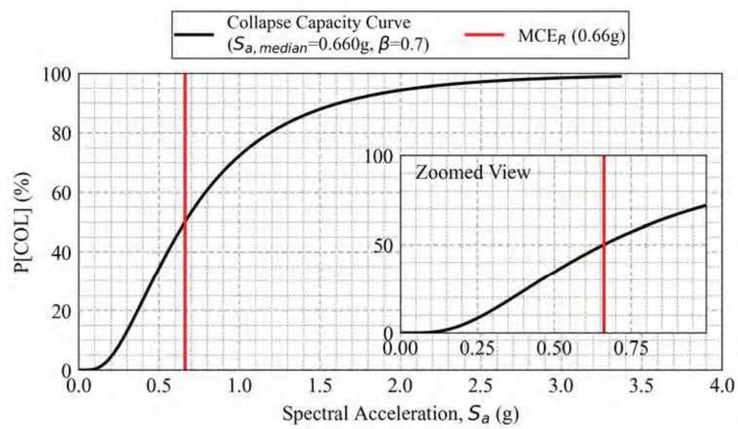

Figure 3. Cumulative distribution function for collapse capacity

7 STRUCTURAL RESPONSE PREDICTIONS FROM THE SP3 STRUCTURAL RESPONSE PREDICTION ENGINE

The SP3 Response Prediction Engine predicts the structural responses (typically providing 100 ground motions per intensity level); this is done by using a combination of three-mode elastic modal analysis, coupled with both elastic and inelastic response modifiers mined from the large SP3 Structural Responses Database (with over 4,000,000 response simulations, and growing). These response predictions track all of the important statistical information in the responses (mean, variability, and correlations); this enables a statistically robust vulnerability curve at the end of the risk assessment process.

7.1 Peak Story Drift

Peak interstory drift ratio is an important metric for both structural and non-structural components in the building. It measures how much the ceiling of a given story moves relative to the floor, normalized to the height of the story. The greater the interstory drift ratio, the greater the damage to the components on that level. Typical components that are damaged from interstory drift ratio are structural components (beams and columns), gypsum partition walls, and exterior cladding and glazing.

Table 7. Peak story drift demands are the same in both directions

Story	90% in 50 years	50% in 30 years	50% in 50 years	50% in 75 years	50% in 100 years	20% in 50 years	10% in 50 years	DE	5% in 50 years	MCE_R	2% in 50 years
8	0.04	0.07	0.10	0.14	0.17	0.22	0.30	0.37	0.41	0.54	0.60
7	0.06	0.10	0.15	0.20	0.24	0.31	0.42	0.53	0.59	0.78	0.86
6	0.07	0.12	0.18	0.24	0.29	0.38	0.51	0.65	0.71	0.95	1.04
5	0.08	0.14	0.20	0.27	0.33	0.42	0.57	0.72	0.79	1.05	1.16
4	0.09	0.15	0.22	0.29	0.35	0.45	0.61	0.77	0.85	1.13	1.24
3	0.09	0.15	0.23	0.30	0.36	0.47	0.64	0.80	0.88	1.18	1.30
2	0.10	0.18	0.26	0.35	0.43	0.55	0.75	0.94	1.03	1.38	1.51
1	0.19	0.33	0.48	0.65	0.78	1.01	1.37	1.73	1.90	2.53	2.78

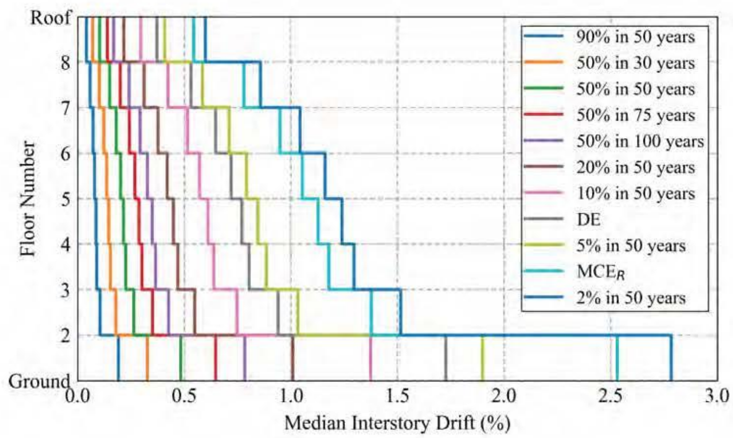

Figure 4. Peak story drift demands are the same in both directions

7.2 Peak Floor Acceleration

Peak floor acceleration is an an important metric for non-structural components in the building. Components such as piping, HVAC, and electrical switchgear are sensitive to the floor accelerations. High accelerations will typically damage a component itself or cause the component's anchorage to fail, both of which may require repair or replacement of the component.

Table 8. Peak floor acceleration demands are the same in both directions

Floor	90% in 50 years	50% in 30 years	50% in 50 years	50% in 75 years	50% in 100 years	20% in 50 years	10% in 50 years	DE	5% in 50 years	MCE_R	2% in 50 years
Roof	0.15	0.25	0.36	0.43	0.50	0.54	0.59	0.64	0.65	0.68	0.69
8	0.13	0.23	0.31	0.37	0.41	0.43	0.48	0.52	0.53	0.57	0.58
7	0.12	0.20	0.28	0.33	0.37	0.39	0.45	0.49	0.51	0.55	0.57
6	0.11	0.18	0.25	0.30	0.32	0.35	0.41	0.46	0.47	0.53	0.55
5	0.10	0.17	0.23	0.28	0.30	0.34	0.41	0.46	0.49	0.56	0.59
4	0.09	0.16	0.22	0.26	0.29	0.33	0.41	0.48	0.50	0.60	0.63
3	0.09	0.15	0.20	0.25	0.28	0.33	0.43	0.51	0.55	0.67	0.71
2	0.08	0.14	0.20	0.24	0.28	0.33	0.45	0.55	0.59	0.74	0.80
Ground	0.08	0.13	0.18	0.23	0.28	0.35	0.50	0.62	0.68	0.87	0.95

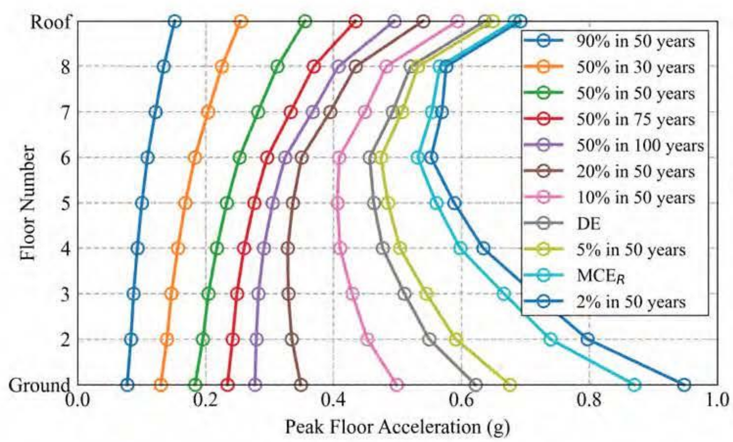

Figure 5. Peak floor acceleration demands are the same in both directions

7.3 Residual Story Drift

Residual drift is a metric that informs the need for structural repairs or building demolition (where excessive drifts are present). Residual drift ratio is a measure of how much the building is "leaning over" after the seismic event has ceased. A residual drift of 2% would indicate that the story is laterally displaced 2% of it's height, which equates to about 3.6 inches for a 15 foot tall story.

Table 9. Residual story drift demands are the same in both directions

Story	90% in 50 years	50% in 30 years	50% in 50 years	50% in 75 years	50% in 100 years	20% in 50 years	10% in 50 years	DE	5% in 50 years	MCE_R	2% in 50 years
8	0.00	0.00	0.00	0.00	0.00	0.00	0.00	0.00	0.00	0.00	0.00
7	0.00	0.00	0.00	0.00	0.00	0.00	0.00	0.00	0.00	0.01	0.02
6	0.00	0.00	0.00	0.00	0.00	0.00	0.00	0.00	0.00	0.03	0.04
5	0.00	0.00	0.00	0.00	0.00	0.00	0.00	0.00	0.01	0.05	0.06
4	0.00	0.00	0.00	0.00	0.00	0.00	0.00	0.01	0.02	0.05	0.07
3	0.00	0.00	0.00	0.00	0.00	0.00	0.00	0.01	0.02	0.06	0.08
2	0.00	0.00	0.00	0.00	0.00	0.00	0.01	0.03	0.04	0.09	0.10
1	0.00	0.00	0.00	0.00	0.01	0.04	0.09	0.13	0.15	0.23	0.26

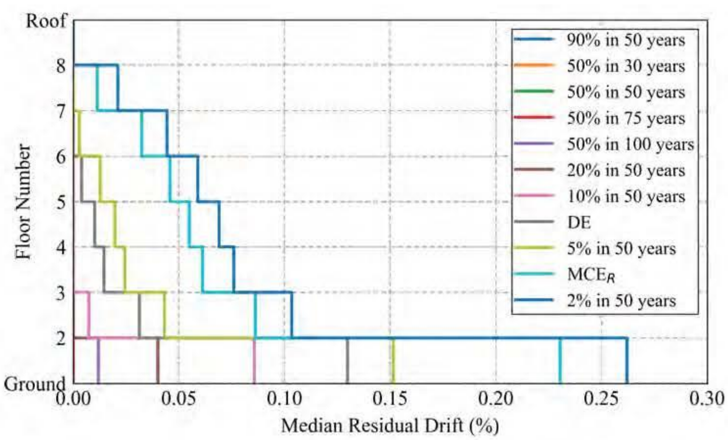

Figure 6. Residual story drift demands are the same in both directions

7.4 Maximum Residual Story Drift

Residual drift is a metric that informs the need for structural repairs or building demolition (where excessive drifts are present). A residual drift of 2% would indicate that the story is laterally displaced 2% of it's height, which equates to about 3.6 inches for a 15 foot tall story. Maximum residual drift is the maximum of the residual drifts on all levels. This is the value used to determine if the building is demolished due to excessive residual drift. Excessive drifts can be visually unsettling and prohibitively expensive (or even impossible) to "straighten" and repair the structural damage. Due to this, the building owner may decide to demolish and rebuild the building if the residual drifts are too large.

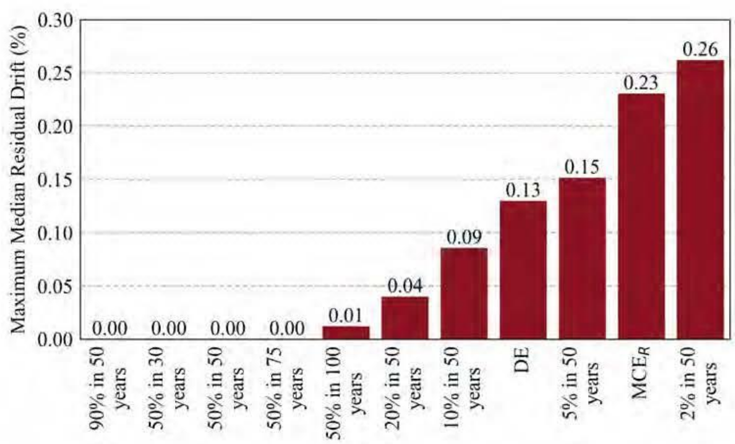

Figure 7. Maximum residual story drift demands are the same in both directions

8 REPAIR COSTS - BY LEVEL OF GROUND MOTION

8.1 Mean and 90^{th} Percentile Repair Costs (SEL and SUL)

The different metrics for repair cost are as follows:

- **Mean (SEL)**: ("Scenario Expected Loss") the average repair cost of the building repair/replacement.
- **Median**: there is a 50% probability that the repair cost will not exceed this value.
- **Fitted SUL**: Fitted value of "Scenario Upper Loss".
- **Counted 90^{th} Percentile**: there is a 90% probability that the repair cost will not exceed this value.

Table 10. Expected loss normalized by building cost

Intensity	PGA (g)	Mean (SEL) (%)	Fitted SUL (%)	Median (%)	Counted 90^{th} Percentile (%)
90% in 50 years	0.08	5.0	9.1	4.2	9.1
50% in 30 years	0.13	11	20	9.0	20
50% in 50 years	0.18	17	29	16	29
50% in 75 years	0.23	25	37	23	37
50% in 100 years	0.28	30	43	27	43
20% in 50 years	0.35	39	58	35	58
10% in 50 years	0.50	55	89	48	100
DE	0.62	68	100	63	100
5% in 50 years	0.68	73	100	72	100
MCE_R	0.87	87	100	100	100
2% in 50 years	0.95	90	100	100	100

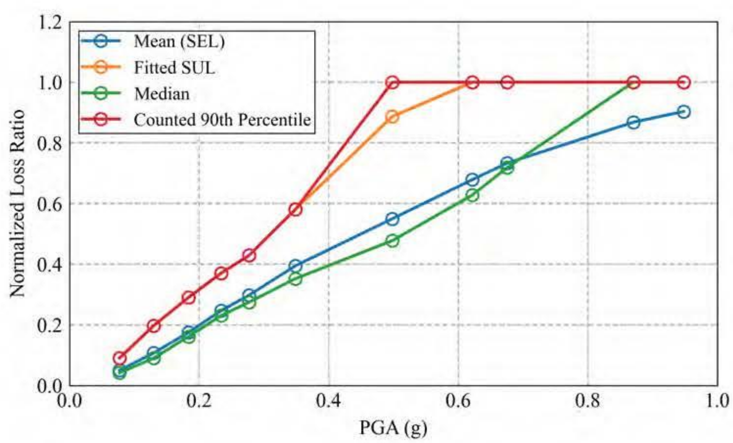

Figure 8. Loss metrics across all intensity levels analyzed

9 REPAIR COST BREAKDOWN BY BUILDING COMPONENTS

9.1 Categories for Repair Cost Breakdowns

Repair costs are binned into eight categories as follows:

- **Collapse**: building demolition and replacement following a collapse.
- **Residual**: building demolition and replacement following unacceptable residual drifts.
- **Structural**: components of the lateral force resisting system or gravity system (e.g. beam column connections, link beams, shear wall, shear tabs, etc.).
- **Partitions**: partition wall components (e.g. wood or metal stud gypsum full height partitions).
- **Exterior**: components placed on the exterior of the building (e.g. cladding, glazing, etc.).
- **Interior**: non-structural components on the interior of the building (e.g. raised access floors, ceilings, lighting).
- **HVAC**: HVAC and plumbing components (e.g. water piping and bracing, sanitary piping, ducting, boilers etc.).
- **Other**: components not included in the categories above (e.g. elevators, user defined components, fire protection components).

9.2 Repair Cost Breakdown for Various Ground Motion Levels

Table 11. Expected mean loss per component group (in percent)

Intensity	Total	Collapse	Structural	Exterior	Residual	Other	HVAC	Partitions	Interior
90% in 50 years	5.0	0.0	1.8	0.3	0.0	1.5	1.5	0.0	0.0
50% in 30 years	11	0.1	5.8	1.3	0.0	1.8	1.7	0.1	0.1
50% in 50 years	17	0.4	10	2.6	0.0	2.0	1.8	0.1	0.1
50% in 75 years	25	1.4	15	3.9	0.0	2.1	1.8	0.2	0.2
50% in 100 years	30	2.7	18	4.6	0.0	2.2	1.8	0.3	0.3
20% in 50 years	39	6.2	22	6.0	0.0	2.3	1.8	0.4	0.4
10% in 50 years	55	18	26	6.9	0.0	2.1	1.6	0.6	0.5
DE	68	28	28	7.5	0.1	1.9	1.4	0.7	0.6
5% in 50 years	73	33	28	7.4	0.4	1.8	1.3	0.7	0.6
MCE_R	87	50	26	6.6	1.7	1.3	1.0	0.7	0.6
2% in 50 years	90	56	24	6.2	2.4	1.2	0.8	0.7	0.5

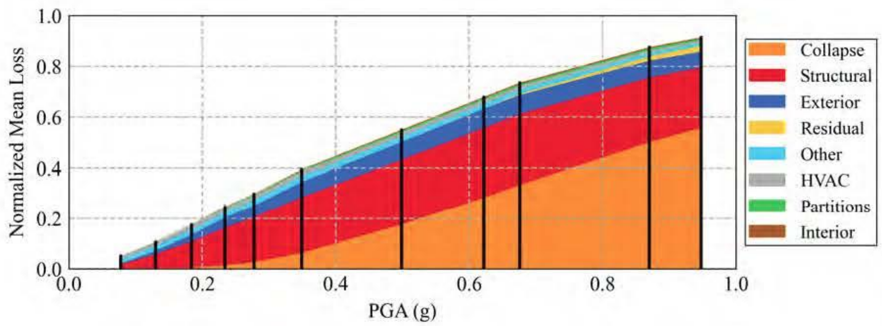

Figure 9. Contribution of building components to mean loss ratio

9.3 Repair Cost Breakdown for Expected Annual Loss

The expected annual loss for this building is $189,689.

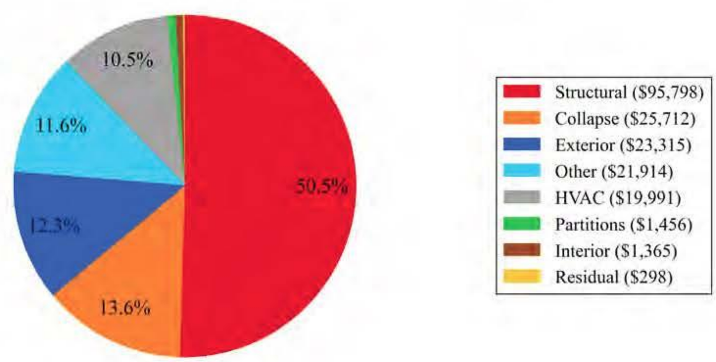

Figure 10. Annualized loss breakdown

10 REPAIR TIME AND BUILDING CLOSURE TIME

The building repair times are computed from the REDi Rating System methodology (Almufti & Willford, 2013). These are the preferred method to compare building repair time because these include detailed repair schedules as part of the calculation process.

- **Re-Occupancy**: This is the time after which the building is deemed safe enough to be used for shelter.
- **Functional Recovery**: This is time required to establish re-occupancy and regain the facility's primary function. This is what is typically used for assessing building closure time.
- **Full Recovery**: This is the time required to restore the building to its original pre-earthquake condition.

For comparison, the methods of calculating building repair time from the FEMA P-58 methodology are as follows. These are typically not used to estimate building closure time.

- **Series**: Repair activities are limited to one floor at a time
- **Parallel**: All floors are repaired at the same time

For a design level or 10% in 50 year event, the REDi methodology is also calibrated to include "impedance factors" associated with the following processes:

- Post-earthquake Inspection
- Engineering Mobilization and Review/Re-design
- Financing
- Contractor Mobilization and Bid Process
- Permitting

These capture the time required to start the repairs, since beginning repairs immediately after an earthquake may not be realistic. **With these impedance factors, the median functional recovery time is 19 months.**

Table 12. Median repair time, without impeding factors

Intensity	FEMA P-58 Parallel	FEMA P-58 Series	REDi Re-Occupancy	REDi Functional Recovery	REDi Full Recovery
90% in 50 years	8 days	2.4 weeks	0 days	14 days	14 days
50% in 30 years	3.2 weeks	2.2 months	3.7 weeks	5.7 weeks	5.7 weeks
50% in 50 years	5.8 weeks	5.0 months	2.2 months	2.6 months	2.6 months
50% in 75 years	7.9 weeks	7.9 months	3.5 months	3.9 months	3.9 months
50% in 100 years	2.1 months	9.5 months	4.3 months	4.7 months	4.7 months
20% in 50 years	2.6 months	12 months	5.6 months	6.0 months	6.0 months
10% in 50 years	3.5 months	17 months	7.8 months	8.2 months	8.2 months
DE	4.8 months	19 months	11 months	11 months	11 months
5% in 50 years	5.4 months	19 months	12 months	13 months	13 months
MCE_R	19 months	19 months	19 months	19 months	19 months
2% in 50 years	19 months	19 months	19 months	19 months	19 months

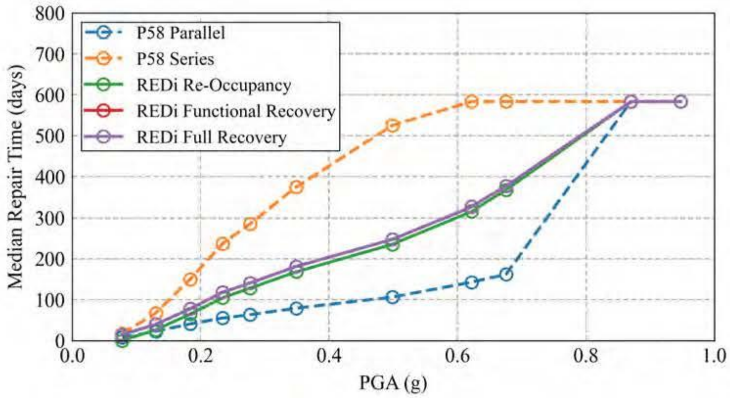

Figure 11. Median repair time, without impeding factors

11 JUSTIFICATION OF SECONDARY MODIFIERS

No justification of secondary inputs was provided.

12 DISCLAIMER

REFERENCES

Almufiti, Ibrahim, & Willford, Michael. 2013. *REDi Rating System*. Arup.

Applied Technology Council. 2015a. *FEMA P-154: Rapid Visual Screening of Buildings for Potential Seismic Hazards: A Handbook.*

Applied Technology Council. 2015b. *FEMA P-155: Rapid Visual Screening of Buildings for Potential Seismic Hazards: Supporting Documentation.*

Applied Technology Council. 2018. *FEMA P-58: Seismic Perfromance Assessment of Buildings.*

International Conference of Building Officials. 1961. *Uniform Building Code 1961 Edition*. International Conference of Building Officials.

H5. Detailed Analysis – Existing Franz (With Test Data)

CONTENTS

1 SUMMARY OF INPUTS AND RISK RESULTS

Risk Model Inputs

Primary

Project Name:	4 Franz-Pritzker
Model Name:	S.F. (w/test data) reduced top joints
Building Type:	RC: Space Frame
Year of Construction:	1967
Number of Stories:	8
Occupancy:	Commercial Office
Address: 502 Portola Plaza Los Angeles, CA, 90095	
Latitude:	34.06985°
Longitude:	-118.44125°

Analysis Options

Include Collapse in Analysis:	Yes
Consider Residual Drift:	Yes

Building Layout Information

Cost per Square Foot:	–
Total Square Feet:	84,211
Aspect Ratio:	–
First Story Height (ft):	14
Upper Story Heights (ft):	13
Vertical Irregularity:	Moderate
Plan Irregularity:	–

Ground Motion and Soil Information

Site Class:	C
Site Hazard:	SP3 Default

Building Design Info

Level of Detailing (Dir. 1, 2):	Ordinary, Ordinary
Drift Limit (Dir. 1, 2):	2.000%, 2.000%
Risk Category:	I/II
Seismic Importance Factor, I_e:	1
Component Importance Factor, I_p:	–
Include Retrofit Information?	No

Structural Properties

Property	Dir. 1	Dir. 2
Base Shear Strength (g):	0.128	0.128
Yield Drift (%):	0.69	0.69
1^{st} Mode Period (T_1) (s):	1.35	1.35
2^{nd} Mode Period (T_2) (s):	–	–
3^{rd} Mode Period (T_3) (s):	–	–

Component Information

Do your stairs have seismic joints?	No
Is your ceiling laterally supported?	Yes
Is your lighting seismically rated?	Yes
Is your piping seismically rated?	Yes
Is your HVAC system seismically anchored?	Yes
Is your electrical equipment seismically rated?	Yes
Percent of Building Glazed:	–

Building Stability

Median Collapse Capacity:	–
Beta (Dispersion):	–

Responses

No responses provided

Repair Time Options

Factors Delaying Start of Repairs	
Inspection	Yes
Financing	Yes
Permitting	Yes
Engineering Mobilization	Yes
Contractor Mobilization	Yes
Mitigation Factors	
Inspector on Retainer	No
Engineer on Retainer	No
Engineer on Retainer	No
Funding Source	Private Loans

Expected Loss

Expected loss in percent of total building value

Shaking Intensity	Return Period	SEL (%)	SUL (%)
90% in 50 years	22 Years	3.3	5.4
50% in 30 years	43 Years	5.1	8.7
50% in 50 years	72 Years	7.9	14
50% in 75 years	108 Years	11	20
50% in 100 years	144 Years	15	28
20% in 50 years	224 Years	23	43
10% in 50 years	475 Years	41	69
DE	791 Years	57	92
5% in 50 years	975 Years	64	100
MCE_R	1956 Years	83	100
2% in 50 years	2475 Years	88	100

Repair Time

Median repair time, without impeding factors

Intensity	FEMA P-58 Parallel	FEMA P-58 Series	REDi Re-Occupancy	REDi Functional Recovery	REDi Full Recovery
90% in 50 years	5 days	7 days	0 days	8 days	8 days
50% in 30 years	7 days	12 days	1 days	13 days	13 days
50% in 50 years	11 days	3.6 weeks	5 days	2.9 weeks	2.9 weeks
50% in 75 years	2.5 weeks	6.8 weeks	14 days	4.2 weeks	4.2 weeks
50% in 100 years	3.4 weeks	2.5 months	3.6 weeks	5.7 weeks	5.7 weeks
20% in 50 years	5.8 weeks	4.6 months	7.7 weeks	2.3 months	2.3 months
10% in 50 years	3.0 months	11 months	4.8 months	5.3 months	5.3 months
DE	4.6 months	19 months	8.3 months	8.7 months	8.7 months
5% in 50 years	5.5 months	19 months	10 months	11 months	11 months
MCE_R	8.5 months	19 months	18 months	18 months	18 months
2% in 50 years	9.7 months	19 months	19 months	19 months	19 months

2 BASIS OF ANALYSIS

This analysis is based on the SP3-RiskModel of the Seismic Performance Prediction Program (SP3) software platform. The underlying analysis methods are based on the FEMA P-58 analytical method, which is a transparent and well documented method developed through a 15 year project (Applied Technology Council, 2018). This project leveraged the previous decades of academic research, funded by a $16 million investment by the Federal Emergency Management Agency (FEMA). In contrast to many risk assessment methods based on judgment and past earthquake experience, the FEMA P-58 and SP3 analysis are based on engineering-oriented risk evaluation methods.

3 DOCUMENTATION OF SITE AND BUILDING INPUT DATA

Project Name: 4 Franz-Pritzker
Model Name: S.F. (w/test data) reduced top joints

3.1 Site Information

Address: 502 Portola Plaza, Los Angeles, CA, 90095
Latitude: 34.06985°
Longitude: -118.44125°

3.2 Building Information

Material Type:	Cast-in-Place Concrete
Number of Stories:	8
Total Building Square Footage:	84,211
Occupancy Type:	Commercial Office
Total Expected Building Replacement Value:	$22,110,841

4 SITE HAZARD INFORMATION

This section presents the site's seismic hazard information. The V_{S30} value is the shear wave velocity in the soil at a depth of 30 meters. This value and the associated site class are presented in Table 1.

Table 1. Site soil information

V_{S30} (m/s):	537.0
Site Class:	C

Table 2 and Figure 1 present the spectral acceleration information for this site. The spectral acceleration is a measure of how much force the building will attract in an earthquake. This amount of force is dependent on the intensity of the ground shaking (e.g. 10% in 50 years), as well as a dynamic property of the building known as the "fundamental period". Shorter buildings tend to have smaller fundamental periods and taller buildings tend to have larger fundamental periods. As indicated by Figure 1, smaller fundamental periods (with the exception of very short fundamental periods) will attract more force in an earthquake.

The Design Earthquake (DE) and Maximum Considered Earthquake (MCE) are based on the modern code maximum direction spectra and are converted to geometric mean for comparison.

Table 2. Geometric mean spectral acceleration values (in g)

Shaking Intensity	Return Period	PGA	$S_a(0.2s)$	$S_a(1.0s)$	$S_a(1.4s)$
90% in 50 years	22 years	0.08	0.18	0.05	0.04
50% in 30 years	43 years	0.13	0.30	0.09	0.07
50% in 50 years	72 years	0.18	0.44	0.13	0.11
50% in 75 years	108 years	0.23	0.56	0.18	0.14
50% in 100 years	144 years	0.28	0.67	0.21	0.17
20% in 50 years	224 years	0.35	0.84	0.28	0.23
10% in 50 years	475 years	0.50	1.22	0.43	0.34
DE	791 years	0.62	1.53	0.55	0.44
5% in 50 years	975 years	0.68	1.66	0.61	0.49
MCE_R	1956 years	0.87	2.18	0.82	0.66
2% in 50 years	2475 years	0.95	2.36	0.91	0.73

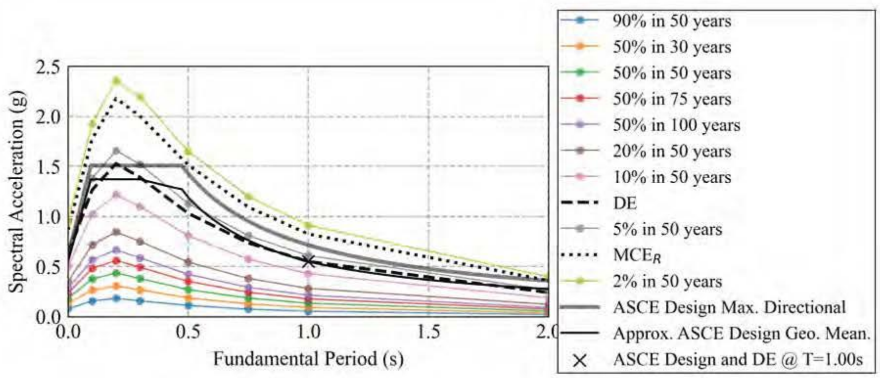

Figure 1. Hazard curves for this site. All curves are geometric mean unless otherwise stated.

5 BUILDING DESIGN SUMMARY FROM THE *SP3 BUILDING CODE DESIGN DATABASE*

5.1 Building Code Design Parameters

The seismic design parameters used to compute the seismic base shear coefficients for this building are presented in Table 3. These parameters are specific to the 1961 edition of the Uniform Building Code (International Conference of Building Officials, 1961).

Table 3. Code design parameters

(a) UBC 1961 structural system parameters

Parameter	Dir. 1	Dir. 2
C_d	1	1
k	1	1

(b) UBC 1961 site specific parameters

Parameter	Value
Z	1
Seismic Zone	3

5.2 Modern Building Code Design Parameters

For comparison to modern code, the modern code parameters are presented in Table 4.

Table 4. Modern code design parameters

(a) ASCE/SEI 7-2010 structural system parameters

Parameter	Dir. 1	Dir. 2
C_t	0.016	0.016
C_d	5.5	5.5
x	0.9	0.9
R	8	8
Ω_0	3	3

(b) ASCE/SEI 7-2010 site specific parameters

Parameter	Value
S_s	2.263
S_1	0.825
S_{ds}	1.508
S_{d1}	0.715
SDC	E
C_u	1.4
$\mathrm{MCE}_{R,max}(g)$	0.794
$\mathrm{MCE}_{R,geomean}(g)$	0.611
$\mathrm{DE}_{max}(g)$	0.529
$\mathrm{DE}_{geomean}(g)$	0.407

5.3 Structural Properties

This section summarizes the main structural properties of the building in each direction. These structural properties are used as inputs to the SP3 Structural Response Prediction Engine.

Table 5. Structural properties table

Parameter	Direction 1	Direction 2
General		
Structural System	RC: Space Frame	RC: Space Frame
Building Edge Length (ft)	102	102
Detailing Level	Ordinary	Ordinary
Strength		
Seismic Design Base Shear Ratio, C_s	0.034	0.034
Ultimate Base Shear Ratio, v_{ult}	0.128*	0.128*
Stiffness		
$T_{1,design}$ (s)	1.79	1.79
T_1 with structural overstiffness (s)	1.54	1.54
T_1 with gravity system (s)	1.53	1.53
T_1 with non-structural components (s)	1.45	1.45
T_1 empirical lower bound (s)	0.91	0.91
T_1 empirical upper bound (s)	1.71	1.71
T_1 Final (s)	1.35	1.35

*User defined, not SP3 default

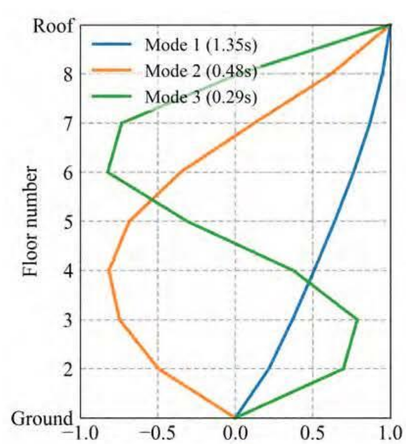

Figure 2. Mode shapes

6 BUILDING STABILITY

The FEMA P-154 collapse capacity score was calculated as follows using the "very high" seismicity level. The terminology used in this section is consistent with the FEMA P-154 methodology (Applied Technology Council, 2015a):

- P$[COL|MCE_R]_{P-154}$: the probability that the building will be in the HAZUS complete structural damage state when subjected to MCER shaking, times the collapse factor
- P$[COL|MCE_R]_{P-58}$: the probability that the building will be in the HAZUS complete structural damage state when subjected to MCER shaking, times the collapse factor
- Collapse Factor: expected ratio of collapsed area to total area given that the building is in the HAZUS Complete structural damage state

For a more in-depth explanation of "collapse," refer to Section 4.4.1.5 of FEMA P-155 Third Edition available here (Applied Technology Council, 2015b).

Table 6. Breakdown of FEMA P-154 score assignment

FEMA ID:	C1
Basic Score	1
Soil	0
Year	0
Plan Irregularity	0
Vertical Irregularity	-0.4
Risk Category* (Cat I/II)	0
Sum:	0.6
Minimum Allowed:	0.3
Score:	**0.6**
Dispersion (β):	0.7

*Non-standard property implemented by SP3

The FEMA P-154 probability of collapse at the MCE_R level event is then calculated as:

$$\begin{aligned} \text{P}[COL|MCE_R]_{P-154} &= 10^{-\text{score}} \\ &= 10^{-0.6} \qquad \text{(FEMA P-155 eqn. 4-1)} \\ &= 25.1\% \end{aligned}$$

Taking into account the fraction of floor area collapsed (1 in this case), the probability of collapse is:

$$\begin{aligned} \text{P}[COL|MCE_R]_{P-58} &= \text{P}[COL|MCE_R]_{P-154} \text{ / Collapse Factor} \\ &= 25.1\% / 1 \\ &= 25.1\% \end{aligned}$$

The median collapse capacity is calculated as:

$$\begin{aligned} S_{a,\ collapse\ median,\ P-58} &= \exp\left(\ln(S_{a,MCE_R}) - \text{norminv}\left(P[COL|MCE_R]_{P-58}\right) \cdot \beta\right) \\ &= \exp\left(\ln(0.662g) - \text{norminv}\left(25.1\%\right) \cdot 0.7\right) \\ &= 1.06g \end{aligned}$$

where `norminv` is the inverse of the standard normal cumulative distribution function (CDF).

Figure 3 shows the collapse capacity cumulative distribution function used in the analysis.

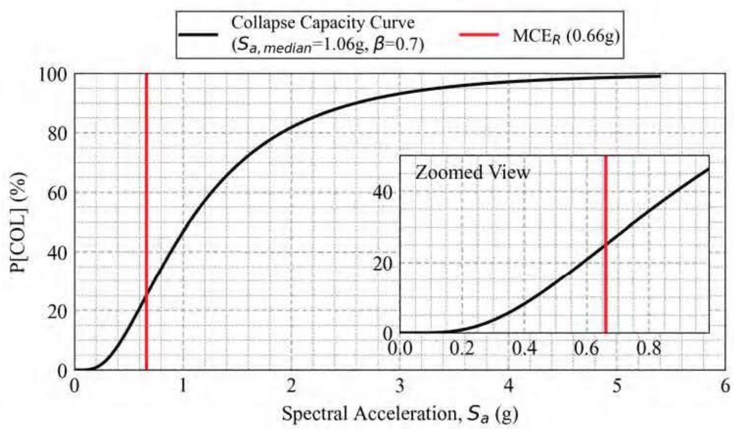

Figure 3. Cumulative distribution function for collapse capacity

7 STRUCTURAL RESPONSE PREDICTIONS FROM THE SP3 STRUCTURAL RESPONSE PREDICTION ENGINE

The SP3 Response Prediction Engine predicts the structural responses (typically providing 100 ground motions per intensity level); this is done by using a combination of three-mode elastic modal analysis, coupled with both elastic and inelastic response modifiers mined from the large SP3 Structural Responses Database (with over 4,000,000 response simulations, and growing). These response predictions track all of the important statistical information in the responses (mean, variability, and correlations); this enables a statistically robust vulnerability curve at the end of the risk assessment process.

7.1 Peak Story Drift

Peak interstory drift ratio is an important metric for both structural and non-structural components in the building. It measures how much the ceiling of a given story moves relative to the floor, normalized to the height of the story. The greater the interstory drift ratio, the greater the damage to the components on that level. Typical components that are damaged from interstory drift ratio are structural components (beams and columns), gypsum partition walls, and exterior cladding and glazing.

Table 7. Peak story drift demands are the same in both directions

Story	90% in 50 years	50% in 30 years	50% in 50 years	50% in 75 years	50% in 100 years	20% in 50 years	10% in 50 years	DE	5% in 50 years	MCE_R	2% in 50 years
8	0.05	0.08	0.12	0.16	0.19	0.25	0.34	0.43	0.47	0.63	0.69
7	0.07	0.11	0.17	0.23	0.27	0.35	0.48	0.60	0.67	0.89	0.98
6	0.08	0.14	0.20	0.27	0.33	0.42	0.58	0.73	0.80	1.07	1.17
5	0.09	0.15	0.23	0.30	0.36	0.47	0.64	0.80	0.88	1.18	1.30
4	0.09	0.16	0.24	0.32	0.39	0.50	0.68	0.85	0.94	1.25	1.38
3	0.10	0.17	0.25	0.33	0.40	0.52	0.71	0.89	0.98	1.30	1.43
2	0.11	0.19	0.27	0.37	0.45	0.57	0.78	0.98	1.08	1.44	1.58
1	0.15	0.25	0.37	0.49	0.59	0.77	1.04	1.31	1.44	1.92	2.11

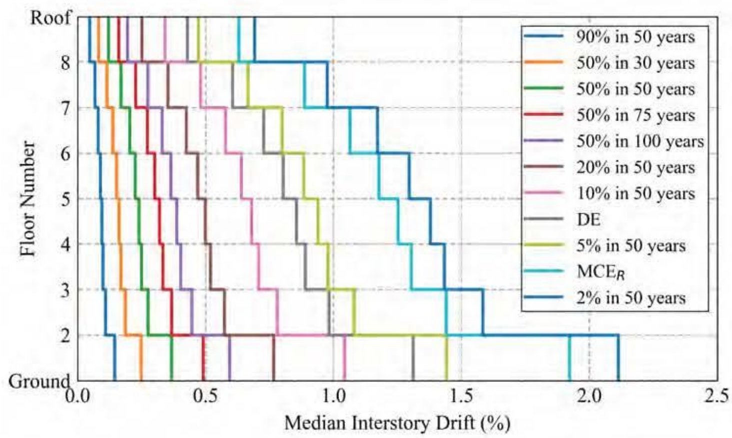

Figure 4. Peak story drift demands are the same in both directions

7.2 Peak Floor Acceleration

Peak floor acceleration is an an important metric for non-structural components in the building. Components such as piping, HVAC, and electrical switchgear are sensitive to the floor accelerations. High accelerations will typically damage a component itself or cause the component's anchorage to fail, both of which may require repair or replacement of the component.

Table 8. Peak floor acceleration demands are the same in both directions

Floor	90% in 50 years	50% in 30 years	50% in 50 years	50% in 75 years	50% in 100 years	20% in 50 years	10% in 50 years	DE	5% in 50 years	MCE_R	2% in 50 years
Roof	0.16	0.27	0.38	0.47	0.53	0.57	0.63	0.67	0.69	0.72	0.73
8	0.14	0.24	0.33	0.39	0.43	0.46	0.51	0.55	0.56	0.60	0.61
7	0.13	0.21	0.30	0.35	0.38	0.41	0.47	0.51	0.53	0.58	0.59
6	0.11	0.19	0.26	0.31	0.34	0.37	0.43	0.48	0.50	0.56	0.58
5	0.10	0.18	0.24	0.29	0.32	0.35	0.42	0.48	0.51	0.58	0.61
4	0.10	0.16	0.23	0.27	0.30	0.34	0.43	0.50	0.52	0.62	0.66
3	0.09	0.15	0.21	0.26	0.29	0.34	0.44	0.53	0.56	0.68	0.73
2	0.08	0.14	0.20	0.25	0.28	0.34	0.46	0.56	0.60	0.75	0.81
Ground	0.08	0.13	0.18	0.23	0.28	0.35	0.50	0.62	0.68	0.87	0.95

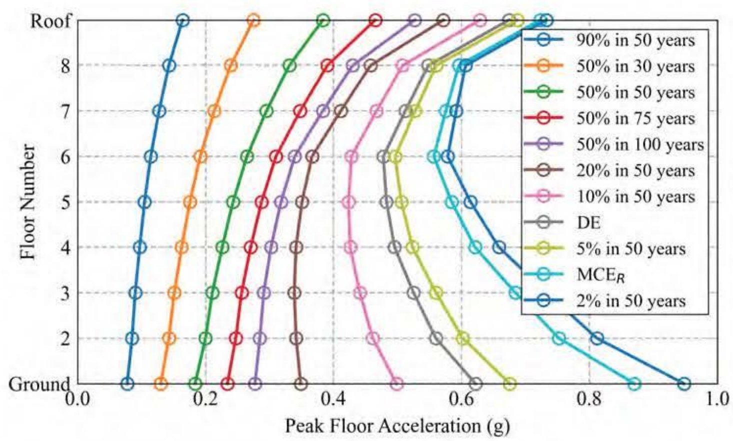

Figure 5. Peak floor acceleration demands are the same in both directions

7.3 Residual Story Drift

Residual drift is a metric that informs the need for structural repairs or building demolition (where excessive drifts are present). Residual drift ratio is a measure of how much the building is "leaning over" after the seismic event has ceased. A residual drift of 2% would indicate that the story is laterally displaced 2% of it's height, which equates to about 3.6 inches for a 15 foot tall story.

Table 9. Residual story drift demands are the same in both directions

Story	90% in 50 years	50% in 30 years	50% in 50 years	50% in 75 years	50% in 100 years	20% in 50 years	10% in 50 years	DE	5% in 50 years	MCE_R	2% in 50 years
8	0.00	0.00	0.00	0.00	0.00	0.00	0.00	0.00	0.00	0.00	0.00
7	0.00	0.00	0.00	0.00	0.00	0.00	0.00	0.00	0.00	0.02	0.04
6	0.00	0.00	0.00	0.00	0.00	0.00	0.00	0.00	0.01	0.05	0.06
5	0.00	0.00	0.00	0.00	0.00	0.00	0.00	0.01	0.02	0.06	0.08
4	0.00	0.00	0.00	0.00	0.00	0.00	0.00	0.02	0.03	0.07	0.09
3	0.00	0.00	0.00	0.00	0.00	0.00	0.00	0.03	0.04	0.08	0.09
2	0.00	0.00	0.00	0.00	0.00	0.00	0.01	0.04	0.05	0.09	0.11
1	0.00	0.00	0.00	0.00	0.00	0.01	0.04	0.08	0.09	0.15	0.18

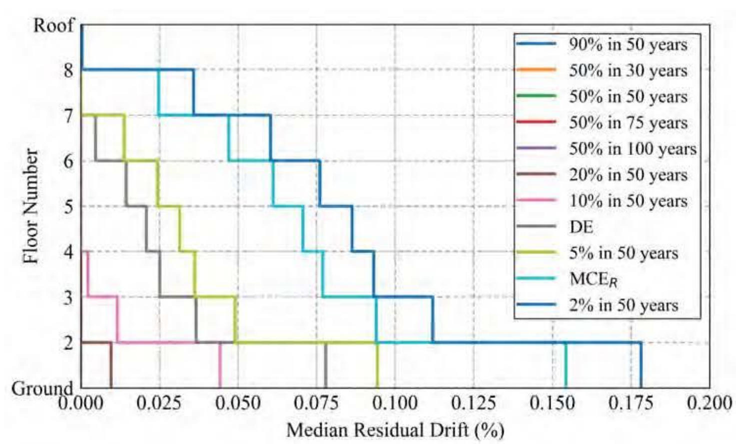

Figure 6. Residual story drift demands are the same in both directions

7.4 Maximum Residual Story Drift

Residual drift is a metric that informs the need for structural repairs or building demolition (where excessive drifts are present). A residual drift of 2% would indicate that the story is laterally displaced 2% of it's height, which equates to about 3.6 inches for a 15 foot tall story. Maximum residual drift is the maximum of the residual drifts on all levels. This is the value used to determine if the building is demolished due to excessive residual drift. Excessive drifts can be visually unsettling and prohibitively expensive (or even impossible) to "straighten" and repair the structural damage. Due to this, the building owner may decide to demolish and rebuild the building if the residual drifts are too large.

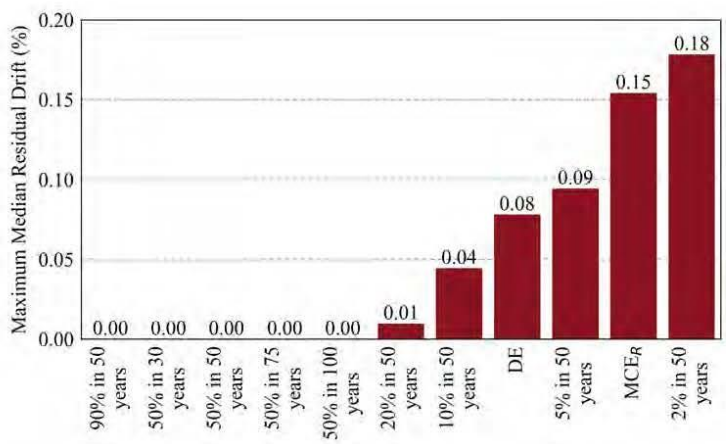

Figure 7. Maximum residual story drift demands are the same in both directions

8 REPAIR COSTS - BY LEVEL OF GROUND MOTION

8.1 Mean and 90^{th} Percentile Repair Costs (SEL and SUL)

The different metrics for repair cost are as follows:

- **Mean (SEL)**: ("Scenario Expected Loss") the average repair cost of the building repair/replacement.
- **Median**: there is a 50% probability that the repair cost will not exceed this value.
- **Fitted SUL**: Fitted value of "Scenario Upper Loss".
- **Counted 90^{th} Percentile**: there is a 90% probability that the repair cost will not exceed this value.

Table 10. Expected loss normalized by building cost

Intensity	PGA (g)	Mean (SEL) (%)	Fitted SUL (%)	Median (%)	Counted 90^{th} Percentile (%)
90% in 50 years	0.08	3.3	5.4	3.1	5.4
50% in 30 years	0.13	5.1	8.7	4.3	8.7
50% in 50 years	0.18	7.9	14	6.5	14
50% in 75 years	0.23	11	20	9.6	20
50% in 100 years	0.28	15	28	12	28
20% in 50 years	0.35	23	43	18	45
10% in 50 years	0.50	41	69	35	77
DE	0.62	57	92	54	100
5% in 50 years	0.68	64	100	63	100
MCE_R	0.87	83	100	100	100
2% in 50 years	0.95	88	100	100	100

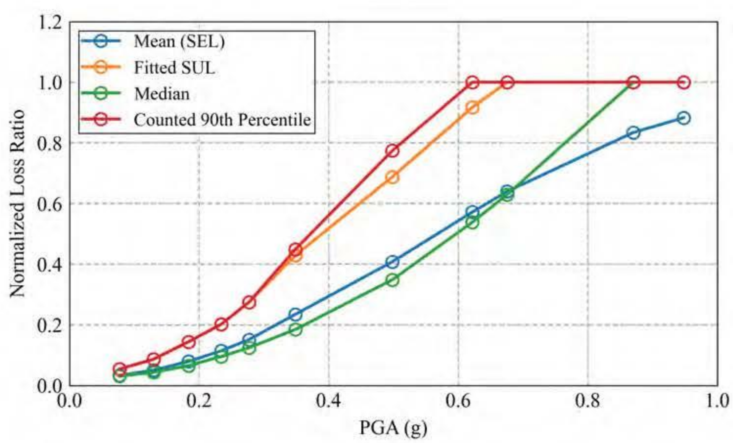

Figure 8. Loss metrics across all intensity levels analyzed

9 REPAIR COST BREAKDOWN BY BUILDING COMPONENTS

9.1 Categories for Repair Cost Breakdowns

Repair costs are binned into eight categories as follows:

- **Collapse**: building demolition and replacement following a collapse.
- **Residual**: building demolition and replacement following unacceptable residual drifts.
- **Structural**: components of the lateral force resisting system or gravity system (e.g. beam column connections, link beams, shear wall, shear tabs, etc.).
- **Partitions**: partition wall components (e.g. wood or metal stud gypsum full height partitions).
- **Exterior**: components placed on the exterior of the building (e.g. cladding, glazing, etc.).
- **Interior**: non-structural components on the interior of the building (e.g. raised access floors, ceilings, lighting).
- **HVAC**: HVAC and plumbing components (e.g. water piping and bracing, sanitary piping, ducting, boilers etc.).
- **Other**: components not included in the categories above (e.g. elevators, user defined components, fire protection components).

9.2 Repair Cost Breakdown for Various Ground Motion Levels

Table 11. Expected mean loss per component group (in percent)

Intensity	Total	Structural	Collapse	Exterior	Other	HVAC	Partitions	Interior	Residual
90% in 50 years	3.3	0.0	0.0	0.3	1.5	1.5	0.0	0.0	0.0
50% in 30 years	5.1	0.2	0.0	1.3	1.8	1.7	0.0	0.1	0.0
50% in 50 years	7.9	0.9	0.1	2.9	2.0	1.8	0.1	0.2	0.0
50% in 75 years	11	2.7	0.2	4.1	2.2	1.8	0.2	0.2	0.0
50% in 100 years	15	4.9	0.5	5.0	2.3	1.9	0.3	0.4	0.0
20% in 50 years	23	10	1.4	6.4	2.4	1.9	0.5	0.4	0.0
10% in 50 years	41	22	5.4	8.3	2.4	1.9	0.7	0.6	0.0
DE	57	32	11	9.7	2.4	1.8	0.9	0.8	0.0
5% in 50 years	64	37	13	10.0	2.3	1.7	1.0	0.8	0.2
MCE_R	83	49	25	11	2.1	1.5	1.2	1.0	0.5
2% in 50 years	88	52	30	11	2.0	1.4	1.2	1.1	0.8

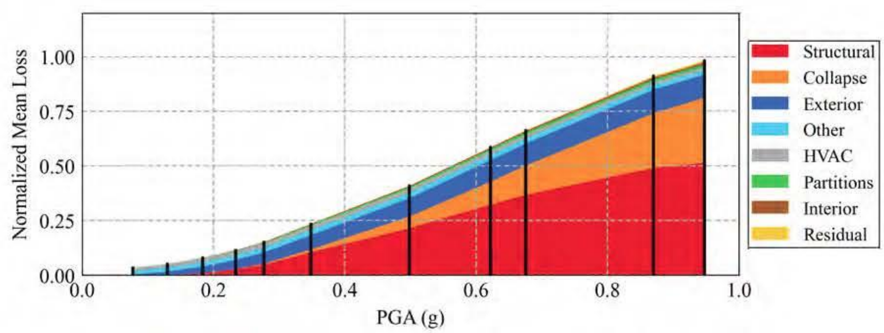

Figure 9. Contribution of building components to mean loss ratio

9.3 Repair Cost Breakdown for Expected Annual Loss

The expected annual loss for this building is $112,912.

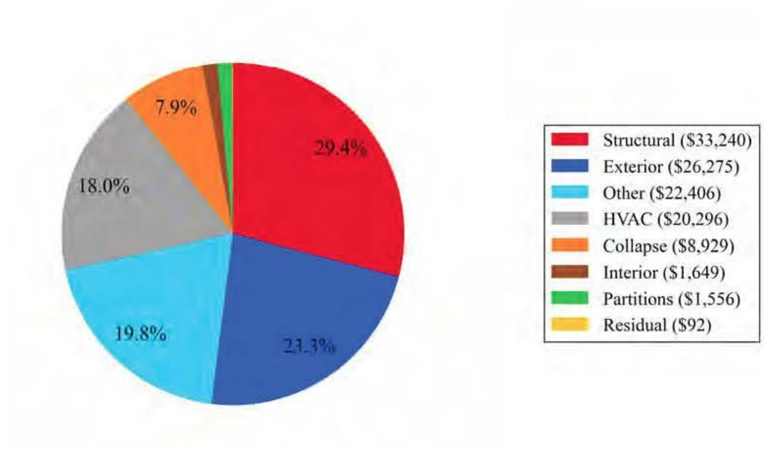

Figure 10. Annualized loss breakdown

10 REPAIR TIME AND BUILDING CLOSURE TIME

The building repair times are computed from the REDi Rating System methodology (Almufiti & Willford, 2013). These are the preferred method to compare building repair time because these include detailed repair schedules as part of the calculation process.

- **Re-Occupancy**: This is the time after which the building is deemed safe enough to be used for shelter.
- **Functional Recovery**: This is time required to establish re-occupancy and regain the facility's primary function. This is what is typically used for assessing building closure time.
- **Full Recovery**: This is the time required to restore the building to its original pre-earthquake condition.

For comparison, the methods of calculating building repair time from the FEMA P-58 methodology are as follows. These are typically not used to estimate building closure time.

- **Series**: Repair activities are limited to one floor at a time
- **Parallel**: All floors are repaired at the same time

For a design level or 10% in 50 year event, the REDi methodology is also calibrated to include "impedance factors" associated with the following processes:

- Post-earthquake Inspection
- Engineering Mobilization and Review/Re-design
- Financing
- Contractor Mobilization and Bid Process
- Permitting

These capture the time required to start the repairs, since beginning repairs immediately after an earthquake may not be realistic. **With these impedance factors, the median functional recovery time is 16 months.**

Table 12. Median repair time, without impeding factors

Intensity	FEMA P-58 Parallel	FEMA P-58 Series	REDi Re-Occupancy	REDi Functional Recovery	REDi Full Recovery
90% in 50 years	5 days	7 days	0 days	8 days	8 days
50% in 30 years	7 days	12 days	1 days	13 days	13 days
50% in 50 years	11 days	3.6 weeks	5 days	2.9 weeks	2.9 weeks
50% in 75 years	2.5 weeks	6.8 weeks	14 days	4.2 weeks	4.2 weeks
50% in 100 years	3.4 weeks	2.5 months	3.6 weeks	5.7 weeks	5.7 weeks
20% in 50 years	5.8 weeks	4.6 months	7.7 weeks	2.3 months	2.3 months
10% in 50 years	3.0 months	11 months	4.8 months	5.3 months	5.3 months
DE	4.6 months	19 months	8.3 months	8.7 months	8.7 months
5% in 50 years	5.5 months	19 months	10 months	11 months	11 months
MCE_R	8.5 months	19 months	18 months	18 months	18 months
2% in 50 years	9.7 months	19 months	19 months	19 months	19 months

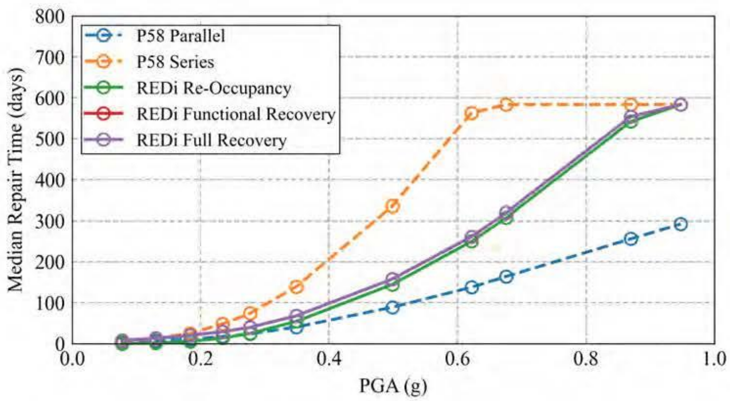

Figure 11. Median repair time, without impeding factors

11 JUSTIFICATION OF SECONDARY MODIFIERS

No justification of secondary inputs was provided.

12 DISCLAIMER

REFERENCES

Almufiti, Ibrahim, & Willford, Michael. 2013. *REDi Rating System*. Arup.

Applied Technology Council. 2015a. *FEMA P-154: Rapid Visual Screening of Buildings for Potential Seismic Hazards: A Handbook.*

Applied Technology Council. 2015b. *FEMA P-155: Rapid Visual Screening of Buildings for Potential Seismic Hazards: Supporting Documentation.*

Applied Technology Council. 2018. *FEMA P-58: Seismic Perfromance Assessment of Buildings.*

International Conference of Building Officials. 1961. *Uniform Building Code 1961 Edition*. International Conference of Building Officials.

H6. Detailed Analysis – Franz Tower Retrofit with BRB (No Test Data)

CONTENTS

1 SUMMARY OF INPUTS AND RISK RESULTS

Risk Model Inputs

Primary

Project Name:	6 Franz-Pritzker
Model Name:	BRB Retrofit (021a,b)
Building Type:	Steel: BRBF Generic FEMA P-58
Year of Construction:	1967
Number of Stories:	8
Occupancy:	Commercial Office
Address: 502 Portola Plaza Los Angeles, CA, 90095	
Latitude:	34.06985°
Longitude:	-118.44125°

Analysis Options

Include Collapse in Analysis:	Yes
Consider Residual Drift:	Yes

Building Layout Information

Cost per Square Foot:	–
Total Square Feet:	84,211
Aspect Ratio:	–
First Story Height (ft):	14
Upper Story Heights (ft):	13
Vertical Irregularity:	None
Plan Irregularity:	–

Ground Motion and Soil Information

Site Class:	C
Site Hazard:	SP3 Default

Building Design Info

Level of Detailing (Dir. 1, 2):	Special, Special
Drift Limit (Dir. 1, 2):	2.000%, 2.000%
Risk Category:	I/II
Seismic Importance Factor, I_e:	1
Component Importance Factor, I_p:	–
Include Retrofit Information?	No

Structural Properties

Property	Dir. 1	Dir. 2
Base Shear Strength (g):	–	–
Yield Drift (%):	–	–
1^{st} Mode Period (T_1) (s):	–	–
2^{nd} Mode Period (T_2) (s):	–	–
3^{rd} Mode Period (T_3) (s):	–	–

Component Information

Do your stairs have seismic joints?	No
Is your ceiling laterally supported?	Yes
Is your lighting seismically rated?	Yes
Is your piping seismically rated?	Yes
Is your HVAC system seismically anchored?	Yes
Is your electrical equipment seismically rated?	Yes
Percent of Building Glazed:	–

Building Stability

Median Collapse Capacity:	–
Beta (Dispersion):	–

Responses

No responses provided

Repair Time Options

Factors Delaying Start of Repairs	
Inspection	Yes
Financing	Yes
Permitting	Yes
Engineering Mobilization	Yes
Contractor Mobilization	Yes
Mitigation Factors	
Inspector on Retainer	No
Engineer on Retainer	No
Engineer on Retainer	No
Funding Source	Private Loans

Expected Loss

Expected loss in percent of total building value

Shaking Intensity	Return Period	SEL (%)	SUL (%)
90% in 50 years	22 Years	3.1	4.8
50% in 30 years	43 Years	3.7	5.7
50% in 50 years	72 Years	4.7	7.1
50% in 75 years	108 Years	6.4	10
50% in 100 years	144 Years	8.1	13
20% in 50 years	224 Years	12	22
10% in 50 years	475 Years	20	37
DE	791 Years	28	49
5% in 50 years	975 Years	34	59
MCE_R	1956 Years	61	97
2% in 50 years	2475 Years	68	100

Repair Time

Median repair time, without impeding factors

Intensity	FEMA P-58 Parallel	FEMA P-58 Series	REDi Re-Occupancy	REDi Functional Recovery	REDi Full Recovery
90% in 50 years	5 days	6 days	0 days	8 days	8 days
50% in 30 years	7 days	10 days	0 days	13 days	13 days
50% in 50 years	10 days	2.6 weeks	1 days	2.6 weeks	2.6 weeks
50% in 75 years	14 days	4.5 weeks	7 days	3.5 weeks	3.5 weeks
50% in 100 years	2.8 weeks	7.2 weeks	2.5 weeks	4.5 weeks	4.5 weeks
20% in 50 years	3.9 weeks	2.8 months	4.8 weeks	6.6 weeks	6.6 weeks
10% in 50 years	6.8 weeks	5.7 months	2.4 months	2.8 months	2.8 months
DE	2.4 months	9.0 months	4.0 months	4.3 months	4.3 months
5% in 50 years	3.1 months	11 months	5.1 months	5.3 months	5.3 months
MCE_R	5.7 months	19 months	10 months	10 months	10 months
2% in 50 years	7.6 months	19 months	14 months	14 months	14 months

2 BASIS OF ANALYSIS

This analysis is based on the SP3-RiskModel of the Seismic Performance Prediction Program (SP3) software platform. The underlying analysis methods are based on the FEMA P-58 analytical method, which is a transparent and well documented method developed through a 15 year project (Applied Technology Council, 2018). This project leveraged the previous decades of academic research, funded by a $16 million investment by the Federal Emergency Management Agency (FEMA). In contrast to many risk assessment methods based on judgment and past earthquake experience, the FEMA P-58 and SP3 analysis are based on engineering-oriented risk evaluation methods.

3 DOCUMENTATION OF SITE AND BUILDING INPUT DATA

Project Name: 6 Franz-Pritzker
Model Name: BRB Retrofit (021a,b)

3.1 Site Information

Address: 502 Portola Plaza, Los Angeles, CA, 90095
Latitude: 34.06985°
Longitude: -118.44125°

3.2 Building Information

Material Type:	Steel
Number of Stories:	8
Total Building Square Footage:	84,211
Occupancy Type:	Commercial Office
Total Expected Building Replacement Value:	$22,098,238

4 SITE HAZARD INFORMATION

This section presents the site's seismic hazard information. The V_{S30} value is the shear wave velocity in the soil at a depth of 30 meters. This value and the associated site class are presented in Table 1.

Table 1. Site soil information

V_{S30} (m/s):	537.0
Site Class:	C

Table 2 and Figure 1 present the spectral acceleration information for this site. The spectral acceleration is a measure of how much force the building will attract in an earthquake. This amount of force is dependent on the intensity of the ground shaking (e.g. 10% in 50 years), as well as a dynamic property of the building known as the "fundamental period". Shorter buildings tend to have smaller fundamental periods and taller buildings tend to have larger fundamental periods. As indicated by Figure 1, smaller fundamental periods (with the exception of very short fundamental periods) will attract more force in an earthquake.

The Design Earthquake (DE) and Maximum Considered Earthquake (MCE) are based on the modern code maximum direction spectra and are converted to geometric mean for comparison.

Table 2. Geometric mean spectral acceleration values (in g)

Shaking Intensity	Return Period	PGA	$S_a(0.2s)$	$S_a(1.0s)$	$S_a(1.1s)$
90% in 50 years	22 years	0.08	0.18	0.05	0.05
50% in 30 years	43 years	0.13	0.30	0.09	0.09
50% in 50 years	72 years	0.18	0.44	0.13	0.13
50% in 75 years	108 years	0.23	0.56	0.18	0.17
50% in 100 years	144 years	0.28	0.67	0.21	0.20
20% in 50 years	224 years	0.35	0.84	0.28	0.27
10% in 50 years	475 years	0.50	1.22	0.43	0.41
DE	791 years	0.62	1.53	0.55	0.52
5% in 50 years	975 years	0.68	1.66	0.61	0.58
MCE_R	1956 years	0.87	2.18	0.82	0.79
2% in 50 years	2475 years	0.95	2.36	0.91	0.87

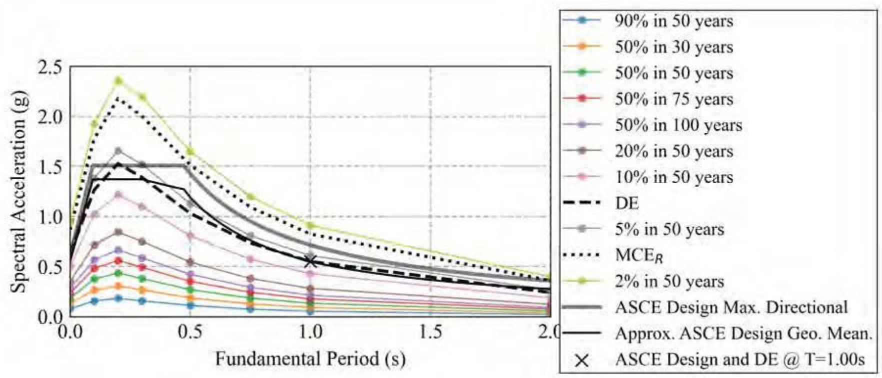

Figure 1. Hazard curves for this site. All curves are geometric mean unless otherwise stated.

5 BUILDING DESIGN SUMMARY FROM THE *SP3 BUILDING CODE DESIGN DATABASE*

5.1 Building Code Design Parameters

The seismic design parameters used to compute the seismic base shear coefficients for this building are presented in Table 3. These parameters are specific to the 1961 edition of the Uniform Building Code (International Conference of Building Officials, 1961).

Table 3. Code design parameters

(a) UBC 1961 structural system parameters

Parameter	Dir. 1	Dir. 2
C_d	1	1
k	1.33	1.33

(b) UBC 1961 site specific parameters

Parameter	Value
Z	1
Seismic Zone	3

5.2 Modern Building Code Design Parameters

For comparison to modern code, the modern code parameters are presented in Table 4.

Table 4. Modern code design parameters

(a) ASCE/SEI 7-2010 structural system parameters

Parameter	Dir. 1	Dir. 2
C_t	0.03	0.03
C_d	5	5
x	0.75	0.75
R	8	8
Ω_0	2.5	2.5

(b) ASCE/SEI 7-2010 site specific parameters

Parameter	Value
S_s	2.263
S_1	0.825
S_{ds}	1.508
S_{d1}	0.715
SDC	E
C_u	1.4
$\mathrm{MCE}_{R,max}(g)$	0.989
$\mathrm{MCE}_{R,geomean}(g)$	0.761
$\mathrm{DE}_{max}(g)$	0.66
$\mathrm{DE}_{geomean}(g)$	0.507

5.3 Structural Properties

This section summarizes the main structural properties of the building in each direction. These structural properties are used as inputs to the SP3 Structural Response Prediction Engine.

Table 5. Structural properties table

Parameter	Direction 1	Direction 2
General		
Structural System	Steel: BRBF Generic FEMA P-58	Steel: BRBF Generic FEMA P-58
Building Edge Length (ft)	102	102
Detailing Level	Special	Special
Strength		
Seismic Design Base Shear Ratio, C_s	0.050	0.050
Ultimate Base Shear Ratio, v_{ult}	0.193	0.193
Stiffness		
$T_{1,design}$ (s)	1.25	1.25
T_1 with structural overstiffness (s)	1.19	1.19
T_1 with gravity system (s)	1.15	1.15
T_1 with non-structural components (s)	1.08	1.08
T_1 empirical lower bound (s)	0.97	0.97
T_1 empirical upper bound (s)	1.69	1.69
T_1 Final (s)	1.08	1.08

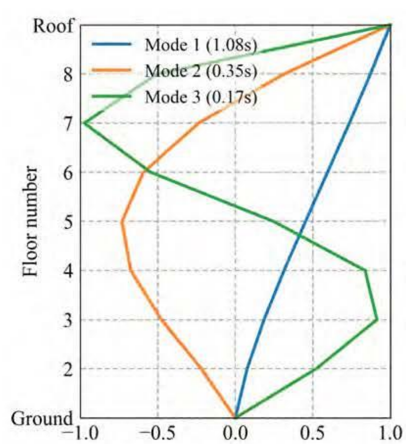

Figure 2. Mode shapes

6 BUILDING STABILITY

The FEMA P-154 collapse capacity score was calculated as follows using the “very high” seismicity level. The terminology used in this section is consistent with the FEMA P-154 methodology (Applied Technology Council, 2015a):

- P$[COL|MCE_R]_{P-154}$: the probability that the building will be in the HAZUS complete structural damage state when subjected to MCER shaking, times the collapse factor
- P$[COL|MCE_R]_{P-58}$: the probability that the building will be in the HAZUS complete structural damage state when subjected to MCER shaking, times the collapse factor
- Collapse Factor: expected ratio of collapsed area to total area given that the building is in the HAZUS Complete structural damage state

For a more in-depth explanation of “collapse,” refer to Section 4.4.1.5 of FEMA P-155 Third Edition available here (Applied Technology Council, 2015b).

Table 6. Breakdown of FEMA P-154 score assignment

FEMA ID:	S2
Basic Score	1.4
Soil	0
Year	0
Plan Irregularity	0
Vertical Irregularity	0
Risk Category* (Cat I/II)	0
Sum:	1.4
Minimum Allowed:	0.5
Score:	**1.4**
Dispersion (β):	0.59

*Non-standard property implemented by SP3

The FEMA P-154 probability of collapse at the MCE_R level event is then calculated as:

$$\begin{aligned} \mathrm{P}[COL|MCE_R]_{P-154} &= 10^{-\text{score}} \\ &= 10^{-1.4} \qquad \text{(FEMA P-155 eqn. 4-1)} \\ &= 3.98\% \end{aligned}$$

Taking into account the fraction of floor area collapsed (0.5 in this case), the probability of collapse is:

$$\begin{aligned} \mathrm{P}[COL|MCE_R]_{P-58} &= \mathrm{P}[COL|MCE_R]_{P-154} \text{ / Collapse Factor} \\ &= 3.98\% / 0.5 \\ &= 7.96\% \end{aligned}$$

The median collapse capacity is calculated as:

$$\begin{aligned} S_{a,\ collapse\ median,\ P-58} &= \exp\left(\ln(S_{a,MCE_R}) - \text{norminv}\left(P[COL|MCE_R]_{P-58}\right) \cdot \beta\right) \\ &= \exp\left(\ln(0.786g) - \text{norminv}\left(7.96\%\right) \cdot 0.59\right) \\ &= 1.80g \end{aligned}$$

where `norminv` is the inverse of the standard normal cumulative distribution function (CDF).

Figure 3 shows the collapse capacity cumulative distribution function used in the analysis.

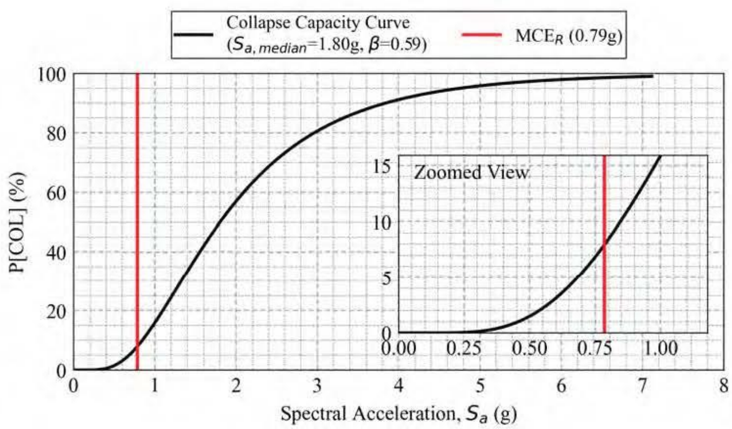

Figure 3. Cumulative distribution function for collapse capacity

7 STRUCTURAL RESPONSE PREDICTIONS FROM THE SP3 STRUCTURAL RESPONSE PREDICTION ENGINE

The SP3 Response Prediction Engine predicts the structural responses (typically providing 100 ground motions per intensity level); this is done by using a combination of three-mode elastic modal analysis, coupled with both elastic and inelastic response modifiers mined from the large SP3 Structural Responses Database (with over 4,000,000 response simulations, and growing). These response predictions track all of the important statistical information in the responses (mean, variability, and correlations); this enables a statistically robust vulnerability curve at the end of the risk assessment process.

7.1 Peak Story Drift

Peak interstory drift ratio is an important metric for both structural and non-structural components in the building. It measures how much the ceiling of a given story moves relative to the floor, normalized to the height of the story. The greater the interstory drift ratio, the greater the damage to the components on that level. Typical components that are damaged from interstory drift ratio are structural components (beams and columns), gypsum partition walls, and exterior cladding and glazing.

Table 7. Peak story drift demands are the same in both directions

Story	90% in 50 years	50% in 30 years	50% in 50 years	50% in 75 years	50% in 100 years	20% in 50 years	10% in 50 years	DE	5% in 50 years	MCE_R	2% in 50 years
8	0.09	0.15	0.22	0.30	0.35	0.41	0.49	0.51	0.51	0.56	0.58
7	0.09	0.15	0.22	0.29	0.35	0.40	0.48	0.51	0.51	0.55	0.57
6	0.09	0.15	0.22	0.29	0.34	0.40	0.47	0.50	0.50	0.54	0.55
5	0.09	0.15	0.21	0.28	0.34	0.41	0.54	0.62	0.66	0.81	0.88
4	0.08	0.14	0.21	0.28	0.33	0.41	0.59	0.74	0.82	1.09	1.19
3	0.08	0.13	0.20	0.26	0.31	0.41	0.63	0.84	0.95	1.32	1.47
2	0.07	0.11	0.17	0.22	0.27	0.37	0.63	0.89	1.03	1.49	1.68
1	0.04	0.08	0.11	0.15	0.18	0.28	0.54	0.83	0.99	1.51	1.71

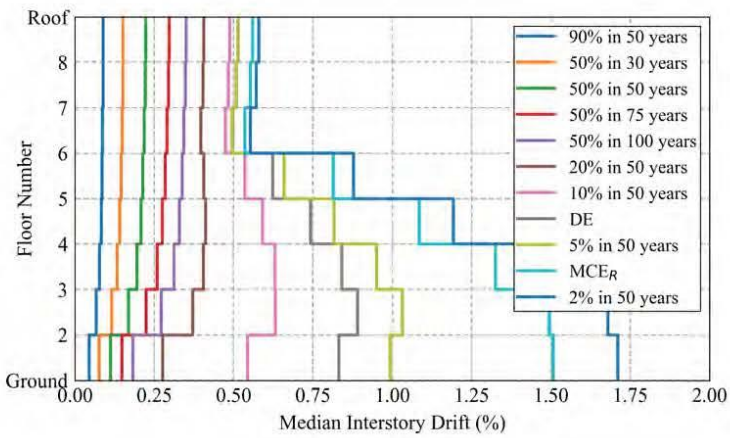

Figure 4. Peak story drift demands are the same in both directions

7.2 Peak Floor Acceleration

Peak floor acceleration is an an important metric for non-structural components in the building. Components such as piping, HVAC, and electrical switchgear are sensitive to the floor accelerations. High accelerations will typically damage a component itself or cause the component's anchorage to fail, both of which may require repair or replacement of the component.

Table 8. Peak floor acceleration demands are the same in both directions

Floor	90% in 50 years	50% in 30 years	50% in 50 years	50% in 75 years	50% in 100 years	20% in 50 years	10% in 50 years	DE	5% in 50 years	MCE_R	2% in 50 years
Roof	0.20	0.34	0.48	0.62	0.77	0.90	1.02	1.12	1.15	1.27	1.34
8	0.15	0.26	0.37	0.47	0.55	0.66	0.79	0.91	0.95	1.12	1.18
7	0.13	0.21	0.30	0.38	0.46	0.55	0.66	0.77	0.81	0.96	1.02
6	0.12	0.21	0.30	0.38	0.45	0.54	0.66	0.77	0.82	0.98	1.04
5	0.11	0.18	0.26	0.33	0.39	0.48	0.60	0.70	0.75	0.90	0.96
4	0.11	0.18	0.26	0.33	0.39	0.47	0.60	0.72	0.76	0.93	1.00
3	0.09	0.16	0.22	0.28	0.33	0.41	0.53	0.64	0.69	0.85	0.91
2	0.09	0.14	0.20	0.26	0.31	0.38	0.51	0.62	0.66	0.83	0.90
Ground	0.08	0.13	0.18	0.23	0.28	0.35	0.50	0.62	0.68	0.87	0.95

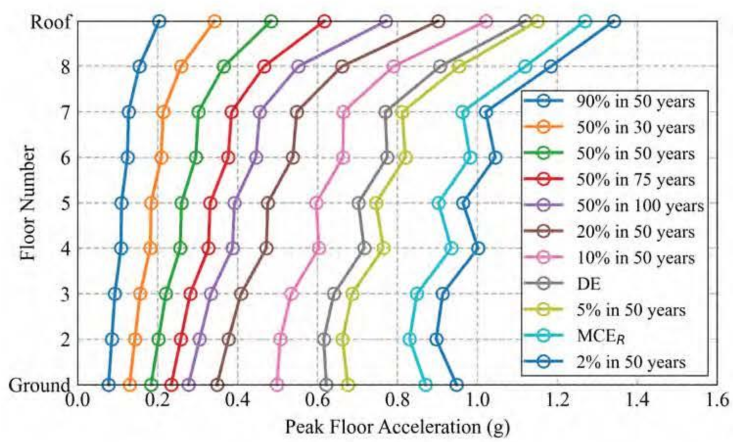

Figure 5. Peak floor acceleration demands are the same in both directions

7.3 Residual Story Drift

Residual drift is a metric that informs the need for structural repairs or building demolition (where excessive drifts are present). Residual drift ratio is a measure of how much the building is "leaning over" after the seismic event has ceased. A residual drift of 2% would indicate that the story is laterally displaced 2% of it's height, which equates to about 3.6 inches for a 15 foot tall story.

Table 9. Residual story drift demands are the same in both directions

Story	90% in 50 years	50% in 30 years	50% in 50 years	50% in 75 years	50% in 100 years	20% in 50 years	10% in 50 years	DE	5% in 50 years	MCE_R	2% in 50 years
8	0.00	0.00	0.01	0.03	0.04	0.05	0.07	0.08	0.08	0.09	0.10
7	0.00	0.00	0.01	0.03	0.04	0.05	0.07	0.08	0.08	0.09	0.09
6	0.00	0.00	0.01	0.02	0.04	0.05	0.07	0.08	0.08	0.09	0.09
5	0.00	0.00	0.01	0.02	0.04	0.05	0.09	0.11	0.12	0.16	0.17
4	0.00	0.00	0.00	0.02	0.03	0.05	0.10	0.14	0.16	0.29	0.38
3	0.00	0.00	0.00	0.02	0.03	0.05	0.11	0.16	0.19	0.48	0.60
2	0.00	0.00	0.00	0.01	0.02	0.04	0.11	0.17	0.25	0.62	0.77
1	0.00	0.00	0.00	0.00	0.00	0.02	0.09	0.16	0.22	0.63	0.79

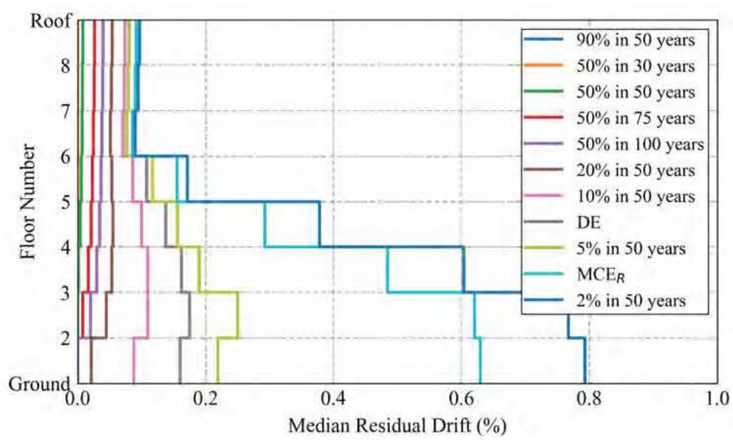

Figure 6. Residual story drift demands are the same in both directions

7.4 Maximum Residual Story Drift

Residual drift is a metric that informs the need for structural repairs or building demolition (where excessive drifts are present). A residual drift of 2% would indicate that the story is laterally displaced 2% of it's height, which equates to about 3.6 inches for a 15 foot tall story. Maximum residual drift is the maximum of the residual drifts on all levels. This is the value used to determine if the building is demolished due to excessive residual drift. Excessive drifts can be visually unsettling and prohibitively expensive (or even impossible) to "straighten" and repair the structural damage. Due to this, the building owner may decide to demolish and rebuild the building if the residual drifts are too large.

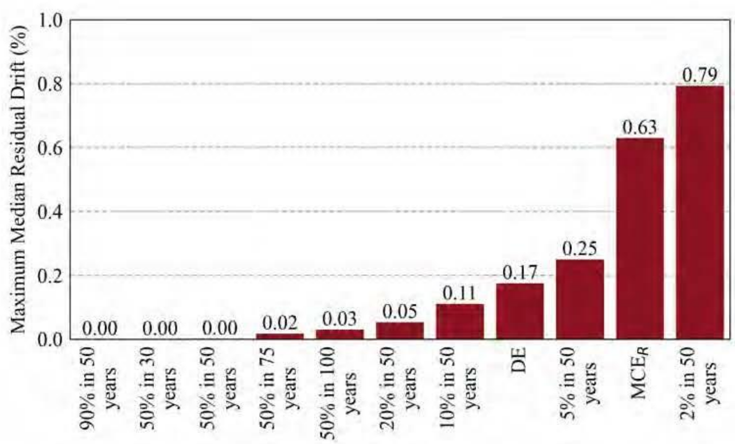

Figure 7. Maximum residual story drift demands are the same in both directions

8 REPAIR COSTS - BY LEVEL OF GROUND MOTION

8.1 Mean and 90^{th} Percentile Repair Costs (SEL and SUL)

The different metrics for repair cost are as follows:

- **Mean (SEL)**: ("Scenario Expected Loss") the average repair cost of the building repair/replacement.
- **Median**: there is a 50% probability that the repair cost will not exceed this value.
- **Fitted SUL**: Fitted value of "Scenario Upper Loss".
- **Counted 90^{th} Percentile**: there is a 90% probability that the repair cost will not exceed this value.

Table 10. Expected loss normalized by building cost

Intensity	PGA (g)	Mean (SEL) (%)	Fitted SUL (%)	Median (%)	Counted 90^{th} Percentile (%)
90% in 50 years	0.08	3.1	4.8	3.0	4.7
50% in 30 years	0.13	3.7	5.7	3.6	5.4
50% in 50 years	0.18	4.7	7.1	4.3	7.1
50% in 75 years	0.23	6.4	10	5.4	10
50% in 100 years	0.28	8.1	13	6.8	13
20% in 50 years	0.35	12	22	9.3	22
10% in 50 years	0.50	20	37	16	37
DE	0.62	28	49	23	49
5% in 50 years	0.68	34	59	29	59
MCE_R	0.87	61	97	52	100
2% in 50 years	0.95	68	100	72	100

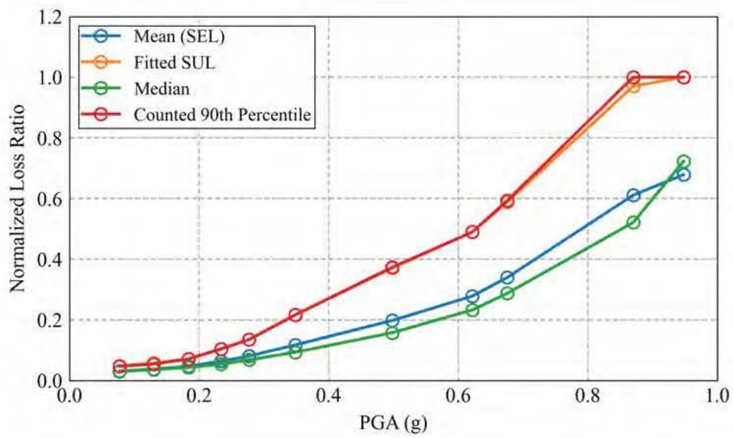

Figure 8. Loss metrics across all intensity levels analyzed

9 REPAIR COST BREAKDOWN BY BUILDING COMPONENTS

9.1 Categories for Repair Cost Breakdowns

Repair costs are binned into eight categories as follows:

- **Collapse**: building demolition and replacement following a collapse.
- **Residual**: building demolition and replacement following unacceptable residual drifts.
- **Structural**: components of the lateral force resisting system or gravity system (e.g. beam column connections, link beams, shear wall, shear tabs, etc.).
- **Partitions**: partition wall components (e.g. wood or metal stud gypsum full height partitions).
- **Exterior**: components placed on the exterior of the building (e.g. cladding, glazing, etc.).
- **Interior**: non-structural components on the interior of the building (e.g. raised access floors, ceilings, lighting).
- **HVAC**: HVAC and plumbing components (e.g. water piping and bracing, sanitary piping, ducting, boilers etc.).
- **Other**: components not included in the categories above (e.g. elevators, user defined components, fire protection components).

9.2 Repair Cost Breakdown for Various Ground Motion Levels

Table 11. Expected mean loss per component group (in percent)

Intensity	Total	Residual	Structural	Collapse	Interior	Other	HVAC	Partitions	Exterior
90% in 50 years	3.1	0.0	0.0	0.0	0.0	1.5	1.6	0.0	0.0
50% in 30 years	3.7	0.0	0.1	0.0	0.1	1.8	1.8	0.0	0.0
50% in 50 years	4.7	0.0	0.5	0.0	0.2	2.0	1.9	0.1	0.0
50% in 75 years	6.4	0.0	1.7	0.0	0.4	2.1	1.9	0.1	0.0
50% in 100 years	8.1	0.0	2.8	0.0	0.7	2.3	2.0	0.2	0.0
20% in 50 years	12	0.0	5.7	0.1	1.1	2.4	2.1	0.3	0.0
10% in 50 years	20	0.2	12	0.6	1.6	2.5	2.1	0.6	0.0
DE	28	0.7	18	1.8	2.0	2.6	2.1	0.8	0.0
5% in 50 years	34	3.0	21	2.7	2.1	2.5	2.0	0.8	0.0
MCE_R	61	30	17	8.0	1.8	1.7	1.3	0.7	0.0
2% in 50 years	68	37	15	11	1.6	1.4	1.1	0.6	0.0

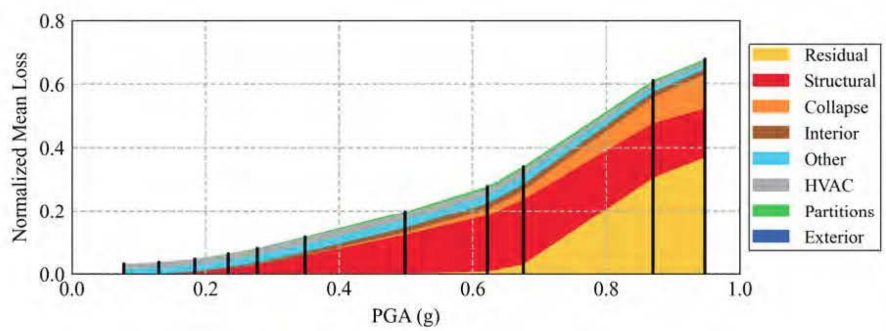

Figure 9. Contribution of building components to mean loss ratio

9.3 Repair Cost Breakdown for Expected Annual Loss

The expected annual loss for this building is $72,115.

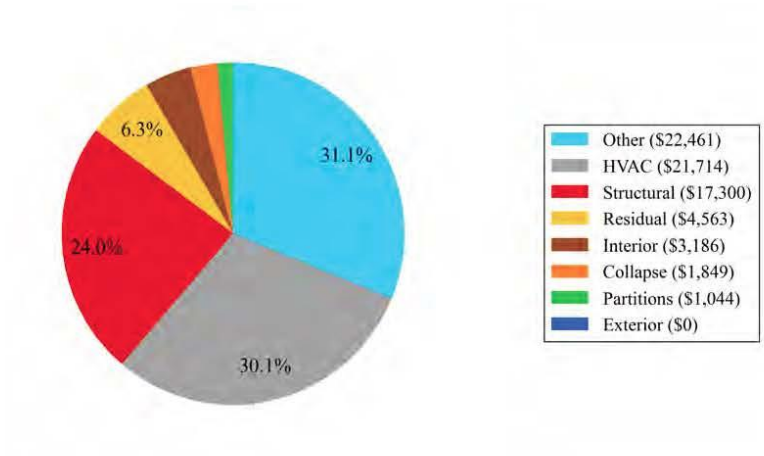

Figure 10. Annualized loss breakdown

10 REPAIR TIME AND BUILDING CLOSURE TIME

The building repair times are computed from the REDi Rating System methodology (Almufiti & Willford, 2013). These are the preferred method to compare building repair time because these include detailed repair schedules as part of the calculation process.

- **Re-Occupancy**: This is the time after which the building is deemed safe enough to be used for shelter.
- **Functional Recovery**: This is time required to establish re-occupancy and regain the facility's primary function. This is what is typically used for assessing building closure time.
- **Full Recovery**: This is the time required to restore the building to its original pre-earthquake condition.

For comparison, the methods of calculating building repair time from the FEMA P-58 methodology are as follows. These are typically not used to estimate building closure time.

- **Series**: Repair activities are limited to one floor at a time
- **Parallel**: All floors are repaired at the same time

For a design level or 10% in 50 year event, the REDi methodology is also calibrated to include "impedance factors" associated with the following processes:

- Post-earthquake Inspection
- Engineering Mobilization and Review/Re-design
- Financing
- Contractor Mobilization and Bid Process
- Permitting

These capture the time required to start the repairs, since beginning repairs immediately after an earthquake may not be realistic. **With these impedance factors, the median functional recovery time is 12 months.**

Table 12. Median repair time, without impeding factors

Intensity	FEMA P-58 Parallel	FEMA P-58 Series	REDi Re-Occupancy	REDi Functional Recovery	REDi Full Recovery
90% in 50 years	5 days	6 days	0 days	8 days	8 days
50% in 30 years	7 days	10 days	0 days	13 days	13 days
50% in 50 years	10 days	2.6 weeks	1 days	2.6 weeks	2.6 weeks
50% in 75 years	14 days	4.5 weeks	7 days	3.5 weeks	3.5 weeks
50% in 100 years	2.8 weeks	7.2 weeks	2.5 weeks	4.5 weeks	4.5 weeks
20% in 50 years	3.9 weeks	2.8 months	4.8 weeks	6.6 weeks	6.6 weeks
10% in 50 years	6.8 weeks	5.7 months	2.4 months	2.8 months	2.8 months
DE	2.4 months	9.0 months	4.0 months	4.3 months	4.3 months
5% in 50 years	3.1 months	11 months	5.1 months	5.3 months	5.3 months
MCE_R	5.7 months	19 months	10 months	10 months	10 months
2% in 50 years	7.6 months	19 months	14 months	14 months	14 months

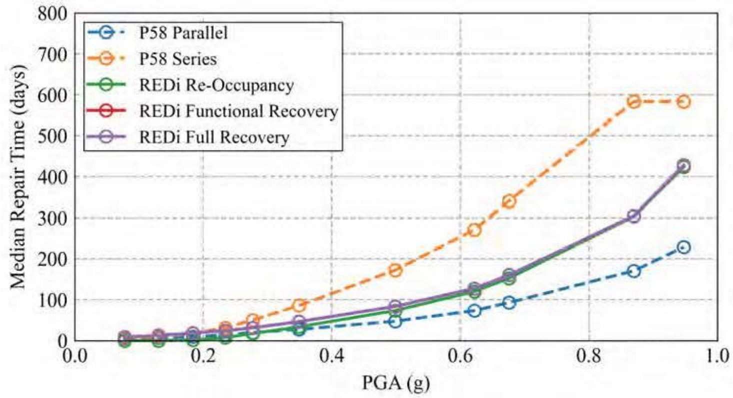

Figure 11. Median repair time, without impeding factors

11 JUSTIFICATION OF SECONDARY MODIFIERS

No justification of secondary inputs was provided.

12 DISCLAIMER

REFERENCES

Almufiti, Ibrahim, & Willford, Michael. 2013. *REDi Rating System*. Arup.

Applied Technology Council. 2015a. *FEMA P-154: Rapid Visual Screening of Buildings for Potential Seismic Hazards: A Handbook.*

Applied Technology Council. 2015b. *FEMA P-155: Rapid Visual Screening of Buildings for Potential Seismic Hazards: Supporting Documentation.*

Applied Technology Council. 2018. *FEMA P-58: Seismic Perfromance Assessment of Buildings.*

International Conference of Building Officials. 1961. *Uniform Building Code 1961 Edition*. International Conference of Building Officials.

H7. Detailed Analysis – Franz Tower Retrofit with CMF (No Test Data)

CONTENTS

1 SUMMARY OF INPUTS AND RISK RESULTS

Risk Model Inputs

Primary

Project Name:	6 Franz Pritzker)
Model Name:	CMF Retrofit (0.21a,b)
Building Type:	RC: Perimeter Frame
Year of Construction:	1967
Number of Stories:	8
Occupancy:	Commercial Office
Address: 502 Portola Plaza Los Angeles, CA, 90095	
Latitude:	34.06985°
Longitude:	-118.44125°

Analysis Options

Include Collapse in Analysis:	Yes
Consider Residual Drift:	Yes

Building Layout Information

Cost per Square Foot:	–
Total Square Feet:	84,211
Aspect Ratio:	–
First Story Height (ft):	14
Upper Story Heights (ft):	13
Vertical Irregularity:	None
Plan Irregularity:	–

Ground Motion and Soil Information

Site Class:	C
Site Hazard:	SP3 Default

Building Design Info

Level of Detailing (Dir. 1, 2):	Special, Special
Drift Limit (Dir. 1, 2):	2.000%, 2.000%
Risk Category:	I/II
Seismic Importance Factor, I_e:	1
Component Importance Factor, I_p:	–
Include Retrofit Information?	No

Structural Properties

Property	Dir. 1	Dir. 2
Base Shear Strength (g):	–	–
Yield Drift (%):	–	–
1^{st} Mode Period (T_1) (s):	–	–
2^{nd} Mode Period (T_2) (s):	–	–
3^{rd} Mode Period (T_3) (s):	–	–

Component Information

Do your stairs have seismic joints?	No
Is your ceiling laterally supported?	Yes
Is your lighting seismically rated?	Yes
Is your piping seismically rated?	Yes
Is your HVAC system seismically anchored?	Yes
Is your electrical equipment seismically rated?	Yes
Percent of Building Glazed:	–

Building Stability

Median Collapse Capacity:	–
Beta (Dispersion):	–

Responses

No responses provided

Repair Time Options

Factors Delaying Start of Repairs	
Inspection	Yes
Financing	Yes
Permitting	Yes
Engineering Mobilization	Yes
Contractor Mobilization	Yes
Mitigation Factors	
Inspector on Retainer	No
Engineer on Retainer	No
Engineer on Retainer	No
Funding Source	Private Loans

Expected Loss

Shaking Intensity	Return Period	SEL (%)	SUL (%)
90% in 50 years	22 Years	3.0	4.7
50% in 30 years	43 Years	3.8	5.8
50% in 50 years	72 Years	5.0	7.6
50% in 75 years	108 Years	7.1	12
50% in 100 years	144 Years	9.1	15
20% in 50 years	224 Years	14	25
10% in 50 years	475 Years	25	41
DE	791 Years	34	54
5% in 50 years	975 Years	39	62
MCE_R	1956 Years	54	87
2% in 50 years	2475 Years	59	94

Expected loss in percent of total building value

Repair Time

Intensity	FEMA P-58 Parallel	FEMA P-58 Series	REDi Re-Occupancy	REDi Functional Recovery	REDi Full Recovery
90% in 50 years	5 days	6 days	0 days	8 days	8 days
50% in 30 years	7 days	11 days	0 days	13 days	13 days
50% in 50 years	10 days	3.1 weeks	3 days	2.7 weeks	2.7 weeks
50% in 75 years	2.2 weeks	5.6 weeks	12 days	3.9 weeks	3.9 weeks
50% in 100 years	2.8 weeks	2.1 months	3.3 weeks	5.3 weeks	5.3 weeks
20% in 50 years	4.5 weeks	3.9 months	6.8 weeks	2.0 months	2.0 months
10% in 50 years	2.0 months	8.7 months	3.9 months	4.2 months	4.2 months
DE	2.6 months	13 months	5.7 months	6.0 months	6.0 months
5% in 50 years	3.0 months	15 months	6.8 months	7.0 months	7.0 months
MCE_R	4.0 months	19 months	9.8 months	10 months	10 months
2% in 50 years	4.3 months	19 months	11 months	11 months	11 months

Median repair time, without impeding factors

2 BASIS OF ANALYSIS

This analysis is based on the SP3-RiskModel of the Seismic Performance Prediction Program (SP3) software platform. The underlying analysis methods are based on the FEMA P-58 analytical method, which is a transparent and well documented method developed through a 15 year project (Applied Technology Council, 2018). This project leveraged the previous decades of academic research, funded by a $16 million investment by the Federal Emergency Management Agency (FEMA). In contrast to many risk assessment methods based on judgment and past earthquake experience, the FEMA P-58 and SP3 analysis are based on engineering-oriented risk evaluation methods.

3 DOCUMENTATION OF SITE AND BUILDING INPUT DATA

Project Name: 6 Franz Pritzker)
Model Name: CMF Retrofit (0.21a,b)

3.1 Site Information

Address: 502 Portola Plaza, Los Angeles, CA, 90095
Latitude: 34.06985°
Longitude: -118.44125°

3.2 Building Information

Material Type:	Cast-in-Place Concrete
Number of Stories:	8
Total Building Square Footage:	84,211
Occupancy Type:	Commercial Office
Total Expected Building Replacement Value:	$22,072,868

4 SITE HAZARD INFORMATION

This section presents the site's seismic hazard information. The V_{S30} value is the shear wave velocity in the soil at a depth of 30 meters. This value and the associated site class are presented in Table 1.

Table 1. Site soil information

V_{S30} (m/s):	537.0
Site Class:	C

Table 2 and Figure 1 present the spectral acceleration information for this site. The spectral acceleration is a measure of how much force the building will attract in an earthquake. This amount of force is dependent on the intensity of the ground shaking (e.g. 10% in 50 years), as well as a dynamic property of the building known as the "fundamental period". Shorter buildings tend to have smaller fundamental periods and taller buildings tend to have larger fundamental periods. As indicated by Figure 1, smaller fundamental periods (with the exception of very short fundamental periods) will attract more force in an earthquake.

The Design Earthquake (DE) and Maximum Considered Earthquake (MCE) are based on the modern code maximum direction spectra and are converted to geometric mean for comparison.

Table 2. Geometric mean spectral acceleration values (in g)

Shaking Intensity	Return Period	PGA	$S_a(0.2s)$	$S_a(1.0s)$	$S_a(1.5s)$
90% in 50 years	22 years	0.08	0.18	0.05	0.04
50% in 30 years	43 years	0.13	0.30	0.09	0.06
50% in 50 years	72 years	0.18	0.44	0.13	0.09
50% in 75 years	108 years	0.23	0.56	0.18	0.12
50% in 100 years	144 years	0.28	0.67	0.21	0.15
20% in 50 years	224 years	0.35	0.84	0.28	0.20
10% in 50 years	475 years	0.50	1.22	0.43	0.30
DE	791 years	0.62	1.53	0.55	0.38
5% in 50 years	975 years	0.68	1.66	0.61	0.43
MCE_R	1956 years	0.87	2.18	0.82	0.58
2% in 50 years	2475 years	0.95	2.36	0.91	0.64

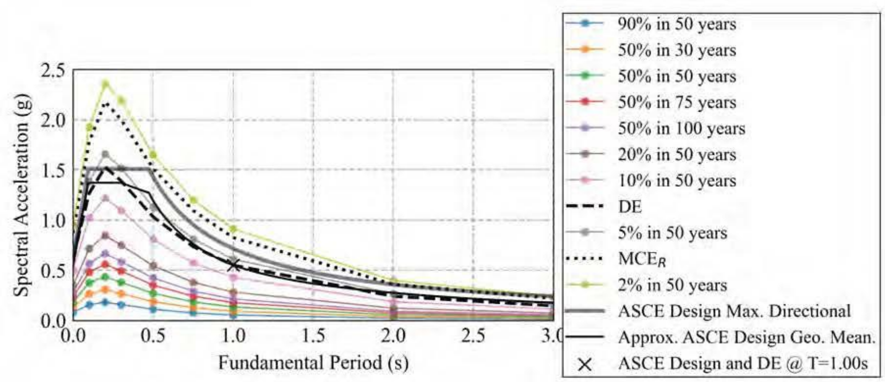

Figure 1. Hazard curves for this site. All curves are geometric mean unless otherwise stated.

5 BUILDING DESIGN SUMMARY FROM THE *SP3 BUILDING CODE DESIGN DATABASE*

5.1 Building Code Design Parameters

The seismic design parameters used to compute the seismic base shear coefficients for this building are presented in Table 3. These parameters are specific to the 1961 edition of the Uniform Building Code (International Conference of Building Officials, 1961).

Table 3. Code design parameters

(a) UBC 1961 structural system parameters

Parameter	Dir. 1	Dir. 2
C_d	1	1
k	1.33	1.33

(b) UBC 1961 site specific parameters

Parameter	Value
Z	1
Seismic Zone	3

5.2 Modern Building Code Design Parameters

For comparison to modern code, the modern code parameters are presented in Table 4.

Table 4. Modern code design parameters

(a) ASCE/SEI 7-2010 structural system parameters

Parameter	Dir. 1	Dir. 2
C_t	0.016	0.016
C_d	5.5	5.5
x	0.9	0.9
R	8	8
Ω_0	3	3

(b) ASCE/SEI 7-2010 site specific parameters

Parameter	Value
S_s	2.263
S_1	0.825
S_{ds}	1.508
S_{d1}	0.715
SDC	E
C_u	1.4
$\text{MCE}_{R,max}(g)$	0.699
$\text{MCE}_{R,geomean}(g)$	0.538
$\text{DE}_{max}(g)$	0.466
$\text{DE}_{geomean}(g)$	0.358

5.3 Structural Properties

This section summarizes the main structural properties of the building in each direction. These structural properties are used as inputs to the SP3 Structural Response Prediction Engine.

Table 5. Structural properties table

Parameter	Direction 1	Direction 2
General		
Structural System	RC: Perimeter Frame	RC: Perimeter Frame
Building Edge Length (ft)	102	102
Detailing Level	Special	Special
Strength		
Seismic Design Base Shear Ratio, C_s	0.047	0.047
Ultimate Base Shear Ratio, v_{ult}	0.184	0.184
Stiffness		
$T_{1,design}$ (s)	1.99	1.99
T_1 with structural overstiffness (s)	1.69	1.69
T_1 with gravity system (s)	1.63	1.63
T_1 with non-structural components (s)	1.53	1.53
T_1 empirical lower bound (s)	0.91	0.91
T_1 empirical upper bound (s)	1.61	1.61
T_1 Final (s)	1.53	1.53

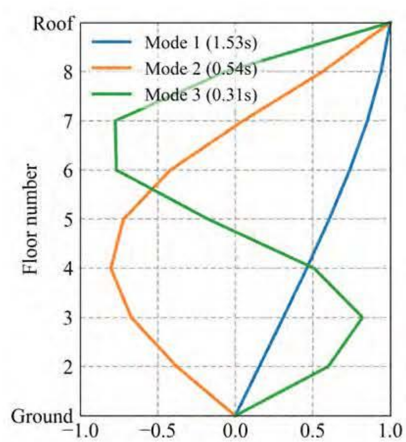

Figure 2. Mode shapes

6 BUILDING STABILITY

The FEMA P-154 collapse capacity score was calculated as follows using the "very high" seismicity level. The terminology used in this section is consistent with the FEMA P-154 methodology (Applied Technology Council, 2015a):

- P$[COL|MCE_R]_{P-154}$: the probability that the building will be in the HAZUS complete structural damage state when subjected to MCER shaking, times the collapse factor
- P$[COL|MCE_R]_{P-58}$: the probability that the building will be in the HAZUS complete structural damage state when subjected to MCER shaking, times the collapse factor
- Collapse Factor: expected ratio of collapsed area to total area given that the building is in the HAZUS Complete structural damage state

For a more in-depth explanation of "collapse," refer to Section 4.4.1.5 of FEMA P-155 Third Edition available here (Applied Technology Council, 2015b).

Table 6. Breakdown of FEMA P-154 score assignment

FEMA ID:	C1
Basic Score	1
Soil	0
Year	0
Plan Irregularity	0
Vertical Irregularity	0
Risk Category* (Cat I/II)	0
Sum:	1
Minimum Allowed:	0.3
Score:	**1**
Dispersion (β):	0.7

*Non-standard property implemented by SP3

The FEMA P-154 probability of collapse at the MCE_R level event is then calculated as:

$$\begin{aligned} \text{P}[COL|MCE_R]_{P-154} &= 10^{-\text{score}} \\ &= 10^{-1} \qquad \text{(FEMA P-155 eqn. 4-1)} \\ &= 10.0\% \end{aligned}$$

Taking into account the fraction of floor area collapsed (1 in this case), the probability of collapse is:

$$\begin{aligned} \text{P}[COL|MCE_R]_{P-58} &= \text{P}[COL|MCE_R]_{P-154} \ / \ \text{Collapse Factor} \\ &= 10.0\% \ / \ 1 \\ &= 10.0\% \end{aligned}$$

The median collapse capacity is calculated as:

$$\begin{aligned} S_{a,\ collapse\ median,\ P-58} &= \exp\left(\ln(S_{a,MCE_R}) - \text{norminv}\left(P[COL|MCE_R]_{P-58}\right) \cdot \beta\right) \\ &= \exp\left(\ln(0.577g) - \text{norminv}\left(10.0\%\right) \cdot 0.7\right) \\ &= 1.41g \end{aligned}$$

where `norminv` is the inverse of the standard normal cumulative distribution function (CDF).

Figure 3 shows the collapse capacity cumulative distribution function used in the analysis.

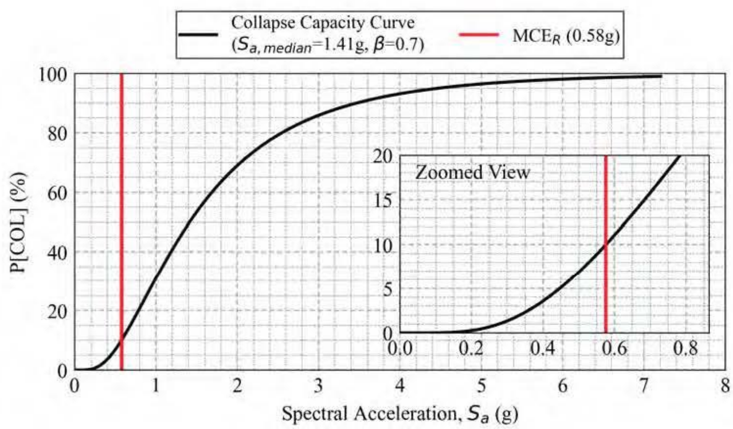

Figure 3. Cumulative distribution function for collapse capacity

7 STRUCTURAL RESPONSE PREDICTIONS FROM THE SP3 STRUCTURAL RESPONSE PREDICTION ENGINE

The SP3 Response Prediction Engine predicts the structural responses (typically providing 100 ground motions per intensity level); this is done by using a combination of three-mode elastic modal analysis, coupled with both elastic and inelastic response modifiers mined from the large SP3 Structural Responses Database (with over 4,000,000 response simulations, and growing). These response predictions track all of the important statistical information in the responses (mean, variability, and correlations); this enables a statistically robust vulnerability curve at the end of the risk assessment process.

7.1 Peak Story Drift

Peak interstory drift ratio is an important metric for both structural and non-structural components in the building. It measures how much the ceiling of a given story moves relative to the floor, normalized to the height of the story. The greater the interstory drift ratio, the greater the damage to the components on that level. Typical components that are damaged from interstory drift ratio are structural components (beams and columns), gypsum partition walls, and exterior cladding and glazing.

Table 7. Peak story drift demands are the same in both directions

Story	90% in 50 years	50% in 30 years	50% in 50 years	50% in 75 years	50% in 100 years	20% in 50 years	10% in 50 years	DE	5% in 50 years	MCE_R	2% in 50 years
8	0.07	0.12	0.18	0.24	0.29	0.37	0.51	0.61	0.66	0.81	0.87
7	0.09	0.15	0.22	0.30	0.36	0.47	0.64	0.78	0.84	1.05	1.13
6	0.10	0.17	0.26	0.34	0.42	0.54	0.75	0.91	0.99	1.24	1.34
5	0.11	0.19	0.28	0.37	0.45	0.59	0.82	1.00	1.08	1.37	1.48
4	0.12	0.20	0.30	0.40	0.48	0.63	0.88	1.09	1.19	1.54	1.68
3	0.12	0.21	0.31	0.41	0.50	0.65	0.94	1.18	1.29	1.72	1.90
2	0.13	0.22	0.32	0.43	0.52	0.69	1.02	1.32	1.47	2.06	2.32
1	0.12	0.21	0.31	0.41	0.50	0.65	0.98	1.26	1.41	1.98	2.22

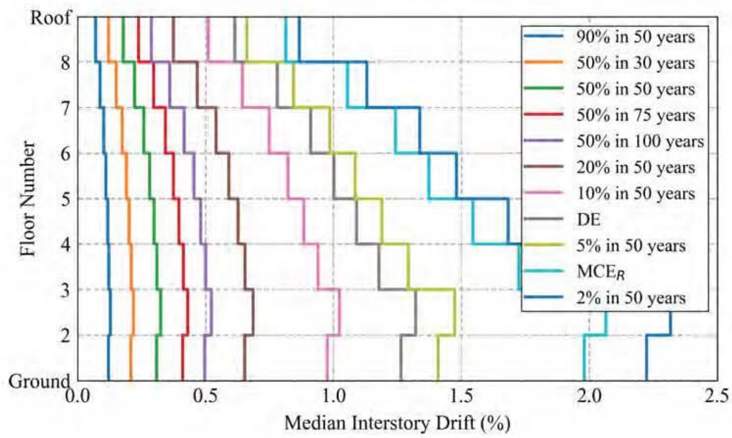

Figure 4. Peak story drift demands are the same in both directions

7.2 Peak Floor Acceleration

Peak floor acceleration is an an important metric for non-structural components in the building. Components such as piping, HVAC, and electrical switchgear are sensitive to the floor accelerations. High accelerations will typically damage a component itself or cause the component's anchorage to fail, both of which may require repair or replacement of the component.

Table 8. Peak floor acceleration demands are the same in both directions

Floor	90% in 50 years	50% in 30 years	50% in 50 years	50% in 75 years	50% in 100 years	20% in 50 years	10% in 50 years	DE	5% in 50 years	MCE_R	2% in 50 years
Roof	0.17	0.28	0.40	0.51	0.59	0.66	0.70	0.74	0.75	0.81	0.83
8	0.13	0.22	0.31	0.40	0.46	0.52	0.58	0.61	0.63	0.68	0.70
7	0.12	0.20	0.29	0.36	0.42	0.48	0.55	0.59	0.61	0.67	0.70
6	0.11	0.18	0.25	0.32	0.37	0.43	0.51	0.56	0.58	0.65	0.68
5	0.10	0.17	0.24	0.30	0.36	0.42	0.50	0.56	0.59	0.67	0.71
4	0.10	0.16	0.23	0.29	0.34	0.40	0.49	0.56	0.59	0.70	0.74
3	0.09	0.15	0.21	0.27	0.31	0.38	0.49	0.57	0.61	0.74	0.79
2	0.08	0.14	0.20	0.25	0.30	0.36	0.49	0.59	0.63	0.78	0.84
Ground	0.08	0.13	0.18	0.23	0.28	0.35	0.50	0.62	0.68	0.87	0.95

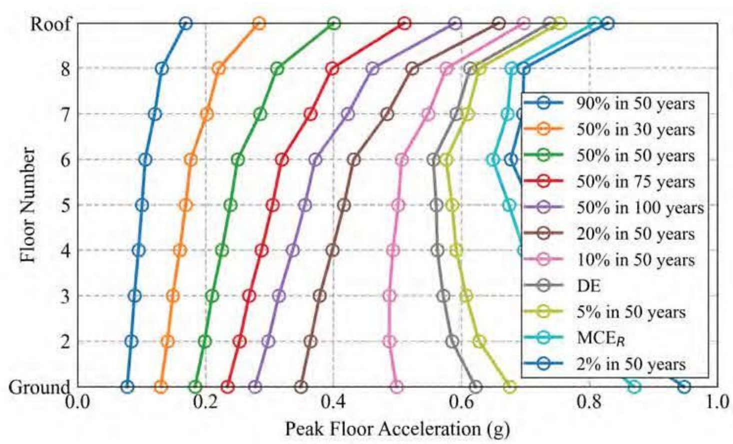

Figure 5. Peak floor acceleration demands are the same in both directions

7.3 Residual Story Drift

Residual drift is a metric that informs the need for structural repairs or building demolition (where excessive drifts are present). Residual drift ratio is a measure of how much the building is "leaning over" after the seismic event has ceased. A residual drift of 2% would indicate that the story is laterally displaced 2% of it's height, which equates to about 3.6 inches for a 15 foot tall story.

Table 9. Residual story drift demands are the same in both directions

Story	90% in 50 years	50% in 30 years	50% in 50 years	50% in 75 years	50% in 100 years	20% in 50 years	10% in 50 years	DE	5% in 50 years	MCE_R	2% in 50 years
8	0.00	0.00	0.00	0.00	0.00	0.00	0.00	0.00	0.00	0.01	0.01
7	0.00	0.00	0.00	0.00	0.00	0.00	0.00	0.00	0.01	0.04	0.05
6	0.00	0.00	0.00	0.00	0.00	0.00	0.00	0.02	0.03	0.06	0.07
5	0.00	0.00	0.00	0.00	0.00	0.00	0.01	0.03	0.04	0.08	0.09
4	0.00	0.00	0.00	0.00	0.00	0.00	0.02	0.04	0.05	0.10	0.12
3	0.00	0.00	0.00	0.00	0.00	0.00	0.02	0.05	0.07	0.12	0.14
2	0.00	0.00	0.00	0.00	0.00	0.00	0.03	0.07	0.09	0.16	0.20
1	0.00	0.00	0.00	0.00	0.00	0.00	0.03	0.06	0.08	0.15	0.18

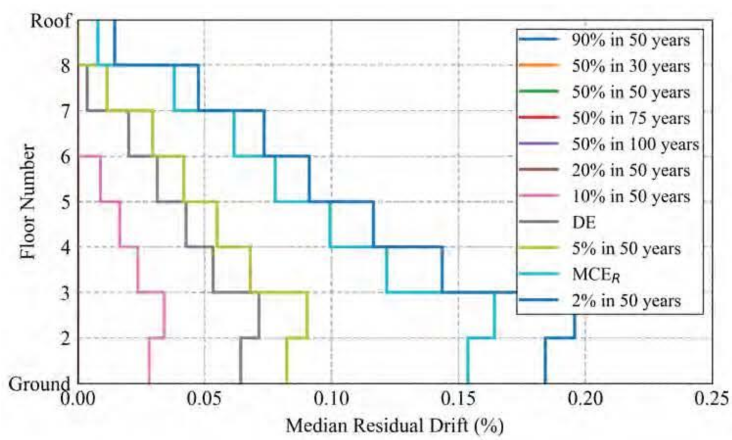

Figure 6. Residual story drift demands are the same in both directions

7.4 Maximum Residual Story Drift

Residual drift is a metric that informs the need for structural repairs or building demolition (where excessive drifts are present). A residual drift of 2% would indicate that the story is laterally displaced 2% of it's height, which equates to about 3.6 inches for a 15 foot tall story. Maximum residual drift is the maximum of the residual drifts on all levels. This is the value used to determine if the building is demolished due to excessive residual drift. Excessive drifts can be visually unsettling and prohibitively expensive (or even impossible) to "straighten" and repair the structural damage. Due to this, the building owner may decide to demolish and rebuild the building if the residual drifts are too large.

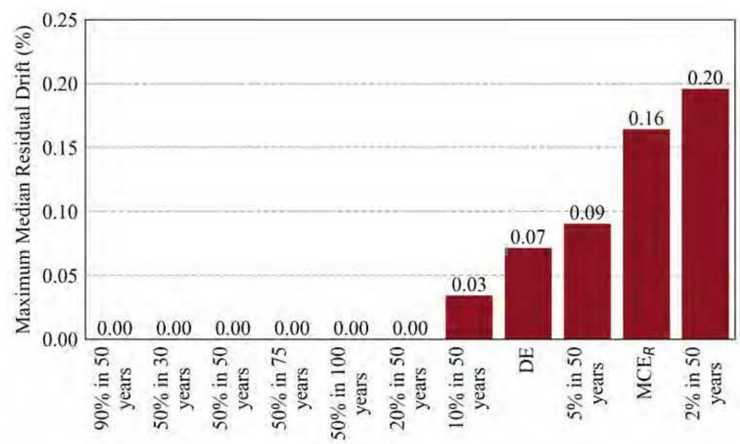

Figure 7. Maximum residual story drift demands are the same in both directions

8 REPAIR COSTS - BY LEVEL OF GROUND MOTION

8.1 Mean and 90^{th} Percentile Repair Costs (SEL and SUL)

The different metrics for repair cost are as follows:

- **Mean (SEL)**: ("Scenario Expected Loss") the average repair cost of the building repair/replacement.
- **Median**: there is a 50% probability that the repair cost will not exceed this value.
- **Fitted SUL**: Fitted value of "Scenario Upper Loss".
- **Counted 90^{th} Percentile**: there is a 90% probability that the repair cost will not exceed this value.

Table 10. Expected loss normalized by building cost

Intensity	PGA (g)	Mean (SEL) (%)	Fitted SUL (%)	Median (%)	Counted 90^{th} Percentile (%)
90% in 50 years	0.08	3.0	4.7	2.9	4.6
50% in 30 years	0.13	3.8	5.8	3.6	5.7
50% in 50 years	0.18	5.0	7.6	4.5	7.6
50% in 75 years	0.23	7.1	12	6.1	12
50% in 100 years	0.28	9.1	15	7.7	15
20% in 50 years	0.35	14	25	12	25
10% in 50 years	0.50	25	41	22	41
DE	0.62	34	54	31	54
5% in 50 years	0.68	39	62	36	62
MCE_R	0.87	54	87	50	100
2% in 50 years	0.95	59	94	56	100

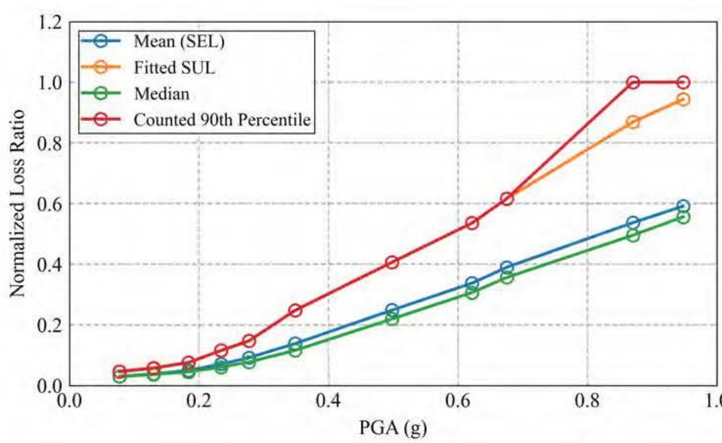

Figure 8. Loss metrics across all intensity levels analyzed

9 REPAIR COST BREAKDOWN BY BUILDING COMPONENTS

9.1 Categories for Repair Cost Breakdowns

Repair costs are binned into eight categories as follows:

- **Collapse**: building demolition and replacement following a collapse.
- **Residual**: building demolition and replacement following unacceptable residual drifts.
- **Structural**: components of the lateral force resisting system or gravity system (e.g. beam column connections, link beams, shear wall, shear tabs, etc.).
- **Partitions**: partition wall components (e.g. wood or metal stud gypsum full height partitions).
- **Exterior**: components placed on the exterior of the building (e.g. cladding, glazing, etc.).
- **Interior**: non-structural components on the interior of the building (e.g. raised access floors, ceilings, lighting).
- **HVAC**: HVAC and plumbing components (e.g. water piping and bracing, sanitary piping, ducting, boilers etc.).
- **Other**: components not included in the categories above (e.g. elevators, user defined components, fire protection components).

9.2 Repair Cost Breakdown for Various Ground Motion Levels

Table 11. Expected mean loss per component group (in percent)

Intensity	Total	Structural	Collapse	Other	HVAC	Partitions	Interior	Residual	Exterior
90% in 50 years	3.0	0.0	0.0	1.5	1.5	0.0	0.0	0.0	0.0
50% in 30 years	3.8	0.2	0.0	1.8	1.7	0.1	0.1	0.0	0.0
50% in 50 years	5.0	0.9	0.0	2.0	1.8	0.2	0.2	0.0	0.0
50% in 75 years	7.1	2.3	0.0	2.2	1.9	0.3	0.3	0.0	0.0
50% in 100 years	9.1	3.9	0.1	2.3	2.0	0.4	0.5	0.0	0.0
20% in 50 years	14	7.9	0.2	2.4	2.0	0.6	0.7	0.0	0.0
10% in 50 years	25	17	1.3	2.6	2.0	1.0	0.9	0.0	0.0
DE	34	24	3.1	2.6	2.0	1.3	1.1	0.0	0.0
5% in 50 years	39	27	4.3	2.6	2.0	1.4	1.2	0.0	0.0
MCE_R	54	35	10	2.6	1.9	1.7	1.5	1.0	0.0
2% in 50 years	59	37	13	2.5	1.8	1.7	1.6	1.4	0.0

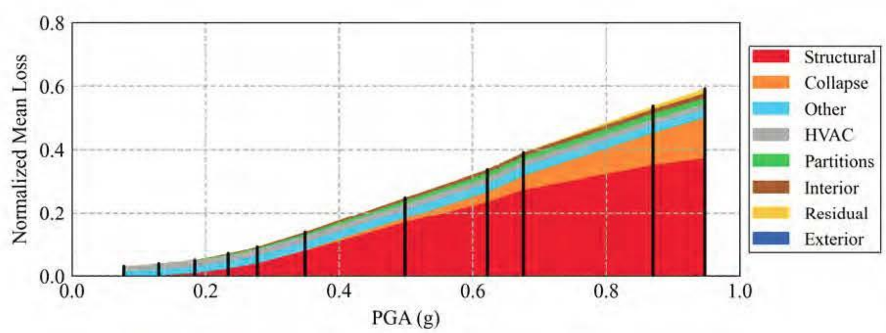

Figure 9. Contribution of building components to mean loss ratio

9.3 Repair Cost Breakdown for Expected Annual Loss

The expected annual loss for this building is $76,442.

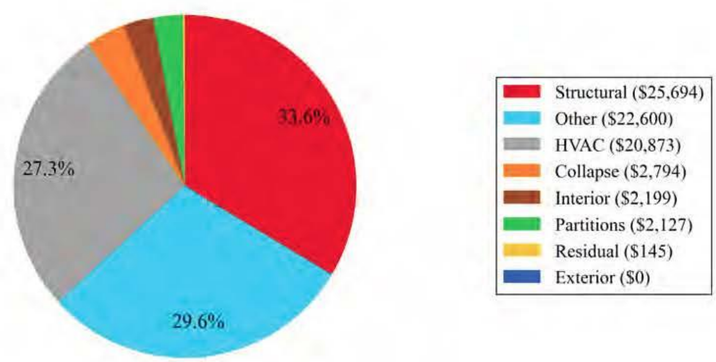

Figure 10. Annualized loss breakdown

10 REPAIR TIME AND BUILDING CLOSURE TIME

The building repair times are computed from the REDi Rating System methodology (Almufiti & Willford, 2013). These are the preferred method to compare building repair time because these include detailed repair schedules as part of the calculation process.

- **Re-Occupancy**: This is the time after which the building is deemed safe enough to be used for shelter.
- **Functional Recovery**: This is time required to establish re-occupancy and regain the facility's primary function. This is what is typically used for assessing building closure time.
- **Full Recovery**: This is the time required to restore the building to its original pre-earthquake condition.

For comparison, the methods of calculating building repair time from the FEMA P-58 methodology are as follows. These are typically not used to estimate building closure time.

- **Series**: Repair activities are limited to one floor at a time
- **Parallel**: All floors are repaired at the same time

For a design level or 10% in 50 year event, the REDi methodology is also calibrated to include "impedance factors" associated with the following processes:

- Post-earthquake Inspection
- Engineering Mobilization and Review/Re-design
- Financing
- Contractor Mobilization and Bid Process
- Permitting

These capture the time required to start the repairs, since beginning repairs immediately after an earthquake may not be realistic. **With these impedance factors, the median functional recovery time is 13 months.**

Table 12. Median repair time, without impeding factors

Intensity	FEMA P-58 Parallel	FEMA P-58 Series	REDi Re-Occupancy	REDi Functional Recovery	REDi Full Recovery
90% in 50 years	5 days	6 days	0 days	8 days	8 days
50% in 30 years	7 days	11 days	0 days	13 days	13 days
50% in 50 years	10 days	3.1 weeks	3 days	2.7 weeks	2.7 weeks
50% in 75 years	2.2 weeks	5.6 weeks	12 days	3.9 weeks	3.9 weeks
50% in 100 years	2.8 weeks	2.1 months	3.3 weeks	5.3 weeks	5.3 weeks
20% in 50 years	4.5 weeks	3.9 months	6.8 weeks	2.0 months	2.0 months
10% in 50 years	2.0 months	8.7 months	3.9 months	4.2 months	4.2 months
DE	2.6 months	13 months	5.7 months	6.0 months	6.0 months
5% in 50 years	3.0 months	15 months	6.8 months	7.0 months	7.0 months
MCE_R	4.0 months	19 months	9.8 months	10 months	10 months
2% in 50 years	4.3 months	19 months	11 months	11 months	11 months

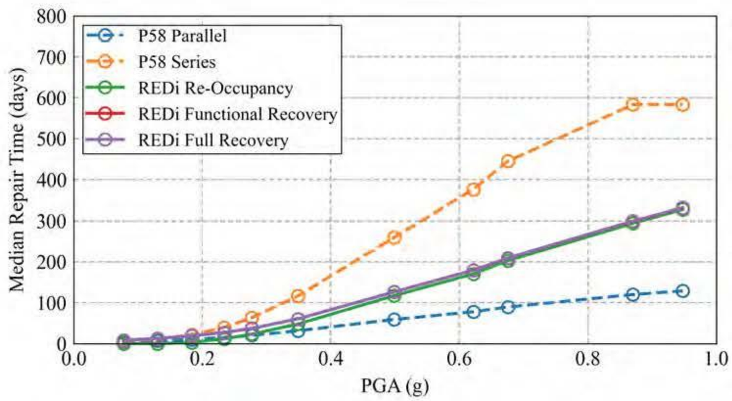

Figure 11. Median repair time, without impeding factors

11 JUSTIFICATION OF SECONDARY MODIFIERS

No justification of secondary inputs was provided.

12 DISCLAIMER

REFERENCES

Almufiti, Ibrahim, & Willford, Michael. 2013. *REDi Rating System*. Arup.

Applied Technology Council. 2015a. *FEMA P-154: Rapid Visual Screening of Buildings for Potential Seismic Hazards: A Handbook.*

Applied Technology Council. 2015b. *FEMA P-155: Rapid Visual Screening of Buildings for Potential Seismic Hazards: Supporting Documentation.*

Applied Technology Council. 2018. *FEMA P-58: Seismic Perfromance Assessment of Buildings.*

International Conference of Building Officials. 1961. *Uniform Building Code 1961 Edition*. International Conference of Building Officials.

H8. Detailed Analysis – Franz Tower Retrofit with VD + Test Data

CONTENTS

1 SUMMARY OF INPUTS AND RISK RESULTS

Risk Model Inputs

Primary

Project Name:	5 Franz-Pritzker
Model Name:	VD Retrofit w/test data (reduced joints / IMF)
Building Type:	RC: Space Frame
Year of Construction:	1967
Number of Stories:	8
Occupancy:	Commercial Office
Address: 502 Portola Plaza Los Angeles, CA, 90095	
Latitude:	34.06985°
Longitude:	-118.44125°

Analysis Options

Include Collapse in Analysis:	Yes
Consider Residual Drift:	Yes

Building Layout Information

Cost per Square Foot:	–
Total Square Feet:	84,211
Aspect Ratio:	–
First Story Height (ft):	14
Upper Story Heights (ft):	13
Vertical Irregularity:	None
Plan Irregularity:	–

Ground Motion and Soil Information

Site Class:	C
Site Hazard:	SP3 Default

Building Design Info

Level of Detailing (Dir. 1, 2):	Ordinary, Ordinary
Drift Limit (Dir. 1, 2):	2.000%, 2.000%
Risk Category:	I/II
Seismic Importance Factor, I_e:	1
Component Importance Factor, I_p:	–
Include Retrofit Information?	No

Structural Properties

Property	Dir. 1	Dir. 2
Base Shear Strength (g):	0.128	0.128
Yield Drift (%):	0.69	0.69
1^{st} Mode Period (T_1) (s):	1.35	1.35
2^{nd} Mode Period (T_2) (s):	–	–
3^{rd} Mode Period (T_3) (s):	–	–

Component Information

Do your stairs have seismic joints?	No
Is your ceiling laterally supported?	Yes
Is your lighting seismically rated?	Yes
Is your piping seismically rated?	Yes
Is your HVAC system seismically anchored?	Yes
Is your electrical equipment seismically rated?	Yes
Percent of Building Glazed:	–

Building Stability

Median Collapse Capacity:	–
Beta (Dispersion):	–

Responses

No responses provided

Repair Time Options

Factors Delaying Start of Repairs	
Inspection	Yes
Financing	Yes
Permitting	Yes
Engineering Mobilization	Yes
Contractor Mobilization	Yes
Mitigation Factors	
Inspector on Retainer	No
Engineer on Retainer	No
Engineer on Retainer	No
Funding Source	Private Loans

Expected Loss

Expected loss in percent of total building value

Shaking Intensity	Return Period	SEL (%)	SUL (%)
90% in 50 years	22 Years	3.0	4.7
50% in 30 years	43 Years	3.6	5.5
50% in 50 years	72 Years	4.3	6.5
50% in 75 years	108 Years	5.2	7.8
50% in 100 years	144 Years	6.3	9.9
20% in 50 years	224 Years	8.6	14
10% in 50 years	475 Years	14	25
DE	791 Years	21	38
5% in 50 years	975 Years	25	46
MCE_R	1956 Years	41	69
2% in 50 years	2475 Years	46	77

Repair Time

Median repair time, without impeding factors

Intensity	FEMA P-58 Parallel	FEMA P-58 Series	REDi Re-Occupancy	REDi Functional Recovery	REDi Full Recovery
90% in 50 years	5 days	6 days	0 days	8 days	8 days
50% in 30 years	6 days	10 days	0 days	12 days	12 days
50% in 50 years	9 days	2.3 weeks	1 days	2.4 weeks	2.4 weeks
50% in 75 years	11 days	3.5 weeks	3 days	2.9 weeks	2.9 weeks
50% in 100 years	2.1 weeks	4.9 weeks	8 days	3.4 weeks	3.4 weeks
20% in 50 years	2.8 weeks	1.9 months	2.7 weeks	4.7 weeks	4.7 weeks
10% in 50 years	4.3 weeks	3.7 months	6.3 weeks	7.9 weeks	7.9 weeks
DE	6.8 weeks	5.9 months	2.6 months	2.9 months	2.9 months
5% in 50 years	2.0 months	7.7 months	3.4 months	3.7 months	3.7 months
MCE_R	3.3 months	14 months	6.6 months	6.8 months	6.8 months
2% in 50 years	3.7 months	17 months	7.8 months	8.0 months	8.0 months

2 BASIS OF ANALYSIS

This analysis is based on the SP3-RiskModel of the Seismic Performance Prediction Program (SP3) software platform. The underlying analysis methods are based on the FEMA P-58 analytical method, which is a transparent and well documented method developed through a 15 year project (Applied Technology Council, 2018). This project leveraged the previous decades of academic research, funded by a $16 million investment by the Federal Emergency Management Agency (FEMA). In contrast to many risk assessment methods based on judgment and past earthquake experience, the FEMA P-58 and SP3 analysis are based on engineering-oriented risk evaluation methods.

3 DOCUMENTATION OF SITE AND BUILDING INPUT DATA

Project Name: 5 Franz-Pritzker
Model Name: VD Retrofit w/test data (reduced joints / IMF)

3.1 Site Information

Address: 502 Portola Plaza, Los Angeles, CA, 90095
Latitude: 34.06985°
Longitude: -118.44125°

3.2 Building Information

Material Type:	Cast-in-Place Concrete
Number of Stories:	8
Total Building Square Footage:	84,211
Occupancy Type:	Commercial Office
Total Expected Building Replacement Value:	$22,110,841

4 SITE HAZARD INFORMATION

This section presents the site's seismic hazard information. The V_{S30} value is the shear wave velocity in the soil at a depth of 30 meters. This value and the associated site class are presented in Table 1.

Table 1. Site soil information

V_{S30} (m/s):	537.0
Site Class:	C

Table 2 and Figure 1 present the spectral acceleration information for this site. The spectral acceleration is a measure of how much force the building will attract in an earthquake. This amount of force is dependent on the intensity of the ground shaking (e.g. 10% in 50 years), as well as a dynamic property of the building known as the "fundamental period". Shorter buildings tend to have smaller fundamental periods and taller buildings tend to have larger fundamental periods. As indicated by Figure 1, smaller fundamental periods (with the exception of very short fundamental periods) will attract more force in an earthquake.

The Design Earthquake (DE) and Maximum Considered Earthquake (MCE) are based on the modern code maximum direction spectra and are converted to geometric mean for comparison.

Table 2. Geometric mean spectral acceleration values (in g)

Shaking Intensity	Return Period	PGA	$S_a(0.2s)$	$S_a(1.0s)$	$S_a(1.4s)$
90% in 50 years	22 years	0.08	0.18	0.05	0.04
50% in 30 years	43 years	0.13	0.30	0.09	0.07
50% in 50 years	72 years	0.18	0.44	0.13	0.11
50% in 75 years	108 years	0.23	0.56	0.18	0.14
50% in 100 years	144 years	0.28	0.67	0.21	0.17
20% in 50 years	224 years	0.35	0.84	0.28	0.23
10% in 50 years	475 years	0.50	1.22	0.43	0.34
DE	791 years	0.62	1.53	0.55	0.44
5% in 50 years	975 years	0.68	1.66	0.61	0.49
MCE_R	1956 years	0.87	2.18	0.82	0.66
2% in 50 years	2475 years	0.95	2.36	0.91	0.73

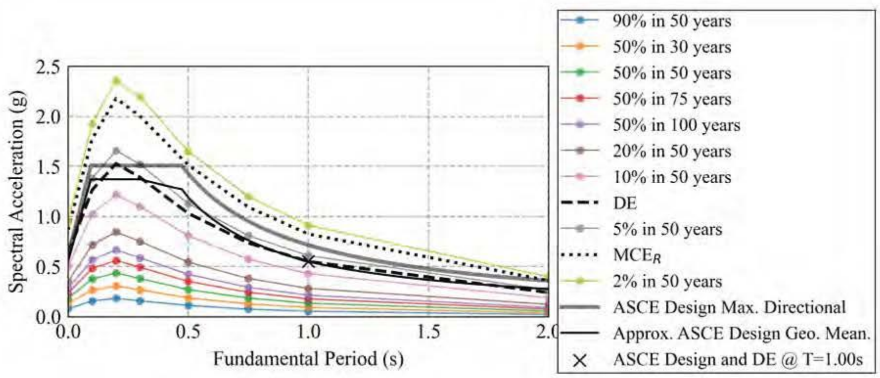

Figure 1. Hazard curves for this site. All curves are geometric mean unless otherwise stated.

5 BUILDING DESIGN SUMMARY FROM THE *SP3 BUILDING CODE DESIGN DATABASE*

5.1 Building Code Design Parameters

The seismic design parameters used to compute the seismic base shear coefficients for this building are presented in Table 3. These parameters are specific to the 1961 edition of the Uniform Building Code (International Conference of Building Officials, 1961).

Table 3. Code design parameters

(a) UBC 1961 structural system parameters

Parameter	Dir. 1	Dir. 2
C_d	1	1
k	1	1

(b) UBC 1961 site specific parameters

Parameter	Value
Z	1
Seismic Zone	3

5.2 Modern Building Code Design Parameters

For comparison to modern code, the modern code parameters are presented in Table 4.

Table 4. Modern code design parameters

(a) ASCE/SEI 7-2010 structural system parameters

Parameter	Dir. 1	Dir. 2
C_t	0.016	0.016
C_d	5.5	5.5
x	0.9	0.9
R	8	8
Ω_0	3	3

(b) ASCE/SEI 7-2010 site specific parameters

Parameter	Value
S_s	2.263
S_1	0.825
S_{ds}	1.508
S_{d1}	0.715
SDC	E
C_u	1.4
$\text{MCE}_{R,max}(g)$	0.794
$\text{MCE}_{R,geomean}(g)$	0.611
$\text{DE}_{max}(g)$	0.529
$\text{DE}_{geomean}(g)$	0.407

5.3 Structural Properties

This section summarizes the main structural properties of the building in each direction. These structural properties are used as inputs to the SP3 Structural Response Prediction Engine.

Table 5. Structural properties table

Parameter	Direction 1	Direction 2
General		
Structural System	RC: Space Frame	RC: Space Frame
Building Edge Length (ft)	102	102
Detailing Level	Ordinary	Ordinary
Strength		
Seismic Design Base Shear Ratio, C_s	0.035	0.035
Ultimate Base Shear Ratio, v_{ult}	0.128*	0.128*
Stiffness		
$T_{1,design}$ (s)	1.86	1.86
T_1 with structural overstiffness (s)	1.57	1.57
T_1 with gravity system (s)	1.56	1.56
T_1 with non-structural components (s)	1.48	1.48
T_1 empirical lower bound (s)	0.91	0.91
T_1 empirical upper bound (s)	1.61	1.61
T_1 Final (s)	1.35	1.35

*User defined, not SP3 default

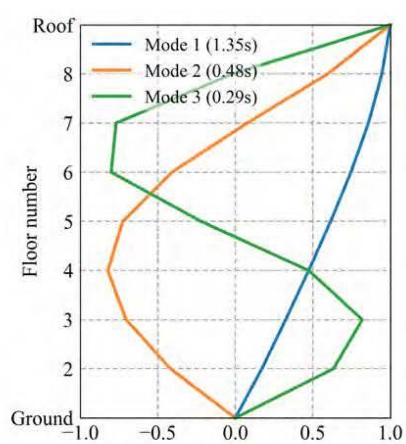

Figure 2. Mode shapes

6 BUILDING STABILITY

The FEMA P-154 collapse capacity score was calculated as follows using the "very high" seismicity level. The terminology used in this section is consistent with the FEMA P-154 methodology (Applied Technology Council, 2015a):

- P$[COL|MCE_R]_{P-154}$: the probability that the building will be in the HAZUS complete structural damage state when subjected to MCER shaking, times the collapse factor
- P$[COL|MCE_R]_{P-58}$: the probability that the building will be in the HAZUS complete structural damage state when subjected to MCER shaking, times the collapse factor
- Collapse Factor: expected ratio of collapsed area to total area given that the building is in the HAZUS Complete structural damage state

For a more in-depth explanation of "collapse," refer to Section 4.4.1.5 of FEMA P-155 Third Edition available here (Applied Technology Council, 2015b).

Table 6. Breakdown of FEMA P-154 score assignment

FEMA ID:	C1
Basic Score	1
Soil	0
Year	0
Plan Irregularity	0
Vertical Irregularity	0
Risk Category* (Cat I/II)	0
Sum:	1
Minimum Allowed:	0.3
Score:	**1**
Dispersion (β):	0.7

*Non-standard property implemented by SP3

The FEMA P-154 probability of collapse at the MCE_R level event is then calculated as:

$$\begin{aligned} \text{P}[COL|MCE_R]_{P-154} &= 10^{-\text{score}} \\ &= 10^{-1} \qquad \text{(FEMA P-155 eqn. 4-1)} \\ &= 10.0\% \end{aligned}$$

Taking into account the fraction of floor area collapsed (1 in this case), the probability of collapse is:

$$\begin{aligned} \text{P}[COL|MCE_R]_{P-58} &= \text{P}[COL|MCE_R]_{P-154} \text{ / Collapse Factor} \\ &= 10.0\% / 1 \\ &= 10.0\% \end{aligned}$$

The median collapse capacity is calculated as:

$$\begin{aligned} S_{a,\ collapse\ median,\ P-58} &= \exp\left(\ln(S_{a,MCE_R}) - \text{norminv}\left(P[COL|MCE_R]_{P-58}\right) \cdot \beta\right) \\ &= \exp\left(\ln(0.662g) - \text{norminv}\,(10.0\%) \cdot 0.7\right) \\ &= 1.62g \end{aligned}$$

where `norminv` is the inverse of the standard normal cumulative distribution function (CDF).

Figure 3 shows the collapse capacity cumulative distribution function used in the analysis.

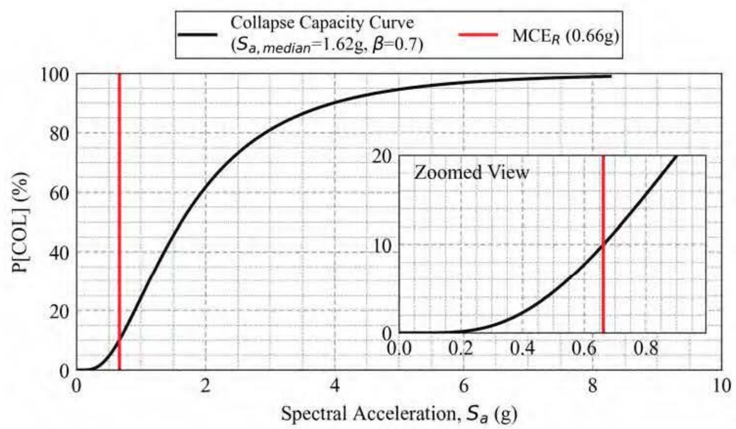

Figure 3. Cumulative distribution function for collapse capacity

7 STRUCTURAL RESPONSE PREDICTIONS FROM THE SP3 STRUCTURAL RESPONSE PREDICTION ENGINE

The SP3 Response Prediction Engine predicts the structural responses (typically providing 100 ground motions per intensity level); this is done by using a combination of three-mode elastic modal analysis, coupled with both elastic and inelastic response modifiers mined from the large SP3 Structural Responses Database (with over 4,000,000 response simulations, and growing). These response predictions track all of the important statistical information in the responses (mean, variability, and correlations); this enables a statistically robust vulnerability curve at the end of the risk assessment process.

7.1 Peak Story Drift

Peak interstory drift ratio is an important metric for both structural and non-structural components in the building. It measures how much the ceiling of a given story moves relative to the floor, normalized to the height of the story. The greater the interstory drift ratio, the greater the damage to the components on that level. Typical components that are damaged from interstory drift ratio are structural components (beams and columns), gypsum partition walls, and exterior cladding and glazing.

Table 7. Peak story drift demands are the same in both directions

Story	90% in 50 years	50% in 30 years	50% in 50 years	50% in 75 years	50% in 100 years	20% in 50 years	10% in 50 years	DE	5% in 50 years	MCE_R	2% in 50 years
8	0.05	0.09	0.13	0.18	0.21	0.27	0.37	0.47	0.52	0.69	0.76
7	0.07	0.12	0.18	0.24	0.30	0.38	0.52	0.65	0.72	0.96	1.05
6	0.09	0.15	0.22	0.29	0.35	0.45	0.62	0.78	0.86	1.14	1.25
5	0.09	0.16	0.24	0.32	0.39	0.50	0.68	0.86	0.94	1.26	1.38
4	0.10	0.17	0.25	0.34	0.41	0.53	0.72	0.91	1.00	1.33	1.46
3	0.10	0.18	0.26	0.35	0.43	0.55	0.75	0.94	1.04	1.38	1.52
2	0.11	0.19	0.28	0.37	0.45	0.58	0.79	0.99	1.09	1.45	1.60
1	0.12	0.20	0.29	0.39	0.47	0.61	0.83	1.04	1.15	1.53	1.68

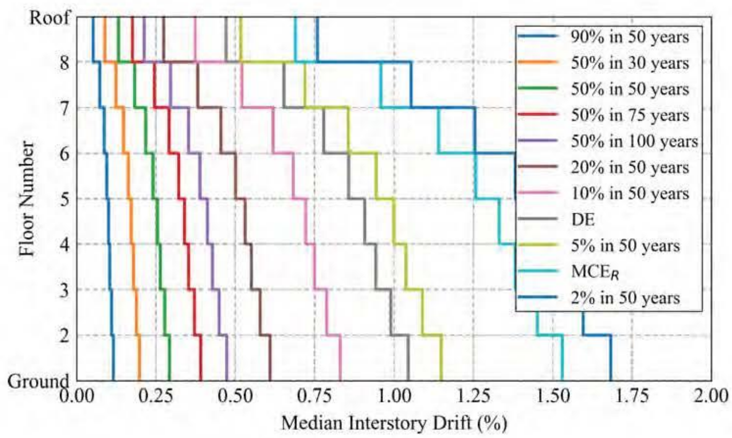

Figure 4. Peak story drift demands are the same in both directions

7.2 Peak Floor Acceleration

Peak floor acceleration is an an important metric for non-structural components in the building. Components such as piping, HVAC, and electrical switchgear are sensitive to the floor accelerations. High accelerations will typically damage a component itself or cause the component's anchorage to fail, both of which may require repair or replacement of the component.

Table 8. Peak floor acceleration demands are the same in both directions

Floor	90% in 50 years	50% in 30 years	50% in 50 years	50% in 75 years	50% in 100 years	20% in 50 years	10% in 50 years	DE	5% in 50 years	MCE_R	2% in 50 years
Roof	0.17	0.29	0.40	0.48	0.54	0.58	0.64	0.68	0.70	0.73	0.74
8	0.15	0.25	0.34	0.40	0.44	0.47	0.52	0.56	0.57	0.61	0.62
7	0.13	0.22	0.30	0.36	0.39	0.42	0.48	0.52	0.54	0.59	0.60
6	0.12	0.20	0.27	0.32	0.35	0.38	0.44	0.49	0.51	0.57	0.59
5	0.11	0.18	0.25	0.29	0.33	0.36	0.43	0.50	0.52	0.60	0.63
4	0.10	0.17	0.23	0.28	0.31	0.35	0.44	0.51	0.54	0.63	0.67
3	0.09	0.15	0.22	0.26	0.30	0.35	0.45	0.53	0.57	0.70	0.75
2	0.09	0.14	0.20	0.25	0.29	0.34	0.46	0.56	0.61	0.76	0.82
Ground	0.08	0.13	0.18	0.23	0.28	0.35	0.50	0.62	0.68	0.87	0.95

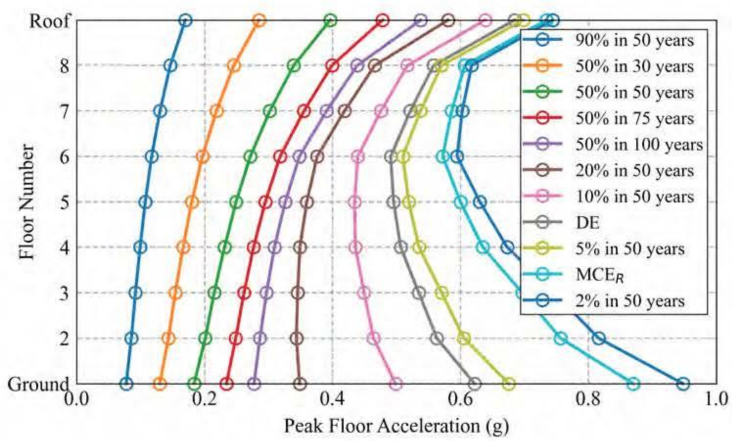

Figure 5. Peak floor acceleration demands are the same in both directions

7.3 Residual Story Drift

Residual drift is a metric that informs the need for structural repairs or building demolition (where excessive drifts are present). Residual drift ratio is a measure of how much the building is "leaning over" after the seismic event has ceased. A residual drift of 2% would indicate that the story is laterally displaced 2% of it's height, which equates to about 3.6 inches for a 15 foot tall story.

Table 9. Residual story drift demands are the same in both directions

Story	90% in 50 years	50% in 30 years	50% in 50 years	50% in 75 years	50% in 100 years	20% in 50 years	10% in 50 years	DE	5% in 50 years	MCE_R	2% in 50 years
8	0.00	0.00	0.00	0.00	0.00	0.00	0.00	0.00	0.00	0.00	0.01
7	0.00	0.00	0.00	0.00	0.00	0.00	0.00	0.00	0.00	0.03	0.05
6	0.00	0.00	0.00	0.00	0.00	0.00	0.00	0.01	0.02	0.06	0.07
5	0.00	0.00	0.00	0.00	0.00	0.00	0.00	0.02	0.03	0.07	0.09
4	0.00	0.00	0.00	0.00	0.00	0.00	0.00	0.03	0.04	0.08	0.10
3	0.00	0.00	0.00	0.00	0.00	0.00	0.01	0.03	0.04	0.09	0.10
2	0.00	0.00	0.00	0.00	0.00	0.00	0.01	0.04	0.05	0.10	0.11
1	0.00	0.00	0.00	0.00	0.00	0.00	0.02	0.04	0.06	0.11	0.12

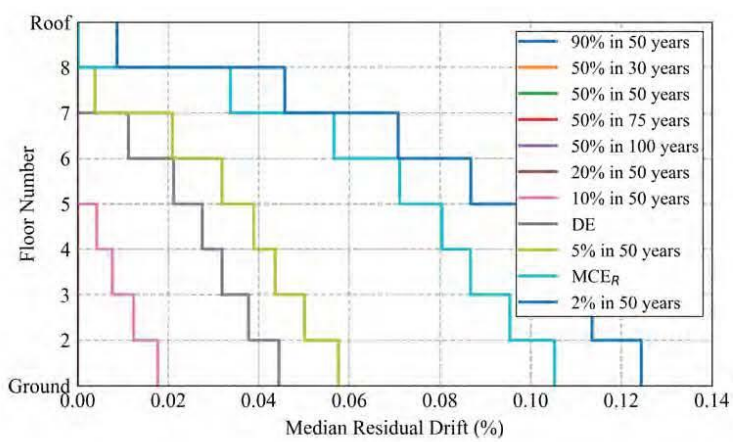

Figure 6. Residual story drift demands are the same in both directions

7.4 Maximum Residual Story Drift

Residual drift is a metric that informs the need for structural repairs or building demolition (where excessive drifts are present). A residual drift of 2% would indicate that the story is laterally displaced 2% of it's height, which equates to about 3.6 inches for a 15 foot tall story. Maximum residual drift is the maximum of the residual drifts on all levels. This is the value used to determine if the building is demolished due to excessive residual drift. Excessive drifts can be visually unsettling and prohibitively expensive (or even impossible) to "straighten" and repair the structural damage. Due to this, the building owner may decide to demolish and rebuild the building if the residual drifts are too large.

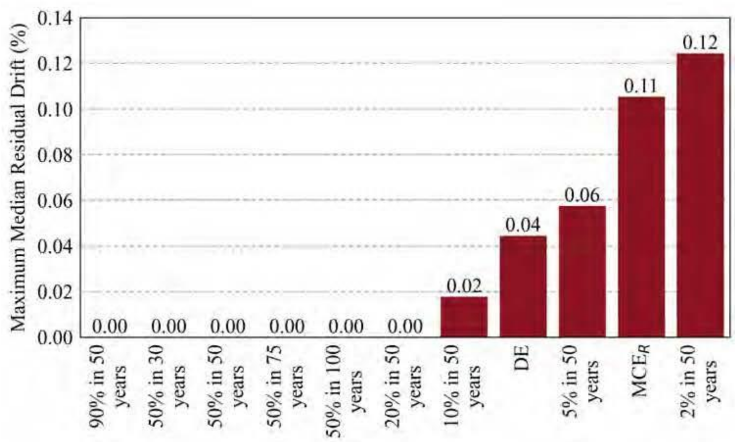

Figure 7. Maximum residual story drift demands are the same in both directions

8 REPAIR COSTS - BY LEVEL OF GROUND MOTION

8.1 Mean and 90th Percentile Repair Costs (SEL and SUL)

The different metrics for repair cost are as follows:

- **Mean (SEL)**: ("Scenario Expected Loss") the average repair cost of the building repair/replacement.
- **Median**: there is a 50% probability that the repair cost will not exceed this value.
- **Fitted SUL**: Fitted value of "Scenario Upper Loss".
- **Counted 90th Percentile**: there is a 90% probability that the repair cost will not exceed this value.

Table 10. Expected loss normalized by building cost

Intensity	PGA (g)	Mean (SEL) (%)	Fitted SUL (%)	Median (%)	Counted 90th Percentile (%)
90% in 50 years	0.08	3.0	4.7	2.9	4.6
50% in 30 years	0.13	3.6	5.5	3.5	5.3
50% in 50 years	0.18	4.3	6.5	4.1	6.3
50% in 75 years	0.23	5.2	7.8	4.7	7.7
50% in 100 years	0.28	6.3	9.9	5.5	9.9
20% in 50 years	0.35	8.6	14	7.1	14
10% in 50 years	0.50	14	25	11	25
DE	0.62	21	38	16	38
5% in 50 years	0.68	25	46	20	46
MCE$_R$	0.87	41	69	35	100
2% in 50 years	0.95	46	77	41	100

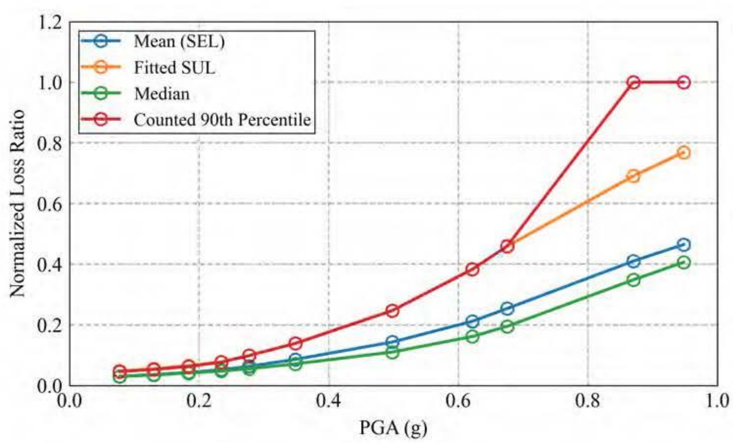

Figure 8. Loss metrics across all intensity levels analyzed

9 REPAIR COST BREAKDOWN BY BUILDING COMPONENTS

9.1 Categories for Repair Cost Breakdowns

Repair costs are binned into eight categories as follows:

- **Collapse**: building demolition and replacement following a collapse.
- **Residual**: building demolition and replacement following unacceptable residual drifts.
- **Structural**: components of the lateral force resisting system or gravity system (e.g. beam column connections, link beams, shear wall, shear tabs, etc.).
- **Partitions**: partition wall components (e.g. wood or metal stud gypsum full height partitions).
- **Exterior**: components placed on the exterior of the building (e.g. cladding, glazing, etc.).
- **Interior**: non-structural components on the interior of the building (e.g. raised access floors, ceilings, lighting).
- **HVAC**: HVAC and plumbing components (e.g. water piping and bracing, sanitary piping, ducting, boilers etc.).
- **Other**: components not included in the categories above (e.g. elevators, user defined components, fire protection components).

9.2 Repair Cost Breakdown for Various Ground Motion Levels

Table 11. Expected mean loss per component group (in percent)

Intensity	Total	Structural	Collapse	Other	HVAC	Partitions	Interior	Residual	Exterior
90% in 50 years	3.0	0.0	0.0	1.5	1.5	0.0	0.0	0.0	0.0
50% in 30 years	3.6	0.0	0.0	1.8	1.7	0.0	0.1	0.0	0.0
50% in 50 years	4.3	0.2	0.0	2.0	1.8	0.1	0.2	0.0	0.0
50% in 75 years	5.2	0.7	0.0	2.2	1.9	0.2	0.3	0.0	0.0
50% in 100 years	6.3	1.3	0.1	2.3	1.9	0.3	0.4	0.0	0.0
20% in 50 years	8.6	3.0	0.2	2.4	2.0	0.5	0.5	0.0	0.0
10% in 50 years	14	7.0	1.3	2.5	2.0	0.8	0.7	0.0	0.0
DE	21	12	3.1	2.6	1.9	1.0	0.9	0.0	0.0
5% in 50 years	25	14	4.3	2.6	1.9	1.1	1.0	0.0	0.0
MCE_R	41	24	10	2.5	1.9	1.4	1.2	0.3	0.0
2% in 50 years	46	26	13	2.5	1.8	1.5	1.3	0.3	0.0

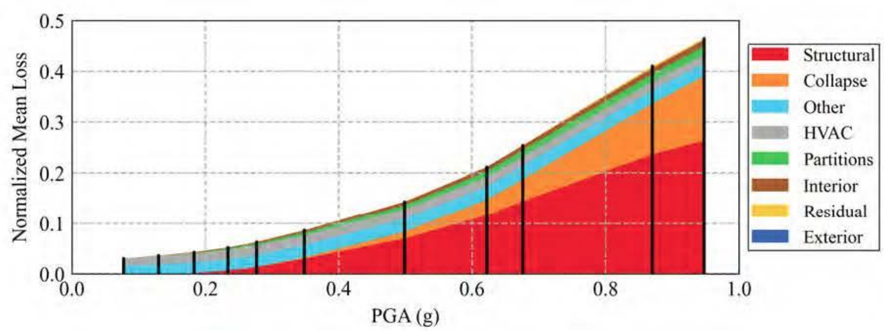

Figure 9. Contribution of building components to mean loss ratio

9.3 Repair Cost Breakdown for Expected Annual Loss

The expected annual loss for this building is $61,207.

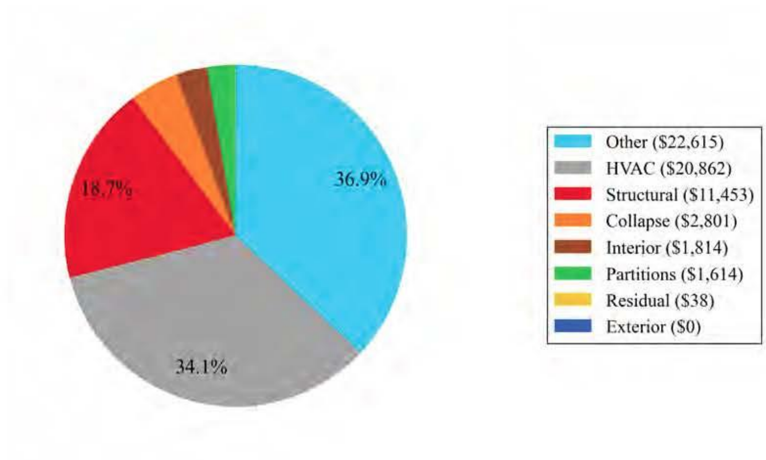

Figure 10. Annualized loss breakdown

10 REPAIR TIME AND BUILDING CLOSURE TIME

The building repair times are computed from the REDi Rating System methodology (Almufiti & Willford, 2013). These are the preferred method to compare building repair time because these include detailed repair schedules as part of the calculation process.

- **Re-Occupancy**: This is the time after which the building is deemed safe enough to be used for shelter.
- **Functional Recovery**: This is time required to establish re-occupancy and regain the facility's primary function. This is what is typically used for assessing building closure time.
- **Full Recovery**: This is the time required to restore the building to its original pre-earthquake condition.

For comparison, the methods of calculating building repair time from the FEMA P-58 methodology are as follows. These are typically not used to estimate building closure time.

- **Series**: Repair activities are limited to one floor at a time
- **Parallel**: All floors are repaired at the same time

For a design level or 10% in 50 year event, the REDi methodology is also calibrated to include "impedance factors" associated with the following processes:

- Post-earthquake Inspection
- Engineering Mobilization and Review/Re-design
- Financing
- Contractor Mobilization and Bid Process
- Permitting

These capture the time required to start the repairs, since beginning repairs immediately after an earthquake may not be realistic. **With these impedance factors, the median functional recovery time is 10 months.**

Table 12. Median repair time, without impeding factors

Intensity	FEMA P-58 Parallel	FEMA P-58 Series	REDi Re-Occupancy	REDi Functional Recovery	REDi Full Recovery
90% in 50 years	5 days	6 days	0 days	8 days	8 days
50% in 30 years	6 days	10 days	0 days	12 days	12 days
50% in 50 years	9 days	2.3 weeks	1 days	2.4 weeks	2.4 weeks
50% in 75 years	11 days	3.5 weeks	3 days	2.9 weeks	2.9 weeks
50% in 100 years	2.1 weeks	4.9 weeks	8 days	3.4 weeks	3.4 weeks
20% in 50 years	2.8 weeks	1.9 months	2.7 weeks	4.7 weeks	4.7 weeks
10% in 50 years	4.3 weeks	3.7 months	6.3 weeks	7.9 weeks	7.9 weeks
DE	6.8 weeks	5.9 months	2.6 months	2.9 months	2.9 months
5% in 50 years	2.0 months	7.7 months	3.4 months	3.7 months	3.7 months
MCE_R	3.3 months	14 months	6.6 months	6.8 months	6.8 months
2% in 50 years	3.7 months	17 months	7.8 months	8.0 months	8.0 months

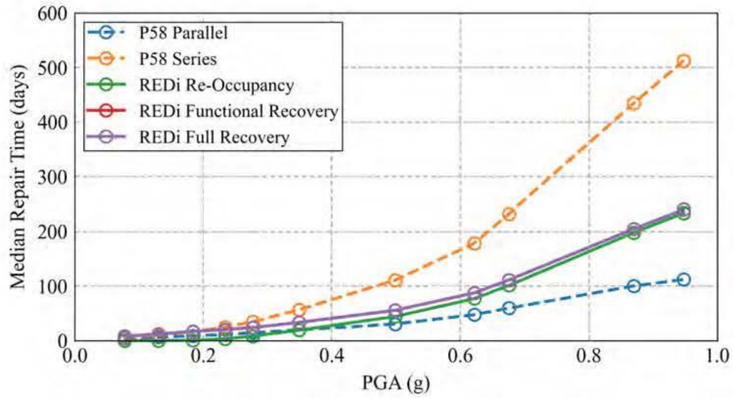

Figure 11. Median repair time, without impeding factors

11 JUSTIFICATION OF SECONDARY MODIFIERS

No justification of secondary inputs was provided.

12 DISCLAIMER

REFERENCES

Almufiti, Ibrahim, & Willford, Michael. 2013. *REDi Rating System*. Arup.

Applied Technology Council. 2015a. *FEMA P-154: Rapid Visual Screening of Buildings for Potential Seismic Hazards: A Handbook.*

Applied Technology Council. 2015b. *FEMA P-155: Rapid Visual Screening of Buildings for Potential Seismic Hazards: Supporting Documentation.*

Applied Technology Council. 2018. *FEMA P-58: Seismic Perfromance Assessment of Buildings.*

International Conference of Building Officials. 1961. *Uniform Building Code 1961 Edition*. International Conference of Building Officials.

H9. Detailed Analysis – Franz Tower Retrofit with VD + Test Data + User Input Ground Motions

CONTENTS

1 SUMMARY OF INPUTS AND RISK RESULTS

Risk Model Inputs

Primary

Project Name:	7 Franz-Pritzker
Model Name:	VD Retrofit w/test data (reduced joints / IMF) User GMs
Building Type:	RC: Space Frame
Year of Construction:	1967
Number of Stories:	8
Occupancy:	Commercial Office
Address: 502 Portola Plaza Los Angeles, CA, 90095	
Latitude:	34.06985°
Longitude:	-118.44125°

Analysis Options

Include Collapse in Analysis:	Yes
Consider Residual Drift:	Yes

Building Layout Information

Cost per Square Foot:	–
Total Square Feet:	84,211
Aspect Ratio:	–
First Story Height (ft):	14
Upper Story Heights (ft):	13
Vertical Irregularity:	None
Plan Irregularity:	–

Ground Motion and Soil Information

Site Class:	C
Site Hazard:	User Defined

Building Design Info

Level of Detailing (Dir. 1, 2):	Ordinary, Ordinary
Drift Limit (Dir. 1, 2):	2.000%, 2.000%
Risk Category:	I/II
Seismic Importance Factor, I_e:	1
Component Importance Factor, I_p:	–
Include Retrofit Information?	No

Structural Properties

Property	Dir. 1	Dir. 2
Base Shear Strength (g):	0.128	0.128
Yield Drift (%):	0.69	0.69
1^{st} Mode Period (T_1) (s):	1.35	1.35
2^{nd} Mode Period (T_2) (s):	–	–
3^{rd} Mode Period (T_3) (s):	–	–

Component Information

Do your stairs have seismic joints?	No
Is your ceiling laterally supported?	Yes
Is your lighting seismically rated?	Yes
Is your piping seismically rated?	Yes
Is your HVAC system seismically anchored?	Yes
Is your electrical equipment seismically rated?	Yes
Percent of Building Glazed:	–

Building Stability

Median Collapse Capacity:	–
Beta (Dispersion):	–

Responses

No responses provided

Repair Time Options

Factors Delaying Start of Repairs	
Inspection	Yes
Financing	Yes
Permitting	Yes
Engineering Mobilization	Yes
Contractor Mobilization	Yes
Mitigation Factors	
Inspector on Retainer	No
Engineer on Retainer	No
Engineer on Retainer	No
Funding Source	Private Loans

Expected Loss

Expected loss in percent of total building value

Shaking Intensity	Return Period	SEL (%)	SUL (%)
20% in 50 years	225 Years	12	21
10% in 50 years	475 Years	21	39
5% in 50 years	975 Years	35	60
2% in 50 years	2475 Years	59	95

Repair Time

Median repair time, without impeding factors

Intensity	FEMA P-58 Parallel	FEMA P-58 Series	REDi Re-Occupancy	REDi Functional Recovery	REDi Full Recovery
20% in 50 years	3.6 weeks	2.8 months	4.4 weeks	6.4 weeks	6.4 weeks
10% in 50 years	6.6 weeks	5.8 months	2.5 months	2.9 months	2.9 months
5% in 50 years	2.7 months	11 months	5.0 months	5.3 months	5.3 months
2% in 50 years	4.9 months	19 months	11 months	11 months	11 months

2 BASIS OF ANALYSIS

This analysis is based on the SP3-RiskModel of the Seismic Performance Prediction Program (SP3) software platform. The underlying analysis methods are based on the FEMA P-58 analytical method, which is a transparent and well documented method developed through a 15 year project (Applied Technology Council, 2018). This project leveraged the previous decades of academic research, funded by a $16 million investment by the Federal Emergency Management Agency (FEMA). In contrast to many risk assessment methods based on judgment and past earthquake experience, the FEMA P-58 and SP3 analysis are based on engineering-oriented risk evaluation methods.

3 DOCUMENTATION OF SITE AND BUILDING INPUT DATA

Project Name: 7 Franz-Pritzker
Model Name: VD Retrofit w/test data (reduced joints / IMF) User GMs

3.1 Site Information

Address: 502 Portola Plaza, Los Angeles, CA, 90095
Latitude: 34.06985°
Longitude: -118.44125°

3.2 Building Information

Material Type:	Cast-in-Place Concrete
Number of Stories:	8
Total Building Square Footage:	84,211
Occupancy Type:	Commercial Office
Total Expected Building Replacement Value:	$22,110,841

4 SITE HAZARD INFORMATION

This section presents the site's seismic hazard information. The V_{S30} value is the shear wave velocity in the soil at a depth of 30 meters. This value and the associated site class are presented in Table 1.

Table 1. Site soil information

V_{S30} (m/s):	537.0
Site Class:	C

Table 2 and Figure 1 present the spectral acceleration information for this site. The spectral acceleration is a measure of how much force the building will attract in an earthquake. This amount of force is dependent on the intensity of the ground shaking (e.g. 10% in 50 years), as well as a dynamic property of the building known as the "fundamental period". Shorter buildings tend to have smaller fundamental periods and taller buildings tend to have larger fundamental periods. As indicated by Figure 1, smaller fundamental periods (with the exception of very short fundamental periods) will attract more force in an earthquake.

The Design Earthquake (DE) and Maximum Considered Earthquake (MCE) are based on the modern code maximum direction spectra and are converted to geometric mean for comparison.

Table 2. Geometric mean spectral acceleration values (in g)

Shaking Intensity	Return Period	PGA	$S_a(0.2s)$	$S_a(1.0s)$	$S_a(1.4s)$
20% in 50 years	225 years	0.39	0.93	0.36	0.29
10% in 50 years	475 years	0.52	1.13	0.55	0.44
5% in 50 years	975 years	0.70	1.70	0.73	0.59
2% in 50 years	2475 years	0.93	2.15	1.10	0.88

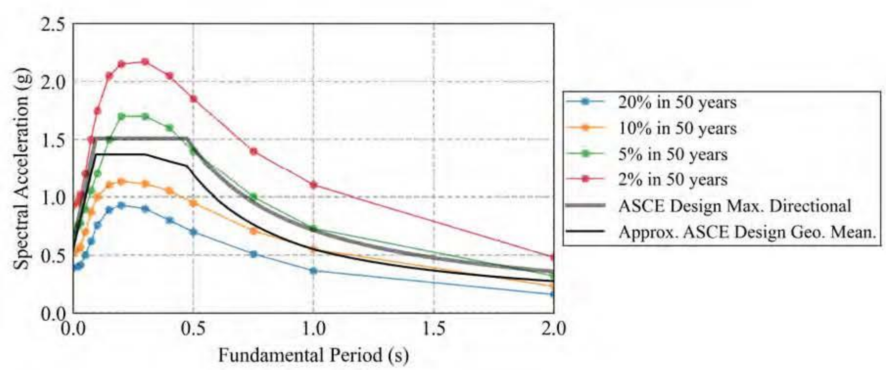

Figure 1. Hazard curves for this site. All curves are geometric mean unless otherwise stated.

5 BUILDING DESIGN SUMMARY FROM THE *SP3 BUILDING CODE DESIGN DATABASE*

5.1 Building Code Design Parameters

The seismic design parameters used to compute the seismic base shear coefficients for this building are presented in Table 3. These parameters are specific to the 1961 edition of the Uniform Building Code (International Conference of Building Officials, 1961).

Table 3. Code design parameters

(a) UBC 1961 structural system parameters

Parameter	Dir. 1	Dir. 2
C_d	1	1
k	1	1

(b) UBC 1961 site specific parameters

Parameter	Value
Z	1
Seismic Zone	3

5.2 Modern Building Code Design Parameters

For comparison to modern code, the modern code parameters are presented in Table 4.

Table 4. Modern code design parameters

(a) ASCE/SEI 7-2010 structural system parameters

Parameter	Dir. 1	Dir. 2
C_t	0.016	0.016
C_d	5.5	5.5
x	0.9	0.9
R	8	8
Ω_0	3	3

(b) ASCE/SEI 7-2010 site specific parameters

Parameter	Value
S_s	2.263
S_1	0.825
S_{ds}	1.508
S_{d1}	0.715
SDC	E
C_u	1.4
$\text{MCE}_{R,max}(g)$	0.794
$\text{MCE}_{R,geomean}(g)$	0.611
$\text{DE}_{max}(g)$	0.529
$\text{DE}_{geomean}(g)$	0.407

5.3 Structural Properties

This section summarizes the main structural properties of the building in each direction. These structural properties are used as inputs to the SP3 Structural Response Prediction Engine.

Table 5. Structural properties table

Parameter	Direction 1	Direction 2
General		
Structural System	RC: Space Frame	RC: Space Frame
Building Edge Length (ft)	102	102
Detailing Level	Ordinary	Ordinary
Strength		
Seismic Design Base Shear Ratio, C_s	0.035	0.035
Ultimate Base Shear Ratio, v_{ult}	0.128*	0.128*
Stiffness		
$T_{1,design}$ (s)	1.86	1.86
T_1 with structural overstiffness (s)	1.57	1.57
T_1 with gravity system (s)	1.56	1.56
T_1 with non-structural components (s)	1.48	1.48
T_1 empirical lower bound (s)	0.91	0.91
T_1 empirical upper bound (s)	1.61	1.61
T_1 Final (s)	1.35	1.35

*User defined, not SP3 default

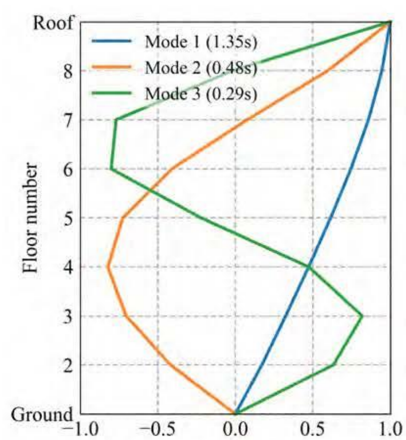

Figure 2. Mode shapes

6 BUILDING STABILITY

The FEMA P-154 collapse capacity score was calculated as follows using the "very high" seismicity level. The terminology used in this section is consistent with the FEMA P-154 methodology (Applied Technology Council, 2015a):

- $P[COL|MCE_R]_{P-154}$: the probability that the building will be in the HAZUS complete structural damage state when subjected to MCER shaking, times the collapse factor
- $P[COL|MCE_R]_{P-58}$: the probability that the building will be in the HAZUS complete structural damage state when subjected to MCER shaking, times the collapse factor
- Collapse Factor: expected ratio of collapsed area to total area given that the building is in the HAZUS Complete structural damage state

For a more in-depth explanation of "collapse," refer to Section 4.4.1.5 of FEMA P-155 Third Edition available here (Applied Technology Council, 2015b).

Table 6. Breakdown of FEMA P-154 score assignment

FEMA ID:	C1
Basic Score	1
Soil	0
Year	0
Plan Irregularity	0
Vertical Irregularity	0
Risk Category* (Cat I/II)	0
Sum:	1
Minimum Allowed:	0.3
Score:	**1**
Dispersion (β):	0.7

*Non-standard property implemented by SP3

The FEMA P-154 probability of collapse at the MCE_R level event is then calculated as:

$$\begin{aligned} P[COL|MCE_R]_{P-154} &= 10^{-\text{score}} \\ &= 10^{-1} \qquad \text{(FEMA P-155 eqn. 4-1)} \\ &= 10.0\% \end{aligned}$$

Taking into account the fraction of floor area collapsed (1 in this case), the probability of collapse is:

$$\begin{aligned} P[COL|MCE_R]_{P-58} &= P[COL|MCE_R]_{P-154} \text{ / Collapse Factor} \\ &= 10.0\% / 1 \\ &= 10.0\% \end{aligned}$$

The median collapse capacity is calculated as:

$$\begin{aligned} S_{a,\ collapse\ median,\ P-58} &= \exp\left(\ln(S_{a,MCE_R}) - \text{norminv}\left(P[COL|MCE_R]_{P-58}\right) \cdot \beta\right) \\ &= \exp\left(\ln(0.611g) - \text{norminv}\left(10.0\%\right) \cdot 0.7\right) \\ &= 1.50g \end{aligned}$$

where `norminv` is the inverse of the standard normal cumulative distribution function (CDF).

Figure 3 shows the collapse capacity cumulative distribution function used in the analysis.

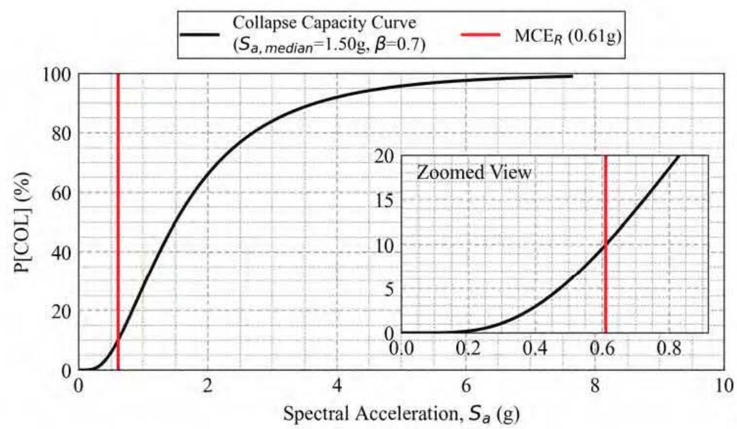

Figure 3. Cumulative distribution function for collapse capacity

7 STRUCTURAL RESPONSE PREDICTIONS FROM THE SP3 STRUCTURAL RESPONSE PREDICTION ENGINE

The SP3 Response Prediction Engine predicts the structural responses (typically providing 100 ground motions per intensity level); this is done by using a combination of three-mode elastic modal analysis, coupled with both elastic and inelastic response modifiers mined from the large SP3 Structural Responses Database (with over 4,000,000 response simulations, and growing). These response predictions track all of the important statistical information in the responses (mean, variability, and correlations); this enables a statistically robust vulnerability curve at the end of the risk assessment process.

7.1 Peak Story Drift

Peak interstory drift ratio is an important metric for both structural and non-structural components in the building. It measures how much the ceiling of a given story moves relative to the floor, normalized to the height of the story. The greater the interstory drift ratio, the greater the damage to the components on that level. Typical components that are damaged from interstory drift ratio are structural components (beams and columns), gypsum partition walls, and exterior cladding and glazing.

Table 7. Peak story drift demands are the same in both directions

Story	20% in 50 years	10% in 50 years	5% in 50 years	2% in 50 years
8	0.34	0.47	0.61	0.91
7	0.47	0.65	0.85	1.26
6	0.56	0.77	1.02	1.50
5	0.61	0.85	1.12	1.66
4	0.65	0.90	1.19	1.76
3	0.68	0.94	1.23	1.82
2	0.71	0.98	1.29	1.91
1	0.75	1.04	1.36	2.02

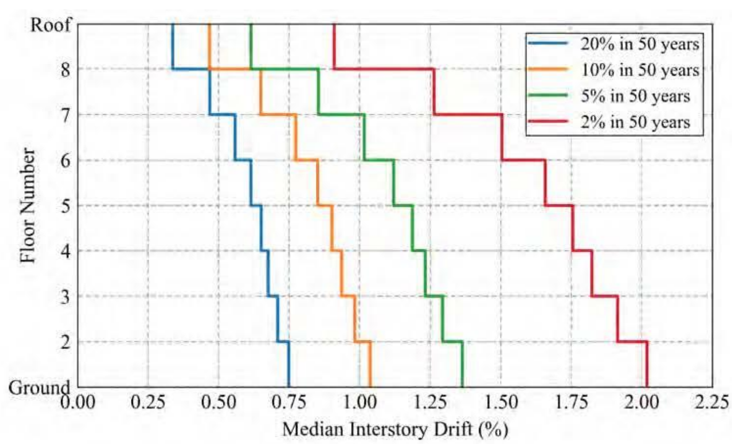

Figure 4. Peak story drift demands are the same in both directions

7.2 Peak Floor Acceleration

Peak floor acceleration is an an important metric for non-structural components in the building. Components such as piping, HVAC, and electrical switchgear are sensitive to the floor accelerations. High accelerations will typically damage a component itself or cause the component's anchorage to fail, both of which may require repair or replacement of the component.

Table 8. Peak floor acceleration demands are the same in both directions

Floor	20% in 50 years	10% in 50 years	5% in 50 years	2% in 50 years
Roof	0.55	0.58	0.64	0.70
8	0.44	0.47	0.53	0.59
7	0.40	0.44	0.50	0.57
6	0.37	0.41	0.49	0.57
5	0.36	0.42	0.50	0.61
4	0.36	0.42	0.53	0.65
3	0.36	0.45	0.57	0.73
2	0.37	0.47	0.62	0.80
Ground	0.39	0.52	0.70	0.93

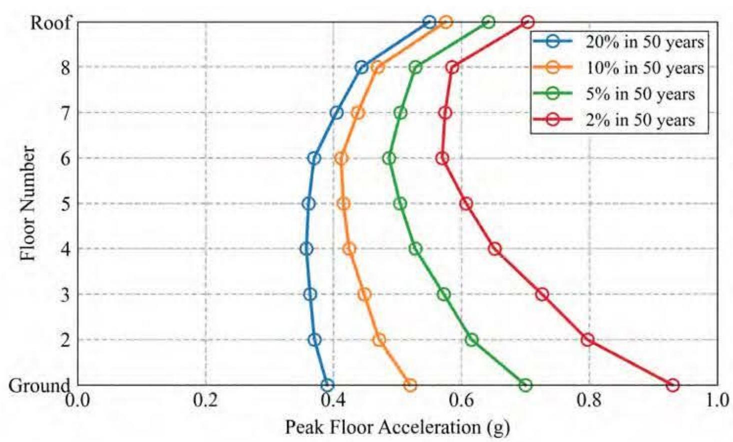

Figure 5. Peak floor acceleration demands are the same in both directions

7.3 Residual Story Drift

Residual drift is a metric that informs the need for structural repairs or building demolition (where excessive drifts are present). Residual drift ratio is a measure of how much the building is "leaning over" after the seismic event has ceased. A residual drift of 2% would indicate that the story is laterally displaced 2% of it's height, which equates to about 3.6 inches for a 15 foot tall story.

Table 9. Residual story drift demands are the same in both directions

Story	20% in 50 years	10% in 50 years	5% in 50 years	2% in 50 years
8	0.00	0.00	0.00	0.03
7	0.00	0.00	0.02	0.07
6	0.00	0.01	0.04	0.10
5	0.00	0.02	0.05	0.12
4	0.00	0.03	0.06	0.13
3	0.00	0.03	0.07	0.14
2	0.00	0.04	0.08	0.15
1	0.01	0.04	0.08	0.17

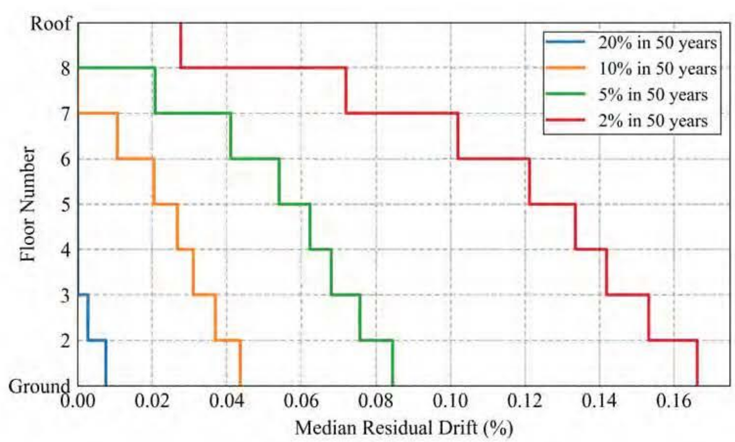

Figure 6. Residual story drift demands are the same in both directions

7.4 Maximum Residual Story Drift

Residual drift is a metric that informs the need for structural repairs or building demolition (where excessive drifts are present). A residual drift of 2% would indicate that the story is laterally displaced 2% of it's height, which equates to about 3.6 inches for a 15 foot tall story. Maximum residual drift is the maximum of the residual drifts on all levels. This is the value used to determine if the building is demolished due to excessive residual drift. Excessive drifts can be visually unsettling and prohibitively expensive (or even impossible) to "straighten" and repair the structural damage. Due to this, the building owner may decide to demolish and rebuild the building if the residual drifts are too large.

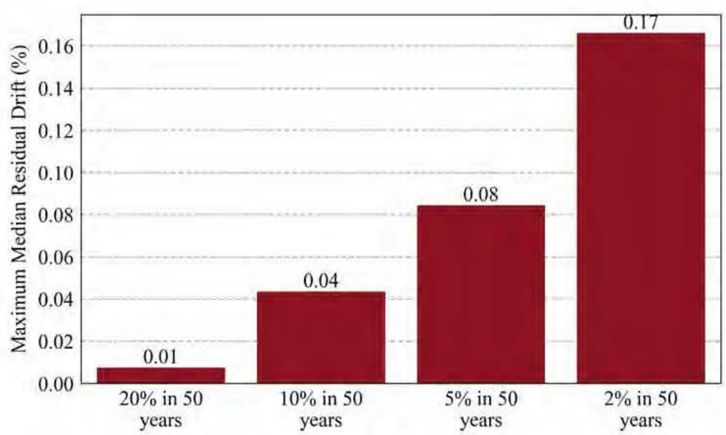

Figure 7. Maximum residual story drift demands are the same in both directions

8 REPAIR COSTS - BY LEVEL OF GROUND MOTION

8.1 Mean and 90^{th} Percentile Repair Costs (SEL and SUL)

The different metrics for repair cost are as follows:

- **Mean (SEL)**: ("Scenario Expected Loss") the average repair cost of the building repair/replacement.
- **Median**: there is a 50% probability that the repair cost will not exceed this value.
- **Fitted SUL**: Fitted value of "Scenario Upper Loss".
- **Counted 90^{th} Percentile**: there is a 90% probability that the repair cost will not exceed this value.

Table 10. Expected loss normalized by building cost

Intensity	PGA (g)	Mean (SEL) (%)	Fitted SUL (%)	Median (%)	Counted 90^{th} Percentile (%)
20% in 50 years	0.39	12	21	8.9	21
10% in 50 years	0.52	21	39	16	39
5% in 50 years	0.70	35	60	28	75
2% in 50 years	0.93	59	95	54	100

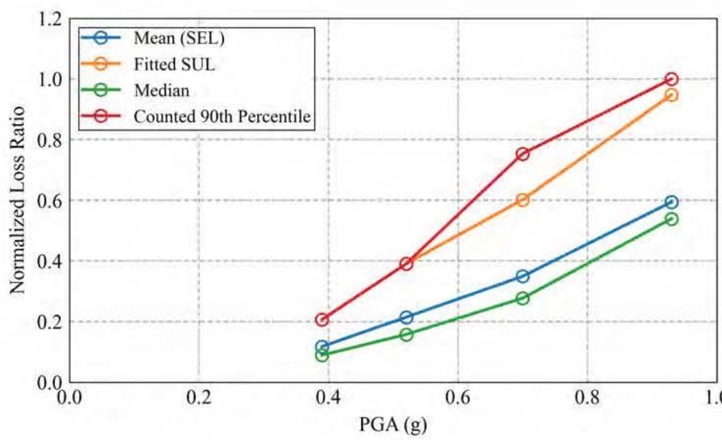

Figure 8. Loss metrics across all intensity levels analyzed

9 REPAIR COST BREAKDOWN BY BUILDING COMPONENTS

9.1 Categories for Repair Cost Breakdowns

Repair costs are binned into eight categories as follows:

- **Collapse**: building demolition and replacement following a collapse.
- **Residual**: building demolition and replacement following unacceptable residual drifts.
- **Structural**: components of the lateral force resisting system or gravity system (e.g. beam column connections, link beams, shear wall, shear tabs, etc.).
- **Partitions**: partition wall components (e.g. wood or metal stud gypsum full height partitions).
- **Exterior**: components placed on the exterior of the building (e.g. cladding, glazing, etc.).
- **Interior**: non-structural components on the interior of the building (e.g. raised access floors, ceilings, lighting).
- **HVAC**: HVAC and plumbing components (e.g. water piping and bracing, sanitary piping, ducting, boilers etc.).
- **Other**: components not included in the categories above (e.g. elevators, user defined components, fire protection components).

9.2 Repair Cost Breakdown for Various Ground Motion Levels

Table 11. Expected mean loss per component group (in percent)

Intensity	Total	Structural	Collapse	Other	Partitions	HVAC	Residual	Interior	Exterior
20% in 50 years	12	5.3	1.0	2.4	0.7	1.9	0.0	0.4	0.0
10% in 50 years	21	12	3.9	2.5	1.0	1.9	0.0	0.6	0.0
5% in 50 years	35	19	9.0	2.5	1.3	1.8	0.0	0.8	0.0
2% in 50 years	59	29	23	2.2	1.6	1.6	1.1	1.1	0.0

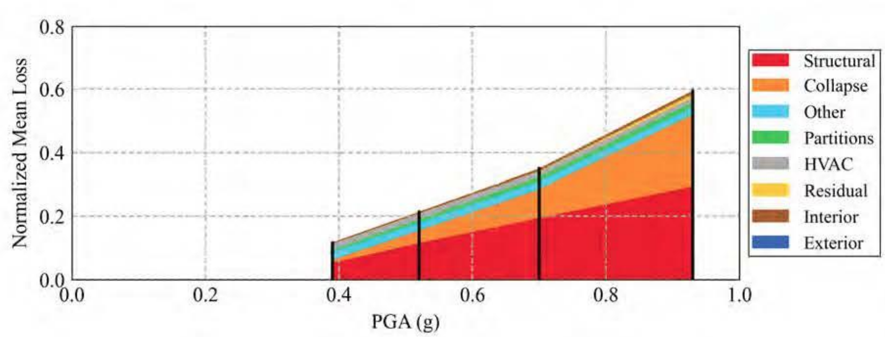

Figure 9. Contribution of building components to mean loss ratio

9.3 Repair Cost Breakdown for Expected Annual Loss

The expected annual loss for this building is $27,483.

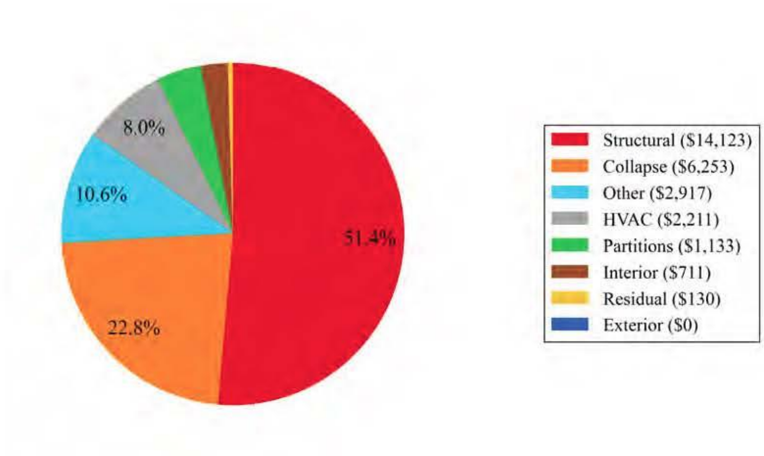

Figure 10. Annualized loss breakdown

10 REPAIR TIME AND BUILDING CLOSURE TIME

The building repair times are computed from the REDi Rating System methodology (Almufiti & Willford, 2013). These are the preferred method to compare building repair time because these include detailed repair schedules as part of the calculation process.

- **Re-Occupancy**: This is the time after which the building is deemed safe enough to be used for shelter.
- **Functional Recovery**: This is time required to establish re-occupancy and regain the facility's primary function. This is what is typically used for assessing building closure time.
- **Full Recovery**: This is the time required to restore the building to its original pre-earthquake condition.

For comparison, the methods of calculating building repair time from the FEMA P-58 methodology are as follows. These are typically not used to estimate building closure time.

- **Series**: Repair activities are limited to one floor at a time
- **Parallel**: All floors are repaired at the same time

For a design level or 10% in 50 year event, the REDi methodology is also calibrated to include "impedance factors" associated with the following processes:

- Post-earthquake Inspection
- Engineering Mobilization and Review/Re-design
- Financing
- Contractor Mobilization and Bid Process
- Permitting

These capture the time required to start the repairs, since beginning repairs immediately after an earthquake may not be realistic. **With these impedance factors, the median functional recovery time is 10 months.**

Table 12. Median repair time, without impeding factors

Intensity	FEMA P-58 Parallel	FEMA P-58 Series	REDi Re-Occupancy	REDi Functional Recovery	REDi Full Recovery
20% in 50 years	3.6 weeks	2.8 months	4.4 weeks	6.4 weeks	6.4 weeks
10% in 50 years	6.6 weeks	5.8 months	2.5 months	2.9 months	2.9 months
5% in 50 years	2.7 months	11 months	5.0 months	5.3 months	5.3 months
2% in 50 years	4.9 months	19 months	11 months	11 months	11 months

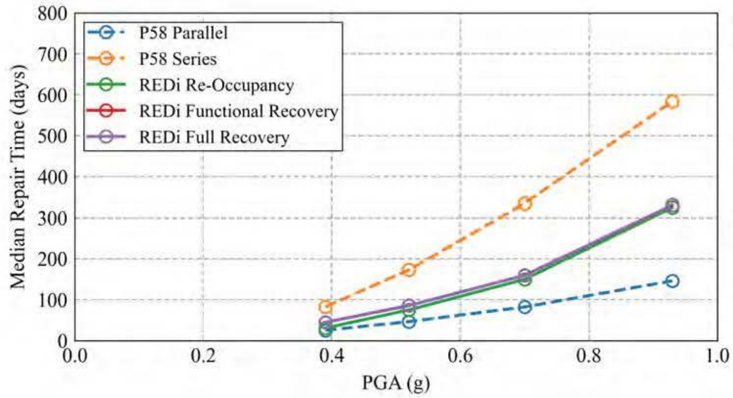

Figure 11. Median repair time, without impeding factors

11 JUSTIFICATION OF SECONDARY MODIFIERS

No justification of secondary inputs was provided.

12 DISCLAIMER

REFERENCES

Almufiti, Ibrahim, & Willford, Michael. 2013. *REDi Rating System.* Arup.

Applied Technology Council. 2015a. *FEMA P-154: Rapid Visual Screening of Buildings for Potential Seismic Hazards: A Handbook.*

Applied Technology Council. 2015b. *FEMA P-155: Rapid Visual Screening of Buildings for Potential Seismic Hazards: Supporting Documentation.*

Applied Technology Council. 2018. *FEMA P-58: Seismic Perfromance Assessment of Buildings.*

International Conference of Building Officials. 1961. *Uniform Building Code 1961 Edition.* International Conference of Building Officials.

REFERENCES

[1] Abdullah, S. A., & Wallace, J. W. (2019). *Reinforced Concrete Structural Walls: Test Database and Modeling Parameters.* Los Angeles.

[2] ACI 318. (2014). ACI 318 Committee. *Building Code Requirements for Structural Concrete*. Farmington Hills, Michigan: American Concrete Institute.

[3] ACI 318, A. C. (2019, 07 01). *A Short History of the ACI 318 Structural Concrete Building Code*. Retrieved from American Concrete Institute (www.concrete.org): https://www.concrete.org/news/newsdetail.aspx?f=51718061

[4] Aktan, A., & Bertero, V. (1984, August). Seismic Response of R/C Frame-Wall Structures. *Jounral of Structural Engineering, 110*(8), 1803-1821.

[5] Alfirevic, D., & Alfirevic, S. S. (2017). Brutalism in Serbian Architecture: Style or Necessity? *Facta universitatis - series Architecture and Civil Engineering 15(3)*, 317-331.

[6] Almufti, I., & Willford, M. (2013). *Resilience-based Earthquake Design Initiative for the Next Generation of Buildings.* Arup.

[7] Alsiwat, J., & Saatcioglu, M. (1992). Reinforcement Anchorage Slip under Monotonic Loading. *Journal of Structural Engineering, 118*(9), 2421-2438.

[8] ASCE/SEI 41-06. (n.d.). . eismic rehabilitation of existing buildings/ American Society of Civil Engineers. Reston, Va.: American Society of Civil Engineers; 2007. .

[9] ATC. (2017). *Recommended Modeling Parameters and Acceptance Criteria for Non-linear Analysis in Support of Seismic Evaluation, Retrofit, and Design.* Gaithersburg: National Institute of Standards and Technology NIST GCR 17-917-45.

[10] ATC. (2020). *FEMA P-58 ATC Council*. Retrieved from FEMA P-58 ATC Council: https://femap58.atcouncil.org/reports

[11] ATC, & FEMA P-58. (2012). *FEMA P-58*. Retrieved from Applied Technology Council (ATC): https://femap58.atcouncil.org/

[12] ATC, & FEMA P-58-1. (2018). *Seismic Performance Assessment of Buildings Volume 1 – Methodology (2nd Edition).* Washington D.C.: Federal Emergency Management Agency.

[13] Baradaran S., M. (2013). *Collapse Assessment of Concrete Buildings: An Application to Non-Ductile Reinforced Concrete Moment Frames* . Vancouver: University of British Columbia.

[14] Baradaran S., M., Elwood, K. J., & Yang, T. Y. (2012, June 24). *Seismic loss estimation of non-ductile reinforced concrete buildings*. Retrieved from John Wiley & Sons, Ltd.: https://doi.org/10.1002/eqe.2213

[15] Barney, K., Rabbat, B., Fiorato, A. E., Russell, H. G., & Corley, W. G. (1980). Behavior of Coupling Beams under Load Reversals. *Portland Cement Association*.

[16] Binney, J. (1972). *Diagonally Reinforced Coupling Beams.* MS Thesis, University of Canterbury, Christchurch, New Zealand.

[17] Biskinis, D., & Fardis, M. N. (2007). *Effect of Lap Splices on Flexural Resistance and Cyclic Deformation Capacity of RC Members.* Berlin: Beton- und Stahlbetonbau.

[18] Boston, M., & Mitrani-Reiser, J. (2018). Applying Resilient Rating Systems for Predicting Continued Operability of Hospitals after Earthquakes. *17th U.S.-Japan-New Zealand Workshop on the Improvement of Structural Engineering and Resilience* (pp. P3-4-1 to P3-4-8). Queenstown: 17th U.S.-Japan-New Zealand Workshop on the Improvement of Structural Engineering and Resilience.

[19] Bower, O. (2008). *Analytical Investigation into the Effect of Axial Restraint on the Stiffness and Ductility of Diagonally Reinforced Concrete Coupling Beams.* MS Thesis, University of Cincinnati.

[20] Brena, S., & Ihtiyar, O. (2011). Preformance of conventinoally reinforced coupling beams subjectd to cyclic loading. *Journal of Structural Engineering, 137*, 665-676.

[21] Bristowe, S. (2000). *Seismic response of normal and high-strength concrete members.* PhD Thesis, McGill University, Canada.

[22] California State University, N. (2019, 07 16). *Northridge Earthquake Photo Collection*. Retrieved from https://digital-library.csun.edu/northridge-earthquake-photos

[23] Cho, J. Y., & Pincheira, J. A. (2006). Inelastic analysis of reinforced concrete columns with short lap splices subjected to reversed cyclic loads . *ACI Structural Journal*, 280-290.

[24] Coleman, & Spacone. (2001, November). Localization Issues in Force-Based Frame Elements. *Jounral of Structural Engineering, 127*(11), 1257-1265.

[25] Comartin, C. A. (2008). *The Concrete Coalition: Building a Network to Address Nonductile Concrete Buildings.* Beijing: 14WCEE.

[26] CUREe. (1998). *Proceedings of the NEHRP Conference and Workshop on Research on the Northridge, California Earthquake of January 17, 1994.* Richmond: California Universities for Research in Earthquake Engineering.

[27] Dugas, D. (2003). *Seismic response of diagonally reinforced coupling beams with headed bars.* MS Thesis, McGill University, Canada.

[28] Elwood, K. J., & Eberhard, M. O. (2009). Effective Stiffness of Reinforced Concrete Columns. *ACI Structural Journal*, 476-484.

[29] Elwood, K. J., & Moehle, J. P. (2008). Dynamic Shear and Axial-Load Failure of Reinforced Concrete Columns. *ASCE Journal of Structural Engineering, 134(7)*, 1189-1198.

[30] Elwood, K. J., & Moehle, J. P. (2008). Dynamic Shear and Axial-Load Failure of Reinforced Concrete Columns. *ASCE Journal of Structural Engineering*, 1189-1198.

[31] Elwood, K. J., Matamoros, A. B., Wallace, J. W., Lehman, D. E., Heintz, J. A., Mitchell, A. D., . . . Moehle, J. P. (2007). Update to ASCE/SEI 41 Concrete Provisions. *Earthquake Spectra*, 493-523.

[32] Elwood, K. J., Wallace, J. W., Lehman, D., Heintz, J., Mitchell, A., Moore, M., . . . Moehle, J. P. (2007). *Update to ASCE/SEI 41 Concrete Provisions.* Berkeley: PEER.

[33] Engineering, C. U. (1998). *Proceedings of the NEHRP Conference and Workshop on Research on the Northridge, California Earthquake of January 17, 1994.* Richmond: California Universities for Research in Earthquake Engineering.

[34] FEMA 356. (n.d.). . Prestandard and commentary for the seismic rehabilitation of buildings/prepared by the American Society of Civil Engineers; prepared for Federal Emergency Management Agency. Reston, Va.: American Society of Civil Engineers; Washington, DC: Federal Emergency Management Agency; 2000. .

[35] Fischinger, M., Isaković, T., & Kante, P. (2006). Shaking Table Response of a Thin H-shaped Coupled Wall. *Managing Risk in Earthquake Country - 100th Anniversary Earthquake Conference : Centennial Meeting.* San Francisco, USA: Earthquake Engineering Research institute, Berkeley, CD ROM.

[36] Fisher, E. C., Stringer, M., & Horiuchi, C. (2017). What structural engineers need to know about resilience. *Structure Magazine*, 34-37.

[37] Fortney, P. (2005). *The Next Generation of Coupling Beams.* PhD Thesis, University of Cincinnati.

[38] Fortney, P., Rassati, G., & Shahrooz, B. (2008). Investigation on effect of transverse reinforcement on performance of diagonally reinforced coupling beams. *ACI Structural Journal, 105*, 781-788.

[39] Galano, L., & Vignoli, A. (2000). Seismic behavior of short coupling beams with different reinforcement layouts. *ACI Structural Journal, 97*, 876-885.

[40] Gavridou, S. (2015). *Shake Table Testing and Analytical Modeling of a Full-Scale, Four-Story Unbonded Post-Tensioned Concrete Wall Building.* Los Angeles: University of California, Los Angeles.

[41] Ghannoum, W. M., & Matamoros, A. B. (n.d.). *Non-linear modeling parameters and acceptance criteria for concrete columns.* ResearchGate.

[42] Gould, N. C., Kallros, M. K., & Dowty, S. M. (2019). Concrete Parking Structures and the Northridge Earthquake. *Structure Magazine*, 48-54.

[43] Hognestad, E. (1951). *A study on combined bending and axial load in reinforced concrete members.* Univ. of Illinois Engineering Experiment Station, Univ. of Illinois at Urbana-Champaign, IL, 43-36.

[44] Holmes, W. T. (2014). Identification and Mitigation of Collapse Prone Concrete Buildings. *10th US National Conference on Earthquake Engineering* (p. 8). Anchorage: 10NCEE.

[45] ICC, I. C. (2017). *The Future of Hazard Resilience: Building Codes and Best Practices.* Columbus: International Code Council.

[46] Islam, S. M. (1996, September). Analysis of the Northridge earthquake response of a damaged non-ductile concrete frame building. *The Structural Design of Tall Buildings*,

151-182. Retrieved from John Wiley & Sons, Ltd.: https://doi.org/10.1002/(SICI)1099-1794(199609)5:3<151::AID-TAL76>3.0.CO;2-4

[47] Kimura, Y. (n.d.). Experimental Study on Seismic Behavior of R/C Diagonally Reinforced Short Beams. *Eleventh World Conference on Earthquake Engineering.*

[48] Kwan, A., & Zhao, Z. (2002). Cyclic behaviour of deep reinforced concrete coupling beams. . *Proc Inst Civil Eng: Struct Build, 152*, 283-293.

[49] Kwan, A., & Zhao, Z. (2002). Testing of coupling beams with equal end rotations maintained and local joint deformation allowed. *Proc Inst Civil Eng: Struct Build, 152*, 67-78.

[50] Lang, S. C., & Wallace, J. W. (2008). *Building Specific Component Testing for Seismic Rehabilitation.* Los Angeles: UCLA.

[51] Lehman, Turgeon, Birely, Hart, Marley, Kuchma, & Lowes. (2013, August). Seismic Behavior of a Modern Concrete Coupled Wall. *Journal of Structural Engineering ASCE, 139*, 1371-1381.

[52] Lim, E., Hwang, S.-J., Cheng, C.-H., & Lin, P.-Y. (2016). Cyclic Tests of Reinforced Concrete Coupling Beam with Intermediate Span-Depth Ratio. *ACI Structural Journal*, *113*(03), 515-524.

[53] Lynn, A. C. (2001). *Seismic Evaluation of Existing Reinforced Concrete Building Columns.* Berkeley.

[54] Mahrenholtz, C., Lin, P.-C., Wu, A.-C., Tsai, K.-C., Hwang, S.-J., Lin, R.-Y., & Bhayusukma, M. Y. (2015). Retrofit of reinforced concrete frames with buckling-restrained braces. *Earthquake Engineering & Structural Dynamics* , 44:59-78.

[55] Mander, Priestley, & Park. (1988, August). Observed Stress-Strain Behavior of Confined Concrete. *Journal of Structural Engineering, 114*(8), 1827-1849.

[56] Mander, Priestley, & Park. (1988, August). Theoretical Stress-Strain Model for Confined Concrete. *Jounral of Structural Engineering, 114*(8), 1804-1826.

[57] Massone , L. M., & Wallace, J. W. (2006). *RC wall shear-flexure interaction: Analytical and experimental responses.* Los Angeles: University of California, Los Angeles.

[58] Matamoros, A. B., Matchulat, L., & Woods, C. (2008). *Axial Load Failure of Shear Critical Columns Subjected to High Levels of Axial Load.* Beijing: 14WCEE.

[59] Mayes, R. L., & Reis, E. (2015). The U.S. Resiliency Council (USRC) and the Building Rating System. *ASCE and ATC*, 754-764.

[60] Melek, M., & Wallace, J. W. (2004). Performance of Columns with Short Lap Splices. *13th World Conference on Earthquake Engineering.* Vancouver: 13th World Conference on Earthquake Engineering.

[61] Moehle, Ghodsi, Hooper, Fields, & Gedhada. (2012). *Seismic Design of Cast-in-Place Concrete Special Structural Walls and Coupling Beams, A Guide for Practicing Engineers.* National Institute of Standards adn Technology, U.S. Department of Commerce. -: NEHRP NIST GCR 11-917-11REV-1.

[62] Moehle, J. (2014). *Seismic Design of Reinforced Concrete Buildings.* McGraw Hilla.

[63] Mortezaei, A. (2014). Columns, Plastic Hinge Length of RC under the Combined Effect of Near-Fault Vertical and Horizontal Ground Motions. *Periodica Polytechnica*, 243-253.

[64] Naish, D. A., & Wallace, J. W. (2010). *Testing and Modeling of Reinforced Concrete Coupling Beams.* Los Angeles: UCLA.

[65] NIST GCR 12-917-21. (2012). *Soil-Structure Interaction for Building Structures by NEHRP Consultants Joint Venture.* U.S. Department of Commerce. National Institute of Standards and Technology.

[66] NIST GCR 14-917-28. (2013). *Review of Past Performance and Further Development of Modeling Techniques for Collapse Assessment of Existing Reinforced Concrete Buildings.* NIST.

[67] OSHPD. (2001). *Summary of Hospital Seismic Performance Ratings.* Sacramento: OSHPD.

[68] Ozselcuk, A. (1990). *Experimental and Analytical Studies of Coupled Wall Structures.* Berkeley: University of California, Berkeley.

[69] Park, R., Priestley, M. J., & Wayne, G. D. (1982). Ductility of Square-Confined Concrete Columns. *Journal of the Structural Division Vol. 108, Issue 4*, 929-950.

[70] Paulay, T. (1969). *The Coupling of Shear Walls.* PhD Thesis, University of Canterbury, Christchurch, New Zealand.

[71] Paulay, T. (1971). Coupling Beams of Reinforced Concrete Shear Walls. *Journal of the Structural Division, American Society of Civil Engineers, 97*(3), 843-862.

[72] Paulay, T., & Priestley, M. J. (1992). *Seismic Design of Reinforced Concrete and Masonry Buildings.* New York: John Wiley & Sons, Inc.

[73] PEER. (2009). *Evaluation of Ground Motion Selection and Modification Methods: Predicting Median Interstory Drift Response of Buildings.* Berkeley: Pacific Engineering Research Center.

[74] PEER Report 2014/18. (2014). *Three-Dimensional Beam-Truss Model for Reinforced-Concrete Walls and Slabs Subjected to Cyclic Static or Dynamic Loading* . Lu, Y.;

Panagiotou, M.; Koutromanos, I.;. Berkeley, CA: Pacific Earthquake Engineering Research Center .

[75] PEER/ATC-72-1. (2010). *Modeling and Acceptance Criteria for Seismic Design and Analysis of Tall Buildings* . Redwood City, Califonia: Applied Technology Cuncil.

[76] Pekelnicky, R., Hagen, G., & Martin, D. (2017). A Summary of Significant Updates in ASCE 41-17. *2017 SEAOC Convention Proceeding* (pp. 1-10). 2017 SEAOC Convention .

[77] Powell, G. (2007). *Detailed Example of a Tall Shear Wall Building using CSI's Perform-3D Non-linear Dynamic Analysis.* Computers & Structures Inc.

[78] Rojahn, C. (2008). *The Applied Technology Council: A Historical Perspective.* Beijing: World Conference on Earthquake Engineering.

[79] Saatcioglu, M., & Razvi, S. (1992). Strength and Ductility of Confined Concrete. *ASCE Journal of Structural Engineering, 1186,* 1590-1607.

[80] Saatcioglu, M., & Razvi, S. R. (1992). Strength and Ductility of Confined Concrete . *Journal of Structural Engineering, American Society of Civil Engineers, 118*(6), 1590-1607.

[81] Segura, C. L., & Wallace, J. W. (2017). *Seismic Performance Limitations of Slender Reinforced Concrete Structural Walls.* Los Angeles.

[82] Sezen, H. (2002). *Seismic behavior and modeling of reinforced concrete building columns.* Berkeley.

[83] Sezen, H., & Moehle, J. P. (2006). Seismic Tests of Concrete Columns with Light Transverse Reinforcement. *ACI Structural Journal Technical Paper, 103*(S85), 842-849.

[84] SP3, R. (2021). *Seismic Performance Prediction Platform*. Retrieved from Seismic Performance Prediction Platform: https://sp3risk.com/

[85] Standards New Zealand - NZS 3101. (1995). Concrete Structures Standard. Wellington: Standards Neew Zealand.

[86] Sugaya, K. (2003). *Experimental Study on Variation Mechanism of Carrying shear force at the time of the earthquake of Coupling Beams with T-shaped Continuous Layer Coupled Wall* . PhD Thesis, Japan.

[87] Sugaya, Teshigawara, & Kato. (2000). Experimental Study on Carrying Shear Force Ratio of 12 Story Coupled Shear Wall. *12WCEEE 2000*. -: 12WCEE.

[88] Tassios, T., Moretti, M., & Bezas, A. (1996). On the behavior and ductility of reinforced concrete coupling beams of shear walls. *ACI Structural Journal, 93*, 711-720.

[89] Taylor-Lang, S. C., & Wallace, J. W. (2008). *Building Specific Component Testing for Seismic Rehabilitation.* Los Angeles: UCLA.

[90] Taylor-Lange, S. C., Wallace, J. W., Salamanca, A., Gavan, J. R., Reynolds, A. D., & Toranzo, L. (2007). Seismic Rehabilitation – Benefits of Component Testing. *Structural Engineers Association of California Convention (SEAOC)* (p. 8). Lake Tahoe: SEAOC.

[91] Thomsen, J. H., & Wallace, J. W. (2004). Experimental verification of Displacement-Based Design Procedures for Slender Reinforced Concrete Structural Walls . *Journal of Structural Engineering, American Society of Civil Engineers, 130*(4), 618-630.

[92] Todd, D., Carino, N., Chung, R. M., Lew, H. S., Taylor, A. W., & Walton, W. D. (1994). *1994 Northridge Earthquake.* Washington: NIST Special Publication.

[93] Tuna, Z. (2012). *ic Performance, Modeling, and Failure Assessment of Reinforced Concrete Shear Wall Buildings.* PhD Thesis, University of California, Los Angeles.

[94] TWH Press, T. W. (2016, 05 10). *The White House President Obama*. Retrieved from The White House President Obama Blog (https://obamawhitehouse.archives.gov): https://obamawhitehouse.archives.gov/blog/2016/05/10/advancing-resilience-through-building-codes-and-standards

[95] UCP, C. A. (2017). *University of California Seismic Safety Policy*. University of California Policy.

[96] USRC, U. (2020). *https://www.usrc.org/usrc-rating-system/*. Retrieved from https://www.usrc.org/usrc-rating-system/: https://www.usrc.org/usrc-rating-system/

[97] Wallace, J. W. (1994). A New Methodology for Seismic Design of Reinforced Concrete Shear Walls . *Journal of Structural Engineering, American Society of Civil Engineers , 120*(3), 863-884.

[98] Wallace, J. W. (2007). Modeling Issues for Tall Reinforced Concrete Core Wall Buildings . *The Structural Design of Tall and Special Buildings , 16*(5), 615-632.

[99] Wallace, J. W. (2012, March). Behavior, Design, and Modeling of Structural Walls and Coupling Beams – Lessons from Recent Laboratory Tests and Earthquakes . *International Journal of Concrete Structures and Materials, 6*(1), 3-18.

[100] Wu, C.-L., Kuo, W.-W., Yang, Y.-S., Hwang, S.-J., Elwood, K. J., Loh, C.-H., & Moehle, J. P. (2008, October 20). *Collapse of a nonductile concrete frame: Shaking table tests*. Retrieved from John Wiley & Sons, Ltd.: https://doi.org/10.1002/eqe.853

[101] Xiao, Y., Esmaeily-Ghasemabadi, A., & Wu, H. (1999). High-Strength Concrete Short Beams Subjected to Cyclic Shear . *Structural Journal, American Concrete Institute, 96*(3), 392-399.

[102] Yavari, S., Elwood, K. J., & Wu, C.-l. (2008, October 16). *Collapse of a nonductile concrete frame: Evaluation of analytical models*. Retrieved from John Wiley & Sons, Ltd.: https://doi.org/10.1002/eqe.855

[103] Zhu, L., Elwood, K. J., & Haukaas, T. (2007). Classification and Seismic Safety Evaluation of Existing Reinforced Concrete Columns. *Journal of Structural Engineering (ASCE)*, 1316-1330.